

JULY 2017

AJNR

VOLUME 38 • PP 1275-1461

AJNR

AMERICAN JOURNAL OF NEURORADIOLOGY

JULY 2017
VOLUME 38
NUMBER 7
WWW.AJNR.ORG

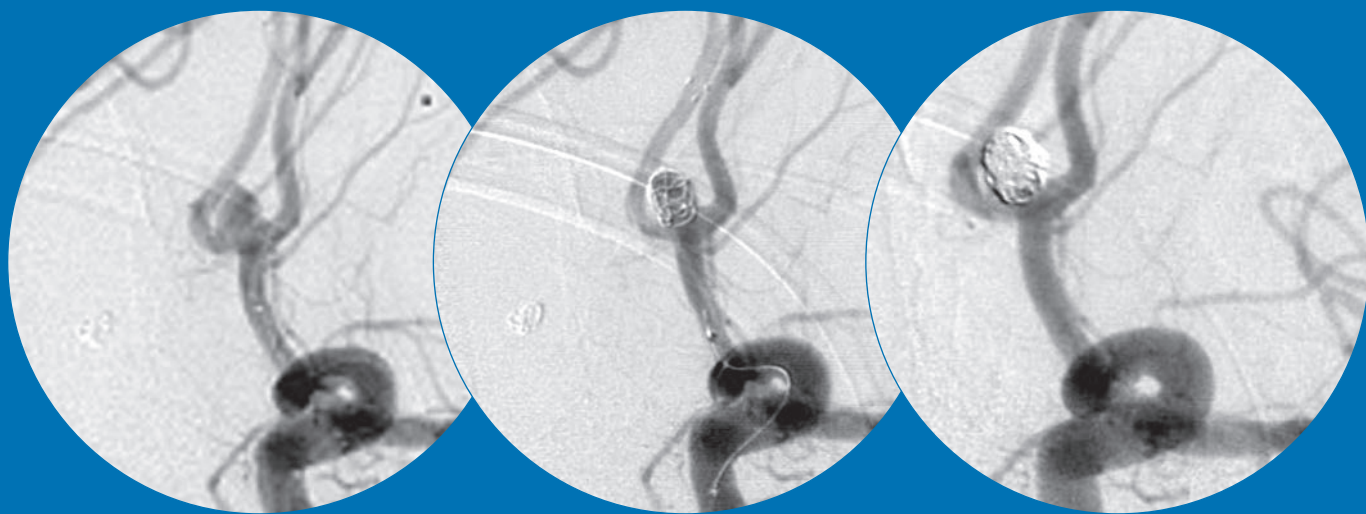
THE JOURNAL OF DIAGNOSTIC AND
INTERVENTIONAL NEURORADIOLOGY

Temporary stent-assisted coil embolization of aneurysms

Diffusional kurtosis and outcome in acute stroke

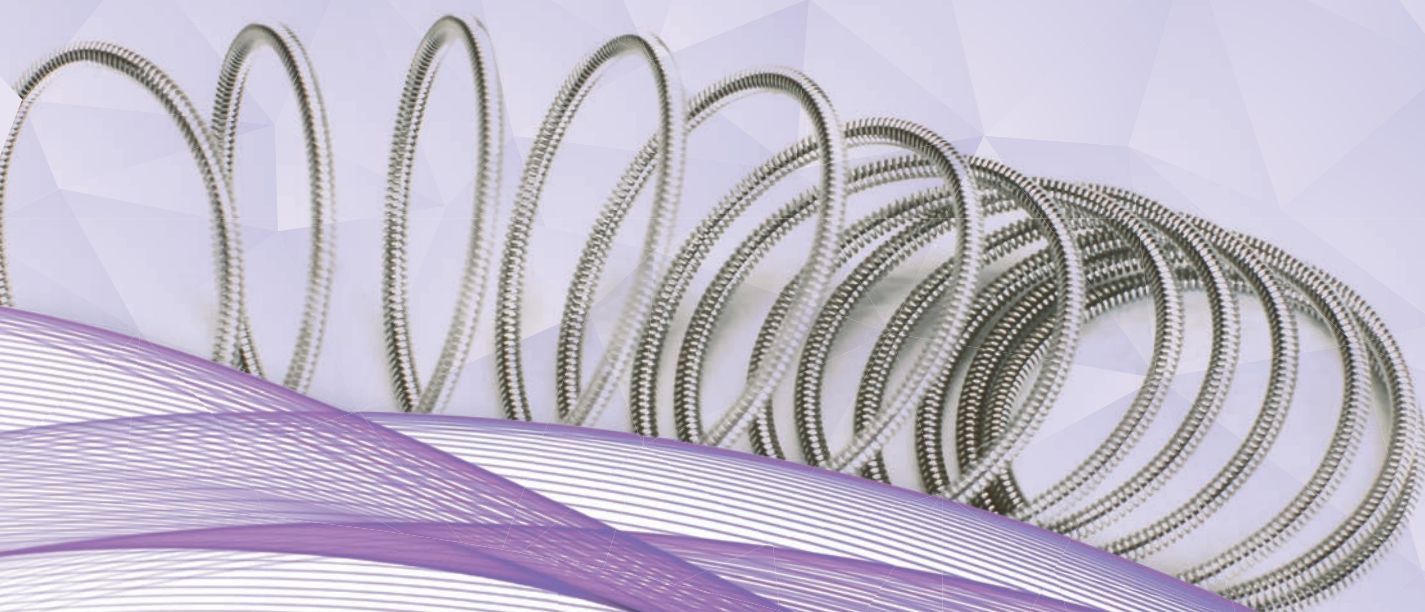
Traumatic MRI findings in professional fighters

Official Journal ASNR • ASFNR • ASHNR • ASPNR • ASSR



A Complete Coil Portfolio

MicroVention's comprehensive portfolio features clinically proven Hydrogel coils, which can be used exclusively or in combination with our trusted Platinum coils to treat a wide range of aneurysms and neurovascular lesions.



REFERENCES:

1. Brinjikji et al, GEL-THE-NEC: a prospective registry evaluating the safety, ease of use and efficacy of the HydroSoft coil as a finishing device. JNIS 2017.
2. ISC 2017 Meeting – Houston, TX – MV Symposium – Results of the GREAT Study – Presented by Christian Taschner, MD, Department of Neuroradiology, Medical Centre – University of Freiburg, Germany

INDICATIONS FOR USE:

The HydroCoil® Embolic System (HES) and MicroPlex Coil System (MCS) are intended for the endovascular embolization of intracranial aneurysms and other neurovascular abnormalities such as arteriovenous malformations and arteriovenous fistulae. The HES and MCS are also intended for vascular occlusion of blood vessels within the neurovascular system to permanently obstruct blood flow to an aneurysm or other vascular malformation and for arterial and venous embolizations in the peripheral vasculature.

The device should only be used by physicians who have undergone pre-clinical training in all aspects of HES/MCS procedures as prescribed by MicroVention.

MICROVENTION, MicroPlex and HydroCoil are registered trademarks of MicroVention, Inc. Refer to Instructions for Use, contraindications and warnings for additional information. Federal (USA) law restricts this device for sale by or on the order of a physician.



Smooth and stable.

Target Detachable Coils deliver consistently smooth deployment and exceptional microcatheter stability. Designed to work seamlessly together for framing, filling and finishing. Target Coils deliver the high performance you demand.

For more information, please visit www.strykerneurovascular.com/Target or contact your local Stryker Neurovascular sales representative.



Target[®]
DETACHABLE COILS



Not for sale within the territory of the United States

PERFECT INTERPLAY

APERIO® Thrombectomy Device

Reliable stent retriever featuring a hybrid cell-design for fast flow restoration in acute ischemic strokes. Available in four sizes for tailored treatment.

RELIABLE. VARIABLE. SAFE.

www.acandis.com

acandis®

ENGINEERING STROKE SOLUTIONS

Breakthrough Hydrogel Technology

- Less Retreatment Compared to Platinum^{1,2}
- Less Recurrence Compared to Platinum^{1,2}
- High Progressive Occlusion^{1,2}

For more information or a product demonstration,
contact your local MicroVention representative:



MicroVention, Inc.
Worldwide Headquarters

1311 Valencia Avenue
Tustin, CA 92780 USA
MicroVention UK Limited
MicroVention Europe, S.A.R.L.
MicroVention Deutschland GmbH
microvention.com

PH +1.714.247.8000

PH +44 (0) 191 258 6777
PH +33 (1) 39 21 77 46
PH +49 211 210 798-0

NEW

Indication for Trevo[®] Retrievers

A New Standard of Care in Stroke



FIRST

mechanical thrombectomy device
indicated to reduce disability in stroke.*

FIRST

new treatment indication for
stroke in 20 years.

Trevo XP

PROVUE RETRIEVER

Success accelerated.

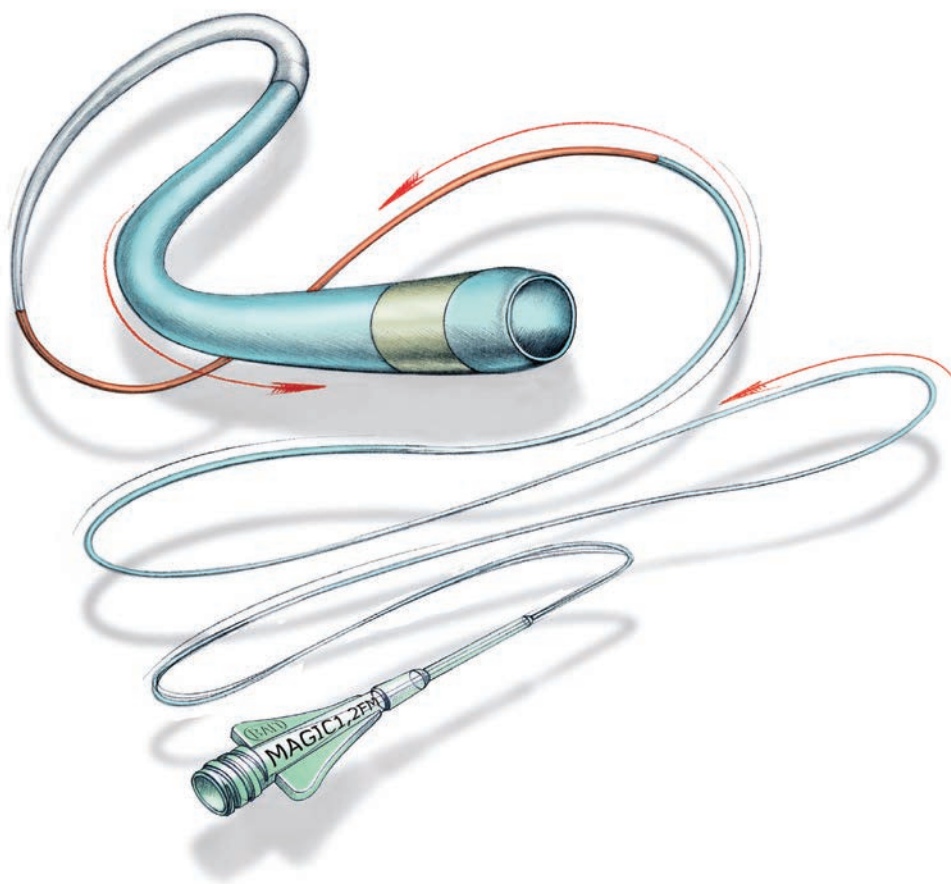
*The Trevo Retriever is indicated for use to restore blood flow in the neurovasculature by removing thrombus for the treatment of acute ischemic stroke to reduce disability in patients with a persistent, proximal anterior circulation, large vessel occlusion, and smaller core infarcts who have first received intravenous tissue plasminogen activator (IV t-PA). Endovascular therapy with the device should start within 6 hours of symptom onset.

Magic



FLOW-DEPENDENT MICROCATHETER

NOW AVAILABLE THROUGH BLOCKADE™ MEDICAL



ORDERMAGICS@BLOCKADEMEDICAL.COM

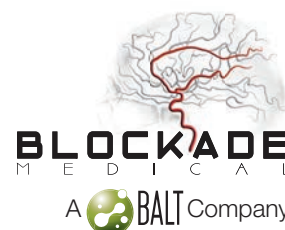
MAGIC catheters are designed for general intravascular use. They may be used for the controlled, selective regional infusion of therapeutic agents or embolic materials into vessels.¹

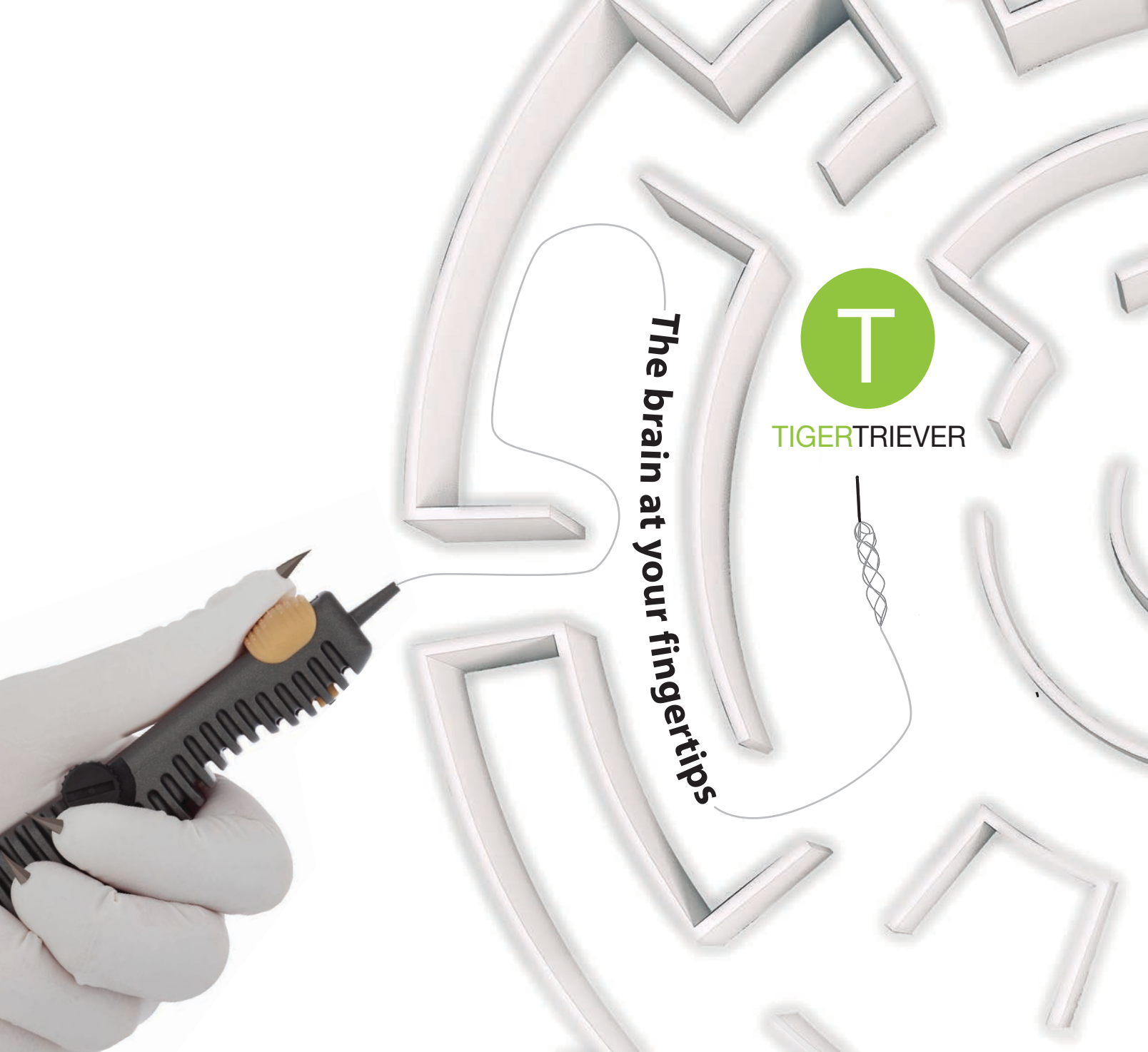
1. Magic Catheters IFU – Ind 19

MKTG-068 Rev. A

18 Technology Drive #169, Irvine Ca 92618

P 949.788.1443 | F 949.788.1444





TIGERTRIEVER

The brain at your fingertips

 **Rapid Medical**

// www.rapid-medical.com

ASNR 56th Annual Meeting & The Foundation of the ASNR Symposium 2018

June 2 - 7, 2018 | Vancouver, B.C., CANADA



The Vancouver Convention Centre East
© 2013 Vancouver Convention Centre

Welcome and Greetings

Please join us in Vancouver, CANADA for the **56th Annual Meeting of the American Society of Neuroradiology** on June 2–7, 2018 at the Vancouver Convention Centre East. Surrounded by the coastal mountains and located on the waterfront, you can enjoy these spectacular views in the heart of downtown Vancouver. With its undeniable charm and friendly atmosphere, Vancouver is known around the world as both a popular tourist attraction and one of the best places to live.

ASNR enthusiastically presents **Neuroradiology: Adding Value and Improving Healthcare** at the Symposium of the Foundation of the ASNR, as well as the common thread throughout the Annual Meeting. Implementing a value-based strategy in imaging has grasped the attention of nearly every healthcare provider; in particular with Radiologists understanding that the future will demand their imaging practices deliver better value. Value in healthcare is typically defined as those imaging strategies that yield improved outcomes, lower costs, or both. As payment transitions from a fee-for-service to a value-based system, thus creating a fundamentally different marketplace dynamic, measuring good outcomes are at the center of this changeover. At this time of uncertainty what little remains clear is that without a well-defined knowledge of their outcomes, no medical specialty will be able to succeed in the future value-based system. The Symposium will feature how Neuroradiology, in its many subspecialty areas, adds value to clinical care pathways by directing healthcare practice towards better outcomes. The annual meeting programming will continue on this theme emphasizing imaging that improves health outcomes, while considering costs, thus adding value. Our discussions will incorporate many innovative approaches to how neuroimaging currently does and will continue to improve overall healthcare performance.

As the Program Chair for ASNR 2018, it is my pleasure and honor to welcome you to Vancouver, CANADA for our annual meeting! Vancouver is known for being a very walkable city with a compact downtown core hosting many places to enjoy. So pack your comfortable walking shoes and let's tour together with our colleagues and friends!

Pina Sanelli

Pina C. Sanelli, MD, MPH, FACR
ASNR 2018 Program Chair/President-Elect



ASNR 2018 ■ VANCOUVER

ASFNR ASHNR ASPNR ASSR SNIS

THE FOUNDATION OF THE ASNR 

Pina C. Sanelli, MD, MPH, FACR

ASNR 2018 Program Chair/President-Elect

Programming developed in cooperation with the...

American Society of Functional Neuroradiology (ASFNR)

Max Wintermark, MD

American Society of Head and Neck Radiology (ASHNR)

Deborah R. Shatzkes, MD

American Society of Pediatric Neuroradiology (ASPNR)

Ashok Panigrahy, MD

American Society of Spine Radiology (ASSR)

John D. Barr, MD, FACR, FSIR, FAHA

Society of NeuroInterventional Surgery (SNIS)

Maresh V. Jayaraman, MD

ASNR Health Policy (HPC) Committee

Robert M. Barr, MD, FACR

ASNR Computer Sciences & Informatics (CSI) Committee

John L. Go, MD, FACR

ASNR Research Scientist Programming Committee

Dikoma C. Shungu, PhD, Timothy P.L. Roberts, PhD

The International Hydrocephalus Imaging Working Group (IHIWG) / CSF Flow Group

William G. Bradley, Jr., MD, PhD, FACR, Harold L. ReKate, MD and Bryn A. Martin, PhD



Fairmont Waterfront Hotel
© Copyright 2017 FRHI



Pan Pacific Hotel
© 2017 Pan Pacific Hotels and Resorts

ASNR 56th Annual Meeting

c/o American Society of Neuroradiology
800 Enterprise Drive, Suite 205
Oak Brook, Illinois 60523-4216
Phone: 630-574-0220 + Fax: 630 574-0661
2018.asnr.org



51st Annual Meeting

American Society of
**Head & Neck
Radiology**

Head and Neck Imaging in the City of Lights



Caesars Palace • Las Vegas, NV

September 16 – 20, 2017
(Saturday - Wednesday)

Please contact Educational Symposia at 813-806-1000 or ASHNR@edusymp.com or visit www.ASHNR.org for additional information.



WE'VE MOVED TO FALL 2017!



*11th Annual Meeting of the
American Society of*

FUNCTIONAL NEURORADIOLOGY

October 9-11, 2017 • the Nines • Portland, Oregon

Optional Hands-on BOLD fMRI Workshop • October 8, 2017



PLEASE CONTACT EDUCATIONAL SYMPOSIA AT

813-806-1000 or ASFNR@edusymp.com or visit www.ASFNR.org for additional information.

Trevo® XP ProVue Retrievers

See package insert for complete indications, complications, warnings, and instructions for use.

INDICATIONS FOR USE

1. The Trevo Retriever is indicated for use to restore blood flow in the neurovasculature by removing thrombus for the treatment of acute ischemic stroke to reduce disability in patients with a persistent, proximal anterior circulation, large vessel occlusion, and smaller core infarcts who have first received intravenous tissue plasminogen activator (IV t-PA). Endovascular therapy with the device should start within 6 hours of symptom onset.
2. The Trevo Retriever is intended to restore blood flow in the neurovasculature by removing thrombus in patients experiencing ischemic stroke within 8 hours of symptom onset. Patients who are ineligible for intravenous tissue plasminogen activator (IV t-PA) or who fail IV t-PA therapy are candidates for treatment.

COMPLICATIONS

Procedures requiring percutaneous catheter introduction should not be attempted by physicians unfamiliar with possible complications which may occur during or after the procedure. Possible complications include, but are not limited to, the following: air embolism; hematoma or hemorrhage at puncture site; infection; distal embolization; pain/headache; vessel spasm, thrombosis, dissection, or perforation; emboli; acute occlusion; ischemia; intracranial hemorrhage; false aneurysm formation; neurological deficits including stroke; and death.

COMPATIBILITY

3x20mm retrievers are compatible with Trevo® Pro 14 Microcatheters (REF 90231) and Trevo® Pro 18 Microcatheters (REF 90238). 4x20mm retrievers are compatible with Trevo® Pro 18 Microcatheters (REF 90238). 4x30mm retrievers are compatible with Excelsior® XT-27® Microcatheters (150cm x 6cm straight REF 275081) and Trevo® Pro 18 Microcatheters (REF 90238). 6x25mm Retrievers are compatible with Excelsior® XT-27® Microcatheters (150cm x 6cm straight REF 275081). Compatibility of the Retriever with other microcatheters has not been established. Performance of the Retriever device may be impacted if a different microcatheter is used.

Balloon Guide Catheters (such as Merci® Balloon Guide Catheter and FlowGate® Balloon Guide Catheter) are recommended for use during thrombus removal procedures.

Retrievers are compatible with the Abbott Vascular DOC® Guide Wire Extension (REF 22260).

Retrievers are compatible with Boston Scientific RHV (Ref 421242).

SPECIFIC WARNINGS FOR INDICATION 1

- The safety and effectiveness of the Trevo Retrievers in reducing disability has not been established in patients with large core infarcts (i.e., ASPECTS ≤ 7). There may be increased risks, such as intracerebral hemorrhage, in these patients.
- The safety and effectiveness of the Trevo Retrievers in reducing disability has not been established or evaluated in patients with occlusions in the posterior circulation (e.g., basilar or vertebral arteries) or for more distal occlusions in the anterior circulation.

WARNINGS APPLIED TO BOTH INDICATIONS

- Administration of IV t-PA should be within the FDA-approved window (within 3 hours of stroke symptom onset).
- Contents supplied STERILE, using an ethylene oxide (EO) process. Nonpyrogenic.
- To reduce risk of vessel damage, adhere to the following recommendations:
 - Take care to appropriately size Retriever to vessel diameter at intended site of deployment.
 - Do not perform more than six (6) retrieval attempts in same vessel using Retriever devices.
 - Maintain Retriever position in vessel when removing or exchanging Microcatheter.
- To reduce risk of kinking/fracture, adhere to the following recommendations:
 - Immediately after unsheathing Retriever, position Microcatheter tip marker just proximal to shaped section. Maintain Microcatheter tip marker just proximal to shaped section of Retriever during manipulation and withdrawal.
 - Do not rotate or torque Retriever.
 - Use caution when passing Retriever through stented arteries.
- Do not resterilize and reuse. Structural integrity and/or function may be impaired by reuse or cleaning.
- The Retriever is a delicate instrument and should be handled carefully. Before use and when possible during procedure, inspect device carefully for damage. Do not use a device that shows signs of damage. Damage may prevent device from functioning and may cause complications.



Concentric Medical
301 East Evelyn Avenue
Mountain View, CA 94041

Stryker Neurovascular
47900 Bayside Parkway
Fremont, CA 94538

strykerneurovascular.com

Date of Release: SEP/2016

EX_EN_US

Copyright © 2016 Stryker
NV00018973.AB

Target® Detachable Coil

See package insert for complete indications, contraindications, warnings and instructions for use.

INTENDED USE / INDICATIONS FOR USE

Target Detachable Coils are intended to endovascularly obstruct or occlude blood flow in vascular abnormalities of the neurovascular and peripheral vessels.

Target Detachable Coils are indicated for endovascular embolization of:

- Intracranial aneurysms
- Other neurovascular abnormalities such as arteriovenous malformations and arteriovenous fistulae
- Arterial and venous embolizations in the peripheral vasculature

CONTRAINDICATIONS

None known.

POTENTIAL ADVERSE EVENTS

Potential complications include, but are not limited to: allergic reaction, aneurysm perforation and rupture, arrhythmia, death, edema, embolus, headache, hemorrhage, infection, ischemia, neurological/intracranial sequelae, post-embolization syndrome (fever, increased white blood cell count, discomfort), TIA/stroke, vasospasm, vessel occlusion or closure, vessel perforation, dissection, trauma or damage, vessel rupture, vessel thrombosis. Other procedural complications including but not limited to: anesthetic and contrast media risks, hypotension, hypertension, access site complications.

WARNINGS

- Contents supplied STERILE using an ethylene oxide (EO) process. Do not use if sterile barrier is damaged. If damage is found, call your Stryker Neurovascular representative.
- For single use only. Do not reuse, reprocess or resterilize. Reuse, reprocessing or resterilization may compromise the structural integrity of the device and/or lead to device failure which, in turn, may result in patient injury, illness or death. Reuse, reprocessing or resterilization may also create a risk of contamination of the device and/or cause patient infection or cross-infection, including, but not limited to, the transmission of infectious disease(s) from one patient to another. Contamination of the device may lead to injury, illness or death of the patient.

- After use, dispose of product and packaging in accordance with hospital, administrative and/or local government policy.
- **This device should only be used by physicians who have received appropriate training in interventional neuroradiology or interventional radiology and preclinical training on the use of this device as established by Stryker Neurovascular.**
- Patients with hypersensitivity to 316LVM stainless steel may suffer an allergic reaction to this implant.
- MR temperature testing was not conducted in peripheral vasculature, arteriovenous malformations or fistulae models.
- The safety and performance characteristics of the Target Detachable Coil System (Target Detachable Coils, InZone Detachment Systems, delivery systems and accessories) have not been demonstrated with other manufacturer's devices (whether coils, coil delivery devices, coil detachment systems, catheters, guidewires, and/or other accessories). Due to the potential incompatibility of non Stryker Neurovascular devices with the Target Detachable Coil System, the use of other manufacturer's device(s) with the Target Detachable Coil System is not recommended.
- To reduce risk of coil migration, the diameter of the first and second coil should never be less than the width of the ostium.
- In order to achieve optimal performance of the Target Detachable Coil System and to reduce the risk of thromboembolic complications, it is critical that a continuous infusion of appropriate flush solution be maintained between a) the femoral sheath and guiding catheter, b) the 2-tip microcatheter and guiding catheters, and c) the 2-tip microcatheter and Stryker Neurovascular guidewire and delivery wire. Continuous flush also reduces the potential for thrombus formation on, and crystallization of infusate around, the detachment zone of the Target Detachable Coil.
- Do not use the product after the "Use By" date specified on the package.
- Reuse of the flush port/dispenser coil or use with any coil other than the original coil may result in contamination of, or damage to, the coil.
- Utilization of damaged coils may affect coil delivery to, and stability inside, the vessel or aneurysm, possibly resulting in coil migration and/or stretching.
- The fluoro-saver marker is designed for use with a Rotating Hemostatic Valve (RHV). If used without an RHV, the distal end of the coil may be beyond the alignment marker when the fluoro-saver marker reaches the microcatheter hub.

- If the fluoro-saver marker is not visible, do not advance the coil without fluoroscopy.
- Do not rotate delivery wire during or after delivery of the coil. Rotating the Target Detachable Coil delivery wire may result in a stretched coil or premature detachment of the coil from the delivery wire, which could result in coil migration.
- Verify there is no coil loop protrusion into the parent vessel after coil placement and prior to coil detachment. Coil loop protrusion after coil placement may result in thromboembolic events if the coil is detached.
- Verify there is no movement of the coil after coil placement and prior to coil detachment. Movement of the coil after coil placement may indicate that the coil could migrate once it is detached.
- Failure to properly close the RHV compression fitting over the delivery wire before attaching the InZone® Detachment System could result in coil movement, aneurysm rupture or vessel perforation.
- Verify repeatedly that the distal shaft of the catheter is not under stress before detaching the Target Detachable Coil. Axial compression or tension forces could be stored in the 2-tip microcatheter causing the tip to move during coil delivery. Microcatheter tip movement could cause the aneurysm or vessel to rupture.
- Advancing the delivery wire beyond the microcatheter tip once the coil has been detached involves risk of aneurysm or vessel perforation.
- The long term effect of this product on extravascular tissues has not been established so care should be taken to retain this device in the intravascular space.

Damaged delivery wires may cause detachment failures, vessel injury or unpredictable distal tip response during coil deployment. If a delivery wire is damaged at any point during the procedure, do not attempt to straighten or otherwise repair it. Do not proceed with deployment or detachment. Remove the entire coil and replace with undamaged product.

- After use, dispose of product and packaging in accordance with hospital, administrative and/or local government policy.

CAUTIONS / PRECAUTIONS

- Federal Law (USA) restricts this device to sale by or on the order of a physician.
- Besides the number of InZone Detachment System units needed to complete the case, there must be an extra InZone Detachment System unit as back up.

- Removing the delivery wire without grasping the introducer sheath and delivery wire together may result in the detachable coil sliding out of the introducer sheath.
- Failure to remove the introducer sheath after inserting the delivery wire into the RHV of the microcatheter will interrupt normal infusion of flush solution and allow back flow of blood into the microcatheter.
- Some low level overhead light near or adjacent to the patient is required to visualize the fluoro-saver marker; monitor light alone will not allow sufficient visualization of the fluoro-saver marker.
- Advance and retract the Target Detachable Coil carefully and smoothly without excessive force. If unusual friction is noticed, slowly withdraw the Target Detachable Coil and examine for damage. If damage is present, remove and use a new Target Detachable Coil. If friction or resistance is still noted, carefully remove the Target Detachable Coil and microcatheter and examine the microcatheter for damage.
- If it is necessary to reposition the Target Detachable Coil, verify under fluoroscopy that the coil moves with a one-to-one motion. If the coil does not move with a one-to-one motion or movement is difficult, the coil may have stretched and could possibly migrate or break. Gently remove both the coil and microcatheter and replace with new devices.
- Increased detachment times may occur when:
 - Other embolic agents are present.
 - Delivery wire and microcatheter markers are not properly aligned.
 - Thrombus is present on the coil detachment zone.
- Do not use detachment systems other than the InZone Detachment System.
- Increased detachment times may occur when delivery wire and microcatheter markers are not properly aligned.
- Do not use detachment systems other than the InZone Detachment System.



Stryker Neurovascular
47900 Bayside Parkway
Fremont, CA 94538

strykerneurovascular.com

Date of Release: MAR/2016

EX_EN_US

Copyright © 2016 Stryker
NV00018669.AB

Official Journal:

American Society of Neuroradiology
American Society of Functional Neuroradiology
American Society of Head and Neck Radiology
American Society of Pediatric Neuroradiology
American Society of Spine Radiology

EDITOR-IN-CHIEF

Jeffrey S. Ross, MD

*Professor of Radiology, Department of Radiology,
Mayo Clinic College of Medicine, Phoenix, AZ*

SENIOR EDITORS

Harry J. Cloft, MD, PhD

*Professor of Radiology and Neurosurgery,
Department of Radiology, Mayo Clinic College of
Medicine, Rochester, MN*

Thierry A.G.M. Huisman, MD

*Professor of Radiology, Pediatrics, Neurology, and
Neurosurgery, Chairman, Department of Imaging
and Imaging Science, Johns Hopkins Bayview,
Director, Pediatric Radiology and Pediatric
Neuroradiology, Johns Hopkins Hospital,
Baltimore, MD*

Yvonne W. Lui, MD

*Associate Professor of Radiology,
Chief of Neuroradiology,
New York University School of Medicine,
New York, NY*

C.D. Phillips, MD, FACR

*Professor of Radiology, Weill Cornell Medical
College, Director of Head and Neck Imaging,
New York-Presbyterian Hospital, New York, NY*

Pamela W. Schaefer, MD

*Clinical Director of MRI and Associate Director of
Neuroradiology, Massachusetts General Hospital,
Boston, Massachusetts, Associate Professor,
Radiology, Harvard Medical School, Cambridge, MA*

Charles M. Strother, MD

*Professor of Radiology, Emeritus, University of
Wisconsin, Madison, WI*

STATISTICAL SENIOR EDITOR

Bryan A. Comstock, MS

*Senior Biostatistician,
Department of Biostatistics,
University of Washington, Seattle, WA*

EDITORIAL BOARD

Ashley H. Aiken, *Atlanta, GA*
Lea M. Alhilali, *Phoenix, AZ*
John D. Barr, *Dallas, TX*
Ari Blitz, *Baltimore, MD*
Barton F. Branstetter IV, *Pittsburgh, PA*
Jonathan L. Brisman, *Lake Success, NY*
Julie Bykowski, *San Diego, CA*
Keith Cauley, *Danville, PA*
Asim F. Choudhri, *Memphis, TN*
Alessandro Cianfoni, *Lugano, Switzerland*
J. Matthew Debnam, *Houston, TX*
Seena Dehkharghani, *New York, NY*
Colin Derdeyn, *Iowa City, IA*
Rahul S. Desikan, *San Francisco, CA*
Yonghong Ding, *Rochester, MN*
Clifford J. Eskey, *Hanover, NH*
Saeed Fakhran, *Phoenix, AZ*
Massimo Filippi, *Milan, Italy*
Allan J. Fox, *Toronto, Ontario, Canada*
Wende N. Gibbs, *Los Angeles, CA*
Christine M. Glastonbury, *San Francisco, CA*
John L. Go, *Los Angeles, CA*
Allison Grayev, *Madison, WI*
Brent Griffith, *Detroit, MI*
Wan-Yuo Guo, *Taipei, Taiwan*
Ajay Gupta, *New York, NY*
Rakesh K. Gupta, *Lucknow, India*
Lotfi Hachein-Bey, *Sacramento, CA*
Christopher P. Hess, *San Francisco, CA*
Andrei Holodny, *New York, NY*
Benjamin Huang, *Chapel Hill, NC*
George J. Hunter, *Boston, MA*
Mahesh V. Jayaraman, *Providence, RI*
Valerie Jewells, *Chapel Hill, NC*
Christof Karmonik, *Houston, TX*
Timothy J. Kaufmann, *Rochester, MN*
Hillary R. Kelly, *Boston, MA*
Toshitomi Kinoshita, *Akita, Japan*
Kenneth F. Layton, *Dallas, TX*
Michael M. Lell, *Nürnberg, Germany*
Michael Lev, *Boston, MA*
Karl-Olof Lovblad, *Geneva, Switzerland*
Franklin A. Marden, *Chicago, IL*
M. Gisele Matheus, *Charleston, SC*
Joseph C. McGowan, *Merion Station, PA*
Stephan Meckel, *Freiburg, Germany*
Christopher J. Moran, *St. Louis, MO*
Takahisa Mori, *Kamakura City, Japan*
Suresh Mukherji, *Ann Arbor, MI*
Amanda Murphy, *Toronto, Ontario, Canada*
Alexander J. Nemeth, *Chicago, IL*
Sasan Partovi, *Cleveland, OH*
Laurent Pierot, *Reims, France*
Jay J. Pillai, *Baltimore, MD*

Whitney B. Pope, *Los Angeles, CA*
M. Judith Donovan Post, *Miami, FL*
Tina Young Poussaint, *Boston, MA*
Joana Ramalho, *Lisbon, Portugal*
Otto Rapalino, *Boston, MA*
Álex Rovira-Cañellas, *Barcelona, Spain*
Paul M. Ruggieri, *Cleveland, OH*
Zoran Rumboldt, *Rovinj-Rovigno, Croatia*
Amit M. Saindane, *Atlanta, GA*
Erin Simon Schwartz, *Philadelphia, PA*
Lubdhra M. Shah, *Salt Lake City, UT*
Aseem Sharma, *St. Louis, MO*
J. Keith Smith, *Chapel Hill, NC*
Maria Vittoria Spampinato, *Charleston, SC*
Gordon K. Sze, *New Haven, CT*
Krishnamoorthy Thamburaj, *Hershey, PA*
Cheng Hong Toh, *Taipei, Taiwan*
Thomas A. Tomsick, *Cincinnati, OH*
Aquila S. Turk, *Charleston, SC*
Willem Jan van Rooij, *Tilburg, Netherlands*
Arastoo Vossough, *Philadelphia, PA*
Elysa Widjaja, *Toronto, Ontario, Canada*
Max Wintermark, *Stanford, CA*
Ronald L. Wolf, *Philadelphia, PA*
Kei Yamada, *Kyoto, Japan*
Carlos Zamora, *Chapel Hill, NC*

EDITORIAL FELLOW

Vahe Zohrabian, *New Haven, CT*

SPECIAL CONSULTANTS TO THE EDITOR

AJNR Blog Editor

Neil Lall, *Denver, CO*

Case of the Month Editor

Nicholas Stence, *Aurora, CO*

Case of the Week Editors

Juan Pablo Cruz, *Santiago, Chile*

Sapna Rawal, *Toronto, Ontario, Canada*

Classic Case Editor

Sandy Cheng-Yu Chen, *Taipei, Taiwan*

Facebook Editor

Peter Yi Shen, *Sacramento, CA*

Health Care and Socioeconomics Editor

Pina C. Sanelli, *New York, NY*

Physics Editor

Greg Zaharchuk, *Stanford, CA*

Podcast Editor

Wende N. Gibbs, *Los Angeles, CA*

Twitter Editor

Jennifer McCarty, *Atlanta, Georgia*

YOUNG PROFESSIONALS ADVISORY COMMITTEE

Asim K. Bag, *Birmingham, AL*
Anna E. Nidecker, *Sacramento, CA*
Peter Yi Shen, *Sacramento, CA*

Founding Editor
Juan M. Taveras

Editors Emeriti
**Mauricio Castillo, Robert I. Grossman,
Michael S. Huckman, Robert M. Quencer**

Managing Editor
Karen Halm

Assistant Managing Editor
Laura Wilhelm

Executive Director, ASNR
Mary Beth Hepp

Director of Communications, ASNR
Angelo Artemakis

We're Inside Every Great Neuroradiologist!

ASNR MEMBERS RECEIVE

American Journal of Neuroradiology (AJNR)

The leading neuroradiology research journal, published monthly

Neurographics

Bimonthly educational journal with CME for members

ASNR Annual Meeting

Discounts for members on the field's premier conference

eCME

Online collection of lectures and articles with SA-CME and Category 1 credit

Advocacy

Coding/reimbursement, quality standards and practice guidelines; demonstrating neuroradiology's value!

Networking

Access to 5,000 peers

... And More!

Join the leaders in neuroradiology today!

Learn more at www.asnr.org/join

ASNR

American Society of Neuroradiology

800 Enterprise Dr., Suite 205, Oak Brook, IL 60523 • (630)574-0220 • membership@asnr.org • www.asnr.org

AJNR

AMERICAN JOURNAL OF NEURORADIOLOGY

JULY 2017
VOLUME 38
NUMBER 7
WWW.AJNR.ORG

Publication Preview at www.ajnr.org features articles released in advance of print. Visit www.ajnrblog.org to comment on AJNR content and chat with colleagues and AJNR's News Digest at <http://ajnrdigest.org> to read the stories behind the latest research in neuroimaging.

1275 **PERSPECTIVES** *J. Kleefield*

REVIEW ARTICLE

-  1276 **Difficult Lumbar Puncture: Pitfalls and Tips from the Trenches**
P.A. Hudgins, et al.

SPINE
















PRACTICE PERSPECTIVES

-  1284 **Baseline Survey of the Neuroradiology Work Environment in the United States with Reported Trends in Clinical Work, Nonclinical Work, Perceptions of Trainees, and Burnout Metrics** *J.Y. Chen, et al.*

HEALTH CARE REFORM VIGNETTE

- 1292 **The Qualified Clinical Data Registry: A Pathway to Success within MACRA** *M.M. Chen, et al.*

GENERAL CONTENTS

-   1297 **What Does the Boxed Warning Tell Us? Safe Practice of Using Ferumoxytol as an MRI Contrast Agent** *C.G. Varallyay, et al.*
-  1303 **Prevalence of Traumatic Findings on Routine MRI in a Large Cohort of Professional Fighters** *J.K. Lee, et al.*
-   1311 **Retention of Gadolinium-Based Contrast Agents in Multiple Sclerosis: Retrospective Analysis of an 18-Year Longitudinal Study** *Y. Forslin, et al.*
-     1317 **The Use of Noncontrast Quantitative MRI to Detect Gadolinium-Enhancing Multiple Sclerosis Brain Lesions: A Systematic Review and Meta-Analysis** *A. Gupta, et al.*
- 1323 **Neuroradiologists Compared with Non-Neuroradiologists in the Detection of New Multiple Sclerosis Plaques** *W. Wang, et al.*
-    1328 **Diffusional Kurtosis Imaging and Motor Outcome in Acute Ischemic Stroke** *M.V. Spampinato, et al.*
-   1335 **APOE*E4 Is Associated with Gray Matter Loss in the Posterior Cingulate Cortex in Healthy Elderly Controls Subsequently Developing Subtle Cognitive Decline** *S. Haller, et al.*
-  1343 **Pontomesencephalic Atrophy and Postural Instability in Wilson Disease** *J. Kalita, et al.*

PATIENT SAFETY
ADULT BRAIN

ADULT BRAIN

ADULT BRAIN
PATIENT SAFETY

ADULT BRAIN

ADULT BRAIN

ADULT BRAIN

ADULT BRAIN

ADULT BRAIN

AJNR (Am J Neuroradiol ISSN 0195-6108) is a journal published monthly, owned and published by the American Society of Neuroradiology (ASNR), 800 Enterprise Drive, Suite 205, Oak Brook, IL 60523. Annual dues for the ASNR include \$170.00 for journal subscription. The journal is printed by Cadmus Journal Services, 5457 Twin Knolls Road, Suite 200, Columbia, MD 21045; Periodicals postage paid at Oak Brook, IL and additional mailing offices. Printed in the U.S.A. POSTMASTER: Please send address changes to American Journal of Neuroradiology, P.O. Box 3000, Denville, NJ 07834, U.S.A. Subscription rates: nonmember \$390 (\$460 foreign) print and online, \$310 online only; institutions \$450 (\$520 foreign) print and basic online, \$895 (\$960 foreign) print and extended online, \$370 online only (basic), extended online \$805; single copies are \$35 each (\$40 foreign). Indexed by PubMed/Medline, BIOSIS Previews, Current Contents (Clinical Medicine and Life Sciences), EMBASE, Google Scholar, HighWire Press, Q-Sensei, RefSeek, Science Citation Index, and SCI Expanded. Copyright © American Society of Neuroradiology.

| | | | | |
|---|---|--|--|------------|
|  | 1348 | Discrimination between Glioma Grades II and III Using Dynamic Susceptibility Perfusion MRI: A Meta-Analysis <i>A.F. Delgado, et al.</i> | ADULT BRAIN | |
|  | 1356 | Mechanical Thrombectomy with the Embolus Retriever with Interlinked Cages in Acute Ischemic Stroke: ERIC, the New Boy in the Class <i>H. Steglich-Arnholm, et al.</i> | INTERVENTIONAL | |
| | 1362 | Impact of Anesthesia on the Outcome of Acute Ischemic Stroke after Endovascular Treatment with the Solitaire Stent Retriever <i>A. Slezak, et al.</i> | INTERVENTIONAL | |
| | 1368 | Correlation of Thrombectomy Maneuver Count with Recanalization Success and Clinical Outcome in Patients with Ischemic Stroke <i>F. Seker, et al.</i> | INTERVENTIONAL | |
|  | 1372 | Temporary Stent-Assisted Coil Embolization as a Treatment Option for Wide-Neck Aneurysms <i>M. Müller, et al.</i> | INTERVENTIONAL | |
| | 1377 | Liquid Embolic Agents for Endovascular Embolization: Evaluation of an Established (Onyx) and a Novel (PHIL) Embolic Agent in an In Vitro AVM Model <i>D.F. Vollherbst, et al.</i> | INTERVENTIONAL | |
| | 1383 | Appropriate Minimal Dose of Gadobutrol for 3D Time-Resolved MRA of the Supra-Aortic Arteries: Comparison with Conventional Single-Phase High-Resolution 3D Contrast-Enhanced MRA <i>S.H. Bak, et al.</i> | EXTRACRANIAL VASCULAR | |
|  |  | 1391 TIPIC Syndrome: Beyond the Myth of Carotidynia, a New Distinct Unclassified Entity <i>A. Lecler, et al.</i> | EXTRACRANIAL VASCULAR | |
| | 1399 | Carotid Bulb Webs as a Cause of “Cryptogenic” Ischemic Stroke <i>P.I. Sajedi, et al.</i> | EXTRACRANIAL VASCULAR | |
| | 1405 | Solid Lymph Nodes as an Imaging Biomarker for Risk Stratification in Human Papillomavirus–Related Oropharyngeal Squamous Cell Carcinoma <i>T.J. Rath, et al.</i> | HEAD & NECK | |
| | 1411 | The Central Bright Spot Sign: A Potential New MR Imaging Sign for the Early Diagnosis of Anterior Ischemic Optic Neuropathy due to Giant Cell Arteritis <i>P. Remond, et al.</i> | HEAD & NECK | |
| | 1416 | Zuckerkind Tubercle of the Thyroid Gland: Correlations between Findings of Anatomic Dissections and CT Imaging <i>H.-J. Won, et al.</i> | HEAD & NECK | |
|  |  | 1421 The Role of Core Needle Biopsy for Thyroid Nodules with Initially Indeterminate Results on Previous Fine-Needle Aspiration: A Systematic Review and Meta-Analysis <i>C.H. Suh, et al.</i> | HEAD & NECK | |
|  |  | 1427 Nonmicrocephalic Infants with Congenital Zika Syndrome Suspected Only after Neuroimaging Evaluation Compared with Those with Microcephaly at Birth and Postnatally: How Large Is the Zika Virus “Iceberg”? <i>M.F.V.V. Aragao, et al.</i> | PEDIATRICS | |
|  |  |  | 1435 Validation of an MRI Brain Injury and Growth Scoring System in Very Preterm Infants Scanned at 29- to 35-Week Postmenstrual Age <i>J.M. George, et al.</i> | PEDIATRICS |
|  |  | 1443 Apparent Diffusion Coefficient Value Changes and Clinical Correlation in 90 Cases of Cytomegalovirus-Infected Fetuses with Unremarkable Fetal MRI Results <i>D. Kotovich, et al.</i> | PEDIATRICS | |
|  |  | 1449 Quantitative Folding Pattern Analysis of Early Primary Sulci in Human Fetuses with Brain Abnormalities <i>K. Im, et al.</i> | PEDIATRICS | |
| | 1456 | Lumbar Puncture Test in Normal Pressure Hydrocephalus: Does the Volume of CSF Removed Affect the Response to Tap? <i>S.K. Thakur, et al.</i> | SPINE | |
| | 1461 | 35 YEARS AGO IN AJNR | | |

ONLINE FEATURES

LETTERS

- 🔑 **E46** **3D-Printed Patient-Specific Models for CT- and MRI-Guided Procedure Planning** *E. George, et al.*
- E48** **3D T2-SPACE versus T2-FSE or T2 Gradient Recalled-Echo: Which Is the Best Sequence?** *M.I. Vargas, et al.*
- E50** **Reply** *F.H. Chokshi, et al.*

BOOK REVIEWS *R.M. Quencer, Section Editor*

Please visit www.ajnrblog.org to read and comment on Book Reviews.



A, Anterior communicating artery aneurysm before coiling. B, The same aneurysm partially coiled with a deployed stent from the left A1 to the right A2 segment. C, Same aneurysm after complete coil embolization, with removal of the stent.



Indicates Editor's Choices selection



Indicates Fellows' Journal Club selection



Indicates open access to non-subscribers at www.ajnr.org



Indicates article with supplemental on-line table



Indicates article with supplemental on-line photo



Indicates article with supplemental on-line video



Evidence-Based Medicine Level 1



Evidence-Based Medicine Level 2



Title: Metropolitan Opera House—Lincoln Center, New York City. Opened only 4 years after the 1962 founding of the ASNR, this breathtaking building has a fully glass front that allows people outside to enjoy the enormous Marc Chagall paintings, seen behind the most lateral bay on each side. The hall is noted for its excellent acoustics and sight lines. Lincoln Center was constructed on the former site of numerous run-down tenements. The rubble of this material served as the "stage" for Robert Wise's fantastic 1961 movie version of Leonard Bernstein's "West Side Story," which won numerous Academy Awards, including Best Picture.

Jonathan Kleeefield, Department of Radiology, Beth Israel Deaconess Medical Center, Boston, Massachusetts

Difficult Lumbar Puncture: Pitfalls and Tips from the Trenches

 P.A. Hudgins,  A.J. Fountain,  P.R. Chapman, and  L.M. Shah



ABSTRACT

SUMMARY: Lumbar puncture has, for many years, been the responsibility of the internal medicine physician or the neurologist. As more patients have undergone spine surgery and with the current increase in body mass index of the general population, the radiologist has been consulted with increasing frequency to perform lumbar puncture with fluoroscopic guidance. Radiology, in fact, is now the dominant overall provider of lumbar puncture procedures. The procedure is more difficult when the needle length increases, and if fluoroscopy is used, landmarks are more difficult to visualize with increasing subcutaneous fat. Our goal with this review was to describe our techniques for lumbar puncture in the difficult patient, with emphasis on using fluoroscopy in the obese patient and to suggest maneuvers that might make the procedure easier. Combining our experience from performing these procedures on an obese population, we would like to share our tips, especially with trainees early in their career.

ABBREVIATIONS: BMI = body mass index; IIH = idiopathic intracranial hypertension; LP = lumbar puncture

Lumbar puncture (LP) has, for many years, been the responsibility of the internal medicine physician or the neurologist. As more patients have undergone spine surgery and with the current increase in body mass index (BMI) of the general population, the radiologist has been consulted with increasing frequency to perform the LP fluoroscopic guidance.¹

Current estimates from the Centers for Disease Control and Prevention are that more than one-third (34.9% or 78.6 million) of adults in the United States are obese.² BMI is calculated as weight in kilograms divided by the square of the height in meters, and obesity is defined as a BMI of >30 . In our practice, patients often weigh >136 kg, with a BMI of >50 . The financial impact of obesity on the health care system is well-known, because this chronic condition contributes to the development of diabetes, cardiovascular issues, and, now increasingly recognized, idiopathic intracranial hypertension (IIH), previously termed “pseudotumor cerebri.”^{3,4}

The impact of obesity on the radiology practice is now being recognized. Patients are not able to fit on imaging equipment,


including procedural equipment, designed for the “average-sized” patient. The obese patient who needs CSF sampling presents multiple potential difficulties. Equipment has weight limits above which table function is not assured, and the fluoroscopy table may not tilt. Increasing BMI has been shown to result in a longer fluoroscopy time for LP access.⁵ LP is more difficult when the needle length increases, and if fluoroscopy is used, landmarks are more difficult to visualize with increasing subcutaneous fat. Conventional imaging parameters are not sufficient to penetrate extra layers of patient fat; the density properties of human tissue become problematic in patients weighing ≥ 113 kg.^{6,7}

Previously, LPs were typically performed without image guidance; however, radiology is now the dominant overall provider of LP procedures.¹ Image guidance is often requested when there is postoperative hardware and/or osseous fusion, extensive degenerative change, or scoliosis⁸; after multiple failed attempts without imaging; and with the inability to identify or palpate spinous processes or the iliac crest, osseous landmarks routinely used to plan LP, such as in the obese patient. One of the most common indications for LP in the obese patient is confirming or treating IIH, a known complication of obesity. For diagnosis alone, CSF pressure measurements may be all that are required. However, for the symptomatic patient, especially with headache or fluctuating vision loss, removing CSF is therapeutic.

Our goal in this review was to describe our techniques for LP in the difficult patient, with emphasis on the obese patient, and suggest maneuvers that might make the procedures easier. Because fluoroscopically guided LP is a common procedure performed by

From the Department of Radiology and Imaging Sciences (P.A.H., A.J.F.), Division of Neuroradiology, Emory University School of Medicine, Atlanta, Georgia; Department of Radiology (P.R.C.), University of Alabama, Tuscaloosa, Alabama; and Department of Radiology and Imaging Sciences (L.M.S.), University of Utah, Salt Lake City, Utah.

Please address correspondence to Patricia A. Hudgins, MD, FACR, Emory University Hospital, 1364 Clifton Rd NE, Atlanta, GA 30322; e-mail: phudgin@emory.edu; @phudge54

 Indicates open access to non-subscribers at www.ajnr.org

<http://dx.doi.org/10.3174/ajnr.A5128>



FIG 1. Adult woman, BMI 55, in a serious motor vehicle collision. Scout CT scan for chest, abdomen, and pelvis shows the hands in the midline, loosely tied with tape so the patient could fit through the CT bore.

the neuroradiologist, experienced physicians likely have their own tricks. Combining our experience in performing these procedures on an obese population with those of other interventionalists with similar challenges, we would like to share our tips, especially with trainees early in their careers.

Fluoroscopy or CT?

Most LPs in our practice are performed with fluoroscopy because it is faster and does not tie up a CT scanner that might be needed for critical inpatients or those in the emergency department. The table load weight limit indicates the z-axis accuracy as the patient goes through the scanner, ensuring the diagnostic quality of the image.⁹ However, if the weight limit is exceeded, the table may bend or break with possible injury to the patient. CT scanners have variable table weight limits, and vendors now offer bariatric tables to accommodate larger patients. Furthermore, the body habitus of many of our patients does not allow them to fit in the scanner with the needle in place. Thus, the usable portion of the anteroposterior diameter is important to know, not just the gantry aperture.⁹ We have occasionally had to tie or tape patients' hands together and loosely bind redundant skin folds to just get a diagnostic CT scan (Fig 1). Additionally, the CT table usually

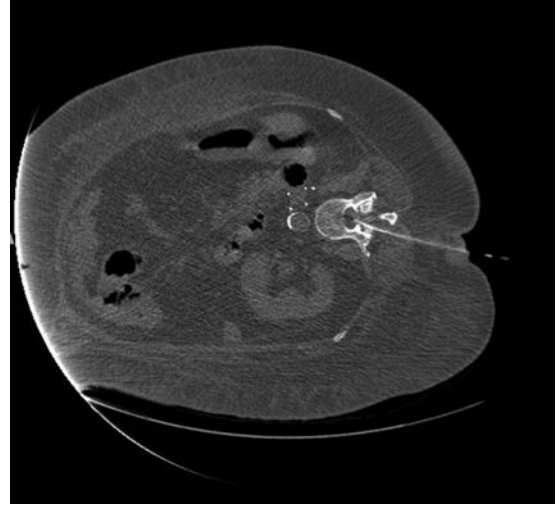


FIG 2. Adult patient, BMI 49, with bowel incarceration requiring an operation, now with altered mental status. LP was requested to exclude meningitis. The patient is in the right lateral decubitus position so that the respiratory technologist can control the tracheostomy and airway. Note the tip of the needle in the mid-spinal canal.

cannot tilt; this maneuver facilitates the flow of CSF. Using a fluoroscopic C-arm is the ideal method because the obese patient often cannot lie prone or even slightly oblique. However, our C-arm fluoroscopic machines are usually scheduled for interventional use, and we initially attempt the LP with conventional fluoroscopy most of the time. It is obviously essential that the fluoroscopy tower clear the patient and the needle; otherwise, a C-arm is essential.

Radiation doses from fluoroscopy versus CT are reportedly comparable for LPs performed in obese patients.¹⁰ Data from phantom studies indicate that obese patients receive higher radiation doses from CT and radiography than nonobese patients.^{11,12} For severely ill or intubated patients in the hospital, obese or not, CT or a biplane image intensifier is invaluable, with the patient in the lateral decubitus position (Fig 2). This allows greater comfort, less respiratory motion, better airway control by the respiratory therapist, and assurance that the patient will fit in the gantry with the LP needle in position.

Planning the Examination

We almost always have prior brain imaging available, ideally within 30 days of the LP, to be sure there is no mass, hydrocephalus, or mass effect that may result in herniation when the spinal pressure is lowered by removing CSF. A recent physical examination with normal findings documented by a neurosurgeon or neurologist can also suffice. Especially if there has been a prior lumbar spine operation, plain radiographs or postoperative cross-sectional imaging is essential. This preprocedural image review helps determine the best level for the procedure and can show surgical complications such as hardware failure, arachnoiditis (Fig 3), or spinal infection. A scar from a prior operation, if mature, is generally not sensitive, but lidocaine is still used subcutaneously. A new postoperative scar tends to be exquisitely sensitive, and if possible, we avoid these levels. Any bone window, whether a normal space or as a result of prior surgery, potentially can be used to gain access.

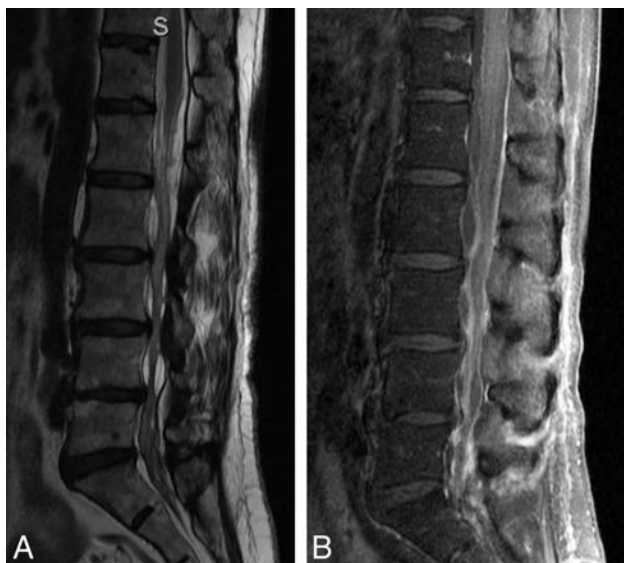


FIG 3. Adult patient with multiple epidural lumbar steroid injections, now recalcitrant to more injections. The patient experienced severe pain during an attempted LP. Note severe arachnoiditis. *A*, T2 sagittal MR image shows marked clumping of the cauda equina in the central thecal sac, but it also adhered to the posterior dural wall. The conus appears irregular, also from arachnoiditis. *B*, T1 sagittal, postgadolinium image with fat saturation shows diffuse enhancement of the nerve roots and meninges. Arachnoiditis does not always enhance. Because meningitis could have a similar appearance, CSF must be obtained to exclude infection, despite the arachnoiditis.

If there is prior lumbar spine MR imaging or abdominal CT imaging, the distance between skin and thecal sac can be measured and use of a longer needle can be planned. Measurement is made typically from the left parasagittal region, the expected site of the proposed LP. The depth of the thecal sac is variable over the length of the lumbar spine but often decreases from inferior to superior. For example, in a given patient, a 3.5-cm needle may be sufficient at the L2–3 level but may be too short to reach at the L5–S1 level. A pillow beneath the hips may decrease the lumbar lordosis and slightly “stretch out” the subcutaneous fat. If there is no imaging available, we palpate the lumbar spinous processes. If they cannot be palpated, it is likely that the standard 3.5-cm needle will not be long enough. This is a relatively crude measurement, but in our experience, it works well. Nayate et al¹³ have proposed a formula [Skin-Canal Distance (inches) = $0.077 \times \text{BMI} + 0.88$] to predict the appropriate needle length in oblique interlaminar-approach LP using the BMI. In some obese patients, there is a large “buttock shelf” with almost a right angle with the back (Fig 4). Occasionally, we may need a second person to gently push this large shelf inferiorly.

Review of prior spine imaging helps avoid levels of spinal stenosis, where the thecal sac is narrowed and nerve roots are clumped. Increased fat in the epidural space, especially at L4 or lower, should also be avoided (Fig 5). At a stenotic level, the patient will likely experience radicular pain with the procedure, and CSF return will be slow or nonexistent. Therefore, it will be beneficial to approach the level above the stenosis to access the subarachnoid space.

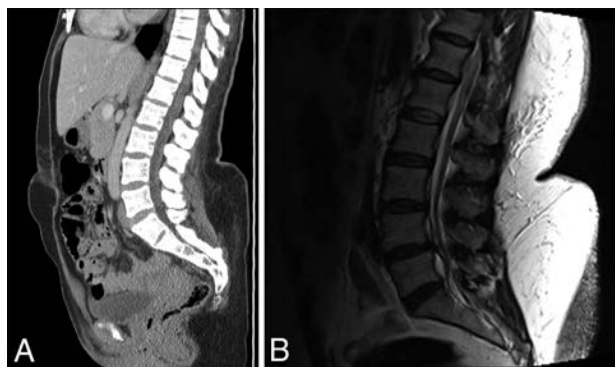


FIG 4. Adult female patients with morbid obesity and large fat shelf on the lower lumbar back. *A*, Sagittal reformation from a noncontrast abdominal and pelvis CT shows the deformity of the back, even with the patient supine. *B*, Sagittal T2 MR image in another patient with marked subcutaneous fat in the lower thoracic and lumbar back. Note an abrupt increase in fat thickness at the L3 level, which makes LP difficult.

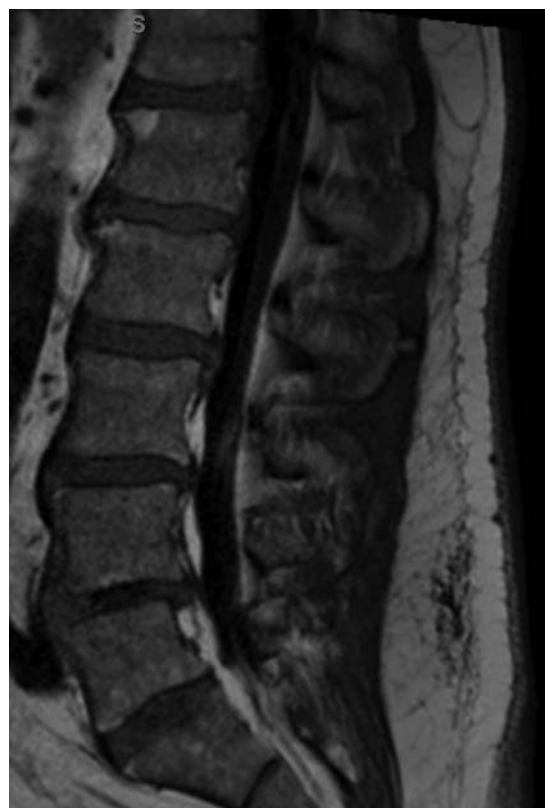


FIG 5. A man with epidural lipomatosis. T1 sagittal MR image shows high-signal-intensity fat around the thecal sac, with marked narrowing at L5.

Patient Experience and Comfort

We have all heard about negative experiences with LP. The goal of the radiologist should be to provide an LP procedure with as little anxiety, discomfort, and pain as possible. While obtaining consent, the radiologist should be calm, relaxed, and unhurried and offer positive reassurance that the goal is to provide a pain-free experience. The details of the procedure and the risks and benefits should be conveyed in layman’s terms. The small risk of spinal headache, infection, and nerve injury is important to communicate but with reassurance that the risks are low. If the patient

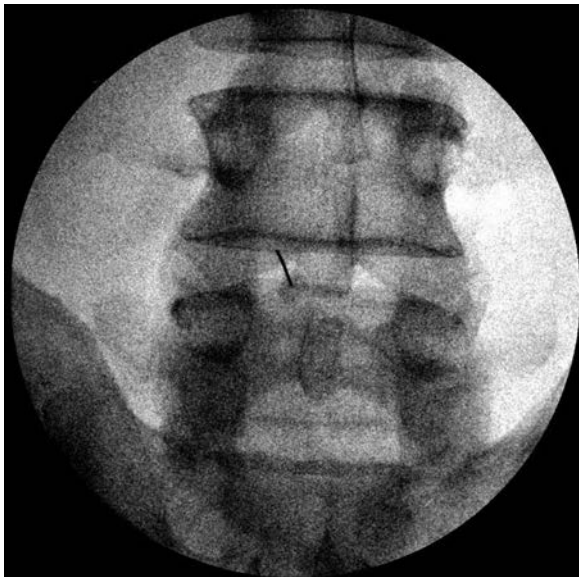


FIG 6. Spot fluoroscopic image showing a 23-ga needle near the lamina for deep anesthesia. It is critical that the lidocaine not be injected into the spinal canal or thecal sac. We never use the anesthesia needle in the thecal sac.

experiences what is likely a low-pressure headache, he or she may be advised to call the radiology department and speak with a neuroradiologist. We discuss the headache with the patient, and advise increasing caffeine intake and bedrest for at least 2 additional days before treatment by a blood patch is considered. Low-pressure headache treatment is institutional-dependent.

The patient should be prone or prone oblique on the fluoroscopy table, with only a thin pillow under the head, arms by the side, and a small bolster at the abdominal level if there is a lordosis. With the patient in the oblique position, we have the top leg, usually the right leg, bent. Local anesthesia is important. While some providers minimize the effects of local anesthesia and may claim that the lidocaine injection is more painful than the lumbar puncture itself, we consider it essential for patient comfort. Lidocaine HCl 1% concentration itself can be painful, but the pain can be reduced by a slower, gentler injection to create a cutaneous and subcutaneous wheal. After we create a skin wheal, the 25-ga needle is advanced through the subcutaneous tissues and several milliliters of lidocaine is injected. We have used 1 mL of bicarbonate solution mixed with 4–5 mL of lidocaine to mitigate the initial sting.

One trick is to use a 25-ga 3.5-cm spinal needle in all patients to deliver anesthesia to the deeper tissues and periosteum (if the needle reaches it). Unlike larger needles, the 25-ga needle can be advanced through the tissues with minimal or no discomfort for the patient. After we numb the skin, the 25-ga needle is advanced through the subcutaneous tissues to the fascia of the paraspinal muscle, the stylet is removed, and several milliliters of lidocaine is injected. The needle can be advanced with the syringe still attached, injecting into the muscle. With fluoroscopy to be sure the needle is not intraspinal, the needle can even be directed to the lamina (either above or below the interlaminar space) (Fig 6). Thus, both the periosteum and the distal medial branches of the dorsal ramus can be numbed to provide anesthesia to the deep

soft tissues and prevent referred radicular pain. This maneuver also determines the depth necessary for the LP.

We recommend never injecting lidocaine through the LP needle because injecting lidocaine into the thecal sac can be dangerous, potentially resulting in motor weakness or arachnoiditis. Also, lidocaine in the needle or hub can make identification of CSF more difficult.

While you advance the spinal needle, it is helpful to secure the hub and brace your hands against the patient to guard against sudden patient movement, which may inadvertently advance the needle. It is critical to recognize that the greatest pain can be produced by advancing the needle into an intradural spinal nerve and producing a lancinating pain to the lower extremity, hip, buttock, or groin. When the needle is at or within the ligamentum flavum, we remind the patient that the needle is approaching nerves that have not been anesthetized and ask the patient to speak up if there is radicular pain (focal sharp pain down 1 leg). The needle is then advanced extremely slowly and gently at this point. If radicular pain is felt, the operator should immediately stop the needle, withdraw it approximately 1 mm, and check for fluid. Remember that 1 mm of movement can be the difference between experiencing pain or not. Pain usually abates within seconds once the needle is off the nerve. If the patient continues to have severe radicular pain, a different approach needs to be taken altogether.

During the examination, some patients, in our experience young males in particular, may have a vasovagal response. The radiologist should be aware of these signs: increased anxiety, paleness, sweating, or comments like, “I feel really hot” or “I feel like I am going to throw up.” Typically, we tell the patient that we are going to break for few moments, put the table in the Trendelenburg position, and offer a cold washcloth to the face. After a minute or so, the procedure can be completed without further progression of the response.

The spinal headache is the most common complication following LP. In our experience, the LP headache occurs far less often in patients with documented IIH. Typically, the headache will be at maximum 1–2 days after the procedure and will take 1–2 days to fully resolve. Most headaches occurring after a single needle stick will resolve spontaneously without a blood patch. Patients are advised to restrict strenuous or athletic activity for 24 hours following the procedure to prevent the headaches. While some authors have suggested the use of an “atraumatic” needle such as the Whitacre needle, we think that the most effective way to prevent postprocedural headache is by limiting the procedure to a single puncture of the posterior thecal sac. Replacing the stylet before removal of the needle may decrease the incidence of postlumbar puncture headache.^{14,15} We have patients lie in the recumbent position for approximately 30 minutes after the LP; however, this has not been shown to be effective in preventing postprocedural headache.¹⁶ If the headache is still present ≥ 4 days after the LP and there is no improvement, we consider referral for an epidural blood patch.

Technique

We routinely use either the prone or prone oblique position and aim for the interlaminar location or “behind the Scotty dog’s



FIG 7. Cross-table lateral film after failure to obtain CSF, thought to be a dry tap. Note the LP approach at the L4–5 disc space and the needle extended through the disc into the retroperitoneum. At this point, the stylet was removed and no blood was returned. The needle was withdrawn at 5-mm increments, each time checking for arterial or venous blood return. There were no complications, but the diagnostic LP was cancelled until the following day.

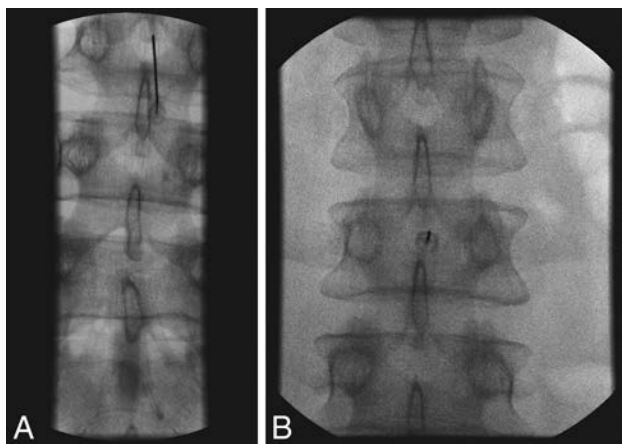


FIG 8. Fluoroscopic spot films obtained during LP, showing parallax artifacts. *A*, Note that on this image, the needle is not centered and the tip appears to abut the inferior spinous process. *B*, The same procedure with no needle adjustment, but now the tip is centered in the image. CSF flow was normal.

neck,” avoiding the disc space level. Because an LP needle can easily extend through the disc itself, terminating in the prevertebral location or retroperitoneum (Fig 7), we avoid the disc space level. If there is inadvertent extension through a disc with the spinal needle, a rare event, we have found that replacing the stylet and removing the needle at $\frac{1}{2}$ -cm intervals, with frequent checks for blood return, is a method to deal with this complication. We have never had venous or arterial blood return, but if that occurred, we would plan to document the blood return, attempt to differentiate venous from arterial blood, and consider a CT angiogram/venogram of the aorta and inferior vena cava after terminating the unsuccessful LP. It is critical that when using fluoroscopy, the needle be centered in the image to avoid parallax artifacts, an effect distinct to radiographs (Fig 8). Parallax is a

difference in the apparent position of an object along 2 different lines of sight.¹⁷

Experienced radiologists are often comfortable with a 25-ga spinal needle, but if a longer needle is needed, a 25-ga needle is more difficult to steer. Our standard needle is 22 ga. For extremely obese patients, we often use a 3.5-inch 18-ga introducer, but this larger gauge should not enter the thecal sac.¹⁸ The introducer is advanced using the same landmarks used in the LP and is hubbed. Although the introducer needle is easy to steer, it is important to have a properly planned trajectory because it can be difficult to correct the path with this larger gauge coaxial needle. The needle is much easier to steer through the introducer. The standard spinal needle is 8.8 cm (3.5 inches). Needles are also available at 13-, 14-, 15-, and 18-cm or even longer lengths.

The 22-ga 19-cm spinal needle is then advanced through the introducer. The needle hub has a notch, which is on the bevel side. Therefore, the side opposite the notch is the “sharp” side. The needle will go toward this sharper side and away from the notch. Therefore, if you are steering the needle, the notch should be opposite the direction you are attempting to steer. Some introducer needles may have the bevel on the opposite side of the notch on the hub. Turning the needle $\frac{1}{4}$ turn every 1 cm or so helps direct the needle in a straight line. The introducer will help with needle position, but it is still important to check periodically with the fluoroscopy for an adequate trajectory. Even with the longer spinal needle, the “pop” through the dura can often be felt. The bevel should be directed cephalad, away from the dura/arachnoid and perpendicular to the course of the nerves, to improve exposure to the fluid, particularly if there is slow flow.

The obese patient usually cannot roll on the table for an opening pressure in the lateral decubitus position, so we obtain the pressure in the prone or prone oblique position, adding the needle length to the final pressure measurement.¹⁹ The normal CSF pressure range is 6–20 cm H₂O in adults and up to 25 cm H₂O in obese patients.²⁰ An opening pressure of >25 cm H₂O is diagnostic of IIH, in the correct clinical setting.²¹

For the diagnostic LP, how much CSF to remove and put in each tube varies on the basis of what has been requested by the referring physician or provider. We routinely attach short tubing to the needle and use a 10-mL syringe after the seal has been broken, to gently remove CSF. The suction is applied very gently, for just 2–3 seconds, then released to avoid affecting a nerve root. This process is then repeated as long as CSF return is present. One of the authors uses a unique technique that allows air release into the tube-hub interface (Fig 9). The connection between the tubing and hub is loose and not airtight, thus preventing oversuction of fluid. For the standard diagnostic LP, CSF is collected in 4 tubes for a total of 8–15 mL.²² If leptomeningeal carcinomatosis is suspected, we get the usual specimen for the initial cell count, protein and glucose levels, and culture; then, fluid for cytology can be placed either in a black-top tube or in one of the standard LP tubes on the tray. We always send the last 1–2 mL for the final cell count.

Flow cytometry in lymphoma or leukemia is unpredictable. The laboratory needs “viable” cells to perform the test, and it is impossible to know how much CSF is truly necessary. It can be done with 3 mL of fluid, depending on the viable cell population.

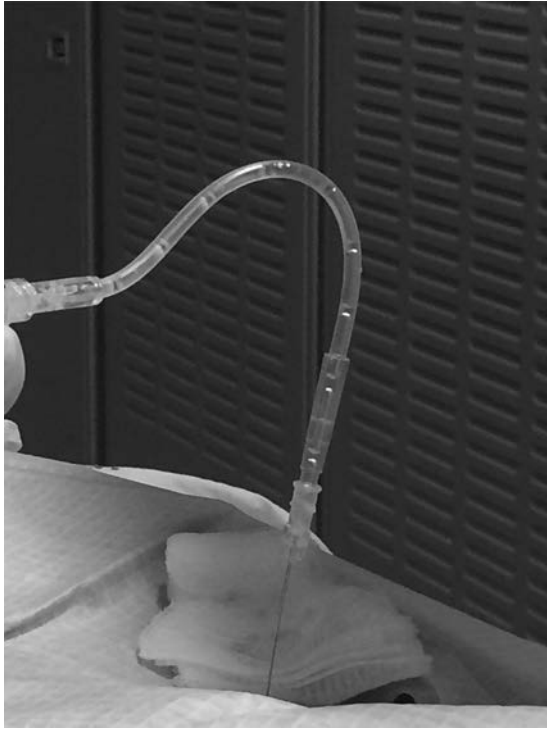


FIG 9. Bubble technique to avoid sucking nerve roots into the spinal needle. The short tubing is literally lying on the LP needle hub so that there is no manipulation of the needle. Both air and CSF fill the tubing and the syringe. With this technique, we have never had nerve root pain reported, and CSF can be easily aspirated.

However, 10 mL of fluid might be inadequate at other times if the load of abnormal cells in the CSF is small. We try to obtain a separate vial of 6–10 mL when flow cytometry is requested. Flow cytometry should be distinguished from cytology.

Therapeutic LP: How Much CSF to Remove?

The therapeutic LP generally implies removal of CSF to both confirm the diagnosis of IIH and treat the symptoms of intracranial hypertension, which in some institutions can mean removal of >30 mL of CSF. When LP is performed to remove CSF, we ask the patient about a headache or visual obscurations before the study and symptom changes during the procedure and then ask again once CSF has been removed. In our experience, a high-volume tap is rarely needed, and there is a risk of low-pressure headaches after the LP. Most patients with IIH do well with a standard amount of CSF removed (15–20 mL). This is likely because the dural defect continues to leak after the tap. In addition, the high intracranial pressure in IIH results in distal transverse venous sinus narrowing; removing CSF decreases the intracranial pressure and reduces venous sinus narrowing, improving venous return with a resultant decrease in symptoms. The opening and closing pressures, the amount of CSF removed, and symptom resolution are documented in the final dictation. The closing pressure is only obtained when performing a therapeutic tap.

Dry Tap

“Dry tap” is defined as an LP with confirmed needle location in the thecal sac, but no egress of CSF. Confirmation of the needle position is by a cross-table lateral radiograph. In our experience,

the dry tap most commonly occurs in the hospitalized patient who has not been eating or drinking and is relatively dehydrated. Before any LP in the hospitalized patient, we ask the team to hydrate the patient, ideally with intravenous fluids. For outpatients, we use no sedating medications, and patients are not NPO and are instructed to drink fluids liberally. Anecdotally, we have noticed that the elderly patient will often have a dry tap and very low CSF pressure, and CSF flow may be very slow. Dry taps can occur in severe spinal stenosis, including thecal sac narrowing from epidural lipomatosis (Fig 5) or arachnoiditis (Fig 3). If a fluoroscopically guided LP has been a truly dry tap, repeating the LP under CT guidance can assure definitive needle tip placement.

Before the LP, be sure the footplate is secured at the end of the fluoroscopy table. After the pop into the thecal sac is felt, advance the needle an additional 2–3 mm and then withdraw the stylet to check for return of CSF. If the spinal needle is 25 ga, CSF return may be very slow. Flow of CSF can be very unpredictable because even tiny alterations in position can affect flow and the rate of flow. It is critical that once CSF flow is confirmed, great care be taken to maintain the same position of the needle throughout the procedure. The hub can be held with the left hand during attachment of the tubing or manometer. Be careful to not let the syringe or tube torque and rotate the needle.

If CSF flow is confirmed and then stops, reinsert the stylet fully, remove it again, and recheck it. Several maneuvers can help with a dry tap. First, have the patient gently cough or perform a Valsalva maneuver, and this will usually start CSF return. Another step is to raise the fluoroscopy table to about 45° to fill the distal thecal sac. After several minutes in this position with provocative maneuvers, recheck the flow by removing the stylet. If there is still no flow, with the stylet out, carefully turn the needle 90° and wait patiently. Continue with this maneuver until a full circle has been achieved. If there is still no flow, the stylet should be replaced and the needle advanced 1–2 mm, followed by a check for CSF return. An additional maneuver is attaching a short tubing and gentle suction with a 10-mL syringe. The suction should be gentle and intermittent, not sustained. Adequately stretch the tubing so that there are few “uphill” kinks through which the CSF has to travel. It may be helpful to hold the tubing lower than the table for gravitational assistance. This is particularly helpful when the table cannot be tilted. In our experience, if CSF flow is initially good, then stops, being patient is most important because usually the flow will start again. Rarely, aspiration is ineffective, and CSF has to be obtained by gravity flow only. This may take up to 30 minutes. The air-leak technique, described previously, can also be attempted.

At this point, a cross-table lateral film if using fluoroscopy or moving the C-arm to confirm the needle position is recommended. If the needle position is confirmed within the canal and there is still no flow, another level can be accessed in the cooperative patient. If a myelography is being performed, 3–5 mL of myelographic-safe contrast can be instilled to determine whether the needle is intrathecal.

Cases that cannot be successfully accessed with fluoroscopy may require biplane or CT guidance.

If another attempt does not result in CSF, there may be thick



FIG 10. Lateral plain film in a patient with recurrent back pain after bilateral pedicle screws at nearly every level. Note dystrophic ossification from a fusion graft. In a patient with extensive postoperative changes, cross-sectional imaging should be obtained to determine whether there is a patent trajectory for the LP.

tenacious secretions in the CSF as may be seen with meningitis, especially in coccidioidomycosis or arachnoiditis ossificans.

If a second level results in no CSF, then it is truly a dry tap. Our preference is to perform a lumbar spine MR imaging to see whether there is a small thecal sac with a narrowed subarachnoid space, such as in patients with epidural lipomatosis. Depending on the clinical setting and need for CSF, the LP can be attempted another day after hydration or performed with CT guidance or a C1–2 puncture can be considered. Before the C1–2 tap, a cervical spine MR imaging is recommended to be sure there is no cerebellar tonsillar ectopia, which can be present in IIH. Particular attention should be paid to the course of the vertebral and posterior inferior cerebellar arteries. Because of low CSF volume in the subarachnoid space with intracranial hypotension, a dry tap is not uncommon. Additional imaging findings of intracranial hypotension include cerebellar tonsillar ectopia, brain stem slumping, lack of CSF about the orbital optic nerves, dural enhancement, venous engorgement, and cerebral and spinal subdural collections.^{23–26} For patients with intracranial hypotension or a prior dry tap, planning the initial or repeat LP under CT guidance is another consideration. The advantage is immediate confirmation of needle position in the thecal sac.

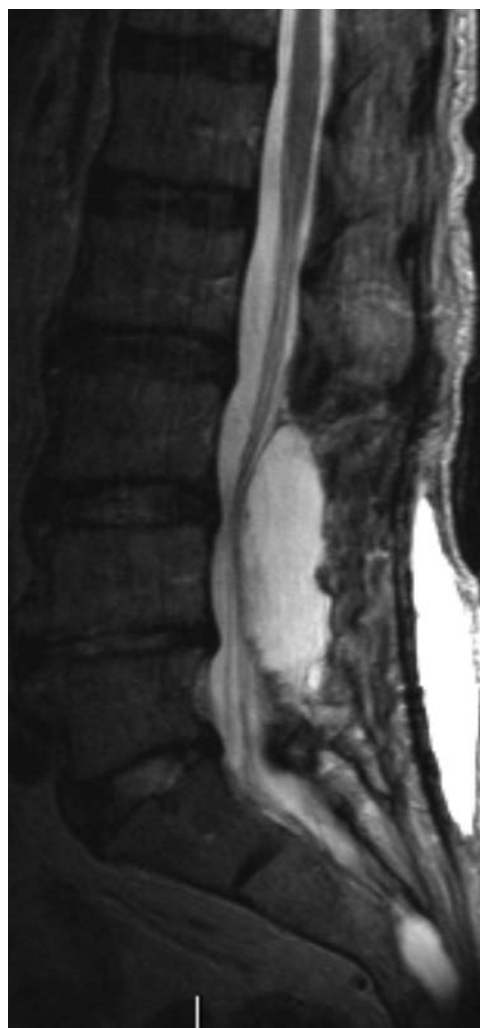


FIG 11. Adult patient with severe back pain following a lumbar spine operation. If LP or myelography is deemed necessary, the needle should be above or below the dorsal intraspinal extradural collection.

The Patient with a Prior Lumbar Spine Surgery

It is critical that prior imaging be reviewed in a patient with a history of lumbar spine surgery. This review helps avoid bulky osteophytes or osseous fusions; determine whether there is arachnoiditis, which may impair CSF return; and finally, determine the easiest site for the LP (Fig 10). We do not hesitate to go through prior surgical sites. We have not experienced increased pain at prior laminectomy sites, but this experience is patient-dependent. 3D surface-rendered images and models can help the proceduralist visualize the trajectory, especially if there are significant degenerative changes.²⁷ In general, a decompressive laminectomy can make the LP easier. However, the procedure can be complicated by arachnoiditis, especially if nerves are adherent to the posterior thecal sac along the course of the needle tract. Postoperative images are also important in determining whether the patient has a dorsal postoperative fluid collection, a seroma, or pseudomeningocele (Fig 11). In general, avoid the fluid collection if you know it is there, to avoid any chance of cross-contamination or confusing imaging or clinical issues with a CSF leak and pseudomeningocele. One of us has inadvertently “sampled” a

LP dictation template

The following are included in our LP template:

Reason for LP: [...]
Level of stick, if additional level was attempted: [...]
Fluoroscopy or C-arm: [...]
Coaxial technique vs single needle: [...]
Anesthetic used, amount, bicarbonate used: [...]
Gauge and length of needle: [...]
Opening pressure and position (prone or on side) when pressure was measured: [...]
Closing pressure (not always performed):
Amount of CSF obtained:
Appearance of CSF:
Symptoms when patient arrived in radiology department:
Resolution of symptoms following LP: [...]
Fluoroscopy time: [...]
Radiation dose: [...]

dorsal seroma in a postoperative patient. If the operation was recent, try to avoid the operative levels, again to prevent infection (or blame for infection) or a confusing picture in a CSF leak. Recent postoperative cases are probably better performed by using CT guidance.

Finally, the Dictation Template

The obese patient often undergoes serial LPs and knowing what worked previously is helpful to the next proceduralist. We always dictate whether fluoroscopy was adequate or whether the C-arm was necessary. Of course, the level for the successful stick, types of needles used, and whether coaxial technique was needed are included in the report. A general estimate of the necessary needle depth is useful to include in the report. Opening pressure, symptom resolution with the LP, and any other technical facts are included. The anesthetic used, whether bicarbonate was used, and the appearance of the CSF, whether clear, cloudy, or blood-tinged with clearing, are dictated. Finally, fluoroscopy time and radiation dose are always mentioned (Table).

REFERENCES

1. Kroll H, Duszak R Jr, Nsiah E, et al. **Trends in lumbar puncture over 2 decades: a dramatic shift to radiology.** *AJR Am J Roentgenol* 2015; 204:15–19 CrossRef Medline
2. Ogden CL, Carroll MD, Kit BK, et al. **Prevalence of childhood and adult obesity in the United States, 2011–2012.** *JAMA* 2014;311: 806–14 CrossRef Medline
3. Hannerz J, Ericson K. **The relationship between idiopathic intracranial hypertension and obesity.** *Headache* 2009;49:178–84 CrossRef Medline
4. Mokdad AH, Ford ES, Bowman BA, et al. **Prevalence of obesity, diabetes, and obesity-related health risk factors, 2001.** *JAMA* 2003; 289:76–79 Medline
5. Boddu SR, Corey A, Peterson R, et al. **Fluoroscopic-guided lumbar puncture: fluoroscopic time and implications of body mass index—a baseline study.** *AJNR Am J Neuroradiol* 2014;35:1475–80 CrossRef Medline
6. Fetterly KA, Schueler BA. **Experimental evaluation of fiber-inter-spaced antiscatter grids for large patient imaging with digital x-ray systems.** *Phys Med Biol* 2007;52:4863–80 CrossRef Medline
7. Bushberg JT. **The AAPM/RSNA physics tutorial for residents: X-ray interactions.** *Radiographics* 1998;18:457–68 CrossRef Medline
8. Eskey CJ, Ogilvy CS. **Fluoroscopy-guided lumbar puncture: decreased frequency of traumatic tap and implications for the assessment of CT-negative acute subarachnoid hemorrhage.** *AJNR Am J Neuroradiol* 2001;22:571–76 Medline
9. Modica MJ, Kanal KM, Gunn ML. **The obese emergency patient: imaging challenges and solutions.** *Radiographics* 2011;31:811–23 CrossRef Medline
10. Brook AD, Burns J, Dauer E, et al. **Comparison of CT and fluoroscopic guidance for lumbar puncture in an obese population with prior failed unguided attempt.** *J Neurointerv Surg* 2014;6:324–28 CrossRef Medline
11. Schindera ST, Nelson RC, Toth TL, et al. **Effect of patient size on radiation dose for abdominal MDCT with automatic tube current modulation: phantom study.** *AJR Am J Roentgenol* 2008;190: W100–05 CrossRef Medline
12. Yanch JC, Behrman RH, Hendricks MJ, et al. **Increased radiation dose to overweight and obese patients from radiographic examinations.** *Radiology* 2009;252:128–39 CrossRef Medline
13. Nayate AP, Nasrallah IM, Schmitt JE, et al. **Using body mass index to predict needle length in fluoroscopy-guided lumbar punctures.** *AJNR Am J Neuroradiol* 2016;37:572–78 CrossRef Medline
14. Strupp M, Brandt T, Müller A. **Incidence of post-lumbar puncture syndrome reduced by reinserting the stylet: a randomized prospective study of 600 patients.** *J Neurol* 1998;245:589–92 CrossRef Medline
15. Evans RW. **Complications of lumbar puncture.** *Neurol Clin* 1998;16: 83–105 CrossRef Medline
16. Wu CL, Rowlingson AJ, Cohen SR, et al. **Gender and post-dural puncture headache.** *Anesthesiology* 2006;105:613–18 CrossRef Medline
17. Curry TS III, Dowdey JE, Murry RC Jr. *Christensen's Physics of Diagnostic Radiology.* 4th ed. Philadelphia: Lea & Febiger; 1990:258–59
18. Johnson JC, Deeb ZL. **Coaxial needle technique for lumbar puncture in the morbidly obese patient.** *Radiology* 1991;179:874 CrossRef Medline
19. Abel AS, Brace JR, McKinney AM, et al. **Practice patterns and opening pressure measurements using fluoroscopically guided lumbar puncture.** *AJNR Am J Neuroradiol* 2012;33:823–25 CrossRef Medline
20. Rando TA, Fishman RA. **Spontaneous intracranial hypotension: report of two cases and review of the literature.** *Neurology* 1992;42: 481–87 CrossRef Medline
21. Corbett JJ, Mehta MP. **Cerebrospinal fluid pressure in normal obese subjects and patients with pseudotumor cerebri.** *Neurology* 1983;33: 1386–88 CrossRef Medline
22. Cauley KA. **Fluoroscopically guided lumbar puncture.** *AJR Am J Roentgenol* 2015;205:W442–50 CrossRef Medline
23. Dillon WP, Fishman RA. **Some lessons learned about the diagnosis and treatment of spontaneous intracranial hypotension.** *AJNR Am J Neuroradiol* 1998;19:1001–02
24. Mokri B, Piepgras DG, Miller GM. **Syndrome of orthostatic headaches and diffuse pachymeningeal gadolinium enhancement.** *Mayo Clin Proc* 1997;72:400–13 CrossRef Medline
25. Schievink WI, Meyer FB, Atkinson JL, et al. **Spontaneous spinal cerebrospinal fluid leaks and intracranial hypotension.** *J Neurosurg* 1996;84:598–605 CrossRef Medline
26. Fishman RA, Dillon WP. **Dural enhancement and cerebral displacement secondary to intracranial hypotension.** *Neurology* 1993;43: 609–11 CrossRef Medline
27. Cramer J, Quigley E, Hutchins T, et al. *Spine Procedures in 3D.* Salt Lake City: Practical Imaging; 2016: version 1.1, iTunes Bookstore. <https://itunes.apple.com/us/book/spine-procedures-in-3d/id1119397210?ls=1&mt=13>. Accessed February 25, 2017

Baseline Survey of the Neuroradiology Work Environment in the United States with Reported Trends in Clinical Work, Nonclinical Work, Perceptions of Trainees, and Burnout Metrics

J.Y. Chen and F.J. Lexa



ABSTRACT

BACKGROUND AND PURPOSE: Neuroradiologists have faced continuously increasing clinical workloads. Our aim was to establish and report a baseline survey of the current neuroradiology work environment in the United States and of experiential changes in recent years.

MATERIALS AND METHODS: A voluntary survey was sent to practicing and out-of-training members of the American Society of Neuroradiology in the United States. Selected measures included workday volume and length, burnout symptoms, participation in academic and practice-building duties; effects on perceived interpretation quality, communication of abnormal results, and consideration of early retirement or career changes, among others.

RESULTS: Four hundred thirty-two respondents across a broad range of experience reported the following: 52.8% (224/424) with teaching responsibilities; 93% (399/430) with workdays extending at least 1 hour past expected, in 45% (193/430) frequently or always; 71.9% (309/430) reading more cases per hour compared to previous years; 79.5% (341/429) sometimes-to-always interpreting cases faster than comfortable for optimal interpretation; and 67.8% (292/431) sometimes or more often with inadequate time to discuss abnormal results. Burnout symptoms ranged between 49% and 75% (211/428 to 322/428) across 4 indices. For academic activities of teaching, mentoring, and research/publications, a mean of 94.3% reported cut-backs during the past few years. For practice-building activities, 92% reported cut-backs, 51.6% (222/429) considered early retirement, and 38.8% (167/429) considered changing careers.

CONCLUSIONS: Increasing clinical demands have coincided with destructive effects in the work environment and the ability and desire of neuroradiologists in the United States to perform academic or practice-building duties with a substantial incidence of burnout symptoms. While this survey does not prove causation, the trends and the correlations should be concerning to the leaders of radiology and warrant further monitoring.

ABBREVIATIONS: ASNR = American Society of Neuroradiology; RVU = relative value unit

In the United States, the work volume of neuroradiologists has mirrored that of radiology and health care in general, with increases in annual work productivity (number of Relative Value Units [RVUs]) during the past decade.¹ This is part of a longer term trend in increased workloads that occurred in the prior de-

cade.² The rise in productivity demand has resulted in some practices requiring the use of specific work-output RVU targets as thresholds for compensation or hiring without adequate regard for their effects on workers or potential limits to human task performance. Neuroradiologists' target and total RVUs are the highest of radiology subspecialties,³⁻⁵ and neuroradiologists may serve as a bellwether for the broader radiologist population. To date, there has not been a single national survey collecting data on the neuroradiologists' practice work environment evaluating compensation, workplace hiring practices, effects on productivity, and output as well as burnout, to our knowledge.

The emphasis on ever-increasing RVU targets may have downstream effects on radiology, such as increased speed of interpretation, decreased remaining time for training residents and fellows, decreased research output, decreased time for practice building (such as quality projects, administrative committees), and potential burnout of radiologists. Worker burnout is a

Received December 12, 2016; accepted after revision March 3, 2017.

From the Department of Radiology (J.Y.C.), San Diego Veterans Administration Health System, San Diego, California; Department of Radiology (J.Y.C.), Division of Neuroradiology, University of California San Diego Health System, San Diego, California; The Global Consulting Practicum and Department of Marketing (F.J.L.), The Wharton School, University of Pennsylvania, Philadelphia, Pennsylvania; and Radiology Leadership Institute of the American College of Radiology (F.J.L.), Reston, Virginia.

Paper previously presented, in part, at: American College of Radiology–Radiology Business Management Association Forum, January 13–15, 2017; Orlando, Florida.

Please address correspondence to James Y. Chen, MD, 3350 La Jolla Village Dr, MC 114, La Jolla, CA 92161; e-mail: jamesychen@ucsd.edu

Indicates article with supplemental on-line appendix and tables.

<http://dx.doi.org/10.3174/ajnr.A5215>

known contributor to workplace errors and is costly in terms of personal and institutional impact. Burnout of radiologists and other physicians is becoming an important topic, not just in the United States, but also in other countries.⁶⁻⁸

This survey of neuroradiologists was performed to establish a national baseline for work patterns in the United States to allow tracking and comparison with future surveys. The survey will be repeated and updated biennially to allow tracking and comparisons as the work environment in the United States continues to change. This schedule will provide better data to practitioners and practice managers for understanding, measuring, and (perhaps) modifying the work environment.

MATERIALS AND METHODS

A voluntary on-line survey was sent to practicing neuroradiologists in the United States who are members of the American Society of Neuroradiology (ASNR). It was inclusive of the neuroradiologists in the United States and excludes neuroradiologist members who were outside the United States. The survey was launched at the beginning of August 2016 and was open until October 5, 2016. The current membership includes practicing physicians and fellows in training. We excluded the latter because many of the questions interrogated trends and changes with a baseline that was longer than the training period. Although participation was voluntary, an incentive was offered in the form of a drawing for a gift certificate valued at \$250, given the length of the survey.

The survey (On-line Appendix) was collected electronically by using Survey Monkey (<http://www.surveymonkey.com>), a survey Web site that allows viewing of survey responses only by the owner of the survey. The American Society of Neuroradiology agreed to send the survey out to members in the United States by e-mail. Members who chose to participate did so by clicking the e-mail link to open the Survey Monkey Web page containing the survey and completed it on their device. No direct contact occurred between the study Principal Investigator or the survey respondents except for announcement to the respondents of the winner of the prize associated with the lottery.

The e-mail addresses and surveys were initially linked temporarily only if the participant chose to participate in the prize lottery. The e-mail address was collected only for the lottery and then was separated from the survey response. The survey responses were then de-linked from any e-mail address in the investigator's response data base. Until the e-mail addresses were separated from the responses, they were considered confidential. Once the responses were separated from the e-mail addresses, there was no mechanism for tracking responses back to a specific e-mail address.

Survey data were then checked for quality and to remove duplicates. Internet Protocol addresses, survey submission time, and e-mails were cross-referenced to identify responses that could be considered duplicates.

In 1 case, duplicate answers from the same ASNR member were reconciled before inclusion in the analysis. Initial data display was performed by using the on-line survey tool output; then, more advanced data analysis was performed by importing the data into an Excel (Microsoft, Redmond, Washington)

spreadsheet. Statistical comparison of selected yes/no results between groups was performed by using n-1 comparison.

Results were broken into several groups for analysis: overall results, respondents who routinely teach trainees versus respondents who do not routinely teach trainees, and roughly by demographic generation with practice experience as a proxy. If one assumed contiguous education and training with completion of the fellowship at 32 years of age, dividing respondents at and below 20 years of experience would roughly divide respondents into 2 major demographic generations. This division would approximately divide respondents at a date of birth of 1964, roughly "Generation X" including 1 or 2 years of "Millennials" versus "Baby Boomers" and "Greatest Generation" with >20 years of experience.

RESULTS

Article length constraints limit text reporting of the results to the overall results and selected subgroups. The results tables (Tables 1–3 and On-line Tables 1–3) provide more detailed comparisons of subgroups, including teaching versus nonteaching, and <20 years of experience versus >20 years of experience.

Only 1 duplicate response from 1 Internet Protocol address was discovered. Once the duplicated responses were reconciled and the 20 member-in-training responses were excluded, a total of 432 participants were included for further analysis. There was minimal survey fatigue; although questions could be skipped, 99.3% (429/432) of the respondents answered the last question. The results below are based on the percentage of participants who responded to a question.

Demographic Results

A slight majority of respondents, 52.8% versus 47.2%, reported that they routinely teach radiology residents or fellows, giving the survey a relatively well-balanced sample of both training settings and nontraining sites of neuroradiology work.

The dataset was also fairly well-distributed by experience from the first 5 years out of training to those with >31 years of post-training work experience (Fig 1).

The survey group encompassed a fairly wide spread of respondents with regard to the anticipated number of years remaining in their careers. Fourteen percent of the respondents were within ≤5 years of planned retirement, with a peak of 20% planning to work 11–15 years and 19.5% planning to work ≥26 years. There was less diversity with regard to the number of jobs held: Three of 4 of the respondents (77.8%) had not changed employers in past few years, while 17.4 had changed employers once, 3.9% had changed twice, and <1% had changed ≥3 times.

Reported Compensation and Time Off

Slightly less than half, 48.5%, reported that their compensation versus the prior year was unchanged; 28.4% reported an increase; and 23.1% reported a decrease. Time off the clinical schedule (vacation and nonclinical professional time) was more stable, with 73% reporting no change since the prior year, but with a more concerning trend in that those reporting a decrease (18.7%) outnumbered those with an increase (8.4%). Similarly, if we looked at weeks rather than days, 70.8% reported no change, but

Table 1: Respondent demographics

| | Overall | | | Teaching | | | Nonteaching | | | <20 Years' Experience | | | ≥20 Years' Experience | | |
|--|---------|-----|---------|----------|-----|---------|-------------|-----|---------|-----------------------|-----|---------|-----------------------|-----|---------|
| | % | No. | Skipped | % | No. | Skipped | % | No. | Skipped | % | No. | Skipped | % | No. | Skipped |
| 1) Do you teach radiology trainees? | | | 8 | | | 0 | | | 0 | | | 3 | | | 5 |
| Yes | 52.8% | 224 | | 100.0% | 224 | | 0.0% | 0 | | 54.4% | 141 | | 50.3% | 83 | |
| No | 47.2% | 200 | | 0.0% | 0 | | 100.0% | 208 | | 45.6% | 118 | | 49.7% | 82 | |
| 2) How long have you been in practice? | | | 0 | | | 0 | | | 0 | | | 0 | | | 0 |
| Still in training | 0.0% | 0 | | 0.0% | 0 | | 0.0% | 0 | | 0.0% | 0 | | 0.0% | 0 | |
| 1–5 yr beyond training | 16.2% | 70 | | 17.0% | 38 | | 15.5% | 31 | | 26.7% | 70 | | 0.0% | 0 | |
| 6–10 yr beyond training | 19.4% | 84 | | 24.1% | 54 | | 15.0% | 30 | | 32.1% | 84 | | 0.0% | 0 | |
| 11–15 yr beyond training | 13.2% | 57 | | 12.5% | 28 | | 14.0% | 28 | | 21.8% | 57 | | 0.0% | 0 | |
| 16–20 yr beyond training | 11.8% | 51 | | 9.4% | 21 | | 14.5% | 29 | | 19.5% | 51 | | 0.0% | 0 | |
| 21–25 yr beyond training | 16.7% | 72 | | 12.9% | 29 | | 20.5% | 41 | | 0.0% | 0 | | 42.4% | 72 | |
| 26–30 yr beyond training | 13.0% | 56 | | 12.9% | 29 | | 12.5% | 25 | | 0.0% | 0 | | 32.9% | 56 | |
| ≥31 yr beyond training | 9.7% | 42 | | 11.2% | 25 | | 8.0% | 16 | | 0.0% | 0 | | 24.7% | 42 | |
| 3) When do you intend to retire from radiology practice? | | | 2 | | | 1 | | | 1 | | | 0 | | | 2 |
| 0–5 yr | 14.0% | 60 | | 10.8% | 24 | | 17.1% | 34 | | 1.5% | 4 | | 33.3% | 56 | |
| 6–10 yr | 17.4% | 75 | | 15.7% | 35 | | 19.1% | 38 | | 9.5% | 25 | | 29.8% | 50 | |
| 11–15 yr | 20.7% | 89 | | 17.9% | 40 | | 24.1% | 48 | | 17.9% | 47 | | 25.0% | 42 | |
| 16–20 yr | 14.7% | 63 | | 13.5% | 30 | | 16.6% | 33 | | 21.4% | 56 | | 4.2% | 7 | |
| 21–25 yr | 13.7% | 59 | | 16.6% | 37 | | 11.1% | 22 | | 22.1% | 58 | | 0.6% | 1 | |
| 26–30 yr | 11.6% | 50 | | 13.5% | 30 | | 9.5% | 19 | | 17.9% | 47 | | 1.8% | 3 | |
| ≥31 yr | 7.9% | 34 | | 12.1% | 27 | | 2.5% | 5 | | 9.5% | 25 | | 5.4% | 9 | |

Table 2: Burnout measures

| | Overall | | | Teaching | | | Nonteaching | | | <20 Years' Experience | | | ≥20 Years' Experience | | |
|--|---------|-----|---------|----------|-----|---------|-------------|-----|---------|-----------------------|-----|---------|-----------------------|-----|---------|
| | % | No. | Skipped | % | No. | Skipped | % | No. | Skipped | % | No. | Skipped | % | No. | Skipped |
| 27) Compared with 5 years ago, have you experienced | | | | | | | | | | | | | | | |
| Greater fatigue? | | | 4 | | | 2 | | | 2 | | | 4 | | | 0 |
| Yes | 75.2% | 322 | | 77.9% | 173 | | 71.2% | 141 | | 76.4% | 197 | | 73.5% | 125 | |
| No | 24.8% | 106 | | 22.1% | 49 | | 28.8% | 57 | | 23.6% | 61 | | 26.5% | 45 | |
| Difficulty relaxing after work? | | | 4 | | | 2 | | | 2 | | | 4 | | | 0 |
| Yes | 59.3% | 254 | | 62.2% | 138 | | 55.1% | 109 | | 65.1% | 168 | | 50.6% | 86 | |
| No | 40.7% | 174 | | 37.8% | 84 | | 44.9% | 89 | | 34.9% | 90 | | 49.4% | 84 | |
| Greater anxiety or depression? | | | 4 | | | 2 | | | 2 | | | 4 | | | 0 |
| Yes | 49.3% | 211 | | 49.5% | 110 | | 49.0% | 97 | | 52.7% | 136 | | 44.1% | 75 | |
| No | 50.7% | 217 | | 50.5% | 112 | | 51.0% | 101 | | 47.3% | 122 | | 55.9% | 95 | |
| Diminished sense of enthusiasm or effectiveness at work? | | | 5 | | | 3 | | | 2 | | | 5 | | | 0 |
| Yes | 68.1% | 291 | | 72.9% | 161 | | 63.1% | 125 | | 69.6% | 179 | | 65.9% | 112 | |
| No | 31.9% | 136 | | 27.1% | 60 | | 36.9% | 73 | | 30.4% | 78 | | 34.1% | 58 | |

Table 3: Administrative adjustments to workplace and thoughts of personal changes in career and retirement

| | Overall | | | Teaching | | | Nonteaching | | | <20 Years' Experience | | | ≥20 Years' Experience | | |
|---|---------|-----|---------|----------|-----|---------|-------------|-----|---------|-----------------------|-----|---------|-----------------------|-----|---------|
| | % | No. | Skipped | % | No. | Skipped | % | No. | Skipped | % | No. | Skipped | % | No. | Skipped |
| 28) Over the last few years, have your practice administrators made concrete changes to the practice to balance changes of your clinical workload with your nonclinical duties? | | | 2 | | | 1 | | | 1 | | | 1 | | | 1 |
| Yes | 14.2% | 61 | | 15.7% | 35 | | 12.6% | 25 | | 13.8% | 36 | | 14.8% | 25 | |
| No | 66.5% | 286 | | 74.4% | 166 | | 58.3% | 116 | | 69.0% | 180 | | 62.7% | 106 | |
| NA | 19.3% | 83 | | 9.9% | 22 | | 29.1% | 58 | | 17.2% | 45 | | 22.5% | 38 | |
| 29) Have you considered retiring earlier than you had initially intended when first starting practice? | | | 3 | | | 0 | | | 3 | | | 3 | | | 0 |
| Yes | 51.7% | 222 | | 51.3% | 115 | | 51.8% | 102 | | 57.9% | 150 | | 42.4% | 72 | |
| No | 48.3% | 207 | | 48.7% | 109 | | 48.2% | 95 | | 42.1% | 109 | | 57.6% | 98 | |
| 30) In the last few years, have you considered changing careers? | | | 3 | | | 2 | | | 1 | | | 1 | | | 2 |
| Yes | 38.9% | 167 | | 40.5% | 90 | | 37.7% | 75 | | 46.0% | 120 | | 28.0% | 47 | |
| No | 61.1% | 262 | | 59.5% | 132 | | 62.3% | 124 | | 54.0% | 141 | | 72.0% | 121 | |

those reporting working more weeks (23.2%) outnumbered those reporting working fewer (6.0%).

Perceptions of Clinical Workload and Time at Work

Close to one-third (32.5%) of respondents said that radiology compensation was determined by RVU targets. At a personal level, most

(62.7%) reported that during the past few years, their RVU production had increased, while 6.5% reported a decrease, 16.4% reported that it was the same, and 14.4% did not know. Reporting on the trend of the number of hours worked per day during the past few years, almost half (49.7%) reported working longer days, while a slightly smaller number, 46.9%, reported that they worked about the same,

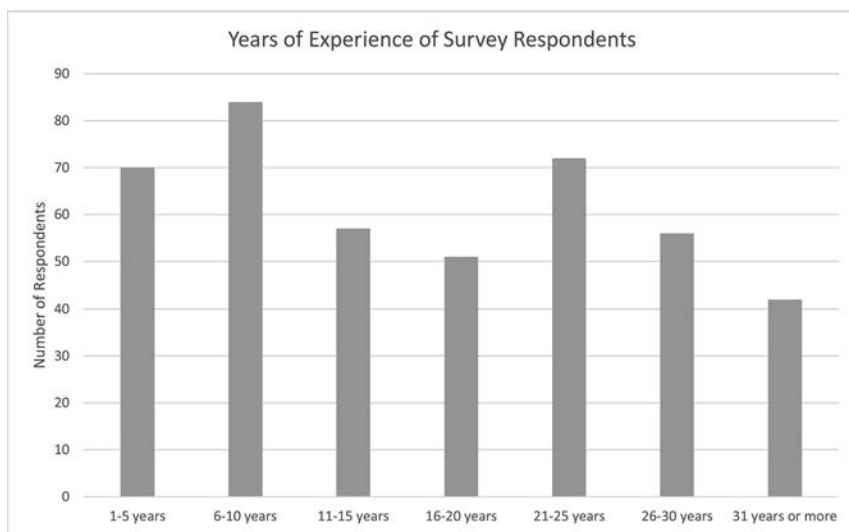


FIG 1. Five-year periods of practice experience of survey respondents.

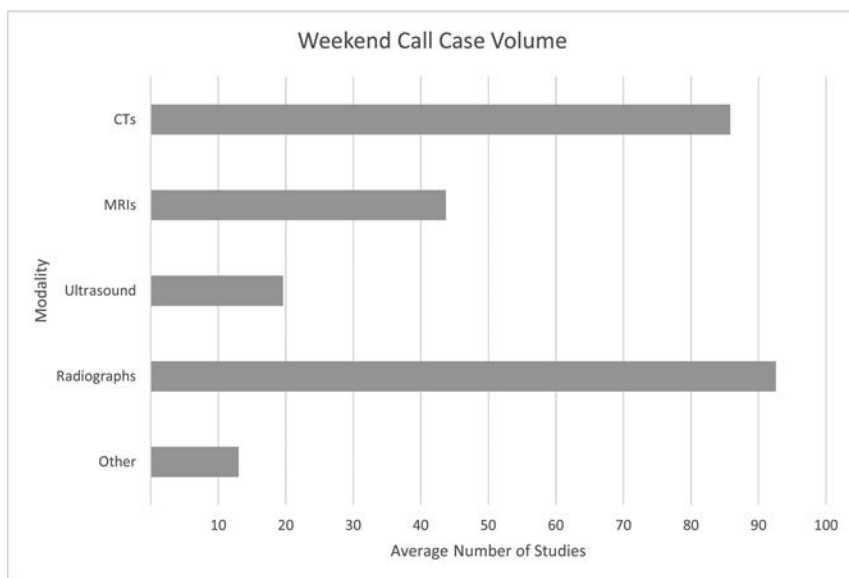


FIG 2. Number of studies by technique interpreted during a weekend between Friday evening and Monday morning. This is a gross overstatement of individual workload, as these numbers do not account for case number and modality differences between fully subspecialized and partly subspecialized call responsibilities.

and only 3.5% reported a shorter workday. In a related question, the participants were asked how often they had to stay ≥ 1 hour beyond the expected workday. Here only slightly more than one-quarter reported that a longer stay never or rarely occurred (27.4%, sum of 2 responses). More than half the respondents reported that it happened sometimes or frequently (57.2%, sum of 2 responses), and most interesting were the 15.4% who said they always stayed an hour or more past the end of the “expected workday.”

With the regard to the number of workdays in the year, more than half (54.1%) reported that this was stable during the past few years. Of the remainder, 38.0% reported working more days and 7.9% reported working fewer.

With regard to the trends in the intensity of work, 24% reported reading the same number of cases per hour, while only 4.2% reported reading fewer, and most, 71.9%, were reading

more per hour. When asked how often a participant thought that they were reading faster than they were comfortable with, only around one-fifth (20.5%) reported that reading faster was rare or never occurred. Almost half (44.1%) reported that this occurred sometimes; 29.1% said that this was frequent; and 6.3% of the participants said that this occurred “always.” When it came to reports, a similar distribution occurred with 8.1% reporting that they always signed reports faster than they were “comfortable for optimal communication and clarity.” When asked if they had too little time to discuss important abnormal results with clinicians, about one-third (32.3%) responded that the lack of time rarely or never happened, while 35.3% said that it occurred sometimes, 27.4% stated it was frequent, and for 5.1% this always happened. In reporting abnormal results, there was a similar distribution, with 4.7% of respondents stating that they always had too little time to report abnormal results.

When asked about reading cases when sleep-deprived, approximately half (48.72%) said this was a rare or never occurrence, while 36.0% reported doing this sometimes, 13.5% did it frequently, and 1.9% did it “always.”

On-Call Responsibilities and Perceptions

For the number of duty day/nights of call coverage, 54.1% of respondents reported no change, while in the remainder, those reporting an increase, 36.6%, outnumbered those reporting a decrease, 9.3%. Regarding the perception of on-call duty, only a little more than one-third

(35.5%) reported that the difficulty of on call was stable, while of the remainder, those reporting greater difficulty, 59.7%, outnumbered those who thought their on-call duty was easier, 4.9%.

Participants were asked to provide information about what they read on weekend call, defined as Friday evening to Monday morning. The following averages were obtained from 328 respondents: 86 CTs, 44 MRIs, 20 ultrasounds, 93 radiographs, and 13 other (Fig 2), which likely grossly overestimates studies interpreted due to limitations of context in the survey instrument. Important contextual information not obtained as part of the survey included the number of hours on-call, whether calls were fully subspecialized, and whether final or preliminary interpretation was provided, among others.

Of respondents, 62.2% thought that the number of poorly indicated or unindicated studies had increased, while only 4.0% thought that they had decreased, with 33.8% reporting a stable amount.

Trends in Perceptions of Trainees

Of those who train neuroradiology fellows, most thought that the ability of the trainees was the same as in the past, but of those

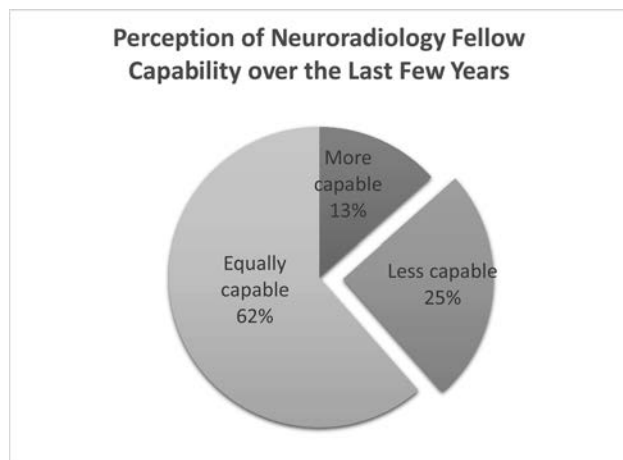


FIG 3. Faculty reported change in the capabilities of fellows-in-training.

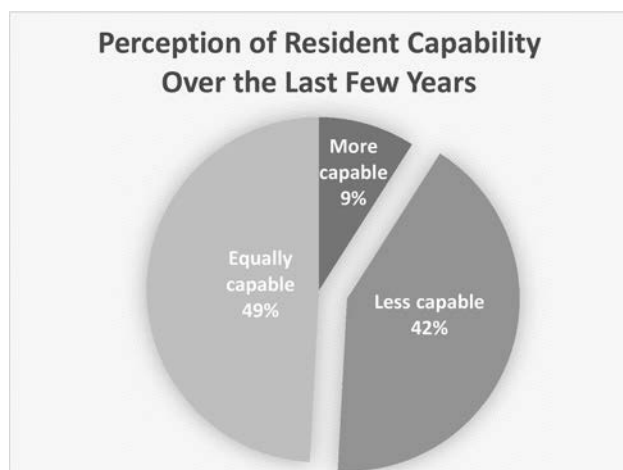


FIG 4. Faculty reported change in the capabilities of residents-in-training.

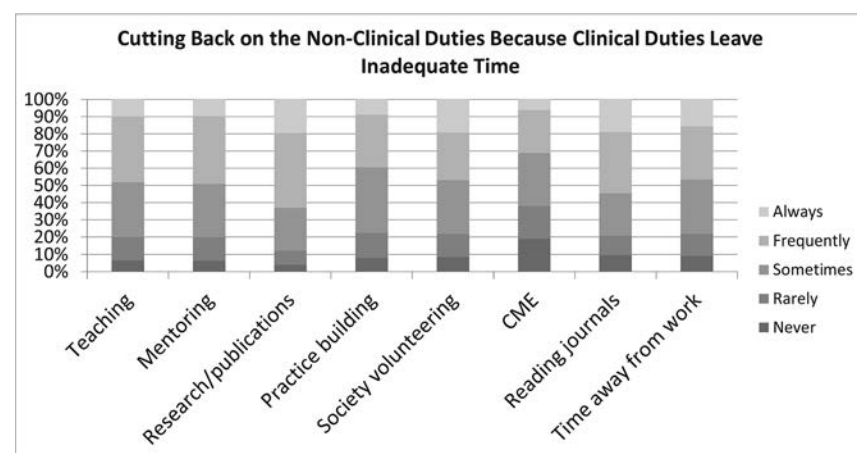


FIG 5. The percentage of respondents reporting cutting back time spent performing various nonclinical duties who consider those duties part of their job description. This specifically excludes respondents who answered, "Not Applicable" to those duties.

reporting a change, almost twice as many thought that abilities had declined (Fig 3).

Of respondents who train residents, of those who noticed a change in the past few years, >4 times as many respondents found a reduction in resident ability than an increase (Fig 4).

Changes in Nonclinical Activities Occurring in Parallel with Increased Clinical Work

Most respondents reported cutting back on ≥ 1 key nonclinical professional activity (Fig 5 and On-line Table 3) in the past few years. This included key elements of the "academic triad," including teaching and research, as well as mentoring, volunteer work for professional societies, practice building, and personal medical education. Concordant with the earlier results, most of the respondents also reported an impact on the amount of time they have away from work.

Excluding respondents for whom these activities are "Not Applicable," only a small minority of respondents (2 categories combined) never or rarely needed to cut back on the following activities, whereas most (3 categories combined) reported sometimes, frequently, or always cutting back (Fig 5). Regarding cutting back on teaching, of the 60.9% of respondents who teach, 80.0% of those responded that they cut back between "sometimes" and "all the time," with 20.0% who reported never or rarely cutting back. Similar results were obtained regarding the 62.4% of respondents who mentor, 80.1% of whom reported cutting back sometimes or more frequently, with a minority, 19.9%, saying that they never or rarely cut back. Of the 57.9% of respondents who perform and publish research, there was a sharper decrease, with only 12.2% never or rarely cutting back, compared with 87.8% who did. Regarding the 87.8% of respondents who would participate in practice-building activities, 22.4% never or rarely cut back, compared with 77.6% who did. Of the 69.6% of respondents who voluntarily serve in radiology and academic societies, 21.8% of respondents never or rarely cut back on their service compared with 78.2% who did. The 95.6% of respondents who participate in Continuing Medical Education activities were most

resistant to cut back, with 38.0% of respondents never or rarely cutting back compared with 62.0% who did. Of the 97.2% of respondents who read journals, 20.7% never or rarely cut back, compared with the 79.3% who did. Most interesting, only 97.2% of respondents reported spending time away from work, and of those, 21.8% never or rarely cut back on nonwork time, compared with 78.2% who did.

Burnout Indices

In answer to 4 commonly considered parameters of burnout or burning out workers, more than half of the respondents said that they had experienced increases in fatigue, difficulty relaxing after work, and diminished enthusiasm

or effectiveness at work. On the fourth question regarding anxiety and depression, slightly less than half reported an increase. When asked if their practice administrators had made changes to help balance clinical and nonclinical work, only about 1 in 7 (14.2%) said yes. More than half the respondents said that they considered retiring earlier than originally planned (51.8%) and 38.9% have considered changing careers.

Statistically significant differences were found for several measures divided by experience. Neuroradiologists with <20 years of experience were more likely to have difficulty relaxing after work (65.1%) versus those with ≥ 20 years of experience (50.6%, $P = .003$). Neuroradiologists with <20 years of experience were more likely to consider retiring earlier than initially intended (57.9%) versus those with ≥ 20 years of experience (42.4%, $P = .002$). Neuroradiologists with <20 years of experience were more likely to consider changing careers (46.0%) versus those with ≥ 20 years of experience (28.0%, $P < .001$).

DISCUSSION

This article reports the results of the first survey of practicing members of the ASNR of their current work, their perceptions of changes in their clinical work, changes in their nonclinical work, their perceptions of their trainees, and 4 commonly used measures of burnout. Radiologists are among the most educated and highly trained professionals in the United States, requiring a minimum of 13 years of education after high school. Neuroradiologists require an additional year (or more) of fellowship training. Staying current requires a strong commitment not only to their work but also to maintaining certification through a combination of Continuing Medical Education and performing service and quality projects. Neuroradiologists thus represent not only a major personal commitment but also a substantial societal investment to create knowledge professionals.

The 21st century has been a time of rapid change in medicine in the United States. Implementation of cost reductions and the shift from volume- to value-based reimbursement have had a strong impact on how radiologists practice. Private practice physicians in many parts of the United States have seen reductions in their autonomy, and others have shifted to employed practice (either voluntary or not); both of these trends have additional impact on the way radiologists practice.

This survey was implemented to begin a periodic process of understanding how neuroradiologists in the United States practice and how they view the quality of their work and its impact. This understanding is important for several reasons.

Sustainability

First, these results suggest crowding out of important nonclinical tasks that academic and private practice radiologists need to do to sustain their careers and their groups/departments. In 2000, Eschelman et al⁹ reported an inverse relationship between clinical productivity and academic productivity. If clinical demands crowd out academic work and practice building, then the academic mission will be compromised and the ability of radiologists to build and maintain their practices will be challenged. An important report from a leading academic neuroradiology

practice showed that approximately one-fifth of productivity was non-RVU-generating.¹⁰

Second, the sustainability of the radiology enterprise depends on intergenerational work and cooperation. If clinical demands crowd out time for effective teaching, mentoring, and academic project work, the profession itself is at risk. While correlation is not proof of causation, 93.5% (243/260) of our respondents who teach reported a degree of cutting back on teaching, with almost half reporting cutting back frequently or always, 48.1% (125/260). Mentoring activities showed similar degrees of reported reductions. These are professionals acknowledging that they are not doing important tasks for the future of the profession.

The perceptions of neuroradiologists that there has been a decline in the quality of trainees is concerning for the future of the profession and should be investigated further because it could be due to many factors, including the following: generational misunderstandings, burnout in the current teaching cadre leading to overly harsh evaluations, declining educational standards at the medical school level, and/or a decline in the quality of trainees self-selecting into a radiology career.

Potential for Future Workforce Shortage

Although considering early retirement or career change does not necessarily equal intention, it raises the possibility of a shrinking workforce, compounded by recent trends in the general diagnostic radiology National Resident Matching Program.

The historical data from 2004 to 2015,¹¹⁻¹⁵ years for which information was available at the time this manuscript was written, show a divergence beginning in 2011 in the number of offered training positions from the number of filled positions (Fig 6) in diagnostic radiology residencies. Regarding neuroradiology fellowship positions, there was a milder and delayed divergence between offered positions and filled positions beginning in 2014 (Fig 7), which may be expected, given that fellowship applications occur 4 years after diagnostic residency applications in the third year of residency.

Data from the 2016 National Resident Matching Program,^{16,17} however, show an increase in the fill percentage of both diagnostic radiology programs (96.4%) and neuroradiology fellowships (80.5%) compared with the 2015 year (86.3% and 74.5%, respectively), a deviation from the trend of the previous 5 years.

Depending on whether the 2016 data are an anomaly compared with the trailing trend of the past half-decade versus an important inflection point for reversal of the trend, the implication for the availability of future trainees to replace retiring neuroradiologists is great. If the 2016 data are an anomaly, radiology and thus neuroradiology may find itself unable to replace both radiologists who retire as planned when first beginning their careers and any who may retire early or change careers due to burnout. That situation could create a negative cycle, exacerbating the problem. On the other hand, if the 2016 data represent an inflection point, the possibility of a future workforce shortage may be less. More future data points will be needed to evaluate these possibilities.

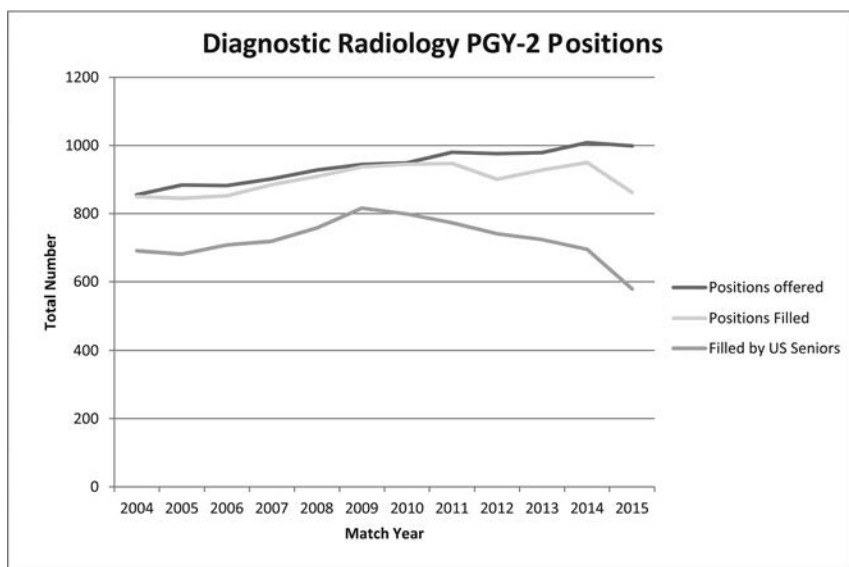


FIG 6. Positions offered in the diagnostic radiology match of the National Resident Matching Program compared with number of positions filled in total and by seniors in the United States. Beginning in 2011, there is a divergence between number of offered positions and filled positions, with a sharper drop in the number of positions filled by seniors in the United States. PGY-2 indicates postgraduate year 2, or first year of a typical radiology residency.

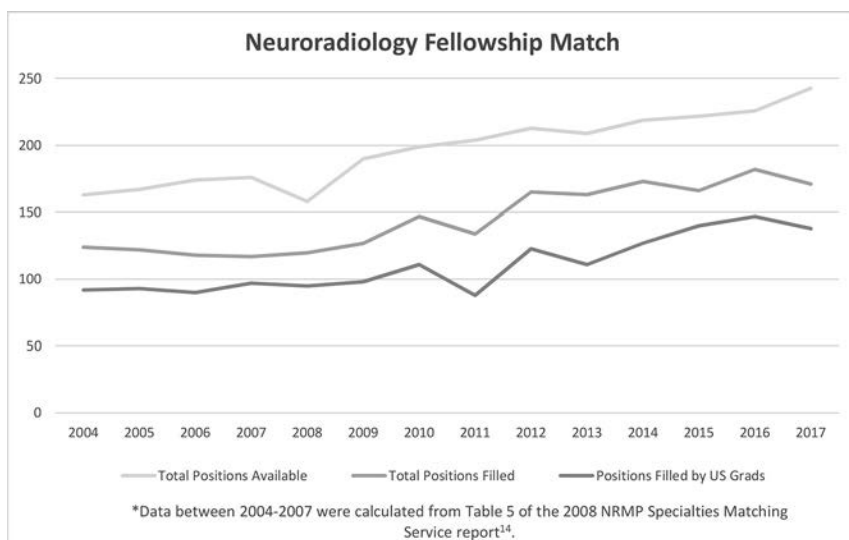


FIG 7. Positions offered in the neuroradiology fellowship match of the National Resident Matching Program compared with number of positions filled in total and by graduates in the United States. The total number of filled positions in 2014 and 2015 appears to have leveled off, despite the larger number of offered positions compared with previous years.

Burnout

Burnout is a serious threat for this cadre of neuroradiologists. A study of physician happiness comparing specialties reported in 2015 that radiologists were the least happy of 27 types of specialists on a Likert scale.¹⁸ Another report with different methodology also showed radiologists in the lower half of a large group of major medical specialties in reported happiness at work.¹⁹ Burnout is often misunderstood by physicians and administrators. Delay in diagnosis can occur if there is an ignorance of early warning signs. The late indicators include poor work performance, visible anger-yelling, throwing things, verbal abuse, and so forth as well as inappropriate be-

havior and medical malpractice. By the time these indicators are manifest, serious personal and professional impairment has already occurred.

Workplace unhappiness extends far beyond the employment setting. It affects relationships, including divorce, and can lead to substance abuse and sleep and eating disorders and neglect of hygiene and health. In a 2015 report, burnout in physicians correlated with the following: a lower rate of volunteerism, worse health, lower exercise, greater likelihood of obesity, less savings, and more likely never being married and being alone.²⁰ Burnout is also linked to a higher rate of depression; not surprisingly perhaps, the suicide rate among physicians in the United States is higher than that in the general population and is worse for female physicians.²¹

Earlier warning signs of burnout include what have been called the “3 D’s”: disengagement, disinterest, and disconnection. Also, watch for loss of communication, truancy, heightened cynicism, and aggression.

A second problem with accurate diagnosis and treatment of burnout is that burnout is often misunderstood as a character flaw. For example, one may ask why one radiologist cannot work as hard or as long as another? There must be something wrong and so forth. Like posttraumatic stress disorder, burnout can happen to the best of neuroradiologists, despite good character, good training, and so forth. The focus on the individual can also distract leaders and administrators from addressing environmental issues. While some may burn out sooner than others, if a group or department is seeing advanced burnout in one member, that should be a warning to others as well.

The same article that noted the level of unhappiness in radiologists compared with other specialties also noted that 10% of radiologists in the United States were severely burned out.¹⁸ In a different article, 49% of radiologists reported at least some burnout.^{18,22} Radiology was not the specialty with highest rate of burnout (urology and critical care were the worst), but it was in the top half of specialties examined and reported.¹⁸

Burnout is increasing in the United States. A report in the *Mayo Clinic Proceedings* from 2011 to 2014 showed that the percentage of physicians reporting at least 1 symptom of burnout increased from 45.5% to 54.4%, while satisfaction with

work-life balance fell from 48.5% to 40.9%.²² These changes in the medical profession should be considered serious, particularly given that the general population of the United States showed only minimal changes in the same time period.²² Similarly, another report showed increasing rates of physician burnout from 2013 to 2016, with consistently greater rates in women than men.¹⁹

A recent report from an American College of Radiology Commission focusing on the issue of burnout suggested several remedies for preventing burnout. The highest impact recommendation was to provide adequate staffing.²³

Limitations

This survey has several limitations. It was voluntary, and it is possible that responders are different from the broader neuroradiology community. This is a survey and not an audit of radiologists' work. It is thus open to response and recall biases.

Other authors have noted bias issues in how radiologists and their groups report workload.^{2,24} The survey may underestimate changes in workload and difficulty because it does not distinguish between neuroradiologists who work full-time versus neuroradiologists who work part-time or have recently cut back their clinical time.

The number of studies interpreted on-call is likely a gross overexaggeration because it mixes those who take full-subspecialty neuroradiology calls (likely nearly entirely CT and MR imaging) with more general calls (which likely include other modalities beyond CT and MR imaging) and is further confounded by the lack of detail captured in the survey to give those responses context. The survey did not distinguish between preliminary on-call interpretations versus final interpretations or the number of total on-call hours spent interpreting studies, among other confounds.

CONCLUSIONS

This is the first survey in a planned series of surveys of the American Society of Neuroradiology to track changes in radiologists' work, their work environment, and the effects on the quality of their profession and personal lives. Increasing clinical work demands have coincided with destructive effects in the work environment and the ability and desire of radiologists to perform academic or practice-building duties, with a substantial incidence of burnout symptoms in neuroradiologists in the United States. While this survey does not prove causation, the trends and the correlations should be concerning to radiologists, their groups/departments, and their leaders and warrant further monitoring.

REFERENCES

- McDonald RJ, Schwartz KM, Eckel LJ, et al. **The effects of changes in utilization and technological advancements of cross-sectional imaging on radiologist workload.** *Acad Radiol* 2015;22:1191–98 CrossRef Medline
- Bhargavan M, Kaye AH, Forman HP, et al. **Workload of radiologists in United States in 2006–2007 and trends since 1991–1992.** *Radiology* 2009;252:458–67 CrossRef Medline
- Ridley EL. Workload analysis helps enable subspecialized reading. *AuntMinnie*. February 10, 2014. <http://www.auntminnie.com/index.aspx?sec=sup&sub=pac&pag=dis&ItemID=106458>. Accessed October 29, 2016
- Lu Y, Arenson RL. **The academic radiologist's clinical productivity: an update.** *Acad Radiol* 2005;12:1211–23 CrossRef Medline
- Lu Y, Zhao S, Chu PW, et al. **An update survey of academic radiologists' clinical productivity.** *J Am Coll Radiol* 2008;5:817–26 CrossRef Medline
- Hankiss J. **Burn-out...the big danger?** [in Hungarian]. *Orv Hetil* 2015;156:1188 CrossRef Medline
- Du H, Qin L, Jia H, et al. **Relationship between job burnout and cognitive function and influencing factors of job burn out among medical staff** [in Chinese]. *Zhonghua Lao Dong Wei Sheng Zhi Ye Bing Za Zhi* 2015;33:676–78 Medline
- Frutos-Llanes R, Jiménez-Blanco S, Blanco-Montagut LE. **Burnout syndrome in general practitioners of Avila** [in Spanish]. *Semergen* 2014;40:357–65 CrossRef Medline
- Eschelman DJ, Sullivan KL, Parker L, et al. **The relationship of clinical and academic productivity in a university hospital radiology department.** *AJR Am J Roentgenol* 2000;174:27–31 CrossRef Medline
- Wintermark M, Zeineh M, Zaharchuk G, et al. **Non-relative value unit-generating activities represent one-fifth of academic neuroradiologist productivity.** *AJNR Am J Neuroradiol* 2016;37:1206–08 CrossRef Medline
- National Resident Matching Program. *Results and Data: 2005 Main Residency Match*. Washington, DC: National Resident Matching Program; 2005
- National Resident Matching Program. *Results and Data: 2010 Main Residency Match*. Washington, DC: National Resident Matching Program; 2010
- National Resident Matching Program. *Results and Data: 2015 Main Residency Match*. Washington, DC: National Resident Matching Program; 2015
- National Resident Matching Program. *Results and Data: Specialties Matching Service 2008 Appointment Year*. Washington, DC: National Resident Matching Program; 2008
- National Resident Matching Program. *Results and Data: Specialties Matching Service 2010 Appointment Year*. Washington, DC: National Resident Matching Program; 2010
- National Resident Matching Program. *Results and Data: 2016 Main Residency Match*. Washington, DC: National Resident Matching Program; 2016
- National Resident Matching Program. *Results and Data: Specialties Matching Service 2016 Appointment Year*. Washington, DC: National Resident Matching Program; 2016
- Peckham C. Physician burnout: it just keeps getting worse. http://www.medscape.com/viewarticle/838437_2. Accessed May 6, 2016
- Peckham C. Medscape lifestyle report 2016: bias and burnout. <http://www.medscape.com/features/slideshow/lifestyle/2016/public/overview>. Accessed May 9, 2016
- Peckham C. Medscape physician lifestyle report 2015. <http://www.medscape.com/features/slideshow/lifestyle/2015/public/overview>. Accessed January 2, 2017
- Andrew LB. Physician suicide. Medscape. Updated October 3, 2016. <http://emedicine.medscape.com/article/806779-overview>. Accessed May 11, 2016
- Shanafelt TD, Hasan O, Dyrbye LN, et al. **Changes in burnout and satisfaction with work-life balance in physicians and the general US working population between 2011 and 2014.** *Mayo Clin Proc* 2015;90:1600–13 CrossRef Medline
- Harolds JA, Parikh JR, Bluth EI, et al. **Burnout of radiologists: frequency, risk factors, and remedies—a report of the American College of Radiology Commission on Human Resources.** *J Am Coll Radiol* 2016;13:411–16 CrossRef Medline
- Sunshine JH, Burkhardt JH. **Radiology groups' workload in relative value units and factors affecting it.** *Radiology* 2000;214:815–22 CrossRef Medline

The Qualified Clinical Data Registry: A Pathway to Success within MACRA

 M.M. Chen,  A.B. Rosenkrantz,  G.N. Nicola,  E. Silva III,  G. McGinty,  L. Manchikanti, and  J.A. Hirsch

ABBREVIATIONS: ACR = American College of Radiology; CMS = Centers for Medicare & Medicaid Services; MACRA = Medicare Access and CHIP Reauthorization Act; MIPS = Merit-based Incentive Payment System; NRDR = National Radiology Data Registry; PQRS = Physician Quality Reporting System; QCDR = Qualified Clinical Data Registry

Clinical data registries are data bases that collect anonymous patient information focused around a specific diagnosis or health condition for scientific, clinical, or policy purposes. Registries help to assess real-world outcomes in the practice of medicine.¹ By comparing a practice's process and outcome measures to regional and national performance benchmarks, registries have the potential to improve the quality of patient care by facilitating the development of quality improvement projects.²

A Qualified Clinical Data Registry (QCDR) is a distinct designation from a clinical data registry or qualified registry. The Centers for Medicare & Medicaid Services (CMS) defines a QCDR as an entity that "collects medical and/or clinical data for the purpose of patient and disease tracking with the goal of improved patient care."³ Critically, a QCDR is specifically approved by CMS as one of the mechanisms for reporting into the new Merit-based Incentive Payment System (MIPS) as part of the new Quality Payment Program. The details of this new value-based payment system have been outlined in prior reviews.⁴⁻⁶ Despite the new administration after the 2016 federal elections, the Quality Payment Program, and specifically the MIPS pathway, is expected to remain in place.⁷

The QCDR was initially conceived by the American Taxpayer Relief Act of 2012⁸ as a mechanism to allow specialty societies to develop relevant specialty-specific metrics for reporting to the Physician Quality and Reporting System (PQRS) as an alternative to the existing, narrower in scope, generic measures previously

accepted by CMS. However, QCDRs must reach a higher level of rigor than other registries, fulfilling CMS requirements regarding the demonstration of improvements in quality and efficiency. Some of the specific requirements imposed by CMS include: being established for at least 1 year before the first data-collecting year as a QCDR; having a minimum participation of 50 groups; not being locally owned or managed by an individual or single-specialty practice; the ability to publicly report quality measure results; and transparency on data collection, specific data elements, and risk models.⁹ The QCDR first served as a reporting mechanism for PQRS in 2014.^{8,10}

CMS has incentivized the usage of QCDRs under the new MIPS through the Medicare Access and CHIP (Children's Health Insurance Program) Reauthorization Act (MACRA). In the early years of the Quality Payment Program mandated by MACRA, MIPS will be the most common payment pathway for radiologists.³ In the MACRA Final Rule, CMS expressed that by allowing for the use of QCDRs to report data into the 3 MIPS performance categories that require data submission, QCDRs "will become a viable option for MIPS-eligible clinicians."¹¹ CMS further asserted "these flexible options will allow MIPS-eligible clinicians to more easily meet the submission criteria for MIPS, which in turn will positively affect their final score." The MIPS final score will determine the negative and positive payment adjustments. The potential negative payment adjustment in 2017 is 4%, increasing to 9% by 2022.¹¹

QCDRs have evolved in response to long-standing legislative mandates and reports from governmental organizations. This article provides a historical perspective of clinical data registries, the evolution of quality reporting, and the critical role QCDRs will play in MIPS reporting.

HISTORICAL CONTEXT

In 1986, the Health Care Financing Administration, now known as CMS, released raw mortality data for coronary artery bypass grafting operations stratified by institution.¹² However, the government published this data without risk stratifying patients, thus

From the Department of Radiology (M.M.C.), The University of Texas MD Anderson Cancer Center, Houston, Texas; Department of Radiology (A.B.R.), NYU Langone Medical Center, New York, New York; Hackensack Radiology Group (G.N.N.), Riveredge, New Jersey; South Texas Radiology Group (E.S.), San Antonio, Texas; Department of Radiology (G.M.), Weill Cornell Medical College, New York; Department of Anesthesiology and Perioperative Medicine (L.M.), University of Louisville, Louisville, Kentucky; and Department of Radiology (J.A.H.), Massachusetts General Hospital, Boston, Massachusetts.

Please address correspondence to Melissa M. Chen, MD, Department of Radiology, The University of Texas MD Anderson Cancer Center, 1400 Pressler St, Unit 1482, Room #FCT 16.5032, Houston, TX 77030; e-mail: melissa.mei.chen@gmail.com; @MelissaChenMD

<http://dx.doi.org/10.3174/ajnr.A5220>

failing to take into account patient-level factors that affect post-operative mortality and clinical outcomes. The data cast hospitals and providers with higher-risk patients and seemingly worse outcomes in an unfavorable light. In response, the Society of Thoracic Surgery (STS) formulated a novel plan to develop its own classification system to combat this oversimplification of quality reporting. The Society established the first data registry in 1989.^{13,14} The STS National Database has grown to include 3 different clinical areas: adult cardiac, general thoracic, and congenital heart surgery. It is now one of the most established clinical data registries and considered the “gold standard.”¹⁵

The Institute of Medicine’s publication *Crossing the Quality Chasm: A New Health System for the 21st Century* outlined a strategic plan for how to improve the delivery of health care.¹⁶ The report, published in 2001, highlighted the importance of aligning payment policy with financial incentives and paved the way for the legislatively mandated establishment of “pay for performance” programs.¹⁷ Specifically, the Tax Relief and Health Care Act of 2006 established PQRS.¹⁸ PQRS became a permanent program under the Medicare Improvements for Patients and Providers Act in 2008.^{19,20} The payment adjustments under PQRS have evolved from bonus payments for successful reporting (1.5% at the inception of the program) to penalties for unsuccessful reporting (starting in 2015).

The Tax Relief and Health Care Act of 2006 also mandated that eligible professionals should be able to provide data on quality measures through an appropriate medical registry, specifically citing the STS National Database as an example.¹⁸ Support for clinical data registries continued with the American Taxpayer Relief Act of 2012, which prompted the establishment of QCDRs as an approved reporting mechanism for PQRS, as previously discussed. Despite this legislative momentum toward adoption, adoption of QCDRs as a reporting mechanism has remained historically low.

QCDR FOR RADIOLOGY

As a response to the shifting focus toward quality and value-based payments, the American College of Radiology (ACR), in collaboration with other specialty societies, developed its own clinical data registry, the National Radiology Data Registry (NRDR).² The development of the ACR’s NRDR began with the National Oncology PET Registry, a joint effort with the Academy of Molecular Imaging and the American College of Radiology Imaging Network, which became functional on March 6, 2008. The registry was developed in response to a CMS-proposed expansion of coverage for PET using ¹⁸F-FDG. PET imaging for cancers and indications previously not reimbursed by CMS were eligible for reimbursement if the referring physician and billing providers submitted data to a clinical registry. In April 2009, based in part on peer-reviewed data registry results, CMS officially expanded coverage of PET to include the evaluation of nearly all types of cancer and also allowed the use of PET in subsequent treatment strategy evaluations for an expanded number of cancers.²¹ Building on this experience, and further recognizing the importance of expanding their data base of metrics for radiologists, the ACR developed several other registries.²² Some of the relevant metrics that neuroradiologists can report by using the NRDR include the

measurement of carotid stenosis, appropriate imaging follow-up for incidental thyroid nodules, and door-to-puncture time for endovascular stroke treatment.

Importantly, in 2015, CMS approved the ACR’s NRDR, through a self-nomination process, as a QCDR that will enable radiologists to succeed in the MIPS pathway.²³ The NRDR was 1 of 36 approved QCDRs in the initial year, which has nearly doubled in size to 69 CMS-approved QCDRs for 2016.^{24,25}

Other registries specific to neuroradiologists include the Neurovascular Quality Initiative and the North American Spine Society Spine Registry. The Neurovascular Quality Initiative allows neurointerventionalists to compare processes, complication rates, and lengths of stay as well as medical device effectiveness. The Society of NeuroInterventional Surgery has announced plans to convert the Neurovascular Quality Initiative into a QCDR. The North American Spine Society Spine Registry is a diagnosis-based outcomes data registry that will track patient care and patient-reported outcomes. Although still in its pilot phase and not an approved Neurovascular Quality Initiative, the North American Spine Society Spine Registry may be an opportunity for neuroradiologists.²⁶ Members of the American Society of Neuroradiology will be well positioned to participate in the NRDR, Neurovascular Quality Initiative, or North American Spine Society Spine Registry.²⁷

CRITICAL ROLE OF QCDRs

In the MACRA Final Rule released in October 2016, CMS finalized its intention to incorporate data submitted via QCDRs into the MIPS.¹¹ MIPS consolidates into a single program 3 previously existing federal quality programs: PQRS, the Medicare EHR (electronic health record) Incentive Program (formerly known as Meaningful Use), and the Value-Based Modifier. The Quality category replaces PQRS, the Advancing Care Information category replaces the Medicare EHR Incentive Program, and the Cost category replaces the Value-Based Modifier. MIPS also incorporates a new category called Improvement Activities, which addresses patient access, beneficiary engagement, and population health efforts. QCDRs will satisfy reporting into 3 of the 4 MIPS categories: Quality, Advancing Care Information, and Improvement Activities. The fourth category, Cost, will not require physicians to report and will be assessed by CMS based on administrative claims data obtained from submitted clinician billing claims. Under MIPS, clinicians’ performance in these 4 categories will contribute to a “Final Score” determined on a 100-point scale. The weighting of the 4 categories in computing the Final Score will be gradually phased in over the first 3 years of the program. For example, the Cost category will be weighted to 0% for all providers in the first performance year of 2017, not contributing to the Final Score until subsequent years. In addition, the weighting will be adjusted to give special considerations to clinicians with infrequent face-to-face patient interaction. Further details of this scoring system have been previously described and are beyond the scope of this review.²⁷

MIPS will adjust payments based on the actual level of performance within each category, measure, and activity. In the MIPS Quality category, participating clinicians will be required to submit 6 quality metrics, including 1 outcome measure if available.

2017 Finalized MIPS radiology measure set

| MIPS Measures | Data Submission Method |
|--|------------------------|
| Exposure dose or time reported for procedures using fluoroscopy | Registry |
| Inappropriate use of “Probably Benign” assessment category in mammography screening | Claims, Registry |
| Correlation with existing imaging studies for all patients undergoing bone scintigraphy | Claims, Registry |
| Stenosis measurement in carotid imaging reports | Claims, Registry |
| Reminder system for screening mammograms | Claims, Registry |
| Use of a standardized nomenclature for CT imaging | Registry |
| Count of potential high-dose radiation imaging studies: CT and cardiac nuclear medicine studies | Registry |
| Reporting to a radiation dose index registry | Registry |
| CT images available for patient follow-up and comparison purposes | Registry |
| Search for prior CT studies through a secure, authorized, media-free, shared archive | Registry |
| Follow-up CT imaging for incidentally detected pulmonary nodules according to recommended guidelines | Registry |
| Appropriate follow-up imaging for incidental abdominal lesions | Claims, Registry |
| Appropriate follow-up imaging for incidental thyroid nodules in patients | Claims, Registry |
| Use of dose-lowering techniques | Claims, Registry |
| Biopsy follow-up | Registry |

Mechanisms for submitting Quality metrics to MIPS will include: claims data, electronic health record submission, a CMS Web interface (only for groups of 25 or more), a qualified registry, and, as previously noted, a QCDR. This listing of options by CMS highlights the distinct nature of a qualified registry and a QCDR.

For radiologists within a single-specialty practice, the submission options for the Quality category are claims-based, a qualified registry, or a QCDR. Claims-based submission can only be reported at an individual level, not at the group level, and requires the successful reporting of 6 measures. The Quality Payment Program Final Rule lists MIPS measures for individual specialties. A total of 7 measures are listed for diagnostic radiology when using claims-based reporting.¹¹ Radiologists practicing primarily at a subspecialty level have a more limited number of MIPS measures available to them when using claims or qualified registry reporting mechanisms and, therefore, may find it difficult to reach the minimum threshold of 6 measures (Table). But radiologists may more easily satisfy the MIPS Quality category requirements by using a qualified registry or QCDR through the Group Practice

Reporting Option. For example, a dedicated neuroradiologist who is only able to report by using MIPS measures may only have 2–3 total applicable measures: stenosis measurement in carotid imaging reports and appropriate follow-up imaging for incidental thyroid nodules in patients. Accordingly, many neuroradiologists reporting individually could not meet the Quality reporting requirements under MIPS. With the Group Practice Reporting Option, groups may submit by using a qualified registry or a QCDR to consolidate quality measures across the practice, more easily meeting the requirement of 6 measures. Moreover, QCDRs include non-MIPS measures, which are specific to the QCDR and distinct from MIPS measures such as median dose-length product for CT head/brain without contrast and Report Turnaround Time: CT.⁹ Because QCDRs may report both MIPS and non-MIPS measures, this increased flexibility enables successful reporting congruent with MACRA’s and CMS’ intention to encourage the use of QCDRs.

The use of QCDRs has other advantages such as bonus points in the Quality category. Each reported measure in the Quality category will be scored on a decile-based, 10-point scale by using established benchmarks obtained 2 years before the performance period. Bonus points are available if reporting high-priority measures based on specific national quality domains such as outcome, appropriate use, patient safety, efficiency, patient experience, and care coordination. The ACR NRDR QCDR gives users access to a larger number of high-priority measures, and hence, bonus points, compared with the other MIPS reporting mechanisms. Bonus points in the Quality category are also available for reporting measures by using “end-to-end” electronic reporting based on certified electronic health record technology.¹¹ End-to-end electronic reporting refers to the use of automated software to aggregate measurement data, calculate measures, perform filtering of measurement data, and submit electronically to CMS via a Web interface. Although the exact CMS guidelines for bonus points based on end-to-end reporting require further clarification from CMS as of this writing, it is possible that several measures within the ACR NRDR QCDR may be eligible if properly captured and submitted.

Another key benefit of the QCDR is the provision of more frequent feedback to providers than CMS currently provides through the Quality and Resource Use Reports.²⁸ The Quality and Resource Use Reports are a biannual report that demonstrates how groups and solo practitioners perform on quality and cost measures. Quality measures included in the Quality and Resource Use Reports are drawn from PQRS measures, Consumer Assessment of Health Care Providers and Systems (CAHPS) for PQRS surveys, and claims-based quality outcome measures. Cost measures are calculated by using CMS administrative claims. Each group practice receives composite scores in quality and cost. Scores in each of these 2 areas are classified as either “high,” “average,” or “low.” This scoring system has been phased in from 2014–2016 to determine positive, neutral, or negative payment adjustments under the Value Modifier program. Although CMS provides midyear feedback, the data included is from June of the prior year to July of the current year, which may limit a group’s ability to understand its performance in a particular calendar year. The NRDR provides more frequent quarterly feedback,

thereby allowing for groups to make process improvements to potentially improve their performance in a measure before the year's end, with the ultimate goal of improved quality and outcomes.

The use of QCDRs can facilitate the reporting of other MIPS performance categories as well. For example, participation in the NRDR provides opportunities for Improvement Activities not available in other reporting mechanisms in this newly introduced MIPS performance.²⁹ Although too numerous to list, a few examples include "participation in a QCDR that promotes": collaborative learning network opportunities that are interactive, use of patient-engagement tools, processes and tools that engage patients for adherence to a treatment plan, and leveraging a QCDR to promote the use of patient-reported outcome tools. Although some of the listed Improvement Activities are not relevant to radiology, the specific inclusion of QCDR as a tool for these activities highlights the importance and future potential opportunities for radiology. A few proposed Improvement Activities for radiologists include using clinical decision support to optimize the use of imaging examinations and decrease low value imaging examinations, using the ACR NRDR to receive performance feedback to assess practice and identify areas of improvement, and improving the timeliness of radiology reports to referring physicians to use in developing treatment plans by monitoring radiology report turnaround times through participation in the ACR NRDR.³⁰

BENEFITS BEYOND MACRA

As demonstrated by the impact of the National Oncology PET Registry reporting on PET/CT, registries play a key role in expanding Medicare coverage for important techniques and procedures. More recently, in response to efforts by the ACR and a coalition of other patient-advocacy groups, CMS approved reimbursement for lung cancer screening with the requirement of reporting to a "CMS-approved registry" (ie, the NRDR Lung Cancer Screening Registry).³¹ This trend of linking reimbursement to registry reporting is likely to continue and will facilitate radiologists in demonstrating their value to patient care. Indeed, clinical registries stand to be a centerpiece of CMS' increasing embracement of evidence-based coverage determination.

The NRDR offers an opportunity to improve patient care by providing national benchmark data on a variety of radiology-specific process and outcome measures. Multiple registries within the NRDR benchmark radiation dose to improve patient safety. The National Mammography Database, CT Colonography Registry, and Lung Cancer Screening Registry benchmark the positive predictive value of the radiologist's diagnosis, which is the ultimate value the radiologist provides to patient care.²² The well-established Society of Thoracic Surgery has already demonstrated that this cycle of feedback and comparison of results heightens awareness, encourages self-assessment and analysis of processes, and ultimately improves patient outcomes.³²

Aside from improving quality of care and preserving reimbursements, physicians will need to ensure that their professional reputation is maintained. The Affordable Care Act mandated a Web site, Physician Compare,³³ that provides publicly available quality information regarding physicians and other health care professionals enrolled in Medicare.¹⁸ This Web site is intended to

increase transparency and allow patients to directly compare their providers. Performance data from MIPS will be incorporated into the information included on Physician Compare. Physicians who do not participate in MIPS reporting may be perceived as inferior to their peers using this platform.²⁷ This level of public transparency through this tool further increases the importance for radiologists to pursue actions, such as the use of QCDRs, to ensure their success under MIPS.

FUTURE DIRECTIONS

Despite the potential repeal of the Affordable Care Act, the payment reform mandated by MACRA and subsequently implemented by CMS, which heavily links physician reimbursements to quality, will continue. The intent of MACRA is to move physicians into Alternative Payment Models.³⁴ Neuroradiologists will need to focus their research efforts on real-world cost comparisons of imaging recommendations. In particular, when determining guidelines for follow-up of incidental findings, neuroradiologists need to analyze the cost to follow or not follow a finding. In addition, neuroradiologists should become leaders in their local health networks to increase their visibility and demonstrate their value. By actively engaging with their health networks, neuroradiologists can help to direct the transition to Alternative Payment Models.

CONCLUSIONS

Legislation dating back to 2006 took incremental steps toward encouraging the use of clinical registries for quality reporting. In 2012, the notion of a QCDR was codified legislatively. QCDR use is expected to dramatically increase as its utility is emphasized and rewarded in MACRA. Organized radiology helped pioneer the use of QCDRs through the NRDR. Participation in QCDRs, including but not specifically the NRDR, will help radiologists achieve a high Final Score in the MIPS pathway in MACRA, which will be critical for their reimbursements and public reputation alike. As a result, QCDRs are poised to experience dramatically increased use in the near term and, in turn, help radiologists improve the quality of patient care.

Disclosures: Andrew B. Rosenkrantz—RELATED: Grant: Harvey L. Neiman Health Policy Institute*. Laxmaiah Manchikanti—UNRELATED: Consultancy: Semnur Pharmaceuticals Inc, Comments: provided limited consulting services to Semnur Pharmaceuticals, which is developing nonparticulate steroids; Employment: PMC of Paducah, Comments: medical director. Joshua Hirsch—UNRELATED: Consultancy: Medtronic, Carefusion, Globus, Codman, Comments: Medtronic: ongoing; Carefusion and Globus: one-time events; Codman: data safety monitoring board membership. *Money paid to the institution.

REFERENCES

1. Registries for Evaluating Patient Outcomes: A User's Guide. <https://effectivehealthcare.ahrq.gov/index.cfm/search-for-guides-reviews-and-reports/?pageaction=displayproduct&productid=12#26>. Accessed December 31, 2016
2. van Moore A Jr. Metrics and NRDR: what is "near dear" and how will it affect radiology's future? *J Am Coll Radiol* 2006;3:723–24 CrossRef Medline
3. 2016 Physician Quality Reporting System (PQRS): Qualified Clinical Data Registry (QCDR) Training Guide. <https://www.cms.gov/Medicare/Quality-Initiatives-Patient-Assessment-Instruments/PQRS/Downloads/2016QCDRTrainingGuide.pdf>. Accessed November 28, 2016

4. Hirsch JA, Leslie-Mazwi TM, Patel AB, et al. **MACRA: background, opportunities and challenges for the neurointerventional specialist.** *J Neurointerv Surg* 2016;8:868–74 CrossRef Medline
5. Hirsch JA, Harvey HB, Barr RM, et al. **Sustainable growth rate re-pealed, MACRA revealed: historical context and analysis of recent changes in Medicare physician payment methodologies.** *AJNR Am J Neuroradiol* 2016;37:210–14 CrossRef Medline
6. Rosenkrantz AB, Nicola GN, Allen B Jr, et al. **MACRA, MIPS, and the new Medicare Quality Payment Program: an update for radiologists.** *J Am Coll Radiol* 2017;14:316–23 CrossRef Medline
7. Rosenkrantz AB, Nicola GN, Hirsch JA. **Anticipated impact of the 2016 federal election on federal health care legislation.** *J Am Coll Radiol* 2017;14:490–93 CrossRef Medline
8. American Taxpayer Relief Act of 2012. <https://www.congress.gov/bill/112th-congress/house-bill/8/text>. Accessed November 28, 2016
9. 2015 PQRS Qualified Clinical Data Registry Criteria. <https://www.acr.org/~media/ACR/Documents/P4P/Resources/2015/NRDR-2015-QCDDR-Criteria.pdf>. Accessed January 15, 2017
10. Bhatt DL, Drozda JP Jr, Shahian DM, et al. **ACC/AHA/STS statement on the future of registries and the performance measurement enterprise: a report of the American College of Cardiology/American Heart Association Task Force on Performance Measures and the Society of Thoracic Surgeons.** *J Am Coll Cardiol* 2015;66:2230–45 CrossRef Medline
11. Medicare Program; Merit-Based Incentive Payment System (MIPS) and Alternative Payment Model (APM) Incentive under the Physician Fee Schedule, and criteria for Physician-Focused Payment Models. <https://www.gpo.gov/fdsys/pkg/FR-2016-05-09/pdf/2016-10032.pdf>. Accessed November 28, 2016
12. Executive Summary: Medicare Program; Merit-based Incentive Payment System (MIPS) and Alternative Payment Model (APM) Incentive under the Physician Fee Schedule, and criteria for Physician-Focused Payment Models. https://qpp.cms.gov/docs/QPP_Executive_Summary_of_Final_Rule.pdf. Accessed December 19, 2016
13. Clark RE. **The STS National Database: alive, well, and growing.** *Ann Thorac Surg* 1991;52:5 CrossRef Medline
14. Clark R. **The Society of Thoracic Surgeons National Database status report.** *Ann Thorac Surg* 1994;57:20–26 CrossRef Medline
15. Porter M, Teisberg EO. *Redefining Health Care: Creating Value-Based Competition on Results.* Boston: Harvard Business Press; 2013
16. America COQOHCI, Institute of Medicine. *Crossing the Quality Chasm: A New Health System for the 21st Century.* Washington, D.C.: National Academies Press; 2001
17. Hirsch JA, Leslie-Mazwi TM, Nicola GN, et al. **PQRS and the MACRA: value-based payments have moved from concept to reality.** *AJNR Am J Neuroradiol* 2016;37:2195–200 CrossRef Medline
18. H.R. 6111 - Tax Relief and Health Care Act of 2006. <https://www.congress.gov/bill/109th-congress/house-bill/6111/text>. Accessed November 28, 2016
19. Loftus ML, Sanelli PC. **Physician quality reporting system: 2013 update.** *AJNR Am J Neuroradiol* 2013;34:1137–38 CrossRef Medline
20. Manchikanti L. **Physician Quality Reporting System (PQRS) for interventional pain management practices: challenges and opportunities.** *Pain Physician* 2016;19:E15–E32 Medline
21. The National Oncology PET Registry (NOPR). <http://www.cancerpetregistry.org/what.htm>. Accessed December 30, 2016
22. ACR National Data Registry. <https://www.acr.org/Quality-Safety/National-Radiology-Data-Registry>. Accessed December 30, 2016
23. 2015 PQRS Qualified Clinical Data Registry. <https://www.acr.org/Quality-Safety/National-Radiology-Data-Registry/Qualified-Clinical-Data-Registry/2015-QCDDR>. Accessed January 14, 2017
24. 2014 Physician Quality Reporting System Qualified Clinical Data Registries. <https://www.cms.gov/medicare/quality-initiatives-patient-assessment-instruments/pqrs/downloads/2014qcdrposting.pdf>. Published June 25, 2014. Accessed January 15, 2017
25. 2016 Physician Quality Reporting System Qualified Clinical Data Registries. <https://www.cms.gov/Medicare/Quality-Initiatives-Patient-Assessment-Instruments/PQRS/Downloads/2016QCDDRPosting.pdf>. Published June 10, 2016. Accessed January 15, 2017
26. NASS Spine Registry. <https://www.spine.org/Portals/0/Documents/ResearchClinicalCare/NASSSpineRegistryFlyer.pdf>. Accessed March 5, 2017
27. Hirsch JA, Rosenkrantz AB, Ansari SA, et al. **MACRA 2.0: are you ready for MIPS?** *J Neurointerv Surg* 2016 Nov 24. [Epub ahead of print] CrossRef Medline
28. How to Understand Your 2015 Annual Quality and Resource Use Report. <https://www.cms.gov/Medicare/Medicare-Fee-for-Service-Payment/PhysicianFeedbackProgram/Downloads/2015-UnderstandingYourAQRUR.pdf>. Accessed December 28, 2016
29. Explore Measures: Improvement Activities. <https://qpp.cms.gov/measures/ia>. Accessed December 28, 2016
30. Suggested Improvement Activities. https://www.acr.org/~media/ACR/Documents/PDF/QualitySafety/Quality-Measurement/Quality-Payment-Program/IA_Activities_Suggested-Radiology-Activities-Feb-2017.xlsx?la=en. Accessed March 8, 2017
31. Silva E 3rd. **The time for registry participation is now.** *J Am Coll Radiol* 2015;12:733–34 CrossRef Medline
32. STS Manuscript Report Publications. <http://www.sts.org/sites/default/files/documents/STS%20Manuscript-Feb82013.pdf>. Accessed January 22, 2017
33. Physician Compare Website. <https://www.medicare.gov/physician-compare/>. Accessed November 26, 2016
34. Rosenkrantz AB, Nicola GN, Allen B, et al. **MACRA, Alternative Payment Models, and the Physician-Focused Payment Model: implications for radiology.** *J Am Coll Radiol* 2017 Jan 26. [Epub ahead of print] CrossRef Medline

What Does the Boxed Warning Tell Us? Safe Practice of Using Ferumoxytol as an MRI Contrast Agent

C.G. Varallyay, G.B. Toth, R. Fu, J.P. Netto, J. Firkins, P. Ambady, and E.A. Neuwelt



ABSTRACT

BACKGROUND AND PURPOSE: Despite the label change and the FDA's boxed warning added to the Feraheme (ferumoxytol) label in March 2015, radiologists have shown increasing interest in using ferumoxytol as an MR imaging contrast agent as a supplement or alternative to gadolinium. The goals of this study were to provide information regarding ferumoxytol safety as an imaging agent in a single center and to assess how the Feraheme label change may affect this potential, currently off-label indication.

MATERIALS AND METHODS: This retrospective study evaluated the overall frequency of ferumoxytol-related adverse events when used for CNS MR imaging. Patients with various CNS pathologies were enrolled in institutional review board–approved imaging studies. Ferumoxytol was administered as multiple rapid bolus injections. The risk of adverse events was correlated with demographic data/medical history.

RESULTS: The safety of 671 ferumoxytol-enhanced MR studies in 331 patients was analyzed. No anaphylactic, life-threatening, or fatal (grade 4 or 5) adverse events were recorded. The overall proportion of ferumoxytol-related grade 1–3 adverse events was 10.6% (8.6% occurring within 48 hours), including hypertension (2.38%), nausea (1.64%), diarrhea (1.04%), and headache (1.04%). History of 1 or 2 allergies was associated with an increased risk of adverse events (14.61% versus 7.51% [no history]; $P = .007$).

CONCLUSIONS: The frequency of mild ferumoxytol-related adverse events was comparable with literature results, and no serious adverse event was recorded. Although the recommendations in the boxed warning should be followed, serious adverse events appear to be rare, and with proper precautions, ferumoxytol may be a valuable MR imaging agent.

ABBREVIATIONS: AE = adverse event; CTCAE = Common Terminology Criteria for Adverse Events; HSR = hypersensitivity reaction

Ferumoxytol, marketed as Feraheme (AMAG Pharmaceuticals, Waltham, Massachusetts), is an ultra-small iron oxide nanoparticle approved to treat iron deficiency anemia in adults with chronic kidney disease.¹ Because of its superparamagnetic prop-

erties, ferumoxytol can be used as an MR imaging contrast agent.² Despite the label change and the FDA's boxed warning about possible serious hypersensitivity reactions (HSR) added to the Feraheme label in March 2015, radiologists have shown increasing interest in using ferumoxytol as an MR imaging contrast agent because the long plasma half-life and the lack of early leakage allow imaging of the intravascular space early after injection.^{3–7} Delayed MR imaging (24 hours after ferumoxytol administration) shows blood-brain barrier defects similar to gadolinium agents, which makes it a potential alternative if gadolinium-based contrast agents are contraindicated.^{8,9} Delayed ferumoxytol imaging can also take advantage of intracellular uptake of the nanoparticles to image inflammation¹⁰ or assess the lymph nodes for tumor staging.^{11–14}

There are limited safety data of ferumoxytol as an MR imaging contrast agent in the literature. A recent study analyzing 65 cases of children and young adults from institutional review board–approved imaging studies concluded that ferumoxytol was well tolerated as an MR imaging agent.¹⁵ Another publication re-

Received December 22, 2016; accepted after revision February 17, 2017.

From the Departments of Radiology (C.G.V., J.P.N.), Neurology (C.G.V., G.B.T., J.P.N., J.F., P.A., E.A.N.), Medical Informatics and Clinical Epidemiology (R.F.), and Neurosurgery (E.A.N.) and School of Public Health (R.F.), Oregon Health & Science University, Portland, Oregon; and Portland Veterans Affairs Medical Center (E.A.N.), Portland, Oregon.

This work was supported by National Institutes of Health grants NS053468, CA199111, and CA137488-1S1, in part with Federal funds from the National Cancer Institute, National Institutes of Health, under Contract No. HHSN261200800001E, and by the Walter S. and Lucienne Driskill Foundation (all to E.A.N.).

Paper previously presented at: Annual Meeting of the Radiological Society of North America, November 29–December 4, 2015; Chicago, Illinois.

Please address correspondence to Edward A. Neuwelt, MD, Oregon Health & Science University, 3181 SW Sam Jackson Park Rd, L603, Portland, OR 97239; e-mail: neuwelte@ohsu.edu

Indicates open access to non-subscribers at www.ajnr.org

Indicates article with supplemental on-line tables.

<http://dx.doi.org/10.3174/ajnr.A5188>

ported a single anaphylactoid reaction in 2000 off-label uses of ferumoxytol for MR imaging,¹⁶ whereas a recently published single-center investigation with 217 patients showed no serious adverse events (AEs) with the diagnostic use of ferumoxytol.¹⁷ Our institution has more than 10 years of experience using ferumoxytol as an MR imaging contrast agent in the CNS in patients with or without compromised renal function and, as of December 31, 2015, had completed 671 MR imaging studies with ferumoxytol in 8 institutional review board–approved imaging protocols in which AEs were closely monitored. These are the largest single-institution safety data of ferumoxytol used in imaging research protocols. Detailed demographic information was collected, and patients were followed-up for 6 weeks after ferumoxytol administration. The goals of this study were to provide information regarding the safety of ferumoxytol as an MR imaging contrast agent and to assess how the ferumoxytol label change may affect this potential, currently off-label indication.

MATERIALS AND METHODS

Ferumoxytol Administration

This retrospective, single-center study analyzed the safety data of 671 ferumoxytol injections in 331 patients between June 2004 and December 2015. The average age of the patients was 51.08 years (SD, ± 16.82 years), and the female-male ratio was 1:1.33. All patients signed informed consent and were enrolled in 1 of the 8 institutional review board–approved ferumoxytol imaging protocols (On-line Table 1).

In all cases, ferumoxytol was given during MR imaging by using 1 or multiple IV bolus injections (1:1 or 1:2 diluted ferumoxytol, 3 mL/s flow rate, with 20-mL saline flush at the same flow rate). In most studies, the first 1 mg/kg (or 75 mg) was used for dynamic perfusion imaging, with the remaining dose administered in 1 or 2 subsequent bolus injections. The full 4–7 mg/kg or 510 mg was never given as a single injection. Subsequent to the label changes and boxed warning, infusion parameters were modified in all protocols, as Fig 1 indicates. Patients were evaluated for AEs after each ferumoxytol injection. Blood pressure, pulse, and oxygen saturation were recorded before and after each injection. Patients were observed for at least 30 minutes after the completion of ferumoxytol administration. A research nurse or physician was always present during ferumoxytol administration, the postcontrast MR imaging acquisition, and the following observation period.

Recording Adverse Events

Data on AEs were recorded according to Common Terminology Criteria for Adverse Events v3.0 or v4.0 (CTCAE),^{18,19} including the description of the toxicity event, toxicity category, toxicity grade, time of occurrence after ferumoxytol injection, and toxicity attribute. Attribute describes the likelihood that the AE was caused by ferumoxytol based on clinical judgment and has 5 categories: 1, unrelated; 2, unlikely; 3, possible; 4, probably; and 5, definite. We only included AEs that occurred within 6 weeks (42 days) of each ferumoxytol injection. Patients were contacted by phone by a research nurse or completed a clinic visit 6 weeks after administration of ferumoxytol to assess for any AEs. Patient characteristics such as age, race, sex, existence of allergies, steroid use, pathology, and administered ferumoxytol dose were also re-

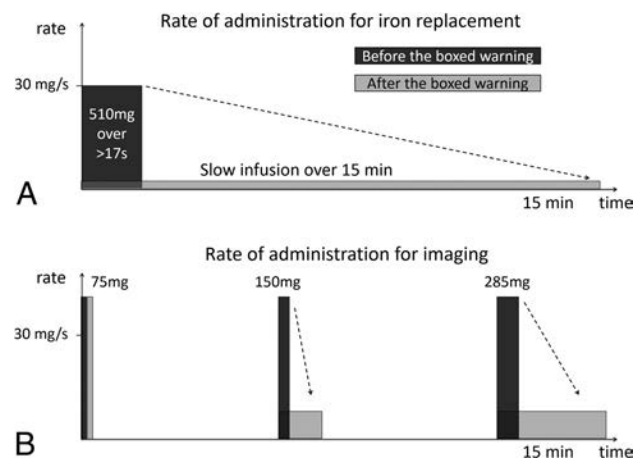


FIG 1. Rate of ferumoxytol administration; for iron replacement (A), the prior label allowed bolus injection of 510 mg of ferumoxytol not faster than 17 seconds (equivalent to 30 mg/s Fe). The current label recommends slow infusion of diluted ferumoxytol over 15 minutes. For imaging, which is still an off-label indication, we used to administer ferumoxytol in 2 or 3 rapid bolus injections. Panel B shows ferumoxytol administration of protocol #1562, in which a full vial of 510 mg was given. As a response to the boxed warning, only the initial 75 mg is injected as before (3 mL/s of 1:1 diluted ferumoxytol, equivalent to 45 mg/s Fe), and dynamic perfusion data are acquired. The other ongoing protocols have been adjusted accordingly; only the first 1 mg/kg being injected as a bolus.

corded. On-line Table 2 shows the potential AEs with ferumoxytol classified to CTCAE and FDA categories. Note that CTCAE grade 3 (severe) AEs may or may not be serious based on FDA classification.^{18–20} Serious AEs are associated with specific outcomes (eg, life-threatening or hospitalization). In contrast, a “severe nosebleed” may not qualify as being categorized as serious.

Statistical Methods

Descriptive statistics were used to summarize patient demographics and clinical characteristics. AEs with an attribute of 3, 4, or 5 were characterized, including at least 1 AE in an infusion, early AE (occurring within 48 hours of ferumoxytol administration), and AE by event type by using proportions. Association between at least 1 AE in an infusion and patient characteristics was assessed by using a logistic generalized estimating equation model while taking into account the correlation of multiple infusions within a patient. The statistical package SAS 9.4 (SAS Institute, Cary, North Carolina) was used.

RESULTS

Among the 671 ferumoxytol infusions, grade 1, 2, or 3 AEs occurred in 71 infusions (10.6%) recorded within 6 weeks. Most AEs occurred within 48 hours after ferumoxytol infusion (in 58 cases [8.6% of the infusions]). There were no life-threatening or fatal (grade 4 or 5) AEs. The most frequent mild and moderate AEs were hypertension (2.38%), nausea (1.64%), diarrhea (1.04%), and headache (1.04%) (Fig 2). Only 2 grade 3 AEs were recorded (0.30%). One patient had a rapid rash on his trunk, both upper extremities, and thighs after the imaging. He received IV dexamethasone, and after several hours of observation, all symptoms disappeared with no further treatment needed. Another patient, who developed red sclera with burning/tingling sensation after an otherwise uneventful ferumoxytol MR imaging, returned for a

second study visit 6 months later. Immediately after the initial 1 mg/kg ferumoxytol administration, he reported severe nausea and moderate degree of shortness of breath along with lower back pain. The patient was removed from the scanner, and no further ferumoxytol was given. He was treated with albuterol and diphenhydramine, and the symptoms completely subsided after 2 hours.

In the logistic generalized estimating equation model, patients with 1 or 2 pre-existing allergies were more likely to have at least 1 AE after ferumoxytol infusion compared with patients without any pre-existing allergy (14.6% versus 7.5%; $P = .007$). No other patient characteristics showed significant association with the occurrence of AE (Table 1).

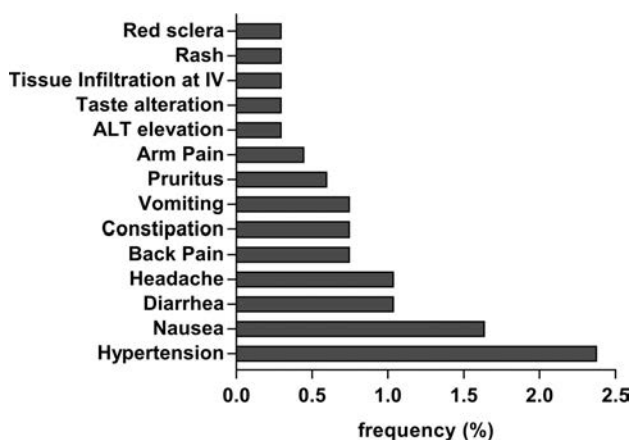


FIG 2. Frequency of AEs potentially related to ferumoxytol. Events that occurred in at least 2 cases are displayed. Note that multiple AEs (symptoms, abnormal lab values) may be associated with a single injection according to the CTCAE recording guidelines.

Table 1: Patient characteristics

| Characteristics | Infusions, No. | Infusions With At Least 1 Event | % of Infusions With At Least 1 Event | Odds Ratio | P Value ^a |
|------------------------------|----------------|---------------------------------|--------------------------------------|-------------------|----------------------|
| Age | | | | | |
| <70 yrs | 634 | 67 | 10.6 | Reference | .91 |
| >70 yrs | 37 | 4 | 10.8 | 1.06 (0.37, 3.02) | |
| Race | | | | | |
| White | 645 | 68 | 10.5 | Reference | .87 |
| Non-white | 26 | 3 | 11.5 | 1.10 (0.35, 3.50) | |
| Gender | | | | | |
| Female | 272 | 33 | 12.1 | Reference | .38 |
| Male | 399 | 38 | 9.5 | 0.79 (0.47, 1.33) | |
| Number of existing allergies | | | | | |
| 0 | 333 | 25 | 7.5 | Reference | .026 ^b |
| 1 or 2 | 268 | 39 | 14.6 | 2.13 (1.23, 3.70) | .007 ^c |
| >2 allergies | 70 | 7 | 10 | 1.35 (0.58, 3.17) | .49 |
| Ferumoxytol dose | | | | | |
| ≤2 mg/kg | 121 | 8 | 6.6 | Reference | .40 ^b |
| 2–4 mg/kg | 303 | 34 | 11.2 | 1.77 (0.69, 4.54) | .23 |
| >4 mg/kg | 247 | 29 | 11.7 | 1.86 (0.75, 4.58) | .18 |
| Steroid use | | | | | |
| None | 461 | 44 | 9.5 | Reference | .13 |
| On decadron | 183 | 25 | 13.7 | 1.56 (0.92, 2.67) | |
| Pathology | | | | | |
| Non-tumor | 54 | 5 | 9.3 | Reference | .71 |
| Tumor | 617 | 66 | 10.7 | 1.20 (0.47, 3.04) | |

^a P values are obtained from the logistic generalized estimating equation model.

^b Overall P value for the number of existing allergies or ferumoxytol dose.

^c Statistically significant.

DISCUSSION

Contrast materials are frequently used in imaging and provide valuable information, often changing the course of treatment. Contrast agents are known to be generally safe, with minimal risk of HSR.²¹ Our results showed that overall ferumoxytol-related AE occurred in 10.6% of infusions, most of them occurring within 48 hours (8.6%), in concordance with 10%–14.6% of AE published in the literature based on 3 randomized trials for iron replacement.^{22–24} Based on our data, the frequency of AE with Feraheme is equivalent to ionic iodinated contrast media, approximately 15 times higher than gadolinium MR contrast agents, and 4 times higher than non-ionic iodinated contrast agents,^{25,26} which is summarized in Table 2. Severe reactions, based on literature data, occur 6–7 times more often with ferumoxytol compared with gadolinium or currently used nonionic iodinated agents.

At our institution, we have not recorded any serious AEs with ferumoxytol. However, we acknowledge that our sample size may not be adequate to record this rare event. It is worth mentioning that our patient population may differ from populations reported in prior studies because most of our patients had brain tumors; it has been shown that patients with tumor can be anergic^{27–29} and are often on corticosteroids, which may cause immunosuppression and, in theory, help prevent HSR.³⁰ Our results, however, did

Table 2: Frequency of adverse events using various contrast media from the literature and our data

| Contrast Media | Adverse Events | Severe Adverse Events |
|------------------------------------|----------------|-----------------------|
| Gadolinium ²⁵ | 0.8% | 0.03% |
| Iodinated (ionic) ²⁶ | 12.66% | 0.22% |
| Iodinated (nonionic) ²⁶ | 3.13% | 0.04% |
| Ferumoxytol (Feraheme label) | 3.7% | 0.2% |
| Ferumoxytol (our data) | 10.6% | 0% |

not show any risk reduction in patients with long-term corticosteroid use, nor in those with tumor pathology. The benefit of premedication before IV iron products remains controversial in the literature and is generally not advised.³¹

Although the 2 grade 3 reactions were possibly HSR-related, most of the AEs recorded in this study are likely unrelated to HSR. Hypertension, recorded most frequently after ferumoxytol injection, may be anxiety-related, which normalized without intervention by the time the patient left the MR imaging suite. No ferumoxytol-related blood pressure drop has been detected. Our study found a significant association between 1 or 2 existing allergies and the frequency of mild AEs. The exact mechanism of iron HSR is still unclear. Bioactive, labile iron, which is present in all IV iron products, may be an important causative factor. Complement activation-related pseudoallergy, triggered by iron nanoparticles, is probably a more frequent mechanism in acute reactions to current IV formulations than is an immunologic IgE-mediated response.³²

The boxed warning of FeraHeme is intended to mitigate the risk and potential morbidity of HSR, thus enhancing patient safety. Recommendations are to observe patients up to 30 minutes after injection and monitor heart rate and blood pressure at baseline and after (each) ferumoxytol administration, which was re-emphasized in this warning and which we strictly adhere to in our imaging protocols. Rapid bolus injection (previously up to 30 mg/s) was eliminated from the package insert, and infusion of the diluted ferumoxytol over 15 minutes became the recommendation. Although there are currently no data using ferumoxytol to support that slow infusion is indeed safer than bolus injection, slow infusion is recommended with other iron products³² and it also allows observation of the patient during ferumoxytol administration and termination of the infusion if HSR occurs.

For MR imaging, to best comply with FDA recommendations, rapid bolus should be avoided. Our imaging protocols have eliminated rapid injection, and only the first 1 mg/kg is given as a bolus to gain clinically valuable dynamic imaging data. The lack of contrast agent leakage has been demonstrated as a benefit compared with low molecular weight agents, though the latter ones may be corrected with mathematical algorithms.³³ For most imaging applications, such as high-resolution steady-state blood volume mapping, steady-state angiography, and visualization of delayed ferumoxytol enhancement/inflammation, no bolus injection is necessary; therefore, high flow rate injection may be completely avoided.

The new prescribing information as of March 2015 provides additional information regarding the potential for more severe HSR in elderly patients with multiple or serious comorbidities and increased risk of HSR to FeraHeme in patients with a history of multiple drug allergies. This information may be useful when considering risk and benefit.

A detailed analysis and guideline have been published by an international group to minimize the risk and severity of IV iron supplement-related AEs. There is emphasis on observation, prompt recognition of symptoms, and severity-related interventions by well-trained medical and nursing staff.³² On-line Table 3 summarizes our recommendations in managing hypersensitivity related to IV iron, when used as an MR contrast agent.

Contrast agent safety is a relevant clinical issue. HSR is just one of the contrast agent-related AEs; in gadolinium-based agents, the incidence of nephrogenic systemic fibrosis has been minimized since the guidelines and boxed warning. Given the emerging safety record of macrocyclic contrast agents in patients with renal failure, remaining contraindications are rare and limited essentially to a history of rare severe allergic reaction to gadolinium-based agents. Gadolinium deposition in the nervous system is a recent finding, which occurs even in patients with normal renal function, and its clinical impact is still unknown.³⁴ Although no serious AE with ferumoxytol was observed in 671 administrations at our institution, it is important to understand the potential risks and be prepared in case a severe reaction occurs. Having trained staff and appropriate medications available would be considered good medical practice in any facility using any imaging contrast agent.

The limitations of ferumoxytol imaging include potential iron overload in patients with iron metabolism disorders. The maximum administered dose (510 mg) is equivalent with 2 units of blood, which is unlikely to cause acute or chronic toxicity in patients with normal iron metabolism.¹⁵ Ferumoxytol is taken up by the liver, spleen, and bone marrow, which may cause signal change on the MR imaging for months. In the CNS, contrast enhancement may be detectable a few days after administration. Adding another contrast agent (ie, if used in addition to gadolinium-based contrast agents) may increase the costs, in addition to MR imaging time, if additional imaging is used. Our research protocols included up to 3 consecutive days of scanning, and MR imaging times were long: between 60–90 minutes on days when contrast agent was given and 30–45 minutes to image late ferumoxytol enhancement. In clinical practice, however, more focused imaging is applied to answer the clinical question. High-resolution blood volume maps may be obtained with only an additional 5 minute scan time.⁵ Steady-state angiography requires only a few minutes of scan time, whereas late enhancement/imaging inflammation/lymph node imaging requires a separate MR imaging scanning session, which is likely the length of a noncontrast MR imaging study. Multiphase contrast administration was used to test the optimal doses for various applications, but in clinical use, a single infusion of the most appropriate dose is sufficient. Applications, such as visualizing the micro- and macrovasculature and visualizing inflammation, hold promise, but future trials have to prove their impact on improving clinical diagnosis and clinical management.

Limitations of this study include the variable patient characteristics and ferumoxytol doses. Although our sample size of 671 was the highest reported in a single center, this number is still too low to evaluate the frequency of rare, but serious HSR.

CONCLUSIONS

The safety of 671 well-documented cases of using ferumoxytol as an MR imaging agent was reported in this study. The overall occurrence of AEs is in agreement with prior ferumoxytol safety studies, and no serious AE was observed. Although the AE is more frequent compared with gadolinium, and there may be increased costs, emerging new MR imaging applications may justify the use of ferumoxytol as an MR imaging contrast agent. The recommen-

dations in the boxed warning should be followed to further improve the safety of imaging with ferumoxytol.

Disclosures: Rongwei Fu—UNRELATED: Grants/Grants Pending: Oregon Health & Science University*. Jenny Firkins—RELATED: Grants/Grants Pending: Driskill Foundation grant and R01*; UNRELATED: Employment: Driskill Foundation grant and R01. Edward Neuwelt—RELATED: Grants/Grants Pending: National Institutes of Health, Driskill Foundation, Comments: This work was supported in part by National Institutes of Health grants NS053468, CA199111, and CA137488–1S1, in part with Federal funds from the National Cancer Institute, National Institutes of Health, under Contract No. HHSN261200800001E, and by the Walter S. and Lucienne Driskill Foundation, all to E.A.N.; UNRELATED: Grants/Grants Pending: AMAG Pharmaceuticals, Comments: Dr. Neuwelt's studies involving ferumoxytol were entirely funded by National Institutes of Health research grants and the Driskill Foundation, with the ferumoxytol ultra-small superparamagnetic iron oxide nanoparticles donated by AMAG Pharmaceuticals. Oregon Health & Science University has received a small sponsored research agreement from AMAG Pharmaceuticals to partially fund clinical trials of MRI with ferumoxytol. None of the authors has financial interest in this agent or in its developer AMAG Pharmaceuticals.* Money paid to the institution.

REFERENCES

- Lu M, Cohen MH, Rieves D, et al. **FDA report: ferumoxytol for intravenous iron therapy in adult patients with chronic kidney disease.** *Am J Hematol* 2010;85:315–19 CrossRef Medline
- Bashir MR, Bhatti L, Marin D, et al. **Emerging applications for ferumoxytol as a contrast agent in MRI.** *J Magn Reson Imaging* 2015;41:884–98 CrossRef Medline
- Hope MD, Hope TA, Zhu C, et al. **Vascular imaging with ferumoxytol as a contrast agent.** *AJR Am J Roentgenol* 2015;205:W366–73 CrossRef Medline
- Nayak AB, Luhan A, Hanudel M, et al. **High-resolution, whole-body vascular imaging with ferumoxytol as an alternative to gadolinium agents in a pediatric chronic kidney disease cohort.** *Pediatr Nephrol* 2015;30:515–21 CrossRef Medline
- Varallyay CG, Nesbit E, Fu R, et al. **High-resolution steady-state cerebral blood volume maps in patients with central nervous system neoplasms using ferumoxytol, a superparamagnetic iron oxide nanoparticle.** *J Cereb Blood Flow Metab* 2013;33:780–86 CrossRef Medline
- Christen T, Ni W, Qiu D, et al. **High-resolution cerebral blood volume imaging in humans using the blood pool contrast agent ferumoxytol.** *Magn Reson Med* 2013;70:705–10 CrossRef Medline
- Finn JP, Nguyen KL, Han F, et al. **Cardiovascular MRI with ferumoxytol.** *Clin Radiol* 2016;71:796–806 CrossRef Medline
- Neuwelt EA, Hamilton BE, Varallyay CG, et al. **Ultrasmall superparamagnetic iron oxides (USPIOs): a future alternative magnetic resonance (MR) contrast agent for patients at risk for nephrogenic systemic fibrosis (NSF)?** *Kidney Int* 2009;75:465–74 CrossRef Medline
- Neuwelt EA, Varallyay CG, Manninger S, et al. **The potential of ferumoxytol nanoparticle magnetic resonance imaging, perfusion, and angiography in central nervous system malignancy: a pilot study.** *Neurosurgery* 2007;60:601–11; discussion 611–12 CrossRef Medline
- Storey P, Arbini AA. **Bone marrow uptake of ferumoxytol: a preliminary study in healthy human subjects.** *J Magn Reson Imaging* 2014;39:1401–10 CrossRef Medline
- Guthrie PJ, Thomas JV, Peker D, et al. **Perivesical unicentric Castleman disease initially suspected to be metastatic prostate cancer.** *Urol Ann* 2016;8:245–48 CrossRef Medline
- Liu L, Tseng L, Ye Q, et al. **A new method for preparing mesenchymal stem cells and labeling with ferumoxytol for cell tracking by MRI.** *Sci Rep* 2016;6:26271 CrossRef Medline
- Pouw JJ, Grootendorst MR, Bezooijen R, et al. **Pre-operative sentinel lymph node localization in breast cancer with superparamagnetic iron oxide MRI: the SentiMAG Multicentre Trial imaging subprotocol.** *Br J Radiol* 2015;88:20150634 CrossRef Medline
- Wang YX. **Current status of superparamagnetic iron oxide contrast agents for liver magnetic resonance imaging.** *World J Gastroenterol* 2015;21:13400–02 CrossRef Medline
- Muehe AM, Feng D, von Eyben R, et al. **Safety report of ferumoxytol for magnetic resonance imaging in children and young adults.** *Invest Radiol* 2016;51:221–27 CrossRef Medline
- Vasanawala SS, Nguyen KL, Hope MD, et al. **Safety and technique of ferumoxytol administration for MRI.** *Magn Reson Med* 2016;75:2107–11 CrossRef Medline
- Nguyen KL, Yoshida T, Han F, et al. **MRI with ferumoxytol: a single center experience of safety across the age spectrum.** *J Magn Reson Imaging* 2017;45:804–12 CrossRef Medline
- Common Terminology Criteria for Adverse Events v3.0 (CTCAE).** Published August 9, 2006. https://ctep.cancer.gov/protocolDevelopment/electronic_applications/docs/ctcae3.pdf. Accessed April 3, 2017
- Common Terminology Criteria for Adverse Events (CTCAE) Version 4.0.** Published 2010. https://ctep.cancer.gov/protocolDevelopment/electronic_applications/ctc.htm. Accessed April 3, 2017
- What is a serious adverse event? U.S. Food and Drug Administration. <https://www.fda.gov/safety/medwatch/howtoreport/ucm053087.htm>. Accessed May 4, 2017
- Brockow K, Sánchez-Borges M. **Hypersensitivity to contrast media and dyes.** *Immunol Allergy Clin North Am* 2014;34:547–64, viii CrossRef Medline
- Vadhan-Raj S, Strauss W, Ford D, et al. **Efficacy and safety of IV ferumoxytol for adults with iron deficiency anemia previously unresponsive to or unable to tolerate oral iron.** *Am J Hematol* 2014;89:7–12 CrossRef Medline
- MacDougall IC, Strauss WE, McLaughlin J, et al. **A randomized comparison of ferumoxytol and iron sucrose for treating iron deficiency anemia in patients with CKD.** *Clin J Am Soc Nephrol* 2014;9:705–12 CrossRef Medline
- Hetzel D, Strauss W, Bernard K, et al. **A phase III, randomized, open-label trial of ferumoxytol compared with iron sucrose for the treatment of iron deficiency anemia in patients with a history of unsatisfactory oral iron therapy.** *Am J Hematol* 2014;89:646–50 CrossRef Medline
- Bleicher AG, Kanal E. **Assessment of adverse reaction rates to a newly approved MRI contrast agent: review of 23,553 administrations of gadobenate dimeglumine.** *AJR Am J Roentgenol* 2008;191:W307–11 CrossRef Medline
- Katayama H, Yamaguchi K, Kozuka T, et al. **Adverse reactions to ionic and nonionic contrast media. A report from the Japanese Committee on the Safety of Contrast Media.** *Radiology* 1990;175:621–28 CrossRef Medline
- Evans C, Dalgleish AG, Kumar D. **Review article: immune suppression and colorectal cancer.** *Aliment Pharmacol Ther* 2006;24:1163–77 CrossRef Medline
- Kawakami Y, Yaguchi T, Sumimoto H, et al. **Cancer-induced immunosuppressive cascades and their reversal by molecular-targeted therapy.** *Ann N Y Acad Sci* 2013;1284:80–86 CrossRef Medline
- Pumhirun P, Wasuwat P. **Anergy testing in patients with head and neck cancer.** *Asian Pac J Allergy Immunol* 2003;21:189–92 Medline
- Braaten K, Holcombe RF, Kim SS. **Premedication with IV steroids effectively prevented anaphylactic reactions following ferumoxytol given as IV push in hematology and oncology patients.** *Am J Hematol* 2015;90:E207 CrossRef Medline
- Bircher AJ, Auerbach M. **Hypersensitivity from intravenous iron products.** *Immunol Allergy Clin North Am* 2014;34:707–23, x-xi CrossRef Medline
- Rampton D, Folkersen J, Fishbane S, et al. **Hypersensitivity reactions to intravenous iron: guidance for risk minimization and management.** *Haematologica* 2014;99:1671–76 CrossRef Medline
- Gahramanov S, Muldoon LL, Varallyay CG, et al. **Pseudoprogression of glioblastoma after chemo- and radiation therapy: diagnosis by using dynamic susceptibility-weighted contrast-enhanced perfusion MR imaging with ferumoxytol versus gadoteridol and correlation with survival.** *Radiology* 2013;266:842–52 CrossRef Medline
- Kanda T, Ishii K, Kawaguchi H, et al. **High signal intensity in the dentate nucleus and globus pallidus on unenhanced T1-weighted MR images: relationship with increasing cumulative dose of a gad-**

- olmium-based contrast material. *Radiology* 2014;270:834–41 CrossRef Medline
35. Gahramanov S, Raslan AM, Muldoon LL, et al. **Potential for differentiation of pseudoprogression from true tumor progression with dynamic susceptibility-weighted contrast-enhanced magnetic resonance imaging using ferumoxytol vs. gadoteridol: a pilot study.** *Int J Radiat Incol Biol Phys* 2011;79:514–23 CrossRef Medline
36. Hamilton BE, Nesbit GM, Dosa E, et al. **Comparative analysis of ferumoxytol and gadoteridol enhancement using T1- and T2-weighted MRI in neuroimaging.** *AJR Am J Roentgenol* 2011;197:981–88 CrossRef Medline
37. Nasser M, Gahramanov S, Netto JP, et al. **Evaluation of pseudo-progression in patients with glioblastoma multiforme using dynamic magnetic resonance imaging with ferumoxytol calls RANO criteria into question.** *Neuro Oncol* 2014;16:1146–54 CrossRef Medline
38. Dósa E, Tuladhar S, Muldoon LL, et al. **MRI using ferumoxytol improves the visualization of central nervous system vascular malformations.** *Stroke* 2011;42:1581–88 CrossRef Medline
39. Dósa E, Guillaume DJ, Haluska M, et al. **Magnetic resonance imaging of intracranial tumors: intra-patient comparison of gadoteridol and ferumoxytol.** *Neuro Oncol* 2011;13:251–60 CrossRef Medline
40. Farrell BT, Hamilton BE, Dósa E, et al. **Using iron oxide nanoparticles to diagnose CNS inflammatory diseases and PCNSL.** *Neurology* 2013;81:256–63 CrossRef Medline
41. Hamilton BE, Woltjer RL, Prola-Netto J, et al. **Ferumoxytol-enhanced MRI differentiation of meningioma from dural metastases: a pilot study with immunohistochemical observations.** *J Neurooncol* 2016;129:301–09 CrossRef Medline
42. Thompson EM, Guillaume DJ, Dósa E, et al. **Dual contrast perfusion MRI in a single imaging session for assessment of pediatric brain tumors.** *J Neurooncol* 2012;109:105–14 CrossRef Medline
43. UpToDate: Evidence-Based Clinical Decision Support System. Waltham, Massachusetts: Wolters Kluwer; 1992 [updated in 2016]. <https://www.uptodate.com>. Accessed April 3, 2017
44. ACR Committee on Drugs and Contrast Media. *ACR Manual on Contrast Media*. Version 10.2. Published June 2016. https://www.acr.org/~media/ACR/Documents/PDF/QualitySafety/Resources/Contrast-Manual/2016_Contrast_Media.pdf. Accessed April 3, 2017

Prevalence of Traumatic Findings on Routine MRI in a Large Cohort of Professional Fighters

J.K. Lee, J. Wu, S. Banks, C. Bernick, M.G. Massand, M.T. Modic, P. Ruggieri, and S.E. Jones



ABSTRACT

BACKGROUND AND PURPOSE: Previous studies investigating MR imaging abnormalities among fighters have had small sample sizes. This investigation assessed a large number of fighters using the same conventional sequences on the same scanner.

MATERIALS AND METHODS: Conventional 3T MR imaging was used to assess 499 fighters (boxers, mixed martial artists, and martial artists) and 62 controls for nonspecific WM changes, cerebral microhemorrhage, cavum septum pellucidum, and cavum vergae. The lengths of the cavum septum pellucidum and cavum vergae and the ratio of cavum septum pellucidum to the septum pellucidum lengths were assessed.

RESULTS: The prevalence of nonspecific WM changes was similar between groups. Fighters had a prevalence of cerebral microhemorrhage (4.2% versus 0% for controls, $P = .152$). Fighters had a higher prevalence of cavum septum pellucidum versus controls (53.1% versus 17.7%, $P < .001$) and cavum vergae versus controls (14.4% versus 0%, $P < .001$). The lengths of the cavum septum pellucidum plus the cavum vergae ($P < .001$), cavum septum pellucidum ($P = .025$), and cavum septum pellucidum to the septum pellucidum length ratio ($P = .009$) were higher in fighters than in controls. The number of fights slightly correlated with cavum septum pellucidum plus cavum vergae length ($R = 0.306$, $P < .001$) and cavum septum pellucidum length ($R = 0.278$, $P < .001$). When fighters were subdivided into boxers, mixed martial artists, and martial artists, results were similar to those in the whole-group analysis.

CONCLUSIONS: This study assessed MR imaging findings in a large cohort demonstrating a significantly increased prevalence of cavum septum pellucidum among fighters. Although cerebral microhemorrhages were higher in fighters than in controls, this finding was not statistically significant, possibly partially due to underpowering of the study.

ABBREVIATIONS: CMH = cerebral microhemorrhage; CSP = cavum septum pellucidum; CSPV = cavum septum pellucidum and vergae; CV = cavum vergae; NSWMC = nonspecific white matter change; MA = martial artists; MMA = mixed martial artists; PFBHS = Professional Fighters Brain Health Study

Multiple sports such as boxing, mixed martial arts, football, and soccer involve repetitive head trauma in young people, and this trauma is accumulated over many years. Many studies have attempted to describe conventional MR imaging findings associated with repetitive head trauma in the hope that an early in vivo diagnosis may preclude further trauma and help guide possible treatment.^{1–9} However, these studies have often involved a small number of athletes, leading to variable findings and a low significance of results.^{10,11} In some

studies, MR imaging results were normal for athletes with head trauma,^{7,9} whereas other studies demonstrated a variably increased prevalence of cerebral microhemorrhage (CMH),^{4,5} nonspecific WM changes (NSWMCs),¹¹ or cavum septum pellucidum (CSP)/cavum septum pellucidum and vergae (CSPV).^{1,2,10}

Regarding professional fighting, previous studies have similarly demonstrated the occurrence of imaging abnormalities, with imaging findings ranging from smaller volumes in structures such as the thalamus, vermis, and hippocampus and microhemorrhages in the parenchyma to macrohemorrhages such as subdural hematomas and parenchymal contusions.^{4–6,8,12,13} However, these studies were also limited by small sample sizes and a relatively low prevalence of microhemorrhages, so the calculated increased prevalence was not found to be statistically significant.^{4,5}

Other studies have demonstrated a higher incidence of CSP among fighters, with some research finding a trend toward significance in fighters versus controls.¹⁰ However, an early large study

Received July 20, 2016; accepted after revision February 10, 2017.

From the Imaging Institute (J.K.L., J.W., M.G.M., M.T.M., P.R., S.E.J.) and Lou Ruvo Center for Brain Health (S.B., C.B.), Cleveland Clinic, Cleveland, Ohio.

This work was supported by HBO, the Lincy Foundation, Ultimate Fighting Championship, Spike TV/Bellator MMA, Top Rank Promotions, Golden Boy Promotions, the August Rapone Family Foundation, and Haymon Boxing.

Please address correspondence to Jonathan K. Lee, MD, Imaging Institute, Cleveland Clinic, 9500 Euclid Ave, L10, Cleveland, OH 44195; e-mail: leej3@ccf.org

<http://dx.doi.org/10.3174/ajnr.A5175>

of fighters demonstrated increased CSP prevalence in controls rather than in fighters.³ More recent studies in retired professional American football players found that the prevalence and size of the CSP were increased in the athletes versus controls.^{2,14} Comparing these studies is complicated by differences in patient populations (eg, different sports, various age groups, current athletes versus retired athletes).^{2,4,5,14} Additionally, even though an increased prevalence of CSP has been demonstrated among fighters in previous research, neuroradiologists disagree over whether this is a manifestation of trauma or simply a normal variant.

Other conventional MR imaging findings in patients with repetitive head trauma include the presence of NSWMCs.⁷ However, some research into repetitive head trauma has demonstrated normal imaging findings in these patients.¹¹ This finding is consistent with our anecdotal experience.

In this study, we chose to focus on a sport with a known high incidence of repetitive head trauma (professional fighters), using a large sample size and ensuring that all fighters were scanned with the same protocol on the same 3T MR imaging scanner. We sought to assess the prevalence of NSWMCs, CMH, and CSP/CSPV among these fighters versus the prevalence of these imaging abnormalities among healthy controls.

MATERIALS AND METHODS

Fighter Population

The Professional Fighters Brain Health Study (PFBHS) is an ongoing observational study of active professional fighters (boxers, mixed martial artists [MMA], and martial artists [MA] fighters), retired professional fighters, and age-matched healthy controls.¹⁵ This study was approved by the local institutional review board, and informed consent was obtained from all participants. The purpose of this study is to follow imaging and psychological metrics across time as fighters practice their craft and experience repetitive head trauma, allowing researchers to explore the relationships among head trauma exposure, changes in brain imaging, and neurologic/behavioral functioning. However, this article only focuses on conventional imaging findings between fighters and controls at the current time. Further correlations between imaging findings and neurologic/behavioral functioning and longitudinal follow-up of imaging findings are currently being investigated.

Fighters eligible for enrollment in the PFBHS were those who hold a license to fight professionally. Study patients were required to be at least 18 years of age, with at least a fourth-grade reading level, fluency in English or Spanish, and a willingness to undergo annual evaluations, including 3T MR imaging, neurocognitive testing, and blood sampling for genotyping and exploratory biomarker studies. We obtained extensive details about fighting history for all study patients before performing MR imaging, including information about the type of fighting (boxing or mixed martial arts), the number of fights, years of fighting, and the number of knockouts.

The PFBHS control group included age- and sex-matched participants without a history of head trauma or participation in a sport associated with head injuries at a high school level or beyond. A medical history was self-reported by both the fighters and controls, including any diagnosed medical conditions, all medications, performance-enhancing drugs, and other drug use.

MR Imaging Acquisition

All participants were scanned on a Verio 3T system (Siemens, Erlangen, Germany). Conventional sagittal 3D MPRAGE T1 (voxel size = $1 \times 1 \times 1.2$ mm, TR/TE/TI = 2300/2.98/900 ms, scan time = 9 minutes 14 seconds), axial TSE T2 (voxel size = $0.8 \times 0.8 \times 4$ mm TR/TE = 5000/2.98 ms, 38 sections, scan time = 57 seconds), axial TSE FLAIR (voxel size = $0.8 \times 0.8 \times 4$ mm, TR/TE/TI = 7000/81/2220 ms, 38 sections, scan time = 2 minutes 36 seconds), and axial SWI (voxel size = $0.9 \times 0.9 \times 0.9$ mm, TR/TE = 20/27 ms, 36 sections, scan time = 1 minute 17 seconds) sequences were used for this study. These sequences were evaluated for the presence of CMH, CSP, and NSWMC. The scans were assessed for the presence of CMH by 4 neuroradiologists (experience: M.T.M., 38 years; S.E.J., 10 years; M.G.M., 10 years; and P.R., 24 years) and a neuroradiology fellow. Initial disagreements were resolved by consensus. A neuroradiology fellow and a radiology resident assessed the scans for the presence of CSP, and a neuroradiology fellow assessed the scans for the presence of NSWMC. The raters were blinded to whether the images belonged to fighters or controls.

Image Analysis

NSWMCs were defined as focal areas of T2 and FLAIR signal hyperintensity relative to the adjacent WM in 1 of 3 subregions: subcortical, deep, and periventricular WM. NSWMC foci were excluded if they were <3 mm or if they were associated with another abnormality such as a microhemorrhage or encephalomalacia. NSWMCs were defined as absent, punctate foci, the beginning of coalescence, or large areas of coalescence based on the Fazekas score.¹⁶

CMHs were defined as well-defined areas of abnormal susceptibility hypointensity that were focal, rounded, <5 mm, not on the pial or ependymal surface, and not due to vessel or normal variant anomalies such as developmental venous anomalies. Cavernous malformations were also excluded from this definition on the basis of characteristic features seen on SWI and T2 sequences.

CSP was defined and measured in a manner similar to that used in recently published studies on retired professional American football players.^{2,14} A CSP was defined as a cystic space between the 2 leaflets of the preforniceal septum pellucidum as viewed on coronal 3D MPRAGE T1-weighted images and whose signal characteristics followed those of CSF. Continuation of the cyst into the postforniceal septum was termed a cavum vergae (CV). The length and transverse diameter of the CSP and/or CV were measured on axial reconstructed T1 images cross-referenced to the last coronal image on which the CSP was seen (Fig 1). If the cystic space measured ≤ 1 mm in length, it was not counted as a CSP. To account for possible increased size of the CSP with increased head and ventricular size, we measured the septum pellucidum on sagittal T1 imaging from the dorsal margin of the genu of the corpus callosum to the ventral margin of the splenium and calculated a ratio of CSP length to septum length (Fig 1).

All images were reviewed by using an IMPAX 6.6 DICOM viewer (Agfa, Mortsel, Belgium) on flat panel LCD monitors.

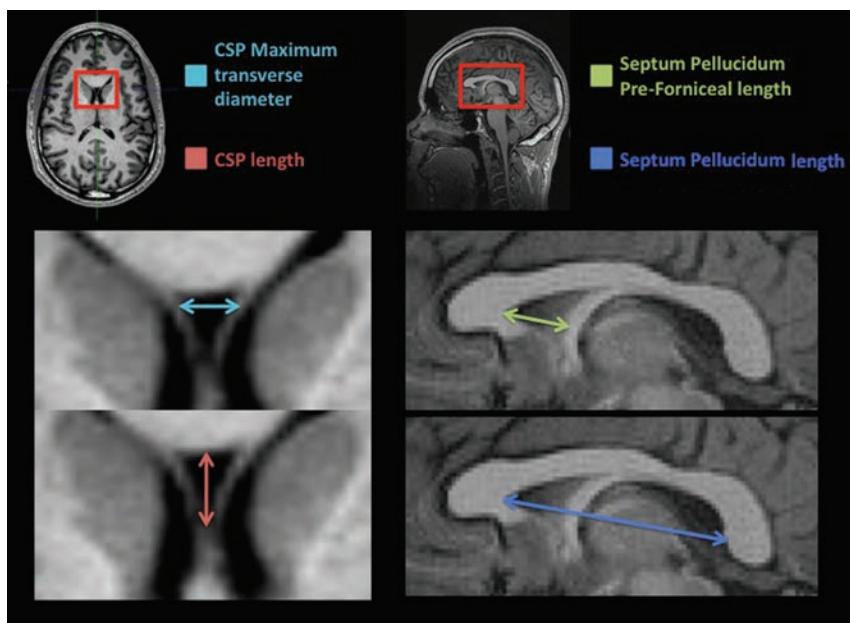


FIG 1. Example of CSP and septum pellucidum measurements.

Imaging findings in fighters and controls

| Imaging Findings | Fighters (<i>n</i> = 499 ^a) (No.) (%) | Controls (<i>n</i> = 62) (No.) (%) | <i>P</i> Value |
|------------------|---|--|----------------|
| NSWMC | 118 (23.6) | 12 (19.4) | .525 |
| CMH | 21 (4.2) | 0 (0) | .152 |
| CSP | 265 (53.1) | 11 (17.7) | <.001 |
| CV | 72 (14.4) | 0 (0) | <.001 |

^a Except for CMH, which had 498 because 1 fighter did not have SWI.

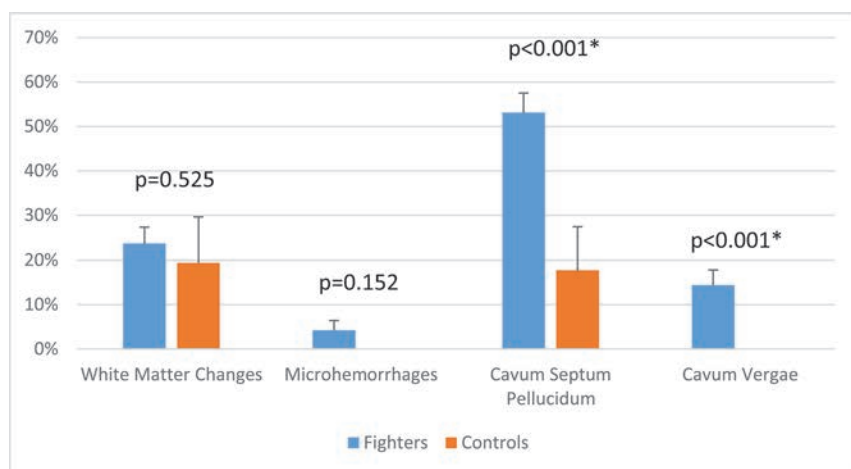


FIG 2. Prevalence of MR imaging findings in fighters versus controls.

Statistical Analysis

All statistics were calculated by using SPSS (IBM, Armonk, New York). The prevalence of CMHs, CSP, and NSWMCs was compared between the 2 groups by using a χ^2 test, and the extent of these findings was compared with the Fisher exact test. A 2-sided χ^2 test was used to test the hypothesis that fighters would have a greater prevalence of NSWMCs, CMHs, and CSPs than the control group. Given the low percentages of CMH, a post hoc power analysis was also performed.

Subsequently, fighters were also subdivided into boxers,

mixed martial artists, and martial artists. The total number of fighters in the subgroups does not equal the total number of fighters because some fighters have multiple fighting styles and they were not included in the subanalysis. A 2-sided χ^2 test was used to compare the incidence of NSWMC, CMH, and CSPV in each subgroup compared with controls and subsequently with each other subgroup.

The Student *t* test was used to compare the number of fights for fighters with CSP, CV, CMHs, or NSWMC versus the number of fights for fighters without these abnormalities. The Student *t* test was also used to compare septum pellucidum length, CSP length, CV length, CSPV length, and CSP to septum pellucidum ratio in fighters versus controls. The Pearson correlation was used to identify any association between the number of fights and CSP or CSPV length.

RESULTS

Four hundred ninety-nine fighters and 62 controls from the PFBHS were assessed for evidence of NSWMC, CMH, and CSPV. Fighters had a mean age of 30 years and controls had a mean age of 31 years ($P = .406$). Four hundred sixty-two fighters were male (92.6%), while 37 fighters were female. Fifty-six (90.3%) controls were men, while 6 controls were women ($P = .457$).

NSWMCs were present in 118/499 (23.6%) fighters and 12/62 (19.4%) controls ($P = .525$; Table and Fig 2). CMHs were present in 21/498 (4.2%, 1 fighter did not have SWI) fighters and 0/62 controls (0%, $P = .152$) (Table and Fig 3 as an example). Post hoc power analysis with an α of .05 showed a power ($1 - \beta$) of 18.5%. CSP was present in 265/499 (53.1%) fighters and 11/62 (17.7%) controls ($P < .001$) (Table). CV was present in 72/499 (14.4%) fighters and 0/62 (0%) controls ($P < .001$) (Table).

Twenty fighters had SWI abnormalities that the 4 neuroradiologists believed, in consensus, to be cases of cavernous malformation, capillary telangiectasia, or vascular structures such as developmental venous anomalies. If these normal variants had been included in the count of CMHs, 41 (7.9%) fighters and 3 controls (4.8%) would have been assessed as having positive findings on SWI.

We identified 59 CMHs: One fighter had 14 CMHs, 1 fighter

had 10, and the remaining 35 CMHs were found in 19 fighters (mean, 1.5 CMHs per fighter) (Fig 4). Almost all CMHs were located near the cortex, with only a few in the deep white matter and periventricular margins. In the posterior fossa, most cases of CMH were in the inferior aspects of the cerebellum. There were relatively few CMHs in the supraorbital convexities, deep gray matter, or corpus callosum.

Figure 5 shows the distribution of NSWMCs overlaid on a sketch of representative axial brain sections. Five controls were randomly selected from among the controls for NSWMC, with a total of 15 foci. For visual comparison, 5 fighters were randomly selected from among the fighters with NSWMC. This subset of fighters showed a total of 12 foci. Not included were 2 fighters with a very large number of NSWMCs, one with approximately 30 foci and the other with approximately 20 foci. All foci were in subcortical locations, except for 2 foci that were in periventricular locations.

Fighters with NSWMC and those with CSP trended toward having a higher average of total fights (60 fights versus 46 in those

without NSWMCs, $P = .098$; 56 versus 42 in those without CSP, $P = .054$) (Fig 6). Fighters with CMH had a higher average of total fights than those without CMH, though this was not statistically significant (85 versus 47, $P = .530$), and fighters with CV had a significantly higher number of total fights than those without CV (88 versus 43, $P < .001$).

The length of the septum pellucidum was not significantly different between fighters and controls (50.8 versus 52.4 mm, $P = .180$); this finding suggests that head sizes were similar between the 2 groups (Fig 7). The lengths of the CSP and CSPV were both significantly higher in fighters than in controls. In fighters with CSP, the average length was 10.9 versus 7.6 mm in controls ($P = .025$) (Fig 7); in fighters with CSPV, the average length was 16.2 versus 7.6 mm in controls ($P < .001$). The ratio of CSP to septum length was similarly higher in fighters than in controls (0.21 versus 0.14, $P = .009$) (Fig 8). The maximum transverse diameter of the CSP was similar for fighters and controls (3.7 versus 2.8 mm, $P = .107$). There was a small-but-positive correlation between the number of fights and CSPV/CSP length; specifically, as the number of fights increased, the CSPV length ($R = 0.306$; $P < .001$) and CSP length ($R = 0.278$; $P < .001$) both increased slightly.

After we subdivided the fighters into boxers, MMA, and MA and compare them with controls, NSWMCs were present in 52 (27.4%) of 190 boxers ($P = .242$), 42 (21.1%) of 199 MMA ($P = .859$), and 5 (17.2%) of 29 MA ($P = 1.0$). CMHs were present in 6 (3.2%) of 189 boxers (1 boxer did not have SWI, $P = .341$), 12 (6%) of 199 MMA ($P = .075$), and 0 (0%) of 29 MA. CSPs were present in 122 (64.2%) of 190 boxers ($P < .001$), 88 (44.2%) of 199 MMA ($P < .001$), and 14 (48.3%) of 29 MA ($P = .005$). CV were present in 52 (27.4%) of 190 boxers ($P < .001$), 12 (6%) of 199 MMA ($P = .075$), and 1 (3.4%) of 29 MA ($P = .319$).

When we compared the groups of fighters, boxers had significantly more CSP (64.2% versus 44.2%, $P < .001$) and CV (27.4% versus 6%, $P < .001$) than MMA and more CV (27.4% versus 3.4%, $P = .004$) than MAs. No significant differences were seen between MMA and MA.

DISCUSSION

This study presents a large number of fighters who have been exposed to known cumulative head trauma and scanned on the same 3T MR imaging machine by using standardized conventional imaging protocols. We found that CSP and CV occurred more frequently in fighters than in age- and sex-matched controls, whereas there was no statistical difference between groups in the occurrence of NSWMCs. CMHs occurred more frequently in fighters than controls, but this was not statistically significant.

The presence of CMH as a distinct pathologic finding was first discussed in 1924¹⁷ and was soon related to a theory

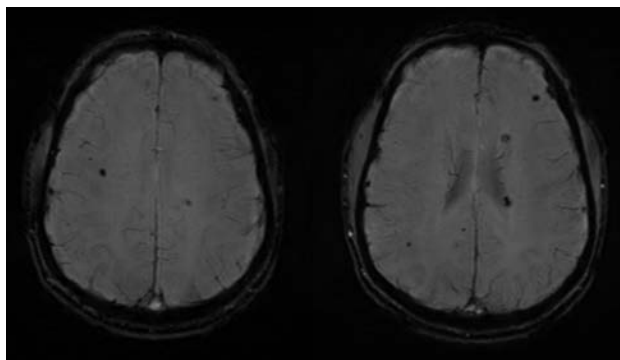


FIG 3. Example of cerebral microhemorrhage in a fighter.

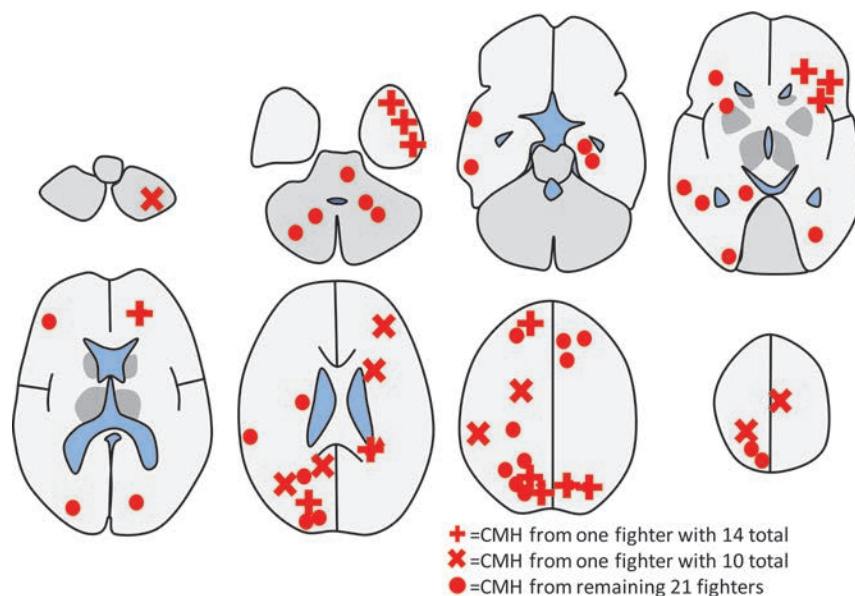


FIG 4. Schematic diagram showing the location of all cerebral microhemorrhages observed from all 21 fighters in the study. Although 50 CMHs were observed, 2 fighters had a disproportionate share, and their CMHs have their own symbol of a cross and a triangle. The simplified diagram does not show all the sulci. Most CMHs were actually located near the cortex, and a few were located in the deep white matter.

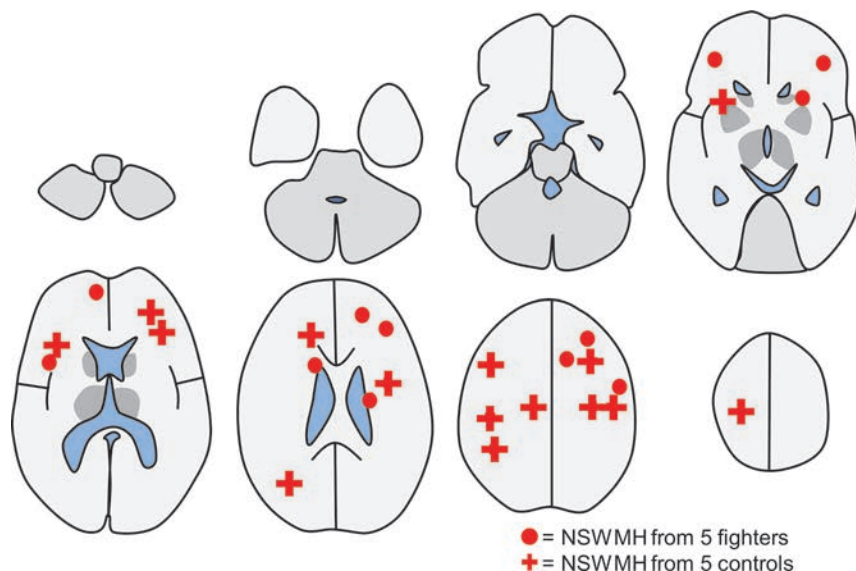


FIG 5. Schematic diagram showing the location of all 15 nonspecific white matter changes observed from 5 randomly selected controls with foci shown by crosses. For comparison of the distribution, 5 randomly selected fighters with NSWMC are shown by circles, which totaled 12. As in Fig 4, the simplified diagram does not show all the sulci, most NSWMCs were actually located near the cortex, and only 2 were located in the periventricular margins.

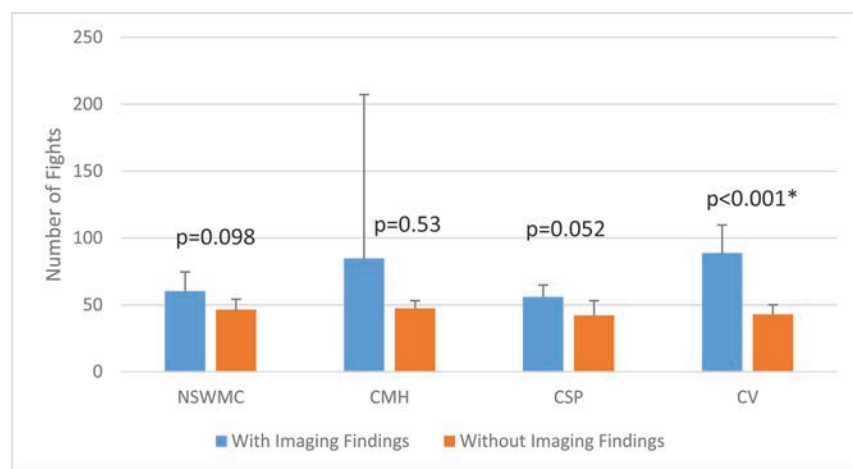


FIG 6. The number of fights in fighters with and without cavum septum pellucidum, cavum vergae, cerebral microhemorrhages, and nonspecific white matter change.

of traumatic brain injury characteristically seen in boxers.¹⁸ Mechanisms of traumatic injury at the microscopic level involve strain (relative stretch) of neural tissue, and the severity of injury depends on the magnitude of the strain. At the smallest magnitude, tissue is elastic and there is no damage; at intermediate magnitudes, there are transient and reversible alterations of membrane potentials (concussions); at the highest magnitudes, irreversible damage and chronic change occur. Along this spectrum are concomitant tissue reactions, including vasogenic and cytotoxic edema (seen acutely on DWI), microhemorrhages (seen chronically on SWI), and focal gliosis and demyelination (seen chronically on FLAIR). Because the fighters in this study were not imaged in the acute setting, imaging findings would likely be manifest as chronic changes on SWI and FLAIR.

Although the reason for microhemorrhages occurring in fighters may seem self-evident, the relatively low prevalence of

CMH might be surprising given the large number of fighters known to receive knockout blows and concussions. In fact, the radiologic appearance of the brain among most fighters with known multiple concussions is normal on conventional MR imaging. However, damage may be present below the capability of conventional MR imaging. For example, in other sports with a high incidence of repetitive head trauma (eg, American football), researchers have established the existence of chronic traumatic encephalopathy during postmortem examinations, which can only be seen under the microscope.¹⁹ Therefore, any damage evident on MR imaging likely represents the “tip of the iceberg,” with much greater microscopic damage extending beyond any visible damage. For many fighters, it is possible that damage and dysfunction accumulate within this microscopic range, which could explain the discrepancy between known mild traumatic brain injury and MR images with clinically normal findings. Some portion of this range could be explored with higher field MR imaging (eg, 7T MR imaging with higher resolution and sensitivity to susceptibility effects) or with advanced MR imaging techniques such as high-resolution DTI.²⁰

In our study, the CMH prevalence among fighters was 4.2%; this is lower than the prevalence observed in previous studies (7.1% and 9.5%)^{4,5} and was not statistically significant from that in our controls. This finding is likely in part due to the study being underpowered with a relatively small number of controls versus fighters, as supported by post hoc power analysis with an α of .05

that showed a power ($1-\beta$) of 18.5%. Generally, a power of 80% is considered adequate in most cases and would have required around double the control population to achieve adequate power, given an α of .05 and an unchanged incidence of CMH in fighters and controls. In regard to the raw percentage CMH, a comparison study of retired National Football League players also demonstrated a prevalence of 9%.²¹ The prevalence in our study may have been lower because we excluded susceptibility-positive healthy variants such as capillary telangiectasia and vascular malformations and nontraumatic pathologies such as cavernous malformations. If we had included these findings, the prevalence of CMH would have been 7.9%. The type of imaging sequence used may also have played a role. T2* and SWI are most commonly used to assess for the presence of CMH. The higher prevalence of CMH observed by Hasiloglu et al⁵ may have been linked to their use of SWI, which is a newer and more sensitive sequence than T2* imaging.

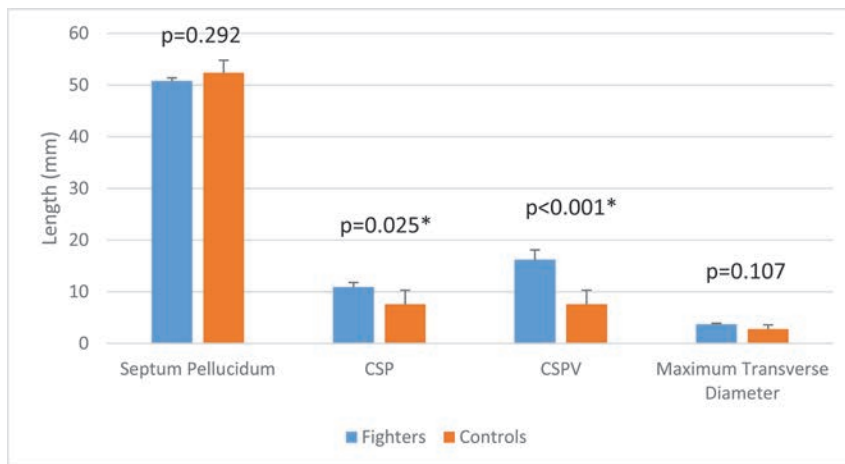


FIG 7. Septum pellucidum length, cavum septum pellucidum length, cavum septum pellucidum plus cavum vergae length, and maximum transverse diameter of the CSP in fighters versus controls.

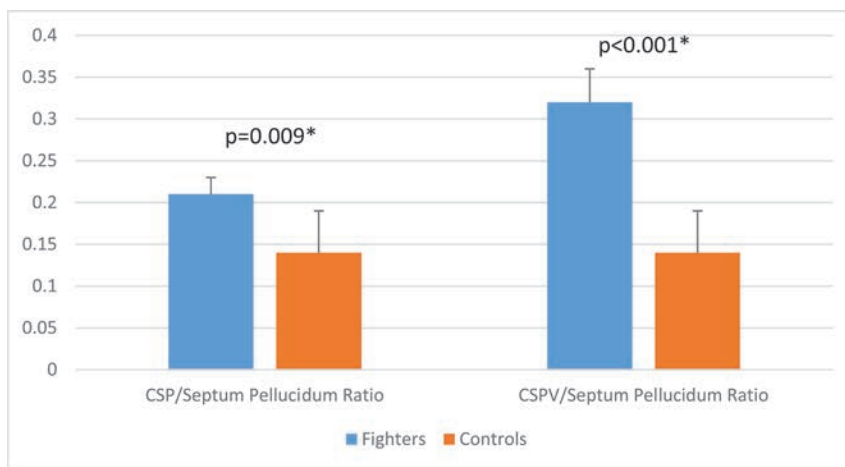


FIG 8. Cavum septum pellucidum and cavum septum pellucidum plus cavum vergae to septum pellucidum ratios in fighters versus controls.

The earliest studies to assess the occurrence of CSP in boxers used pneumoencephalography and found evidence of CSP in 6 of 9 boxers (67%),²² a prevalence slightly higher than we observed in our study (53%). In studies of American football players, Koerte et al¹⁴ and Gardner et al² observed a CSP prevalence of 92% and 94%, respectively. In addition, their prevalence of CSP in healthy controls was 57% and 18%, respectively, with only the latter value comparable with our prevalence of 20%. These differences may be partially explained by differences between the sports in the mechanism of head trauma; boxing blows to the head cause a rotational acceleration, whereas football blows to the head cause a linear acceleration. Other unknown mechanisms could also explain these differences, including genetic differences related to athlete selection. The mean age of each patient population may have also affected the results. The cohort of 72 retired football players in the study by Koerte et al¹⁴ had a higher mean age of 57 years compared with the mean patient age in our study (30 years). The age-dependent prevalence of CSP was illustrated in a large postmortem series of 1032 human brains (from nontraumatic brain injury victims), which demonstrated a CSP prevalence of 18% for boys younger than 10 years of age, 13% for men 25–35 years of age (similar to our age group of controls at 20%), and 24% for men

older than 50 years of age.²³ Another postmortem series demonstrated a CSP prevalence of 18%,²⁴ whereas an MR imaging study of incidental findings of CSP in the pediatric population demonstrated a much lower prevalence of 1.14%, with a mean patient age of 15 years.

These factors do not entirely explain the widely varying range of CSP prevalence observed in previous studies, however. For example, 2 previous MR imaging studies demonstrated a CSP prevalence in adults of 2.1%²⁵ and 68%.²⁶ In another study among football players, the CSP prevalence was 7%, but the researchers included only large CSPs.²¹ This finding suggests that there may be considerable variation in how CSP has been defined in the literature. In our study, most CSPs were very small, appearing as small triangles or trapezoids just posterior to the genu of the corpus callosum (an average length of 10.9 mm in fighters). For future investigations, it would be helpful to derive a consensus opinion regarding size definitions for CSP.

The mechanism for increased CSP/CV prevalence and length with head trauma is still unknown. Pathologists have described 4 types of cava, including noncommunicating and communicating, further complicating the issue.²⁴ One theory for the increase in length and

prevalence of CSP/CV among patients with head trauma is that transient increased intracranial pressure results in passage of CSF through small tears in septal leaflets.¹⁰ Such tears were described in the postmortem examination of a former boxer as multiple perforations of the septal leaflets with a latticelike appearance.²² These tears could be accentuated by shear forces resulting from rapid rotation of the head, allowing CSF to enter the potential space of the septum pellucidum and slowly dissect a cavity. A second theory involves ex vacuo expansion of the potential space in the septum pellucidum due to central volume loss caused by repeated trauma.^{2,27} Future research might benefit from dedicated microscopic postmortem examinations of former athletes.

An interesting hypothesis that may explain the disparity of published CSP prevalence is that traumatic brain injury does not necessarily increase the prevalence of CSP, but the size. Using MR imaging in a pediatric cohort of 98 survivors of traumatic brain injury and 34 healthy controls, Silk et al²⁸ concluded that there was no statistical difference between groups in the prevalence of CSP; however, CSPs were larger among patients with head trauma than among controls. In a similar postmortem study of patients with and without head trauma, the CSP prevalence was 38% and

54%, respectively.²⁹ However, patients with head trauma demonstrated a distinct morphology of CSP termed a “cleft cavum,” which was comorbid with diffuse axonal injury and represented 13% of all head trauma victims. The researchers suggested that this finding represents the acute effect of severe head trauma superimposed on an underlying baseline prevalence of nontraumatic CSP.

In our study, the prevalence of NSWMC was similar between fighters and controls; this finding suggests that no sequelae from repeated head trauma manifested as focal FLAIR hyperintensity. A recent study of college ice hockey players also found no evidence of new FLAIR lesions in patients with concussions,³⁰ and in a study of 46 military veterans with mild traumatic brain injuries, Clark et al³¹ found that there was no significant increased prevalence of FLAIR WM lesions in patients versus controls. These findings suggest that standard MR imaging sequences such as FLAIR are not useful for the diagnosis of mild traumatic brain injury,³² perhaps because the size of the focal traumatic lesions is too small to be visible on these sequences.

This study had several limitations, including the relative imbalance between the large number of fighters and the smaller number of healthy controls. A greater number of controls would have increased the significance of our results, particularly in the case of CMH, which has a low baseline prevalence. There are only a few relevant studies in the literature that have a large number of healthy controls imaged for CMH. In particular, the studies of Hähnel et al⁴ and Hasiloglu et al⁵ together imaged 58 controls, none of whom had any CMH. Although many other studies reported higher numbers of controls, these studies were not applicable because of their use of T2* gradient recalled-echo sequences rather than SWI,³³ poor age matches (typically elderly controls), or underlying disease states such as hypertension, degenerative disease, multiple sclerosis, and amyloid angiopathy.^{34–37}

CONCLUSIONS

This is a large study of conventional MR imaging findings in a cohort of professional fighters with known repetitive head trauma, all scanned with the same 3T MR imaging scanner and protocol. We observed an increased prevalence of CSP and CSPV in fighters versus controls. The prevalence of CMH was also increased in fighters compared with controls, though this was not statistically significant, and may in part be due to underpowering of the study from a relatively lower number of controls. The prevalence of NSWMCs was also not significantly higher in fighters than in controls.

Disclosures: Jonathan K. Lee—RELATED: Grant: Ultimate Fighting Championship, Spike TV/Bellator MMA, Top Rank, Haymon Boxing, Golden Boy Promotions, Lincy Foundation/UCLA Dream Fund, and HBO.* Charles Bernick—RELATED: Grant: Ultimate Fighting Championship, Spike TV, Top Rank, Haymon Boxing, Golden Boy, HBO, Lincy Foundation/UCLA Dream Fund, Comments: These entities provide ongoing support for the Professional Fighters Brain Health Study from which the data for this article were acquired*; UNRELATED: Payment for Lectures Including Service on Speakers Bureaus: Allergan Plc. Michael T. Modic—UNRELATED: Grants/Grants Pending: Ultimate Fighting Championship, Spike TV/Bellator MMA, Top Rank, Haymon Boxing, Golden Boy Promotions, Lincy Foundation/UCLA Dream Fund, and HBO.* Stephen E. Jones—RELATED: Grant: Ultimate Fighting Championship, Spike TV/Bellator MMA, Top Rank, Haymon Boxing, Golden Boy Promotions, Lincy Foundation/UCLA Dream Fund, and HBO*; UNRELATED: Grants/Grants Pending: National Institutes of Health*; Payment for Lectures Including Service

on Speakers Bureaus: Siemens, Monteris, RadNet, Cleveland Clinic lectures. *Money paid to the institution.

REFERENCES

1. Bodensteiner JB, Schaefer GB. **Dementia pugilistica and cavum septi pellucidi: born to box?** *Sports Med* 1997;24:361–65 CrossRef Medline
2. Gardner RC, Hess CP, Brus-Ramer M, et al. **Cavum septum pellucidum in retired American pro-football players.** *J Neurotrauma* 2016; 33:157–61 CrossRef Medline
3. Haglund Y, Bergstrand G. **Does Swedish amateur boxing lead to chronic brain damage? 2: a retrospective study with CT and MRI.** *Acta Neurol Scand* 1990;82:297–302 Medline
4. Hähnel S, Stippich C, Weber I, et al. **Prevalence of cerebral microhemorrhages in amateur boxers as detected by 3T MR imaging.** *AJNR Am J Neuroradiol* 2008;29:388–91 CrossRef Medline
5. Hasiloglu ZI, Albayram S, Selcuk H, et al. **Cerebral microhemorrhages detected by susceptibility-weighted imaging in amateur boxers.** *AJNR Am J Neuroradiol* 2011;32:99–102 CrossRef Medline
6. Jordan BD, Zimmerman RD. **Computed tomography and magnetic resonance imaging comparisons in boxers.** *JAMA* 1990;263: 1670–74 Medline
7. Koerte IK, Ertl-Wagner B, Reiser M, et al. **White matter integrity in the brains of professional soccer players without a symptomatic concussion.** *JAMA* 2012;308:1859–61 CrossRef Medline
8. Orrison WW, Hanson EH, Alamo T, et al. **Traumatic brain injury: a review and high-field MRI findings in 100 unarmed combatants using a literature-based checklist approach.** *J Neurotrauma* 2009;26: 689–701 CrossRef Medline
9. Zhang L, Heier LA, Zimmerman RD, et al. **Diffusion anisotropy changes in the brains of professional boxers.** *AJNR Am J Neuroradiol* 2006;27:2000–04 Medline
10. Aviv RI, Tomlinson G, Kendall B, et al. **Cavum septi pellucidi in boxers.** *Can Assoc Radiol J* 2010;61:29–32; quiz 21–22 CrossRef Medline
11. Levin HS, Lippold SC, Goldman A, et al. **Neurobehavioral functioning and magnetic resonance imaging findings in young boxers.** *J Neurosurg* 1987;67:657–67 CrossRef Medline
12. Bernick C, Banks SJ, Shin W, et al. **Repeated head trauma is associated with smaller thalamic volumes and slower processing speed: the Professional Fighters' Brain Health Study.** *Br J Sports Med* 2015; 49:1007–11 CrossRef Medline
13. Costanza A, Weber K, Gandy S, et al. **Review: contact sport-related chronic traumatic encephalopathy in the elderly—clinical expression and structural substrates.** *Neuropathol Appl Neurobiol* 2011;37: 570–84 CrossRef Medline
14. Koerte IK, Hufschmidt J, Muehlmann M, et al. **Cavum septi pellucidi in symptomatic former professional football players.** *J Neurotrauma* 2016;33:346–53 CrossRef Medline
15. Bernick C, Banks S, Phillips M, et al. **Professional fighters brain health study: rationale and methods.** *Am J Epidemiol* 2013;178: 280–86 CrossRef Medline
16. Fazekas F, Chawluk JB, Alavi A, et al. **MR signal abnormalities at 1.5 T in Alzheimer's dementia and normal aging.** *AJR Am J Roentgenol* 1987;149:351–56 CrossRef Medline
17. Cassasa CB. **Multiple traumatic cerebral hemorrhages.** *Proc New York Path Soc* 1924;24:101
18. Martland HS. **Punch drunk.** *JAMA* 1928;91:1103–07
19. Omalu BI, DeKosky ST, Minster RL, et al. **Chronic traumatic encephalopathy in a National Football League player.** *Neurosurgery* 2006;58:E1003 CrossRef Medline
20. Shin W, Mahmoud SY, Sakaie K, et al. **Diffusion measures indicate fight exposure-related damage to cerebral white matter in boxers and mixed martial arts fighters.** *AJNR Am J Neuroradiol* 2014;35:285–90 CrossRef Medline
21. Casson IR, Viano DC, Haacke EM, et al. **Is there chronic brain damage in retired NFL players? Neuroradiology, neuropsychology, and neurology examinations of 45 retired players.** *Sports Health* 2014;6: 384–95 CrossRef Medline

22. Mawdsley C, Ferguson FR. **Neurologic disease in boxers.** *Lancet* 1963;2:795–801 [Medline](#)
23. Schwidde JT. **Incidence of cavum septi pellucidi and cavum vergae in 1,032 human brains.** *AMA Arch Neurol Psychiatry* 1952;67:625–32 [CrossRef Medline](#)
24. Oteruelo FT. **On the cavum septi pellucidi and the cavum vergae.** *Anat Anz* 1986;162:271–78 [Medline](#)
25. Pauling KJ, Bodensteiner JB, Hogg JP, et al. **Does selection bias determine the prevalence of the cavum septi pellucidi?** *Pediatr Neurol* 1998;19:195–98 [CrossRef Medline](#)
26. Born CM, Meisenzahl EM, Frodl T, et al. **The septum pellucidum and its variant: an MRI study.** *Eur Arch Psychiatry Clin Neurosci* 2004;254:295–302 [Medline](#)
27. Banks SJ, Mayer B, Obuchowski N, et al. **Impulsiveness in professional fighters.** *J Neuropsychiatry Clin Neurosci* 2014;26:44–50 [CrossRef Medline](#)
28. Silk T, Beare R, Crossley L, et al. **Cavum septum pellucidum in pediatric traumatic brain injury.** *Psychiatry Res* 2013;213:186–92 [CrossRef Medline](#)
29. Pittella JE, Gusmão S. **Cleft cavum of the septum pellucidum in victims of fatal road traffic accidents: a distinct type of cavum associated with severe diffuse axonal injury.** *Surg Neurol* 2005;63(suppl 1):S30–34; discussion S34–35 [CrossRef Medline](#)
30. Jarrett M, Tam R, Hernández-Torres E, et al. **A prospective pilot investigation of brain volume, white matter hyperintensities, and hemorrhagic lesions after mild traumatic brain injury.** *Front Neurol* 2016;7:11 [CrossRef Medline](#)
31. Clark AL, Sorg SF, Schiehser DM, et al. **Deep white matter hyperintensities affect verbal memory independent of PTSD symptoms in veterans with mild traumatic brain injury.** *Brain Inj* 2016;30:864–71 [CrossRef Medline](#)
32. Hughes DG, Jackson A, Mason DL, et al. **Abnormalities on magnetic resonance imaging seen acutely following mild traumatic brain injury: correlation with neuropsychological tests and delayed recovery.** *Neuroradiology* 2004;46:550–58 [Medline](#)
33. Cordonnier C, Al-Shahi Salman R, Wardlaw J. **Spontaneous brain microbleeds: systematic review, subgroup analyses and standards for study design and reporting.** *Brain* 2007;130:1988–2003 [CrossRef Medline](#)
34. Huang YL, Kuo YS, Tseng YC, et al. **Susceptibility-weighted MRI in mild traumatic brain injury.** *Neurology* 2015;84:580–85 [CrossRef Medline](#)
35. Koerte IK, Lin AP, Willems A, et al. **A review of neuroimaging findings in repetitive brain trauma.** *Brain Pathol* 2015;25:318–49 [CrossRef Medline](#)
36. Vernooij MW, Ikram MA, Tanghe HL, et al. **Incidental findings on brain MRI in the general population.** *N Engl J Med* 2007;357:1821–28 [CrossRef Medline](#)
37. Qureshi AI, Chughtai M, Malik AA, et al. **Incidental asymptomatic intracerebral hemorrhages and risk of subsequent cardiovascular events and cognitive decline in elderly persons.** *J Stroke Cerebrovasc Dis* 2015;24:1217–22 [CrossRef Medline](#)

Retention of Gadolinium-Based Contrast Agents in Multiple Sclerosis: Retrospective Analysis of an 18-Year Longitudinal Study

Y. Forslin, S. Shams, F. Hashim, P. Aspelin, G. Bergendal, J. Martola, S. Fredrikson, M. Kristoffersen-Wiberg, and T. Granberg



ABSTRACT

BACKGROUND AND PURPOSE: Gadolinium-based contrast agents have been associated with lasting high T1-weighted signal intensity in the dentate nucleus and globus pallidus, with histopathologically confirmed gadolinium retention. We aimed to longitudinally investigate the relationship of multiple gadolinium-based contrast agent administrations to the Signal Intensity Index in the dentate nucleus and globus pallidus and any associations with cognitive function in multiple sclerosis.

MATERIALS AND METHODS: The Signal Intensity Index in the dentate nucleus and globus pallidus was retrospectively evaluated on T1-weighted MR imaging in an 18-year longitudinal cohort study of 23 patients with MS receiving multiple gadolinium-based contrast agent administrations and 23 healthy age- and sex-matched controls. Participants also underwent comprehensive neuropsychological testing.

RESULTS: Patients with MS had a higher Signal Intensity Index in the dentate nucleus ($P < .001$), but not in the globus pallidus ($P = .19$), compared with non-gadolinium-based contrast agent–exposed healthy controls by an unpaired t test. Increasing numbers of gadolinium-based contrast agent administrations were associated with an increased Signal Intensity Index in the dentate nucleus ($\beta = 0.45$, $P < .001$) and globus pallidus ($\beta = 0.60$, $P < .001$). This association remained stable with corrections for the age, disease duration, and physical disability for both the dentate nucleus ($\beta = 0.43$, $P = .001$) and globus pallidus ($\beta = 0.58$, $P < .001$). An increased Signal Intensity Index in the dentate nucleus among patients with MS was associated with lower verbal fluency scores, which remained significant after correction for several aspects of disease severity ($\beta = -0.40$, $P = .013$).

CONCLUSIONS: Our data corroborate previous reports of lasting gadolinium retention in brain tissues. An increased Signal Intensity Index in the dentate nucleus and globus pallidus was associated with lower verbal fluency, which does not prove causality but encourages further studies on cognition and gadolinium-based contrast agent administration.

ABBREVIATIONS: DN = dentate nucleus; EDSS = Expanded Disability Status Scale; GBCA = gadolinium-based contrast agent; GP = globus pallidus; SII = Signal Intensity Index

Gadolinium-based contrast agents (GBCAs) are an important aid in MR imaging diagnostics for improving the detection and characterization of pathologic processes. Approximately 30 million contrast-enhanced MRIs are performed every year, with an estimated 300 million administered thus far.¹ In multiple sclerosis,

GBCAs play a key role in detecting disease activity. Gadolinium has paramagnetic properties that shorten the T1 relaxation in tissues, resulting in an increased signal on T1-weighted imaging. Because gadolinium (Gd^{3+}) is toxic, it is chelated to stabilize the compound and mitigate these effects.² Macrocyclic GBCAs are kinetically more stable than linear GBCAs with less dissociation of gadolinium, while nonionic linear GBCAs are the least stable.³ Dissociation of gadolinium has been implicated in the development of nephrogenic systemic fibrosis, which is typically seen in patients with impaired renal function.² This implication has led to the recommendation to primarily use macrocyclic GBCAs in patients with renal impairment.⁴

We know from earlier studies that gadolinium is deposited in the bone, liver,^{5,6} and skin.⁷ In 2014, Kanda et al⁸ showed an association between the number of administrations of linear GBCA and a higher T1 intensity in the dentate nucleus (DN) and globus pallidus (GP), suggestive of gadolinium retention in the

Received October 22, 2016; accepted after revision March 3, 2017.

From the Departments of Clinical Science Intervention and Technology (Y.F., S.S., F.H., P.A., G.B., J.M., M.K.-W., T.G.), Radiology (Y.F., S.S., F.H., P.A., G.B., J.M., M.K.-W., T.G.), Neurology (G.B., S.F.), and Clinical Neuroscience (S.F.), Karolinska Institutet, Stockholm, Sweden.

This research was funded by the Stockholm County Council and Karolinska Institutet through the regional agreement on medical training and clinical research.

Please address correspondence to Yngve Forslin, MD, Department of Clinical Science, Intervention and Technology, CI-46, Karolinska University Hospital, 141 86 Stockholm, Sweden; e-mail: yngve.forslin@ki.se

Indicates open access to non-subscribers at www.ajnr.org

Indicates article with supplemental on-line table.

<http://dx.doi.org/10.3174/ajnr.A5211>

Demography and mean SII in the study population and healthy controls^a

| | Patients with MS, Baseline | Patients with MS, 9-Year Follow-Up | Patients with MS, 18-Year Follow-Up | Healthy Controls |
|--|-------------------------------|---------------------------------------|--|--------------------------|
| Female/male (No.) | 18:5 | 18:5 | 18:5 | 18:5 |
| Age (yr) | 39 ± 8.1 | 48 ± 8.1 | 57 ± 8.0 | 57 ± 7.2 |
| Disease duration (yr) | 10 ± 7 | 19 ± 7 | 27 ± 7 | — |
| MS subtype: RR/SP/PP (No.) | 18/5/0 | 13/10/0 | 3/20/0 | — |
| Disease-modifying therapy (No.) (%) | 13 (57%) | 13 (57%) | 5 (22%) | — |
| Gadolinium administrations (median) (range) | 1 (0–3) | 3 (2–10) | 6 (3–12) | 0 |
| Dentate nucleus SII, middle cerebellar peduncle as a reference | 1.01 ± 0.02 | 1.03 ± 0.03 | 1.06 ± 0.05 | 1.01 ± 0.03 ^b |
| Globus pallidus SII, thalamus as a reference | 1.04 ± 0.05 | 1.06 ± 0.04 | 1.09 ± 0.06 | 1.10 ± 0.04 ^c |

Note:—PP indicates primary-progressive; RR, relapsing-remitting; SP, secondary-progressive.

^a Values are reported as means, unless otherwise specified.

^b The difference in SIIs between controls and patients with MS: unpaired *t* test (*P* < .001).

^c The difference in SIIs between controls and patients with MS: unpaired *t* test (*P* = .19).

brain. This finding has since been confirmed by other human studies,^{9–11} animal studies, and histopathologically.^{10,12–14} Concerns have therefore been raised regarding the safety profile of GBCAs and whether retention in brain tissue may have any long-term negative neurologic side effects.¹⁵ Recently, a large study in individuals with contrast-enhanced nonbrain MR imaging without a history of Parkinsonism failed to show any associations between administration of GBCA and Parkinsonism, but studies on cognitive aspects are lacking.¹⁶

We aimed to retrospectively investigate the association between the number of GBCA administrations and a higher Signal Intensity Index (SII) in the DN and GP in a longitudinal MS cohort with an 18-year follow-up and to compare these results with non-GBCA-exposed matched healthy controls. We also explored possible associations between a higher SII and cognitive disability in MS.

MATERIALS AND METHODS

Study Population

On the basis of a consecutively recruited prospective cohort of 23 patients with MS followed for 18 years, we performed a retrospective analysis with regard to the SII. The cohort was originally recruited from the Department of Neurology in Huddinge, Karolinska University Hospital. The inclusion criterion at baseline was a diagnosis of MS according to the concurrent diagnostic criteria,¹⁷ while the exclusion criterion was neurologic comorbidities or MR imaging contraindications. For the study duration, all patients had at least 3 brain MR imaging scans. For the last MR imaging follow-up, we also recruited 23 age- and sex-matched healthy controls who were volunteers without neurologic diseases who were scanned with the same MR imaging protocol for the research project. The demography of the study population is presented in the Table. None of the participants had any history of renal or liver failure, and when available, renal and liver function blood test results were normal. The study was approved by the ethics review board in Stockholm, Sweden, and written informed consent was obtained from all participants.

GBCA Administrations

All patients with MS in the cohort received both linear non-ionic gadodiamide (Omniscan; GE Healthcare, Piscataway, New Jersey) and linear ionic gadopentetate dimeglumine (Magnevist; Bayer HealthCare Pharmaceuticals, Wayne, New Jersey). Six patients had received macrocyclic gadoterate me-

glumine (Dotarem; Guerbet, Aulnay-sous-Bois, France) on 1 occasion in the last 2 years before the last follow-up. The information on the number of administrations and class of GBCA was based on documentation in the digital radiologic information system, along with patient charts, to determine that no additional contrast-enhanced MR imaging had been performed at other sites.

Imaging and Volumetry

All patients underwent MR imaging of the brain at baseline, after 9 years, and after 18 years. MR imaging scans obtained between these time points were also included. MR imaging examinations were acquired with native 5-mm-thick T1-weighted spin-echo sequences at up to 3 time points (at least at baseline and 18-year follow-up). MPAGE sequences (resolution, 1 × 1 × 1.5 mm) were available at up to 4 time points during the last 9 years of the study (at least at 9- and 18-year follow-ups). The On-line Table details the MR imaging acquisition parameters.

The longitudinal stream of FreeSurfer 5.3.0 (<http://surfer.nmr.mgh.harvard.edu>) was used to obtain brain parenchymal fraction measurements from the MPAGE scans with semi-manual correction of topologic errors.¹⁸ Lesion segmentations were performed by using the combination of MPAGE and FLAIR scans with the lesion growth algorithm in the Segmentation Toolbox 1.2.3 (Technische Universität, München, Munich, Germany) for SPM8 software (<http://www.fil.ion.ucl.ac.uk/spm/software/spm12>).¹⁹

Radiologic Evaluation

The SII was calculated according to the following formula: SII = Signal Intensity_{ROI}/Signal Intensity_{Reference Region}. The radiologic measurements were performed by placing ROIs bilaterally in the GP and DN, with the thalamus and left middle cerebellar peduncle measured in the same image section as the reference points, respectively. The radiologic evaluation was blinded to the examination date, the original radiologic reading, and all clinical information. The specific region for each measurement was decided by consensus, by a radiology resident (Y.F.) and a neuroradiologist (F.H.), with simultaneous assessment of T2-weighted images to improve the delineation of the DN and avoid placement of ROIs in lesioned areas. In 7 scans, measurements were not performed in the GP due to lesions in the ROIs and/or in the reference regions.

Clinical Data

Patients were neurologically and neuropsychologically evaluated at 3 time points during the study (baseline, 9-year follow-up, and 18-year follow-up). Physical disability was assessed by a senior consultant in neurology (S.F.) with the Expanded Disability Status Scale (EDSS).²⁰ The patients with MS underwent extensive neuropsychological testing performed by a senior neuropsychologist (G.B.), including the following: the Symbol Digit Modalities Test to assess information-processing speed; the F-A-S Test for evaluating phonologic verbal fluency; the Rey–Osterrieth Complex Figure Test-Copy for evaluating visuospatial ability; and the Rey Auditory Verbal Learning Test with encoding and delayed recall at 30 minutes for episodic auditory-verbal memory. The raw test scores were converted to normalized z-scores on the basis of age, sex, and educational level.²¹

Statistical Analysis

Descriptive statistics are presented as means and SDs. The SIIs of the right and left DN and GP were analyzed as individual data points because they were not always available in a paired fashion because the lesioned areas were not measured. The SII values for the GP and the cognitive z-scores for the Rey Auditory Verbal Learning Test and Rey–Osterrieth Complex Figure Test-Copy were negatively skewed and therefore underwent a reflect and logarithmic transformation [$\text{Lg}10(\text{Largest Score in Data} + 1) - \text{Data}$] to reach normal distribution. An unpaired *t* test was used to compare the SII between controls and patients with MS obtained in the same scanner.

Multiple linear regression analyses were performed in only the patients with MS. They were used to evaluate associations between SIIs in the GP/DN (dependent variables) and the total number of both linear and all types of GBCA administrations (independent variable), corrected for MR imaging scanner, sequence, and age. Additional analyses corrected for MS disease severity were performed to avoid MS disease progression as a possible confounder. In a first step, disease duration and EDSS scores were added to the model. Second, the model was also corrected for lesion volume and brain parenchymal fraction (when volumetric data were available during the later 9 years of the study). Repeated-measures analysis of variance on the increasing number of GBCA administrations (stratified as 0, 1–4, and >5 administrations) was performed to assess longitudinal change. Associations with cognition were similarly investigated with multiple linear regression analysis between cognitive z-scores (dependent variable) and the SII (independent variable) with the same correction steps. All regression coefficients are presented as the standardized coefficient, β . SPSS (Version 22.0 for Mac; IBM, Armonk, New York) was used for statistical analysis. An α level of .05 was considered statistically significant, equaling a corrected level of .029 after adjustments for the false discovery rate according to the Benjamini-Hochberg procedure.²²

RESULTS

GBCA Administration and Signal Intensity

As detailed in the Table, the SII in the DN was higher in patients with MS than in healthy controls ($P < .001$, by the unpaired *t*

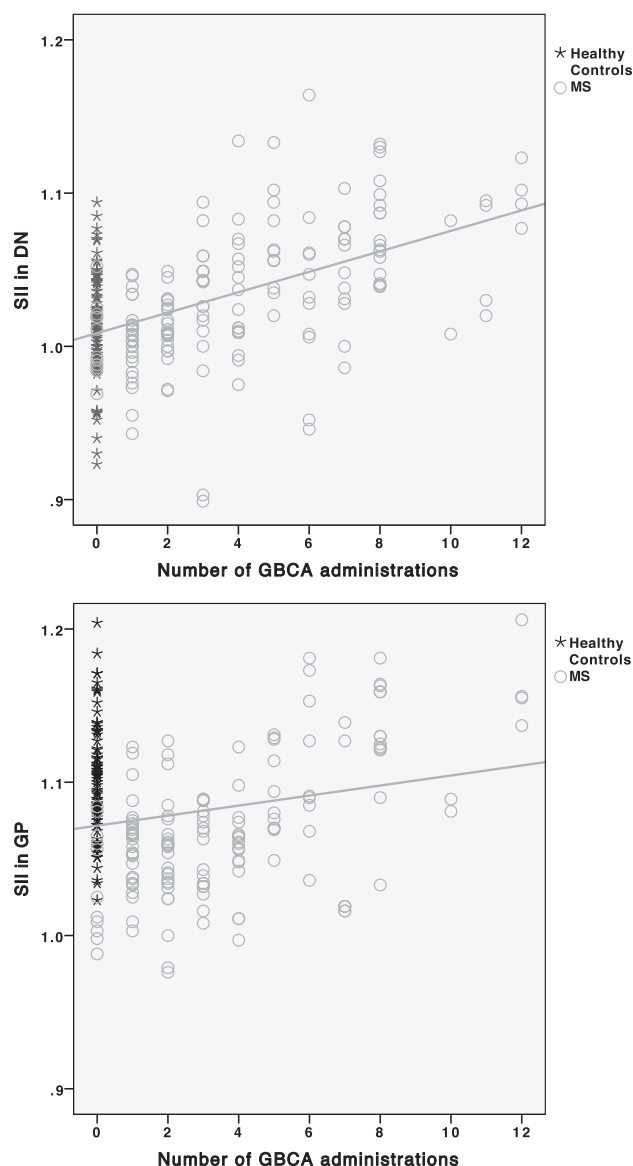


FIG 1. Scatterplots with linear regression lines showing that the number of GBCA administrations is associated with a higher SII in the DN and GP ($\beta = 0.45$, $P < .001$ and $\beta = 0.60$, $P < .001$, respectively) with corrections for age, scanner, and sequence type.

test), while there was no significant difference for the GP ($P = .19$). Within the MS group, an increased number of GBCA administrations was associated with increased SIIs in both the DN ($\beta = 0.45$, $P < .001$) and GP ($\beta = 0.60$, $P < .001$), illustrated in Fig 1. The associations between high SIIs in the DN ($\beta = 0.45$, $P < .001$) and GP ($\beta = 0.58$, $P < .001$) remained significant when using only the number of linear GBCAs as an independent variable. When adding corrections for MS disease duration and EDSS, a higher number of GBCA administrations was still associated with higher SIIs in the DN ($\beta = 0.43$, $P < .001$) and GP ($\beta = 0.58$, $P < .001$). When we analyzed the later time points when lesion volume and brain parenchymal fraction were available (as a further characterization of disease severity) and by adding correction for those factors in the regression model, a higher number of GBCA administrations remained associated with higher SIIs in the DN ($\beta = 0.39$, $P = .007$) and GP ($\beta = 0.64$, $P < .001$).

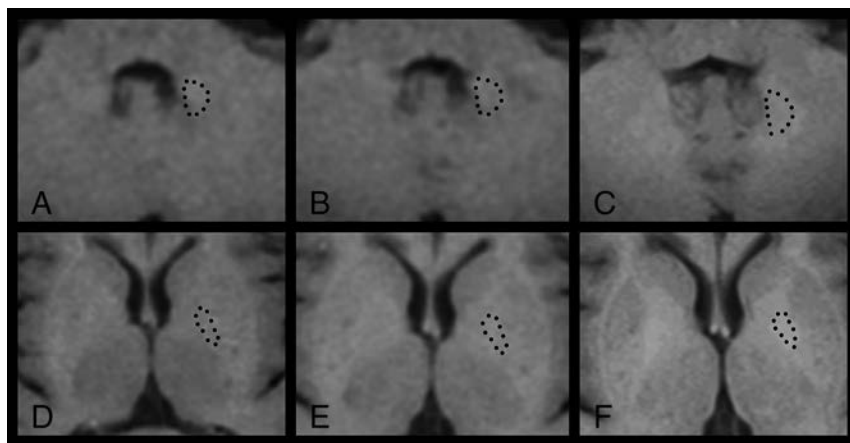


FIG 2. Longitudinal T1-weighted spin-echo signal-intensity changes in the DN (A–C) and GP (D–F) in a female patient with MS after receiving 0 (A and D), 1 (B and E), and 8 (C and F) GBCA administrations. This patient had an increasingly higher SII in both regions: DN 1.03 (A), 1.05 (B), 1.09 (C), GP 1.00 (D), 1.12 (E), 1.16 (F). Dotted lines illustrate the outlining of the ROIs.

.001). Figure 2 illustrates the longitudinal increase in DN signal intensity in relation to more GBCA administrations in 1 patient with MS.

From a longitudinal analysis perspective, the average SII change between baseline and the 18-year follow-up in patients was 0.06 in the DN and 0.07 in the GP, equaling a change of 0.009 in both the DN and GP per additional GBCA administration. Repeated-measures ANOVA (with the Greenhouse-Geisser correction) showed that the SIIs were significantly different with respect to the number of administrations for the DN [$F(2) = 22.98, P < .001$] and the GP [$F(1.07, 10.67) = 6.29, P = .028$]. Pair-wise comparisons were significant between 0 and 5–12 administrations for both the DN (1.01 ± 0.24 and $1.08 \pm 0.032, P < .001$) and the GP (0.96 ± 0.128 and $1.09 \pm 0.53, P = .013$). Similar trends were seen in the comparison between 0 and 1–4 administrations (DN, $P = .049$; GP, $P = .064$).

Associations with Cognition in Patients with MS

A high SII in the GP ($\beta = -0.45, P < .001$) was associated with low verbal fluency performance, and a similar trend was seen for the DN ($\beta = -0.25, P = .03$). After we corrected for disease duration and the EDSS, the associations were significant in both the DN ($\beta = -0.28, P = .012$) and GP ($\beta = -0.49, P < .001$). A higher SII in the GP ($\beta = -0.35, P = .003$), but not in the DN, was associated with low auditory verbal learning encoding ($\beta = -0.35, P = .003$) and low auditory verbal learning retention ($\beta = -0.29, P = .01$). These associations remained significant when correcting for disease duration and EDSS (encoding, $\beta = -0.33, P = .006$; retention, $\beta = -0.34, P = .004$). There were no significant associations between the SII in the DN or GP with either the Rey–Osterrieth Complex Figure Test or the Symbol Digit Modalities Test. After we corrected for disease duration and EDSS, a higher SII in the GP tended to be associated with a lower Symbol Digit Modalities Test score ($\beta = -0.24, P = .043$). When we analyzed the later time points and added correction for lesion volume and brain parenchymal fraction, only the association between a higher SII and low verbal fluency remained significant in

the DN ($\beta = -0.40, P = .013$), with a similar trend in the GP ($\beta = -0.36, P = .034$).

DISCUSSION

In the current study, we show that an increasing number of GBCA administrations is longitudinally associated with a higher SII in both the DN and GP in patients with MS, adding to the growing body of evidence of gadolinium retention in the brain. We further show some initial tentative results regarding associations of the SII in these structures with cognitive performance, which remained significant for verbal fluency when correcting for MS disease severity.

Investigations on gadolinium retention in the brain have studied different types of GBCAs. Multiple studies have

demonstrated associations between the SII in the DN and the number of linear GBCA administrations.²³ More recently, a similar initial association was reported for macrocyclic GBCAs,²⁴ and small amounts of retained gadolinium were recently found in human brain tissue after macrocyclic GBCA.¹³ However, more recent imaging studies regarding gadolinium retention support the use of macrocyclic GBCA as a safer choice even for patients with normal renal function.^{23,25,26} In our study, all patients received linear GBCAs, and 6 of 23 patients also received 1 administration of a macrocyclic GBCA. However, when we studied the patients with MS who received a linear GBCA (gadodiamide and gadopentetic acid) solely, the results were relatively unchanged.

Some studies have used the pons as a reference region for the DN, but here we chose the left middle cerebellar peduncle instead because it was easier to find nonlesioned areas for reference that were not affected by phase-dependent artifacts on T1-weighted spin-echo scans.^{9,11,25} In line with previous studies, the thalamus was used as a reference point for the GP with special care to avoid lesions, though we note that diffuse MS disease-related changes in the thalamus may be a possible confounder.²⁷

We have tried to carefully mitigate the confounding effects of MS pathology or progression in our analysis. However, MS typically causes hypointensities in both white and gray matter on T1-weighted imaging,²⁸ which would likely cause an underestimation of the SII rather than an overestimation in the ROI. On the other hand, we note that a hyperintense DN on native T1-weighted MR imaging has previously been reported in secondary-progressive MS.²⁹ Whether these previous results have been confounded by GBCA administrations (before current knowledge) or actually reflect disease-related signal changes remains unclear. The different scanners and sequences used are a limitation but also unavoidable when performing a long-term study with such long-term follow-up because there is a clinical need for scanner upgrades with time. Because these patients were part of a prospective MS study, they had been scanned with the follow-up similar to that of MR imaging protocols for T1 spin-echo and MPRAGE, respectively, but on different scanners during the years. A subgroup analysis in

a previous study did not show any significant difference when using different sequences.²³ However, a later study showed that this significantly influenced the results, highlighting the importance of using the same sequences and scanners if possible.^{30,31} On the basis of these previous results, we therefore corrected the measurements for these factors to mitigate any scanner-related effects.

In the current study, we showed that a higher SII in the DN in patients with MS is associated with lower word fluency scores, which was the only cognitive measurement that remained associated with the SII after correction for several aspects of MS severity. Most interesting, executive function, including verbal fluency, is less frequently affected compared with episodic memory and information-processing speed in MS.³² Verbal fluency also declines after pallidotomy and cerebellar damage; this finding highlights the importance of these structures in verbal fluency.^{33,34} Furthermore, a recent study in MS showed that higher functional connectivity between the DN and prefrontal, motor, and parietal cortices is associated with lower structural parenchymal damage and less clinical impairment.³⁵ However, many other areas of the brain are affected by MS, which may be more closely related to the decline in our neuropsychological test results.³² Naturally, it is of great clinical interest to explore any possible negative neurologic or cognitive adverse effects of gadolinium retention. It is, however, important to stress that our retrospective results must be interpreted with caution and do not necessarily imply causation.

It is not clear to what degree factors such as renal failure, liver dysfunction, and genetic variations might influence the risk of developing a higher SII in the brain after repeated GBCA administrations. MS is one of the largest patient groups receiving repeat GBCA administrations and may, therefore, be at special risk of accumulation in the brain.³⁶ MS also has a negative impact on cognitive function.³² Consequently, it is difficult to separate the effects of MS progression and a hypothetic effect on cognition attributed to GBCA, though we statistically corrected for the potential impact of disease severity. Furthermore, disease duration, lesion volume, and brain parenchymal fraction might not fully adjust for an MS-dependent decline of brain function because MS is a heterogeneous disease with individualized treatment regimens, different progression rates, and cognitive reserve,³⁷ which are not completely represented by these biomarkers. Last, another limitation was the lack of a matched MS group not exposed to GBCAs or solely to macrocyclic GBCAs, because it was not possible to find a large-enough group of such patients with a disease duration similar to that of the studied cohort.

The strengths of the study are the long follow-up with available clinical, laboratory, and radiologic information and a study population representative of the MS panorama with different subtypes, disease duration, and EDSS scores.

CONCLUSIONS

Our data add support to the existing framework that gadolinium may have lasting effects on the T1-weighted intensities in the DN and GP. Although we show that a higher SII is associated with worse verbal fluency scores, these results are only exploratory and have to be interpreted with caution. Future studies are important to further investigate these cognitive aspects and other clinical

outcome variables in other cohorts with a repeat number of GBCA administrations to understand their clinical implications.

ACKNOWLEDGMENTS

We thank the study participants for making this study possible.

Disclosures: Yngve Forslin—*RELATED: Grant:* ALF, *Comments:* This research was funded by Stockholm County Council and Karolinska Institutet through the regional agreement on medical training and clinical research (ALF grant)*. Farouk Hashim—*RELATED: Grant:* ALF*. Gösta Bergendal—*RELATED: Grant:* ALF*. Sten Fredrikson—*UNRELATED: Board Membership:* Chairman of the Educational and Examination Committee of the Swedish Neurological Society and Swedish delegate of the EFNS, European Board of Neurology and MSIF International Medical and Scientific Board; *OTHER RELATIONSHIPS:* received honorarium for lectures, educational activities, and/or consultancy from Genzyme/Sanofi, Merck, Novartis, and Teva Pharmaceutical Industries. Tobias Granberg—*RELATED: Grant:* Stockholm City Council*. *Money paid to the institution.

REFERENCES

- Lohrke J, Frenzel T, Endrikat J, et al. **25 years of contrast-enhanced MRI: developments, current challenges and future perspectives.** *Adv Ther* 2016;33:1–28 [CrossRef Medline](#)
- Idée JM, Fretellier N, Robic C, et al. **The role of gadolinium chelates in the mechanism of nephrogenic systemic fibrosis: a critical update.** *Crit Rev Toxicol* 2014;44:895–913 [CrossRef Medline](#)
- Frenzel T, Lengsfeld P, Schirmer H, et al. **Stability of gadolinium-based magnetic resonance imaging contrast agents in human serum at 37 degrees C.** *Invest Radiol* 2008;43:817–28 [CrossRef Medline](#)
- Thomsen HS, Morcos SK, Almén T, et al; ESUR Contrast Medium Safety Committee. **Nephrogenic systemic fibrosis and gadolinium-based contrast media: updated ESUR Contrast Medium Safety Committee guidelines.** *Eur Radiol* 2013;23:307–18 [CrossRef Medline](#)
- White GW, Gibby WA, Tweedle MF. **Comparison of Gd(DTPA-BMA) (Omniscan) versus Gd(HP-DO3A) (ProHance) relative to gadolinium retention in human bone tissue by inductively coupled plasma mass spectroscopy.** *Invest Radiol* 2006;41:272–78 [CrossRef Medline](#)
- Idée JM, Port M, Dencausse A, et al. **Involvement of gadolinium chelates in the mechanism of nephrogenic systemic fibrosis: an update.** *Radiol Clin North Am* 2009;47:855–69, vii [CrossRef Medline](#)
- Roberts DR, Lindhorst SM, Welsh CT, et al. **High levels of gadolinium deposition in the skin of a patient with normal renal function.** *Invest Radiol* 2016;51:280–89 [CrossRef Medline](#)
- Kanda T, Ishii K, Kawaguchi H, et al. **High signal intensity in the dentate nucleus and globus pallidus on unenhanced T1-weighted MR images: relationship with increasing cumulative dose of a gadolinium-based contrast material.** *Radiology* 2014;270:834–41 [CrossRef Medline](#)
- Errante Y, Cirimele V, Mallio CA, et al. **Progressive increase of T1 signal intensity of the dentate nucleus on unenhanced magnetic resonance images is associated with cumulative doses of intravenously administered gadodiamide in patients with normal renal function, suggesting dechelation.** *Invest Radiol* 2014;49:685–90 [CrossRef Medline](#)
- McDonald RJ, McDonald JS, Kallmes DF, et al. **Intracranial gadolinium deposition after contrast-enhanced MR imaging.** *Radiology* 2015;275:772–82 [CrossRef Medline](#)
- Quattrocchi CC, Mallio CA, Errante Y, et al. **Gadodiamide and dentate nucleus T1 hyperintensity in patients with meningioma evaluated by multiple follow-up contrast-enhanced magnetic resonance examinations with no systemic interval therapy.** *Invest Radiol* 2015;50:470–72 [CrossRef Medline](#)
- Kanda T, Fukusato T, Matsuda M, et al. **Gadolinium-based contrast agent accumulates in the brain even in subjects without severe renal dysfunction: evaluation of autopsy brain specimens with inductively coupled plasma mass spectroscopy.** *Radiology* 2015;276:228–32 [CrossRef Medline](#)
- Murata N, Gonzalez-Cuyar LF, Murata K, et al. **Macrocyclic and**

- other non-group 1 gadolinium contrast agents deposit low levels of gadolinium in brain and bone tissue: preliminary results from 9 patients with normal renal function. *Invest Radiol* 2016;51:447–53 CrossRef Medline
14. Robert P, Lehericy S, Grand S, et al. T1-weighted hypersignal in the deep cerebellar nuclei after repeated administrations of gadolinium-based contrast agents in healthy rats: difference between linear and macrocyclic agents. *Invest Radiol* 2015;50:473–80 CrossRef Medline
 15. Goischke HK. MRI with gadolinium-based contrast agents: practical help to ensure patient safety. *J Am Coll Radiol* 2016;13:890 CrossRef Medline
 16. Welk B, McArthur E, Morrow SA, et al. Association between gadolinium contrast exposure and the risk of parkinsonism. *JAMA* 2016; 316:96–98 CrossRef Medline
 17. Poser CM, Paty DW, Scheinberg L, et al. New diagnostic criteria for multiple sclerosis: guidelines for research protocols. *Ann Neurol* 1983;13:227–31 CrossRef Medline
 18. Reuter M, Schmansky NJ, Rosas HD, et al. Within-subject template estimation for unbiased longitudinal image analysis. *Neuroimage* 2012;61:1402–18 CrossRef Medline
 19. Schmidt P, Gaser C, Arsic M, et al. An automated tool for detection of FLAIR-hyperintense white-matter lesions in multiple sclerosis. *Neuroimage* 2012;59:3774–83 CrossRef Medline
 20. Kurtzke JF. Rating neurologic impairment in multiple sclerosis: an expanded disability status scale (EDSS). *Neurology* 1983;33:1444–52 CrossRef Medline
 21. Lezak MD, ed. *Neuropsychological Assessment*. 5th ed. Oxford: Oxford University Press; 2012
 22. Benjamini Y, Krieger AM, Yekutieli D. Adaptive linear step-up procedures that control the false discovery rate. *Biometrika* 2006;93: 491–507 CrossRef
 23. Radbruch A, Weberling LD, Kieslich PJ, et al. Gadolinium retention in the dentate nucleus and globus pallidus is dependent on the class of contrast agent. *Radiology* 2015;275:783–91 CrossRef Medline
 24. Stojanov DA, Aracki-Trenkic A, Vojinovic S, et al. Increasing signal intensity within the dentate nucleus and globus pallidus on unenhanced T1W magnetic resonance images in patients with relapsing-remitting multiple sclerosis: correlation with cumulative dose of a macrocyclic gadolinium-based contrast agent, gadobutrol. *Eur Radiol* 2016;26:807–15 CrossRef Medline
 25. Kanda T, Osawa M, Oba H, et al. High signal intensity in dentate nucleus on unenhanced T1-weighted MR images: association with linear versus macrocyclic gadolinium chelate administration. *Radiology* 2015;275:803–09 CrossRef Medline
 26. Thomsen HS. T1 hyperintensity in the brain after multiple intravenous injections of gadolinium-based contrast agents. *Acta Radiol* 2016;57:389–91 CrossRef Medline
 27. Minagar A, Barnett MH, Benedict RH, et al. The thalamus and multiple sclerosis: modern views on pathologic, imaging, and clinical aspects. *Neurology* 2013;80:210–19 CrossRef Medline
 28. Filippi M, Rocca MA, Barkhof F, et al; Attendees of the Correlation between Pathological MRI Findings in MS Workshop. Association between pathological and MRI findings in multiple sclerosis. *Lancet Neurol* 2012;11:349–60 CrossRef Medline
 29. Roccatagliata L, Vuolo L, Bonzano L, et al. Multiple sclerosis: hyperintense dentate nucleus on unenhanced T1-weighted MR images is associated with the secondary progressive subtype. *Radiology* 2009; 251:503–10 CrossRef Medline
 30. Ramalho J, Ramalho M, AlObaidy M, et al. T1 signal-intensity increase in the dentate nucleus after multiple exposures to gadodiamide: intra-individual comparison between 2 commonly used sequences. *AJNR Am J Neuroradiol* 2016;37:1427–31 CrossRef Medline
 31. Ramalho J, Ramalho M, AlObaidy M, et al. Technical aspects of MRI signal change quantification after gadolinium-based contrast agents' administration. *Magn Reson Imaging* 2016;34:1355–58 CrossRef Medline
 32. Rocca MA, Amato MP, Enzinger C, et al; MAGNIMS Study Group. Clinical and imaging assessment of cognitive dysfunction in multiple sclerosis. *Lancet Neurol* 2015;14:302–17 CrossRef Medline
 33. Tröster AI, Woods SP, Fields JA. Verbal fluency declines after pallidotomy: an interaction between task and lesion laterality. *Appl Neuropsychol* 2003;10:69–75 CrossRef Medline
 34. Mariën P, Ackermann H, Adamaszek M, et al. Consensus paper: language and the cerebellum—an ongoing enigma. *Cerebellum* 2014;13:386–410 CrossRef Medline
 35. Sbardella E, Upadhyay N, Tona F, et al. Dentate nucleus connectivity in adult patients with multiple sclerosis: functional changes at rest and correlation with clinical features. *Mult Scler* 2017;23:546–55 CrossRef Medline
 36. Filippi M, Rocca MA, De Stefano N, et al. Magnetic resonance techniques in multiple sclerosis: the present and the future. *Arch Neurol* 2011;68:1514–20 CrossRef Medline
 37. Sandroff BM, Schwartz CE, DeLuca J. Measurement and maintenance of reserve in multiple sclerosis. *J Neurol* 2016;263:2158–69 CrossRef Medline

The Use of Noncontrast Quantitative MRI to Detect Gadolinium-Enhancing Multiple Sclerosis Brain Lesions: A Systematic Review and Meta-Analysis

A. Gupta, K. Al-Dasuqi, F. Xia, G. Askin, Y. Zhao, D. Delgado, and Y. Wang



ABSTRACT

BACKGROUND: Concerns have arisen about the long-term health effects of repeat gadolinium injections in patients with multiple sclerosis and the incomplete characterization of MS lesion pathophysiology that results from relying on enhancement characteristics alone.

PURPOSE: Our aim was to perform a systematic review and meta-analysis analyzing whether noncontrast MR imaging biomarkers can distinguish enhancing and nonenhancing brain MS lesions.

DATA SOURCES: Our sources were Ovid MEDLINE, Ovid Embase, and the Cochrane data base from inception to August 2016.

STUDY SELECTION: We included 37 journal articles on 985 patients with MS who had MR imaging in which T1-weighted postcontrast sequences were compared with noncontrast sequences obtained during the same MR imaging examination by using ROI analysis of individual MS lesions.

DATA ANALYSIS: We performed random-effects meta-analyses comparing the standard mean difference of each MR imaging metric taken from enhancing-versus-nonenhancing lesions.

DATA SYNTHESIS: DTI-based fractional anisotropy values are significantly different between enhancing and nonenhancing lesions ($P = .02$), with enhancing lesions showing decreased fractional anisotropy compared with nonenhancing lesions. Of the other most frequently studied MR imaging biomarkers (mean diffusivity, magnetization transfer ratio, or ADC), none were significantly different (P values of 0.30, 0.47, and 0.19, respectively) between enhancing and nonenhancing lesions. Of the limited studies providing diagnostic accuracy measures, gradient-echo-based quantitative susceptibility mapping had the best performance in discriminating enhancing and nonenhancing MS lesions.

LIMITATIONS: MR imaging techniques and patient characteristics were variable across studies. Most studies did not provide diagnostic accuracy measures. All imaging metrics were not studied in all 37 studies.

CONCLUSIONS: Noncontrast MR imaging techniques, such as DTI-based FA, can assess MS lesion acuity without gadolinium.

ABBREVIATIONS: FA = fractional anisotropy; GRE = gradient recalled-echo; MD = mean diffusivity; MTR = magnetization transfer ratio; MWF = myelin water fraction; QSM = quantitative susceptibility mapping; SMD = standardized mean difference

Multiple sclerosis represents a specific disease process for which recent investigations have shown evidence of gadolinium deposition in the brain after multiple contrast-enhanced

brain MRIs.^{1,2} Patients with MS are likely to undergo repeat contrast-enhanced MR imaging to monitor disease status. As a result, patients with MS are at high risk for cumulative deposition of gadolinium given the relatively early disease onset, which can potentially necessitate many years of disease surveillance imaging.

Received January 4, 2017; accepted after revision February 22.

From the Department of Radiology (A.G., K.A.-D., F.X., Y.W.); Clinical and Translational Neuroscience Unit (A.G.), Feil Family Brain and Mind Research Institute; Department of Healthcare Policy and Research (G.A., Y.Z.); and Samuel J. Wood Library and C.V. Starr Biomedical Information Center (D.D.), Weill Cornell Medicine, New York, New York; and Department of Biomedical Engineering (F.X., Y.W.), Cornell University, Ithaca, New York.

This work was supported National Institutes of Health grants R01NS090464 (Y.W., A.G.) and T35EB006732 (F.X.).

Please address correspondence to Ajay Gupta, MD, Weill Cornell Medicine, 525 East 68th St, Starr 8A, Box 141, New York, NY 10065; e-mail: ajg9004@med.cornell.edu

Indicates open access to non-subscribers at www.ajnr.org

Indicates article with supplemental on-line appendix and tables.

Indicates article with supplemental on-line photo.

<http://dx.doi.org/10.3174/ajnr.A5209>

Such repeat doses of gadolinium administration in patients with MS have been correlated with increased T1-weighted signal intensity in the dentate nucleus in the cerebellum,¹ a finding that has been associated with secondary-progressive MS and increased clinical disability.³ Although the precise causal role, if any, that repeat gadolinium injections plays in MS pathogenesis remains unknown, in 2016, officials from the National Institutes of Health issued guidelines recommending that the necessity of gadolinium administration in specific clinical indications should be carefully re-evaluated, given the uncertain long-term public health impact of the deposition of gadolinium in the brain.⁴

Gadolinium enhancement of MS lesions is a well-established method to evaluate disease status,⁵ with contrast-enhancing lesions reflective of the blood-brain barrier breakdown and inflammatory response known to occur in acutely demyelinating lesions. Several quantitative MR imaging biomarkers may provide diagnostic information capable of discriminating between enhancing and nonenhancing MS lesions. Such MR imaging markers may also have the added benefit of providing insight into MS pathobiology not possible by the simple dichotomous characterization of the presence or absence of contrast enhancement. Identifying the most promising MR imaging biomarkers of MS lesion inflammatory activity is important to inform future MS imaging research in which such biomarkers could be further standardized and evaluated. We therefore performed a systematic review and meta-analysis of the existing scientific literature to evaluate whether quantitative noncontrast MR imaging metrics are able to accurately discriminate between enhancing and nonenhancing MS brain lesions.

MATERIALS AND METHODS

We followed both the Meta-Analysis of Observational Studies in Epidemiology group guidelines⁶ and the Preferred Reporting Items for Systematic Reviews and Meta-Analyses statement in our study protocol.⁷

Data Sources and Searches

An experienced medical librarian performed comprehensive searches of on-line data bases including Ovid MEDLINE, Ovid Embase, and the Cochrane Library from data base inception to August 15, 2016. Key words included “MR imaging,” “multiple sclerosis,” “gadolinium,” “enhancement,” “susceptibility,” “diffusion,” and “perfusion.” We searched first in Ovid MEDLINE and then adapted headings and keywords for other data bases and identified additional records by using the “Cited by” and “View references” features in Scopus (see the On-line Appendix for search methodology details).

Study Selection

We included peer-reviewed journal articles focused on patients with MS who had MR imaging brain studies in which T1-weighted postcontrast sequences were compared with noncontrast sequences obtained during the same MR imaging examination. Specific study criteria were as follows: 1) patients with MS who underwent MR imaging of the brain with and without the administration of a gadolinium-based intravenous contrast agent; 2) evaluation of MS lesion gadolinium enhancement on

T1-weighted postcontrast images; and 3) ROI comparison of MR imaging biomarker values obtained in the location of gadolinium-enhancing lesions versus values obtained in T2 hyperintense, non-enhancing lesions. We included studies evaluating any of the following noncontrast quantitative MR imaging measures: gradient recalled-echo (GRE) derived quantitative susceptibility mapping (QSM); DWI-derived ADC; DTI-derived fractional anisotropy (FA) or mean diffusivity (MD); PWI-derived assessment of CBF; myelin water imaging–derived assessment of myelin water fraction (MWF); or quantitative MR imaging techniques allowing the absolute quantification of longitudinal relaxation, transverse relaxation, proton density, and magnetization transfer ratio; and 4) studies including ≥ 5 subjects to avoid the inclusion of case reports or very small case series. We chose to include only peer-reviewed journal articles rather than conference abstracts so that the studies included would have sufficient detail for systematic review and meta-analysis. If data from a single patient cohort were published more than once, the single article with the largest sample size was included to minimize analysis of duplicate study samples. We contacted via e-mail the corresponding author for additional details to clarify our data extraction as needed.

Data Extraction and Quality Assessment

After the titles and abstracts of preliminary articles were read, potentially eligible articles were shortlisted on the basis of the information contained with the abstract. Two readers (K.A.-D. and F.X., research fellows each with ~ 2 years of experience in brain imaging research) read the shortlisted articles in their entirety to determine eligibility, with disagreements resolved by consensus. We extracted data in duplicate by using a data-collection template, with a third tie-breaking reader (A.G., faculty neuroradiologist) resolving disagreements in data extraction. We extracted the following study characteristics: first author, study design (prospective versus retrospective), major study inclusion criteria, total number of subjects, basic study demographics, median MS disease duration, median Expanded Disability Status Scale, and specific MR imaging techniques used. We performed our analysis at the level of each MS lesion, and divided regions of the brain into 2 categories: enhancing lesions and nonenhancing, T2 hyperintense lesions. When they were available, we collected receiver operating characteristic and diagnostic accuracy measures based on proposed threshold values to describe the ability of the MR imaging biomarkers to discriminate between enhancing and nonenhancing lesions. We also evaluated the risk of bias in each study by generating 7 specific questions to evaluate potential selection, detection, reporting, and confounding bias. Two study investigators (K.A.-D. and F.X.) assessed risks of bias with disagreements in assessment resolved by a third tie-breaking evaluator (A.G.). We did not use a threshold to exclude studies based on a bias scoring system.

Data Synthesis and Analysis

We calculated a standardized mean difference (SMD), comparing the difference of values of each MR imaging metric taken from enhancing-versus-nonenhancing lesions. If at least 5 studies were present that evaluated a given imaging biomarker, we statistically pooled data and performed meta-analyses of the individual quan-

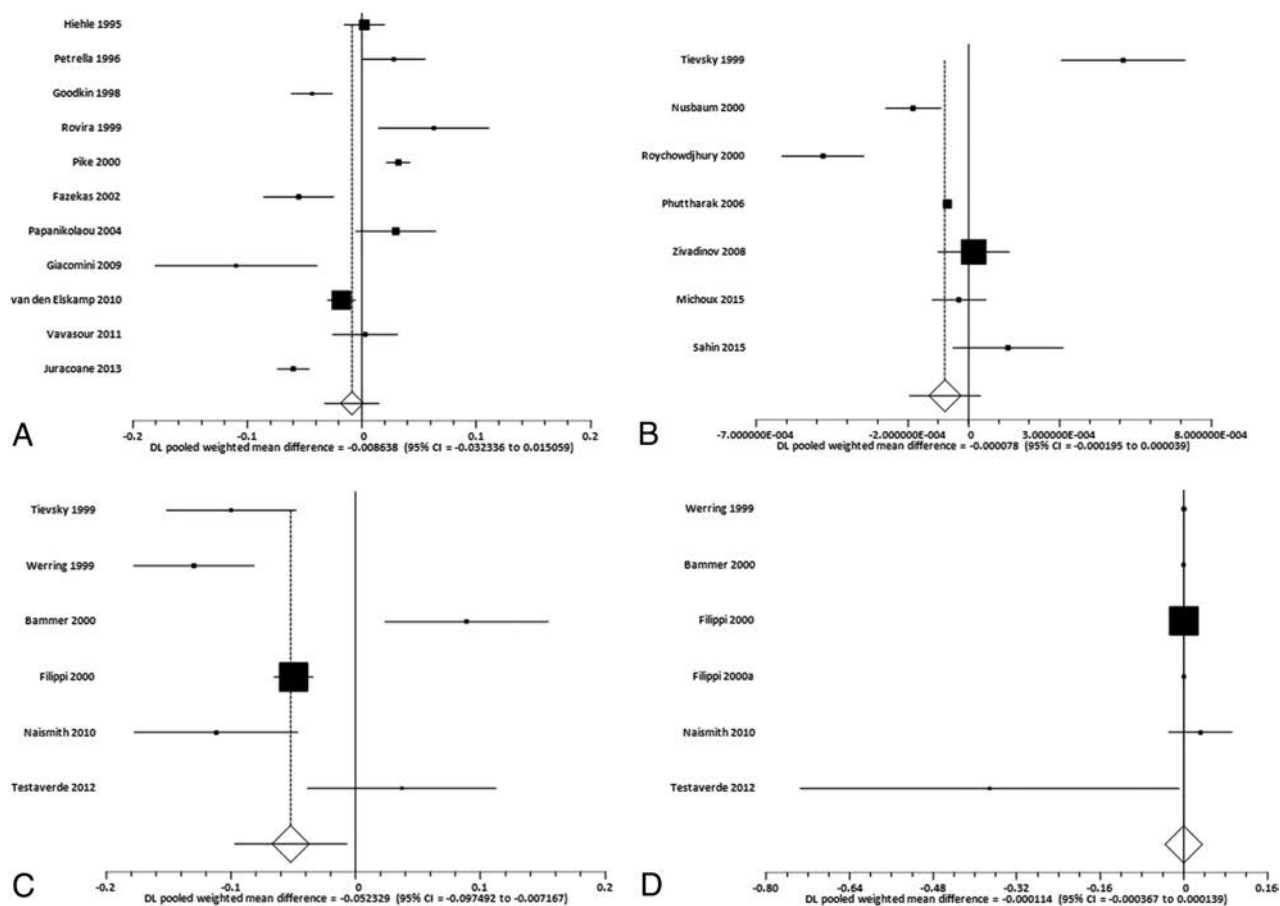


FIGURE. Random-effects forest plots showing the SMD for specific MR imaging biomarker values between enhancing and nonenhancing lesions. *Squares* represent the point estimate for the SMD of each study, with the size of each *square* being proportional to the inverse of the variance of the estimate. The *horizontal lines* represent the 95% confidence intervals of each study. The *diamond* represents the pooled SMD estimate with the width of the *diamond* showing the 95% confident interval. A, SMD for MTR between enhancing lesions and nonenhancing lesions. B, SMD for ADC between enhancing lesions and nonenhancing lesions. C, SMD for FA between enhancing lesions and nonenhancing lesions. D, SMD for MD between enhancing lesions and nonenhancing lesions.

tative MR imaging SMDs. We used a random-effects rather than a fixed-effects model because we adopted the conservative assumption that individual studies did not have the same effect size, given the likelihood of between-study heterogeneity in terms of subject characteristics and MR imaging methods. We performed the I^2 statistical heterogeneity test to evaluate the combinability of each study. The presence of publication bias was evaluated through the Begg-Mazumdar rank correlation test. We considered all P values $< .05$ statistically significant.

RESULTS

Study Selection and Characteristics

From a total of 6129 articles produced by our data base searching, we identified a total of 37 articles⁸⁻⁴⁴ that met inclusion for our systematic review (On-line Figure). In total, the studies included 985 patients comprising 1495 enhancing and 8529 nonenhancing MS lesions from which we were able to extract data (On-line Table 1). Most studies were prospective, and each included an average of 25 patients (range, 5–89 patients). The mean age range for patients with MS in the included studies was between 27.5 and 50 years, with all studies containing cohorts of patients who were predominantly female. Four MR imaging metrics studied in 27 unique articles had an adequate number of published studies

(>4) whose raw data were presented in a manner amenable for meta-analysis: magnetization transfer ratio (MTR) ($n = 11$),^{12,17-20,27,28,30,31,36,39} ADC ($n = 7$),^{23,25,29,32,33,35,44} FA ($n = 6$),^{8,13,24,34,35,40} and MD ($n = 6$).^{8,13,14,24,34,40} There were 4 or fewer studies focused on specific quantitative MR imaging tissue parameters such as GRE-QSM or T1 or T2 relaxation times. We found no studies comparing noncontrast PWI metrics with enhancing-versus-nonenhancing MS lesions. Only 3 studies^{9,23,45} provided optimal threshold values to distinguish enhancing from nonenhancing lesions with area under the curve measurements, with 1 study⁴⁵ showing an area under the curve of 0.95 for QSM to distinguish enhancing-versus-nonenhancing lesions. The remainder of the studies ($n = 34$) reported differences in summary values of biomarker values in enhancing-versus-nonenhancing lesions without diagnostic accuracy measures. The specific MR imaging protocols used by each study and the detailed breakdown of MR imaging test values are provided in On-line Tables 2 and 3, respectively.

Meta-Analysis Results

Magnetization Transfer Ratio. The SMD (Fig 1A) between measurements of enhancing and nonenhancing lesions for MTR was

0.009 (95% CI, -0.032 – -0.015 ; $P = .47$). The publication bias test (Egger) was not statistically significant for publication bias ($P = .74$). The heterogeneity statistic revealed $I^2 = 94.4\%$, consistent with strong heterogeneity.

Apparent Diffusion Coefficient. The SMD (Fig 1B) between measurements of enhancing and nonenhancing lesions for ADC was -0.00008 (95% CI, -0.00020 – -0.00004 ; $P = .19$). There was no evidence of publication bias ($P = .85$), though there was significant between-study heterogeneity, with $I^2 = 92.5\%$.

Fractional Anisotropy. The SMD (Fig 1C) between measurements of enhancing and nonenhancing lesions for FA was -0.052 (95% CI, -0.097 to -0.007 ; $P = .02$). There was no evidence of publication bias ($P = .92$). Finally, there was evidence of strong heterogeneity, with $I^2 = 91.4\%$.

Mean Diffusivity. The SMD (Fig 1D) between measurements of enhancing and nonenhancing lesions for MD was -0.0001 (95% CI, -0.0003 – -0.0001 ; $P = .30$). No significant publication bias was present ($P = .03$), while $I^2 = 92.3\%$ was suggestive of strong heterogeneity.

Assessment of the Quality of Included Studies

Most studies provided detailed imaging methodology and patient inclusion/exclusion criteria that would allow the study to be reproduced (On-line Tables 4–8). We found that most included studies were prospective and all involved some form of blinding to ensure that the presence of gadolinium enhancement occurred without knowledge of the results of the MR imaging quantitative biomarker being studied. Most studies did not use >1 investigator to analyze quantitative MR imaging biomarker imaging data; therefore, most included studies did not report measures of inter-rater reproducibility.

DISCUSSION

The presence of lesion gadolinium contrast enhancement is a well-established marker of MS lesion inflammation and relative acuity and has figured prominently in the diagnosis and monitoring of patients with MS. Given the emergence of promising imaging biomarkers in MS and mounting concerns over the unknown long-term health consequences of repeat gadolinium administration to patients, we sought to critically analyze the body of literature evaluating differences in quantitative MR imaging markers between enhancing and nonenhancing lesions. In this systematic review and meta-analysis, we found that DTI-based FA values are significantly different between enhancing and nonenhancing lesions, with enhancing lesions showing decreased FA compared with nonenhancing lesions. Concerning the other MR imaging biomarkers we identified in the literature that most frequently addressed this question (MD, MTR, or ADC), when pooling data across studies, no other imaging markers were significantly different between enhancing and nonenhancing lesions.

In our study, we found that only 3 studies^{9,23,45} provided an area under the curve showing the performance of the proposed imaging biomarker to differentiate enhancing-versus-nonenhancing lesions. It is possible that most studies did not report diagnostic accuracy measures because the investigators did not explicitly have the goal of determining whether a given MR imag-

ing biomarker could function as a replacement for gadolinium enhancement as a diagnostic test of lesion acuity. Indeed, most of the literature we studied was published before the recent reports that initially surfaced in 2015 over the deposition of gadolinium in the brain, and our pooled analyses of this existing body of literature suggest that re-evaluating whether these noncontrast quantitative MR imaging techniques are a viable alternative to gadolinium-based techniques in MS may now be warranted.

The differences between enhancing and nonenhancing lesions in terms of FA was a robust finding in our analysis. White matter fiber tracts are composed of aligned myelinated axons that limit the free diffusivity of water along the axis of the axonal fibers. The lower mean FA value found in enhancing MS lesions is consistent with the pathobiology of acute MS lesions in which inflammation-mediated disruption of myelin sheath integrity and an increase in local tissue vasogenic edema would together be expected to cause increased 3D diffusivity of water (lower FA).^{13,24} The relatively higher FA found in nonenhancing MS lesions raises the possibility that as lesions transition from enhancing to nonenhancing, some degree of axonal remyelination and/or a decrease in vasogenic edema may underlie increasing FA values following blood-brain barrier closure.²¹ Most interesting, we found no significant difference in ADC between enhancing and nonenhancing lesions, perhaps reflecting immune cell concentration in enhancing lesions being balanced by FA-associated myelin content immediately following blood-brain barrier closure. Because both cellular and myelin content affect ADC, the multidirectional nature of DTI may allow a more sensitive differentiation of enhancing from nonenhancing lesions compared with an ADC map alone.

Furthermore, although only 1 included study⁴⁵ focused on the relatively new technique of QSM, investigators noted high diagnostic accuracy measures using specific relative susceptibility values to distinguish enhancing from nonenhancing lesions. The ability of QSM to detect acute enhancing lesions is a natural extension of the recent observational data showing that the magnetic susceptibility of an MS lesion increases as it changes from enhancing to nonenhancing. Another study⁴¹ included in our systematic review that focused on MR frequency shifts derived from gradient-echo data also found reduced quantitative susceptibility in enhancing-versus-nonenhancing lesions. The usefulness of tissue susceptibility in monitoring MS disease status may reflect the role played by activated macrophages and microglia in removing diamagnetic myelin fragments and depositing iron within MS lesions, which results in enhancing lesions demonstrating lower susceptibility values than nonenhancing lesions.

Our study has some limitations in the underlying literature that can serve to improve future research in evaluating emerging MR imaging biomarkers of MS. First, there were differences in pulse sequence parameters, postprocessing techniques, and methods of evaluating each lesion that may limit our ability to pool studies and provide absolute point estimates for specific pooled MR imaging biomarkers. For example, though most studies provided mean biomarker values by using ROI analysis in all enhancing-versus-nonenhancing lesions, some but not all studies performed subgroup analyses on the pattern of enhancement (homogeneous versus heterogeneous) and the nature of the non-

enhancing lesions (“black hole” versus no associated T1 hypointensity). Although such heterogeneity is an inherent challenge in the interpretation of quantitative MR imaging data across institutions and among patients, we attempted to minimize this impact in our meta-analysis by pooling within-subject data from each study and by reporting standardized mean differences, which should help minimize the lack of standardization that would be present if absolute biomarker quantification were used in our analysis.

Furthermore, we pooled studies using the more conservative random-effects model rather than a fixed-effects model to statistically account for between-study heterogeneity. Second, we found study design limitations in the literature, including the lack of blinding of investigators to enhancement status in a few studies and the failure to provide interreader reproducibility measures of imaging metrics in most studies. Finally, patient-level heterogeneity in terms of disease severity and duration was present in our pooled analysis. These limitations call for larger prospective observational studies with well-defined clinical cohorts who undergo MR imaging interpreted via a rigorous, multireader blinded study design.

Our study further illustrates important knowledge gaps in understanding of the role of non-gadolinium-based techniques in characterizing MS lesions. First, although the studies included in our analysis all compared the value of quantitative biomarkers in brain regions that were enhancing-versus-nonenhancing, only a small minority presented receiver operating characteristics, from which diagnostic accuracy measures, such as sensitivity and specificity, can be derived.⁴⁶ In addition to the wide range of MS lesion biology that can be elucidated by quantitative MR imaging techniques, such receiver operating characteristic data are critical to evaluate the extent to which a specific noncontrast quantitative MR imaging technique is viable as an accurate replacement for contrast-enhanced imaging. Second, most of the included studies evaluated individual noncontrast MR imaging biomarkers in isolation, rather than in a combined, multiple parameter approach. Future studies evaluating the most promising quantitative imaging biomarkers, such as SWI and DTI metrics, in a composite, multiparametric approach are now warranted. For example, because low FA and low QSM values are independently associated with relatively acute lesions, it would be informative to perform receiver operating characteristic analysis and calculate the area under the curve of a composite imaging biomarker of low FA and low QSM in differentiating enhancing from nonenhancing MS lesions.

Although our focus was whether noncontrast quantitative MR imaging techniques are capable of detecting contrast-enhancing MS lesions, it will be critical for future research to also focus on the added value that these approaches provide to our understanding of MS lesion pathogenesis as a complement to the information provided by gadolinium enhancement. Gadolinium enhancement has been an attractive MR imaging biomarker in MS because it provides strong indirect evidence of blood-brain barrier breakdown in acute demyelinating lesions. However, the simple dichotomous characterization of MS lesions as enhancing or nonenhancing fails to capture the wide range of potentially clinically important pathophysiologic states of MS lesions, such as the chronic inflammation known to occur after the blood-brain barrier seals in MS lesions,⁴⁷ for which

non-contrast-dependent quantitative MR imaging biomarkers appear to hold significant promise.

CONCLUSIONS

Although the most widely used MS clinico-radiologic classification schemes have relied heavily on contrast enhancement as a diagnostic criterion, our systematic review and meta-analysis have revealed numerous investigations evaluating the ability of noncontrast MR imaging biomarkers to detect acute MS lesions. From this body of literature, we have found strong evidence in support of DTI-based FA as a promising approach in providing insight into lesion activity. Building on this understanding, we believe that the overall aim of future research should be to determine whether taking into account additional features of MS pathogenesis elucidated by noncontrast quantitative MR imaging techniques can increase the accuracy of MS diagnosis, improve disease prognostication, and provide a more robust marker of treatment response.

ACKNOWLEDGMENTS

The authors acknowledge Alina Jurcoane and Scott Kolbe for providing unpublished data used in this meta-analysis and to Michelle Demetres for providing peer review of the Ovid MEDLINE search strategy.

Disclosures: Ajay Gupta—RELATED: Grant: National Institutes of Health, Comments: R01NS090464*. Fei Xia—RELATED: Grant: National Institutes of Health, Comments: T35EB006732*. Yi Wang—RELATED: Grant: National Institutes of Health, Comments: R01NS072370, NS090464, NS095562*. *Money paid to the institution.

REFERENCES

1. Stojanov DA, Aracki-Trenkic A, Vojinovic S, et al. **Increasing signal intensity within the dentate nucleus and globus pallidus on unenhanced T1W magnetic resonance images in patients with relapsing-remitting multiple sclerosis: correlation with cumulative dose of a macrocyclic gadolinium-based contrast agent, gadobutrol.** *Eur Radiol* 2016;26:807–15 [CrossRef Medline](#)
2. Schlemm L, Chien C, Bellmann-Strobl J, et al. **Gadopentetate but not gadobutrol accumulates in the dentate nucleus of multiple sclerosis patients.** *Mult Scler* 2016 Sep 1. [Epub ahead of print] [CrossRef Medline](#)
3. Roccatagliata L, Vuolo L, Bonzano L, et al. **Multiple sclerosis: hyperintense dentate nucleus on unenhanced T1-weighted MR images is associated with the secondary progressive subtype.** *Radiology* 2009; 251:503–10 [CrossRef Medline](#)
4. Malayeri AA, Brooks KM, Bryant LH, et al. **National Institutes of Health Perspective on Reports of Gadolinium Deposition in the Brain.** *J Am Coll Radiol* 2016;13:237–41 [CrossRef Medline](#)
5. Polman CH, Reingold SC, Edan G, et al. **Diagnostic criteria for multiple sclerosis: 2005 revisions to the “McDonald Criteria.”** *Ann Neurol* 2005;58:840–46 [CrossRef Medline](#)
6. Stroup DF, Berlin JA, Morton SC, et al. **Meta-analysis of observational studies in epidemiology: a proposal for reporting—Meta-analysis Of Observational Studies in Epidemiology (MOOSE) group.** *JAMA* 2000;283:2008–12 [CrossRef Medline](#)
7. Liberati A, Altman DG, Tetzlaff J, et al. **The PRISMA statement for reporting systematic reviews and meta-analyses of studies that evaluate health care interventions: explanation and elaboration.** *Ann Intern Med* 2009;151:W65–94 [Medline](#)
8. Bammer R, Augustin M, Strasser-Fuchs S, et al. **Magnetic resonance diffusion tensor imaging for characterizing diffuse and focal white matter abnormalities in multiple sclerosis.** *Magn Reson Med* 2000; 44:583–91 [CrossRef Medline](#)
9. Blystad I, Hakansson I, Tisell A, et al. **Quantitative MRI for analysis of**

- active multiple sclerosis lesions without gadolinium-based contrast agent. *AJNR Am J Neuroradiol* 2016;37:94–100 CrossRef Medline
10. Droogan AG, Clark CA, Werring DJ, et al. Comparison of multiple sclerosis clinical subgroups using navigated spin echo diffusion-weighted imaging. *Magn Reson Imaging* 1999;17:653–61 CrossRef Medline
11. Faizy TD, Thaler C, Kumar D, et al. Heterogeneity of multiple sclerosis lesions in multislice myelin water imaging. *PLoS One* 2016;11:e0151496 CrossRef Medline
12. Fazekas F, Ropele S, Enzinger C, et al. Quantitative magnetization transfer imaging of pre-lesional white-matter changes in multiple sclerosis. *Mult Scler* 2002;8:479–84 CrossRef Medline
13. Filippi M, Cercignani M, Inglese M, et al. Diffusion tensor magnetic resonance imaging in multiple sclerosis. *Neurology* 2001;56:304–11 CrossRef Medline
14. Filippi M, Iannucci G, Cercignani M, et al. A quantitative study of water diffusion in multiple sclerosis lesions and normal-appearing white matter using echo-planar imaging. *Arch Neurol* 2000;57:1017–21 CrossRef Medline
15. Filippi M, Rocca MA, Martino G, et al. Magnetization transfer changes in the normal appearing white matter precede the appearance of enhancing lesions in patients with multiple sclerosis. *Ann Neurol* 1998;43:809–14 CrossRef Medline
16. Fox RJ, Cronin T, Lin J, et al. Measuring myelin repair and axonal loss with diffusion tensor imaging. *AJNR Am J Neuroradiol* 2011;32:85–91 CrossRef Medline
17. Giacomini PS, Levesque IR, Ribeiro L, et al. Measuring demyelination and remyelination in acute multiple sclerosis lesion voxels. *Arch Neurol* 2009;66:375–81 Medline
18. Goodkin DE, Rooney WD, Sloan R, et al. A serial study of new MS lesions and the white matter from which they arise. *Neurology* 1998;51:1689–97 CrossRef Medline
19. Hiehle JF Jr, Grossman RI, Ramer KN, et al. Magnetization transfer effects in MR-detected multiple sclerosis lesions: comparison with gadolinium-enhanced spin-echo images and nonenhanced T1-weighted images. *AJNR Am J Neuroradiol* 1995;16:69–77 Medline
20. Jurcoane A, Wagner M, Schmidt C, et al. Within-lesion differences in quantitative MRI parameters predict contrast enhancement in multiple sclerosis. *J Magn Reson Imaging* 2013;38:1454–61 CrossRef Medline
21. Levesque IR, Giacomini PS, Narayanan S, et al. Quantitative magnetization transfer and myelin water imaging of the evolution of acute multiple sclerosis lesions. *Magn Reson Med* 2010;63:633–40 CrossRef Medline
22. Liu Y, Mitchell PJ, Kilpatrick TJ, et al. Diffusion tensor imaging of acute inflammatory lesion evolution in multiple sclerosis. *J Clin Neurosci* 2012;19:1689–94 CrossRef Medline
23. Michoux N, Guillet A, Rommel D, et al. Texture analysis of T2-weighted MR images to assess acute inflammation in brain MS lesions. *PLoS One* 2015;10:e0145497 CrossRef Medline
24. Naismith RT, Xu J, Tutlam NT, et al. Increased diffusivity in acute multiple sclerosis lesions predicts risk of black hole. *Neurology* 2010;74:1694–701 CrossRef Medline
25. Nusbaum AO, Lu D, Tang CY, et al. Quantitative diffusion measurements in focal multiple sclerosis lesions: correlations with appearance on T1-weighted MR images. *AJR Am J Roentgenol* 2000;175:821–25 CrossRef Medline
26. Oh J, Han ET, Lee MC, et al. Multislice brain myelin water fractions at 3T in multiple sclerosis. *J Neuroimaging* 2007;17:156–63 CrossRef Medline
27. Papanikolaou N, Papadaki E, Karampekios S, et al. T2 relaxation time analysis in patients with multiple sclerosis: correlation with magnetization transfer ratio. *Eur Radiol* 2004;14:115–22 CrossRef Medline
28. Petrella JR, Grossman RI, McGowan JC, et al. Multiple sclerosis lesions: relationship between MR enhancement pattern and magnetization transfer effect. *AJNR Am J Neuroradiol* 1996;17:1041–49 Medline
29. Phuttharak W, Galassi W, Laopaiboon V, et al. ADC measurements in various patterns of multiple sclerosis lesions. *J Med Assoc Thai* 2006;89:196–204 Medline
30. Pike GB, De Stefano N, Narayanan S, et al. Multiple sclerosis: magnetization transfer MR imaging of white matter before lesion appearance on T2-weighted images. *Radiology* 2000;215:824–30 CrossRef Medline
31. Rovira A, Alonso J, Cucurella G, et al. Evolution of multiple sclerosis lesions on serial contrast-enhanced T1-weighted and magnetization-transfer MR images. *AJNR Am J Neuroradiol* 1999;20:1939–45 Medline
32. Roychowdhury S, Maldjian JA, Grossman RI. Multiple sclerosis: comparison of trace apparent diffusion coefficients with MR enhancement pattern of lesions. *AJNR Am J Neuroradiol* 2000;21:869–74 Medline
33. Sahin T, Bozgeyik Z, Menziloglu MS, et al. Importance of diffusion weighted magnetic resonance imaging in evaluation of the treatment efficacy in multiple sclerosis patients with acute attacks. *Pol J Radiol* 2015;80:544–48 CrossRef Medline
34. Testaverde L, Caporali L, Venditti E, et al. Diffusion tensor imaging applications in multiple sclerosis patients using 3T magnetic resonance: a preliminary study. *Eur Radiol* 2012;22:990–97 CrossRef Medline
35. Tievsky AL, Ptak T, Farkas J. Investigation of apparent diffusion coefficient and diffusion tensor anisotropy in acute and chronic multiple sclerosis lesions. *AJNR Am J Neuroradiol* 1999;20:1491–99 Medline
36. van den Elskamp IJ, Knol DL, Vrenken H, et al. Lesional magnetization transfer ratio: a feasible outcome for remyelinating treatment trials in multiple sclerosis. *Mult Scler* 2010;16:660–69 CrossRef Medline
37. van Waesberghe JH, van Walderveen MA, Castelijns JA, et al. Patterns of lesion development in multiple sclerosis: longitudinal observations with T1-weighted spin-echo and magnetization transfer MR. *AJNR Am J Neuroradiol* 1998;19:675–83 Medline
38. Vargas WS, Monohan E, Pandya S, et al. Measuring longitudinal myelin water fraction in new multiple sclerosis lesions. *Neuroimage Clin* 2015;9:369–75 CrossRef Medline
39. Vavasour IM, Laule C, Li DK, et al. Is the magnetization transfer ratio a marker for myelin in multiple sclerosis? *J Magn Reson Imaging* 2011;33:713–18 CrossRef Medline
40. Werring DJ, Clark CA, Barker GJ, et al. Diffusion tensor imaging of lesions and normal-appearing white matter in multiple sclerosis. *Neurology* 1999;52:1626–32 CrossRef Medline
41. Wiggermann V, Hernández Torres E, Vavasour IM, et al. Magnetic resonance frequency shifts during acute MS lesion formation. *Neurology* 2013;81:211–18 CrossRef Medline
42. Yurtsever I, Hakyemez B, Taskapiloglu O, et al. The contribution of diffusion-weighted MR imaging in multiple sclerosis during acute attack. *Eur J Radiol* 2008;65:421–26 CrossRef Medline
43. Zhang Y, Gauthier SA, Gupta A, et al. Longitudinal change in magnetic susceptibility of new enhanced multiple sclerosis (MS) lesions measured on serial quantitative susceptibility mapping (QSM). *J Magn Reson Imaging* 2016;44:426–32 CrossRef Medline
44. Zivadinov R, Bergsland N, Stosic M, et al. Use of perfusion- and diffusion-weighted imaging in differential diagnosis of acute and chronic ischemic stroke and multiple sclerosis. *Neurol Res* 2008;30:816–26 CrossRef Medline
45. Zhang Y, Gauthier SA, Gupta A, et al. Magnetic susceptibility from quantitative susceptibility mapping can differentiate new enhancing from nonenhancing multiple sclerosis lesions without gadolinium injection. *AJNR Am J Neuroradiol* 2016 Jun 30. [Epub ahead of print] Medline
46. Fryback DG, Thornbury JR. The efficacy of diagnostic imaging. *Med Decis Making* 1991;11:88–94 CrossRef Medline
47. Vellinga MM, Oude Engberink RD, Seewann A, et al. Pluriformity of inflammation in multiple sclerosis shown by ultra-small iron oxide particle enhancement. *Brain* 2008;131:800–07 CrossRef Medline

Neuroradiologists Compared with Non-Neuroradiologists in the Detection of New Multiple Sclerosis Plaques

 W. Wang,  J. van Heerden,  M.A. Tacey, and  F. Gaillard

ABSTRACT

BACKGROUND AND PURPOSE: Multiple sclerosis monitoring is based on the detection of new lesions on brain MR imaging. Outside of study populations, MS imaging studies are reported by radiologists with varying expertise. The aim of this study was to investigate the accuracy of MS reporting performed by neuroradiologists (someone who had spent at least 1 year in neuroradiology subspecialty training) versus non-neuroradiologists.

MATERIALS AND METHODS: Patients with ≥ 2 MS studies with 3T MR imaging that included a volumetric T2 FLAIR sequence performed between 2009 and 2011 inclusive were recruited into this study. The reports for these studies were analyzed for lesions detected, which were categorized as either progressed or stable. The results from a previous study using a semiautomated assistive software for lesion detection were used as the reference standard.

RESULTS: There were 5 neuroradiologists and 5 non-neuroradiologists who reported all studies. In total, 159 comparison pairs (ie, 318 studies) met the selection criteria. Of these, 96 (60.4%) were reported by a neuroradiologist. Neuroradiologists had higher sensitivity (82% versus 42%), higher negative predictive value (89% versus 64%), and lower false-negative rate (18% versus 58%) compared with non-neuroradiologists. Both groups had a 100% positive predictive value.

CONCLUSIONS: Neuroradiologists detect more new lesions than non-neuroradiologists in reading MR imaging for follow-up of MS. Assistive software that aids in the identification of new lesions has a beneficial effect for both neuroradiologists and non-neuroradiologists, though the effect is more profound in the non-neuroradiologist group.

ABBREVIATIONS: NNR = non-neuroradiologist; NR = neuroradiologist; VT = VisTarsier

Multiple sclerosis is the most common disease of the central nervous system in young patients, with a major impact on patients' lives.¹ Over the past decade, a number of disease-modifying drugs that are especially effective during early disease have been developed. Neurologists increasingly are aiming for zero disease progression and, in many instances, will alter management when progression is detected.² Because most demyelinating lesions are clinically occult, MR imaging has become the primary biomarker for disease progression. Both physical and cognitive disability have been shown to have a nonplateauing association with white matter demyelinating lesion burden as seen on T2-weighted and T2-weighted FLAIR sequences.^{2–6} Detecting new

lesions can be an arduous task, particularly when there is a large number of pre-existing lesions.

Outside of study populations, MS MR imaging studies are reported by radiologists with varying expertise, ranging from general radiologists to fellowship-trained neuroradiologists. Although the accuracy of neuroradiologists (NRs) versus non-neuroradiologists (NNRs) has been examined in a number of settings, with varying results,^{7,8} to our knowledge, no studies to date have investigated the efficacy of NR versus NNR reporting for MS.

We aimed to investigate the accuracy of MS reporting performed by NRs versus NNRs, with results from a previously published validated semiautomated assistive software platform (VisTarsier; VT) as a "gold standard." In this study, we hypothesized that nonspecialty reporters would perform at a slightly lower accuracy compared with subspecialty reporters.

MATERIALS AND METHODS

Patient Recruitment

Institutional ethics board approval was obtained at the Royal Melbourne Hospital. The hospital PACS was queried for MR imaging

Received December 15, 2016; accepted after revision February 9, 2017.

From the Department of Radiology (W.W., F.G.) and Melbourne Epicentre (M.A.T.), the Royal Melbourne Hospital, Parkville, Victoria, Australia; and Perth Radiological Clinic (J.v.H.), Subiaco, Western Australia, Australia.

Please address correspondence to Dr Wayland Wang, Department of Radiology, the Royal Melbourne Hospital, Grattan St, Parkville 3050, Melbourne, Victoria, Australia; e-mail: wayland.wang@gmail.com

<http://dx.doi.org/10.3174/ajnr.A5185>

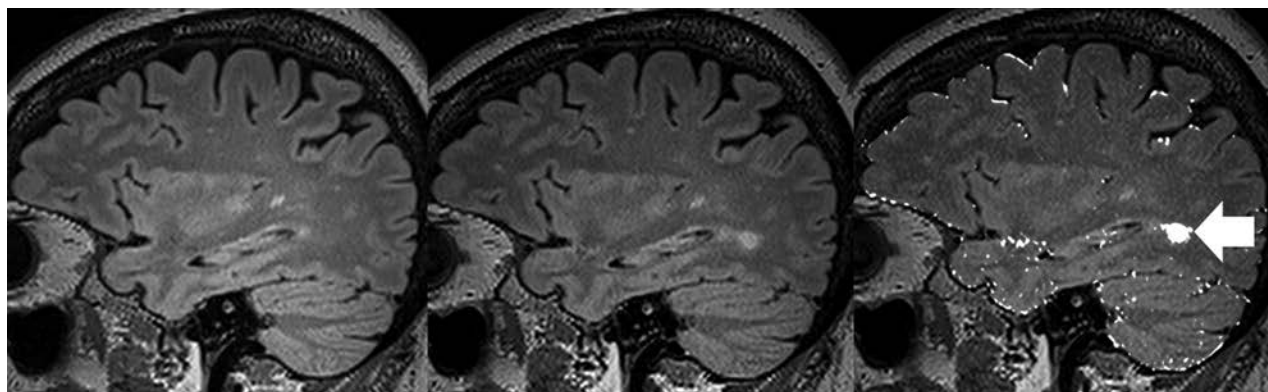


FIG 1. Example of VisTarsier output. From left: volumetric sagittal T2 FLAIR of previous study; volumetric sagittal T2 FLAIR of current study; and “New Lesions” map. NB: the usual output of the “New Lesions” map is colored in orange, whereas it is shown here colored *white*. The new lesion has been highlighted (*arrow*). There are slight misregistration errors at the edges of the brain, which can be dismissed as such by comparing the 2 studies on the left.

brain demyelination-protocol studies performed on a single 3T magnet (Tim Trio, 12-channel head coils; Siemens, Erlangen, Germany), between 2009 and 2011 inclusive, for patients who had ≥ 2 studies during that period. Eligibility criteria were the following: consecutive studies in patients with a confirmed diagnosis of MS (based on information provided on requisition forms), reported by a radiologist working at our institution, and availability of a diagnostic-quality MR imaging volumetric T2 FLAIR sequence (FOV, 250; 160 sections; section thickness, 0.98 mm; matrix, 258×258 ; TR, 5000 ms; TE, 350 ms; TI, 1800 ms; 72 sel inversion recovery magnetic preparation).

Data Analysis

A semiautomated software package (VT) has previously been validated and shown to detect an increased number of new lesions in patients with MS compared with conventional side-by-side comparison.⁹ The development of the software processing tool and data processing procedure has been described in that earlier study. All of the patients included in this study have been reported previously.⁹ The prior article described the development, implementation, and outcome of the semiautomated software package, whereas the current study reports the differences between NRs and NNRs in reporting MS studies by using the outcomes from the previous study as a “gold standard.”

All MS MR imaging studies were performed for routine clinical purposes and analyzed by a full-time academic radiologist at our institution (the Royal Melbourne Hospital) without the benefit of VT. These clinical radiology reports were obtained retrospectively from the institutional radiology information system archive. Each report was analyzed for new demyelinating lesions detected, which was recorded as a binary value of either “progression” (1 or more new lesions) or “stable” (no new lesions). For each reporting radiologist, we summarized the total number of reports and whether any new lesions were detected. This dataset had already been analyzed by 2 blinded neuroradiology-trained readers (J.v.H., F.G.) using VT and was used as a “gold standard” for lesion detection. An example of the VT output is displayed in Fig 1. Importantly, the reporting radiologists had the full diagnostic gamut of conventional imaging sequences available for review, excluding VT change maps, whereas the VT dataset used only the

change maps from VT (by using volumetric T2 FLAIR) in new lesion detection.⁹

Reporting radiologists were categorized as NR, defined as someone who had spent at least 1 year in a neuroradiology fellowship program, or NNR, defined as someone who has not had specific subspecialist training in neuroradiology.

Statistics

There were 5 neuroradiologists and 5 non-neuroradiologists in our group. Patient demographic data were analyzed with a Student *t* test (unpaired) to test differences between the ages in the NR and NNR groups, and χ^2 tests were applied to test for differences between sex distributions in the 2 groups.

Sensitivity, specificity, positive predictive value, and negative predictive value were calculated for each group by using VT outcomes as the “gold standard.” A false-negative rate was also calculated for each group. These are presented as descriptive values.

As a further breakdown of NR versus NNR MS reporting, the variables associated with a false-negative reporting status were also assessed, with univariate analysis considering the effects of sex, age, number of lesions, and radiologist subgroup on the false-negative status. Variables identified with a *P* value $< .20$ from univariate analysis were included in the multivariate model, and manual backwards stepwise regression techniques were used to identify those variables independently associated with false-negative status.

A 2-tailed *P* value $< .05$ was considered to indicate statistical significance. STATA statistical analysis software (version 12.1) was used (StataCorp, College Station, Texas).

RESULTS

In total, 159 comparison pairs (318 studies) met the above inclusion criteria. These pairs were drawn from 146 individual patients, of which 111 were women (76.0%) with a mean age of 44.9 years ± 10.7 (SD). Of the 159 pairs, 96 (60.4%) were reported by the 5 NRs, and 63 (39.6%) were reported by the 5 NNRs. Individual radiologist reporting numbers ranged from 7–43 for the NR group and 2–24 for the NNR group. There were no differences in patient demographics between the NR and NNR read groups

(mean age \pm SD, 44.3 years \pm 9.7 versus 45.8 years \pm 12.0; $P = .415$; proportion of women, 76.4% versus 75.4%; $P = .664$).

The VT-aided assessments reported 70 studies showing progression (ie, 1 or more new lesions). Of these, 39 were in the NR group and 31 in the NNR group. In comparison, 32 NR reports recorded progression, and 13 NNR reports recorded progression. The sensitivity, specificity, positive predictive value, and negative predictive value of NRs, NNRs, and the entire cohort in relation to new lesion detection are presented in Table 1. There was a higher level of sensitivity (82% versus 42%) and negative predictive value (89% versus 64%) in the NR group compared with the NNR group, with an associated lower level of false-negative reports (18% versus 58%) when treating VT-aided assessments as the “gold standard.”

An individual breakdown of true-positives and false-negatives

Table 1: Sensitivity, specificity, positive predictive value, negative predictive value, and false-negative rate for neuroradiologists, non-neuroradiologists, and the combined cohort

| | NR | NNR | Combined |
|-------------|--------------|--------------|--------------|
| Sensitivity | 82% (32/39) | 42% (13/31) | 64% (45/70) |
| Specificity | 100% (57/57) | 100% (32/32) | 100% (89/89) |
| PPV | 100% (32/32) | 100% (13/13) | 100% (45/45) |
| NPV | 89% (57/64) | 64% (32/50) | 78% (89/114) |
| FN rate | 18% (7/39) | 58% (18/31) | 36% (25/70) |

Note:—FN indicates false-negative; NPV, negative predictive value; PPV, positive predictive value.

Table 2: Reporting radiologist breakdown

| | Total | TP | FN ^a | FN Rate |
|------|-------|----|-----------------|---------|
| NR1 | 10 | 4 | 0 | 0.0% |
| NR2 | 21 | 11 | 1 | 4.8% |
| NR3 | 15 | 7 | 1 | 6.7% |
| NR4 | 43 | 14 | 3 | 7.0% |
| NR5 | 7 | 3 | 2 | 29% |
| NNR1 | 21 | 9 | 4 | 19% |
| NNR2 | 5 | 0 | 1 | 20% |
| NNR3 | 24 | 13 | 6 | 25% |
| NNR4 | 11 | 6 | 5 | 45% |
| NNR5 | 2 | 0 | 2 | 100% |

Note:—FN indicates false-negative; TP, true positive.

^a A false-negative is defined as at least one new lesion detected using VT that was not detected in the clinical assessment of the study without the use of VT.

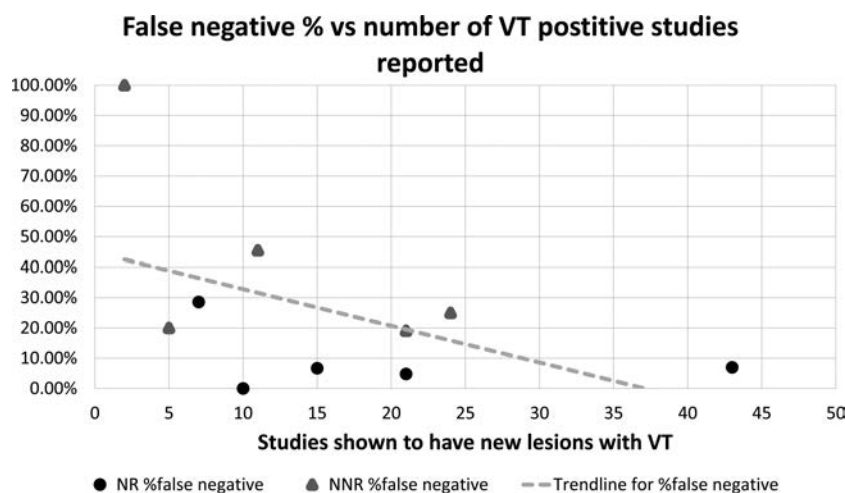


FIG 2. False-negative percent versus all reported studies for all radiologists included in this study.

for each reporting radiologist is presented in Table 2. These data are also presented as a graph in Fig 2.

An assessment of the effect of age and sex on false-negative rates was not significant ($P = .452$ for age and $P = 1.00$ for sex) (Table 3). The NR group outperformed the NNR group, with 7/96 false-negatives compared with 18/63 ($P < .001$). As expected, all false-negatives occurred when VT detected at least 1 new lesion, with the number of lesions also found to be higher for those patients with a false-negative status ($P < .001$).

Multivariate analysis showed that the NNR group had a much higher false-negative rate compared with the NR group (OR, 7.88; 95% CI, 3.10–19.4; $P < .001$), with having more than 1 lesion also being independently associated with false-negative status (OR, 11.94; 95% CI, 4.72–30.19; $P < .001$).

DISCUSSION

The practice of MR imaging radiology is fairly heterogeneous depending on country, size of practice, and personal preference, with studies reported in some instances by general radiologists and at other times by subspecialty radiologists. Conventional MS follow-up study reading techniques have been shown to be subjective and dependent on the skill and consistency of the reader.¹⁰ There have been many proposed solutions to facilitate time-efficient, reproducible, and accurate lesion detection, including semiautomated and fully automated techniques. Although many of these various proposed methods show promising results, the results are usually in small samples and generally have not entered routine clinical use.¹¹

A previous study has shown that a semiautomated assistive platform is fast, robust, and detects many more new lesions on MR imaging of patients with MS than conventional side-by-side comparison.⁹ The same software has also been shown to perform similarly when used by readers of different radiology experience, including readers with minimal radiology experience.¹² This new approach allowed us to use it as a new “gold standard” against which we can measure the performance of radiologists of various levels of subspecialty experience.

Other studies have shown no significant difference in NR versus NNR in stroke CT imaging,¹³ significant discrepancy between NNR and second-opinion NR reporting,⁷ and increased accuracy of interpretation in brain MR imaging by tertiary center NRs compared with external institutions.⁸ Some of the aforementioned studies have showed the utility of second-opinion subspecialty reporting in neuroradiology.^{7,8} However, in these studies, the original reports were over-read by an NR, whereas in our study, the 2 groups are independent of one another.

To our knowledge, no previous study has directly compared the performance of NNRs with subspecialty NRs in reporting a cohort of MR imaging for the same indication against a validated external “gold standard.”

Table 3: Univariate associations between variables and false-negative reporting status

| Variable | Correct | False-Negative | P Value |
|---|-----------------|-----------------|---------|
| Total, no. (%) | 134 (84.3) | 25 (15.7) | N/A |
| Age, yr (Mean \pm SD) | 44.5 \pm 10.6 | 46.2 \pm 10.3 | .452 |
| Gender, no. (%) | | | 1.000 |
| Female | 100 (74.6) | 19 (76.0) | |
| Male | 34 (25.4) | 6 (24.0) | |
| Lesions found with VT | 0 (0–1) | 2 (1–3) | <.001 |
| Lesions found with VT category, no. (%) | | | .031 |
| ≤ 2 | 111 (82.8) | 16 (64.0) | |
| > 2 | 23 (17.2) | 9 (36.0) | |
| Lesions found with VT category, no. (%) | | | <.001 |
| ≤ 1 | 102 (76.1) | 7 (28.0) | |
| > 1 | 32 (23.9) | 18 (72.0) | |
| Lesions found with VT category, no. (%) | | | <.001 |
| ≤ 0 | 89 (66.4) | 0 | |
| > 0 | 45 (33.6) | 25 (100.0) | |
| Group, no. (%) | | | <.001 |
| NR | 89 (66.4) | 7 (28.0) | |
| NNR | 45 (33.6) | 18 (72.0) | |
| Reporter, no. (%) | | | .277 |
| NR | | | |
| Reporter 1 | 10 (11.2) | 0 | |
| Reporter 2 | 40 (44.9) | 3 (42.9) | |
| Reporter 3 | 14 (15.7) | 1 (14.3) | |
| Reporter 4 | 5 (6.6) | 2 (28.6) | |
| Reporter 5 | 20 (22.5) | 1 (14.3) | |
| NNR | | | .123 |
| Reporter 1 | 0 | 2 (11.1) | |
| Reporter 2 | 4 (8.9) | 1 (5.6) | |
| Reporter 3 | 17 (37.8) | 4 (22.2) | |
| Reporter 4 | 18 (40.0) | 6 (33.3) | |
| Reporter 5 | 6 (13.3) | 5 (27.8) | |

Note:—N/A indicates not available.

The main finding of our study is that NRs performed better than NNRs in the conventional reading of MS studies in terms of better sensitivity, better negative predictive value, and lower false-negative rate. Specificity and positive predictive value were at an expected 100%, as there were no false-positives in our cohort. Among individual radiologists, the false-negative rate ranged from 0%–29% for NRs and 19%–100% for NNRs. The caveat is that the radiologist with a 100% false-negative rate had only reported 2 MS studies during the recruitment period.

In addition, we have also demonstrated that even when only grouping results into 2 or more lesions, versus 1 or 0 lesions, there is a much higher false-negative rate among NNRs compared with NRs (OR, 7.88) when taking into account other variables such as number of studies and patient demographics. This is potentially an important finding because, in some circumstances, a solitary asymptomatic lesion may not be sufficient for neurologists to consider treatment change.

There is a trend toward subspecialty reporting in North America. This is also the case in many other countries, though it is our direct experience that until all neuroradiology studies are reported by subspecialty-trained radiologists, general radiologists will choose to report studies that are perceived to require less subspecialty expertise. Follow-up MS studies are anecdotally of-

ten thought of as only requiring identification of new lesions, a task that is felt to be both cognitively simple and requiring less interpretation. Our findings suggest that this assumption is incorrect and that experience has a significant impact on the accuracy of detecting new lesions. As such, we believe this study not only supports the general move toward subspecialty reporting, but also suggests that there may not be such a thing as an “easy” study.

This study has a number of weaknesses. The largest and most difficult to control for is the fact that subspecialty-trained NRs also tend to report the greatest number of neuroradiology studies and would, in most cases, have done so more consistently over a longer period of time. We attempted to control for the overall number of neuroradiology studies reported by the included radiologist, though this proved to be impractical because of differences in years of experience, number of days worked during the study period, and variability in the type of studies some radiologists chose to report. As such, establishing the effect size of subspecialty training versus experience was not possible. Having said that, if looking at only the 2 most prolific reporters of MS studies from each group, each with more than 20 studies (having reported 64/96 of the studies from the NR group and 45/63 from the NNR group), the results are fairly similar to the entire cohort in that the false-negative rate in the NR group is much lower (6.3% versus 22%). Thus, we feel that the conclusion that NRs are more accurate than NNRs is broadly valid, even if the reason for this is not clear. It is important to note that we are not suggesting a simple direct causative link between subspecialty fellowship training and diagnostic accuracy, but rather using fellowship training as a pragmatic marker of a number of related factors that are likely to be contributory.

Another limitation of this study is that each study pair was reviewed by a single radiologist. Ideally, all 159 study pairs would have been read by each of the involved radiologists. However, this was beyond the scope of this study, which used pre-existing, retrospective data from an earlier study. In some ways, this is not a weakness, in that the clinical reports used are truly reflective of everyday practice rather than a somewhat artificial trial setting.

Future Work

This work has focused on differences in traditional side-by-side comparison interpretation of MS MR imaging studies. It would be interesting, and is our plan, to evaluate how much individual benefit would be gained by radiologists of different subspecialty experience by using assistive software (VT). Another avenue of research is to plot the number of studies per year against performance and determine whether there is a plateau, which could inform a minimum of studies that should be read per year to maintain competence, as is the case in some countries for cardiac CT and CT colonoscopy.

CONCLUSIONS

Neuroradiologists detect more new lesions than non-neuroradiologists in reading MR imaging for follow-up of MS. Assistive software that aids in the identification of new lesions has a beneficial effect for both neuroradiologists and non-neuroradiolo-

gists, though the effect is more profound in the non-neuroradiologist group.

REFERENCES

1. Jones JL, Coles AJ. **New treatment strategies in multiple sclerosis.** *Exp Neurol* 2010;225:34–39 [CrossRef Medline](#)
2. Weiner HL. **The challenge of multiple sclerosis: how do we cure a chronic heterogeneous disease?** *Ann Neurol* 2009;65:239–48 [CrossRef Medline](#)
3. Mortazavi D, Kouzani AZ, Soltanian-Zadeh H. **Segmentation of multiple sclerosis lesions in MR images: a review.** *Neuroradiology* 2012;54:299–320 [CrossRef Medline](#)
4. Caramanos Z, Francis SJ, Narayanan S, et al. **Large, nonplateauing relationship between clinical disability and cerebral white matter lesion load in patients with multiple sclerosis.** *Arch Neurol* 2012;69: 89–95 [CrossRef Medline](#)
5. Sormani MP, Rovaris M, Comi G, et al. **A reassessment of the plateauing relationship between T2 lesion load and disability in MS.** *Neurology* 2009;73:1538–42 [CrossRef Medline](#)
6. Fisniku LK, Brex PA, Altmann DR, et al. **Disability and T2 MRI lesions: a 20-year follow-up of patients with relapse onset of multiple sclerosis.** *Brain* 2008;131(Pt 3):808–17 [CrossRef Medline](#)
7. Briggs GM, Flynn PA, Worthington M, et al. **The role of specialist neuroradiology second opinion reporting: is there added value?** *Clin Radiol* 2008;63:791–95 [CrossRef Medline](#)
8. Zan E, Yousem DM, Carone M, et al. **Second-opinion consultations in neuroradiology.** *Radiology* 2010;255:135–41 [CrossRef Medline](#)
9. van Heerden J, Rawlinson D, Zhang AM, et al. **Improving multiple sclerosis plaque detection using a semiautomated assistive approach.** *AJNR Am J Neuroradiol* 2015;36:1465–71 [CrossRef Medline](#)
10. Abraham AG, Duncan DD, Gange SJ, et al. **Computer-aided assessment of diagnostic images for epidemiological research.** *BMC Med Res Methodol* 2009;9:74 [CrossRef Medline](#)
11. Vrenken H, Jenkinson M, Horsfield MA, et al. **Recommendations to improve imaging and analysis of brain lesion load and atrophy in longitudinal studies of multiple sclerosis.** *J Neurol* 2013;260: 2458–71 [CrossRef Medline](#)
12. Dahan A, Wang W, Tacey MA, et al. **Can medical professionals with minimal-to-no neuroradiology training monitor MS disease progression using semiautomated imaging software?** *Neurology* 2016; 86(16 Supplement):P2.151
13. Jordan YJ, Jordan JE, Lightfoote JB, et al. **Quality outcomes of reinterpretation of brain CT studies by subspecialty experts in stroke imaging.** *AJR Am J Roentgenol* 2012;199:1365–70 [CrossRef Medline](#)

Diffusional Kurtosis Imaging and Motor Outcome in Acute Ischemic Stroke

M.V. Spampinato, C. Chan, J.H. Jensen, J.A. Helpert, L. Bonilha, S.A. Kautz, P.J. Nietert, and W. Feng



ABSTRACT

BACKGROUND AND PURPOSE: Motor impairment is the most common deficit after stroke. Our aim was to evaluate whether diffusional kurtosis imaging can detect corticospinal tract microstructural changes in the acute phase for patients with first-ever ischemic stroke and motor impairment and to assess the correlations between diffusional kurtosis imaging–derived diffusion metrics for the corticospinal tract and motor impairment 3 months poststroke.

MATERIALS AND METHODS: We evaluated 17 patients with stroke who underwent brain MR imaging including diffusional kurtosis imaging within 4 days after the onset of symptoms. Neurologic evaluation included the Fugl-Meyer Upper Extremity Motor scale in the acute phase and 3 months poststroke. For the corticospinal tract in the lesioned and contralateral hemispheres, we estimated with diffusional kurtosis imaging both pure diffusion metrics, such as the mean diffusivity and mean kurtosis, and model-dependent quantities, such as the axonal water fraction. We evaluated the correlations between corticospinal tract diffusion metrics and the Fugl-Meyer Upper Extremity Motor scale at 3 months.

RESULTS: Among all the diffusion metrics, the largest percentage signal changes of the lesioned hemisphere corticospinal tract were observed with axial kurtosis, with an average 12% increase compared with the contralateral corticospinal tract. The strongest associations between the 3-month Fugl-Meyer Upper Extremity Motor scale score and diffusion metrics were found for the lesioned/contralateral hemisphere corticospinal tract mean kurtosis ($\rho = -0.85$) and axial kurtosis ($\rho = -0.78$) ratios.

CONCLUSIONS: This study was designed to be one of hypothesis generation. Diffusion metrics related to kurtosis were found to be more sensitive than conventional diffusivity metrics to early poststroke corticospinal tract microstructural changes and may have potential value in the prediction of motor impairment at 3 months.

ABBREVIATIONS: CST = corticospinal tract; D_a = intra-axonal diffusivity; DKI = diffusional kurtosis imaging; FA = fractional anisotropy; FM-UE = Fugl-Meyer Upper Extremity Motor; $K_{||}$ = axial kurtosis; K_{\perp} = radial kurtosis; $\lambda_{||}$ = axial diffusivity; λ_{\perp} = radial diffusivity; MD = mean diffusivity; MK = mean kurtosis

Motor impairment caused by injury of the motor pathways is the most common deficit after stroke.¹ While a proportion of patients with acute stroke with motor deficits will have func-

tional recovery, the degree of motor recovery is highly variable.² Clinical assessment of motor impairment in the acute phase is a significant predictor of chronic motor outcome.³ However, for patients with severe initial motor impairment, long-term motor outcome is only weakly predicted by the degree of motor impairment in the acute phase.⁴ Thus, it remains difficult to make an accurate motor outcome prediction for an individual patient with information collected in the acute phase. If clinicians had access to an early marker of motor pathway injury and were able to predict motor outcome, stroke recovery could be greatly improved by delivering treatment to those individuals who are likely to benefit from intervention.

The integrity of the corticospinal tract (CST) is critical for

Received August 8, 2016; accepted after revision February 13, 2017.

From the Department of Radiology and Radiological Science (M.V.S., C.C., J.H.J., J.A.H.), Center for Biomedical Imaging (M.V.S., C.C., J.H.J., J.A.H.), Department of Health Sciences and Research (S.A.K.), Department of Public Health Sciences (P.J.N., W.F.), and Department of Neurology (L.B., W.F., J.A.H.), Medical University of South Carolina, Charleston, South Carolina; and Ralph H. Johnson VA Medical Center (S.A.K.), Charleston, South Carolina.

This work was supported, in part, by the South Carolina Clinical and Translational Research Institute at the Medical University of South Carolina, funded by the National Institutes of Health, National Center for Advancing Translational Science (grant No. UL1TR001450). Dr Feng was supported by American Heart Association (14SDG1829003) and Drs Feng, Bonilha, and Kautz were supported by National Institute of Health (P20 GM109040).

Please address correspondence to Maria Vittoria Spampinato, MD, Department of Radiology and Radiological Science, Medical University of South Carolina, 96 Jonathan Lucas, MSC 323, Charleston, SC 29425; e-mail: spampin@musc.edu; @mvspampinato

Indicates open access to non-subscribers at www.ajnr.org

Indicates article with supplemental on-line table.

<http://dx.doi.org/10.3174/ajnr.A5180>

recovery of motor function in stroke.⁵ Identification of early CST microstructural changes in patients with acute stroke would improve our ability to predict motor recovery and plan rehabilitative treatment. DTI can quantify early CST microstructural changes in patients with stroke with motor impairment.^{6–10} However, a limitation of DTI is that the data analysis approximates the water diffusion dynamics within brain tissue as being a Gaussian process, though substantial non-Gaussian diffusion effects are observed throughout the brain. Hence, DTI does not fully characterize water diffusion in the brain. Diffusional kurtosis imaging (DKI) is a clinically feasible diffusion MR imaging method, which extends the DTI model to include non-Gaussian diffusion effects.^{11,12} As a result, DKI has the potential to provide more sensitive biomarkers for probing microscopic structural changes.¹³ In addition, white matter tract integrity metrics can be obtained from the DKI dataset by using a model that describes the microstructural characteristics in the extra- and intra-axonal compartments of WM.¹⁴ To our knowledge, no prospective studies have previously assessed the role of DKI in the prediction of motor outcome after stroke.

Our objectives were to evaluate whether DKI-derived diffusion metrics can detect early CST microstructural changes 1–4 days after first-ever acute ischemic stroke and motor impairment and to assess the correlations between CST DKI-derived metrics and 3-month motor outcome measured by using the Fugl-Meyer Upper Extremity Motor (FM-UE) scale.

MATERIALS AND METHODS

Subjects

The local institutional review board approved the study. Patients with first-ever ischemic stroke with various degrees of motor impairment were enrolled in this prospective observational study. Written informed consent was obtained from all patients or their legal representatives. Inclusion criteria were the following: 18–80 years of age; first-ever ischemic stroke involving only 1 hemisphere, confirmed by MR imaging; brain MR imaging, including DKI, performed between 1 and 4 days after stroke onset; prestroke mRS ≤ 1 ; and unilateral motor impairment at baseline with an FM-UE scale score of ≤ 56 of 66 (to avoid recovery ceiling effect). We excluded any subject with intracranial hemorrhage, other neurologic disorders affecting limb motor function, severe dementia, recurrent stroke, or death during the 3-month follow-up.

A detailed neurologic examination was performed by a stroke neurologist in the acute phase and at a 3-month follow-up visit. The baseline examination included the FM-UE scale and the NIHSS (Table 1). During the 3-month follow-up examination, the FM-UE scale, NIHSS, and mRS scores were obtained. The FM-UE scale, a motor assessment scale with excellent intra- and interrater reliability, represented the primary motor outcome variable (the maximum score is 66 points; higher scores indicate less severe impairment).¹⁵ We also calculated the percentage change of the FM-UE scale between the baseline and 3-month evaluation. For descriptive purposes, patients were divided into 3 cohorts based on the 3-month FM-UE scale: 1) upper limb remained essentially plegic (FM-UE ≤ 9); 2) patients with well-defined upper limb mass flexion and extension synergy-dependent movements (FM-UE = 10–18); and 3) patients with

Table 1: Patient clinical characteristics and demographics (N = 17)

| Demographics and Characteristics | |
|--|-------------|
| Age (yr) ^a | 55.7 (12.3) |
| Men | 64.7% |
| Race (white/African American) | 12/5 |
| Lesion side (right) | 70.6% |
| Stroke etiology | |
| Small-vessel disease | 35.3% |
| Cardioembolism | 17.6% |
| Large-vessel atherosclerosis | 29.4% |
| Unknown | 17.6% |
| rtPA or reperfusion therapy | 41.2% |
| Hypertension | 82.4% |
| Diabetes mellitus | 35.3% |
| Dyslipidemia | 70.6% |
| Atrial fibrillation | 23.5% |
| Coronary artery disease | 11.8% |
| Antiplatelet use | 88.2% |
| Anticoagulation use | 17.6% |
| Statin on discharge | 82.3% |
| Smoking on admission | 47.1% |
| Length of hospital stay (days) ^a | 5.8 (3.8) |
| Clinical assessment | |
| Days between stroke onset and MRI ^a | 2.0 (1.0) |
| Days from stroke onset to baseline assessment ^a | 2.6 (1.5) |
| Days from admission to follow-up visit ^a | 94.1 (9.6) |
| Median No. of days of rehabilitation therapy | 34 (18.1) |
| Baseline NIHSS score ^a | 11.2 (6.5) |
| 3-mo NIHSS score ^a | 4.9 (3.9) |
| Baseline FM-UE scale ^a | 19.1 (16.9) |
| 3-month FM-UE scale ^a | 29.1 (22.0) |
| Median 3-mo mRS (range) | 3 (1–4) |
| Location of infarction (No.) (%) | |
| Right hemisphere | 12 (70.5) |
| Left hemisphere | 5 (29.5) |
| Motor cortex | 6 (35.3) |
| Premotor cortex | 5 (29.5) |
| Centrum semiovale | 4 (23.5) |
| Corona radiata | 9 (52.9) |
| Posterior limb of the internal capsule | 9 (52.9) |
| Brain stem | 4 (23.5) |

^a Mean (SD).

recovery of isolated upper limb movements (FM-UE ≥ 19).¹⁶ We also recorded the total number of days each patient received rehabilitative therapy (including physical therapy and/or occupational therapy during rehabilitation, at home, and during outpatient visits) between the stroke and the 3-month follow-up.

Imaging

Brain MRIs were performed on a 1.5T MR imaging scanner. A sagittal T1-weighted MPRAGE (voxel size, $1 \times 1 \times 1 \text{ mm}^3$) sequence was performed. Axial diffusion-weighted images were acquired with 3 b-values (0, 1000, and 2000 s/mm^2) along 30 diffusion-encoding directions by using a single-shot twice-refocused spin-echo EPI sequence with NEX = 1 (NEX = 10 for $b=0$). Imaging parameters of the diffusion sequence were the following: voxel size = $3 \times 3 \times 3 \text{ mm}^3$, number of sections = 40, TR/TE = 5500/99 ms, FOV = $222 \times 222 \text{ mm}^2$, acquisition matrix = 74×74 , bandwidth/pixel = 1325 Hz, acceleration factor = 2, acquisition time ≈ 7 minutes.

Using Diffusional Kurtosis Estimator software¹⁷ (Version 2.6; <https://www.nitrc.org/projects/dke/>) implemented in Matlab (MathWorks, Natick, Massachusetts), we calculated the diffusion

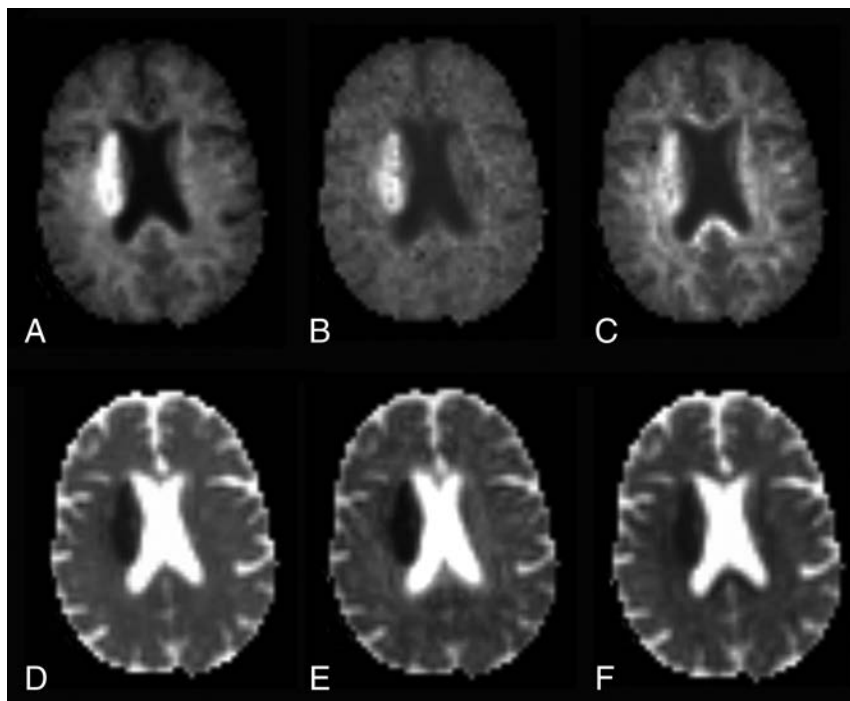


FIG 1. Mean kurtosis (A), axial kurtosis (B), radial kurtosis (C), mean diffusivity (D), axial diffusivity (E), and radial diffusivity (F) maps obtained from the DKI dataset in a representative patient with acute ischemic infarct of the right corona radiata.

and kurtosis tensors on a voxel-by-voxel basis. Parametric maps for the following metrics were obtained from the DKI dataset: 1) diffusivity metrics: fractional anisotropy (FA), mean diffusivity (MD), axial (λ_{\parallel}), and radial diffusivity (λ_{\perp}); 2) kurtosis metrics: mean kurtosis (MK), axial (K_{\parallel}), and radial kurtosis (K_{\perp}) (Fig 1),¹¹ in which MK is the average kurtosis over all diffusion directions, K_{\parallel} is the kurtosis in the direction of the diffusion tensor eigenvector with the largest diffusion eigenvalue (typically along the direction of the axons), and K_{\perp} is the average kurtosis over all directions perpendicular to the diffusion eigenvector with the largest eigenvalue (typically all directions perpendicular to the axons); and 3) white matter tract integrity metrics: axonal water fraction, intra-axonal diffusivity (D_a), axial extra-axonal diffusivity, and radial extra-axonal diffusivity. White matter tract integrity metrics were obtained from the DKI dataset in WM voxels consisting of aligned fiber bundles (defined here as $FA \geq 0.3$).¹⁴ In the white matter tract integrity model, axonal fiber bundles are idealized as impermeable, cylindric tubes, and the axonal water fraction represents the fraction of diffusion MR imaging-visible water contained within the tubes. Water within myelin is thus neglected because it contributes little to the diffusion MR imaging signal due to its short T2 relaxation time. Qualitatively, the axonal water fraction can be regarded as an index of axonal fiber density. D_a is a measure of intrinsic diffusivity inside the axons. The remainder of the WM is modeled as the extra-axonal space, and axial extra-axonal diffusivity and radial extra-axonal diffusivity are markers of changes in extra-axonal diffusivity.

Fiber tracking of the CST was performed by using DSI Studio (<http://dsi-studio.labsolver.org>) with a generalized deterministic tracking algorithm that uses quantitative anisotropy as the termination index.¹⁸ The CST was reconstructed as previously de-

scribed¹⁹ in accordance with the following steps: The tractography seed point was obtained by manually placing an ROI on each CST at the level of the rostral pons on the color-coded FA maps, and the tractography end point was obtained by manually placing a gray matter ROI on the ipsilateral precentral gyrus (anisotropy threshold = 0.2; angular threshold = 40°; step size = 1 mm; track length = ≥ 50 mm; number of seeds = 10,000). The lesioned hemisphere CST could be reliably identified at the rostral pons in all subjects, even in patients with large infarctions. We added a logical “and” function so that only streamlines passing through both ROIs were included for further analysis. Fiber tracts were generated of the left and right CST. A neuroradiologist, blinded to demographic information and clinical data, visually inspected the CST tracts overlaid on the FA map for quality control purposes. Then, left and right CST tracts were converted to VOIs in native diffusion space. Average diffusion values of the CST VOIs were computed for all diffusion metrics and

subjects by using Matlab. Lesioned hemisphere/contralateral hemisphere CST ratios were computed for all diffusion metrics.

Multisection VOIs of the infarct were identified by a neuroradiologist, blinded to demographic and clinical information, on the diffusion-weighted images with b-values of 2000 s/mm² with the intensity filter module of MRICron (<http://www.mccauslandcenter.sc.edu/crnl/mricron/>). The volumes of the infarct VOI, ipsilateral CST VOI, and the intersection between the CST and infarct VOIs were calculated by using MRICron.

Statistical analyses were performed by using SPSS, Version 22 (IBM, Armonk, New York). Comparisons of the ipsilateral and contralateral CST diffusion metrics were performed by using the paired Wilcoxon signed rank test. Associations between average CST diffusion metrics and the 3-month FM-UE scale were evaluated by using Spearman rank correlation tests. Results were considered significant with $P < .05$. Because this study was designed largely to be one of hypothesis generation, P values were not corrected for multiple comparisons.

RESULTS

Clinical Data

Twenty-one patients were recruited for this study. Subsequently, 3 patients were excluded because they were lost to follow-up and 3-month follow-up data were not available. One patient was excluded because the DKI dataset was degraded by artifacts from bulk motion. Hence, 17 patients were included in the analysis (Table 1). All patients received rehabilitation therapy (median number of days of therapy = 34 ± 18). Overall, the FM-UE scale score significantly improved between the baseline and the 3-month neurologic examination ($P = .001$), with motor func-

Table 2: Diffusion metrics of lesioned and contralateral corticospinal tract in stroke with motor impairment

| Diffusion Metric | Lesioned CST ^a | Contralateral CST ^a | P Value |
|---------------------------------|---------------------------|--------------------------------|---------|
| MD | 0.91 (0.07) | 0.96 (0.03) | .003 |
| Axial diffusivity | 1.35 (0.12) | 1.44 (0.06) | .002 |
| Radial diffusivity | 0.70 (0.05) | 0.72 (0.04) | .031 |
| Fractional anisotropy | 0.41 (0.03) | 0.43 (0.03) | .025 |
| MK | 1.19 (0.12) | 1.10 (0.07) | .002 |
| Axial kurtosis | 0.94 (0.11) | 0.84 (0.03) | .001 |
| Radial kurtosis | 1.48 (0.18) | 1.43 (1.13) | .193 |
| AWF | 0.41 (0.02) | 0.40 (0.02) | .246 |
| Intra-axonal diffusivity | 0.71 (0.09) | 0.78 (0.06) | .001 |
| Extra-axonal axial diffusivity | 1.95 (0.17) | 2.05 (0.10) | .002 |
| Extra-axonal radial diffusivity | 1.07 (0.07) | 1.10 (0.05) | .049 |

Note:—AWF indicates axial water fraction.

^a Mean (SD).

tion improvement in 14 subjects, no changes in 2 subjects, and worsening function in 1 subject. At 3 months, 3 patients had little if any upper extremity motor function; 5 patients had well-defined upper limb mass flexion and extension synergy-dependent movements; and 9 patients had isolated upper limb movements. There was no significant correlation between the number of days of rehabilitation therapy and the baseline FM-UE scale score ($r = -0.340$, $P = .181$) or the 3-month FM-UE scale score ($r = -0.373$, $P = .140$).

Imaging Data

Please see Table 1 for details regarding infarct location and Table 2 for CST diffusion metrics. CST MD, FA, λ_{\parallel} , λ_{\perp} , D_a , axial extra-axonal diffusivity, and radial extra-axonal diffusivity were lower in the lesioned than in the contralateral hemisphere. MK and K_{\parallel} were greater in the lesioned than in the contralateral hemisphere CST. The On-line Table demonstrates infarct volume, CST volume, their intersection, and diffusion metrics for the entire cohort and for patients stratified on the basis of the degree of recovery at 3 months. There was a strong association between baseline and 3-month FM-UE scale ($\rho = 0.8$, $P = .001$). We found significant correlations among the 3-month FM-UE scale, percentage change of FM-UE scale between the baseline and 3-month visit, diffusion metrics of the lesioned hemisphere, and lesioned/contralateral hemisphere CST ratios (Table 3). The strongest associations were found between the 3-month FM-UE scale score and MK, and the 3-month FM-UE scale score and K_{\parallel} , among kurtosis metrics; and between the 3-month FM-UE scale score and MD, among diffusivity metrics (Fig 2). We did not find any significant correlation between the number of days of rehabilitation therapy and kurtosis metrics. For example, there was no significant association between the number of days of rehabilitation therapy and lesioned/contralateral MK ($\rho = 0.212$, $P = .398$), K_{\parallel} ($\rho = 0.282$, $P = .257$), MD ($\rho = -0.318$, $P = .198$), λ_{\parallel} ($\rho = -0.330$, $P = .181$), and FA ($\rho = -0.78$, $P = .759$).

DISCUSSION

We conducted a prospective observational study designed to explore the hypothesis that DKI-derived metrics can be useful in assessing CST microstructural changes and predicting motor outcome after stroke. Due to the relatively small sample size, this proof-of-concept study is mainly for hypothesis generation, and

Table 3: Correlations among the baseline FM-UE scale score, corticospinal tract diffusion metrics, and 3-month FM-UE scale score

| | Lesioned Hemisphere CST | | Lesioned/Contralateral CST Ratio | |
|---------------------------------|-------------------------|---------|----------------------------------|---------|
| | ρ | P Value | ρ | P Value |
| 3-mo FM-UE scale | | | | |
| MD | 0.65 | .007 | 0.69 | .002 |
| Axial diffusivity | 0.55 | .022 | 0.73 | .001 |
| Radial diffusivity | 0.53 | .030 | 0.60 | .011 |
| FA | 0.08 | .761 | 0.40 | .111 |
| MK | −0.72 | .001 | −0.85 | <.001 |
| Axial kurtosis | −0.75 | .001 | −0.78 | <.001 |
| Radial kurtosis | −0.33 | .196 | −0.47 | .056 |
| AWF | −0.45 | .072 | −0.63 | .007 |
| Intra-axonal diffusivity | 0.51 | .035 | 0.48 | .054 |
| Axial extra-axonal diffusivity | 0.45 | .070 | 0.61 | .009 |
| Radial extra-axonal diffusivity | 0.37 | .142 | 0.45 | .072 |
| Change of FM-UE scale (%) | | | | |
| MD | 0.64 | .006 | 0.47 | .055 |
| Axial diffusivity | 0.49 | .046 | 0.66 | .004 |
| Radial diffusivity | 0.69 | .002 | 0.42 | .098 |
| FA | −0.01 | .974 | 0.47 | .060 |
| MK | −0.61 | .010 | −0.72 | .001 |
| Axial kurtosis | −0.65 | .005 | −0.65 | .004 |
| Radial kurtosis | −0.28 | .269 | −0.48 | .049 |
| AWF | −0.54 | .026 | −0.59 | .013 |
| Intra-axonal diffusivity | 0.42 | .095 | 0.43 | .083 |
| Axial extra-axonal diffusivity | 0.42 | .090 | 0.56 | .019 |
| Radial extra-axonal diffusivity | 0.53 | .028 | 0.24 | .349 |

Note:—AWF indicates axial water fraction.

our results will require validation in future studies with larger sample sizes. Both diffusivity and kurtosis diffusion metrics could detect early microstructural changes of the CST in the acute post-stroke phase, with larger differences between the ipsilateral and contralateral CST being observed for the kurtosis metrics. We also found moderately strong associations between motor outcome with the 3-month FM-UE scale and several diffusion metrics. The strongest motor outcome correlations were with MK ($\rho = -0.72$) and K_{\parallel} ($\rho = -0.75$) of the lesioned CST, and with the lesioned/contralateral hemisphere CST MK ($\rho = -0.85$) and K_{\parallel} ($\rho = -0.78$) ratios.

The observation of early CST diffusion changes is consistent with the known dynamics of acute neuronal damage after stroke, a phenomenon known as Wallerian degeneration.⁸ In agreement with prior studies, we found that diffusivity metrics differed between the lesioned hemisphere CST and the contralateral CST,²⁰ with greater acute–early subacute changes in λ_{\parallel} and MD compared with λ_{\perp} .²¹ Kurtosis metrics, specifically MK, K_{\parallel} , D_a , and axial extra-axonal diffusivity, could identify early microstructural changes of the CST. The kurtosis parameters provide microstructural information not available by using conventional DTI,¹¹ and it is important to assess whether the enhanced sensitivity to microstructural changes provided by DKI translates into improved motor outcome prediction. Larger absolute percentage changes for kurtosis metrics than for diffusivity metrics have been consistently reported in ischemic stroke in the animal and human literature.^{13,22,23} Here, we find that kurtosis metrics also have greater sensitivity to the detection of CST microstructural alterations, as reflected by their larger absolute percentage changes. For example, we found an average 12% increase in K_{\parallel} and an average 6.5% decrease in λ_{\parallel} of the ipsilateral compared with the contralateral

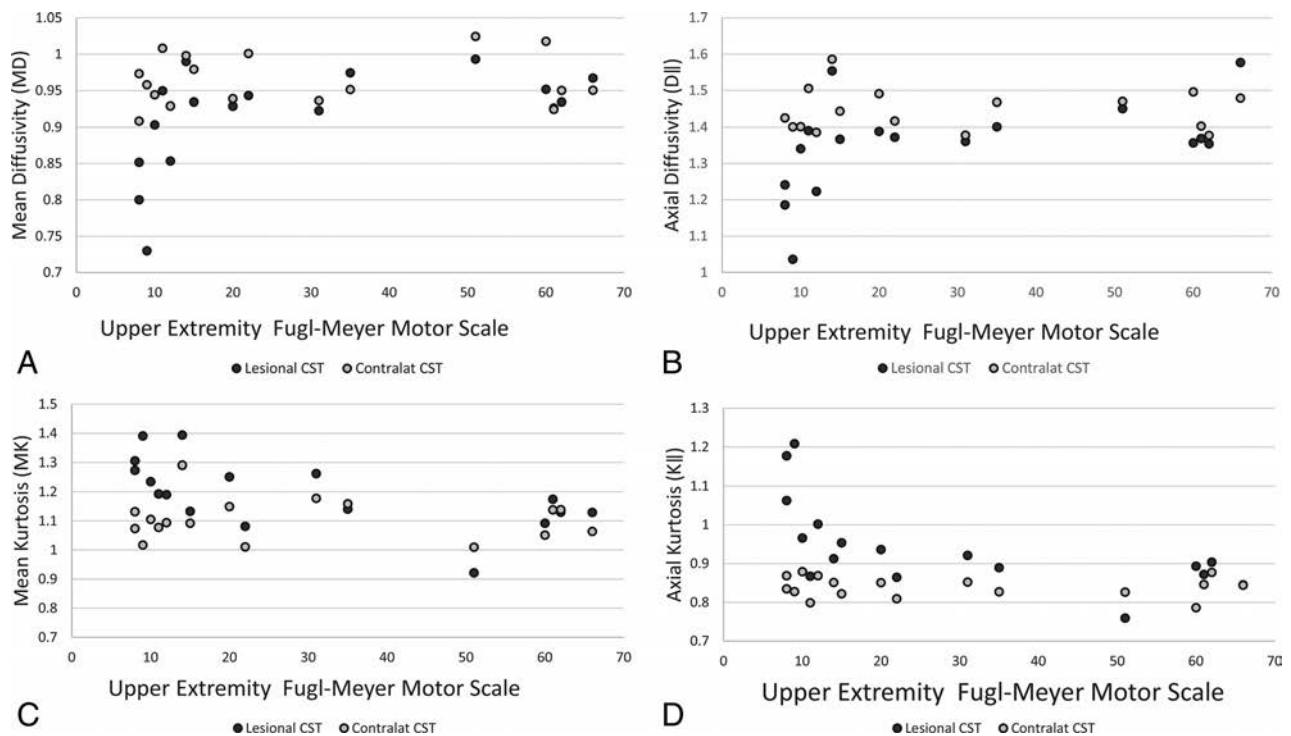


FIG 2. Scatterplots for the Upper Extremity Fugl-Meyer Motor scale versus mean diffusivity (A), axial diffusivity (B), mean kurtosis (C), and axial kurtosis (D) of the corticospinal tracts.

CST. Absolute percentage changes were larger along the axial direction than along the radial direction of the CST WM.²⁴ As expected, absolute percentage changes of λ_{\parallel} and K_{\parallel} of the lesioned-hemisphere CST were smaller than the absolute percentage changes of λ_{\parallel} and K_{\parallel} of the core infarct, respectively 58% and -32%, in a previous study.²⁴

The pathologic correlates of increased MK in acute infarct and the downstream effect along the affected WM tracts are still incompletely understood. Acute infarct leading to early CST Wallerian degeneration may result in swelling or beading of downstream axons and dendrites.²³⁻²⁵ Alternatively, ischemia could cause increased intra-axonal tortuosity, viscosity changes, microglia upregulation, and mitochondrial or endoplasmic reticulum changes, which may result in decreased D_a .^{22,23,26} In agreement with Hui et al,²⁴ we found that the decrease in MD of the CST is mainly due to a drop in D_a , consistent with a proposed mechanism of axonal beading, though the CST axial extra-axonal diffusivity was also decreased.

Previous studies have assessed the correlations between DTI-derived measures of CST integrity and functional motor impairment in acute stroke. Doughty et al²⁷ identified subtle changes in FA values of the CST in the vicinity of the lesion early after acute ischemic stroke; however, the degree of FA reduction did not significantly improve on the predictive value of the baseline FM-UE scale for 3-month motor outcome.²⁷ Similarly, Puig et al^{10,28} did not find significant correlations between 30-day motor outcome after stroke and CST FA measured in the pons in the acute phase, specifically <12 hours and 3 days poststroke. Feng et al²⁹ developed the weighted CST lesion load, a novel imaging marker obtained by overlaying lesion maps obtained from DWI in the acute phase with a canonical CST. The weighted CST lesion

load was found to be a significant predictor of 3-month motor outcome. However, this metric is not a direct measure of CST injury and does not take into account CST pathophysiologic changes after stroke. There is an unfulfilled clinical need for an early imaging marker of CST injury that would complement clinical assessment in the prediction of motor outcome and patient response to rehabilitation therapy. Our work demonstrates that DKI-derived diffusion metrics can detect early microstructural changes of the CST associated with acute stroke. Furthermore, DKI-derived metrics obtained in the acute phase show promising correlations with 3-month motor outcome. If these associations are validated in a future larger prospective study, then these metrics may ultimately prove to be powerful adjuncts to clinical assessment in triaging patients who may benefit from neurorehabilitation treatment.

Stroke rehabilitative treatments are resource-intensive, and patient selection is critical to identify individuals who are likely to benefit from the treatment.³⁰ Proposed motor outcome predictors, such as stroke location and volume,³¹ and the degree of CST involvement,^{6,29} may not provide adequate information to predict motor outcome, and a substantial amount of variance remains unexplained. Our results suggest that kurtosis metrics may prove valuable in determining motor pathway integrity. Specifically, we found that elevated MK/K_{\parallel} and decreased MD of the CST indicate a poor prognosis, and MK and K_{\parallel} had the strongest associations with the 3-month FM-UE scale. Patients with unfavorable diffusion markers may be less likely to benefit from motor rehabilitation programs. Although our preliminary observations will need confirmation in studies with larger cohorts, the use of imaging biomarkers of CST integrity could enable improved selection strategies in future stroke-recovery trials.

This study has several limitations. We evaluated a small patient cohort, which limits our ability to evaluate the role of diffusion metrics in the context of other prognostic factors. On the other hand, all data were prospectively acquired, and imaging data were obtained with the same MR imaging protocol and scanner. Future studies should include a larger series of patients, which would allow one to determine whether the diffusion metrics are truly independent predictors of motor recovery, over and above the traditional clinical prognostic variables. We did not evaluate the subsequent temporal evolution of the observed CST diffusion measures. Furthermore, we included patients with acute stroke and motor impairment regardless of the vascular territory involved. Our purpose was to evaluate the effects of acute ischemia on CST microstructure regardless of where the core infarct was located along the motor pathways. This study design has been used in previous imaging-based studies on motor outcome after stroke.^{27,29}

CONCLUSIONS

Our preliminary study reveals that early CST microstructural changes immediately following stroke can be detected by using kurtosis metrics, specifically MK and $K_{||}$. We have preliminarily found strong associations between kurtosis metrics obtained at early time points after stroke and long-term motor outcome. A major limitation of this study is the small sample size. This study was designed largely to be one of hypothesis generation, and the usefulness of these imaging markers as independent predictors of disability in the context of other motor outcome predictors must be validated in future studies with larger sample sizes.

ACKNOWLEDGMENTS

We acknowledge Rachael L. Deardorff for assisting with manuscript preparation.

Disclosures: M. Vittoria Spampinato—**RELATED: Grant:** South Carolina Translational Research Institute, *Comments:* National Institutes of Health National Center for Advancing Translational Sciences UL1TR001450*. Jens H. Jensen—**UNRELATED: Patents (Planned, Pending or Issued):** US patent 8811706, issued August 19, 2014, *Comments:* This is a patent on the DKI technology used in our study. To date, I have not received any royalties from this patent. Joseph A. Helpert—**UNRELATED: Patents (Planned, Pending or Issued):** New York University and Siemens, *Comments:* patent for DKI owned by New York University licensed to Siemens*. Leonardo Bonilha—**UNRELATED: Grants/Grants Pending:** National Institutes of Health, American Heart Association, *Comments:* IR01DC014021 (National Institutes of Health/National Institute on Deafness and Other Communication Disorders, Principal Investigator; July 1, 2014, to July 1, 2019), Brain Connectivity Supporting Language Recovery in Aphasia, major goal: to investigate how residual structural connectivity enables recovery from aphasia in individuals with stroke; Principal Investigator in 15SFDNR26030003 (American Heart Association; July 1, 2015, to July 1, 2019), Influence of Pre-Morbid Brain Health on Stroke Recovery; major goal: to investigate how prestroke brain health can affect recovery from stroke with regard to focal neurological deficits and quality of life. Steven Kautz—**RELATED: Grant:** National Institutes of Health, *Comments:* P20GM109040*. Paul J. Nietert—**RELATED: Grant:** National Institutes of Health, *Comments:* National Center for Advancing Translational Sciences grant No. UL1TR001450*. W. Feng—**RELATED: Grant:** Prediction and Imaging Biomarker for Post-stroke Motor Recovery (American Heart Association: 14SDG1829003). *Money paid to the institution.

REFERENCES

- Langhorne P, Coupar F, Pollock A. **Motor recovery after stroke: a systematic review.** *Lancet Neurol* 2009;8:741–54 CrossRef Medline
- Hendricks HT, van Limbeek J, Geurts AC, et al. **Motor recovery after stroke: a systematic review of the literature.** *Arch Phys Med Rehabil* 2002;83:1629–37 CrossRef Medline
- Duncan PW, Goldstein LB, Matchar D, et al. **Measurement of motor recovery after stroke: outcome assessment and sample size requirements.** *Stroke* 1992;23:1084–89 CrossRef Medline
- Prabhakaran S, Zarahn E, Riley C, et al. **Inter-individual variability in the capacity for motor recovery after ischemic stroke.** *Neurorehabil Neural Repair* 2008;22:64–71 Medline
- Ward NS, Newton JM, Swayne OB, et al. **Motor system activation after subcortical stroke depends on corticospinal system integrity.** *Brain* 2006;129:809–19 CrossRef Medline
- Puig J, Pedraza S, Blasco G, et al. **Acute damage to the posterior limb of the internal capsule on diffusion tensor tractography as an early imaging predictor of motor outcome after stroke.** *AJNR Am J Neuroradiol* 2011;32:857–63 CrossRef Medline
- Kumar P, Kathuria P, Nair P, et al. **Prediction of upper limb motor recovery after subacute ischemic stroke using diffusion tensor imaging: a systematic review and meta-analysis.** *J Stroke* 2016;18:50–59 CrossRef Medline
- Yu C, Zhu C, Zhang Y, et al. **A longitudinal diffusion tensor imaging study on Wallerian degeneration of corticospinal tract after motor pathway stroke.** *Neuroimage* 2009;47:451–58 CrossRef Medline
- Groisser BN, Copen WA, Singhal AB, et al. **Corticospinal tract diffusion abnormalities early after stroke predict motor outcome.** *Neurorehabil Neural Repair* 2014;28:751–60 CrossRef Medline
- Puig J, Pedraza S, Blasco G, et al. **Wallerian degeneration in the corticospinal tract evaluated by diffusion tensor imaging correlates with motor deficit 30 days after middle cerebral artery ischemic stroke.** *AJNR Am J Neuroradiol* 2010;31:1324–30 CrossRef Medline
- Jensen JH, Helpert JA. **MRI quantification of non-Gaussian water diffusion by kurtosis analysis.** *NMR Biomed* 2010;23:698–710 CrossRef Medline
- Jensen JH, Helpert JA, Tabesh A. **Leading non-Gaussian corrections for diffusion orientation distribution function.** *NMR Biomed* 2014;27:202–11 CrossRef Medline
- Grinberg F, Ciobanu L, Farrher E, et al. **Diffusion kurtosis imaging and log-normal distribution function imaging enhance the visualization of lesions in animal stroke models.** *NMR Biomed* 2012;25:1295–304 CrossRef Medline
- Fieremans E, Jensen JH, Helpert JA. **White matter characterization with diffusional kurtosis imaging.** *Neuroimage* 2011;58:177–88 CrossRef Medline
- Fugl-Meyer AR, Jaasko L, Leyman I, et al. **The post-stroke hemiplegic patient. 1: a method for evaluation of physical performance.** *Scand J Rehabil Med* 1975;7:13–31 Medline
- Shelton FN, Reding MJ. **Effect of lesion location on upper limb motor recovery after stroke.** *Stroke* 2001;32:107–12 CrossRef Medline
- Tabesh A, Jensen JH, Ardekani BA, et al. **Estimation of tensors and tensor-derived measures in diffusional kurtosis imaging.** *Magnetic Reson Med* 2011;65:823–36 CrossRef Medline
- Yeh FC, Verstynen TD, Wang Y, et al. **Deterministic diffusion fiber tracking improved by quantitative anisotropy.** *PLoS One* 2013;8:e80713 CrossRef Medline
- Wakana S, Caprihan A, Panzenboeck MM, et al. **Reproducibility of quantitative tractography methods applied to cerebral white matter.** *Neuroimage* 2007;36:630–44 CrossRef Medline
- Moulton E, Amor-Sahli M, Perlberg V, et al. **Axial diffusivity of the corona radiata at 24 hours post-stroke: a new biomarker for motor and global outcome.** *PLoS One* 2015;10:e0142910 CrossRef Medline
- Bhagat YA, Hussain MS, Stobbe RW, et al. **Elevations of diffusion anisotropy are associated with hyper-acute stroke: a serial imaging study.** *Magn Reson Imaging* 2008;26:683–93 CrossRef Medline
- Cheung JS, Wang E, Lo EH, et al. **Stratification of heterogeneous diffusion MRI ischemic lesion with kurtosis imaging: evaluation of mean diffusion and kurtosis MRI mismatch in an animal model of transient focal ischemia.** *Stroke* 2012;43:2252–54 CrossRef Medline
- Jensen JH, Falangola MF, Hu C, et al. **Preliminary observations of**

- increased diffusional kurtosis in human brain following recent cerebral infarction. *NMR Biomed* 2011;24:452–57 [CrossRef](#) [Medline](#)
24. Hui ES, Fieremans E, Jensen JH, et al. **Stroke assessment with diffusional kurtosis imaging.** *Stroke* 2012;43:2968–73 [CrossRef](#) [Medline](#)
 25. Budde MD, Frank JA. **Neurite beading is sufficient to decrease the apparent diffusion coefficient after ischemic stroke.** *Proc Natl Acad Sci U S A* 2010;107:14472–77 [CrossRef](#) [Medline](#)
 26. Weber RA, Hui ES, Jensen JH, et al. **Diffusional kurtosis and diffusion tensor imaging reveal different time-sensitive stroke-induced microstructural changes.** *Stroke* 2015;46:545–50 [CrossRef](#) [Medline](#)
 27. Doughty C, Wang J, Feng W, et al. **Detection and predictive value of fractional anisotropy changes of the corticospinal tract in the acute phase of a stroke.** *Stroke* 2016;47:1520–26 [CrossRef](#) [Medline](#)
 28. Puig J, Blasco G, Daunis-I-Estadella J, et al. **Decreased corticospinal tract fractional anisotropy predicts long-term motor outcome after stroke.** *Stroke* 2013;44:2016–18 [CrossRef](#) [Medline](#)
 29. Feng W, Wang J, Chhatbar PY, et al. **Corticospinal tract lesion load: an imaging biomarker for stroke motor outcomes.** *Ann Neurol* 2015;78:860–70 [CrossRef](#) [Medline](#)
 30. Stinear C. **Prediction of recovery of motor function after stroke.** *Lancet Neurol* 2010;9:1228–32 [CrossRef](#) [Medline](#)
 31. Chen CL, Tang FT, Chen HC, et al. **Brain lesion size and location: effects on motor recovery and functional outcome in stroke patients.** *Arch Phys Med Rehabil* 2000;81:447–52 [CrossRef](#) [Medline](#)

APOE*E4 Is Associated with Gray Matter Loss in the Posterior Cingulate Cortex in Healthy Elderly Controls Subsequently Developing Subtle Cognitive Decline

 S. Haller,  M.-L. Montandon,  C. Rodriguez,  M. Ackermann,  F.R. Herrmann, and  P. Giannakopoulos



ABSTRACT

BACKGROUND AND PURPOSE: The presence of *apolipoprotein E4* (APOE*E4) is the strongest currently known genetic risk factor for Alzheimer disease and is associated with brain gray matter loss, notably in areas involved in Alzheimer disease pathology. Our objective was to assess the effect of APOE*E4 on brain structures in healthy elderly controls who subsequently developed subtle cognitive decline.

MATERIALS AND METHODS: This prospective study included 382 community-dwelling elderly controls. At baseline, participants underwent MR imaging at 3T, extensive neuropsychological testing, and genotyping. After neuropsychological follow-up at 18 months, participants were classified into cognitively stable controls and cognitively deteriorating controls. Data analysis included whole-brain voxel-based morphometry and ROI analysis of GM.

RESULTS: APOE*E4-related GM loss at baseline was found only in the cognitively deteriorating controls in the posterior cingulate cortex. There was no APOE*E4-related effect in the hippocampus, mesial temporal lobe, or brain areas not involved in Alzheimer disease pathology. Controls in the cognitively deteriorating group had slightly lower GM concentration in the hippocampus at baseline. Higher GM densities in the hippocampus, middle temporal lobe, and amygdala were associated with a decreased risk for cognitively deteriorating group status at follow-up.

CONCLUSIONS: APOE*E4-related GM loss in the posterior cingulate cortex (an area involved in Alzheimer disease pathology) was found only in those elderly controls who subsequently developed subtle cognitive decline but not in cognitively stable controls. This finding might explain the partially conflicting results of previous studies that typically did not include detailed neuropsychological assessment and follow-up. Most important, APOE*E4 status had no impact on GM density in areas affected early by neurofibrillary tangle formation such as the hippocampus and mesial temporal lobe.

ABBREVIATIONS: AD = Alzheimer disease; APOE = *apolipoprotein E*; dCON = cognitively deteriorating controls; MCI = mild cognitive impairment; sCON = cognitively stable controls

The *apolipoprotein E* gene (APOE) has 3 different alleles, APOE*E2, APOE*E3, and APOE*E4. The presence of APOE*E4 is the strongest currently known genetic risk factor for Alzheimer disease (AD).^{1,2} APOE*E3 is the most common variant in the general population, while the APOE*E2 variant is associated with a lower risk of AD. The APOE variant modifies not only the risk of AD but also the age of onset of cognitive symptoms.^{3,4}


Cross-sectional structural MR imaging studies indicated reduced gray matter in elderly APOE*E4 carriers including healthy controls, subjective memory impairment, mild cognitive impairment (MCI), and AD.⁵⁻¹⁴ In MCI and AD, the APOE*E4-related GM decrease seems to affect areas involved in AD pathology, notably the hippocampus, amygdala, and mesial temporal cortex¹⁴⁻¹⁷ but also the left occipital, frontal, and anterior cingulate cortices.^{14,18} In healthy elderly controls, the APOE*E4 effect on brain structure is less clear. Decreased GM volume in the caudate nuclei¹⁴ and the right cingulate gyrus and decreased white matter


Received September 25, 2016; accepted after revision February 17, 2017.

From the Affidea Centre de Diagnostic Radiologique de Carouge (S.H.), Geneva, Switzerland; Faculty of Medicine (S.H., M.-L.M., F.R.H., P.G.), University of Geneva, Switzerland; Departments of Surgical Sciences and Radiology (S.H.), Uppsala University, Uppsala, Sweden; Department of Neuroradiology (S.H.), University Hospital Freiburg, Freiburg, Germany; and Department of Mental Health and Psychiatry (M.-L.M., M.A.), Division of Institutional Measures, Medical Direction (C.R., P.G.), and Division of Geriatrics, Department of Internal Medicine, Rehabilitation and Geriatrics (F.R.H.), University Hospitals of Geneva, Geneva, Switzerland.

This work is supported by Swiss National Foundation grants SNF 3200B0-1161193 and SPUM 33CM30-124111 and an unrestricted grant from the Association Suisse pour la Recherche Alzheimer.

Please address correspondence to Sven Haller, MD, MSc, Affidea Centre de Diagnostic Radiologique de Carouge CDRC, Geneva, Switzerland; Faculty of Medicine of the University of Geneva, Geneva, Switzerland; Departments of Surgical Science and Radiology, Uppsala University, Uppsala, Sweden; Department of Neuroradiology, University Hospital Freiburg, Freiburg, Germany; e-mail: sven.haller@me.com

 Indicates open access to non-subscribers at www.ajnr.org

 Indicates article with supplemental on-line table.

<http://dx.doi.org/10.3174/ajnr.A5184>

integrity in right parahippocampal gyrus¹⁹ were found. However, negative data were also reported.^{15,18,20} In younger *APOE***E4* carriers, the results are also more ambiguous. Some studies demonstrated reduced GM in middle-aged²¹ and young *APOE***E4* carriers^{22,23} compared with the other *APOE* allele carriers, whereas others reported no *APOE***E4* effect throughout adulthood.²⁰

Longitudinal studies also indicated that among MCI converters, those with a positive *APOE***E4* status displayed increased GM atrophy in AD-related brain regions.^{24,25}

The current investigation goes 1 step earlier in the degenerative process and assesses the effect of *APOE* allele status in healthy controls who subsequently developed subtle cognitive decline. To this end, we performed MR imaging and cognitive assessment at baseline in 382 community-dwelling elderly controls. Extensive cognitive assessment was repeated at 18-month follow-up to define a subsample of 181 individuals with a stable condition and 201 with a deteriorating condition. We demonstrated a gradually progressive GM loss in the posterior cingulate cortex as a function of *APOE* alleles (*E2* < *E3* < *E4*) only in deteriorating groups, with preserved GM densities in cognitively stable groups.

MATERIALS AND METHODS

Study Protocol and Participants

All data used in the preparation of this article were obtained from a large, population-based study of community-dwelling older adults who have undergone an 18-month follow-up. These community-dwelling subjects were recruited via advertisements in local newspapers and media. All participants had normal or corrected-to-normal visual acuity, and none reported a history of neurologic or psychiatric disorders or alcohol or drug abuse. To avoid contamination by reversible forms of cognitive decline, subjects with vitamin B12 or folic acid deficiency and those with infectious diseases were excluded. Subjects with regular use of neuroleptics, antidepressants, mood stabilizers, anticonvulsant drugs, or psychostimulants and those with contraindications to MR imaging were excluded. Initially, 433 patients were screened. Thirty-seven refused to continue after the first evaluation (no death or illness, but for personal reasons). Fourteen were not considered due to the above-mentioned exclusion criteria. Five among them had substantial abnormal findings on MR imaging at baseline.

The education level was defined according to the Swiss scholar system, in which level 1 = <9 years (primary school), level 2 = between 9 and 12 years (high school), and level 3 = >12 years (university). All participants provided written informed consent after formal approval by the local ethics committee.

Neuropsychological Assessment

At baseline, all individuals were evaluated with an extensive neuropsychological battery, including the Mini-Mental State Examination,²⁶ the Hospital Anxiety and Depression Scale,²⁷ and the Lawton Instrumental Activities of Daily Living.²⁸ Cognitive assessment included the following: 1) attention (Digit-Symbol-Coding,²⁹ Trail-Making Test A,³⁰); 2) working memory (verbal: Digit Span Forward³¹; visuospatial: visual memory span [Corsi]³²); 3) episodic memory (verbal: RI-48 Cued Recall Test³³; visual: Shapes Test³⁴); 4) executive functions (Trail-Making Test B,³⁰ Wisconsin

Card Sorting Test, and Phonemic Verbal Fluency Test); 5) language (Boston Naming Test³⁵); 6) visual gnosis (Ghent Overlapping Figures); and 7) apraxia: ideomotor,³⁶ reflexive,³⁷ and constructional (Consortium to Establish a Registry for Alzheimer Disease; figure copy test³⁸). All individuals were also evaluated with the Clinical Dementia Rating scale.³⁹

Those who met dementia the *Diagnostic and Statistical Manual of Mental Disorders*, 4th edition, diagnostic criteria based on the neuropsychological and clinical assessments were excluded. In agreement with the criteria of Petersen et al,⁴⁰ participants with a Clinical Dementia Rating scale score of 0.5 but no dementia and a score of >1.5 SDs below the age-appropriate mean in any of the previously mentioned tests were also excluded from the present study. Participants with neither dementia nor MCI were classified as cognitively healthy older controls and underwent full neuropsychological assessment at follow-up by the same neuropsychologist, on average 18 months later. Those whose cognitive scores remained stable and those whose performance at follow-up was at least 0.5 SD lower compared with the baseline evaluation in at least 2 cognitive tests were classified as stable (sCON) and deteriorating (dCON), respectively. Two neuropsychologists clinically assessed all individuals independently. The final classification of sCON versus dCON was made by a trained neuropsychologist who took into account both the neuropsychological test results and overall clinical assessment.⁴¹ In her final appreciation, the trained neuropsychologist considered the most relevant test performances, usually altered in the course of Alzheimer disease (verbal episodic memory: RI-48 Cued Recall Test; attention: Trail-Making Test A; executive functions: Trail-Making Test B³⁰ and Phonemic Verbal Fluency Test). Among the 2 tests needed for dCON classification, altered cognitive scores in at least 1 of these tests were mandatory.

MR Imaging Acquisition

Imaging data were acquired on a clinical routine whole-body 3T MR scanner (Tim Trio; Siemens, Erlangen, Germany). The structural 3D T1 sequence was performed with the following fundamental parameters: 256 × 256 matrix; 176 sections; 1 × 1 × 1 mm³; TE, 2.3 ms; TR, 2300 ms. Additional sequences (T2WI, susceptibility-weighted imaging, diffusion tensor imaging) were used to exclude incidental brain lesions.

Genetic Testing

Whole-blood samples were collected at baseline for all subjects for *APOE* genotyping. Standard DNA extraction was performed by using either 9-mL ethylenediaminetetraacetic acid tubes (Sarstedt AG, Nümbrecht, Germany) or the Oragene Saliva DNA Kit (DNA Genotek; Kanata, Ontario, Canada); tubes were stored at −20°C. *APOE* genotyping was performed on the LightCycler (Roche Diagnostics, Basel, Switzerland) as described previously.⁴²

Statistical Analysis

The voxel-based morphometry analysis was performed by using the FSL software package (<http://www.fmrib.ox.ac.uk/fsl/>), according to the standard procedure. The essential processing steps included brain extraction with the FSL Brain Extraction Tool (<http://fsl.fmrib.ox.ac.uk/fsl/fslwiki/BET>), tissue-type segmenta-

Table 1: Essential demographic data of the included study groups of stable and deteriorating elderly control participants^a

| Group | sCON Alleles | | | dCON Alleles | | | APOE Allele Effect 3/3 vs 3/2 (P Value) | APOE Allele Effect 4/3 vs 3/2 (P Value) | Group Effect (P Value) | Interaction 1 (P Value) | Interaction 2 (P Value) |
|----------------|--------------|------|------|--------------|------|------|--|--|---------------------------|----------------------------|----------------------------|
| | 3/2 | 3/3 | 4/3 | 3/2 | 3/3 | 4/3 | | | | | |
| No. | 22 | 132 | 27 | 21 | 142 | 38 | | | | | |
| Sex | | | | | | | .734 | .411 | .172 | .261 | .359 |
| Female | 13 | 83 | 19 | 8 | 86 | 26 | | | | | |
| Male | 9 | 49 | 8 | 13 | 56 | 12 | | | | | |
| Education (yr) | | | | | | | .466 | .324 | .676 | .808 | .450 |
| <9 | 3 | 23 | 4 | 3 | 27 | 3 | | | | | |
| 9–12 | 8 | 53 | 14 | 9 | 72 | 20 | | | | | |
| >12 | 11 | 56 | 9 | 9 | 43 | 15 | | | | | |
| Age (yr) | | | | | | | .980 | .969 | .377 | .952 | .539 |
| Mean | 73.7 | 73.7 | 73.8 | 74.8 | 74.9 | 73.9 | | | | | |
| SD | 3.2 | 3.9 | 4.2 | 4.4 | 4.2 | 4.0 | | | | | |

^aData in columns 2–7 are number.

tion with the FMRIB Automated Segmentation Tool (<http://fsl.fmrib.ox.ac.uk/fsl/fslwiki/fast>), nonlinear transformation into Montreal Neurological Institute reference space, and creation of a study-specific GM template to which the native GM images were then nonlinearly reregistered. The modulated segmented images were then smoothed with an isotropic Gaussian kernel with a σ of 2 mm. Finally, the voxelwise FSL General Linear Model (<http://fsl.fmrib.ox.ac.uk/fsl/fslwiki/GLM>) was applied by using permutation-based nonparametric testing with the FSL Randomize tool (<http://fsl.fmrib.ox.ac.uk/fsl/fslwiki/Randomise/>) with threshold-free cluster enhancement correction for multiple comparisons,⁴³ considering fully corrected *P* values < .05 as significant. The analysis was performed to compare regions and *APOE* genotypes with the percentage of GM as a dependent variable with age, sex, and education as potential confounders. Furthermore, we created a mask for the bilateral mesial temporal cortex, posterior cingulate cortex, hippocampus, amygdala, caudate nuclei, and parietal and occipital lobes that was then applied to the GM image of the study-specific template.

Demographic and neuropsychological data were compared among groups by using regression models with group (stable versus deteriorating), *APOE* genotype (3/2, 3/3, 4/3), and a group \times genotype interaction term as predictors. Logistic, ordered logistic, and linear regression models were used for binary, ordinal, and respectively continuous variables. Group effects (stable versus deteriorating) were compared by using the *Z*-test for plain and ordered logistic regressions and the *t* test for linear regression.

Logistic regression models were built to assess the relationship between cognitive status (dependent variable) and *APOE* genotyping, GM densities in the 3 areas of interest (posterior cingulate, hippocampus, mesial temporal lobe), age, sex, and education levels (independent variables). Because GM density values were all ranging between 0.32 and 0.87, we transformed them by using *z* scores (subtracting the overall mean and dividing by the overall SD) and thus calculated the standardized odds ratio, which represents the decrease in estimated risk for a 1-SD change in GM density.

RESULTS

Demographic and Neuropsychological Data

The final sample included 382 subjects with 3D T1 scans available and *APOE* genotyping. We grouped these subjects into 3 groups: 43 with *APOE**E2 (mean age, 74.1 ± 3.8 years; 22 with sCON and

21 with dCON), 274 with *APOE**E3 (mean age, 74.1 ± 4.1 years; 132 with sCON and 142 with dCON), and 65 with *APOE**E4 (mean age, 73.6 ± 4.1 years; 27 with sCON and 38 with dCON) genotypes. Demographic data and neuropsychological performances at baseline did not differ between sCON and dCON groups (data not shown). As expected, there were group differences at follow-up, with worse cognitive performances of dCON for the Trail-Making Test B (*P* = .015), Verbal Fluency (*P* = .045), and the Wisconsin Card Sorting Test (number of categories) (*P* = .034). The *APOE**E4 allele had a negative impact on verbal fluency performance at follow-up (*P* = .011) with a significant group \times *APOE* interaction (*P* = .003 for dCON). There was no other significant association between *APOE* genotyping and neuropsychological performances at follow-up (Table 1 and Online Table).

Whole-Brain Voxel-Based Morphometry

In a first step, we performed a voxelwise analysis across the entire brain. The posterior cingulate cortex demonstrated a significant difference between *APOE**E3 > *APOE**E4 for the dCON group (Fig 1).

ROI Analysis: APOE Effect on GM Densities in dCON and sCON

In a second step, we additionally performed an ROI analysis in 7 regions of particular interest in the context of cognitive decline (posterior cingulate cortex, hippocampus, mesial temporal lobe, parietal lobe, amygdala, and caudate nucleus) with the occipital lobe as a control region.

In the posterior cingulate, the GM concentration decreased from E2 to E3 to E4 across all participants. When we separated the patients into stable-versus-deteriorating controls, this decrease in GM concentration was present in only the dCON group (Fig 2A and Table 2). Moreover, we found a significant difference between sCON versus dCON in *APOE**E4-positive individuals. Concerning the hippocampus, patients with dCON had lower GM concentrations compared with those with sCON, which was significant only in the *APOE**E3 group, presumably due to the large sample size (Fig 2B and Table 3). In the amygdala, there was a decrease in GM concentration from *APOE**E2 to *APOE**E3 to *APOE**E4 in all participants, and this effect was present only in the sCON but not in the dCON subgroups (Fig 2C and Table 3). In the parietal lobe, the pattern was inverse, with increased GM con-

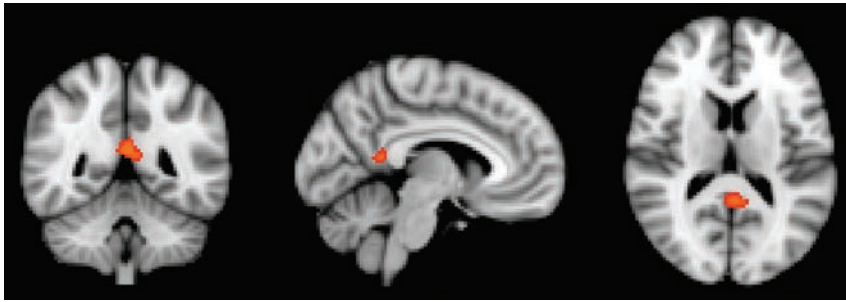


FIG 1. Whole-brain voxel-based morphometry analysis demonstrating higher GM density for the comparison of $APOE^*E3 > APOE^*E4$ in the posterior cingulate cortex. $P < .05$ corrected.

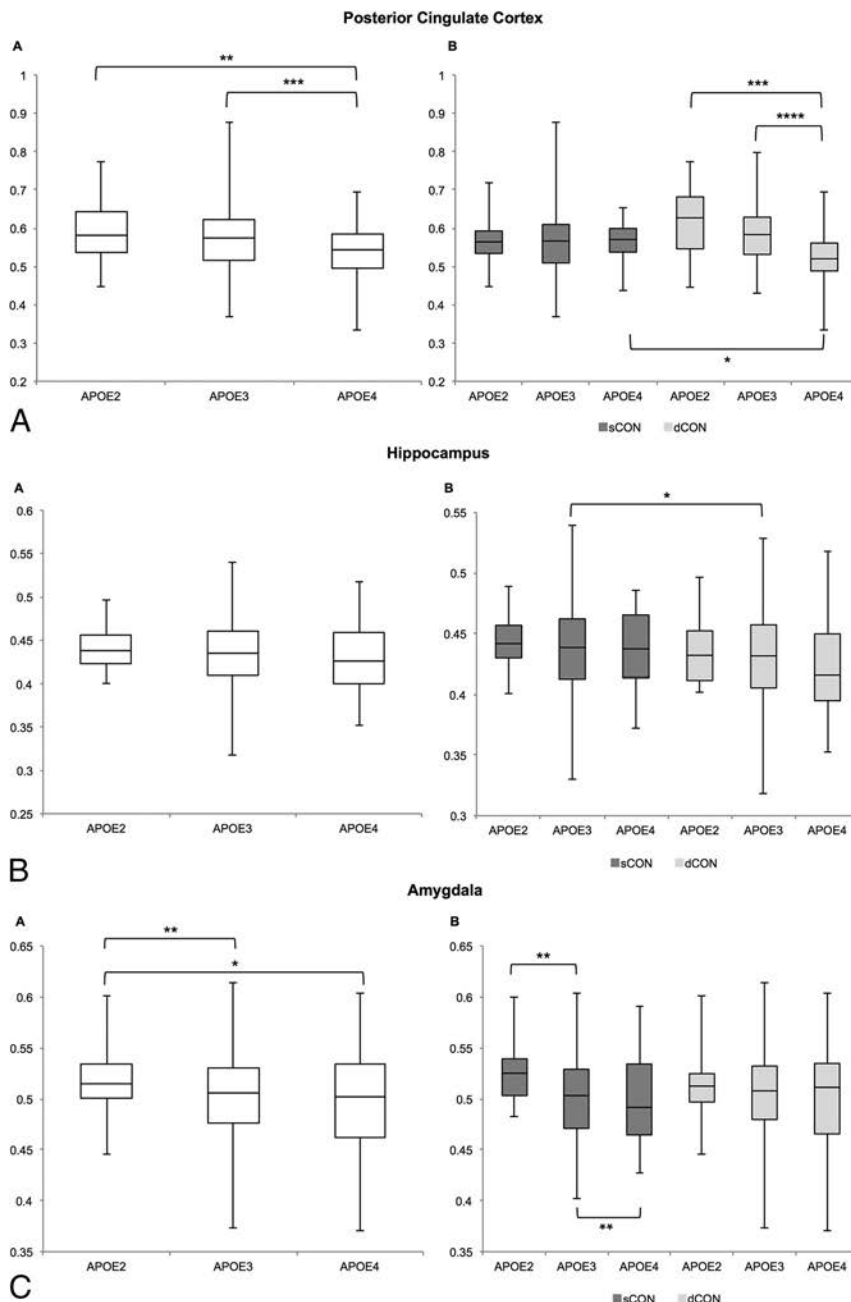


FIG 2. ROI analysis of GM density depending on $APOE$ status for the 7 target regions for all elderly controls (left-hand side) and separately for subjects with sCON and dCON (right-hand side). One asterisk indicates $P < .05$; 2 asterisks, $P < .01$; 3 asterisks, $P < .001$; 4 asterisks, $P < .0001$.

centration in those with dCON, notably in those with $APOE^*E3$ and $APOE^*E4$ (Fig 2D and Table 3). No significant differences were found in the mesial temporal lobe, occipital lobe, or caudate nuclei (Fig 2E–G and Table 3).

Logistic Regression Models

Higher GM densities in the hippocampus, middle temporal lobe, and amygdala were all associated with a decreased risk for dCON status at follow-up (hippocampus: standardized OR = 0.75; 95% CI, 0.61–0.92; $P = .006$; middle temporal lobe: standardized OR = 0.80; 95% CI, 0.65–0.98; $P = .028$; and amygdala: standardized OR = 0.75; 95% CI, 0.61–0.93, $P = .008$). Although significant, these associations explained $<1.5\%$ of cognitive variability. $APOE$ genotyping, age, sex, and duration did not predict dCON status at follow-up. When categorizing GM densities into quintiles, we confirmed the assumption of a linearity of their association with the log odds, because the odds ratios displayed a gradient that is statistically significant for quintile 4 (threshold ≥ 0.4426118) and quintile 5 (threshold ≥ 0.48496512), with ORs of 0.51 ($P = .044$) and 0.44 ($P = .013$).

DISCUSSION

Several studies demonstrated that the presence of the $APOE^*E4$ allele modulates the expression of brain atrophy in MCI and clinically overt AD, increasing the vulnerability of the areas prone to early neurodegeneration such as the hippocampus, amygdala, and mesial temporal lobe.^{15–17} Although higher cortical amyloid β load and decreased metabolism in the above-mentioned areas were reported in the $APOE^*E4$ allele, cross-sectional MR imaging studies failed to identify consistent GM decreases associated with this genotype in elderly controls (for a review see Fouquet et al⁴⁴). The finding in the current investigation that $APOE^*E4$ was related to GM loss in only the subsequently deteriorating but not in the cognitively stable groups might explain these partially conflicting results of previous studies, which typically do not include detailed neuropsychological assessment and follow-up.

The present data show that the $APOE^*E4$ genotype is not associated

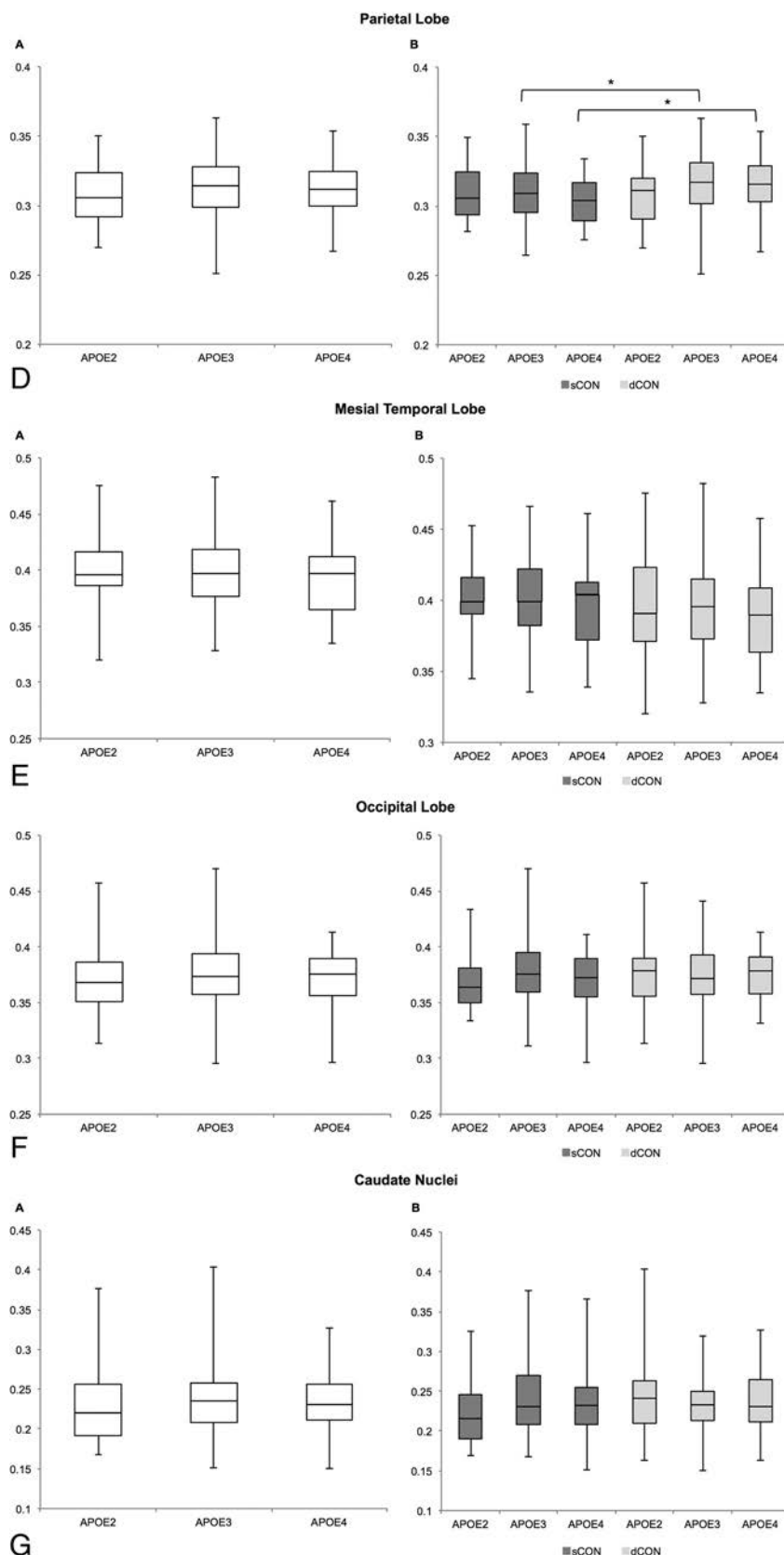


FIG 2. Continued.

with an increased risk of dCON status at follow-up. Consistent with previous reports in elderly controls,^{15,18,20} no *APOE* genotyping-related effect was identified in the hippocampus and me-

sial temporal cortex in subjects with both sCON and dCON. In agreement with previous observations in this field, these observations indicate that the *APOE***E4* allele detrimental effect in terms of structural changes and clinical progression becomes evident only in elderly individuals with significant cognitive deterioration (MCI) or clinically overt symptoms of dementia (early AD).¹⁴⁻¹⁷

The posterior cingulate cortex is known to be affected early in the AD process with significant hypometabolism in cognitively healthy individuals and those with MCI (both converters and nonconverters; for review see Teipel and Grothe⁴⁵). In more advanced stages of the degenerative process, this area exhibits subtle atrophy and hypometabolism in subjects with amnesic amyloid-negative AD.⁴⁶ Rare cross-sectional studies addressed the impact of *APOE* genotyping on the structural and functional integrity of the posterior cingulate cortex. Early contributions from the Cardiovascular Health Study indicated an *APOE***E4*-independent age-related atrophy in the hippocampus and posterior cingulate cortex in healthy elderly controls.⁴⁷ More recently, an altered energy metabolism was reported in this area in young adult *APOE***E4* carriers.⁴⁸ In the same line, Lu et al⁴⁹ reported cortical atrophy in the right cingulate gyrus in cognitively intact *APOE***E4* carriers. Our observations parallel these findings, suggesting that the presence of this allele may have a detrimental effect on GM density in this vulnerable area.

The strengths of the present study include its longitudinal design, large number of community-dwelling subjects, and detailed neuropsychological testing at inclusion and follow-up. However, some limitations should also be considered. First, in line with recent core clinical criteria for MCI,⁵⁰ the identification of deteriorating controls was based on the objective decline in cognitive functions measured by using serial, comprehensive neuropsychological assessments. However, in the absence of longer follow-up and AD biomarker characterization at baseline (including PET amyloid scans or the CSF τ /amyloid

β 42 ratio), the cognitive fate of these individuals remains uncertain so that they cannot be a priori considered as subjects with incipient AD. Second, the rarity of *APOE***E4* homozygotes pre-

Table 2: ROI analysis of GM concentration in the 7 regions for the comparison of sCON versus dCON^a

| | sCON versus dCON | | | | | | |
|---|---------------------|--------------------|------------------------|--------------------|----------------|----------|----------------|
| | Posterior Cingulate | Hippocampus | Mesial Temporal Cortex | Parietal Lobe | Occipital Lobe | Amygdala | Caudate Nuclei |
| <i>APOE</i> * <i>E2</i> (<i>n</i> = 22/21) | .0524 | .3890 | .4189 | .8146 | .4223 | .3146 | .2863 |
| <i>APOE</i> * <i>E3</i> (<i>n</i> = 132/142) | .0813 | .0261 ^b | .0756 | .0349 ^b | .2425 | .2567 | .1384 |
| <i>APOE</i> * <i>E4</i> (<i>n</i> = 27/38) | .0155 ^b | .1916 | .4076 | .0316 ^b | .2433 | .5410 | .3960 |

^a Data are *P* values.^b *P* < .05.**Table 3: ROI analysis of GM concentration in the 7 regions for the comparison of *APOE***E2* versus *APOE***E3* and *APOE***E2* versus *APOE***E4* and *APOE***E3* versus *APOE***E4***

| | <i>APOE</i> * <i>E2</i> versus <i>APOE</i> * <i>E3</i> | <i>APOE</i> * <i>E2</i> versus <i>APOE</i> * <i>E4</i> | <i>APOE</i> * <i>E3</i> versus <i>APOE</i> * <i>E4</i> |
|----------------------|---|---|---|
| Posterior cingulate | | | |
| sCON | .7816 (<i>n</i> = 22/132) | .9153 (<i>n</i> = 22/27) | .6539 (<i>n</i> = 132/27) |
| dCON | .1989 (<i>n</i> = 21/142) | .0004 ^a (<i>n</i> = 22/38) | .00002 ^b (<i>n</i> = 132/38) |
| Hippocampus | | | |
| sCON | <i>P</i> = .4227 | <i>P</i> = .3954 | <i>P</i> = .7191 |
| dCON | <i>P</i> = .2852 | <i>P</i> = .1937 | <i>P</i> = .5711 |
| Mesial temporal lobe | | | |
| sCON | <i>P</i> = .7285 | <i>P</i> = .313 | <i>P</i> = .3601 |
| dCON | <i>P</i> = .9713 | <i>P</i> = .5361 | <i>P</i> = .3119 |
| Parietal lobe | | | |
| sCON | <i>P</i> = .6977 | <i>P</i> = .4708 | <i>P</i> = .1469 |
| dCON | <i>P</i> = .1433 | <i>P</i> = .2133 | <i>P</i> = .8734 |
| Occipital lobe | | | |
| sCON | <i>P</i> = .0596 | <i>P</i> = .6834 | <i>P</i> = .1617 |
| dCON | <i>P</i> = .9744 | <i>P</i> = .6773 | <i>P</i> = .4631 |
| Amygdala | | | |
| sCON | <i>P</i> = .0025 ^c | <i>P</i> = .0083 ^c | <i>P</i> = .6342 |
| dCON | <i>P</i> = .4174 | <i>P</i> = .3411 | <i>P</i> = .6874 |
| Caudate nuclei | | | |
| sCON | <i>P</i> = .2931 | <i>P</i> = .4369 | <i>P</i> = .8506 |
| dCON | <i>P</i> = .9051 | <i>P</i> = .9427 | <i>P</i> = .9431 |

^a *P* < .001.^b *P* < .0001.^c *P* < .01.

cluded a detailed analysis of gene-dose effect on GM densities. Third, handedness was not considered as a covariate in our MR imaging analysis, which included both left- and right-handed controls.

CONCLUSIONS

Our data reveal that the presence of the *APOE***E4* allele is associated with decreased GM density in the posterior cingulate cortex in dCON, a community-based group of elderly controls who subsequently had subtle cognitive decline at 18-month follow-up. This *APOE* effect was not identified in cognitively stable controls. Most important, the *APOE***E4* allele has no impact on GM density in areas affected early by neurofibrillary tangle formation such as the hippocampus and mesial temporal lobe. These observations suggest that decreased GM density in the posterior cingulate cortex should be systematically detected among *APOE***E4* controls because it could represent a structural marker preceding subtle cognitive deficits in the very early stages of the degenerative process.

Disclosures: Sven Haller—RELATED: Grant: Swiss National Foundation, Comments: grant SNF 3200B0–1161193 and SPUM 33CM30–124111* and an unrestricted grant from the Association Suisse pour la Recherche Alzheimer*. *Money paid to the institution.

REFERENCES

1. Corder EH, Saunders AM, Strittmatter WJ, et al. Gene dose of apolipoprotein E type 4 allele and the risk of Alzheimer's disease in late onset families. *Science* 1993;261:921–23 [CrossRef Medline](#)
2. Strittmatter WJ, Saunders AM, Schmechel D, et al. Apolipoprotein E: high-avidity binding to beta-amyloid and increased frequency of type 4 allele in late-onset familial Alzheimer disease. *Proc Natl Acad Sci U S A* 1993;90:1977–81 [CrossRef Medline](#)
3. Jack CR Jr, Thorneau TM, Wiste HJ, et al. Transition rates between amyloid and neurodegeneration biomarker states and to dementia: a population-based, longitudinal cohort study. *Lancet Neurol* 2016; 15:56–64 [CrossRef Medline](#)
4. Jack CR Jr, Wiste HJ, Weigand SD, et al. Age-specific population frequencies of cerebral β -amyloidosis and neurodegeneration among people with normal cognitive function aged 50–89 years: a cross-sectional study. *Lancet Neurol* 2014;13:997–1005 [CrossRef Medline](#)
5. Lee YM, Ha JK, Park JM, et al. Impact of apolipoprotein E4 polymorphism on the gray matter volume and the white matter integrity in subjective memory impairment without white matter hyperintensities: voxel-based morphometry and Tract-Based Spatial Statistics Study under 3-Tesla MRI. *J Neuroimaging* 2016;26: 144–49 [CrossRef Medline](#)
6. Li B, Shi J, Gutman BA, et al. Influence of APOE genotype on hippocampal atrophy over time: an N=1925 surface-based ADNI study. *PLoS One* 2016;11:e0152901 [CrossRef Medline](#)
7. Shi J, Lepore N, Gutman BA, et al. Genetic influence of apolipoprotein

- tein E4 genotype on hippocampal morphometry: an N = 725 surface-based Alzheimer's disease neuroimaging initiative study. *Hum Brain Mapp* 2014;35:3903–18 CrossRef Medline
8. Gohi J, Cervantes S, Arrondo G, et al. Selective brain gray matter atrophy associated with APOE ϵ 4 and MAPT H1 in subjects with mild cognitive impairment. *J Alzheimers Dis* 2013;33:1009–19 CrossRef Medline
9. Lu PH, Thompson PM, Leow A, et al. Apolipoprotein E genotype is associated with temporal and hippocampal atrophy rates in healthy elderly adults: a tensor-based morphometry study. *J Alzheimers Dis* 2011;23:433–42 CrossRef Medline
10. Honea RA, Vidoni E, Harsha A, et al. Impact of APOE on the healthy aging brain: a voxel-based MRI and DTI study. *J Alzheimers Dis* 2009;18:553–64 Medline
11. Agosta F, Vessel KA, Miller BL, et al. Apolipoprotein E epsilon4 is associated with disease-specific effects on brain atrophy in Alzheimer's disease and frontotemporal dementia. *Proc Natl Acad Sci U S A* 2009;106:2018–22 Medline
12. Wishart HA, Saykin AJ, McAllister TW, et al. Regional brain atrophy in cognitively intact adults with a single APOE epsilon4 allele. *Neurology* 2006;67:1221–24 CrossRef Medline
13. Pennanen C, Testa C, Boccardi M, et al. The effect of apolipoprotein polymorphism on brain in mild cognitive impairment: a voxel-based morphometric study. *Dement Geriatr Cogn Disord* 2006;22:60–66 CrossRef Medline
14. Liu Y, Paajanen T, Westman E, et al. Effect of APOE ϵ 4 allele on cortical thicknesses and volumes: the AddNeuroMed study. *J Alzheimers Dis* 2010;21:947–66 CrossRef Medline
15. Lupton MK, Strike L, Hansell NK, et al. The effect of increased genetic risk for Alzheimer's disease on hippocampal and amygdala volume. *Neurobiol Aging* 2016;40:68–77 CrossRef Medline
16. Wang X, Wang J, He Y, et al. Apolipoprotein E ϵ 4 modulates cognitive profiles, hippocampal volume, and resting-state functional connectivity in Alzheimer's disease. *J Alzheimers Dis* 2015;45:781–95 CrossRef Medline
17. Susanto TA, Pua EP, Zhou J, et al. Cognition, brain atrophy, and cerebrospinal fluid biomarkers changes from preclinical to dementia stage of Alzheimer's disease and the influence of apolipoprotein e. *J Alzheimers Dis* 2015;45:253–68 CrossRef Medline
18. Chen J, Shu H, Wang Z, et al. The interaction of APOE genotype by age in amnesic mild cognitive impairment: a voxel-based morphometric study. *J Alzheimers Dis* 2015;43:657–68 CrossRef Medline
19. Chen Y, Chen K, Zhang J, et al. Disrupted functional and structural networks in cognitively normal elderly subjects with the APOE ϵ 4 allele. *Neuropsychopharmacology* 2015;40:1181–91 CrossRef Medline
20. Habes M, Toledo JB, Resnick SM, et al. Relationship between APOE genotype and structural MRI measures throughout adulthood in the study of health in Pomerania population-based cohort. *AJNR Am J Neuroradiol* 2016;37:1636–42 CrossRef Medline
21. Matura S, Prvulovic D, Jurcoane A, et al. Differential effects of the ApoE4 genotype on brain structure and function. *Neuroimage* 2014;89:81–91 CrossRef Medline
22. Shaw P, Lerch JP, Pruessner JC, et al. Cortical morphology in children and adolescents with different apolipoprotein E gene polymorphisms: an observational study. *Lancet Neurol* 2007;6:494–500 CrossRef Medline
23. O'Dwyer L, Lambertson F, Matura S, et al. Reduced hippocampal volume in healthy young ApoE4 carriers: an MRI study. *PLoS One* 2012;7:e48895 CrossRef Medline
24. Hämäläinen A, Grau-Olivares M, Tervo S, et al. Apolipoprotein E epsilon 4 allele is associated with increased atrophy in progressive mild cognitive impairment: a voxel-based morphometric study. *Neurodegener Dis* 2008;5:186–89 CrossRef Medline
25. Risacher SL, Shen L, West JD, et al. Alzheimer's Disease Neuroimaging Initiative (ADNI). Longitudinal MRI atrophy biomarkers: relationship to conversion in the ADNI cohort. *Neurobiol Aging* 2010;31:1401–18 CrossRef Medline
26. Folstein MF, Folstein SE, McHugh PR. "Mini-mental state": a practical method for grading the cognitive state of patients for the clinician. *J Psychiatr Res* 1975;12:189–98 CrossRef Medline
27. Zigmond AS, Snaith RP. The hospital anxiety and depression scale. *Acta Psychiatr Scand* 1983;67:361–70 CrossRef Medline
28. Barberger-Gateau P, Commenges D, Gagnon M, et al. Instrumental activities of daily living as a screening tool for cognitive impairment and dementia in elderly community dwellers. *J Am Geriatr Soc* 1992;40:1129–34 CrossRef Medline
29. Wechsler DA. *Wechsler Memory Scale*. 3rd ed. San Antonio: Psychological Corporation; 1987
30. Reitan RM. Validity of the Trail Making Test as an indicator of organic brain damage. *Percept Mot Skills* 1958;8:271–76
31. Wechsler D. *Manual for the Wechsler Adult Intelligence Scale*. New York: Psychological Corporation; 1995
32. Milner B. Interhemispheric differences in the localization of psychological processes in man. *Br Med Bull* 1971;27:272–77 CrossRef Medline
33. Buschke H, Sliwinski MJ, Kuslansky G, et al. Diagnosis of early dementia by the Double Memory Test: encoding specificity improves diagnostic sensitivity and specificity. *Neurology* 1997;48:989–97 CrossRef Medline
34. Baddley A, Emslie H, Nimmo-Smith I. *Doors and People. A Test of Visual and Verbal Recall and Recognition*. Bury St. Edmunds: Thames Valley Test Company; 1994
35. Kaplan EF, Goodglass H, Weintraub S. *The Boston Naming Test*. 2nd ed. Philadelphia: Lea & Febiger; 1983
36. Schnider A, Hanlon RE, Alexander DN, et al. Ideomotor apraxia: behavioral dimensions and neuroanatomical basis. *Brain Lang* 1997;58:125–36 CrossRef Medline
37. Poeck K. Clues to the nature of disruption to limb Praxis. In: Roy EA, ed. *Neuropsychological Studies of Apraxia and related Disorders*. Amsterdam: North-Holland; 1985:99–109
38. Welsh KA, Butters N, Mohs RC, et al. The Consortium to Establish a Registry for Alzheimer's Disease (CERAD), Part V: a normative study of the neuropsychological battery. *Neurology* 1994;44:609–14 CrossRef Medline
39. Hughes CP, Berg L, Danziger WL, et al. A new clinical scale for the staging of dementia. *Br J Psychiatry* 1982;140:566–72 CrossRef Medline
40. Petersen RC, Doody R, Kurz A, et al. Current concepts in mild cognitive impairment. *Arch Neurol* 2001;58:1985–92 CrossRef Medline
41. Xekardaki A, Rodriguez C, Montandon ML, et al. Arterial spin labeling may contribute to the prediction of cognitive deterioration in healthy elderly individuals. *Radiology* 2015;274:490–99 CrossRef Medline
42. Nauck M, Hoffmann MM, Wieland H, et al. Evaluation of the apo E genotyping kit on the LightCycler. *Clin Chem* 2000;46:722–24 Medline
43. Smith SM, Nichols TE. Threshold-free cluster enhancement: addressing problems of smoothing, threshold dependence and localisation in cluster inference. *Neuroimage* 2009;44:83–98 CrossRef Medline
44. Fouquet M, Besson FL, Gonneaud J, et al. Imaging brain effects of APOE4 in cognitively normal individuals across the lifespan. *Neuropsychol Rev* 2014;24:290–99 CrossRef Medline
45. Teipel S, Grothe MJ; Alzheimer's Disease Neuroimaging Initiative. Does posterior cingulate hypometabolism result from disconnection or local pathology across preclinical and clinical stages of Alzheimer's disease. *Eur J Nucl Med Mol Imaging* 2016;43:526–36 CrossRef Medline
46. Chételat G, Ossenkoppele R, Villemagne VL, et al. Atrophy, hypometabolism and clinical trajectories in patients with amyloid-negative Alzheimer's disease. *Brain* 2016;139:2528–39 CrossRef Medline
47. Raji CA, Lopez OL, Kuller LH, et al. White matter lesions and brain

- gray matter volume in cognitively normal elders. *Neurobiol Aging* 2012;33:-834.e7–16 [CrossRef](#)
48. Perkins M, Wolf AB, Chavira B, et al. **Altered energy metabolism pathways in the posterior cingulate in young adult apolipoprotein E ϵ 4 carriers.** *J Alzheimers Dis* 2016;53:95–106 [CrossRef](#) [Medline](#)
49. Lu H, Fung AW, Chan SS, et al. **Disturbance of attention network functions in Chinese healthy older adults: an intra-individual perspective.** *Int Psychogeriatr* 2016;28:291–301 [CrossRef](#) [Medline](#)
50. Albert MS, DeKosky ST, Dickson D, et al. **The diagnosis of mild cognitive impairment due to Alzheimer's disease: recommendations from the National Institute on Aging-Alzheimer's Association workgroups on diagnostic guidelines for Alzheimer's disease.** *Alzheimers Dement* 2011;7:270–79 [CrossRef](#) [Medline](#)

Pontomesencephalic Atrophy and Postural Instability in Wilson Disease

J. Kalita, S. Naik, S.K. Bhoi, U.K. Misra, A. Ranjan, and S. Kumar



ABSTRACT

BACKGROUND AND PURPOSE: The MR Parkinsonism index helps in differentiating progressive supranuclear palsy from Parkinson disease and multisystem atrophy. Pontomesencephalic involvement is common in neurologic Wilson disease, but there is no prior study evaluating the MR Parkinsonism index and its indices in Wilson disease. We report the MR Parkinsonism index and its indices in Wilson disease and correlate these changes with clinical severity and postural reflex.

MATERIALS AND METHODS: Thirteen individuals with neurologic Wilson disease were included, and their clinical details, including neurologic severity, postural reflex abnormality, and location of signal changes on MR imaging, were noted. The 3D BRAVO T1 sequence was used for measurement of the MR Parkinsonism index and its indices. The MR Parkinsonism index and its indices were also obtained in 6 age- and sex-matched controls. The morphometric parameters in Wilson disease were compared with those in with healthy controls and among the patients with and without abnormal postural reflex.

RESULTS: The midbrain area was reduced in patients with Wilson disease compared with controls (112.08 ± 27.94 versus 171.95 ± 23.66 mm², $P = .002$). The patients with an abnormal postural reflex had an increased MR Parkinsonism index and pons-to-midbrain ratio compared with controls, whereas these parameters were equivalent in patients with normal postural reflex and controls. The patients with abnormal postural reflex had more severe illness, evidenced by higher Burke-Fahn-Marsden scores (51.0 ± 32.27 versus 13.75 ± 12.37 , $P = .04$) and neurologic severity grades (2.57 ± 0.53 versus 1.67 ± 0.82 , $P = .04$).

CONCLUSIONS: An increase in the MR Parkinsonism index in Wilson disease is mainly due to midbrain atrophy and it correlates with neurologic severity and abnormal postural reflex.

ABBREVIATIONS: MCP = middle cerebellar peduncle; MRPI = MR Parkinsonism index; PD = Parkinson disease; PSP = progressive supranuclear palsy; SCP = superior cerebellar peduncle; WD = Wilson disease

Wilson disease (WD) is an autosomal recessive disorder of copper metabolism due to *ATP7B* mutation on chromosome 13q14.3.¹ It is a rare disease with a world wide prevalence of 1–2/100,000 population.² Neurologic manifestation in WD usually occurs in the second decade and is characterized by cognitive decline, drooling, and varying severity of extrapyramidal and pyramidal symptoms and signs.^{3–5} The characteristic cranial MR

imaging abnormalities in WD are corpus striatal involvement and the “giant Panda sign,” which are reported in 14.3%–71.5% of patients.^{6–8} Involvement of the pons and midbrain may lead to an abnormal postural reflex in WD, which may increase the neurologic disability. Recently, the MR Parkinsonism index (MRPI) has been reported to correctly differentiate progressive supranuclear palsy (PSP) from Parkinson disease (PD) and multisystem atrophy.^{9–11} These studies did not correlate the MRPI with postural reflexes. The loss of neurons in the mesencephalic locomotor region and pedunculo-pontine region has been reported in postmortem studies on PD and PSP.^{12,13} Stroke in these areas has been reported with freezing and impaired gait initiation.^{14–16}

Abnormal postural reflex renders an individual prone to falls, leading to fractures and head injury. The MRPI may be a radiologic marker of abnormal postural reflex but this has not been studied. In neurologic WD, involvement of the midbrain and pons on MR imaging has been reported in up to 66% of patients.^{4,8} There is no study evaluating postural reflex and MRPI in

Received September 14, 2016; accepted after revision February 21, 2017.

From the Departments of Neurology (J.K., S.K.B., U.K.M., A.R.) and Radiology (S.N., S.K.), Sanjay Gandhi Post Graduate Institute of Medical Sciences, Lucknow, India.

This study was approved by Institutional Ethics Committee, Sanjay Gandhi Post Graduate of Medical Sciences, Lucknow India.

Please address correspondence to J. Kalita, MD, DM, Department of Neurology, Sanjay Gandhi Post Graduate Institute of Medical Sciences, Raebareilly Rd, Lucknow 226014, Uttar Pradesh, India; e-mail: jayanteeek@yahoo.com, jkalita@sgpgi.ac.in



Indicates article with supplemental on-line video.

<http://dx.doi.org/10.3174/ajnr.A5207>

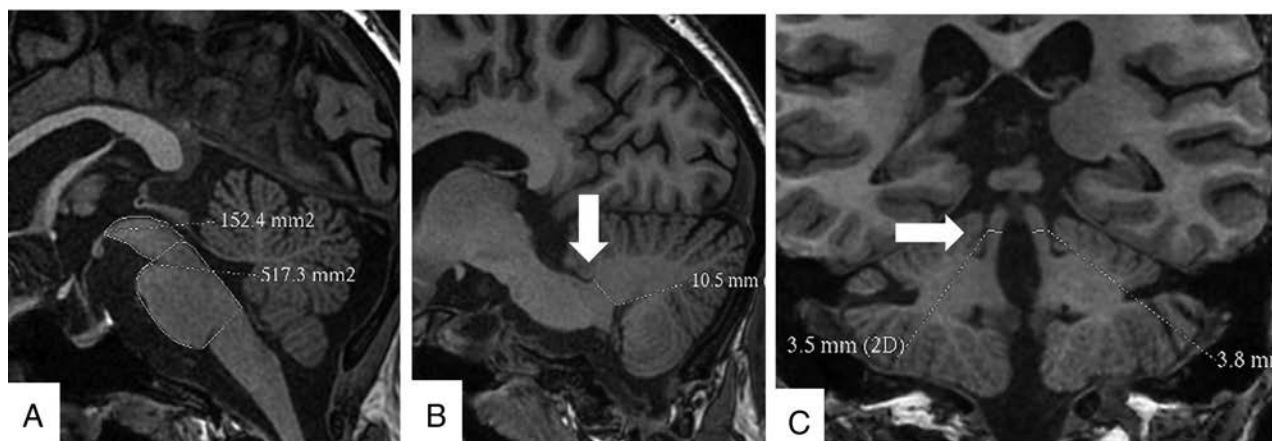


FIG 1. Cranial MR imaging in the BRAVO 3D sequence showing the protocol of measurement of the midbrain and pons areas (A), width of the middle cerebellar peduncle (B), and width of the superior cerebellar peduncle (C).

patients with neurologic WD, to our knowledge. In this communication, we report MRPI parameters in patients with neurologic WD and correlate these with postural reflex and disease severity.

MATERIALS AND METHODS

Patients with WD having neurologic manifestations were prospectively included. The diagnosis of WD was based on characteristic clinical features, a Kayser-Fleischer ring on slit lamp examination, serum ceruloplasmin levels (<20 mg/dL), and 24-hour urinary copper excretion (>40 μ g).^{17,18} The study was approved by the ethics committee of the institution. A detailed clinical history, including duration of illness, cognitive decline, drooling, seizures, abnormal movements, jaundice, and skeletal abnormality, was noted. A pedigree chart was prepared for each index patient. The neurologic severity of WD was grades I–III based on 5 signs (tremor, dysarthria, ataxia, rigidity/bradykinesia, and chorea/dystonia).¹⁹ The severity of dystonia was assessed by the Burke-Fahn-Marsden score.²⁰ Patients were examined for nystagmus, horizontal and vertical gaze, and saccadic and pursuit eye movements. Postural reflex was assessed by the pull test. The examiner stood behind the patient, and the patient was instructed to maintain the same erect, stable posture when subjected to a sudden backward pull on their shoulders. The pull test result was considered abnormal if the patient went >2 steps backward or lost balance.²¹

Investigations

Routine laboratory tests, including clotting parameters, were assessed for any abnormalities. The serum and urinary copper levels were assessed by an atomic absorption spectrophotometer. The serum-free copper level was calculated by subtracting 3 times the serum ceruloplasmin level from the total serum copper level (microgram/deciliter).^{17,22} A sonographic abdomen examination was performed.

Cranial MR Imaging. Cranial MR imaging was performed by using a 3T Signa scanner (GE Healthcare, Milwaukee, Wisconsin). We obtained the following sequences: T1 (TR, 1254 ms; TE, 11.6 ms), T2 (TR, 5600 ms; TE, 95.5 ms), fast fluid-attenuated inversion recovery (TI, 2200 ms; TR, 8802 ms; TE, 85.4 ms), and DWI (TR, 5600 ms; TE, 72.4 ms, at 2 b-values of 0 and 1000 s/mm²). The isotropic diffusion-weighted images were reviewed. All images

were 5-mm-thick with an intersection gap of 0.5 mm. Matrix size was 256×256 with NEX = 1. Abnormal signal, extent, and location were noted.

The T1-weighted 3D BRAVO sequence (GE Healthcare) was performed in 13 patients and 6 controls. We used the following parameters: TR/TE, 8.4/3.3 ms; TI, 400 ms; flip angle, 13°; FOV, 240×240 mm²; matrix, 288×288 ; and section thickness, 1-mm without intersection gap. The acquisition time was 4.08 minutes.

The midbrain and pons areas were measured on the midsagittal 3D BRAVO sequence. A line passing through the superior pontine notch and the inferior edge of the quadrigeminal plate was taken as the demarcating line between midbrain and pons. A second line parallel to the first line passing through the inferior pontine notch was taken as the lower margin of the pons. The midbrain area was traced around the edges of the midbrain tegmentum above the first line. The tectum of the midbrain was not included. The pons area was included craniocaudally between the 2 above-mentioned lines and along the anterior and posterior margins of the pons anteroposteriorly. The width of the middle cerebellar peduncle (MCP) was measured on parasagittal views of the 3D BRAVO sequence. Left and right MCPs were identified on parasagittal views on which the MCP was best exposed between the pons and the cerebellum. The distance between the superior and inferior borders of the MCP was measured, as delineated by the peripeduncular CSF spaces of the pontocerebellar cisterns. Each MCP width (left and right) was measured, and a mean value for the 2 MCPs was calculated. The superior cerebellar peduncles (SCPs) were measured on the coronal views of the 3D BRAVO sequence. In the coronal view, images were inspected in the anteroposterior direction parallel to the axis of the brain stem to identify the SCP. The linear distance between the medial and lateral borders of the superior cerebellar peduncle was measured at the middle of their extension, and an average of the 2 SCPs was calculated. The ratios of pons-to-midbrain area and MCP-to-SCP width (MCP/SCP) were also used, and the MRPI was calculated by Pons Area / Midbrain Area \times MCP width / SCP width (Fig 1).¹¹

Statistical Analysis

The MRPI and its different indices in patients were compared with 6 age- (23.15 ± 8.72 versus 20.50 ± 6.60 , $P = .54$) and sex-

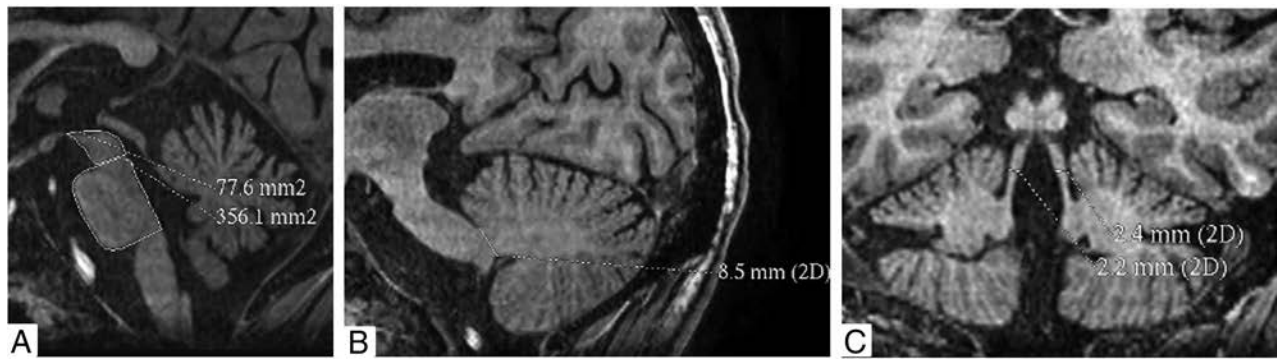


FIG 2. Cranial MR imaging of a 31-year-old woman with Wilson disease shows increased pons-to-midbrain areas (4.59 mm^2) (A), reduced width of the middle cerebellar peduncle (8 mm) (B), and a reduced width of superior cerebellar peduncle (2.3 mm) (C). Her MR Parkinsonism index was increased (16.9). She had impaired postural reflex.

Comparison of MRI morphometric parameters between patients with Wilson disease with neurologic manifestation and healthy controls

| Serial No. | Parameters | Wilson Disease (n = 13) | Controls (n = 6) | P Value |
|------------|------------------------------------|-------------------------|--------------------|---------|
| 1 | Age (mean) (yr) | 23.15 ± 8.72 | 20.50 ± 6.60 | .54 |
| 2 | Female/male | 5:8 | 2:4 | 1.00 |
| 3 | MB area (mean) (mm^2) | 112.08 ± 27.94 | 171.95 ± 23.66 | .002 |
| 4 | Pons area (mean) (mm^2) | 402.45 ± 45.47 | 469.27 ± 45.62 | .02 |
| 5 | Right MCP (mean) (mm) | 8.68 ± 0.76 | 9.78 ± 1.01 | .04 |
| 6 | Left MCP (mean) (mm) | 8.72 ± 0.93 | 9.73 ± 1.15 | .07 |
| 7 | Mean MCP (mean) (mm) | 8.70 ± 0.81 | 9.76 ± 1.12 | .06 |
| 8 | Right SCP (mean) (mm) | 2.90 ± 0.53 | 3.65 ± 0.58 | .03 |
| 9 | Left SCP (mean) (mm) | 3.12 ± 0.49 | 3.73 ± 0.55 | .06 |
| 10 | Mean SCP (mean) (mm) | 3.01 ± 0.50 | 3.71 ± 0.57 | .03 |
| 11 | Pons area/MB area (mean) (mm) | 3.75 ± 0.78 | 2.75 ± 0.20 | .004 |
| 12 | MCP/SCP (mean) (mm) | 2.96 ± 0.56 | 2.67 ± 0.44 | .22 |
| 13 | MR parkinsonism index ^a | 11.01 ± 2.99 | 7.31 ± 1.20 | .002 |

Note:—MB indicates midbrain.

^a MR Parkinsonism index = (Pons area / MB area) \times (MCP width / SCP width).

(M/F, 8:5 versus 4:2; $P = 1.00$) matched healthy controls by using the Mann-Whitney U test. The MRPI and its parameters in WD were also compared with clinical, MR imaging findings; the Burke-Fahn-Marsden score; and the severity of WD by using various parametric and nonparametric tests. The MRPI and its indices were also compared between controls and patients with WD with and without an abnormal postural reflex by 1-way ANOVA with the Tukey multiple comparison test. The statistical analysis was performed by using SPSS, Version 16, software (IBM, Armonk, New York), and graphs were prepared with GraphPad Prism 5 software (GraphPad Software, San Diego, California). The variable was considered significant if the 2-tailed P value was $< .05$.

RESULTS

Thirteen patients with WD with neurologic manifestations were included whose median age was 23 years (range, 12–40 years); 5 were females. The median duration of illness was 18 months (range, 3–84 months). Only 1 patient had a history of jaundice. All patients had varying types and severity of movement disorders, which included dystonia in all, tremor in 10, choreoathetosis in 1, and myoclonus in 1 patient. Seven patients had drooling. The Burke-Fahn-Marsden score ranged between 2 and 84 (median, 24). Three patients had grade I severity, and the remaining patients had grades II and III. Mus-

cle power was normal in all, though tendon reflexes were brisk in 10 patients. Seven patients had abnormal postural reflex on the pull test: Four had > 2 steps backward-stepping and 3 lost their balance (On-line Video 1). Nine patients had slow pursuit and broken saccadic eye movements in both horizontal and vertical gazes.

MR Imaging Findings

Cranial MR imaging findings were abnormal in all and revealed the following involvement: putamen in 11; globus pallidus in 6; caudate in 6; thalamus, midbrain, and pons in 8 each; subcortical white matter in 2; frontal cortex in 1; middle cerebellar peduncle in 2; and cerebellum in 1 patient. These lesions were hyperintense in T2 and FLAIR, and diffusion restriction in a frontal lesion was found in 1 patient.

Morphometric Parameters on MR Imaging

The areas of the pons ($P = .02$) and midbrain ($P = .002$) and the width of the SCP ($P = .03$) were reduced in patients with WD compared with the controls. The midbrain was more atrophied compared with the pons; this finding was evident by an increase in the ratio of the pons to the midbrain area in patients compared with controls ($P = .004$). The ratio of MCP to SCP width, however, was not different between patients and controls ($P = .22$). The MRPI was higher in patients with WD compared with controls (11.01 ± 2.99 versus 7.31 ± 1.20 , $P = .002$; Fig 2). The details are presented in the Table.

Clinical Correlation

The postural reflex was abnormal in 7 and normal in 6 patients; both of these groups had reduced midbrain areas compared with controls ($P < .001$). The patients with abnormal postural reflex had significant reduction in the pons area ($P < .01$), MCP width ($P < .05$), and SCP width ($P < .05$) compared with controls. These 3 parameters, however, were not significantly different between controls and patients with WD with normal postural re-

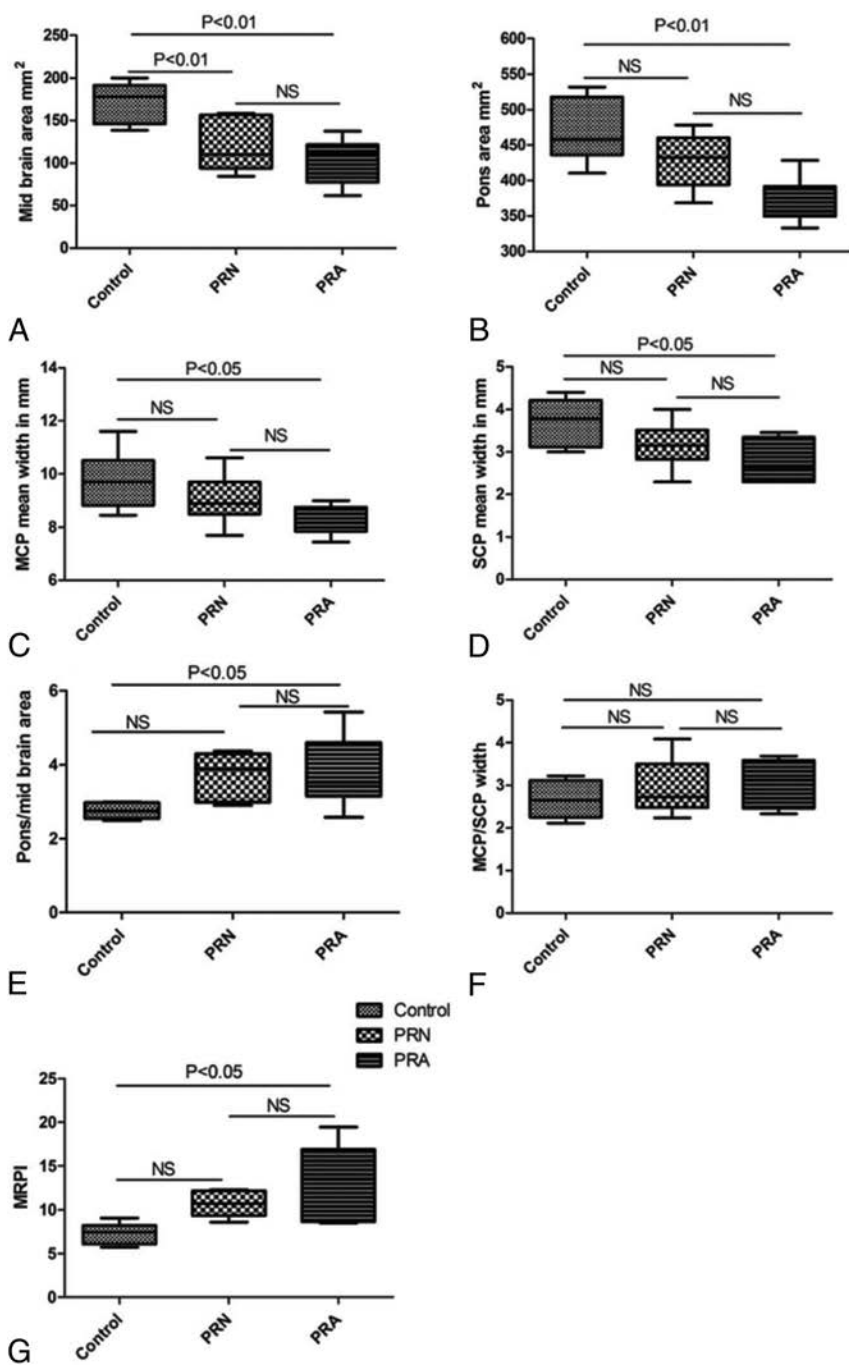


FIG 3. Error bar diagram shows the MR Parkinsonism index and its indices in patients with Wilson disease with postural reflex abnormality compared with patients with WD with normal postural reflex (PRN) and healthy controls. The midbrain area was reduced in patients with WD with and without postural reflex abnormality (PRA), but MRPI and pons-to-midbrain areas were increased and the width of the superior and middle cerebellar peduncles was decreased in patients with WD with postural reflex abnormality but not patients with normal postural reflex compared with controls.

flexes. The pons-to-midbrain ratio ($P < .05$) and MRPI ($P < .05$) were significantly increased in patients with WD with abnormal postural reflexes compared with those with normal postural reflexes and healthy controls. The details are presented in Fig 3.

The presence of abnormal signal changes in the midbrain and pons was not related to the midbrain area (105.83 ± 25.41 versus 119.38 ± 31.30 mm², $P = .77$) and pons area (380.57 ± 39.65 versus 427.97 ± 40.29 mm², $P = .06$). The patients with abnormal

postural reflex had more severe illness, evidenced by higher Burke-Fahn-Marsden scores (51.0 ± 32.27 versus 13.75 ± 12.37 , $P = .04$) and higher grades of neurologic severity (2.57 ± 0.53 versus 1.67 ± 0.82 , $P = .04$).

DISCUSSION

This study revealed an increase in the MRPI and pons-to-midbrain ratio in patients with WD compared with controls. These changes were more marked in patients with abnormal postural reflex, and abnormal postural reflex correlated with neurologic severity. This is the first study reporting morphometric evaluation of brain stem structures and MRPI in WD and correlating these parameters with clinical severity and postural reflex. During the past 20 years, a number of MR imaging features and morphometric parameters have been evaluated to differentiate PSP and multisystem atrophy from PD.⁹⁻¹¹ The overlapping clinical features sometime cause difficulty in differentiating PSP from PD and multisystem atrophy-Parkinson. In a study on 45 patients with clinically unclassifiable parkinsonism, MRPI ≥ 13.55 predicted PSP at 3-year follow-up with 100% sensitivity, 90.3% specificity, and 92.9% accuracy.¹¹ The patients with MRPI ≥ 13.55 had higher Unified Parkinson's Disease Rating Scale scores and more frequent falls compared with those with MRPI < 13.55 . In our study, none of the controls had MRPI > 9 , but 10 of 13 patients with WD had MRPI ≥ 9 . All our patients were children or young adults, and none were older than 40 years of age. We therefore used normal age- and sex-matched controls. The ratio of MCP-to-SCP width was not significantly different in the patients with WD compared with controls. In PSP, the MCP-to-SCP ratio was increased due to greater reduction of the SCP width. Conventional MR imaging did not reveal any signal changes in PSP, multisystem

atrophy, and PD; whereas in WD, midbrain involvement occurred in 32.4%–49% of patients.^{4,8,23}

The involvement of the pons, cerebellum, and cerebellar peduncles, however, is rare in WD. The signal changes in the midbrain and pons in our patients, however, were not related to the midbrain and pons areas, respectively. This finding suggests that the reduction of the midbrain and pons areas may be due to chronic degeneration or apoptosis of the neurons of the midbrain

locomotor region and pedunculopontine neurons. Dopaminergic and other aminergic neurons of the brain stem are metabolically active; therefore, they are vulnerable to oxidative stress. Serum-free copper levels are increased in WD and can cross the blood-brain barrier and may result in oxidative injury. In a study on neurologic WD, serum antioxidants (glutathione and total antioxidant capacity) were reduced and the oxidative marker (malondialdehyde) and tumor necrosis factor- α were increased. These parameters were related to serum-free copper and urinary excretion of copper.²² In another study, an increase in death signal (tumor necrosis factor α , interleukin 8, malondialdehyde) and reduction in survival signal (glutathione and X-link inhibitors of apoptosis protein) have been reported.²³

Posture is a reflex and involves involuntary contraction of antigravity muscles to maintain an erect posture. Human locomotion is presumed to have supraspinal control, whereas animal locomotion is mostly spinal. The pedunculopontine nuclei are located in the pontomesencephalic tegmentum and are thought to be the anatomic substrate of human locomotion. Pedunculopontine nuclei are reciprocally connected to the limbic system, globus pallidus, subthalamic nuclei, substantia nigra, and brain stem reticular formation. The rhythmic activity of pedunculopontine nuclei is under cerebellar control. Reduction in the number of pedunculopontine neurons may result in dopamine-resistant extrapyramidal syndrome, including freezing, postural instability, and sleep disturbance.²⁴ The dystonia in WD is also resistant to dopaminergic drugs.²⁵

The present study is limited by the small number of patients. WD is a rare inherited metabolic disease. Many patients with WD die in the first decade due to liver failure, and only a few survive to develop neurologic manifestations. The results of our study are helpful in understanding the basis of postural instability in WD. Increased MRPI and midbrain-to-pons ratio may be the radiologic markers of postural instability in WD but need confirmation in a larger study. The improvement in postural reflex following chelating treatment may correspond with improvement in MRPI and midbrain-to-pons ratio, which may be explored in a future longitudinal study.

CONCLUSIONS

An increase in MRPI in WD is mainly due to midbrain atrophy, and it correlates with abnormal postural reflex and neurologic severity.

ACKNOWLEDGMENTS

We thank Mr Rakesh Kumar Nigam and Mr Shakti Kumar for the secretarial help.

REFERENCES

1. Bull PC, Thomas GR, Rommens JM, et al. **The Wilson disease gene is a putative copper transporting P-type ATPase similar to the Menkes gene.** *Nat Genet* 1993;5:327–37 CrossRef Medline
2. Jankovic J. **Movement disorder.** In: Daroff RB, Fenichel GM, Jankovic J, et al, eds. *Bradley's Neurology in Clinical Practice*. 6th ed. Philadelphia: Elsevier/Saunders; 2012:1762–1801
3. Kalita J, Kumar V, Ranjan A, et al. **Role of oxidative stress in the worsening of neurologic Wilson disease following chelating therapy.** *Neuromolecular Med* 2015;17:364–72 CrossRef Medline
4. Sinha S, Taly AB, Ravishankar S, et al. **Wilson's disease: cranial MRI observations and clinical correlation.** *Neuroradiology* 2006;48:613–21 CrossRef Medline
5. Broussolle E, Trocello JM, Woimant F, et al. **Samuel Alexander Kinier Wilson: Wilson's disease, Queen Square and neurology.** *Rev Neurol (Paris)* 2013;169:927–35 CrossRef Medline
6. Singh S, Behari M. **Wilson's disease.** *J Assoc Physicians India* 2003;51:183–90 Medline
7. Prashanth LK, Sinha S, Taly AB, et al. **Do MRI features distinguish Wilson's disease from other early onset extrapyramidal disorders? An analysis of 100 cases.** *Mov Disord* 2010;25:672–78 CrossRef Medline
8. Ranjan A, Kalita J, Kumar S, et al. **A study of MRI changes in Wilson disease and its correlation with clinical features and outcome.** *Clin Neurol Neurosurg* 2015;138:31–36 CrossRef Medline
9. Kim YH, Ma HI, Kim YJ. **Utility of the midbrain tegmentum diameter in the differential diagnosis of progressive supranuclear palsy from idiopathic Parkinson's disease.** *J Clin Neurol* 2015;11:268–74 CrossRef Medline
10. Quattrone A, Nicoletti G, Messina D, et al. **MR imaging index for differentiation of progressive supranuclear palsy from Parkinson disease and the Parkinson variant of multiple system atrophy.** *Radiology* 2008;246:214–21 CrossRef Medline
11. Morelli M, Arabia G, Novellino F, et al. **MRI measurements predict PSP in unclassifiable parkinsonisms: a cohort study.** *Neurology* 2011;77:1042–47 CrossRef Medline
12. Zweig RM, Jankel WR, Hedreen JC, et al. **The pedunculopontine nucleus in Parkinson's disease.** *Ann Neurol* 1989;26:41–46 CrossRef Medline
13. Pahapill PA, Lozano AM. **The pedunculopontine nucleus and Parkinson's disease.** *Brain* 2000;123(pt 9):1767–83 CrossRef Medline
14. Kuo SH, Kenney C, Jankovic J. **Bilateral pedunculopontine nuclei strokes presenting as freezing of gait.** *Mov Disord* 2008;23:616–19 CrossRef Medline
15. Masdeu JC, Alampur U, Cavaliere R, et al. **Astasia and gait failure with damage of the pontomesencephalic locomotor region.** *Ann Neurol* 1994;35:619–21 CrossRef Medline
16. Hathout GM, Bhidayasiri R. **Midbrain ataxia: an introduction to the mesencephalic locomotor region and the pedunculopontine nucleus.** *AJR Am J Roentgenol* 2005;184:953–56 CrossRef Medline
17. Kalita J, Kumar V, Misra UK, et al. **A study of oxidative stress, cytokines and glutamate in Wilson disease and their asymptomatic siblings.** *J Neuroimmunol* 2014;274:141–48 CrossRef Medline
18. Roberts EA, Schilsky ML; American Association for Study of Liver Disease (AASLD). **Diagnosis and treatment of Wilson disease: an update.** *Hepatology* 2008;47:2089–111 CrossRef Medline
19. Grimm G, Prayer L, Oder W, et al. **Comparison of functional and structural brain disturbances in Wilson's disease.** *Neurology* 1991;41:272–76 CrossRef Medline
20. Krystkowiak P, du Montcel ST, Vercueil L, et al; SPIDY Group. **Reliability of the Burke-Fahn-Marsden scale in a multicenter trial for dystonia.** *Mov Disord* 2007;22:685–89 CrossRef Medline
21. Fahn S, Elton RL, members of the UPDRS Development Committee. **The Unified Parkinson's Disease Rating Scale.** In: Fahn S, Marsden CD, Calne DB, et al, eds. *Recent Developments in Parkinson's Disease*. Vol. 2. New York: Raven Press; 1986:153–63, 293–304
22. Das SK, Ray K. **Wilson's disease: an update.** *Nat Clin Pract Neurol* 2006;2:482–93 CrossRef Medline
23. Kalita J, Kumar V, Misra UK. **A study on apoptosis and anti-apoptotic status in Wilson disease.** *Mol Neurobiol* 2016;53:6659–67 CrossRef Medline
24. Bartels AL, Leenders KL. **Brain imaging in patients with freezing of gait.** *Mov Disord* 2008;23(suppl 2):S461–67 CrossRef Medline
25. Kalita J, Ranjan A, Misra UK. **Oromandibular dystonia in Wilson disease.** *Movement Disorders Clinical Practice* 2015;2:253–59 CrossRef

Discrimination between Glioma Grades II and III Using Dynamic Susceptibility Perfusion MRI: A Meta-Analysis

Anna F. Delgado and Alberto F. Delgado



ABSTRACT

BACKGROUND: DSC perfusion has been evaluated in the discrimination between low-grade and high-grade glioma but the diagnostic potential to discriminate between glioma grades II and III remains unclear.

PURPOSE: Our aim was to evaluate the diagnostic accuracy of relative maximal CBV from DSC perfusion MR imaging to discriminate glioma grades II and III.

DATA SOURCES: A systematic literature search was performed in PubMed/MEDLINE, Embase, Web of Science, and ClinicalTrials.gov.

STUDY SELECTION: Eligible studies reported on patients evaluated with relative maximal CBV derived from DSC with a confirmed neuropathologic diagnosis of glioma World Health Organization grades II and III. Studies reporting on mean or individual patient data were considered for inclusion.

DATA ANALYSIS: Data were analyzed by using inverse variance with the random-effects model and receiver operating characteristic curves describing optimal cutoffs and areas under the curve. Bivariate diagnostic random-effects meta-analysis was used to calculate diagnostic accuracy.

DATA SYNTHESIS: Twenty-eight studies evaluating 727 individuals were included in the meta-analysis. Individual data were available from 10 studies comprising 190 individuals. The mean difference of relative maximal CBV between glioma grades II and III ($n = 727$) was 1.76 (95% CI, 1.27–2.24; $P < .001$). Individual patient data ($n = 190$) had an area under the curve of 0.77 for discriminating glioma grades II and III at an optimal cutoff of 2.02. When we analyzed astrocytomas separately, the area under the curve increased to 0.86 but decreased to 0.61 when we analyzed oligodendrogliomas.

LIMITATIONS: A substantial heterogeneity was found among included studies.

CONCLUSIONS: Glioma grade III had higher relative maximal CBV compared with glioma grade II. A high diagnostic accuracy was found for all patients and astrocytomas; however, the diagnostic accuracy was substantially reduced when discriminating oligodendroglioma grades II and III.

ABBREVIATIONS: QUADAS-2 = Quality Assessment of Diagnostic Accuracy Studies-2; rCBVmax = relative maximum cerebral blood volume; ROC = receiver operating characteristic; WHO = World Health Organization

Perfusion MR imaging with dynamic susceptibility contrast is a clinical method used to assess brain perfusion in several diseases.^{1,2} DSC has been studied with regard to perfusion in brain tumors such as gliomas, and maximum relative cerebral blood

volume (rCBVmax) has been correlated with World Health Organization (WHO) malignant grade^{3–5} to a higher extent than contrast enhancement in morphologic MR imaging.^{6,7} A higher rCBVmax has been associated with high-grade gliomas (WHO grades III and IV) compared with low-grade gliomas (WHO grades I and II).^{7–13} An optimal cutoff of 1.75 for rCBVmax has been proposed and evaluated in previous studies.^{7,14–16} However, an optimal cutoff between glioma grades II and III has not been assessed previously, to our knowledge.

The current standard criterion for diagnosing and grading

Received December 7, 2016; accepted after revision March 10, 2017.

From the Department of Clinical Neuroscience (Anna F.D.), Karolinska Institute, Stockholm, Sweden; and Department of Surgical Sciences (Alberto F.D.), Uppsala University, Uppsala, Sweden.

One of the authors (Anna F.D.) received funding from Karolinska University Hospital, Department of Neuroradiology.

Please address correspondence to Anna F. Delgado, MD, PhD, Karolinska Institute, Department of Clinical Neuroscience, Administration, Tomtebodavägen 18A, plan 5, 171 77 Stockholm, Sweden.



Indicates article with supplemental on-line tables.

<http://dx.doi.org/10.3174/ajnr.A5218>

glioma is through neuropathologic evaluation.¹⁷ However, not all patients are suitable for surgical resection, and tumor biopsy can lead to a false-negative diagnosis due to an unrepresentative tissue specimen. There is a need for a noninvasive adjunct in discriminating glioma grades at initial diagnosis and at clinical follow-up.

Recently, a meta-analysis studying MR imaging perfusion in low- and high-grade gliomas was published aggregating data on rCBV from DSC imaging, indicating a potential for the clinical use of the method in discrimination of low- and high-grade gliomas.¹⁸ However, no meta-analysis regarding the specific differences in rCBVmax from DSC imaging between glioma grades II and III has been performed.

Grade II gliomas represent low-grade tumors with longer patient survival and treatment options different from those in high-grade (III) gliomas, which show shorter patient survival and a more dismal prognosis.^{17,19} Furthermore, grade III gliomas have a greater propensity to spread outside their macroscopic margins and are thus harder to resect in total with surgery.²⁰ The interest in noninvasive differentiation between glioma grades II and III is attributed to discrepancies in prognosis and treatment options. Noninvasive radiologic evaluation is important in patients not suitable for primary surgery or for longitudinal surveillance in a grade II glioma, with its intrinsic risk of malignant transformation; for treatment follow-up; and as an adjunct to neuropathology.

Several studies analyzing rCBVmax in specific glioma grades have found conflicting results. A number of studies analyzing differences in rCBVmax in glioma grades II and III have failed to show any differences between these malignancy grades.^{6,21–27} Radiologic analyses of differences between low- and high-grade gliomas depend mainly on the specific characteristics of a glioma grade IV (glioblastoma). The added value of physiologic perfusion MR imaging such as DSC is therefore in the distinction between gliomas of lower grades than WHO grade IV, as in the discrimination between glioma grades II and III. The aim of this meta-analysis was to evaluate differences in relative maximal CBV from DSC perfusion MR imaging between glioma grades II and III and to assess the diagnostic accuracy of rCBVmax to discriminate glioma grades II and III.

MATERIALS AND METHODS

This meta-analysis was performed according to the Preferred Reporting Items for Systematic Reviews and Meta-Analyses (PRISMA)²⁸ statement and current recommended methods for meta-analysis of diagnostic accuracy in imaging journals.²⁹

Search Strategy and Information Sources

Relevant articles were searched from the date of inception to October 2016 in PubMed/MEDLINE, Embase, Web of Science, and ClinicalTrials.gov independently, by the 2 authors (Anna F.D., Alberto F.D.).

PubMed/MEDLINE was searched with the following Medical Subject Heading terms: “glioma perfusion,” “MR imaging,” “astrocytoma,” and “oligodendroglioma.” Additional searches were performed with the following terms: “grade,” “grading,”

“DSC,” “oligoastrocytoma” (the full search strategy is in Online Table 1).

Selection Criteria

Study selection was based on the patient, intervention, comparison, and outcome criteria, in which eligible studies analyzed patients with glioma WHO grades II and III. The intervention was defined as measurement of rCBVmax from DSC. The comparison was defined as neuropathologic diagnosis after MR imaging of either glioma grade II or III (astrocytoma, oligoastrocytoma, or oligodendroglioma). Studies reporting on mean or individual patient data for grade II and III gliomas were considered for inclusion. Studies reporting on DSC imaging with no restriction in field strength, postprocessing, or ROI method were included. Only English studies were considered. Both retrospective and prospective studies were eligible. Exclusion criteria were the following: studies reporting on patients posttreatment, pediatric patients (younger than 18 years of age), case studies, reviews, abstracts, technical reports, meta-analyses, duplicate or overlapping cohorts, and longitudinal studies. Studies not classifying gliomas according to WHO were excluded.

Data Extraction

Study characteristics and results were extracted into tables independently by the 2 authors (Anna F.D., Alberto F.D.) with experience in meta-analysis. Data were sought for in the main documents and on-line material.

We extracted the following data: first author, year published, study period, country, perfusion method and MR imaging sequence, MR imaging field strength (1.5T/3T), scanner type (model and company), presaturation of tissue (yes/no), leakage-correction method (yes/no), WHO classification, study design (prospective/retrospective), number of patients with glioma grades II and III respectively, glioma subtypes (astrocytomas, oligoastrocytomas, oligodendrogliomas), ROI method (rCBVmax or histogram parameter), and mean (SD) rCBVmax in glioma grades II and III, respectively, with associated information about the discriminating potential among grades (yes/no) from the individual study.

Available individual patient data on rCBVmax and neuropathologic diagnosis were extracted separately by the 2 authors, initially blinded to each other's data and subsequently checked for consistency. Patients from overlapping study cohorts (same authors, institution, overlapping years of patient recruitment) were considered for inclusion once in the meta-analysis. Any disagreements regarding data extraction were solved through discussion until consensus.

Data Quality Assessment

The risk of bias and quality assessment of included studies were independently assessed by the 2 authors (Anna F.D., Alberto F.D.) through the Quality Assessment of Diagnostic Accuracy Studies-2 (QUADAS-2), evaluating patient selection, analysis of index/reference tests, and the flow/timing of the study.³⁰ Any disagreements were solved through discussion until consensus. Results from QUADAS-2 were evaluated in sensitivity analysis.

Statistical Analysis

Mean Study Data. Mean and SDs of rCBVmax from DSC imaging for each glioma grade (WHO grades II or III) were used for the meta-analysis of mean differences. In studies reporting summary estimates other than mean and SD, data were recalculated according to the Cochrane handbook³¹ and Hozo et al.³²

Syntheses of results were evaluated with a forest plot of mean difference with 95% CIs of the continuous variable rCBVmax with inverse variance with random effects. The overall effect was calculated with the *z* score. To assess whether observed differences in results were compatible with chance alone, we calculated the χ^2 and its significance level. I^2 was calculated to assess any inconsistencies across studies with the estimation of the percentage of the variability in effect estimate due to heterogeneity. The between-study variance in a random-effects meta-analysis was described by τ^2 .

Additional analyses exploring sources of heterogeneity and the risk of bias were prespecified, except exploratory sensitivity analyses based on QUADAS-2. A funnel plot was calculated for the assessment of publication bias as a scatterplot of included studies with the mean difference in rCBVmax plotted on the horizontal axis, and its standard error, on the vertical axis and visually assessed for asymmetry.³³

Individual Patient Data. Individual patient data on rCBVmax and neuropathologic diagnosis were analyzed stratified for grade II and III gliomas and in subgroups of histopathologic subtypes (astrocytomas, oligoastrocytomas, and oligodendrogliomas).

To estimate the diagnostic potential of rCBVmax to discriminate glioma grades II and III, we used data from studies including individual patient data to construct receiver operating characteristic (ROC) curves and calculated the area under the curve. From ROC calculations, the number of patients with true-positive, false-negative, false-positive, and true-negative counts was calculated with maximum accuracy set as the cutoff.

The true-positive, false-negative, false-positive, and true-negative counts were analyzed with the bivariate model of mada³⁴ in R, Version 3.3.1 (R statistical and computing software; <http://www.r-project.org>).³⁵ Descriptive forest plots of sensitivity and specificity were constructed. After we assumed a binomial model conditional on the true sensitivity and false-positive rates of the primary studies and a bivariate normal model for the logit-transformed pairs of sensitivities and false-positive rates, a linear mixed model implemented in the Reitsma function of mada was used (bivariate diagnostic random-effects meta-analysis with restricted maximum likelihood estimation method).³⁴

Statistical analysis was performed by 1 author (Anna F.D.) with the following statistical programs: RevMan 5.3,³⁶ Statistica 12 (<https://2ra5-downloads.phpnuke.org/en/c06229/statistica>), and R 3.3.1.^{34,35} A continuity correction of 0.5 was used when applicable, and $P < .05$ was considered statistically significant, except in χ^2 for which the significance level was set at $P < .10$.

RESULTS

Literature Search

The searches yielded 1977 hits (1458 in PubMed, 172 in Embase, 283 in Web of Science, 64 in ClinicalTrials.gov) that were

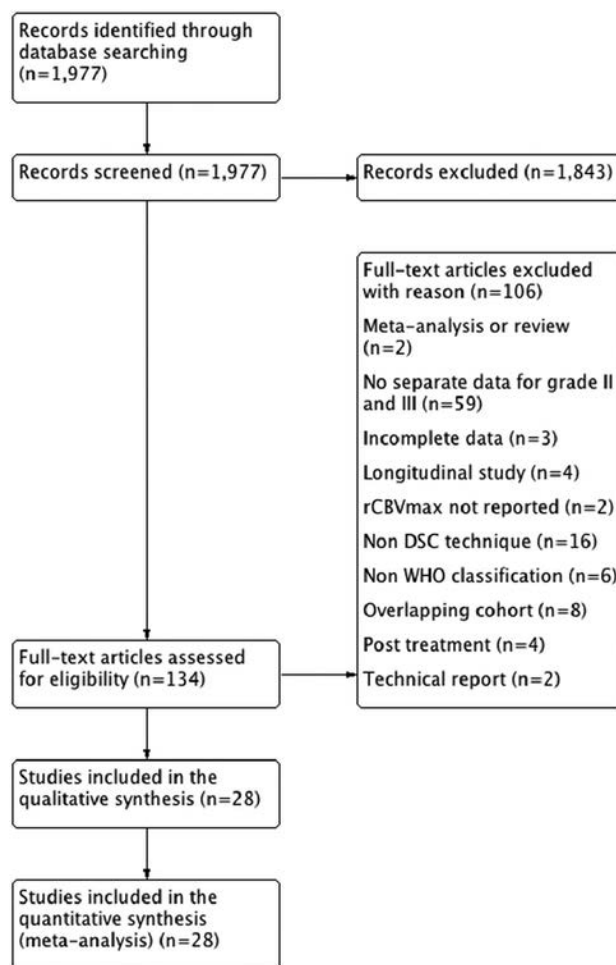


FIG 1. PRISMA flow chart of included and excluded studies.

screened for inclusion in the meta-analysis. Full-text evaluation of 134 articles was performed. Twenty-eight studies comprising 727 patients were included in the qualitative study assessment and quantitative meta-analysis (On-line Table 2). Individual patient data were available in 10 studies comprising 190 patients. A PRISMA flow chart is presented in Fig 1, and the sample search strategy, in On-line Table 1.

Quality Assessment

Quality assessment from QUADAS-2 is presented in On-line Table 3. Included studies showed a general low risk of bias and a low risk of applicability concerns. Biases included lack of information regarding blinding of index and reference tests and lack of information regarding the time between index and reference tests. Applicability concerns were the use of histogram measures as a surrogate for rCBVmax in 3 studies.

Data Analysis

Mean Study Data. Tabulated perfusion data and study characteristics of included studies ($n = 28$) evaluating 727 patients are presented in On-line Table 4. The mean (SD) rCBVmax in glioma grade II was 2.14 (1.04); and it was 3.85 (1.18) in grade III (Mann-Whitney *U* test, $P < .001$).

Of the included studies ($n = 28$), 16 showed statistically signifi-

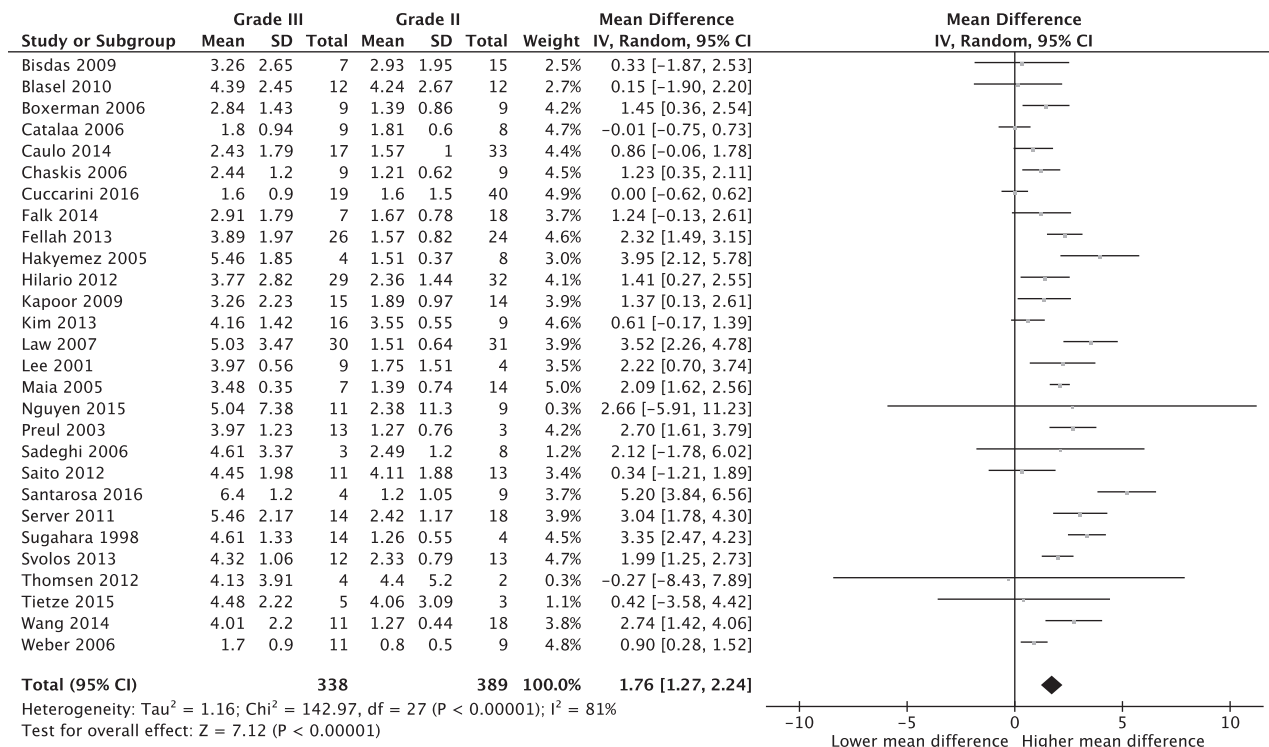


FIG 2. Forest plot of mean differences between glioma grades II and III with a random-effects model.

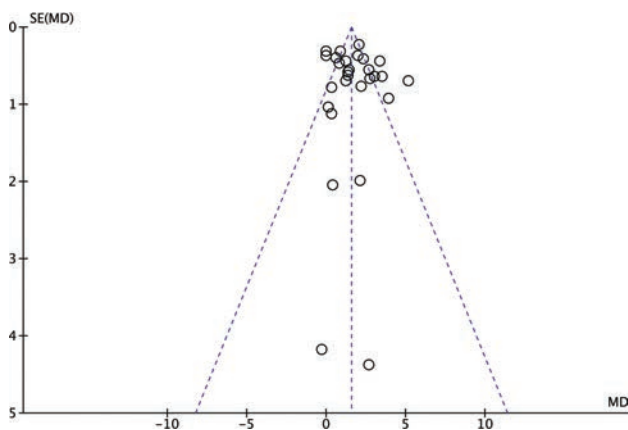


FIG 3. Funnel plot of 28 included studies ($n = 727$ patients) illustrated by open circles with the effect estimate mean difference (MD) of rCBVmax plotted on the horizontal axis, the standard error (SE) of the MD plotted on the vertical axis, and a triangular 95% confidence region. The study distribution is symmetric without apparent publication bias.

cant differences between glioma grades II and III and 12 studies did not (On-line Table 4). Meta-analytic evaluation of included studies ($n = 28$) showed a mean difference in rCBVmax between glioma grades II and III of 1.76 (95% CI, 1.27–2.24; $P < .001$); $I^2 = 81\%$; Fig 2). Visual assessment of the funnel plot revealed no evidence of the existence of publication bias (Fig 3).

Heterogeneity between study results (χ^2), inconsistencies between studies (I^2), and between-study variances (τ^2) are presented in the Table. Three study characteristics increasing heterogeneity (χ^2) across studies were significantly related to studies without published individual patient data ($n = 121$, $\chi^2 = 18$, $P = .07$) and ROI analysis ($n = 25$, $\chi^2 = 116$, $P < .001$) and studies with a

blinded index test evaluation ($n = 14$, $\chi^2 = 98$, $P < .001$). Study characteristics increasing inconsistencies across studies (I^2) were the following: prospective study design ($n = 11$, $I^2 = 89$), optimal flow and timing assessed in QUADAS-2 ($n = 7$, $I^2 = 88$), and blinded index test evaluation ($n = 14$, $I^2 = 87$). Study characteristics with increasing χ^2 were those with correction for contrast agent leakage according to Boxerman et al¹ ($n = 8$, $\tau^2 = 2.58$), those reporting on WHO 2007 classification ($n = 11$, $\tau^2 = 2.07$), and those with a prospective study design ($n = 11$, $\tau^2 = 1.94$).

Individual Patient Data. A total of 190 patients (105 with WHO grade II, 85 with WHO grade III) from 10 studies reported on individual patient data (On-line Table 5). ROC analysis showed discriminatory potential between glioma grades II and III ($n = 190$) with an area under curve of 0.77 with maximum accuracy at an exploratory cutoff of 2.02 (Fig 4). Data were stratified for tumor type: astrocytomas ($n = 102$), with an area under curve of 0.86 and maximum accuracy at cutoff at 2.02, oligoastrocytomas ($n = 28$) with an area under curve of 0.83 and maximum accuracy at cutoff at 3.19, and oligodendrogliomas ($n = 60$) with an area under curve of 0.61 and maximum accuracy at cutoff at 6.23.

Data on true-positive, false-negative, false-positive, and true-negative counts from each study are presented in On-line Table 6. Univariate paired forest plots for individual patient data are presented in Fig 5A, -B.

A bivariate diagnostic random-effects meta-analysis model with a restricted maximum likelihood estimation method described the summary receiver operating characteristic curve in Fig 6 with a sensitivity of 0.71 (95% CI, 0.48–0.86) and a false-positive rate of 0.15 (95% CI, 0.09–0.25).

Factors affecting heterogeneity

| Factor (No. of Studies) | τ^2 | χ^2 (P) | I ² (%) | Mean Differences (95 % CI) Random |
|--|----------|----------------|--------------------|-----------------------------------|
| Studies without significant differences between grades II and III (n = 14) | 0.00 | 6.5 (.84) | 0 | 0.35 (0.01–0.69) |
| Oligodendroglial tumors (n = 3) | 0.04 | 2.17 (.34) | 8 | 1.95 (1.21–2.96) |
| Histogram rCBVmax (n = 3) | 0.10 | 2.88 (.24) | 31 | 0.45 (–0.17–1.08) |
| Published individual patient data (n = 10) | 0.28 | 15.76 (<.001) | 43 | 1.82 (1.28–2.36) |
| Retrospective study design (n = 17) | 0.70 | 52.34 (<.001) | 69 | 1.42 (0.89–1.96) |
| Astrocytic tumors (n = 6) | 1.57 | 20.69 (<.001) | 76 | 2.28 (0.96–3.60) |
| Studies with significant differences between grades II and III (n = 16) | 0.73 | 63.01 (<.001) | 76 | 2.37 (1.87–2.87) |
| Non-WHO 2007 classification (n = 17) | 0.88 | 73.74 (<.001) | 78 | 1.71 (1.16–2.26) |
| No correction for contrast agent leakage according to Boxerman (n = 20) | 0.88 | 86.07 (<.001) | 78 | 1.75 (1.24–2.25) |
| ROI analysis (n = 25) | 1.09 | 116.10 (<.001) | 79 | 1.93 (1.43–2.44) |
| Studies published in 2010 or before (n = 14) | 1.02 | 65.67 (<.001) | 80 | 1.81 (1.17–2.44) |
| No presaturation of tissue (n = 18) | 1.05 | 84.70 (<.001) | 80 | 1.85 (1.27–2.43) |
| All studies (n = 28) | 1.16 | 142.97 (<.001) | 81 | 1.76 (1.27–2.24) |
| 3T (n = 10) | 1.67 | 46.71 (<.001) | 81 | 1.66 (0.69–2.64) |
| Presaturation of tissue (n = 10) | 1.53 | 53.21 (<.001) | 83 | 1.60 (0.68–2.15) |
| Studies published after 2010 (n = 14) | 1.50 | 75.04 (<.001) | 83 | 1.70 (0.93–2.48) |
| 1.5T (n = 16) | 1.17 | 95.95 (<.001) | 84 | 1.83 (1.22–2.45) |
| WHO 2007 classification (n = 11) | 2.07 | 68.39 (<.001) | 85 | 1.85 (0.85–2.86) |
| No published individual patient data (n = 18) | 1.54 | 120.79 (.07) | 86 | 1.75 (1.07–2.42) |
| Blinded reference test evaluation (n = 5) QUADAS-2 | 1.10 | 29.23 (<.001) | 86 | 1.30 (0.29–2.32) |
| Correction for leakage according to Boxerman (n = 8) | 2.58 | 54.12 (<.001) | 87 | 1.83 (0.49–3.16) |
| Blinded index test evaluation (n = 14) QUADAS-2 | 1.57 | 97.79 (<.001) | 87 | 1.77 (1.03–2.51) |
| Optimal flow and timing (n = 7) QUADAS-2 | 1.57 | 49.31 (<.001) | 88 | 1.69 (0.57–2.80) |
| Prospective study design (n = 11) | 1.94 | 89.9 (<.001) | 89 | 2.27 (1.35–3.20) |

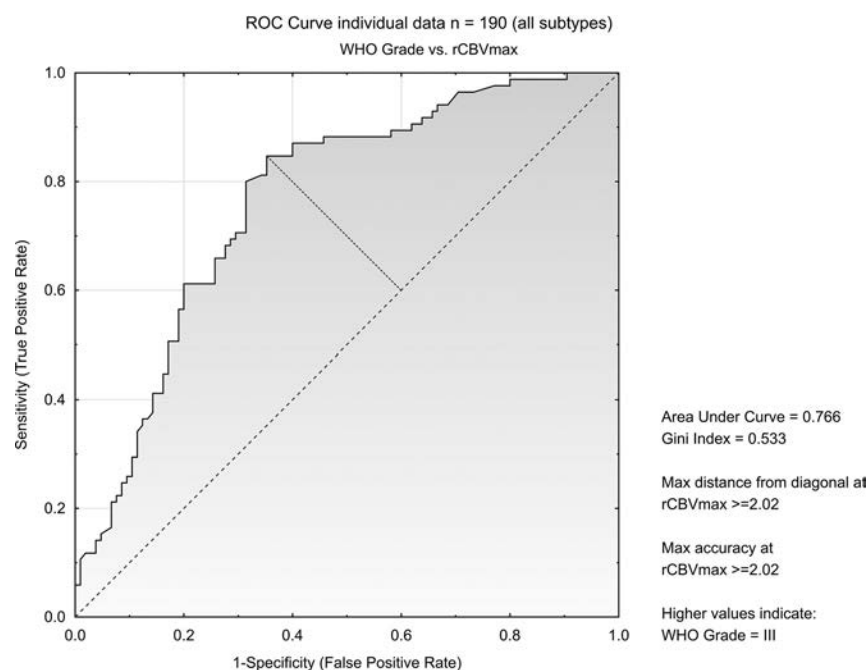


FIG 4. ROC curve on individual patient data from 10 studies including all patients (n = 190).

DISCUSSION

This meta-analysis investigated the potential of DSC perfusion MR imaging to distinguish glioma grades II and III. Our study showed significant differences in rCBVmax between glioma grades II and III, with higher rCBVmax in WHO grade III compared with grade II. Furthermore, we evaluated individual patient data on rCBVmax to explore the diagnostic potential and the optimal cutoff for rCBVmax between glioma grades II and III, stratified for glial subtypes.

The importance of this meta-analysis is mainly that it describes the differences in rCBVmax between glioma grades II and III and that these differences can be measured and applied in a clinical setting. This evidence is based on data from 28 studies including 727 individual patients. This is an interesting finding in a field with small conflicting studies. Non-invasive glioma grade evaluation is an important adjunct to neuropathologic evaluation in patients deemed inoperable or at longitudinal follow-up. It might also be of value in patients with nonrepresentative biopsies that might lead to a false-negative diagnosis. Furthermore, the pooling of data across studies adds precision to estimates and can guide future work.

The quality and bias assessment of included studies showed intermediate-to-low risk of bias and an intermediate-to-high study quality. However, minor concerns about blinding of index and reference tests, flow and timing in the studies,

and the lack of prespecified cutoffs in ROC analysis could have affected the results of the meta-analysis. Although no asymmetry was detected in the funnel plot, evidence of gray literature was searched in ClinicalTrials.gov.

Statistical heterogeneity between studies was substantial. Potential sources for heterogeneity were evaluated but did not alter the main study finding of statistical differences in rCBVmax between glioma grades II and III, except for sensitivity analyses of 3 studies

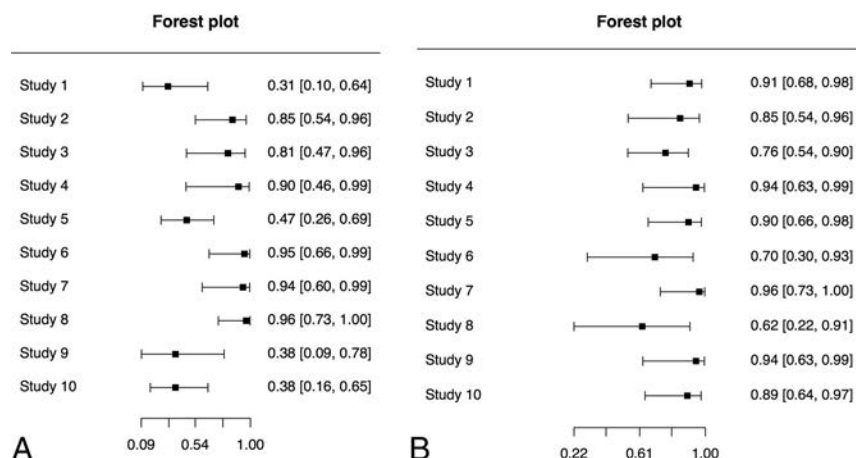


FIG 5. Paired forest plots for individual patient data ($n = 190$). A, Forest plot of sensitivity. B, Forest plot of specificity.

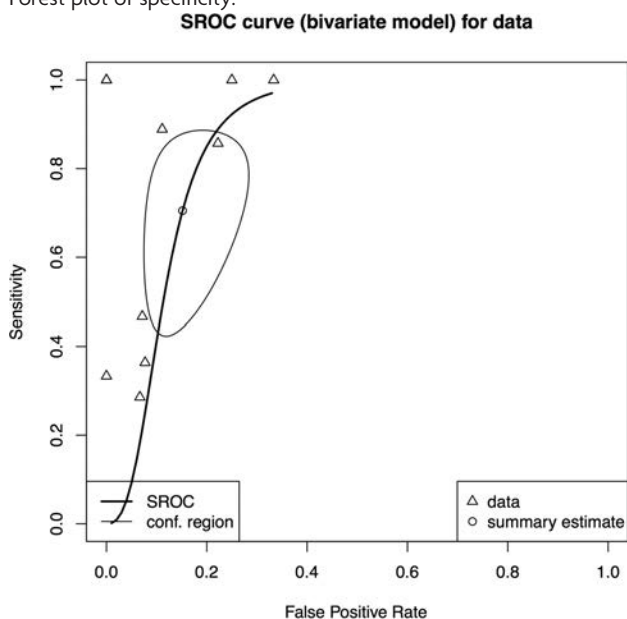


FIG 6. Graph showing a point estimate of the pair of sensitivity and false-positive rates plotted together with a confidence region, without extrapolation beyond the range of the original data (individual patient data, $n = 190$).

with a histogram technique to identify rCBVmax, which showed no statistically significant difference in rCBVmax between groups of glioma grades II and III.^{10,21,37}

Analyzing specific subtypes of glioma grades II and III preoperatively is counterintuitive because subtype attribution is largely unknown before neuropathologic evaluation. Knowledge of differences in rCBVmax between subtypes of gliomas relates to discrepancies in biology, more than it adds to the diagnostic potential in a preoperative clinical setting.^{38–41} However, while sensitivity analysis of studies analyzing oligodendroglial tumors (oligoastrocytomas or oligodendrogliomas) showed differences in rCBVmax among tumor grades similar to those in astrocytomas, the individual patient data analysis stratifying oligodendroglial tumors into oligoastrocytomas and oligodendrogliomas decreased the diagnostic potential when analyzing oligodendrogliomas separately.

DSC might be of added value at the longitudinal follow-up in specific glioma subtypes after initial neuropathologic diagnosis

when assessing malignant transformation. Preoperatively when the tumor subtype is unknown (or only suspected based on the morphologic appearance on CT or MR imaging), a true diagnostic discrepancy by rCBVmax between glioma grades II and III is possibly hampered by the lack of information regarding glial cell subtype. Speaking for the applicability of DSC is the, relative to astrocytomas, lower incidence of oligodendrogliomas, making this method important in most patients.

When evaluating the diagnostic accuracy of DSC in this meta-analysis, we used exploratory evaluations of optimal cutoffs for discrimination between glioma grades II and III. This lack of evaluating diagnostic accuracy from a prespecified cutoff can increase the diagnostic potential presented in the meta-analysis.

A limitation in DSC perfusion MR imaging is the nonlinear relationship between gadolinium concentration and the relaxivity-time curve, and nonexponential relaxation decay.⁴² Consequently, measured rCBV values, despite normalization to healthy white matter, are dependent on TE, injection rate, and total dose and gadolinium preloading and act as potential drivers for heterogeneity.⁴³

When discussing an optimal cutoff between glioma grades II and III, we found maximum accuracy from ROC analysis at rCBVmax = 2.02 (individual patient data, No. of patients = 190, No. of studies = 10). This is a higher cutoff than previously suggested for optimal discrimination between low- (WHO I and II) and high-grade gliomas (WHO III and IV), which might be explained by different compositions of specific grades and subtypes in the groups of low- and high-grade gliomas in previously published material. This cutoff needs to be validated in prospective studies with standardized methodology, taking the differences in biology between glioma subtypes into account.

On the basis of subgroup analyses, the new molecular advances and WHO 2016 classification are applicable to our results regarding astrocytomas and oligodendrogliomas. The main difference pertains to molecular classification of oligoastrocytomas as either astrocytomas or oligodendrogliomas, which are analyzed separately in the individual patient data analysis.¹⁷

CONCLUSIONS

This meta-analysis evaluates DSC MR imaging perfusion in patients with glioma grades II and III. A higher rCBVmax was found in glioma grade III compared with grade II ($n = 727$). A high diagnostic accuracy was found for all patients and when analyzing astrocytomas separately; however, the diagnostic accuracy was substantially reduced when discriminating grade II and III oligodendrogliomas.

REFERENCES

- Boxerman JL, Schmainda KM, Weisskoff RM. **Relative cerebral blood volume maps corrected for contrast agent extravasation sig-**

- nificantly correlate with glioma tumor grade, whereas uncorrected maps do not. *AJNR Am J Neuroradiol* 2006;27:859–67 CrossRef Medline
2. Boxerman JL, Shiroishi MS, Ellingson BM, et al. Dynamic susceptibility contrast MR imaging in glioma: review of current clinical practice. *Magn Reson Imaging Clin N Am* 2016;24:649–70 CrossRef Medline
3. Law M, Young R, Babb J, et al. Histogram analysis versus region of interest analysis of dynamic susceptibility contrast perfusion MR imaging data in the grading of cerebral gliomas. *AJNR Am J Neuroradiol* 2007;28:761–66 Medline
4. Hilario A, Ramos A, Perez-Núñez A, et al. The added value of apparent diffusion coefficient to cerebral blood volume in the preoperative grading of diffuse gliomas. *AJNR Am J Neuroradiol* 2012;33:701–07 CrossRef Medline
5. Wang XC, Zhang H, Tan Y, et al. Combined value of susceptibility-weighted and perfusion-weighted imaging in assessing WHO grade for brain astrocytomas. *J Magn Reson Imaging* 2014;39:1569–74 CrossRef Medline
6. Caulo M, Panara V, Tortora D, et al. Data-driven grading of brain gliomas: a multiparametric MR imaging study. *Radiology* 2014;272:494–503 CrossRef Medline
7. Law M, Yang S, Wang H, et al. Glioma grading: sensitivity, specificity, and predictive values of perfusion MR imaging and proton MR spectroscopic imaging compared with conventional MR imaging. *AJNR Am J Neuroradiol* 2003;24:1989–98 Medline
8. Park MJ, Kim HS, Jahng GH, et al. Semiquantitative assessment of intratumoral susceptibility signals using non-contrast-enhanced high-field high-resolution susceptibility-weighted imaging in patients with gliomas: comparison with MR perfusion imaging. *AJNR Am J Neuroradiol* 2009;30:1402–08 CrossRef Medline
9. Van Cauter S, De Keyser F, Sima DM, et al. Integrating diffusion kurtosis imaging, dynamic susceptibility-weighted contrast-enhanced MRI, and short echo time chemical shift imaging for grading gliomas. *Neuro Oncol* 2014;16:1010–21 CrossRef Medline
10. Kim H, Choi SH, Kim JH, et al. Gliomas: application of cumulative histogram analysis of normalized cerebral blood volume on 3 T MRI to tumor grading. *PLoS One* 2013;8:e63462 CrossRef Medline
11. Emblem KE, Scheie D, Due-Tønnessen P, et al. Histogram analysis of MR imaging-derived cerebral blood volume maps: combined glioma grading and identification of low-grade oligodendroglial subtypes. *AJNR Am J Neuroradiol* 2008;29:1664–70 CrossRef Medline
12. Di Costanzo A, Pollice S, Trojsi F, et al. Role of perfusion-weighted imaging at 3 Tesla in the assessment of malignancy of cerebral gliomas [In English, Italian]. *Radiol Med* 2008;113:134–43 CrossRef Medline
13. Law M, Young R, Babb J, et al. Comparing perfusion metrics obtained from a single compartment versus pharmacokinetic modeling methods using dynamic susceptibility contrast-enhanced perfusion MR imaging with glioma grade. *AJNR Am J Neuroradiol* 2006;27:1975–82 Medline
14. Caseiras GB, Chheang S, Babb J, et al. Relative cerebral blood volume measurements of low-grade gliomas predict patient outcome in a multi-institution setting. *Eur J Radiol* 2010;73:215–20 CrossRef Medline
15. Nasserli M, Gahramanov S, Netto JP, et al. Evaluation of pseudoprogression in patients with glioblastoma multiforme using dynamic magnetic resonance imaging with ferumoxytol calls RANO criteria into question. *Neuro Oncol* 2014;16:1146–54 CrossRef Medline
16. Hu LS, Kelm Z, Korfiatis P, et al. Impact of software modeling on the accuracy of perfusion MRI in glioma. *AJNR Am J Neuroradiol* 2015;36:2242–49 CrossRef Medline
17. Louis DN, Perry A, Reifenberger G, et al. The 2016 World Health Organization Classification of Tumors of the Central Nervous System: a summary. *Acta Neuropathol* 2016;131:803–20 CrossRef Medline
18. Usinskiene J, Ulyte A, Bjornerud A, et al. Optimal differentiation of high- and low-grade glioma and metastasis: a meta-analysis of perfusion, diffusion, and spectroscopy metrics. *Neuroradiology* 2016;58:339–50 CrossRef Medline
19. Crocetti E, Trama A, Stiller C, et al. Epidemiology of glial and non-glial brain tumours in Europe. *Eur J Cancer* 2012;48:1532–42 CrossRef Medline
20. Kelly PJ, Daumas-Duport C, Kispert DB, et al. Imaging-based stereotaxic serial biopsies in untreated intracranial glial neoplasms. *J Neurosurg* 1987;66:865–74 CrossRef Medline
21. Catalaa I, Henry R, Dillon WP, et al. Perfusion, diffusion and spectroscopy values in newly diagnosed cerebral gliomas. *NMR Biomed* 2006;19:463–75 CrossRef Medline
22. Cuccarini V, Erbetta A, Farinotti M, et al. Advanced MRI may complement histological diagnosis of lower grade gliomas and help in predicting survival. *J Neurooncol* 2016;126:279–88 CrossRef Medline
23. Nguyen TB, Cron GO, Perdrizet K, et al. Comparison of the diagnostic accuracy of DSC- and dynamic contrast-enhanced MRI in the preoperative grading of astrocytomas. *AJNR Am J Neuroradiol* 2015;36:2017–22 CrossRef Medline
24. Saito T, Yamasaki F, Kajiura Y, et al. Role of perfusion-weighted imaging at 3T in the histopathological differentiation between astrocytic and oligodendroglial tumors. *Eur J Radiol* 2012;81:1863–69 CrossRef Medline
25. Thomsen H, Steffensen E, Larsson EM. Perfusion MRI (dynamic susceptibility contrast imaging) with different measurement approaches for the evaluation of blood flow and blood volume in human gliomas. *Acta Radiol* 2012;53:95–101 CrossRef Medline
26. Toyooka M, Kimura H, Uematsu H, et al. Tissue characterization of glioma by proton magnetic resonance spectroscopy and perfusion-weighted magnetic resonance imaging: glioma grading and histological correlation. *Clin Imaging* 2008;32:251–58 CrossRef Medline
27. Togao O, Hiwatashi A, Yamashita K, et al. Grading diffuse gliomas without intense contrast enhancement by amide proton transfer MR imaging: comparisons with diffusion- and perfusion-weighted imaging. *Eur Radiol* 2017;27:578–88 CrossRef Medline
28. Moher D, Liberati A, Tetzlaff J, et al. Preferred reporting items for systematic reviews and meta-analyses: the PRISMA statement. *BMJ* 2009;339:b2535 CrossRef Medline
29. McGrath TA, McInnes MD, Korevaar DA, et al. Meta-analyses of diagnostic accuracy in imaging journals: analysis of pooling techniques and their effect on summary estimates of diagnostic accuracy. *Radiology* 2016;281:78–85 CrossRef Medline
30. Whiting PF, Rutjes AW, Westwood ME, et al. QUADAS-2: a revised tool for the quality assessment of diagnostic accuracy studies. *Ann Intern Med* 2011;155:529–36 CrossRef Medline
31. Higgins JP, Green S. *Cochrane Handbook for Systematic Reviews of Interventions*, Version 5.1.0 (updated March 2011). The Cochrane Collaboration, 2011. <http://handbook.cochrane.org/>. Accessed September 6, 2016
32. Hozo SP, Djulbegovic B, Hozo I. Estimating the mean and variance from the median, range, and the size of a sample. *BMC Med Res Methodol* 2005;5:13 CrossRef Medline
33. Light RJ, Pillemer DB. *Summing Up: The Science of Reviewing Research*. Cambridge: Harvard University Press; 1984
34. Doebler P, Holling H. Meta-Analysis of Diagnostic Accuracy with mada. 2015. <https://cran.r-project.org/web/packages/mada/vignettes/mada.pdf>. Accessed September 6, 2016
35. R Development Core Team. *R: A Language and Environment for Statistical Computing*. Vienna: R Foundation for Statistical Computing; 2010
36. Review Manager (RevMan). 5.3 ed. Copenhagen: The Nordic Cochrane Centre: The Cochrane Collaboration; 2014 <http://www.medsci.cn/webeditor/uploadfile/201408/20140815214316360.pdf>. Accessed September 6, 2016
37. Falk A, Fahlström M, Rostrup E, et al. Discrimination between glioma grades II and III in suspected low-grade gliomas using dynamic contrast-enhanced and dynamic susceptibility contrast perfusion MR imaging: a histogram analysis approach. *Neuroradiology* 2014;56:1031–38 CrossRef Medline
38. Cairncross JG, Wang M, Jenkins RB, et al. Benefit from procarb-

- zine, lomustine, and vincristine in oligodendroglial tumors is associated with mutation of IDH. *J Clin Oncol* 2014;32:783–90 [CrossRef](#) [Medline](#)
39. van den Bent MJ, Brandes AA, Taphoorn MJ, et al. Adjuvant procarbazine, lomustine, and vincristine chemotherapy in newly diagnosed anaplastic oligodendroglioma: long-term follow-up of EORTC brain tumor group study 26951. *J Clin Oncol* 2013;31:344–50 [CrossRef](#) [Medline](#)
 40. Eckel-Passow JE, Lachance DH, Molinaro AM, et al. Glioma groups based on 1p/19q, IDH, and TERT promoter mutations in tumors. *N Engl J Med* 2015;372:2499–508 [CrossRef](#) [Medline](#)
 41. Brat DJ, Verhaak RG, Aldape KD et al; Cancer Genome Atlas Research Network. Comprehensive, integrative genomic analysis of diffuse lower-grade gliomas. *N Engl J Med* 2015;372:2481–98 [CrossRef](#) [Medline](#)
 42. Kiselev VG, Posse S. Analytical model of susceptibility-induced MR signal dephasing: effect of diffusion in a microvascular network. *Magn Reson Med* 1999;41:499–509 [Medline](#)
 43. Yablonskiy DA, Haacke EM. Theory of NMR signal behavior in magnetically inhomogeneous tissues: the static dephasing regime. *Magn Reson Med* 1994;32:749–63 [CrossRef](#) [Medline](#)

Mechanical Thrombectomy with the Embolus Retriever with Interlinked Cages in Acute Ischemic Stroke: ERIC, the New Boy in the Class

 H. Steglich-Arnholm,  D. Kondziella,  A. Wagner,  M.E. Cronqvist,  K. Hansen,  T.C. Truelsén,  L.-H. Krarup,  J.L.S. Højgaard,  S. Taudorf,  H.K. Iversen,  D.W. Krieger, and  M. Holtmannspötter



ABSTRACT

BACKGROUND AND PURPOSE: The Embolus Retriever with Interlinked Cages (ERIC) device is a novel stent retriever for mechanical thrombectomy. It consists of interlinked cages and could improve procedural benchmarks and clinical outcome compared with classic stent retrievers. This study compares the rates of recanalization, favorable clinical outcome, procedural adverse events, and benchmarks between the ERIC device and classic stent retrievers.

MATERIALS AND METHODS: From 545 patients treated with thrombectomy between 2012 and 2015, 316 patients were included. The mean age was 69 ± 13 years, the mean baseline NIHSS score was 17 ± 5 , and 174 (55%) were men. The ERIC was used as the primary thrombectomy device in 59 (19%) patients. In a propensity score matched analysis including the NIHSS score, clot location, delay to groin puncture, neurointerventionalist, and anesthetic management, 57 matched pairs were identified.

RESULTS: Patients treated with the ERIC device compared with classic stent retrievers showed equal rates of recanalization (86% versus 81%, $P = .61$), equal favorable 3-month clinical outcome (mRS 0–2: 46% versus 40%, $P = .71$), and procedural adverse events (28% versus 30%, $P = 1.00$). However, in patients treated with the ERIC device, thrombectomy procedures were less time-consuming (67 versus 98 minutes, $P = .009$) and a rescue device was needed less often (18% versus 39%, $P = .02$) compared with classic stent retrievers.

CONCLUSIONS: Mechanical thrombectomy with the ERIC device is effective and safe. Rates of favorable procedural and clinical outcomes are at least as good as those with classic stent retrievers. Of note, the ERIC device might be time-saving and decrease the need for rescue devices. These promising results call for replication in larger prospective clinical trials.

ABBREVIATION: ERIC = Embolus Retriever with Interlinked Cages

The design of thrombectomy devices plays an important role in the efficacy of mechanical thrombectomy for acute ischemic stroke.¹ This is illustrated by the introduction of the stent retriever design, which was a driving factor for the positive results of the randomized controlled trials published in 2015.^{2–6} These studies showed improved recanalization rates and, most important, improved clinical outcome with endovascular therapy compared with medical therapy alone for large-embolic acute ischemic stroke.¹ In contrast to these trials, the negative endovascular ther-

apy trials published in 2013^{7–9} mainly used older thrombectomy devices such as coil retrievers or mechanical clot disintegrators combined with aspiration systems.


Classic stent retrievers have a tubular design and were originally designed to support the endovascular coil treatment of wide-neck intracranial aneurysms by neck remodelling.¹⁰ During mechanical thrombectomy for acute ischemic stroke, stent retrievers function by squeezing the clot against the vessel wall and, during a few minutes, interacting with the clot by entangling it in the meshed network of the stent and sometimes establishing temporary reperfusion of the affected territory. However, the tubular design also means that the clot rests on the surface of the stent retriever (Fig 1A) and may risk fragmentation or shearing off during thrombectomy, causing distal embolization, so-called clot migration. In addition, a large proportion of the surface area of the stent retriever is in contact with and possibly interacts with the endothelium of the vessel wall when deployed; this feature may lead to intimal injuries and/or induced vasospasm during retraction.¹¹

Received August 24, 2016; accepted after revision February 22, 2017.

From the Departments of Neurology (H.S.-A., D.K., K.H., T.C.T., L.-H.K., J.L.S.H., S.T., H.K.I.) and Neuroradiology (A.W., M.E.C., M.H.), Rigshospitalet, Copenhagen, Denmark; and Dubai Healthcare City (D.W.K.), Clinic 2006, Dubai, UAE.

Paper previously presented at: European Stroke Organization Conference, May 10–12, 2016; Barcelona, Spain.

Please address correspondence to Henrik Steglich-Arnholm, MD, Department of Neurology 2082, Rigshospitalet, Blegdamsvej 9, 2100 Copenhagen Ø; e-mail: henrik.steglich@gmail.com

 Indicates article with supplemental on-line tables.

<http://dx.doi.org/10.3174/ajnr.A5201>

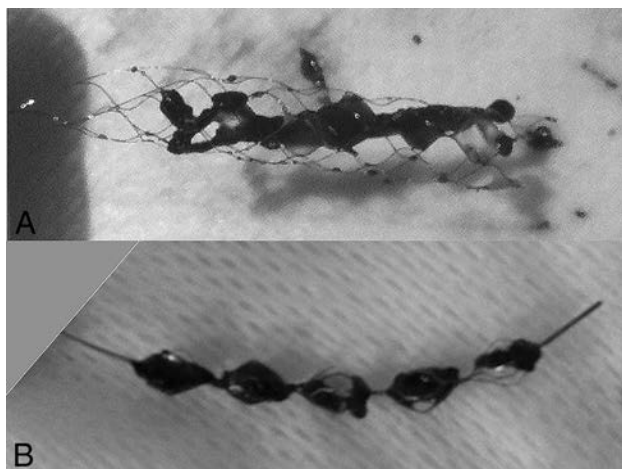


FIG 1. Figure illustrating the differences in clot retainment between the outside of classic stent retrievers (A) and inside the cages of the ERIC device (B).

Second-generation stent retrievers consisting of an interlinked cage design devised specifically for clot removal have recently been introduced. One of these second-generation stent retrievers is the Embolus Retriever with Interlinked Cages (ERIC; MicroVention, Tustin, California). Proposed advantages of the interlinked cage design compared with classic stent retrievers are the following: less fragmentation and shaving of the clot due to retention within or in-between the cages (Fig 1B), less contact and interaction of the stent retriever with the vessel wall, relying less on interaction with the clot, and the possibility of using a thinner delivery system (0.017-inch low-profile microcatheter), allowing improved access in challenging patient anatomy.¹²

Introduction of this new stent retriever design may improve procedural benchmarks and clinical outcome and ensure high rates of procedural success. In this retrospective study from a high-volume tertiary level stroke center, we aimed to examine the safety and efficacy of the ERIC device used as the primary thrombectomy device by comparing outcomes and procedural benchmarks with those of classic stent retrievers.

MATERIALS AND METHODS

This case-control study was approved by the Danish Health Authority (3–3013-1017/1) and the Danish Data Protection Agency (30–1148). All patients were treated within the Declaration of Helsinki.

The endovascular setup at our comprehensive stroke center in Copenhagen has previously been described.¹³ Seven stroke neurologists and 5 neurointerventionalists cover a 24/7 stroke team service with 30-minute response time. Patients were predominantly referred from primary stroke centers where initial clinical assessment and diagnostic imaging were performed and IV rtPA was administered. Stroke severity was assessed according to the NIHSS. We retrospectively reviewed all patients referred to us for anterior circulation acute ischemic stroke from January 2012 to December 2015. Only patients treated with mechanical thrombectomy by using a stent retriever were included in this study. The ERIC device has been available at our center since July 2013. We included all patients treated with classic stent retrievers from 2012

to 2015 for the comparison group. This time period was chosen because patient flow was high and consistent during these 4 years and our clinical setup has not changed since 2012.

Clinical and interventional details were extracted from prospectively recorded patient charts. Patient comorbidity was assessed according to the Charlson comorbidity index.¹⁴ Neuroimages were reviewed by 2 authors (H.S.-A. and M.H.). Clot location was defined on DSA and categorized into ICA bifurcation (ICA-T), MCA before the major bifurcation (MCA-M1) or after the major bifurcation (MCA-M2), or “other” clot location in case of distally located clots or intracranial carotid siphon occlusion without involvement of the bifurcation.

Neurointerventions

Right femoral access was predominantly used. A large-bore long-sheath or coaxial catheter was placed in the ipsilateral carotid artery (eg, Destination sheath, Terumo, Leuven, Belgium; Neuron Max 6F, Penumbra, Alameda, California; or Arrow 8–9F, Teleflex, Limerick, Ireland). A long standard guide catheter with JB1 or SIM2 configuration (Cook, Bloomington, Indiana) was used to guide the sheath or the large-bore coaxial catheter from the aortic arch into the carotid arteries. From a stable position in the proximal ICA or distal common carotid artery, a distal-access catheter (eg, Sofia, MicroVention; Navien guiding catheter, Covidien, Irvine, California; Fargo and Fargomax, Balt, Montmorency, France; or ACE 64 or 5MAX ACE reperfusion catheter, Penumbra) was advanced into the intracranial vasculature, usually in a triaxial fashion via a microcatheter to avoid unnecessary vessel stress. If necessary, an additional proximal balloon-guide catheter (eg, Cello balloon-guide catheter; Covidien) was placed through a large-bore sheath (8F or 9F) before the distal-access catheter was advanced through it.

After the clot location had been confirmed as initially seen on preprocedural CTA, a microcatheter (eg, Prowler Select Plus, Codman & Shurtleff, Raynham, Massachusetts; or Headway 17–21, MicroVention) following a guidewire (eg, Traxcess 0.014-inch, MicroVention; or Transcend platinum 0.014-inch, Stryker Neurovascular, Kalamazoo, Michigan) was navigated through the clot. The guidewire was then substituted for a stent retriever, which was deployed within the clot. In cases using the ERIC device, the largest possible number of cages was placed distal to the clot while still covering the entire clot with the device. Patients who were not treated with the ERIC device had been treated with classic stent retrievers from various companies (eg, Solitaire FR; Covidien, or pREset thrombus retriever, phenox, Bochum, Germany) (On-line Table 1). Thrombectomy was performed in combination with distal or proximal aspiration or a combination of both, and the choice of thrombectomy devices was left to the discretion of the neurointerventionalist. Furthermore, conscious sedation or general anesthesia, extracranial carotid stent placement, and periprocedural antithrombotic therapy were managed on a case-by-case basis.

Postprocedural Management

Patients were observed in a neurointensive care unit at least until 24-hour postprocedural follow-up NCCT had excluded major intracranial hemorrhages or risk of malignant infarction. Intracere-

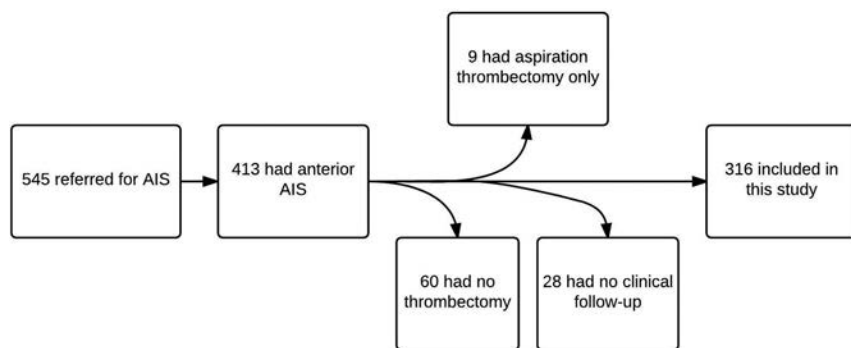


FIG 2. Flow chart of patient inclusion.

Table 1: Baseline characteristics^a

| Characteristics | N = 316 |
|-------------------------------|-----------------------------|
| Age (mean) (yr) | 68.7 ± 13; range 27–94 |
| Sex (male) | 174 (55%) |
| Diabetes | 38 (12%) |
| Hyperlipidemia | 100 (32%) |
| Hypertension | 183 (58%) |
| Known atrial fibrillation | 84 (27%) |
| Prior stroke | 39 (12%) |
| CCI 0 | 158 (50%) |
| CCI 1–3 | 137 (43%) |
| CCI 4–10 | 21 (7%) |
| IV rtPA | 223 (71%) |
| Clot location | |
| ICA-T | 83 (26%) |
| M1 | 177 (56%) |
| M2 | 47 (15%) |
| Other | 9 (3%) |
| NIHSS (mean) | 16.9 ± 5; range, 0–28 |
| Extracranial carotid stenting | 64 (20%) |
| Onset to image (mean) (min) | 97.8 ± 64; range, 10–517 |
| Image to groin (mean) (min) | 149.3 ± 62; range, 27–459 |
| Onset to TICI (mean) (min) | 325.0 ± 106; range, 102–900 |
| General anesthesia | 205 (65%) |

Note:—CCI indicates Charlson comorbidity index.

^a Data are No. (%) unless otherwise indicated.

bral hemorrhages were classified according to the European Cooperative Acute Stroke Study II criteria into hemorrhagic infarcts and parenchymal hemorrhages.¹⁵ In cases where differentiation between residual contrast and hemorrhagic infarction was not possible on 24-hour NCCT, or on a subsequent NCCT within few days, the image was attributed to hemorrhagic infarction. Afterward, patients were discharged for neurorehabilitation, and follow-up was arranged at 3 months poststroke with clinical assessment according to the mRS.

Outcome Measures

The main outcome was favorable recanalization defined as a TICI score of 2b–3.¹⁶ Secondary outcomes included the following: favorable clinical outcome defined as mRS 0–2 at 3 months, procedural adverse events defined as any untoward event occurring during neurointerventions, symptomatic intracerebral hemorrhages defined as any intracranial hemorrhage causing a clinical deterioration of ≥4 points on the NIHSS,¹⁵ and procedural benchmarks (procedural duration [groin puncture to final image], number of thrombectomy passes, and need for >1 thrombectomy device).

Statistical Analysis

Variables are presented as means ± SD and range for continuous variables and number with percentage for categorical variables. Means were compared with the Student *t* test, and 95% confidence intervals of the difference in means are presented. Categorical variables were compared by means of the χ^2 or Fisher exact test when appropriate, and 95% CI of the OR is presented.

We performed a propensity score-matched analysis comparing patients treated with the ERIC device with patients

treated with classic stent retrievers at our center in a 1:1 ratio,¹⁷ with the “nearest available Mahalanobis metric matching within calipers defined by the propensity score” method.¹⁸ The following covariates were used to calculate the propensity score by using a logistic regression model predicting treatment with the ERIC device: stroke severity, the neurointerventionalist in charge of the procedure, clot location, time from neuroimaging to groin puncture, and level of sedation during the procedure. Baseline variables were compared before and after matching to check for reduction of bias.

Due to the unevenly distributed time periods for the ERIC (July 2013 to December 2015) and the classic stent retriever group (January 2012 to December 2015), we planned a time-sensitivity analysis by using only patients treated within the same time period. Furthermore, our results were compared with multivariate regression analyses with backward elimination of covariates with nonsignificant associations to outcomes.

All analyses were performed by using SAS Statistical Software, Version 9.4 (SAS Institute, Cary, North Carolina).

RESULTS

We identified 545 patients with acute ischemic stroke referred for mechanical thrombectomy in the study period. Of these, 413 patients had anterior circulation stroke, and 69 patients not treated with a stent retriever and 28 patients with missing follow-up (referred from a nearby Swedish stroke center, On-line Table 2) were excluded (Fig 2).

Thus, 316 patients were included. Baseline variables including age, sex, comorbidities, cardiovascular risk factors, stroke severity, and clot location are found in Table 1.

We identified 59 patients treated with the ERIC device as the primary thrombectomy device and 257 patients treated with classic stent retrievers as the primary thrombectomy device. Propensity scoring identified 57 matched pairs, and we compared baseline characteristics before and after matching (Table 2).

The ERIC group showed equal rates of favorable recanalization (86% versus 81% [OR 95% CI, 0.54–3.96; *P* = .61]), favorable 3-month clinical outcome (46% versus 40%, [OR 95% CI, 0.59–2.61; *P* = .71]), and procedural adverse events (28% versus 30% [OR 95% CI, 0.41–2.06; *P* = 1.00]) compared with the classic stent retriever group and nonsignificantly fewer parenchymal intracerebral hemorrhages (7% versus 14% [OR 95% CI, 0.13–1.63; *P* = .36]), symptomatic intracerebral hemorrhages (5% versus

Table 2: Comparison of clinical and treatment characteristics before and after propensity score matching^a

| | Before Propensity Score Matching | | | After Propensity Score Matching | | |
|-------------------------------|----------------------------------|--------------------|---------|---------------------------------|-------------------|---------|
| | ERIC (n = 59) | Non-ERIC (n = 257) | P Value | ERIC (n = 57) | Non-ERIC (n = 57) | P Value |
| Age (yr) | 70.0 | 68.4 | .41 | 69.7 | 70.1 | .87 |
| Sex (male) | 29 (49%) | 145 (56%) | .31 | 29 (51%) | 31 (54%) | .85 |
| CCI 0 | 27 (46%) | 131 (51%) | .44 | 27 (47%) | 28 (49%) | .50 |
| CCI 1–3 | 26 (44%) | 111 (43%) | | 25 (44%) | 27 (47%) | |
| CCI ≥4 | 6 (10%) | 15 (6%) | | 5 (9%) | 2 (4%) | |
| Known atrial fibrillation | 15 (25%) | 69 (27%) | .87 | 14 (25%) | 17 (30%) | .67 |
| IV rtPA | 39 (66%) | 184 (72%) | .43 | 38 (67%) | 41 (72%) | .69 |
| Clot location | | | | | | |
| ICA-T | 22 (37%) | 61 (24%) | <.0001 | 22 (39%) | 22 (39%) | .63 |
| M1 | 19 (32%) | 158 (61%) | | 17 (30%) | 21 (37%) | |
| M2 | 13 (22%) | 34 (13%) | | 13 (23%) | 12 (21%) | |
| Other | 5 (8%) | 4 (2%) | | Other: 5 (8%) | 2 (3%) | |
| NIHSS | 17.4 | 16.8 | .36 | 17.4 | 17.5 | .91 |
| Extracranial carotid stenting | 13 (22%) | 51 (20%) | .72 | 13 (23%) | 10 (18%) | .64 |
| Onset to image (min) | 92.3 | 99.0 | .51 | 92.6 | 98.7 | .65 |
| Image to groin (min) | 167.0 | 145.3 | .04 | 167.0 | 150.5 | .20 |
| General anesthesia | 34 (58%) | 171 (67%) | .23 | 33 (58%) | 32 (56%) | 1.00 |
| Neurointerventionalist | | | | | | |
| 1 | 38 (64%) | 53 (21%) | <.0001 | 36 (63%) | 28 (49%) | .51 |
| 2 | 15 (25%) | 45 (18%) | | 15 (26%) | 20 (35%) | |
| 3 | 4 (7%) | 59 (23%) | | 4 (7%) | 6 (11%) | |
| 4 | 0 (0%) | 42 (16%) | | 0 (0%) | 0 (0%) | |
| 5 | 2 (3%) | 58 (23%) | | 2 (4%) | 3 (5%) | |

Note:—CCI indicates Charlson comorbidity index.

^a Data are No. (%) unless otherwise indicated.

Table 3: Comparison of procedural and clinical outcome after propensity score matching for primary and time-sensitivity analysis^a

| | Primary Analysis | | | Time-Sensitivity Analysis | | |
|---------------------------|-------------------|-------------------|---------|---------------------------|-------------------|---------|
| | ERIC (n = 57) | Non-ERIC (n = 57) | P Value | ERIC (n = 37) | Non-ERIC (n = 37) | P Value |
| TICI 2b–3 | 49 (86%) | 46 (81%) | | 32 (86%) | 30 (81%) | |
| OR (95% CI) | 1.46 (0.54–3.96) | | .61 | 1.49 (0.43–5.22) | | .75 |
| mRS 0–2 | 26 (46%) | 23 (40%) | | 17 (46%) | 14 (38%) | |
| OR (95% CI) | 1.24 (0.59–2.61) | | .71 | 1.56 (0.62–3.93) | | .64 |
| Mortality | 11 (19%) | 12 (21%) | | 7 (19%) | 7 (19%) | |
| OR (95% CI) | 0.90 (0.36–2.24) | | 1.00 | 1.17 (0.39–3.45) | | 1.00 |
| Procedural duration (min) | 67.4 | 98.0 | | 74.1 | 90.8 | |
| Mean difference (95% CI) | 30.6 (8.0–53.2) | | .009 | 16.6 (–7.8–41.1) | | .18 |
| No. of passes | 2.5 | 3.1 | | 2.5 | 3.4 | |
| Mean difference (95% CI) | 0.6 (–0.1–1.3) | | .11 | 0.9 (–0.2–2.0) | | .10 |
| Several devices needed | 10 (18%) | 22 (39%) | | 7 (19%) | 16 (43%) | |
| OR (95% CI) | 0.34 (0.14–0.80) | | .02 | 0.31 (0.11–0.87) | | .04 |
| Parenchymal hemorrhages | 4 (7%) | 8 (14%) | | 4 (11%) | 2 (6%) | |
| OR (95% CI) | 0.46 (0.13–1.63) | | .36 | 1.50 (0.24–9.55) | | .67 |
| Symptomatic hemorrhages | 3 (5%) | 9 (16%) | | 3 (8%) | 4 (11%) | |
| OR (95% CI) | 0.30 (0.076–1.16) | | .12 | 0.47 (0.08–2.74) | | 1.00 |
| Distal embolism | 1 (2%) | 5 (9%) | | 1 (3%) | 4 (11%) | |
| OR (95% CI) | 0.19 (0.02–1.64) | | .21 | 0.23 (0.02–2.16) | | .36 |
| Procedural adverse events | 16 (28%) | 17 (30%) | | 11 (30%) | 13 (35%) | |
| OR (95% CI) | 0.92 (0.41–2.06) | | 1.00 | 0.59 (0.22–1.63) | | .80 |

^a Data are No. (%) unless otherwise indicated.

16% [OR 95% CI, 0.076–1.16; $P = .12$]), and distal embolism (2% versus 9%, [OR 95% CI, 0.02–1.64; $P = .21$]) (Table 3). Procedural adverse events are presented in detail in On-line Table 3.

The ERIC group showed significantly shorter procedural durations (67.4 versus 98.0 minutes [95% CI, 8–53 minutes; $P = .009$]) and less frequent use of secondary/rescue devices (18% versus 39% [OR 95% CI, 0.14–0.80; $P = .02$]). The number of thrombectomy passes was not statistically different (2.5 versus 3.1 passes [95% CI, –0.1–1.3 passes; $P = .11$]) compared with the classic stent retriever group (Table 3).

Sensitivity Analyses

In the time-sensitivity analysis on 199 patients treated from July 2013 to December 2015, we only identified 37 matched pairs. This analysis still showed equal rates of favorable recanalization (OR 95% CI, 0.43–5.22; $P = .75$), clinical outcome (OR 95% CI, 0.62–3.93; $P = .64$), procedural adverse events (OR 95% CI, 0.22–1.63; $P = .80$), symptomatic intracerebral hemorrhages (OR 95% CI, 0.08–2.74; $P = 1.00$), and distal embolism (OR 95% CI, 0.02–2.16; $P = .36$) (Table 3). The procedural duration remained numerically shorter in the ERIC group, though this difference was no longer statistically significant (74.1 versus 90.8 minutes [95%

CI, $-8-41$]; $P = .18$). The number of thrombectomy passes remained statistically insignificant (2.5 versus 3.4 passes [95% CI, $-0.16-1.95$]; $P = .10$), and the significantly less frequent use of secondary/rescue device remained (OR 95% CI, $0.11-0.87$; $P = .04$) (Table 3). The multivariate regression analyses confirmed that thrombectomy with the ERIC retriever was not associated with either favorable recanalization or favorable clinical outcome but predicted shorter procedural duration and less need for a secondary device (On-line Table 4).

DISCUSSION

This study examined the efficacy and safety of the ERIC device by comparing it with those of classic stent retrievers and identified equal rates of favorable recanalization and clinical outcome, equal procedural adverse events, and improvements in some procedural benchmarks. Possible drawbacks with the design of the classic stent retrievers are dependency on time-consuming interaction with the clot, which also may be problematic in white, platelet-rich clots,¹⁹ and vulnerability of the clot during retraction because it is retained on the outside of the stent retriever. New generations of thrombectomy devices were designed to overcome these disadvantages. The interlinked cages design of the ERIC and similar devices captures the clot within and between the cages and relies less on interaction with the clot, possibly allowing faster and gentler clot removal. Additionally, the ERIC device has a slimmer profile and can be used through low-profile microcatheters. Although still unproven, stent retrievers designed specifically for clot removal such as the ERIC device may improve procedural benchmarks during thrombectomy and could have a positive effect on clinical outcome. Although previous studies^{20,21} have suggested reasonable efficacy and safety with the ERIC device for mechanical thrombectomy, to our knowledge, our study is the first to compare procedural benchmarks and clinical outcome with classic stent retrievers.

The main finding of our study was equal rates of favorable recanalization between the ERIC group and the classic stent retriever group. Furthermore, our rate was comparable with the findings of 2 published case series both reporting 83% favorable recanalization with the ERIC device for thrombectomy.^{20,21} The rates of favorable recanalization with classic stent retrievers are already high, and it is unlikely that any new device will provide more than the 80%–90% TICI 2b–3 seen in recent randomized controlled trials.^{2–6} These high rates of favorable recanalization were, however, not reflected in equally high rates of favorable clinical outcome; this finding suggests that there may still be the potential for procedure-related improvement. Therefore, it may be more relevant to explore improvement in other procedural benchmarks than the rate of favorable recanalization. We identified a statistically significant shorter procedural duration and less frequent use of secondary endovascular devices with the ERIC compared with classic stent retriever devices. These factors both suggest slightly improved performance of the ERIC device compared with classic stent retrievers. These benchmark improvements were not directly reflected in improved 3-month clinical outcome in which we identified equal rates of favorable clinical outcome, but most interesting, the shorter procedural duration of 30 minutes and the 6% absolute difference in rates of favorable

clinical outcome in favor of the ERIC group in our study correspond very well with previous data, suggesting that every 30-minute delay to reperfusion decreases the rate of favorable 3-month clinical outcome by 3%–8%.^{22,23}

Although we identified an average of 30-minute shorter procedural duration in the ERIC group, the difference may be as little as 8 minutes as illustrated by the lower limit of the confidence interval. Furthermore, we saw a difference in delay to groin puncture between the 2 groups. Even though we attempted to adjust for this difference, Table 2 shows that a bias toward longer delay to groin puncture in the ERIC group may still exist after adjustment, though this was no longer statistically significant. If this time delay was better balanced, the difference in 3-month outcome between the 2 groups may have been even greater. Our rate of favorable clinical outcome (46%) was comparable with that in the 2 case series (33%–48%^{20,21}).

Concerning the safety of mechanical thrombectomy with the ERIC device, we found equal rates of adverse events compared with classic stent retrievers. We observed only 1 patient with distal embolus after thrombectomy in the ERIC group and 5 patients in the classic stent retriever group. Although it is tempting to speculate that this finding might signify improved protection of the clot inside the device during retraction of the ERIC retriever, these numbers are too small and the results need be confirmed by large prospective studies.

In the ERIC group, we identified 6 patients with procedure-related intracranial hemorrhagic complications compared with 2 patients in the classic stent retriever group. Four of the 6 hemorrhages were related to thrombectomy with the ERIC retriever, 1 hemorrhage was caused by a microwire perforation, and 1 hemorrhage was related to thrombectomy with a classic stent retriever. Procedures in all 4 hemorrhages that appeared after thrombectomy with the ERIC device were performed in distal branches (distal MCA–M2/M3), where the risk of thrombectomy may be increased.²⁴ This finding suggests that even though the design of the ERIC device allows for low-profile microcatheters that may have easier access to distal branches, the risk-benefit must be carefully evaluated when performing thrombectomy beyond the MCA–M1/M2 branches.

Even though we identified a few more procedure-related hemorrhages in the ERIC group, most were clinically silent minor subarachnoid hemorrhages, and only 2 of the 6 hemorrhages in the ERIC group were symptomatic. One intracerebral hemorrhage appeared after MCA–M1 thrombectomy with a classic stent retriever used as a rescue device (expired day 5). The other intracerebral hemorrhage appeared after MCA–M3 thrombectomy with an ERIC 3×20 device, which led to coiling of the vessel. The patient deteriorated from NIHSS 18 to NIHSS 27 (3-month mRS = 4). The rate of symptomatic hemorrhage observed in this study was comparable with that in the 2 case series (0%–8%^{20,21}). Although we identified slightly fewer symptomatic hemorrhages in the ERIC group, the rates represent very few cases, and the results need to be interpreted with caution. In the time-sensitivity analysis, we saw even rates of symptomatic hemorrhages between the 2 groups, further supporting the risks of thrombectomy with the ERIC device being equal to those in classic stent retrievers.

Limitations

This study represents experience from a single stroke center with a limited sample size, and results may vary from those in other centers. However, we identified very similar results compared with other studies.^{20,21} Procedural details were recorded before clinical outcome was known, and this study was not designed at the time of clinical outcome assessment of patients. Only the clot location was available and not clot size/burden or clot composition, which may play an important role in the efficacy of a stent retriever.¹⁹ Selection of devices for clot removal was based on the discretion of the neuro-interventionalist; even though no specific criteria were used by our staff, our results may have been affected by selection bias. We observed a considerable reduction of bias after propensity score matching (Table 2), but important factors such as the individual interventionist's skill, speed, and aggressiveness and time-delay to groin puncture, which may affect both the procedural success and clinical outcome, could have been better balanced. To obtain truly comparable groups, a randomized controlled trial would be needed. Although we do not believe that our setup has undergone major changes in the past 4 years, a potential learning curve may have affected our results favoring the ERIC stent. However, the time-sensitivity analysis for patients treated within the same time periods (July 2013 to December 2015) confirmed the results of our primary analysis but with a smaller sample size. Our results are further strengthened by the multivariate analysis of variables associated with outcomes also confirming the results of our primary analysis (On-line Table 4).

CONCLUSIONS

Mechanical thrombectomy with the ERIC device is effective and safe and is associated with at least equal rates of favorable procedural and clinical outcomes compared with classic stent retrievers. The inter-linked cages design of the ERIC device showed improvement in procedural benchmarks, which did not translate into improved clinical outcome, possibly due to low statistical power. These promising results warrant further evaluation by larger prospective clinical trials.

Disclosures: Markus Holtmannspötter—UNRELATED: Consultancy: Sequent Medical, MicroVention, Covidien-Medtronic, Stryker; Payment for Lectures Including Service on Speakers Bureaus: Sequent Medical, MicroVention, Covidien-Medtronic; Travel/Accommodations/Meeting Expenses Unrelated to Activities Listed: Sequent Medical, MicroVention, Covidien-Medtronic, Stryker Neurovascular.

REFERENCES

1. Campbell BC, Donnan GA, Lees KR, et al. **Endovascular stent thrombectomy: the new standard of care for large vessel ischaemic stroke.** *Lancet Neurol* 2015;14:846–54 CrossRef Medline
2. Berkhemer OA, Fransen PSS, Beumer D, et al. **A randomized trial of intraarterial treatment for acute ischemic stroke.** *N Engl J Med* 2015;372:11–20 CrossRef Medline
3. Jovin TG, Chamorro A, Cobo E, et al; REVASCAT Trial Investigators. **Thrombectomy within 8 hours after symptom onset in ischemic stroke.** *N Engl J Med* 2015;372:2296–306 CrossRef Medline
4. Saver JL, Goyal M, Bonafe A, et al; SWIFT PRIME Investigators. **Stent-retriever thrombectomy after intravenous t-PA vs. t-PA alone in stroke.** *N Engl J Med* 2015;372:2285–95 CrossRef Medline
5. Campbell BC, Mitchell PJ, Kleinig TJ, et al; EXTEND-IA Investigators. **Endovascular therapy for ischemic stroke with perfusion-imaging selection.** *N Engl J Med* 2015;372:1009–18 CrossRef Medline
6. Goyal M, Demchuk AM, Menon BK, et al; ESCAPE Trial Investigators. **Randomized assessment of rapid endovascular treatment of ischemic stroke.** *N Engl J Med* 2015;372:1019–30 CrossRef Medline
7. Broderick JP, Palesch YY, Demchuk AM, et al; Interventional Management of Stroke (IMS) III Investigators. **Endovascular therapy after intravenous t-PA versus t-PA alone for stroke.** *N Engl J Med* 2013;368:893–903 CrossRef Medline
8. Kidwell CS, Jahan R, Gornbein J, et al; MR RESCUE Investigators. **A trial of imaging selection and endovascular treatment for ischemic stroke.** *N Engl J Med* 2013;368:914–23 CrossRef Medline
9. Ciccone A, Valvassori L, Nichelatti M, et al; SYNTHESIS Expansion Investigators. **Endovascular treatment for acute ischemic stroke.** *N Engl J Med* 2013;368:904–13 CrossRef Medline
10. Henkes H, Flesser A, Brew S, et al. **A novel microcatheter-delivered, highly-flexible and fully-retrievable stent, specifically designed for intracranial use: technical note.** *Interv Neuroradiol* 2003;9:391–93 CrossRef Medline
11. Arai D, Ishii A, Chihara H, et al. **Histological examination of vascular damage caused by stent retriever thrombectomy devices.** *J Neurointerv Surg* 2016;8:992–95 CrossRef Medline
12. MicroVention-Terumo. ERIC brochure. <http://www.vingmed.se/wp-content/uploads/2013/10/ERIC-Brochure-Intl-A4.pdf>. Accessed October 9, 2015
13. Steglich-Arnholm H, Holtmannspötter M, Kondziella D, et al. **Thrombectomy assisted by carotid stenting in acute ischemic stroke management: benefits and harms.** *J Neurol* 2015;262:2668–75 CrossRef Medline
14. Charlson ME, Pompei P, Ales KL, et al. **A new method of classifying prognostic comorbidity in longitudinal studies: development and validation.** *J Chronic Dis* 1987;40:373–83 CrossRef Medline
15. Trouillas P, von Kummer R. **Classification and pathogenesis of cerebral hemorrhages after thrombolysis in ischemic stroke.** *Stroke* 2006;37:556–61 CrossRef Medline
16. Higashida RT, Furlan AJ, Roberts H, et al; Trial design and reporting standards for intra-arterial cerebral thrombolysis for acute ischemic stroke. **Trial design and reporting standards for intra-arterial cerebral thrombolysis for acute ischemic stroke.** *Stroke* 2003;34:e109–37 CrossRef Medline
17. Austin PC. **Statistical criteria for selecting the optimal number of untreated subjects matched to each treated subject when using many-to-one matching on the propensity score.** *Am J Epidemiol* 2010;172:1092–97 CrossRef Medline
18. Rosenbaum PR, Rubin DB. **Constructing a control group using multivariate matched sampling methods that incorporate the propensity score.** *Am Stat* 1985;39:33–38
19. Mokin M, Morr S, Natarajan SK, et al. **Thrombus density predicts successful recanalization with Solitaire stent retriever thrombectomy in acute ischemic stroke.** *J Neurointerv Surg* 2015;7:104–07 CrossRef Medline
20. Kahles T, Garcia-Esperon C, Zeller S, et al. **Mechanical thrombectomy using the new ERIC retrieval device is feasible, efficient, and safe in acute ischemic stroke: a Swiss Stroke Center experience.** *AJNR Am J Neuroradiol* 2016;37:114–19 CrossRef Medline
21. Raoult H, Redjem H, Bourcier R, et al. **Mechanical thrombectomy with the ERIC retrieval device: initial experience.** *J Neurointerv Surg* 2016 May 17. [Epub ahead of print] CrossRef Medline
22. Menon BK, Sajobi TT, Zhang Y, et al. **Analysis of workflow and time to treatment on thrombectomy outcome in the Endovascular Treatment for Small Core and Proximal Occlusion Ischemic Stroke (ESCAPE) randomized, controlled trial.** *Circulation* 2016;133:2279–86 CrossRef Medline
23. Fransen PS, Berkhemer OA, Lingsma HF, et al; Multicenter Randomized Clinical Trial of Endovascular Treatment of Acute Ischemic Stroke in the Netherlands Investigators. **Time to reperfusion and treatment effect for acute ischemic stroke: a randomized clinical trial.** *JAMA Neurol* 2016;73:190–96 CrossRef Medline
24. Kurre W, Aguilar-Pérez M, Martínez-Moreno R, et al. **Stent retriever thrombectomy of small caliber intracranial vessels using pREset LITE: safety and efficacy.** *Clin Neuroradiol* 2016 Jan 21. [Epub ahead of print] Medline

Impact of Anesthesia on the Outcome of Acute Ischemic Stroke after Endovascular Treatment with the Solitaire Stent Retriever

A. Slezak, R. Kurmann, L. Oppliger, A. Broeg-Morvaj, J. Gralla, G. Schroth, H.P. Mattle, M. Arnold, U. Fischer, S. Jung, R. Greif, F. Neff, P. Mordasini, and M.-L. Mono

ABSTRACT

BACKGROUND AND PURPOSE: General anesthesia during endovascular treatment of acute ischemic stroke may have an adverse effect on outcome compared with conscious sedation. The aim of this study was to examine the impact of the type of anesthesia on the outcome of patients with acute ischemic stroke treated with the Solitaire stent retriever, accounting for confounding factors.

MATERIALS AND METHODS: Four-hundred one patients with consecutive acute anterior circulation stroke treated with a Solitaire stent retriever were included in this prospective analysis. Outcome was assessed after 3 months by the modified Rankin Scale.

RESULTS: One-hundred thirty-five patients (31%) underwent endovascular treatment with conscious sedation, and 266 patients (69%), with general anesthesia. Patients under general anesthesia had higher NIHSS scores on admission (17 versus 13, $P < .001$) and more internal carotid artery occlusions (44.6% versus 14.8%, $P < .001$) than patients under conscious sedation. Other baseline characteristics such as time from symptom onset to the start of endovascular treatment did not differ. Favorable outcome (mRS 0–2) was more frequent with conscious sedation (47.4% versus 32%; OR, 0.773; 95% CI, 0.646–0.925; $P = .002$) in univariable but not multivariable logistic regression analysis ($P = .629$). Mortality did not differ ($P = .077$). Independent predictors of outcome were age (OR, 0.95; 95% CI, 0.933–0.969; $P < .001$), NIHSS score (OR, 0.894; 95% CI, 0.855–0.933; $P < .001$), time from symptom onset to the start of endovascular treatment (OR, 0.998; 95% CI, 0.996–0.999; $P = .011$), diabetes mellitus (OR, 0.544; 95% CI, 0.305–0.927; $P = .04$), and symptomatic intracerebral hemorrhage (OR, 0.109; 95% CI, 0.028–0.428; $P = .002$).

CONCLUSIONS: In this single-center study, the anesthetic management during stent retriever thrombectomy with general anesthesia or conscious sedation had no impact on the outcome of patients with large-vessel occlusion in the anterior circulation.

ABBREVIATIONS: CS = conscious sedation; EVT = endovascular treatment; GA = general anesthesia

Endovascular treatment of acute ischemic stroke due to large-vessel occlusion in the anterior circulation is safe and effective for improving functional outcome.¹ However, there is an ongoing debate about the type of anesthesia to be used, general anesthesia (GA) or conscious sedation (CS). No patient movements, better airway control, and perceived procedural safety and efficacy are

regarded as potential advantages of GA, but more recent data of nonrandomized studies including 1 meta-analysis of 9 studies suggest that CS during endovascular stroke treatment might improve outcome.^{2–5} This finding might be explained by a shorter time to start the intervention, less blood pressure dip, and easier neurologic monitoring during and after CS. However, many confounding factors such as stroke severity, occlusion site, pretreatment with IV rtPA, age, endovascular treatment techniques, and recanalization rates, might influence outcome.^{3,6–11} Recently, the results of the first randomized study, Sedation versus Intubation for Endovascular Stroke Treatment (SIESTA), were published, which showed no differences between GA and CS for the primary end point defined as early neurologic improvement on the NIHSS after 24 hours.¹²

The aim of this study was to examine the impact of the type of anesthesia (GA versus CS) on the outcome of patients with acute ischemic stroke with large-vessel occlusion in the ante-

Received December 1, 2016; accepted after revision February 14, 2017.

From the Departments of Neurology (A.S., R.K., L.O., A.B.-M., H.P.M., M.A., U.F., S.J., M.-L.M.), Diagnostic and Interventional Neuroradiology (J.G., G.S., P.M.), and Anesthesiology and Pain Medicine (R.G., F.N.), University Hospital Bern and University of Bern, Bern, Switzerland.

A. Slezak, R. Kurmann, P. Mordasini, and M.-L. Mono contributed equally to this work.

This study was supported by a grant from the Swiss Heart Foundation.

Please address correspondence to Marie-Luise Mono, MD, Department of Neurology, Inselspital, University Hospital and University of Bern, Freiburgstr, 3010 Bern, Switzerland; e-mail: marie-luise.mono@insel.ch

<http://dx.doi.org/10.3174/ajnr.A5183>

rior circulation who were treated with the Solitaire stent retriever (Covidien, Irvine, California), while accounting for confounding factors.

MATERIALS AND METHODS

Data of 401 consecutive patients with acute ischemic stroke with large-vessel occlusion in the anterior circulation who were treated endovascularly with the Solitaire stent retriever either directly or after intravenous thrombolysis with rtPA were prospectively collected and analyzed. Patients were included between January 2010 and April 2015. The study was approved by the Cantonal Ethics Committee of Bern, and all patients or their relatives gave written consent for participation.

Endovascular treatment (EVT) was performed in 266 patients under GA and in 135 patients with CS. In 10 patients (2.5%), CS was switched to GA. On the basis of the intention-to-treat principle, these patients were added to the CS group. Patient data (demographics, comorbidities, stroke etiology according to the Trial of Org 10172 in Acute Stroke Treatment [TOAST] criteria,¹³ prestroke modified Rankin Scale score, pretreatment and stroke treatment details, complications, and outcome) were recorded in the Bernese Stroke Registry.

EVT within 8 hours after symptom onset was performed immediately after CT or MR imaging under the following conditions: 1) The diagnosis of ischemic stroke was established; 2) the NIHSS score on admission assessed by a neurologist was ≥ 4 points or isolated aphasia or hemianopsia was present or neurologic deficits recurred; 3) CT or MR angiography showed occlusion of the carotid artery, the M1 or M2 segments of the middle cerebral artery, or the A1 segment of the anterior cerebral artery; 4) hemorrhage was excluded; 5) neurologic deficits correlated with the vessel occlusion; and 6) no individual clinical or pre-morbid conditions or laboratory findings contraindicated EVT. When the criteria for EVT were fulfilled, digital subtraction angiography was performed via a transfemoral approach by using a biplane, high-resolution angiography system. All patients underwent complete 4-vessel cerebral angiography performed by fully trained interventional neuroradiologists. The decision for EVT in combination with intravenous thrombolysis or without it was made on an individual basis after interdisciplinary discussion. Intravenous thrombolysis was additionally given if it was indicated (symptom onset of <4.5 hours) and nothing against its use was indicated. The interventional neuroradiologist and neurologist decided on EVT with the Solitaire device and when necessary additional intra-arterial urokinase. At the end of angiography, recanalization was classified by the treating neuroradiologist according to the Thrombolysis in Cerebral Infarction perfusion scale grade.¹⁴

The decision of whether to perform GA or CS was made on an individual basis by the neurologist, neuroradiologist, and anesthesiologist on call considering the patient's physical status, pros and cons of the anesthetic management, and preferences of the neurointerventionalists. Reasons for choosing GA over CS were lack of cooperation or agitation of the patient, expected complexity of the interventions (eg, in case of tandem occlusions or ICA occlusions), expected difficult access anatomy, and restricted general physical or neurologic status of the patient (eg, severe stroke

with need for airway protection, impaired consciousness). When a decision for CS was made, patients underwent continuous monitored anesthesia care with supplemental oxygen via a face mask and standardized monitoring including electrocardiography, pulse oximetry, end-tidal carbon dioxide measurement, and invasive arterial blood pressure measurement, which we usually measure by the side-arm extension tube of the femoral sheath to avoid loss of time for puncture of the radial artery. For sedation, intermittent IV boluses of midazolam (2.5 mg) and fentanyl (50 mcg) or propofol (20 mg) were given at the discretion of the attending anesthesiologist.

After proper patient positioning and preoxygenation, GA was induced with IV fentanyl (1–5 mcg/kg) and propofol (1–2 mg/kg), and rocuronium (0.9 mg/kg) for rapid sequence intubation. General anesthesia was maintained with IV propofol (6–10 mcg/kg/h) and boluses of fentanyl (1–3 mcg/kg) and rocuronium (0.1 mg/kg) according to the needs of the patient. Following tracheal intubation, the patient was mechanically ventilated until the end of the procedure (Hamilton C1; Hamilton Medical, Bonaduz, Switzerland). Patient monitoring during GA was the same as under CS. General anesthesia was terminated, and the patient was extubated as soon as possible after the intervention. All anesthesia-related data including blood pressure dips (maximum blood pressure drop within the intervention), complications during the procedure, and difficulties in patient management (eg, movement and thus conversion from sedation to general anesthesia) were recorded in the anesthetic record (AIS Release 57; COPRA System, Berlin, Germany). The goal of systolic blood pressure during EVT was between 140 and 180 mm Hg according to our institutional standards.

After EVT, all patients were transferred to the Stroke Unit or an intermediate or intensive care unit for at least 24 hours after treatment. Neurologic status, blood pressure, glucose levels, oxygen saturation, and body temperature were monitored closely. CT or MR imaging scans were generally obtained 24 hours after treatment, and additionally in case of clinical deterioration. Symptomatic and asymptomatic intracerebral hemorrhage was graded according to the Prolyse in Acute Cerebral Thromboembolism (PROACT) II and European Cooperative Acute Stroke Study (ECASS) II criteria.^{15,16} Secondary preventive treatment was given according to current evidence and the American Heart Association and American Stroke Association guidelines.¹⁷ Pneumonia was diagnosed when at least 1 of the primary and 1 of the secondary criteria were fulfilled according to the US Centers for Disease Control and Prevention criteria. The primary criteria include abnormal respiratory examination and pulmonary infiltrates in chest x-rays; secondary criteria include productive cough with purulent sputum, microbiological cultures from lower respiratory tract or blood cultures, leukocytosis, and elevation of C-reactive protein. We recorded the following periprocedural complications: dissection of an extra- or intracranial vessel, perforation of an extra- or intracranial vessel, and iatrogenic thrombus dislocation.

Outcome

Clinical outcome was assessed 3 months after the index event by using the modified Rankin Scale.¹⁸ The primary study end point

Table 1: Patient characteristics and procedural details^a

| | CS | GA | P Value |
|---|-------------|-------------|---------|
| No. of patients | 135 | 266 | |
| Age (yr) (mean) (SD) | 70.5 (14.9) | 70.9 (13.9) | .803 |
| Age older than 80 yr | 46 (34.1) | 76 (28.6) | .258 |
| Male sex | 59 (43.7) | 140 (52.6) | .091 |
| Prestroke mRS < 1 | 124 (94.7) | 228 (89.8) | .104 |
| TOAST | | | .162 |
| Large-artery disease | 26 (19.3) | 63 (23.8) | |
| Small-artery disease | 3 (2.2) | 6 (2.3) | |
| Cardioembolism | 64 (47.4) | 95 (35.8) | |
| Stroke of other determined etiology | 15 (11.1) | 23 (8.7) | |
| Stroke of undetermined etiology | 27 (20) | 78 (29.5) | |
| Atrial fibrillation | 39 (31.2) | 84 (36.5) | .164 |
| Hyperlipidemia | 59 (44.4) | 120 (45.8) | .786 |
| Arterial hypertension | 66 (48.9) | 146 (54.9) | .255 |
| Diabetes mellitus | 39 (29.3) | 74 (28.2) | .823 |
| Coronary disease | 21 (17.4) | 65 (27.3) | .037 |
| Smoking | 49 (38.9) | 111 (46.3) | .177 |
| Prior stroke or TIA | 15 (14.2) | 32 (14.4) | .949 |
| Recurrent stroke within 3 mo | 9 (7.8) | 11 (4.9) | .462 |
| NIHSS on admission (mean) (SD) | 13.1 (5.7) | 17.2 (6.6) | <.001 |
| Vessel occlusion site | | | <.001 |
| ICA | 20 (14.8) | 117 (44) | |
| ACA | 1 (0.7) | 0 (0) | |
| MCA | 114 (84.4) | 149 (56) | |
| Time from symptom onset to start of EVT (mean) (SD) (min) | 277 (126) | 299 (157) | .165 |
| Intravenous rtPA and EVT | 44 (32.6) | 78 (29.3) | .501 |
| Mechanical thrombectomy only | 72 (53.3) | 159 (59.8) | .217 |
| Maximal systolic blood pressure (mm Hg) (mean) (SD) | 177 (25) | 176 (25) | .631 |
| Minimal systolic blood pressure (mm Hg) (mean) (SD) | 149 (33) | 133 (42) | <.001 |
| Systolic BP gradient during procedure (mm Hg) (mean) (SD) | 31 (26) | 50 (32) | <.001 |
| BP-increasing drugs | 54 (40.3) | 254 (95.8) | <.001 |
| BP-lowering drugs | 42 (31.1) | 104 (39.1) | .116 |
| TICI 2–3 recanalization | 116 (85.9) | 235 (88.3) | .488 |
| 3-month mRS 0–1 | 37 (27.4) | 56 (21.2) | .154 |
| 3-month mRS 0–2 | 64 (47.4) | 85 (32) | .002 |
| NIHSS after 24 hr (mean) (SD) | 9 (8.3) | 13.9 (11.2) | <.001 |
| Death within 3 months | 28 (20.7) | 77 (28.9) | .077 |

Note:—ACA indicates anterior cerebral artery; BP, blood pressure.

^a Data are No. (%) unless otherwise indicated.

Table 2: Peri- and postprocedural complications of endovascular treatment with the Solitaire stent retriever in anterior circulation stroke^a

| | CS | GA | P Value |
|-------------------------------------|-----------|-----------|---------|
| Pneumonia | 22 (16.5) | 67 (25.3) | .048 |
| Symptomatic ICH (PROACT II) | 9 (6.8) | 20 (7.6) | .755 |
| Symptomatic ICH (ECASS II) | 9 (6.8) | 21 (8) | .658 |
| Systemic bleeding | 4 (3) | 3 (1.1) | .185 |
| Asymptomatic ICH (PROACT II) | 24 (18) | 52 (19.9) | .655 |
| Peri-interventional complications | | | |
| Dissection | 6 (4.5) | 12 (4.6) | .975 |
| Thrombus dislocation | 12 (9) | 33 (12.5) | .302 |
| Perforation of intracranial vessels | 2 (1.5) | 5 (1.9) | .773 |

Note:—ICH indicates intracerebral hemorrhage.

^a Data are No. (%) unless otherwise indicated.

was favorable outcome (mRS 0–2). Secondary end points were excellent outcome (mRS 0–1) and death.

Statistics

Descriptive statistics are expressed as means with SDs or medians with interquartile ranges. Groups (GA and CS) were compared by the χ^2 test for categoric variables and the Student *t* test or, in case of a non-normal distribution, the Mann-Whitney *U* test for continuous

variables. Univariable logistic analysis was performed to determine an association between the type of anesthesia and outcome. To adjust for prognostic baseline factors, we performed a multivariable logistic regression including all variables with probability values of <.1 in univariable analysis. A probability value of *P* < .05 was considered significant.

RESULTS

Baseline and Treatment Characteristics

Baseline characteristics and procedural details are given in Table 1. Coronary heart disease was more common in the GA group (27% versus 17%, *P* = .037). Patients under GA had higher NIHSS scores on admission (17 points versus 13 points, *P* < .001), more often had internal carotid artery occlusions (44% versus 15%, *P* < .001), received more blood pressure-elevating drugs (96% versus 40%, *P* < .001), and experienced greater blood pressure drops during anesthesia (50 versus 31 mm Hg, *P* < .001). Patients with CS showed MCA occlusions more often (84% versus 56%, *P* < .001).

Time from symptom onset to the start of EVT (277 minutes in the CS group versus 299 minutes in the GA group, *P* = .165) and recanalization rates (TICI 2–3 in 88% of the GA group versus 86% of the CS group, *P* = .488) did not differ between the groups.

Peri- and Postprocedural Complications

Peri- and postprocedural complications are summarized in Table 2. Patients under GA had pneumonia more frequently than patients under CS (25% versus 17%, *P* = .048). Other complications such as dissections, perforation of the brain-supplying arteries, or iatrogenic thrombus dislocation were equally distributed.

Outcome

The distribution of the mRS scores at 3 months is presented in the Figure. Fifty-one percent of the patients with CS and 34% of patients with GA had favorable outcome (mRS 0–2) (*P* = .002). Excellent outcome (mRS 0–1) was seen in 30% of the CS and in 22% of the patients with GA (*P* = .154). After 3 months, 22% of the patients with CS and 30% of the patients with GA had died (*P* = .077).

In univariable analysis, GA was associated with less favorable outcome than CS (OR, 0.773; 95% CI, 0.646–0.925; *P* = .002), but after adjusting for baseline factors, the difference was no longer significant (Table 3). Independent predictors of unfavorable outcome were advancing age, higher NIHSS score, longer time from symptom onset to start of EVT, diabetes mellitus, and intracerebral hemorrhage (Table 3).

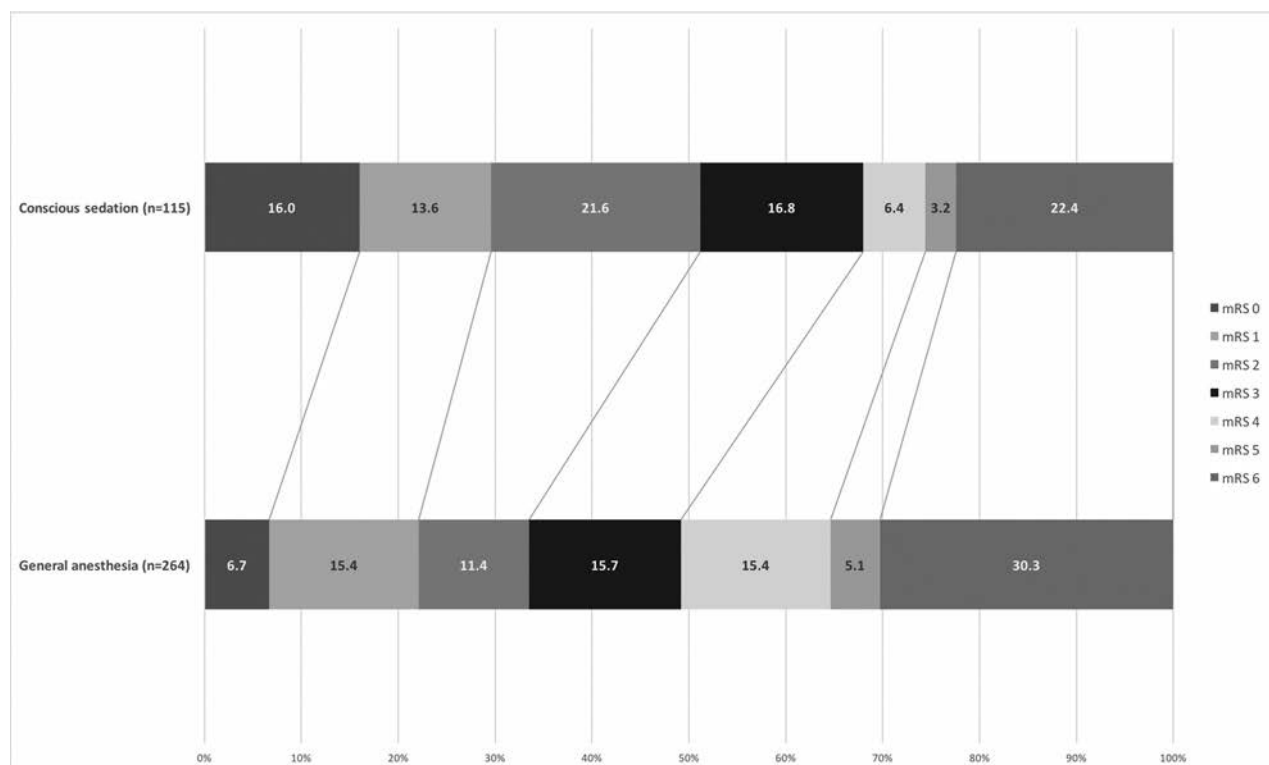


FIGURE. Three-month outcome of patients under GA compared with patients with CS. The figures in the bar indicate the percentage of patients with a given mRS at 3-month follow-up.

Table 3: Predictors of outcome at 3 months (multivariable logistic regression)

| | Odds Ratio (95% CI) | P Value |
|---|---------------------|---------|
| GA | 0.873 (0.505–1.512) | .629 |
| Age | 0.95 (0.932–0.969) | <.001 |
| NIHSS | 0.894 (0.855–0.933) | <.001 |
| Time from symptom onset to start of EVT | 0.998 (0.996–0.999) | .01 |
| Symptomatic ICH | 0.109 (0.028–0.428) | .002 |
| Diabetes mellitus | 0.544 (0.305–0.972) | .04 |

Note:—ICH indicates intracerebral hemorrhage.

DISCUSSION

The anesthetic management during stent retriever thrombectomy, general anesthesia, or conscious sedation has no impact on the outcome of patients with large-vessel occlusion in the anterior circulation. This is the main finding of our analysis of >400 consecutive patients. Univariable analysis showed an advantage for CS, but after multivariable adjustment for baseline characteristics, this difference disappeared. Also, time from symptom onset to the start of EVT, recanalization rates, and mortality did not differ between patients under CS and GA. Patients in the GA group more often had pneumonia.

Our results are in line with the findings of the SIESTA trial, a single-center randomized controlled trial. The SIESTA investigators recently reported the outcomes at 24 hours. Outcomes did not differ in patients who were treated with CS versus those under GA. Unadjusted favorable outcome after 3 months was better in patients undergoing GA than in patients treated in CS (37% versus 18.2, $P = .01$). However, because there was no consistent shift over all mRS categories and the study was not designed to investigate long-term outcome, this result should be interpreted with

caution.¹² Previous studies reported that CS seems to be superior to GA for endovascular stroke treatment.^{4,5,19–22} A recent meta-analysis by Brinjikji et al,³ including 1956 patients from 9 nonrandomized studies, found that GA compared with CS was associated with lower odds of favorable outcome (mRS 0–2) (OR, 0.43; 95% CI, 0.35–0.53; $P < .01$), lower odds of successful recanalization (OR, 0.54; 95% CI, 0.37–0.80; $P < .01$), but higher odds of death (OR, 2.59; 95% CI, 1.87–3.58; $P < .01$) and respiratory complications (OR, 2.09; 95% CI, 1.36–3.23; $P < .01$). Symptomatic and asymptomatic hemorrhage and other vascular complications were similar for both GA and CS, and time to treatment did not differ either (136 minutes for GA versus 117 minutes for CS, $P = .24$). Baseline NIHSS scores were, on average, higher in patients with GA than for those with CS, and when the analysis was adjusted for the NIHSS score, significance got lost.³

The post hoc analysis of the Multicenter Randomized Clinical Trial of Endovascular Treatment for Acute Ischemic Stroke in the Netherlands (MR CLEAN) with balanced baseline NIHSS and occlusion sites between groups indicated higher odds of good clinical outcome with CS (unadjusted OR, 2.1; 95% CI, 1.02–4.31; $P = .04$).⁴ After adjusting for prespecified prognostic factors such as age, occlusion of the internal carotid artery terminus, history of previous stroke, atrial fibrillation, diabetes mellitus, and stroke severity, the difference in outcome was lost (adjusted OR, 1.9; 95% CI, 0.89–4.24; $P =$ not given). Furthermore, there was a significant time delay of 20 minutes with GA compared with CS ($P = .02$). Periprocedural complications and recanalization rates did not differ between GA and CS.⁴

Both GA and CS have their advantages and shortcomings. One potential advantage of CS is the shorter time to treatment as

shown in the post hoc analysis of MR CLEAN.⁴ In our study, the time from symptom onset to the start of EVT was slightly longer in patients undergoing GA, but this was not significant. This finding might be the result of the implementation of a standardized operating procedure to manage patients with stroke, including early notification of the anesthesiologists. These emergency procedures, involving all interprofessional and interdisciplinary health care providers, are based on the consideration of stroke as a potentially lethal and devastating threat to the health of the patient and attribute stroke management as the highest priority. Therefore, the time interval from the call for anesthesia help to needle insertion was set to 30 minutes. The possibility of monitoring the neurologic status during the procedure might be another advantage of CS. Furthermore, blood pressure remains more stable during CS. High blood pressure variability in acute stroke is associated with worse outcome.²³ On the other hand, restless patients under conscious sedation may disturb the intervention, delay time to recanalization, enhance procedure-related complications, and, as a consequence, lead secondarily to GA and intubation.² However, in our series, iatrogenic dissection, perforation of the brain-supplying arteries, or iatrogenic thrombus dislocation did not occur more often under GA.

Furthermore GA leads to more stable working conditions for the interventionalist due to reduced patient movements because of periprocedural anxiety, pain, or agitation. Therefore, the risk of procedure-related complications (eg, dissection or vessel perforation) seems to be reduced. On the other hand, GA carries the risk of drug-related arterial hypotension and cerebral blood flow reduction.²² In our series, blood pressure drop was significantly higher under GA than with CS but had no influence on the outcome. Tracheal intubation and specifically extubation might provoke coughing or retching that raises intrathoracic and intracranial pressure, reducing cerebral blood flow and blood supply to the penumbra. Cerebral blood flow is also reduced when intubated patients are inadvertently hyperventilated leading to hypocapnia-induced vasoconstriction of the intracranial vessels.²⁴ GA and especially an emergency switch from CS to GA carry a high risk of hypotension, aspiration, and pneumonia. As a consequence, this switch may compromise outcome in acute ischemic stroke.^{25–27} In our study, patients under GA had a higher risk of pneumonia, but this did not influence outcome. This result might not be the consequence of GA but rather reflect the higher morbidity of patients undergoing GA on admission. Patients undergoing GA had more severe strokes with impaired consciousness and swallowing problems bearing a higher risk of aspiration already before intubation. The 10 patients in our study with conversion to GA did as well as the others.

In clinical practice, the choice of GA or CS in a given patient is an individual decision considering the patient's physical status and the complexity of the EVT. On the basis of thrombus imaging and visualization of the arteries from the aortic arch up to the pial collaterals by CTA or MRA, which are mandatory parts of our stroke protocol, patients with difficult arterial access (eg, bovine type of aortic arch, tandem occlusions, extensive thrombus burden) can be identified in advance. This identification may explain why CS had to be switched infrequently to GA (2.5%) during the interventions in our series, avoiding time delay, complications,

and, last but not least, stress for the patient and the anesthesiology and neuroradiology teams. According to the Society for Neuroscience in Anesthesiology and Critical Care Expert Consensus Statement on EVT, GA may be preferable in uncooperative or agitated patients or patients with severe strokes who need airway protection. CS seems to be feasible in cooperative patients who understand the procedure and can protect their airways and when advanced stroke imaging predicts straightforward endovascular thrombectomy.²⁸ If GA is chosen, standardized protocols for early postprocedural neurologic assessment and early extubation should be used to minimize postextubation risks. A decision-making tree for selection of the anesthetic management in EVT as suggested by Dhakal et al²⁹ may help avoid delays for EVT.

Our study has the natural limitations of selection bias in a nonrandomized single-center study. The decision as to whether to perform GA or CS was made on an individual basis, which introduces confounding factors limiting comparisons. Furthermore, reasons for the choice of the anesthetic method were not routinely documented for every patient. Therefore, underlying individual patient factors for the choice of GA or CS could not be analyzed. On the other hand, our study also has strengths, mainly the large sample size, the sole use of the Solitaire stent retriever, and strokes only in the anterior circulation. The large sample size allowed a multivariable comparison accounting for many confounding factors influencing stroke outcome.

CONCLUSIONS

Our study shows that outcome did not differ between patients treated with the Solitaire stent retriever who received either GA or CS after adjusting for baseline differences. Time from symptom onset to the start of EVT was similar for both anesthetic management choices. When we considered the pros and cons of GA and CS, the choice of the type of anesthesia seems to depend mainly on individual patient factors, such as the ability to cooperate or the need for airway protection, as well as factors facilitating the optimal conditions for the intervention team. The choice should aim for the best comfort and greatest safety of patients.

Disclosures: Agnieszka Slezak—RELATED: Grant: Swiss Heart Foundation.* Lara Opplinger—RELATED: Grant: Swiss Heart Foundation.* Jan Gralla—UNRELATED: Consulting Fee or Honorarium: Medtronic, Comments: consultant for Medtronic, global Principal Investigator of the STAR study.* Heinrich Mattle—UNRELATED: Board Membership: Steering Committee of the SWIFT PRIME study; Consultancy: Steering Committee of SWIFT PRIME. Marcel Arnold—RELATED: Grant: Swiss Heart Foundation for the Swiss Stroke Registry*; UNRELATED: Board Membership: Advisory Board for NOAK studies for: Bayer Health care, Boehringer Ingelheim, Bristol-Myers Squibb, Covidien, Daiichi Sankyo, Pfizer; Grants/Grants Pending: Swiss Heart Foundation, Swiss National Science Foundation*; Payment for Lectures Including Service on Speakers Bureaus: Bayer Health AG, Bristol-Myers Squibb, Covidien. Marie-Luise Mono—RELATED: Grant: Swiss Heart Foundation*; UNRELATED: Board Membership: Advisory Board Boehringer Ingelheim. *Money paid to the institution.

REFERENCES

- Goyal M, Menon BK, van Zwam WH, et al; HERMES collaborators. Endovascular thrombectomy after large-vessel ischaemic stroke: a meta-analysis of individual patient data from five randomised trials. *Lancet* 2016;387:1723–31 [CrossRef Medline](#)
- Breckenfeld C, Mattle HP, Schroth G. General is better than local anesthesia during endovascular procedures. *Stroke* 2010;41:2716–17 [CrossRef Medline](#)
- Brinjikji W, Murad MH, Rabinstein AA, et al. Conscious sedation

- versus general anesthesia during endovascular acute ischemic stroke treatment: a systematic review and meta-analysis. *AJNR Am J Neuroradiol* 2015;36:525–29 CrossRef Medline
4. van den Berg LA, Koelman DL, Berkhemer OA, et al; MR CLEAN pretrial study group, Participating centers. Type of anesthesia and differences in clinical outcome after intra-arterial treatment for ischemic stroke. *Stroke* 2015;46:1257–62 CrossRef Medline
5. McDonald JS, Brinjikji W, Rabinstein AA, et al. Conscious sedation versus general anaesthesia during mechanical thrombectomy for stroke: a propensity score analysis. *J Neurointerv Surg* 2015;7:789–94 CrossRef Medline
6. Saver JL, Jahan R, Levy EI, et al; SWIFT Trialists. Solitaire flow restoration device versus the Merci retriever in patients with acute ischaemic stroke (SWIFT): a randomised, parallel-group, non-inferiority trial. *Lancet* 2012;380:1241–49 CrossRef Medline
7. König IR, Ziegler A, Bluhmki E, et al; Virtual International Stroke Trials Archive (VISTA) Investigators. Predicting long-term outcome after acute ischemic stroke: a simple index works in patients from controlled clinical trials. *Stroke* 2008;39:1821–26 CrossRef Medline
8. Mandava P, Kent TA. A method to determine stroke trial success using multidimensional pooled control functions. *Stroke* 2009;40:1803–10 CrossRef Medline
9. Smith EE, Shobha N, Dai D, et al. Risk score for in-hospital ischemic stroke mortality derived and validated within the Get With the Guidelines-stroke program. *Circulation* 2010;122:1496–504 CrossRef Medline
10. Linfante I, Starosciak AK, Walker GR, et al. Predictors of poor outcome despite recanalization: a multiple regression analysis of the NASA registry. *J Neurointerv Surg* 2016;8:224–29 CrossRef Medline
11. Zaidat OO, Fitzsimmons BF, Woodward BK, et al. Effect of a balloon-expandable intracranial stent vs medical therapy on risk of stroke in patients with symptomatic intracranial stenosis: the VISSIT randomized clinical trial. *JAMA* 2015;313:1240–48 CrossRef Medline
12. Schönenberger S, Uhlmann L, Hacke W, et al. Effect of conscious sedation vs general anesthesia on early neurological improvement among patients with ischemic stroke undergoing endovascular thrombectomy: a randomized clinical trial. *JAMA* 2016;316:1986–96 CrossRef Medline
13. Adams HP Jr, Bendixen BH, Kappelle LJ, et al. Classification of subtype of acute ischemic stroke: definitions for use in a multicenter clinical trial: TOAST—Trial of Org 10172 in Acute Stroke Treatment. *Stroke* 1993;24:35–41 CrossRef Medline
14. Suh SH, Cloft HJ, Fugate JE, et al. Clarifying differences among thrombolysis in cerebral infarction scale variants: is the artery half open or half closed? *Stroke* 2013;44:1166–68 CrossRef Medline
15. Hacke W, Kaste M, Fieschi C, et al. Randomised double-blind placebo-controlled trial of thrombolytic therapy with intravenous alteplase in acute ischaemic stroke (ECASS II): Second European-Australasian Acute Stroke Study Investigators. *Lancet* 1998;352:1245–51 CrossRef Medline
16. Kase CS, Furlan AJ, Wechsler LR, et al. Cerebral hemorrhage after intra-arterial thrombolysis for ischemic stroke: the PROACT II trial. *Neurology* 2001;57:1603–10 CrossRef Medline
17. Powers WJ, Derdeyn CP, Biller J, et al; American Heart Association Stroke Council. 2015 American Heart Association/American Stroke Association Focused Update of the 2013 Guidelines for the Early Management of Patients with Acute Ischemic Stroke Regarding Endovascular Treatment: a Guideline for Healthcare Professionals from the American Heart Association/American Stroke Association. *Stroke* 2015;46:3020–35 CrossRef Medline
18. van Swieten JC, Koudstaal PJ, Visser MC, et al. Interobserver agreement for the assessment of handicap in stroke patients. *Stroke* 1988;19:604–07 CrossRef Medline
19. Abou-Chebl A, Lin R, Hussain MS, et al. Conscious sedation versus general anesthesia during endovascular therapy for acute anterior circulation stroke: preliminary results from a retrospective, multicenter study. *Stroke* 2010;41:1175–79 CrossRef Medline
20. Davis MJ, Menon BK, Baghirzada LB, et al; Calgary Stroke Program. Anesthetic management and outcome in patients during endovascular therapy for acute stroke. *Anesthesiology* 2012;116:396–405 CrossRef Medline
21. Jumaa MA, Zhang F, Ruiz-Ares G, et al. Comparison of safety and clinical and radiographic outcomes in endovascular acute stroke therapy for proximal middle cerebral artery occlusion with intubation and general anesthesia versus the nonintubated state. *Stroke* 2010;41:1180–84 CrossRef Medline
22. Li F, Deshaies EM, Singla A, et al. Impact of anesthesia on mortality during endovascular clot removal for acute ischemic stroke. *J Neurosurg Anesthesiol* 2014;26:286–90 CrossRef Medline
23. Stead LG, Gilmore RM, Vedula KC, et al. Impact of acute blood pressure variability on ischemic stroke outcome. *Neurology* 2006;66:1878–81 CrossRef Medline
24. Takahashi C, Liang CW, Liebeskind DS, et al. To tube or not to tube? The role of intubation during stroke thrombectomy. *Front Neurol* 2014;5:170 CrossRef Medline
25. Hassan AE, Chaudhry SA, Zacharatos H, et al. Increased rate of aspiration pneumonia and poor discharge outcome among acute ischemic stroke patients following intubation for endovascular treatment. *Neurocrit Care* 2012;16:246–50 CrossRef Medline
26. Koennecke HC, Belz W, Berfelde D, et al; Berlin Stroke Register Investigators. Factors influencing in-hospital mortality and morbidity in patients treated on a stroke unit. *Neurology* 2011;77:965–72 CrossRef Medline
27. Li J, Murphy-Lavoie H, Bugas C, et al. Complications of emergency intubation with and without paralysis. *Am J Emerg Med* 1999;17:141–43 CrossRef Medline
28. Talke PO, Sharma D, Heyer EJ, et al. Republished: Society for Neurosciences in Anesthesiology and Critical Care expert consensus statement—a management of endovascular treatment for acute ischemic stroke. *Stroke* 2014;45:e138–150 CrossRef Medline
29. Dhakal LP, Díaz-Gómez JL, Freeman WD. Role of anesthesia for endovascular treatment of ischemic stroke: do we need neurophysiological monitoring? *Stroke* 2015;46:1748–54 CrossRef Medline

Correlation of Thrombectomy Maneuver Count with Recanalization Success and Clinical Outcome in Patients with Ischemic Stroke

F. Seker, J. Pfaff, M. Wolf, P.A. Ringleb, S. Nagel, S. Schönenberger, C. Herweh, M.A. Möhlenbruch, M. Bendszus, and M. Pham

ABSTRACT

BACKGROUND AND PURPOSE: In the treatment of acute thromboembolic stroke, the effectiveness and success of thrombus removal when using stent retrievers is variable. In this study, we analyzed the correlation of thrombectomy maneuver count with a good clinical outcome and recanalization success.

MATERIALS AND METHODS: One hundred and four patients with acute occlusion of the middle cerebral artery or the terminal internal carotid artery who were treated with thrombectomy were included in this retrospective study. A good clinical outcome was defined as a 90-day mRS of ≤ 2 , and successful recanalization was defined as TICI 2b–3.

RESULTS: The maneuver count ranged between 1–10, with a median of 2. Multivariate logistic regression analyses identified an increasing number of thrombectomy maneuvers as an independent predictor of poor outcome (adjusted OR, 0.59; 95% CI, 0.38–0.87; $P = .011$) and unsuccessful recanalization (adjusted OR, 0.48; 95% CI, 0.32–0.66; $P < .001$). A good outcome was significantly more likely if finished within 2 maneuvers compared with 3 or 4 maneuvers, or even more than 4 maneuvers ($P < .001$).

CONCLUSIONS: An increasing maneuver count correlates strongly with a decreasing probability of both good outcome and recanalization. The probability of successful recanalization decreases below 50% if not achieved within 5 thrombectomy maneuvers. Patients who are recanalized within 2 maneuvers have the best chance of achieving a good clinical outcome.

Recent trials showed that mechanical thrombectomy is effective in acute ischemic stroke caused by large vessel occlusion.^{1–7} The speed and success of thrombus removal is variable.^{8–12} Often, several thrombectomy maneuvers are necessary to restore antegrade flow and cerebral perfusion. However, it is uncertain whether flow restoration after multiple thrombectomy maneuvers is still followed by a good clinical outcome. Currently, there is no consensus on a maximum number of maneuver attempts in cases where the thrombus cannot be removed promptly. Hence, the decision to abort the procedure for technical futility is mostly at the discretion of the individual operator. To address this question, we retrospectively analyzed the impact of thrombectomy maneuver count on recanalization and clinical outcome.

MATERIALS AND METHODS

Patient Selection

Between January 2012 and November 2014, all consecutive patients undergoing thrombectomy for the treatment of acute ischemic stroke were collected in a prospective data base and analyzed retrospectively. Inclusion criteria for this study were acute occlusion of the M1 segment of the middle cerebral artery or terminal internal carotid artery, premorbid mRS score of ≤ 2 , and the primary usage of Solitaire FR (Covidien, Irvine, California) or Trevo (Stryker, Kalamazoo, Michigan) stent retrievers. Patients who underwent concomitant stent placement of intracranial arteries during the procedure were excluded. The study was approved by our local ethics committee.

Data Acquisition

Baseline demographic data, initial NIHSS score, prestroke mRS, and mRS score at 90 days after stroke onset were regularly documented by neurologists. A good clinical outcome was defined as a 90-day mRS score of ≤ 2 . An unfavorable outcome was defined as a 90-day mRS score of > 2 .

Image Analysis

The reader was blinded to clinical data. Baseline ASPECTS was determined on pre-interventional diffusion-weighted sequences

Received November 7, 2016; accepted after revision March 3, 2017.

From the Departments of Neuroradiology (F.S., J.P., M.W., C.H., M.A.M., M.B., M.P.) and Neurology (P.A.R., S.N., S.S.), Heidelberg University Hospital, Heidelberg, Germany; and Department of Neuroradiology (M.P.), Würzburg University Hospital, Würzburg, Germany.

Please address correspondence to Dr. Fatih Seker, Im Neuenheimer Feld 400, 69120 Heidelberg, Germany; e-mail: fatih.seker@med.uni-heidelberg.de

<http://dx.doi.org/10.3174/ajnr.A5212>

Table 1: Univariate analysis of data according to recanalization success

| Characteristics | Successful Recanalization (n = 83) | Unsuccessful Recanalization (n = 21) | P Value |
|-----------------------------------|---------------------------------------|---|---------|
| Age, yr (mean, SD) | 68.8 (15.6) | 69.7 (14.3) | .005 |
| Female, no. (%) | 52 (62.7) | 8 (38.1) | .051 |
| Hypertension, no. (%) | 64 (77.1) | 10 (47.6) | .045 |
| Diabetes mellitus, no. (%) | 15 (18.1) | 2 (9.5) | .733 |
| Prestroke mRS, median (IQR) | 0 (0–1) | 0 (0–1) | .910 |
| Initial NIHSS score, median (IQR) | 17 (14–21.75) | 18 (14.75–23.25) | .420 |
| Initial ASPECTS, median (IQR) | 8 (7–9) | 8 (7–9) | .673 |
| Initial occlusion site, no. (%) | | | .311 |
| Carotid T | 28 (33.7%) | 10 (47.6%) | |
| M1 | 55 (66.3%) | 11 (52.4%) | |
| Intravenous tPA, no. (%) | 56 (67.5%) | 16 (76.2%) | .598 |
| Maneuver count, median (IQR) | 2 (1–3) | 5 (3–7) | <.001 |
| Onset to TICI, min (median, IQR) | 310 (224–401) | 281 (219–324) | .295 |

Note:—Carotid T indicates terminal internal carotid artery; IQR, interquartile range; M1, M1 segment of the middle cerebral artery.

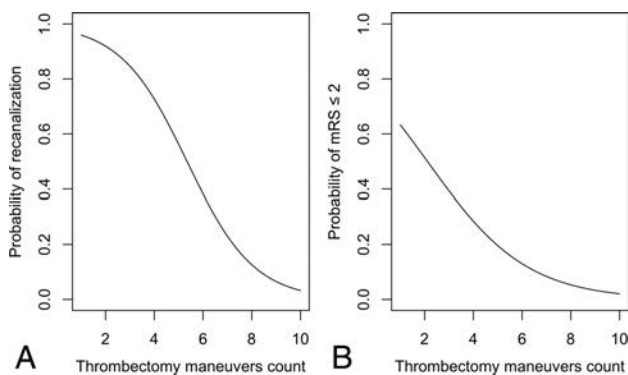


FIGURE. A, Logistic regression curve representing an estimate of the probability of successful recanalization (TICI score of 2b or 3), depending on the thrombectomy maneuver count ($P < .001$). B, Logistic regression curve representing an estimate of the probability of a good clinical outcome (90-day mRS score of ≤ 2), depending on the thrombectomy maneuver count ($P < .001$).

in MR imaging or nonenhanced CT scans. TICI scores were assessed on the final angiographic series. A TICI score of 2b or 3 (subtotal or complete perfusion) was regarded as successful recanalization. The thrombectomy maneuver count was regularly reported by the performing neurointerventionalist. The reported maneuver count included the use of any additional stent retriever during thrombectomy and was not limited to Solitaire FR or Trevo. Sole thrombus aspiration attempts were not evaluated as a thrombectomy maneuver.

Statistical Methods

Statistical analyses were performed with R version 3.2.2 (<http://www.r-project.org/>) and RStudio version 0.99 (<http://rstudio.org/download/desktop>). Ninety-day mRS scores are presented as median and interquartile range. Univariate analyses comparing demographic variables that were potentially relevant for predicting the clinical outcome and recanalization were performed by using a Mann-Whitney U test for continuous data and Fisher exact test for categorical variables. A multivariate model was applied to assess the association of the maneuver count with the TICI score and 90-day mRS score, adjusting for those variables that showed univariate association ($P < .05$). Odds ratios and 95% confidence intervals were estimated. Differences in the 90-day mRS score between various

groups were analyzed by using a Kruskal-Wallis rank sum test. Statistical significance was set at $P < .05$.

RESULTS

Of the 250 reviewed records of stroke patients with any intracranial occlusion undergoing thrombectomy at our institution, 104 patients met the inclusion criteria for this retrospective study. Among these patients, 57.7% were women, and the mean age was $69.0 (\pm 14.3)$ years.

Eighty-eight patients (84.6%) were treated under general anesthesia, and 16 patients (15.4%) were treated under conscious sedation.

The following stent retrievers were used primarily: Solitaire in all cases and Trevo in 7 cases (6.7%). If recanalization could not be achieved by using Solitaire or Trevo, the following devices were used: Catch Mini (Balt, Montmorency, France) in 3 cases (2.9%), ERIC (MicroVention, Tustin, California) in 1 case (0.9%), Capture LP (MindFrame, Irvine, California) in 1 case (0.9%), and Aperio (Acandis, Pforzheim, Germany) in 1 case (0.9%).

The median number of thrombectomy maneuvers was 2 (range, 1–10). Eleven patients (10.6%) underwent concomitant stent placement of the proximal internal carotid artery. A total of 79.8% of the patients were successfully recanalized (TICI score of 2b or 3). A TICI score of 2a was achieved in 14.4%. In 3.8% of the patients, no sufficient recanalization was achieved (TICI score of 0 or 1). A good clinical outcome was recorded in 41.3% of the patients (90-day mRS score of ≤ 2).

In univariate analysis (Table 1), successful recanalization was associated with lower age ($P = .005$), hypertension ($P = .045$), and lower maneuver count ($P < .001$). The univariate analysis also revealed that the chance of successful recanalization decreased below 50% after 5 thrombectomy maneuvers (Fig 1A). In adjusted multivariate logistic regression, the maneuver count was an independent predictor of successful recanalization (adjusted OR, 0.48; 95% CI, 0.32–0.66; $P < .001$).

In another univariate analysis (Table 2), good clinical outcome was significantly associated with lower age ($P < .001$), lower prestroke mRS ($P = .020$), lower initial NIHSS score ($P = .025$), lower maneuver count ($P < .001$), successful recanalization ($P = .042$), and short onset-to-recanalization time ($P = .016$). In a multivariate logistic regression analysis adjusting for these variables, the maneuver count appeared to be an independent predictor of good clinical outcome (adjusted OR, 0.59; 95% CI, 0.38–0.87; $P = .011$). As shown in Fig 1B, patients who were recanalized within 2 thrombectomy maneuvers had a 50%–60% chance of a good outcome ($n = 51$; median 90-day mRS score of 2; interquartile range, 1–4). Chances of a good outcome were significantly lower when 3 or 4 maneuvers ($n = 34$; median 90-day mRS score of 3; interquartile range, 2–4), or even more than 4 maneuvers ($n = 16$; median 90-day mRS score of 4; interquartile range, 3.5–6) were required for recanalization ($P < .001$). Only 1 of 16 patients with more than 4 thrombectomy maneuvers had a good neurologic outcome.

Table 2: Univariate analysis of data according to clinical outcome^a

| Characteristics | Good Outcome (n = 43) | Poor Outcome (n = 59) | P Value |
|-----------------------------------|--------------------------|--------------------------|---------|
| Age, yr (mean, SD) | 61.4 (17.3) | 74.6 (10.8) | <.001 |
| Female, no. (%) | 27 (62.8) | 32 (54.2) | .423 |
| Hypertension, no. (%) | 27 (62.8%) | 46 (78.0%) | .068 |
| Diabetes mellitus, no. (%) | 5 (11.6%) | 12 (20.3%) | .285 |
| Prestroke mRS, median (IQR) | 0 (0–0) | 1 (0–1) | .020 |
| Initial NIHSS score, median (IQR) | 15 (12–20) | 19 (16–22) | .025 |
| Initial ASPECTS, median (IQR) | 8 (7–9) | 8 (7–8) | .155 |
| Initial occlusion site, no. (%) | | | .838 |
| Carotid T | 14 (38%) | 22 (37%) | |
| M1 | 23 (62%) | 38 (63%) | |
| Intravenous tPA, no. (%) | 33 (76.7%) | 37 (62.7%) | .194 |
| Maneuver count, median (IQR) | 2 (1–3) | 3 (2–4.25) | <.001 |
| Onset to TICI, min (median, IQR) | 254 (193.25–357) | 324 (273.5–429) | .016 |
| Recanalization, no. (%) | | | .042 |
| TICI score 0–2a | 4 (9.3%) | 16 (27.1%) | |
| TICI score 2b or 3 | 39 (90.7%) | 43 (72.9%) | |

Note:—Carotid T indicates terminal internal carotid artery; IQR, interquartile range; M1, M1 segment of the middle cerebral artery.

^a Two patients were lost to follow-up.

DISCUSSION

In mechanical thrombectomy, it is still unclear how many maneuvers should be attempted in cases where the occluding thrombus cannot be removed easily (ie, where sufficient recanalization according to TICI 2b/3 cannot be achieved with a single or few maneuvers). The decision of when to abort the thrombectomy procedure after encountering technical difficulties in retrieving the thrombus is made mainly at the discretion of the operator and not based on empirical evidence. Therefore, we retrospectively studied the impact of the thrombectomy maneuver count on recanalization and clinical outcome in patients with acute ischemic stroke caused by occlusion of the terminal internal carotid artery or M1 segment.

This study confirms that achieving flow restoration within a few thrombectomy maneuvers is important. With every thrombectomy maneuver, we found that the probability of a favorable outcome, defined as mRS score ≤ 2 , decreases significantly. In addition, our results demonstrate that the number of thrombectomy maneuvers is strongly correlated with the probability of successful recanalization itself (TICI score of 2b or 3). Patients who were recanalized within 2 maneuvers had the best chance of achieving a good outcome.

The fundamental question is whether the thrombectomy procedure should be aborted if recanalization cannot be achieved within a few maneuvers. In our cohort, sufficient flow restoration was highly unlikely if more than 5 thrombectomy maneuvers were necessary. After 4 thrombectomy maneuvers, there is almost no chance of a good clinical outcome. However, we refrain from suggesting a clear cutoff as a recommendation of how many thrombectomy attempts should be undertaken because, obviously, any such value would be arbitrary. Nonetheless, we provide the first analysis of the association between maneuver count and technical as well as clinical success. These results may help to empirically inform individual decisions for when to abort a procedure and, thus, define it as technically futile.

It is not clear why the thrombectomy maneuver count needed for recanalization varies and why, based on our results, it is closely associated with clinical outcome and with the efficiency of an-

giographic recanalization rated on the TICI scale. A possible variable affecting the clinical outcome might be the prolonged procedure time when multiple thrombectomy maneuvers need to be carried out.¹³ In addition, platelet-rich and thick clots may barely be removed with currently available stent retrievers, leading to unsuccessful recanalization and consequently to poor neurologic outcome.^{8,10,14} Furthermore, progressive infarction during prolonged recanalization attempts may also be associated with filling defects in the distal macrovasculature caused by increased regional vascular resistance.¹⁵

A limitation of this study is its retrospective design. Although the usage of Solitaire or Trevo as the first thrombectomy device was a defining inclusion cri-

terion, other thrombectomy devices may have been used additionally during the procedure. Therefore, the reported maneuver count could not be attributed to 1 specific stent retriever. Aspiration attempts were not performed on a regular basis and, therefore, not evaluated. With this approach as a primary approach, the relationship between the number of maneuvers and recanalization may be different. Operator experience was not analyzed, either. In addition, termination of the thrombectomy procedure was a subjective choice by the operator based on various clinical factors. Thus, there might be some underlying bias.

CONCLUSIONS

The increasing number of thrombectomy maneuvers is strongly correlated with a decreasing probability of recanalization and of favorable neurologic recovery. Especially, the chance of successful recanalization will decrease below 50% if recanalization is not achieved within 5 thrombectomy maneuvers. Patients recanalized within 2 maneuvers have the best chance of achieving a good outcome. After 4 thrombectomy maneuvers, there is nearly no chance of good clinical outcome.

Disclosures: Johannes Pfaff—UNRELATED: Payment for Lectures (including service on Speakers Bureaus); Siemens Healthineers; Travel/Accommodations/Meeting Expenses Unrelated to Activities Listed: Stryker Neurovascular. Peter Ringleb—UNRELATED: Payment for Lectures (including service on Speakers Bureaus); Bayer, Boehringer Ingelheim, Pfizer, Daiichi Sankyo. Simon Nagel—UNRELATED: Consultancy: Brainomix, Boehringer Ingelheim; Grants/Grants Pending: Brainomix*; Payment for Lectures (including service on Speakers Bureaus); Pfizer, Bayer, Medtronic; Travel/Accommodations/Meeting Expenses Unrelated to Activities Listed: Brainomix, Medtronic, Bayer, Boehringer Ingelheim. Christian Herweh—UNRELATED: Consultancy: Brainomix; Payment for Lectures (including service on Speakers Bureaus); Bristol-Myers Squibb; Travel/Accommodations/Meeting Expenses Unrelated to Activities Listed: Stryker. Markus Möhlenbruch—UNRELATED: Board Membership: Codman; Payment for Lectures (including service on Speakers Bureaus): Microvention, Phenox, Stryker. Martin Bendszus—UNRELATED: Board Membership: DSM for Vascular Dynamics; Consultancy: Codman, Roche, Guerbet; Grants/Grants Pending: DFG, Hopp Foundation, Novartis, Siemens, Guerbet, Stryker, Covidien*; Payment for Lectures (including service on Speakers Bureaus): Novartis, Roche, Guerbet, Teva, Bayer, Codman. Mirko Pham—UNRELATED: Grants/Grants Pending: Guerbet, Comments: project grants; Deutsche Forschungsgemeinschaft, Comments: project grant SFB 1158 TPA3*; Payment for Lectures (including service on Speakers Bureaus): Penumbra, Siemens. *Money paid to the institution.

REFERENCES

1. Berkhemer OA, Fransen PS, Beumer D, et al. **A randomized trial of intraarterial treatment for acute ischemic stroke.** *N Engl J Med* 2015; 372:11–20 [CrossRef Medline](#)
2. Broderick JP, Palesch YY, Demchuk AM, et al. **Endovascular therapy after intravenous t-PA versus t-PA alone for stroke.** *N Engl J Med* 2013;368:893–903 [CrossRef Medline](#)
3. Campbell BC, Mitchell PJ, Kleinig TJ, et al. **Endovascular therapy for ischemic stroke with perfusion-imaging selection.** *N Engl J Med* 2015;372:1009–18 [CrossRef Medline](#)
4. Balami JS, Sutherland BA, Edmunds LD, et al. **A systematic review and meta-analysis of randomized controlled trials of endovascular thrombectomy compared with best medical treatment for acute ischemic stroke.** *Int J Stroke* 2015;10:1168–78 [CrossRef Medline](#)
5. Saver JL, Goyal M, Bonafe A, et al. **Stent-retriever thrombectomy after intravenous t-PA vs. t-PA alone in stroke.** *N Engl J Med* 2015; 372:2285–95 [CrossRef Medline](#)
6. Jovin TG, Chamorro A, Cobo E, et al. **Thrombectomy within 8 hours after symptom onset in ischemic stroke.** *N Engl J Med* 2015;372: 2296–306 [CrossRef Medline](#)
7. Goyal M, Demchuk AM, Menon BK, et al. **Randomized assessment of rapid endovascular treatment of ischemic stroke.** *N Engl J Med* 2015;372:1019–30 [CrossRef Medline](#)
8. Kim SK, Yoon W, Kim TS, et al. **Histologic analysis of retrieved clots in acute ischemic stroke: correlation with stroke etiology and gradient-echo MRI.** *AJNR Am J Neuroradiol* 2015;36:1756–62 [CrossRef Medline](#)
9. Tomkins AJ, Schleicher N, Murtha L, et al. **Platelet rich clots are resistant to lysis by thrombolytic therapy in a rat model of embolic stroke.** *Exp Transl Stroke Med* 2015;7:2 [CrossRef Medline](#)
10. Niesten JM, van der Schaaf IC, van Dam L, et al. **Histopathologic composition of cerebral thrombi of acute stroke patients is correlated with stroke subtype and thrombus attenuation.** *PLoS ONE* 2014;9:e88882 [CrossRef Medline](#)
11. Weisstanner C, Gratz PP, Schroth G, et al. **Thrombus imaging in acute stroke: correlation of thrombus length on susceptibility-weighted imaging with endovascular reperfusion success.** *Eur Radiol* 2014;24:1735–41 [CrossRef Medline](#)
12. Seker F, Pfaff J, Wolf M, et al. **Impact of thrombus length on recanalization and clinical outcome following mechanical thrombectomy in acute ischemic stroke.** *J Neurointerv Surg* 2016 Sep 15. [Epub ahead of print] [CrossRef Medline](#)
13. Dorado L, Millán M, Pérez de la Ossa N, et al. **Time to recanalization and risk of symptomatic intracerebral haemorrhage in patients treated with intravenous thrombolysis.** *Eur J Neurol* 2012;19: 1251–55 [CrossRef Medline](#)
14. Lamprecht S, Jansen O, Riedel CH. **Abstract W MP8: Stent retrievers do not encase clots but hook them within seconds.** *Stroke* 2015; 46(suppl 1):AWMP8
15. Pham M, Bendszus M. **Facing time in ischemic stroke: an alternative hypothesis for collateral failure.** *Clin Neuroradiol* 2016;26:141–51 [CrossRef Medline](#)

Temporary Stent-Assisted Coil Embolization as a Treatment Option for Wide-Neck Aneurysms

 M. Müller,  C. Brockmann,  S. Afat,  O. Nikoubashman,  G.A. Schubert,  A. Reich,  A.E. Othman, and  M. Wiesmann



ABSTRACT

BACKGROUND AND PURPOSE: Simple coil embolization is often not a feasible treatment option in wide-neck aneurysms. Stent-assisted coil embolization helps stabilize the coils within the aneurysm. Permanent placement of a stent in an intracranial vessel, however, requires long-term platelet inhibition. Temporary stent-assisted coiling is an alternative technique for the treatment of wide-neck aneurysms. To date, only case reports and small case series have been published. Our purpose was to retrospectively analyze the effectiveness and safety of temporary stent-assisted coiling in a larger cohort.

MATERIALS AND METHODS: Research was performed for all patients who had undergone endovascular aneurysm treatment in our institution (University Hospital Aachen) between January 2010 and December 2015. During this period, 355 consecutive patients had undergone endovascular aneurysm treatment. We intended to treat 33 (9.2%) of them with temporary stent-assisted coiling, and they were included in this study. Incidental and acutely ruptured aneurysms were included.

RESULTS: Sufficient occlusion was achieved in 97.1% of the cases. In 94%, the stent could be fully recovered. Complications occurred in 5 patients (14.7%), whereas in only 1 case was the complication seen as specific to stent-assisted coiling.

CONCLUSIONS: Temporary stent-assisted coiling is an effective technique for the treatment of wide-neck aneurysms. Safety is comparable with that of stent-assisted coiling and coiling with balloon remodeling.

Simple coil embolization is often not a feasible treatment option in wide-neck aneurysms. Stent-assisted coil embolization helps stabilize the coils within the aneurysm.¹ Permanent placement of a stent in an intracranial vessel, however, requires long-term platelet inhibition. Platelet inhibition is known to be associated with a higher bleeding risk.² Particularly in patients who require further treatment in an intensive care unit, such as patients with an acute subarachnoid hemorrhage, a higher bleeding risk should be avoided. In addition, dual platelet inhibition as recommended when stents are deployed permanently, increases the risk for cerebral hemorrhage within potentially existent isch-

emic brain tissue due to vasospasms.³ Hence, avoiding permanent stent placement is an advantage in patients with acute SAH.

In the past, several techniques have been established for the treatment of wide-neck aneurysms. Common techniques are stent-assisted coiling, balloon-assisted coiling, double microcatheter coiling, and aneurysm treatment with dedicated devices such as the Woven EndoBridge (WEB; Sequent Medical, Aliso Viejo, California) device^{4,5} or the Comaneci device (Rapid Medical, Yokneam, Israel).^{6,7} The combination of balloon remodeling and stent-assisted coiling is another treatment option with possible achievement of higher occlusion rates.⁸

Stent-assisted coiling and balloon remodeling seem to have a comparable complication rate in the literature, ranging between 10% and 20%.^{9,10}

Treatment of wide neck-aneurysms is also possible with flow diverter devices with an occlusion rate of about 80%.¹¹ However, with a latency of 4–12 months to aneurysm thrombosis and the need for subsequent platelet inhibition, these are not a primary option in patients with an acutely ruptured intracranial aneurysm.

Another treatment option for wide-neck aneurysms is temporary stent-assisted coiling.^{12,13} For this purpose, 2 microcatheters

Received October 17, 2016; accepted after revision February 22, 2017.

From the Departments of Neuroradiology (M.M., C.B., S.A., O.N., M.W.), Neurosurgery (G.A.S.), and Neurology (A.R.), University Hospital Aachen, Aachen, Germany; Institute of Neuroscience and Medicine 4 (O.N.), Forschungszentrum Jülich GmbH, Jülich, Germany; and Department for Diagnostic and Interventional Radiology (A.E.O.), Eberhard Karls University Tuebingen, University Hospital Tuebingen, Tuebingen, Germany.

Please address correspondence to Marguerite Müller, MD, Department of Neuro-radiology, University Hospital Aachen, Pauwelsstr 30, 52074 Aachen, Germany; e-mail: mamueller@ukaachen.de

<http://dx.doi.org/10.3174/ajnr.A5204>

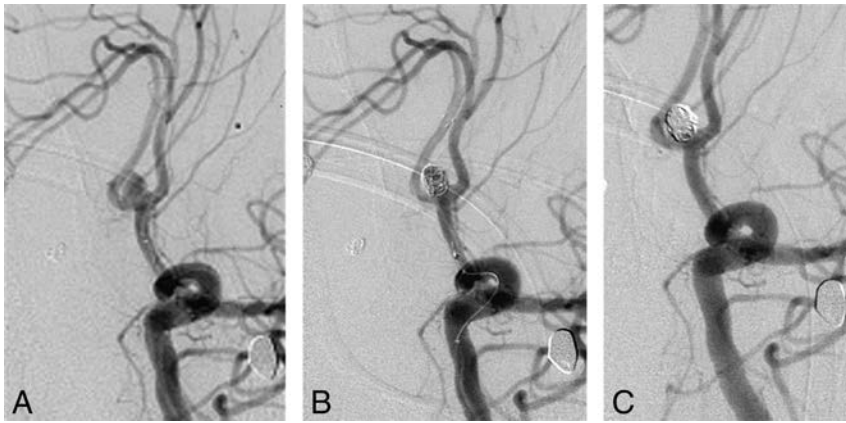


FIG 1. A, An aneurysm of the anterior communicating artery before coiling. B, The same aneurysm partially coiled with a deployed Solitaire stent from the left A1 to the right A2 segment. C, The same aneurysm after complete coil embolization. The Solitaire stent has been recovered.

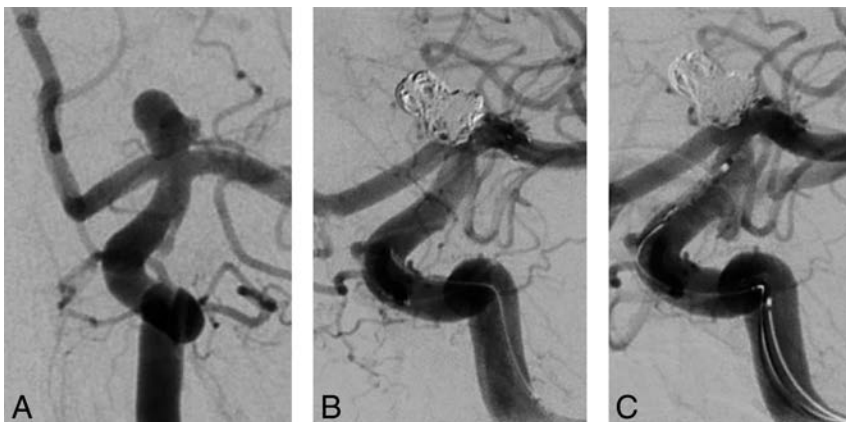


FIG 2. A, A carotid-T aneurysm before coiling. B, The same aneurysm partially coiled with the deployed Solitaire stent from the internal carotid artery to the left M1 segment. C, The same aneurysm after complete coil embolization. The Solitaire stent has been recovered.

are used. The first microcatheter is used to cover the aneurysm neck and deploy the stent. The second microcatheter is advanced into the aneurysm to perform coil embolization. Advancement of the second microcatheter into the aneurysm can be performed either before deployment of the stent or after stent deployment.¹⁴ The stent is deployed to cover the aneurysm neck but is not fully released. After coil embolization has been completed, the stent is recovered (Figs 1 and 2). In the unlikely event of coil protrusion during the process of recovery of the stent, recovery is stopped, the stent is deployed again, and it is released for permanent implantation. Temporary stent-assisted coiling is an established standard technique in our institution for the treatment of wide-neck aneurysms. Because to date, only case reports and small case series have been published, we analyzed a larger cohort of patients treated with temporary stent-assisted coiling.^{12,13} Following, we present a retrospective analysis on the effectiveness and safety of temporary stent-assisted coiling.

MATERIALS AND METHODS

Patients

After approval from our local ethics committee, we retrospectively searched our clinical data base for all patients who had un-

dergone endovascular aneurysm treatment in our institution (University Hospital Aachen) between January 2010 and December 2015. During this period, 355 consecutive patients had undergone endovascular aneurysm treatment. We intended to treat 33 (9.2%) of them with temporary stent-assisted coiling, and they were included in this study. In the same period, 4 (1.1%) patients were treated with balloon remodeling. Incidental and acutely ruptured aneurysms were included.

Clinical and Procedural Data

Evaluation concerned the possibility of stent recovery after coiling, occlusion rate and recurrence of the aneurysm, and the procedure-related complication rate.

Aneurysm occlusion was determined by using the modified Raymond-Roy classification.¹⁵

We also noted the location and the maximal diameter of the aneurysm and the dome-to-neck ratio and the diameter of the parent vessel. Peri-interventional and posttreatment platelet inhibition management was recorded for all patients.

Statistical Analysis

Correlations between variables were calculated by using Pearson Product-Moment Correlation Coefficient. *P* values $\leq .05$ were significant. All statistical

analyses were performed with SPSS 23 software (IBM, Armonk, New York).

RESULTS

Thirty-three patients (25 women) with 34 aneurysms, with the intention to treat by temporary stent-assisted coiling, were included in the retrospective analysis. Twenty of the treated aneurysms were acutely ruptured, 2 were symptomatic but unruptured, and 12 were incidental. Ages ranged from 29 to 79 years with a mean of 55 ± 12 years.

Fifteen aneurysms were located at the anterior communicating artery; 5, at the basilar tip; 11, at the carotid artery (with 6 of these located at the carotid-T); 1, at the middle cerebral artery bifurcation; 1, at the posterior communicating artery; and 1, at the origin of the posterior inferior cerebellar artery.

Maximal aneurysm diameters were 3–18 mm, with a mean maximal diameter of 7 ± 3.4 mm. Parent vessel diameters were 0.9–4.4 mm, with a mean of 2.1 ± 0.75 mm. Dome-to-neck ratios were 0.8–3.33, with a mean of 1.44 ± 0.55 and a median of 1.33.

For temporary stent placement, a Solitaire AB stent (Covidien, Irvine, California) was used in 30 cases. In 3 cases, an Enterprise stent (Codman & Shurtleff, Raynham, Massachusetts) was used,

and 1 aneurysm was treated with a LEO stent (Balt Extrusion, Montmorency, France).

Concerning initial treatment success, 26 aneurysms were completely occluded (class I), 7 aneurysms had a residual dog-ear (class II), and in 1 aneurysm, there was a noted a residuum of the aneurysm (class IIb). Hence, the complete occlusion rate was 76.5%, and a clinically acceptable occlusion rate, including a dog-ear remnant, was 97.1%. Statistical analysis showed no significant correlation between the occlusion rate and diameters of the aneurysm ($P = .50$) or the parent artery ($P = .13$) and no significant correlation to the dome-to-neck ratio ($P = .19$).

For 16 patients, follow-up MR imaging or digital subtraction angiography was available for at least 6 months. Three of 16 had an aneurysm recurrence, and 13 were stable during follow-up, with no significant correlation between recurrence and the diameters of the aneurysm ($P = .30$) or the parent artery ($P = .77$) and no significant correlation to the dome-to-neck ratio ($P = .97$).

For 9 patients, follow-up data were available for at least 2 years. Two of 9 (22.2%) had an aneurysm recurrence, and 7 were stable during long-term follow up.

In 2 of the 34 aneurysms, it was not possible to safely recover the stent, due to impending coil migration into the parent artery. Hence, the overall success rate of stent recovery was 94%. Statistical analysis showed no significant correlation between successful stent recovery and the diameters of the aneurysm ($P = .88$) or the parent artery ($P = .54$) and no significant correlation to the dome-to-neck ratio ($P = .52$).

All patients were treated with platelet inhibition during the procedure with 28 patients receiving intravenous tirofiban, 2 patients receiving IV acetyl salicylic acid, and 3 patients being pretreated with dual platelet inhibition (acetyl salicylic acid and clopidogrel). Pretreatment with antiplatelet drugs in those patients was due to preexisting conditions; 2 had coronary heart disease, and in 1 patient, another aneurysm had previously been treated with stent-assisted coiling.

Posttreatment, 1 of the 2 patients with permanent stent placement was given dual platelet inhibition for 3 months. The other patient with permanent stent placement received mono antiplatelet therapy with acetyl salicylic acid for 3 months. Both patients had acutely ruptured aneurysms.

Concerning the patients with stent recovery, 8 patients (3 with an acutely ruptured aneurysms) were given dual platelet inhibition for 4 weeks to 3 months. Five patients (3 with an acutely ruptured aneurysm) were given a single dose of 500 mg of acetyl salicylic acid subsequent to the procedure. Fourteen patients (8 with an acutely ruptured aneurysm) received mono antiplatelet therapy for 10 days to 6 months. Five patients (4 with an acutely ruptured aneurysms) were not given any subsequent antiplatelet medication.

Periprocedural complications occurred in 5 patients (14.7%). In the first patient, stretching and tearing of a coil occurred. During the process of retrieving the coil, there was thrombus formation in the afferent vessel that was completely resolved by IV rtPA and mechanical recanalization with a Solitaire AB 4/20 (ev3 Neurovascular, Irvine, California). Peri-interventional antiplatelet therapy was performed with tirofiban. The modified Rankin Scale score at discharge was 1.

In the second patient, no peri-interventional emboli were detected, yet postinterventional MR imaging showed multiple emboli in the vascular territory of the parent artery. Peri-interventional antiplatelet therapy was performed with tirofiban. The mRS at discharge was 1, due to a residual pronation.

In the third patient, again no peri-interventional emboli were detected with scattered bi-hemispheric ischemic lesions on postinterventional MR imaging. Peri-interventional antiplatelet therapy was performed with tirofiban. The mRS at discharge was 4, due to hemiparesis. With bi-hemispheric lesions and atrial fibrillation, in this case thromboembolism might also have been of cardiac origin.

In the fourth patient, first an occlusion of the stent lumen and perforation of the right ICA occurred. This complication was managed by an occlusion of the right ICA. Peri-interventional antiplatelet therapy was performed with tirofiban. The mRS at discharge was 5.

In the fifth patient, peri-interventional perforation of the aneurysm occurred during coil deployment. This was quickly managed by further coil embolization. Peri-interventional antiplatelet therapy was administered with tirofiban. The mRS at discharge was 3.

In summary, 4 of these 5 cases were due to thromboembolic events (3 with a Solitaire AB stent and 1 with an Enterprise stent), whereas the remaining complication was due to perforation of the aneurysm during coil deployment. Stent occlusion may be a complication related to the specific procedure, whereas the other complications are the usual ones observed in any technique of aneurysm embolization. There was a moderate negative correlation between the complication rate and dome-to-neck ratio (Pearson Product-Moment Correlation Coefficient = -0.38 , $P = .026$).

Concerning the 4 patients treated with balloon remodeling, 3 aneurysms were located on the internal carotid artery and 1 was of the basilar tip. One was a symptomatic aneurysm, and the other 3 were incidental. None of the aneurysms treated with balloon remodeling were ruptured.

Complete occlusion was achieved in 2 cases: In 1 case, a dog-ear remained, and in 1 case, there was a remaining perfusion of the aneurysm.

Two patients were pretreated with dual platelet inhibition (acetyl salicylic acid and clopidogrel) given for 3 months posttreatment. Two patients received tirofiban during the procedure: One was treated with dual platelet inhibition (acetyl salicylic acid and clopidogrel) for 3 months posttreatment, and 1 received only acetyl salicylic acid for 6 months.

Follow-up data were available for 3 patients for at least 12 months, with 1 recurrence of the aneurysm that had not been completely occluded.

There was 1 complication with a cerebral infarction. In this case, peri-interventional treatment was performed with tirofiban.

Statistical comparison was not performed due to the small sample size in the group treated with balloon remodeling.

DISCUSSION

Our results show that in this small study, temporary stent-assisted coiling is a feasible and effective option for the treatment of wide-neck aneurysms. This technique has been described in previous literature using fully retrievable stents such as the Solitaire

AB.^{12,13} The number of cases in those studies was 3 and 8, respectively. Therefore, this is the first report of a larger collective. Furthermore, we were able to show that this technique is also possible with the Enterprise and LEO stents if not completely deployed during the procedure.

In summary, our results imply that effective stent-assisted coiling with incomplete deployment of a variety of stents can be achieved with a satisfactory complication rate. It was possible to achieve a clinically acceptable occlusion rate (including a dog-ear remnant) in 33/34 (97.1%) cases and to recover the stent after completion of coiling with a success rate of 94%, regardless of the dome-to-neck ratio. Concerning the immediate effectiveness of temporary stent-assisted coiling, we believe a complete occlusion rate of 76.5% (class I)¹⁵ and an occlusion rate including dog-ear remnants (classes I + II) of 97.1% to be rather satisfying and comparable with a previous study that also indicates that a complete occlusion is more likely with stent assistance rather than balloon remodeling.¹⁶

A recurrence rate of 18.8% at 6 months' follow-up and 22.2% at long-term follow-up is comparable with previously mentioned recurrence rates of wide-neck aneurysms treated by stent-assisted coiling or balloon remodeling.¹⁷ Yet, with a higher sample size and more follow-up results, the recurrence rate might be lower because a high occlusion rate is thought to result in a smaller recurrence rate.¹⁸ However, with a sample size of only 16 patients with an available follow-up of at least 6 months, we believe that a safe assumption concerning the long-term results cannot be made with this analysis.

The overall complication rate of 14.7% is comparable with that of stent-assisted coiling with permanent stent placement and balloon remodeling, in which complication rates ranging between 10% and 20% have been reported.⁹ Because most complications were caused by thromboembolic events, we believe that using a sufficient platelet inhibition and an anticoagulation regimen during the procedure with a partially deployed stent is mandatory, despite removal at the end of the procedure. On the basis of a complication rate not higher than that of stent-assisted coiling,⁹ we believe that there is no higher risk involved in an incomplete deployment of the device during the procedure and there does not seem to be a difference between the devices used in our analysis.

Our data, however, do not allow determining whether and how long subsequent (long-term) platelet inhibition is necessary. Posttreatment antiplatelet therapy varied considerably within our patient group. This variation is because in each individual case, the neurointerventionalist has to consider a variety of factors including, for example, the presence of acute hemorrhage, the expected propensity of the coil/parent vessel interface to develop thrombus, surgical procedures potentially required such as CSF drainage, and a variety of other medical conditions. Even though there were no delayed embolisms in the 5 patients who did not receive subsequent platelet inhibition, the relatively small sample size of our study does not allow a valid recommendation. Yet, it seems reasonable that subsequent platelet inhibition should be performed as is common in cases with aneurysms treated only by coiling that has a broad interface with the parent vessel. Therefore, in patients with an unruptured intracranial aneurysm, subsequent platelet inhibition may be reasonable, whereas in patients

with an impending bleeding risk such as those with an acute SAH, further platelet inhibition should not be enforced.

Overall, we believe that temporary stent-assisted coiling is an alternative to balloon remodeling with the advantages of an easier navigation in smaller tortuous vessels and the absence of temporary flow arrest in the parent artery.¹⁹

The limitations of our study are a still rather small sample size and a possible selection bias because the patients were not prospectively randomized to the different treatment techniques for wide-neck aneurysms.

CONCLUSIONS

In this small study, temporary stent-assisted coiling is an effective technique for the treatment of wide-neck aneurysms. Safety is comparable with that of stent-assisted coiling and coiling with balloon remodeling. The major advantage of this treatment is less need for subsequent platelet inhibition, which might cause cerebral hemorrhage or complicate further treatment in an intensive care unit, and is therefore particularly eligible for patients with an acutely ruptured intracranial aneurysm.

Disclosures: Martin Wiesmann—UNRELATED: Consultancy: Stryker Neurovascular; Payment for Lectures Including Service on Speakers Bureaus: Bracco, Siemens, Stryker Neurovascular; Royalties: Springer, Thieme; Payment for Development of Educational Presentations: Abbott Laboratories, ab medica, Acandis, Bayer, Bracco, B. Braun, Codman Neurovascular, Covidien, Dahlhausen, MicroVention, Penumbra, phenox, Philips Healthcare, Siemens, Silk Road Medical, St. Jude Medical, Stryker Neurovascular.* *Money paid to the institution.

REFERENCES

1. Gory B, Klisch J, Bonafé A, et al. **Solitaire AB stent-assisted coiling of wide-necked intracranial aneurysms: mid-term results from the SOLARE study.** *Neurosurgery* 2014;75:215–19; discussion 219 [CrossRef Medline](#)
2. Aradi D, Kirtane A, Bonello L, et al. **Bleeding and stent thrombosis on P2Y12-inhibitors: collaborative analysis on the role of platelet reactivity for risk stratification after percutaneous coronary intervention.** *Eur Heart J* 2015;36:1762–71 [CrossRef Medline](#)
3. Geraghty OC, Kennedy J, Chandratheva A, et al. **Preliminary evidence of a high risk of bleeding on aspirin plus clopidogrel in aspirin-naïve patients in the acute phase after TIA or minor ischaemic stroke.** *Cerebrovasc Dis* 2010;29:460–67 [CrossRef Medline](#)
4. Behme D, Berlis A, Weber W. **Woven EndoBridge intrasaccular flow disrupter for the treatment of ruptured and unruptured wide-neck cerebral aneurysms: report of 55 cases.** *AJNR Am J Neuroradiol* 2015; 36:1501–06 [CrossRef Medline](#)
5. Pierot L, Spelle L, Molyneux A, et al. **Clinical and anatomical follow-up in patients with aneurysms treated with the WEB device: 1-year follow-up report in the cumulated population of 2 prospective, multicenter series (WEBCAST and French Observatory).** *Neurosurgery* 2016;78:133–41 [CrossRef Medline](#)
6. Lawson AL, Chandran A, Puthuran M, et al. **Initial experience of coiling cerebral aneurysms using the new Comaneci device.** *BMJ Case Rep* 2015;2015:pii: bcr2015011726 [CrossRef Medline](#)
7. Gupta R, Kolodgie FD, Virmani R, et al. **Comaneci neck bridging device for the treatment of cerebral aneurysms.** *J Neurointerv Surg* 2016;8:181–85 [CrossRef Medline](#)
8. Gentric JC, Biondi A, Pötin M, et al. **Balloon remodeling may improve angiographic results of stent-assisted coiling of unruptured intracranial aneurysms.** *Neurosurgery* 2015;76:441–45; discussion 445 [CrossRef Medline](#)
9. Chitale R, Chalouhi N, Theofanis T, et al. **Treatment of ruptured intracranial aneurysms: comparison of stenting and balloon remodeling.** *Neurosurgery* 2013;72:953–59 [CrossRef Medline](#)

10. Moon K, Albuquerque FC, Ducruet AF, et al. **Balloon remodeling of complex anterior communicating artery aneurysms: technical considerations and complications.** *J Neurointerv Surg* 2015;7: 418–24 CrossRef Medline
11. Yakovlev SB, Arustamyan SR, Dorokhov PS, et al. **Endovascular treatment of large and giant intracranial aneurysms using flow-diverting stents** [Article in Russian; Abstract available in Russian from the publisher]. *Zh Vopr Neurokhir Im N N Burdenko* 2015;79:19–27 Medline
12. Almekhlafi MA, Hockley A, Wong JH, et al. **Temporary Solitaire stent neck remodeling in the coiling of ruptured aneurysms.** *J Neurointerv Surg* 2013;5(suppl 3):iii76–78 CrossRef Medline
13. Signorelli F, Gory B, Turjman F. **Temporary Solitaire stent-assisted coiling: a technique for the treatment of acutely ruptured wide-neck intracranial aneurysms.** *AJNR Am J Neuroradiol* 2014;35: 984–88 CrossRef Medline
14. Spiotta AM, Wheeler AM, Smithson S, et al. **Comparison of techniques for stent assisted coil embolization of aneurysms.** *J Neurointerv Surg* 2012;4:339–44 CrossRef Medline
15. Stapleton CJ, Torok CM, Rabinov JD, et al. **Validation of the Modified Raymond-Roy classification for intracranial aneurysms treated with coil embolization.** *J Neurointerv Surg* 2016;8:927–33 CrossRef Medline
16. Consoli A, Vignoli C, Renieri L, et al. **Assisted coiling of saccular wide-necked unruptured intracranial aneurysms: stent versus balloon.** *J Neurointerv Surg* 2016;8:52–57 CrossRef Medline
17. Peterson E, Hanak B, Morton R, et al. **Are aneurysms treated with balloon-assisted coiling and stent-assisted coiling different? Morphological analysis of 113 unruptured wide-necked aneurysms treated with adjunctive devices.** *Neurosurgery* 2014;75:145–51; quiz 151 CrossRef Medline
18. Murias Quintana E, Gil Garcia A, Vega Valdes P, et al. **Anatomical results, rebleeding and factors that affect the degree of occlusion in ruptured cerebral aneurysms after endovascular therapy.** *J Neurointerv Surg* 2015;7:892–97 CrossRef Medline
19. Zumofen DW, Sahasrabudhe N, Riina HA, et al. **Temporary stent scaffolding during aneurysm coiling.** *J Clin Neurosci* 2014;21:852–54 CrossRef Medline

Liquid Embolic Agents for Endovascular Embolization: Evaluation of an Established (Onyx) and a Novel (PHIL) Embolic Agent in an In Vitro AVM Model

 D.F. Vollherbst,  C.M. Sommer,  C. Ulfert,  J. Pfaff,  M. Bendszus, and  M.A. Möhlenbruch

ABSTRACT

BACKGROUND AND PURPOSE: Embolization plays a key role in the treatment of arteriovenous malformations. The aim of this study was to evaluate an established (Onyx) and a novel (precipitating hydrophobic injectable liquid [PHIL]) liquid embolic agent in an in vitro AVM model.

MATERIALS AND METHODS: An AVM model was integrated into a circuit system. The artificial nidus (subdivided into 28 honeycomb-like sections) was embolized with Onyx 18 (group Onyx; $n = 8$) or PHIL 25 (group PHIL; $n = 8$) with different pause times between the injections (30 and 60 seconds, $n = 4$ per study group) by using a 1.3F microcatheter. Procedure times, number of injections, embolization success (defined as the number of filled sections of the artificial nidus), volume of embolic agent, and frequency and extent of reflux and draining vein embolization were assessed.

RESULTS: Embolization success was comparable between Onyx and PHIL. Shorter pause times resulted in a significantly higher embolization success for PHIL (median embolization score, 28 versus 18; $P = .011$). Compared with Onyx, lower volumes of PHIL were required for the same extent of embolization (median volume per section of the artificial nidus, 15.5 versus 3.6 μL ; $P < .001$).

CONCLUSIONS: While the embolization success was comparable for Onyx and PHIL, pause time had a considerable effect on the embolization success in an in vitro AVM model. Compared with Onyx, lower volumes of PHIL were required for the same extent of embolization.

ABBREVIATIONS: DMSO = dimethyl-sulfoxide; EVOH = ethylene-vinyl alcohol copolymer; LEA = liquid embolic agent; PHIL = precipitating hydrophobic injectable liquid

Arteriovenous malformations are complex vascular structures composed of feeding arteries, an intervening network of small pathologic blood vessels (the so-called nidus), and draining veins. The lack of an intervening capillary bed allows high-flow arteriovenous shunting of blood. While AVMs can occur throughout the entire body, cerebral AVMs are of particular relevance due to their ability to cause impairing neurologic symptoms and their considerable risk of hemorrhage.¹

Alone or in combination with microneurosurgery and stereotactic radiation therapy, embolization plays an important role in

the management of cerebral AVMs.² The aim of AVM embolization is complete filling of the nidus, while unwanted reflux into the feeding arteries should be minimized and premature embolization of the draining veins should be avoided.³

A wide variety of embolic agents has been and is currently used for embolization of AVMs. At present, the liquid embolic agents (LEAs) ethylene-vinyl alcohol copolymer (EVOH) and *n*-butyl cyanoacrylate are used most frequently.⁴ Although the embolization results have improved since the introduction of EVOH-based LEAs with rates of complete obliteration ranging from 16% to 100%, the success rate of AVM embolization, especially for complex AVMs, is not yet satisfying.^{2,3} Currently, new LEAs are being introduced to improve embolization features, such as embolization efficacy, intraprocedural handling, and control. Furthermore, their use should improve fluoroscopic visibility and reduce artifacts in postinterventional imaging.

The aim of this study was to evaluate an established EVOH-based embolic agent and a novel copolymer-based embolic agent in an in vitro AVM model.

Received January 11, 2017; accepted after revision February 23.

From the Department of Neuroradiology (D.F.V., C.U., J.P., M.B., M.A.M.) and Clinic for Diagnostic and Interventional Radiology (C.M.S.), University Hospital Heidelberg, Heidelberg, Germany; and Clinic for Diagnostic and Interventional Radiology (C.M.S.), Klinikum Stuttgart, Stuttgart, Germany.

This study was technically supported by MicroVention and Medtronic. The authors had full control of the data and its analysis throughout the study.

Please address correspondence to Markus A. Möhlenbruch, MD, Department of Neuroradiology, University Hospital Heidelberg, INF 400, 69120 Heidelberg, Germany; e-mail: markus.moehlenbruch@med.uni-heidelberg.de

<http://dx.doi.org/10.3174/ajnr.A5203>

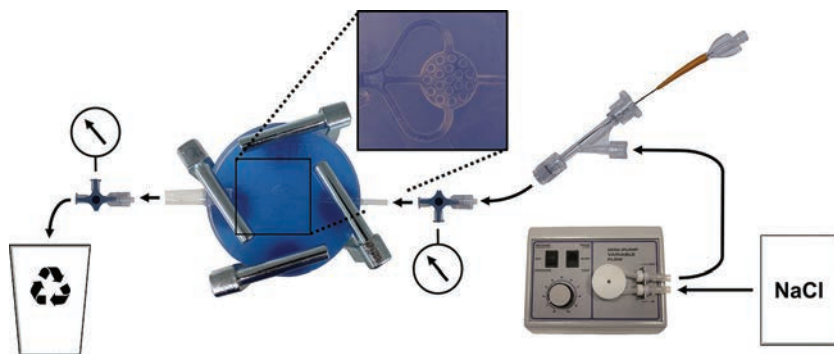


FIG 1. Illustration of the experimental setup. Note that sodium chloride solution (NaCl) was pumped into the circuit system with a constant-flow pump (arrows indicating the direction of flow). A microcatheter was inserted via a hemostatic Y-adaptor. Using 3-way stopcocks, we measured intraluminal pressures (manometer symbols).

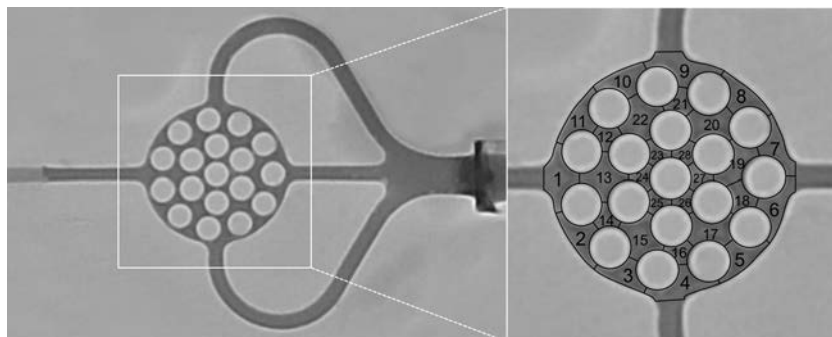


FIG 2. Definition of the embolization success. Note that after we filled the nonembolized AVM model with pure contrast agent, the artificial nidus was subdivided into 28 honeycomb-like sections.

MATERIALS AND METHODS

Embolic Agents

Onyx (Covidien, Irvine, California) is composed of nonadhesive EVOH dissolved in dimethyl-sulfoxide (DMSO) in a mixture with tantalum powder, the latter causing radiopacity. To ensure proper mixing of the tantalum powder, we keep Onyx vials on a shaker (Vortex Genie 2; Scientific Industries, Bohemia, New York) for at least 20 minutes before injection. Three concentrations of Onyx are available: Onyx 18, 20, and 34 (increasing in viscosity; numbers indicating viscosity in centipoise).

Precipitating hydrophobic injectable liquid (PHIL; MicroVention, Tustin, California) is composed of a nonadhesive copolymer (polylactide-co-glycolide and polyhydroxyethylmethacrylate) dissolved in DMSO with an iodine component (triiodophenol) covalently bound to the copolymer, causing radiopacity. PHIL is ready to use in prefilled syringes of 1 mL and does not require shaking before injection. Three concentrations of PHIL are available: PHIL 25, 30, and 35 (increasing in viscosity, numbers indicating concentration in weight/weight).

AVM Model

The in vitro AVM model and the experimental setting are illustrated in Fig 1. The AVM model, made of silicone, consisted of an afferent tube, representing the feeding artery, supplying the artificial nidus; a round, flat, honeycomb-like 3D space; and 3 efferent tubes, representing 3 draining veins. It was placed between 2 congruent glass plates, attached with 4 screw clamps, ensuring

complete tightness of the model. The diameter of the feeding artery and the draining veins was 2 mm; the artificial nidus measured $15 \times 15 \times 3$ mm with a volume of 311 mm^3 . The artificial nidus was subdivided into 28 honeycomb-like sections (Fig 2). The AVM model was integrated into a circuit system with a constant flow of sterile 0.9% (weight/volume) sodium chloride solution with a temperature between 20°C and 25°C and a volume flow of 120 mL/minute. Using 3-way stopcocks, we measured endoluminal pressures proximal and distal to the nonembolized artificial nidus 10 times. Proximal to the AVM model, a hemostatic Y-adaptor was installed for access.

Embolization Technique

A DMSO-compatible 1.3F microcatheter (Headway Duo; MicroVention) was inserted into the circuit system via the Y-adaptor. The catheter tip was positioned 3 mm proximal to the artificial nidus. After flushing the catheter with 1 mL of DMSO, we performed manual embolization with 1-mL DMSO-compatible syringes. Embolization was performed under fluoroscopic guidance (Artis Q biplane system; Siemens, Erlangen, Germany) until reflux, draining vein embolization, or complete embolization of the artificial nidus occurred. In case of reflux or draining vein embolization, embolization was stopped and paused for 30 or 60 seconds (see "Study Groups"). Reflux of 10 mm into the feeding artery and embolization of the proximal 15 mm of the draining veins were tolerated. In case of reflux of >10 mm or draining vein embolization of >15 mm, the embolization procedure was terminated.

Study Groups

In total, 16 embolization procedures were performed. For 8 procedures, Onyx 18 (group Onyx) and for 8 procedures PHIL 25 (group PHIL) were used as the LEA. Pause time between the injections was set to 30 or 60 seconds ($n = 4$ per study group). Accordingly, we defined 4 subgroups: group Onyx_30s ($n = 4$), group Onyx_60s ($n = 4$), group PHIL_30s ($n = 4$), and group PHIL_60s ($n = 4$).

Study Goals

The intention of each embolization procedure was complete filling of the artificial nidus. According to the 28 honeycomb-like sections of the artificial nidus (Fig 2), we graded embolization success from 0/28 sections (no embolization of the artificial nidus) to 28/28 sections (complete embolization of the artificial nidus). The number of filled sections of the artificial nidus at the time of the first reflux or draining vein embolization (first pause)

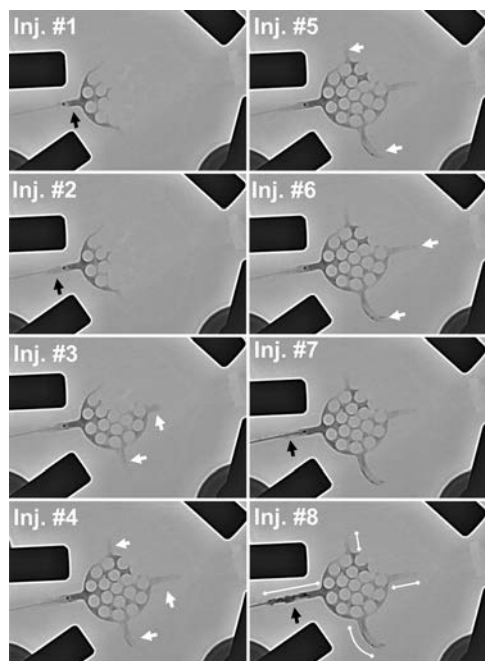


FIG 3. Exemplary embolization procedure. Note the exemplary embolization procedure shown for group Onyx_60s. Eight injections were performed. For 4 injections, embolization of draining veins (white arrows) and, for 4 injections, reflux (black arrows) were the reasons for injection stop. After the eighth injection, the reflux distance exceeded 1.5 cm and the procedure was terminated. After termination, reflux distance and distance of the embolized draining veins were measured (white double arrows injection [Inj.] No. 8) and the filled sections of the artificial nidus were assessed (according to Fig 2).

was determined. Total procedural time, injection time (defined as the duration of all injections per procedure without pause time), time per injection (defined as the time of a single injection until reflux, draining vein embolization, or complete filling of the artificial nidus), and number of injections per procedure were documented. The volume of the LEA per procedure (less the dead space of the microcatheter of 0.35 mL) was assessed, and the volume of the LEA, required for filling 1 section of the artificial nidus, was calculated (less the dead space of the microcatheter and the volume of LEA in the feeding artery and the draining veins). The respective number of reflux events and draining vein embolization events was documented. For each embolization procedure, the extent of reflux and of draining vein embolization was assessed by measuring the embolized distance of the respective structure (Fig 3).

Statistics

GraphPad Prism software (Version 6.00; GraphPad Software, San Diego, California) was used for data analysis. Quantitative data are presented as medians (range [minimum value; maximum value]). To evaluate statistical differences between group Onyx and group PHIL, we performed the Mann-Whitney *U* test. To evaluate statistical differences among the subgroups, we performed the Kruskal-Wallis test with a post hoc Dunn test. A *P* value of < .05 was significant.

RESULTS

All embolization procedures could be performed as planned. No technical failure, such as catheter occlusion or catheter entrap-

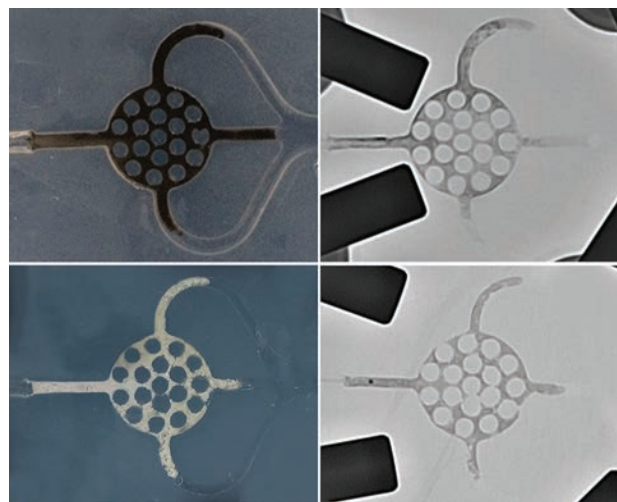


FIG 4. Photographs of Onyx and PHIL after embolization with fluoroscopic correlation. Upper rows, Example from group Onyx_30s. Note the black appearance of the Onyx cast. Lower rows, Example from group PHIL_30s. Note the white appearance of the PHIL cast.

ment, was observed. Endoluminal pressure proximal to the artificial nidus was 70 mm Hg (70 mm Hg, 70 mm Hg), and distal to the artificial nidus, it was 13 mm Hg (13 mm Hg, 13 mm Hg), resulting in a median pressure gradient of 57 mm Hg. Both embolic agents were sufficiently visible under fluoroscopy.

A representative embolization procedure is shown in Fig 3. Representative photographs after embolization with fluoroscopic correlation are shown in Fig 4. Results are presented in Tables 1 and 2 and illustrated in Fig 5.

When we compared group Onyx and group PHIL, the median amount of LEA per embolization procedure was significantly higher for group Onyx (0.48 mL versus 0.15 mL, *P* = .002). This finding was even more distinct for the median amount of LEA per filled section of the artificial nidus (15.5 versus 3.6 μ L, *P* < .001). The median number of filled sections of the artificial nidus at the time of the first reflux or draining vein embolization was significantly higher for group Onyx (13 versus 9, *P* = .032). However, the median number of filled sections of the artificial nidus (embolization success) did not show significant differences between group Onyx and group PHIL (24 versus 20, *P* = .780). Also, total procedural time, injection time, time per injection, number of injections, and the frequency and the extent of reflux and draining vein embolization did not differ.

When we compared group Onyx_30s and group Onyx_60s, subgroup analysis revealed a trend toward a higher median number of filled sections of the artificial nidus for group Onyx_60s, however, without reaching statistical significance (27 versus 21, *P* = .169). The median injection time was considerably higher for group Onyx_30s (34 versus 14 seconds, *P* = .270), also without a statistically significant difference.

When we compared group PHIL_30s and group PHIL_60s, subgroup analysis revealed a significantly higher median number of filled sections of the artificial nidus for group PHIL_30s (28 versus 18, *P* = .011).

Table 1: Procedure times, number of injections per procedure, and required volume of LEA^a

| | Onyx | | PHIL | | P Value ^b P Value ^c subgroups |
|---|------------------|------------------|------------------|------------------|---|
| | Onyx_30s | Onyx_60s | PHIL_30s | PHIL_60s | |
| Total procedure time (sec) | 645 (271–845) | | 561 (375–960) | | .959 |
| | 572 (271–685) | 645 (565–845) | 483 (375–575) | 742 (496–960) | .125 |
| Injection time (sec) | 250 (91–285) | | 152 (88–305) | | .235 |
| | 155 (91–250) | 263 (250–285) | 193 (88–305) | 142 (126–180) | .093 |
| Time per injection (sec) | 23 (7–44) | | 14 (9–33) | | .279 |
| | 14 (7–17) | 34 (29–44) | 21 (9–33) | 11 (11–18) | .067 |
| Injections per procedure (No.) | 9 (6–19) | | 10 (7–14) | | .749 |
| | 13 (7–19) | 8 (6–19) | 10 (7–14) | 11 (7–14) | .240 |
| Volume of LEA per procedure (mL) | 0.48 (0.25–0.65) | | 0.15 (0.10–0.35) | | .002 |
| | 0.53 (0.25–0.65) | 0.45 (0.35–0.50) | 0.23 (0.15–0.35) | 0.13 (0.10–0.20) | .013 |
| Volume of LEA per honeycomb-like section of the artificial nidus (μL) | 15.5 (10.1–27.4) | | 3.6 (0.6–9.5) | | <.001 |
| | 19.5 (14.3–27.4) | 13.3 (10.1–17.5) | 5.2 (2.6–9.5) | 2.9 (0.6–6.5) | .006 |
| | | | | | (Onyx_30s vs PHIL_60s) |

Note:—Onyx indicates Onyx 18; PHIL, PHIL 25.

^a Data presented as median (range).

^b Mann-Whitney *U* test.

^c Kruskal-Wallis test with the post hoc Dunn test.

Table 2: Number of injection stops due to reflux or draining vein embolization, extent of reflux and draining vein embolization, and filled honeycomb-like sections of the artificial nidus^a

| | Onyx | | PHIL | | P Value ^b P Value ^c subgroups |
|--|-----------------|------------------|------------------|------------------|---|
| | Onyx_30s | Onyx_60s | PHIL_30s | PHIL_60s | |
| Injection stops due to reflux (No.) | 5 (1–10) | | 6 (2–11) | | .633 |
| | 7 (4–10) | 3 (1–5) | 6 (2–7) | 5 (3–11) | .251 |
| Injection stops due to embolization of draining veins (No.) | 6 (3–10) | | 5 (3–8) | | .956 |
| | 7 (3–10) | 5 (4–6) | 5 (3–8) | 6 (3–8) | .778 |
| Reflux distance (mm) | 10.3 (5.2–11.4) | | 10.9 (7.7–13.0) | | .156 |
| | 10.3 (5.2–10.7) | 9.7 (7.2–11.4) | 9.6 (7.7–13.0) | 11.5 (10.9–13.0) | .164 |
| Draining vein distance (mm) | 17.2 (5.1–20.6) | | 15.0 (12.9–22.6) | | .683 |
| | 17.2 (5.1–20.6) | 17.5 (14.8–20.2) | 16.3 (13.3–22.6) | 13.8 (12.9–17.5) | .457 |
| Filled honeycomb-like sections of the artificial nidus at first reflux or draining vein embolization (No.) | 13 (8–20) | | 9 (6–14) | | .032 |
| | 12 (8–20) | 13 (13–15) | 9 (7–10) | 10 (6–14) | .109 |
| Filled honeycomb-like sections of the artificial nidus (No.) | 24 (14–28) | | 20 (14–28) | | .791 |
| | 21 (14–24) | 27 (24–28) | 28 (22–28) | 18 (14–18) | .011 |
| | | | | | (PHIL_30s vs. PHIL_60s) |

Note:—Onyx indicates Onyx 18; PHIL, PHIL 25.

^a Data presented as median (range).

^b Mann-Whitney *U* test.

^c Kruskal-Wallis test with the post hoc Dunn test.

DISCUSSION

In this experimental study, the established LEA Onyx and the novel LEA PHIL were evaluated and compared in an in vitro AVM model. As a major finding of this study, the embolization success was comparable for Onyx and PHIL. However, pause time between injections had a considerable influence on the embolization success. For the same extent of embolization, lower volumes of PHIL compared with Onyx were required.

Since its introduction in 1990, the EVOH-based LEA Onyx has gained increasing acceptance as an effective agent for embolization of AVMs and AVFs.^{5–7} The major advantages of Onyx over other embolic agents, such as *n*-BCA, are its low

viscosity and its delayed precipitation, offering increased embolization control and efficacy.⁸ Despite its high embolization potential and the advantages of Onyx over other LEAs, there are still several shortcomings reported by neurointerventionalists, such as long procedure times caused by the relatively long precipitation process of Onyx, impaired visibility during longer embolization procedures, impaired visibility of the microcatheter tip during embolization, artifacts in control imaging and in imaging for irradiation planning, hazards during surgical resection (sparking and combustion), and its preinterventional preparation process.⁹

PHIL is a novel LEA, introduced in 2015 by MicroVention,

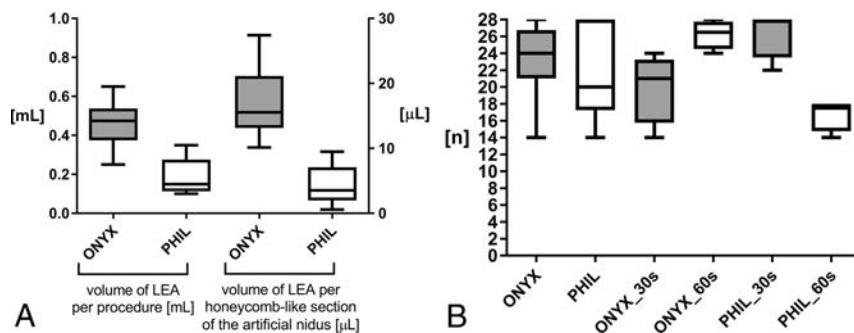


FIG 5. A, Volume of the LEA per procedure (left) and volume of the LEA per honeycomb-like section of the artificial nidus (right). For the same extent of embolization, significantly lower volumes of PHIL were required. B, Filled honeycomb-like sections of the artificial nidus. Embolization success was comparable between group Onyx and group PHIL. A pause time of 60 seconds resulted in a considerable, however not statistically significantly, higher embolization success for Onyx. A pause time of 30 seconds resulted in a significantly higher embolization success for PHIL. Onyx indicates Onyx 18; PHIL indicates PHIL 25.

based on a biocompatible copolymer instead of EVOH. For radiopacity, iodine is covalently bound to the copolymer. Three studies reported their preliminary experience with PHIL for AVM and demonstrated the effectiveness and safety of PHIL for AVM and AVF embolization, albeit for a limited number of cases.¹⁰⁻¹² The potential advantages of PHIL over Onyx discussed in the literature are its ease of use, faster plug formation, more consistent visibility, fewer artifacts in postinterventional imaging, lower required volumes of LEA, a constant degree of embolization effect, and no intraoperative hazards.¹⁰⁻¹²

Two studies with an in vitro AVM model were published recently, and in both studies *n*-BCA was the focus of investigation.^{13,14} In contrast to our AVM model, the model used in these studies consisted of commercially available 1-mL syringes filled with small plastic balls, and in the study of Ishikawa et al,¹³ swine blood instead of electrolyte solution was used. Instead of this 1D artificial nidus, in our study, a complex, 3D AVM model was used. For better standardization of the embolization procedures, we consciously used saline solution instead of heparinized swine blood. The flow rates of cerebral AVMs range from 50 to 550 mL/min.^{15,16} Accordingly and similar to the 2 in vitro studies mentioned above, the flow rate of 120 mL/min in our model represents a moderate-flow AVM nidus.^{13,14} The intraluminal pressures proximal and distal to the artificial nidus (70 and 13 mm Hg) were similar to the intravascular pressures in an AVM (49.3 ± 16.9 and 17.1 ± 6.1 mm Hg).¹⁷

We could demonstrate that compared with Onyx, lower volumes of PHIL are required for the same extent of embolization. In quantitative terms (calculated by using the medians), 0.23 mL of PHIL had the same embolization effect as 1.00 mL of Onyx. This aspect has to be considered when using PHIL in clinical practice.

As initially indicated, the aim of AVM embolization is complete filling of the nidus. Unwanted reflux into the feeding arteries should be minimized because it can cause embolization of non-target arteries or close the access way before complete filling.⁸ For Onyx and also according to the preliminary experiences for PHIL, a certain degree of reflux is intended because it causes plug formation around the catheter tip, which enables and improves antegrade movement of the LEA and deep penetration of the nidus while simultaneously reducing the risk of reflux after successful

plug formation.¹⁰⁻¹² Regarding the frequency or extent of reflux, no significant differences between Onyx and PHIL were observed. The required time for plug formation was short for both LEAs in our experimental setup.

Premature embolization of the draining veins should be avoided because an increase of intranidal pressure can occur, resulting in intra- or postinterventional hemorrhage.^{2,3,9} PHIL is thought to have a column effect, decreasing forward flow into the venous side of an AVM, diminishing venous obliteration, which may reduce the rate of hemorrhage due to venous outflow obstruction.¹⁰ However,

in our study, the frequency and extent of forward flow into the draining veins of the AVM model was comparable for Onyx and PHIL.

The significantly higher number of filled sections of the artificial nidus at the time of the first reflux or draining vein embolization for group Onyx can be interpreted as a sign of higher intranidal forward flow compared with PHIL. However, the primary end point—final filling of the artificial nidus—did not show significant differences.

Although the embolization success was not different between Onyx and PHIL, the pause time between 2 injections had considerable influence on the extent of filling of the artificial AVM nidus. For Onyx, a pause time of 60 seconds was advantageous; however, without statistical significance; and for PHIL, a pause time of 30 seconds was significantly advantageous. This finding is in accordance with the precipitation times provided by the manufacturers of Onyx and PHIL, with 5 and 3 minutes, respectively. For optimal embolization control, the precipitation time of a LEA should be short enough to avoid distal off-target embolization and long enough to avoid premature embolization of the proximal AVM, resulting in subtotal filling of the AVM.^{2,3,9} In this regard, for effective embolization, the pause time of 30 seconds seems to be appropriate for the specific precipitation time of PHIL. The shorter waiting time has to be considered in the clinical use of the novel LEA PHIL.¹⁸

There were some limitations to our study. First, the number of trials was small. Second, transferability of an in vitro model to clinical practice is limited. Third, there might be more or other optimal pause times besides the ones used in this study. Fourth, there was constant and not pulsatile flow in the circuit model.

CONCLUSIONS

Onyx and PHIL showed comparable embolization success in an in vitro AVM model. Pause time between injections had considerable influence on the embolization success. Shorter pause times (30 seconds) resulted in a significantly higher embolization success for PHIL. Compared with Onyx, lower volumes of PHIL were required for the same extent of embolization.

Disclosures: Dominik F. Vollherbst—OTHER: This study was technically supported by MicroVention and Medtronic. Christian Ulfert—UNRELATED: Travel/Accommodations/Meeting Expenses Unrelated to Activities Listed: MicroVention; OTHER: The study was technically supported by Medtronic and MicroVention. Johannes Pfaff—UNRELATED: Payment for Lectures Including Service on Speakers Bureaus: Siemens; Travel/Accommodations/Meeting Expenses Unrelated to Activities Listed: Stryker. Martin Bendszus—UNRELATED: Board Membership: Data and Safety Monitoring Board for Vascular Dynamics; Consultancy: Codman Neurovascular, Roche, Guerbet, Boehringer Ingelheim; Grants/Grants Pending: Deutsche Forschungsgemeinschaft, Hopp Foundation, Novartis, Siemens, Guerbet, Stryker, Covidien*; Payment for Lectures Including Service on Speakers Bureaus: Novartis, Roche, Guerbet, Teva Pharmaceutical Industries, Bayer AG, Codman Neurovascular. Markus A. Möhlenbruch—RELATED: Provision of Writing Assistance, Medicines, Equipment, or Administrative Support: This study was supported by MicroVention and Medtronic with embolic materials and microcatheters; UNRELATED: Payment for Lectures Including Service on Speakers Bureaus: Codman Neurovascular, MicroVention, Medtronic, phenox. *Money paid to the institution.

REFERENCES

- Friedlander RM. **Clinical practice. Arteriovenous malformations of the brain.** *N Engl J Med* 2007;356:2704–12 [CrossRef Medline](#)
- Pierot L, Cognard C, Herbreteau D, et al. **Endovascular treatment of brain arteriovenous malformations using a liquid embolic agent: results of a prospective, multicentre study (BRAVO).** *Eur Radiol* 2013;23:2838–45 [CrossRef Medline](#)
- van Rooij WJ, Sluzewski M, Beute GN. **Brain AVM embolization with Onyx.** *AJNR Am J Neuroradiol* 2007;28:172–77; discussion 178 [Medline](#)
- Gross BA, Du R. **Diagnosis and treatment of vascular malformations of the brain.** *Curr Treat Options Neurol* 2014;16:279 [CrossRef Medline](#)
- Taki W, Yonekawa Y, Iwata H, et al. **A new liquid material for embolization of arteriovenous malformations.** *AJNR Am J Neuroradiol* 1990;11:163–68 [Medline](#)
- Bruno CA Jr, Meyers PM. **Endovascular management of arteriovenous malformations of the brain.** *Interv Neurol* 2013;1:109–23 [CrossRef Medline](#)
- Hu YC, Newman CB, Dashti SR, et al. **Cranial dural arteriovenous fistula: transarterial Onyx embolization experience and technical nuances.** *J Neurointerv Surg* 2011;3:5–13 [CrossRef Medline](#)
- Elsenousi A, Aletich VA, Alaraj A. **Neurological outcomes and cure rates of embolization of brain arteriovenous malformations with n-butyl cyanoacrylate or Onyx: a meta-analysis.** *J Neurointerv Surg* 2016;8:265–72 [CrossRef Medline](#)
- Ayad M, Eskioglu E, Mericle RA. **Onyx: a unique neuroembolic agent.** *Expert Rev Med Devices* 2006;3:705–15 [CrossRef Medline](#)
- Kocer N, Hanımoğlu H, Batur Ş, et al. **Preliminary experience with precipitating hydrophobic injectable liquid in brain arteriovenous malformations.** *Diagn Interv Radiol* 2016;22:184–89 [CrossRef Medline](#)
- Samaniego EA, Kalousek V, Abdo G, et al. **Preliminary experience with Precipitating Hydrophobic Injectable Liquid (PHIL) in treating cerebral AVMs.** *J Neurointerv Surg* 2016 Jan 27. [Epub ahead of print] [CrossRef Medline](#)
- Leyon JJ, Chavda S, Thomas A, et al. **Preliminary experience with the liquid embolic material agent PHIL (precipitating hydrophobic injectable liquid) in treating cranial and spinal dural arteriovenous fistulas: technical note.** *J Neurointerv Surg* 2016;8:596–602 [CrossRef Medline](#)
- Ishikawa M, Horikawa M, Yamagami T, et al. **Embolization of arteriovenous malformations: effect of flow control and composition of n-butyl-2 cyanoacrylate and iodized oil mixtures with and without ethanol in an in vitro model.** *Radiology* 2016;279:910–16 [CrossRef Medline](#)
- Inagawa S, Isoda H, Kougo H, et al. **In-vitro simulation of NBCA embolization for arteriovenous malformation.** *Interv Neuroradiol* 2003;9:351–58 [CrossRef Medline](#)
- Chang W, Loecher MW, Wu Y, et al. **Hemodynamic changes in patients with arteriovenous malformations assessed using high-resolution 3D radial phase-contrast MR angiography.** *AJNR Am J Neuroradiol* 2012;33:1565–72 [CrossRef Medline](#)
- Nornes H, Grip A. **Hemodynamic aspects of cerebral arteriovenous malformations.** *J Neurosurg* 1980;53:456–64 [CrossRef Medline](#)
- Rossitti S. **Pathophysiology of increased cerebrospinal fluid pressure associated to brain arteriovenous malformations: the hydraulic hypothesis.** *Surg Neurol Int* 2013;4:42 [CrossRef Medline](#)
- Frontera JA, Moatti J, de los Reyes KM, et al. **Safety and cost of stent-assisted coiling of unruptured intracranial aneurysms compared with coiling or clipping.** *J Neurointerv Surg* 2014;6:65–71 [CrossRef Medline](#)

Appropriate Minimal Dose of Gadobutrol for 3D Time-Resolved MRA of the Supra-Aortic Arteries: Comparison with Conventional Single-Phase High-Resolution 3D Contrast-Enhanced MRA

S.H. Bak, H.G. Roh, W.-J. Moon, J.W. Choi, and H.S. An

ABSTRACT

BACKGROUND AND PURPOSE: The development of nephrogenic systemic fibrosis and neural tissue deposition is gadolinium dose-dependent. The purpose of this study was to determine the appropriate minimal dose of gadobutrol with time-resolved MRA to assess supra-aortic arterial stenosis with contrast-enhanced MRA as a reference standard.

MATERIALS AND METHODS: Four hundred sixty-two consecutive patients underwent both standard-dose contrast-enhanced MRA and low-dose time-resolved MRA and were classified into 3 groups; group A (a constant dose of 1 mL for time-resolved MRA), group B (2 mL), or group C (3 mL). All studies were independently evaluated by 2 radiologists for image quality by using a 5-point scale (from 0 = failure to 4 = excellent), grading of arterial stenosis (0 = normal, 1 = mild [$<30\%$], 2 = moderate [$30\%–69\%$], 3 = severe to occlusion [$\geq 70\%$]), and signal-to-noise ratio.

RESULTS: The image quality of time-resolved MRA was similar to that of contrast-enhanced MRA in groups B and C, but it was inferior to contrast-enhanced MRA in group A. For the grading of arterial stenosis, there was an excellent correlation between contrast-enhanced MRA and time-resolved MRA ($R = 0.957$ for group A, $R = 0.988$ for group B, $R = 0.991$ for group C). The SNR of time-resolved MRA tended to be lower than that of contrast-enhanced MRA in groups A and B. However, SNR was higher for time-resolved MRA compared with contrast-enhanced MRA in group C.

CONCLUSIONS: Low-dose time-resolved MRA is feasible in the evaluation of supra-aortic stenosis and could be used as an alternative to contrast-enhanced MRA for a diagnostic technique in high-risk populations.

ABBREVIATIONS: CCA = common carotid artery; CE-MRA = contrast-enhanced MRA; GBCA = gadolinium-based contrast agent; TRICKS = time-resolved imaging of contrast kinetics; TR-MRA = time-resolved MRA

Digital subtraction angiography remains the criterion standard for evaluation of supra-aortic steno-occlusive disease, with excellent spatial and temporal resolution. However, it is a time-consuming and invasive technique and is associated with several risks, including transient ischemic attack, permanent neurologic deficit, iodine contrast nephrotoxicity, and exposure to ionizing radiation.^{1–3} Consequently, DSA has largely been reserved for interventions for extracranial and intracranial steno-occlusive disease or in cases of uncertain findings on noninvasive imaging studies.⁴ Noninvasive angiography techniques such as

CTA and MRA are typically used for routine diagnostic procedures. Recently, 3D high-resolution contrast-enhanced MRA (CE-MRA) has become widely used as an excellent alternative imaging technique for the assessment of supra-aortic steno-occlusive disease.⁵

Gadolinium-based contrast agents (GBCAs) were initially thought to be safe in patients with reduced renal function rather than iodine-based contrast agents.⁶ Recently, a positive association between nephrogenic systemic fibrosis and exposure to GBCAs in patients with renal failure has been described.⁷ Several studies showed a relationship between high doses of GBCAs and increased nephrogenic systemic fibrosis risk.^{8–11} Also, in the past 2 years, several studies regarding gadolinium retention in intracranial neuronal tissues have been published.^{12–14} The development of nephrogenic systemic fibrosis with exposure to GBCAs and gadolinium deposition in neuronal tissue is dose-dependent; therefore, caution has been advised when administering GBCAs.^{13,15} There is increasing interest in dose-reduction strategies that maintain diagnostic image quality.¹⁶ Time-resolved MRA (TR-MRA) is used clinically to offer combined anatomic

Received October 12, 2016; accepted after revision February 13, 2017.

From the Department of Radiology (S.H.B., H.G.R., W.-J.M., J.W.C.), Konkuk University Medical Center, Konkuk University School of Medicine, Seoul, Korea; Department of Radiology (S.H.B.), Kangwon National University Hospital, Chuncheon, Korea; and Department of Radiology (H.S.A.), Armed Forces Yangju Hospital, Yangju, Korea.

Please address correspondence to Hong Gee Roh, MD, PhD, Department of Radiology, Konkuk University Medical Center, Konkuk University School of Medicine, Seoul, Korea, 4-12 Hwayang-dong, Gwangjin-gu, Seoul, 143-729, Korea; e-mail: hgroh@kuh.ac.kr

<http://dx.doi.org/10.3174/ajnr.A5176>

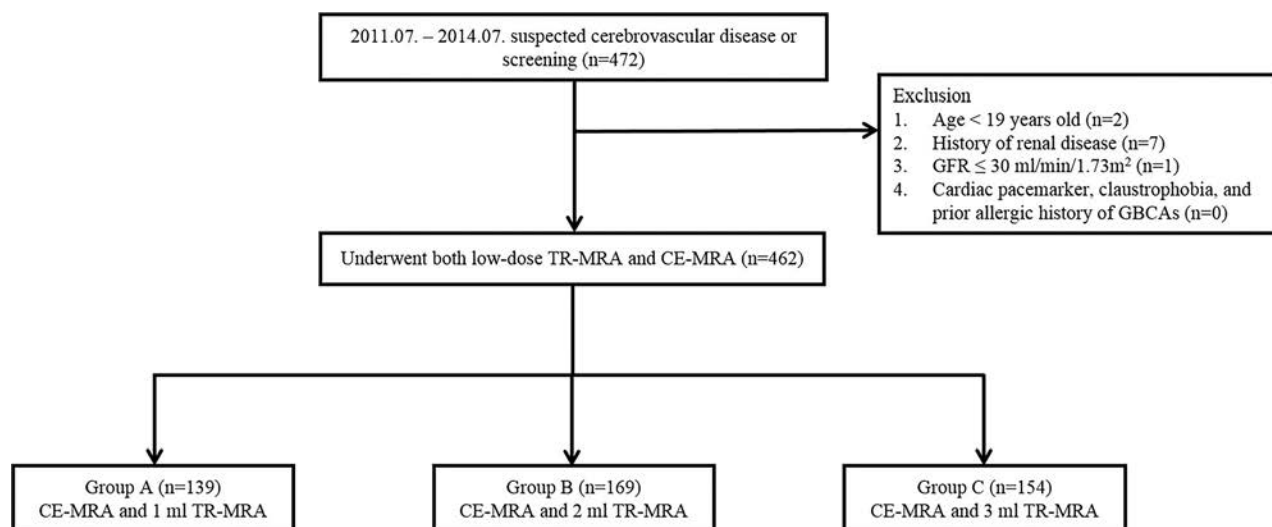


FIG 1. Flow chart of the study population.

and hemodynamic information of the supra-aortic vessels, and another advantage of TR-MRA is the requirement for low-dose GBCAs.^{2,3,16,17} Several studies have demonstrated that TR-MRA with low-dose GBCAs yields comprehensive anatomic and functional information with high sensitivity and negative predictive values.^{2,3,17–20}

The purpose of this study was to determine the appropriate minimal dose for TR-MRA to assess supra-aortic arterial stenosis with CE-MRA as a reference standard.

MATERIALS AND METHODS

Study Population

This retrospective study was approved by the institutional review board of Konkuk University Hospital, and informed consent was waived. Between July 2011 and July 2014, 462 consecutive patients underwent both standard-dose CE-MRA and low-dose TR-MRA. TR-MRA was performed with reducing GBCA doses at intervals of 1 year (3, 2, and 1 mL of 1 mmol/mL of GBCA in each year). Clinical indications for MRA included suspected stroke ($n = 231$), vertigo/dizziness ($n = 119$), headache ($n = 49$), seizure ($n = 10$), general examination ($n = 25$), visual disturbance ($n = 11$), tremor ($n = 7$), carotid stenosis ($n = 4$), aneurysm ($n = 1$), hearing difficulty ($n = 1$), tinnitus ($n = 2$), and metabolic disease ($n = 2$). All patients were classified into 3 groups by contrast dose. Group A ($n = 139$), group B ($n = 169$), and group C ($n = 154$) received a constant dose of 1, 2, and 3 mL of GBCA for TR-MRA, respectively (Fig 1). Exclusion criteria included standard contraindications to MR imaging (eg, cardiac pacemaker, claustrophobia, and prior allergic history of GBCAs), patients younger than 19 years of age, history of renal disease, and a glomerular filtration rate of <30 mL/min/1.73 m².

Image Acquisition

All examinations were performed on a 3T MR imaging system (Signa HDx; GE Healthcare, Milwaukee, Wisconsin) with a 16-channel HNS coil (GE Healthcare). All examinations were performed by experienced technicians and were supervised by experienced neuroradiologists (H.G.R. and J.W.C.).

The imaging protocol for MRA included supra-aortic TR-MRA, followed by CE-MRA. The CE-MRA imaging parameters were as follows: TR/TE = 4.5/1.5 ms, flip angle = 30°, FOV = 300 mm, matrix = 448 × 256, section thickness = 1.2 mm interpolated to 0.6 mm, bandwidth = 83.33 kHz. For CE-MRA, an automatic power injection (Spectris Solaris EP; MedRad, Indianola, Pennsylvania) of 0.1 mmol/kg body weight of gadobutrol (Gadovist; Bayer Schering Pharma, Berlin, Germany) was used at a flow rate of 3 mL/s, followed by a saline chase of 20 mL.

TR-MRA was performed by the repetitive acquisition of coronal 3D imaging slabs extending from the aortic arch to the middle cerebral artery in a caudocranial extent. The TR-MRA method used this study was the commercial technique of time-resolved imaging of contrast kinetics (TRICKS; GE Healthcare) MRA. The TRICKS MRA imaging parameters were as follows: TR/TE = 3.1/1.1 ms, flip angle = 20°, FOV = 320 mm, matrix = 320 × 192, section thickness = 2.8 mm interpolated to 0.7 mm, bandwidth = 83.33 kHz, and temporal resolution = 2.5 seconds. A constant dose of 1 mL (group A), 2 mL (group B), or 3 mL (group C) of gadobutrol was injected at a flow rate of 3 mL/s, followed by a saline flush of 20 mL. TR-MRA was initiated 12 seconds after the injection of contrast medium.

Image Analysis

Two radiologists (S.H.B. and H.S.A.) interpreted the postprocessed coronal maximum-intensity-projection images of CE-MRA and TR-MRA on a dedicated PACS station. The radiologists were blinded to clinical information and contrast agent dose protocol, but they were not blinded to the MRA techniques. Grading was mainly based on the postprocessing MIP images. When MIP images were unclear, source data were used for analysis. For qualitative analysis, the arterial system was divided into 14 segments: right brachiocephalic artery, right and left subclavian arteries, right and left common carotid arteries (CCAs), right and left extracranial internal carotid arteries, right and left intracranial ICAs, right and left vertebral artery orifices, right and left vertebral arteries, and the basilar artery.

Both CE-MRA and TR-MRA datasets were assessed for image quality. Each arterial segment was graded for image quality with a 5-point scale: 0 = failure of segmental visualization, 1 = poorly visualized with severe blurring and/or artifacts, 2 = moderate visualization with moderate blurring and/or artifacts, 3 = good segmental visualization with minimal blurring and/or artifacts, and 4 = excellent segmental depiction with sharp margins and the absence of blurring and artifacts.^{5,20} Grade 3 or 4 was considered diagnostic visualization with clear separation of the lumen from the background, whereas grades 0–2 were classified as nondiagnostic visualization. Each reader assessed the entire vessel from its origin to the termination for qualitative analysis.⁵

Contaminating venous enhancement was assessed by using a 4-point scale: 0 = no venous contamination, 1 = minimal with no influence on image interpretation, 2 = moderate limiting diagnostic confidence, and 3 = severe venous contamination with markedly limited diagnostic interpretation.

Stenosis was rated by using a 4-point scale with 0 = no stenosis, 1 = mild stenosis (<30% luminal reduction), 2 = moderate stenosis (30%–69%), and 3 = severe stenosis to occlusion ($\geq 70\%$).²¹ When ≥ 2 stenoses were detected, the most severe stenosis was selected for grading.

The signal-to-noise ratio was measured by 1 radiologist (S.H.B.). To evaluate the SNR, the ROI for the arterial segment was placed on each of 12 segmental arteries (right brachiocephalic artery, right and left subclavian arteries, right and left CCAs, right and left extracranial ICAs, right and left intracranial ICAs, right and left vertebral arteries, and the basilar artery) and the background ROI was applied at the right MCA level. The SNR was

calculated as the signal intensity of the segmental artery divided by the SD of the background noise.

Statistical Analysis

The Wilcoxon signed rank test was used to evaluate statistical differences between image quality ratings on CE-MRA and TR-MRA. The Kruskal-Wallis test was used to test for statistical differences in image quality scores assigned to the TR-MRA among the 3 groups. Agreement between CE-MRA and TR-MRA for grading of stenoses was assessed by the Spearman correlation coefficients (R). A paired t test was performed for assessment of the significant differences in SNR between CE-MRA and TR-MRA. For TR-MRA, 1-way ANOVA was used to assess the SNR among the 3 groups. Interobserver agreement for the image quality and grading of arterial stenosis between 2 readers was calculated by the κ coefficient ($\kappa = 0$, poor agreement; $\kappa = 0.01$ – 0.2 , slight agreement; $\kappa = 0.21$ – 0.40 , fair agreement; $\kappa = 0.41$ – 0.60 , moderate agreement; $\kappa = 0.61$ – 0.80 , good agreement; $\kappa = 0.80$ – 1.0 , excellent agreement). $P < .05$ was considered statistically significant. All analyses were performed by using SPSS for Windows, Version 22.0 (IBM, Armonk, New York).

RESULTS

All patients completed the examination without complications. There were no adverse effects related to the GBCAs. The characteristics of patients are shown in Table 1. Mean body weight was 63.4 kg in group A (80 men, 59 women; mean age, 60.3 ± 13.6 years), 63.9 kg in group B (94 men, 75 women; mean age, 62.2 ± 13.4 years), and 62.4 kg in group C (83 men, 71 women; mean age, 63.2 ± 14.5 years). Clinical characteristics were not significantly different among 3 groups.

Evaluation of Arterial Visualization

For group A, the mean image-quality scores in 1946 arterial segments were 3.75 (range, 1–4) for CE-MRA and 3.45 (range, 1–4) for TR-MRA. The κ coefficient revealed excellent interobserver agreement in the scoring of image quality for both CE-MRA ($\kappa = 0.985$) and TR-MRA ($\kappa = 0.972$). The distribution of scores of image quality is shown in Table 2. Except for right/left intracranial ICAs, arterial delineation scores of CE-MRA in all arterial seg-

Table 1: Demographic characteristics^a

| | Group A (1 mL) (n = 139) | Group B (2 mL) (n = 169) | Group C (3 mL) (n = 154) | P Value |
|---|--------------------------------|--------------------------------|--------------------------------|------------|
| Age (yr) | 60.3 \pm 13.6 | 62.2 \pm 13.4 | 63.2 \pm 14.5 | .184 |
| Male/female | 80:59 | 94:75 | 83:71 | .821 |
| Body weight (kg) | 63.4 \pm 11.6 | 63.9 \pm 10.3 | 62.4 \pm 10.1 | .498 |
| Contrast dose of CE-MRA (mL) | 6.3 \pm 1.2 | 6.4 \pm 1.0 | 6.2 \pm 1.0 | .498 |
| Time between CE-MRA and TR-MRA (sec) | 224 \pm 21 | 251 \pm 42 | 233 \pm 36 | .532 |

^a Data are means.

Table 2: Comparison of image quality between 2 MRA techniques in the 3 groups

| Arterial Segment | Group A | | | | | Group B | | | | | Group C | | | | |
|--------------------------------|---------|-------|--------|-------|------|---------|-------|--------|-------|-------|---------|-------|--------|-------|------|
| | CE-MRA | | TR-MRA | | P | CE-MRA | | TR-MRA | | P | CE-MRA | | TR-MRA | | P |
| | Mean | Range | Mean | Range | | Mean | Range | Mean | Range | | Mean | Range | Mean | Range | |
| Right brachiocephalic trunk | 3.96 | 3–4 | 3.58 | 2–4 | .000 | 3.97 | 3–4 | 3.91 | 3–4 | .001 | 3.97 | 3–4 | 3.93 | 3–4 | .034 |
| Right subclavian artery | 3.93 | 2–4 | 3.58 | 1–4 | .000 | 3.92 | 1–4 | 3.92 | 1–4 | .655 | 3.93 | 2–4 | 3.94 | 3–4 | .414 |
| Left subclavian artery | 3.77 | 1–4 | 3.27 | 1–4 | .000 | 3.90 | 2–4 | 3.85 | 2–4 | .050 | 3.94 | 3–4 | 3.90 | 3–4 | .058 |
| Right CCA | 3.91 | 2–4 | 3.53 | 1–4 | .000 | 3.95 | 3–4 | 3.91 | 3–4 | .052 | 3.93 | 3–4 | 3.92 | 3–4 | .655 |
| Right extracranial ICA | 3.99 | 3–4 | 3.54 | 3–4 | .000 | 3.99 | 3–4 | 3.96 | 3–4 | .059 | 3.99 | 3–4 | 4.00 | 4–4 | .317 |
| Right intracranial ICA | 3.39 | 1–4 | 3.67 | 2–4 | .000 | 3.45 | 2–4 | 3.88 | 3–4 | .000 | 3.56 | 2–4 | 3.91 | 2–4 | .000 |
| Left CCA | 3.83 | 2–4 | 3.22 | 1–4 | .000 | 3.92 | 3–4 | 3.79 | 3–4 | .000 | 3.94 | 3–4 | 3.92 | 3–4 | .180 |
| Left extracranial ICA | 3.99 | 3–4 | 3.61 | 3–4 | .000 | 3.98 | 3–4 | 3.96 | 3–4 | .180 | 3.99 | 3–4 | 4.00 | 4–4 | .157 |
| Left intracranial ICA | 3.38 | 1–4 | 3.63 | 2–4 | .000 | 3.54 | 2–4 | 3.89 | 3–4 | .000 | 3.62 | 2–4 | 3.90 | 3–4 | .000 |
| Right vertebral artery orifice | 3.79 | 1–4 | 3.33 | 1–4 | .000 | 3.74 | 2–4 | 3.75 | 2–4 | .317 | 3.77 | 3–4 | 3.78 | 3–4 | .705 |
| Right vertebral artery | 3.51 | 1–4 | 3.22 | 1–4 | .000 | 3.62 | 2–4 | 3.81 | 2–4 | .000 | 3.62 | 2–4 | 3.90 | 3–4 | .000 |
| Left vertebral artery orifice | 3.72 | 3–4 | 3.19 | 1–4 | .000 | 3.76 | 3–4 | 3.75 | 2–4 | .405 | 3.77 | 3–4 | 3.77 | 3–4 | .808 |
| Left vertebral artery | 3.55 | 1–4 | 3.20 | 2–4 | .000 | 3.68 | 2–4 | 3.79 | 2–4 | .006 | 3.72 | 2–4 | 3.90 | 2–4 | .000 |
| Basilar artery | 3.85 | 1–4 | 3.69 | 2–4 | .000 | 3.88 | 2–4 | 3.88 | 2–4 | 1.000 | 3.91 | 1–4 | 3.94 | 1–4 | .157 |

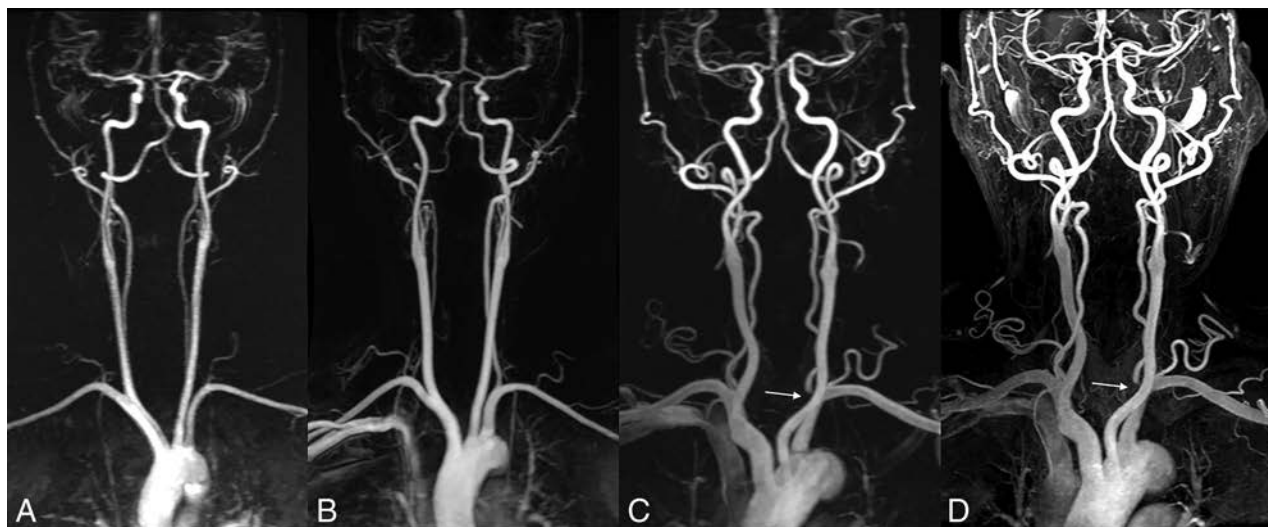


FIG 2. A, TR-MRA with 1 mL of gadobutrol with subtracted coronal MIP images shows good segmental visualization with minimal blurring or undulation of both CCAs, the extracranial ICA, and the vertebral artery. TR-MRA with 2 (B) and 3 mL (C) of gadobutrol with subtraction coronal MIP images shows clear arterial visualization. D, CE-MRA shows mild venous contamination with no influence on the diagnostic interpretation at the intracranial area. TR-MRA with 3 mL of gadobutrol (C) and CE-MRA (D) show severe stenosis of the left vertebral artery origin (arrow) in a 75-year-old man with suspected stroke.

Table 3: Distribution of venous contamination at CE-MRA and TR-MRA in the 3 groups^a

| Arterial Segment | Group A | | | | Group B | | | | Group C | | | |
|--------------------------------|---------|---------|---------|---------|---------|---------|---------|---------|---------|---------|---------|---------|
| | Grade 0 | Grade 1 | Grade 2 | Grade 3 | Grade 0 | Grade 1 | Grade 2 | Grade 3 | Grade 0 | Grade 1 | Grade 2 | Grade 3 |
| Right brachiocephalic trunk | 138/137 | 1/1 | 0/1 | 0/0 | 164/165 | 4/4 | 1/0 | 0/0 | 154/154 | 0/0 | 0/0 | 0/0 |
| Right subclavian artery | 61/118 | 77/19 | 1/2 | 0/0 | 64/123 | 104/40 | 1/6 | 0/0 | 59/115 | 93/35 | 2/4 | 0/0 |
| Left subclavian artery | 128/136 | 11/0 | 0/3 | 0/0 | 164/168 | 5/1 | 0/0 | 0/0 | 142/147 | 10/6 | 2/1 | 0/0 |
| Right CCA | 110/134 | 29/4 | 0/1 | 0/0 | 146/156 | 23/12 | 0/1 | 0/0 | 112/139 | 41/14 | 1/1 | 0/0 |
| Right extracranial ICA | 25/101 | 114/38 | 0/0 | 0/0 | 21/119 | 148/50 | 0/0 | 0/0 | 5/111 | 148/43 | 1/0 | 0/0 |
| Right intracranial ICA | 24/108 | 109/31 | 6/0 | 0/0 | 24/120 | 138/49 | 6/0 | 1/0 | 30/114 | 120/39 | 4/1 | 0/0 |
| Left CCA | 125/133 | 14/5 | 0/1 | 0/0 | 158/167 | 11/2 | 0/0 | 0/0 | 140/148 | 13/5 | 1/1 | 0/0 |
| Left extracranial ICA | 28/103 | 111/36 | 0/0 | 0/0 | 24/111 | 145/58 | 0/0 | 0/0 | 15/109 | 137/45 | 2/0 | 0/0 |
| Left intracranial ICA | 25/97 | 102/40 | 12/2 | 0/0 | 19/115 | 142/53 | 8/1 | 0/0 | 32/112 | 115/42 | 7/0 | 0/0 |
| Right vertebral artery orifice | 122/137 | 17/1 | 0/1 | 0/0 | 151/160 | 17/6 | 1/3 | 0/0 | 132/145 | 22/7 | 0/2 | 0/0 |
| Right vertebral artery | 54/112 | 84/27 | 1/0 | 0/0 | 68/139 | 101/29 | 0/1 | 0/0 | 45/126 | 104/27 | 5/1 | 0/0 |
| Left vertebral artery orifice | 132/139 | 7/0 | 0/0 | 0/0 | 166/167 | 3/1 | 0/1 | 0/0 | 143/151 | 10/3 | 0/0 | 1/0 |
| Left vertebral artery | 51/115 | 86/24 | 2/0 | 0/0 | 63/145 | 105/24 | 1/0 | 0/0 | 51/131 | 101/22 | 2/1 | 0/0 |
| Basilar artery | 29/119 | 103/16 | 6/4 | 1/0 | 51/142 | 105/25 | 13/2 | 0/0 | 36/134 | 111/20 | 7/0 | 0/0 |

^a Data are number of segments for CE-MRA/TR-MRA.

ments was higher than those of TR-MRA, and there was a statistically significant difference between the 2 techniques ($P < .000$).

For group B, mean image quality scores in 2366 arterial segments were 3.81 (range, 1–4) for CE-MRA and 3.86 (range, 1–4) for TR-MRA. The κ coefficient revealed excellent interobserver agreement in the scoring of image quality for both CE-MRA ($\kappa = 0.982$) and TR-MRA ($\kappa = 0.971$). For group C, the mean image-quality scores in a total of 2156 arterial segments were 3.83 (range, 1–4) for CE-MRA and 3.91 (range, 1–4) for TR-MRA. The κ coefficient revealed excellent interobserver agreement in the scoring of image quality for both CE-MRA ($\kappa = 0.991$) and TR-MRA ($\kappa = 0.969$). For groups B and C, most of the arterial segments had no statistically significant difference in scores of image quality between the 2 techniques ($P > .05$). However, arterial delineation scores of TR-MRA in the right/left intracranial ICAs and right/left vertebral arteries were statistically significantly higher than those of CE-MRA in groups B and C (Table 2).

With regard to TR-MRA, age, sex, and body weight-adjusted arterial delineation scores among the 3 groups were statistically different ($P < .000$). As the dose increased, the arterial delineation

scores of TR-MRA showed a tendency to improve (mean = 3.43 for group A, mean = 3.86 for group B, mean = 3.91 for group C) (Fig 2).

Evaluation of Venous Contamination

The distribution of venous contamination at CE-MRA and TR-MRA in the 3 groups is shown in Table 3. The venous contamination of CE-MRA tended to be higher than that of TR-MRA (45.9% versus 13.2% in group A, 45.8% versus 15.6% in group B, 49.2% versus 14.8% in group C). On CE-MRA, group A showed 29 (1.5%) segments, group B showed 31 (1.3%), and group C showed 35 (1.6%) segments with moderate-to-severe venous contamination, while group A showed 15 (0.8%) segments, group B showed 16 (0.7%) segments, and group C showed 12 (0.6%) segments with moderate-to-severe venous contamination on TR-MRA.

Evaluation of Arterial Stenosis

The distribution of stenosis at CE-MRA and TR-MRA in the 3 groups is shown in Table 4. Concerning the grading of arterial

Table 4: Evaluation of stenosis at CE-MRA and TR-MRA in the 3 groups

| CE-MRA | Group A TR-MRA | | | | | Group B TR-MRA | | | | | Group C TR-MRA | | | | |
|--------|----------------|----|----|----|-------|----------------|-----|----|----|-------|----------------|-----|----|----|-------|
| | 0 | 1 | 2 | 3 | Total | 0 | 1 | 2 | 3 | Total | 0 | 1 | 2 | 3 | Total |
| 0 | 1766 | 2 | 3 | 2 | 1773 | 2149 | 1 | 0 | 0 | 2150 | 1947 | 1 | 0 | 0 | 1948 |
| 1 | 6 | 57 | 4 | 0 | 67 | 0 | 98 | 2 | 0 | 100 | 1 | 102 | 1 | 0 | 104 |
| 2 | 1 | 4 | 69 | 1 | 75 | 3 | 3 | 76 | 0 | 82 | 0 | 4 | 75 | 0 | 79 |
| 3 | 0 | 0 | 0 | 31 | 31 | 0 | 0 | 0 | 34 | 34 | 1 | 0 | 0 | 24 | 25 |
| Total | 1773 | 63 | 76 | 34 | 1946 | 2152 | 102 | 78 | 34 | 2366 | 1949 | 107 | 76 | 24 | 2156 |

Table 5: Comparison of SNR between 2 MRA techniques in the 3 groups^a

| Arterial Segment | Group A | | | Group B | | | Group C | | |
|-----------------------------|--------------|--------------|------|---------------|--------------|------|---------------|---------------|------|
| | CE-MRA | TR-MRA | P | CE-MRA | TR-MRA | P | CE-MRA | TR-MRA | P |
| Right brachiocephalic trunk | 211.2 ± 50.6 | 144.0 ± 47.6 | .000 | 203.0 ± 45.3 | 211.2 ± 61.1 | .019 | 204.0 ± 116.0 | 230.8 ± 65.9 | .011 |
| Right subclavian artery | 150.8 ± 41.0 | 97.8 ± 32.0 | .000 | 144.2 ± 36.6 | 154.0 ± 81.9 | .099 | 135.2 ± 37.0 | 167.4 ± 110.7 | .000 |
| Left subclavian artery | 163.3 ± 35.3 | 100.9 ± 29.3 | .000 | 157.0 ± 34.0 | 154.0 ± 40.4 | .276 | 152.3 ± 36.6 | 174.9 ± 45.7 | .000 |
| Right CCA | 172.1 ± 45.5 | 103.9 ± 32.6 | .000 | 164.8 ± 42.1 | 156.4 ± 48.7 | .017 | 157.1 ± 44.9 | 173.8 ± 47.3 | .000 |
| Right extracranial ICA | 190.4 ± 63.9 | 107.0 ± 38.9 | .000 | 177.4 ± 53.5 | 166.4 ± 57.4 | .003 | 176.5 ± 54.5 | 193.1 ± 61.3 | .001 |
| Right intracranial ICA | 280.1 ± 77.4 | 136.3 ± 46.6 | .000 | 289.9 ± 172.2 | 226.3 ± 74.7 | .000 | 274.5 ± 71.3 | 280.1 ± 77.2 | .364 |
| Left CCA | 200.6 ± 48.8 | 112.9 ± 33.3 | .000 | 189.7 ± 45.9 | 172.2 ± 43.2 | .000 | 183.6 ± 50.1 | 200.2 ± 52.0 | .000 |
| Left extracranial ICA | 220.8 ± 66.0 | 120.1 ± 38.5 | .000 | 204.2 ± 59.3 | 184.9 ± 62.0 | .000 | 199.8 ± 61.5 | 224.1 ± 70.8 | .000 |
| Left intracranial ICA | 300.5 ± 73.2 | 144.9 ± 47.1 | .000 | 295.3 ± 63.5 | 240.4 ± 66.1 | .000 | 291.1 ± 70.8 | 301.7 ± 82.5 | .137 |
| Right vertebral artery | 165.3 ± 52.9 | 71.8 ± 27.7 | .000 | 158.4 ± 57.3 | 115.8 ± 57.9 | .000 | 158.0 ± 55.2 | 136.2 ± 56.4 | .000 |
| Left vertebral artery | 169.6 ± 60.7 | 73.7 ± 25.6 | .000 | 167.4 ± 53.8 | 122.1 ± 49.8 | .000 | 170.6 ± 55.3 | 149.1 ± 52.2 | .000 |
| Basilar artery | 223.2 ± 59.5 | 80.7 ± 29.5 | .000 | 229.9 ± 55.4 | 136.1 ± 62.8 | .000 | 230.5 ± 46.9 | 165.5 ± 54.9 | .000 |

^a Data are means.

stenosis, there was an excellent correlation between CE-MRA and TR-MRA in the 3 groups ($R = 0.957$ for group A, $R = 0.988$ for group B, $R = 0.991$ for group C; all $P < .000$). For evaluation of arterial stenosis, interobserver agreement for each MRA technique in the 3 groups indicated excellent agreement ($\kappa = 0.988-0.998$).

Vascular SNR

Table 5 presents a comparison of mean SNR between CE-MRA and TR-MRA in the 3 groups. In groups A and B, the SNR of TR-MRA tended to be significantly lower than that of CE-MRA (204.1 ± 73.3 for CE-MRA, 107.7 ± 43.7 for TR-MRA, $P < .000$ in group A; 199.0 ± 84.2 for CE-MRA, 170.8 ± 71.0 for TR-MRA, $P < .000$ in group B). The SNR was higher for TR-MRA compared with CE-MRA in group C, except for both vertebral arteries and the basilar artery (194.4 ± 77.3 for CE-MRA, 199.7 ± 82.9 for TR-MRA, $P = .004$). With regard to TR-MRA, the measured SNR was highest for group C (199.7 ± 82.9) followed by group B (170.8 ± 71.0) and group A (107.7 ± 43.7) ($P < .000$).

DISCUSSION

CE-MRA has emerged as a powerful noninvasive imaging technique for morphologic assessment of steno-occlusive disease and is widely used in clinical practice.⁵ All GBCAs approved for MRA have been considered to have a relatively wide safety margin (0.1–0.3 mmol/kg) and have been recommended as a substitute for iodine-based contrast agents in patients with reduced renal function in CTA.^{13,22} A significant association between nephrogenic systemic fibrosis and exposure or the dose of GBCAs is well-known; therefore, the use of GBCAs and iodine-based contrast agents is limited in patients with reduced renal function.⁷⁻¹¹ In the past 2 years, studies have suggested that there is a risk of gadolinium deposition in neural tissue following repeat GBCA administration in patients with

normal renal function, and a dose-dependent relationship between gadolinium administration and brain deposition has been described, though the clinical significance of gadolinium retention remains unclear.^{12,14,15,23} A number of attempts have been made to reduce the dose of GBCAs. TR-MRA can provide anatomic or hemodynamic information with a small dose of GBCA.² Therefore, given the findings of nephrogenic systemic fibrosis and gadolinium deposition in the brain, TR-MRA has the potential to be an alternative technique.¹⁶ In our study, low-dose TR-MRA with 1 mL of GBCA produced suboptimal image quality, whereas the image quality of TR-MRA with 2 or 3 mL of GBCA was comparable with that of CE-MRA. When using 3 mL, the SNR of TR-MRA was higher than that of CE-MRA. The data demonstrated that TR-MRA with only 1 mL of GBCA could be useful for detection of supra-aortic arterial stenosis.

In a previous study, TR-MRA with a full dose of GBCA was comparable with DSA for the grading of stenosis.²⁴ Lohan et al²⁰ reported that TR-MRA with 3 mL of Gd-DTPA (0.5 mmol/mL) preserved the overall image quality, whereas image quality with 1.5 mL of contrast dose was associated with more suboptimal quality. Also, Lee et al²⁵ demonstrated that TR-MRA with an injection of 0.03 mmol/kg of gadoterate meglumine was feasible and effective in the diagnosis of supra-aortic arterial stenosis. Gadobutrol is a macrocyclic and nonionic agent that has the lowest risk of nephrogenic systemic fibrosis but it can also result in neural tissue deposition.^{6,13,14,26} Similar to previous studies, our study showed that the image quality of TR-MRA with 1 mL of gadobutrol was inferior to that of CE-MRA, whereas the image quality of TR-MRA with 2 and 3 mL was not statistically different from that of CE-MRA. Several studies demonstrated that low-dose TR-MRA showed highly concordant results for the evaluation of stenosis.^{2,3,20} Our study showed complementary results. In

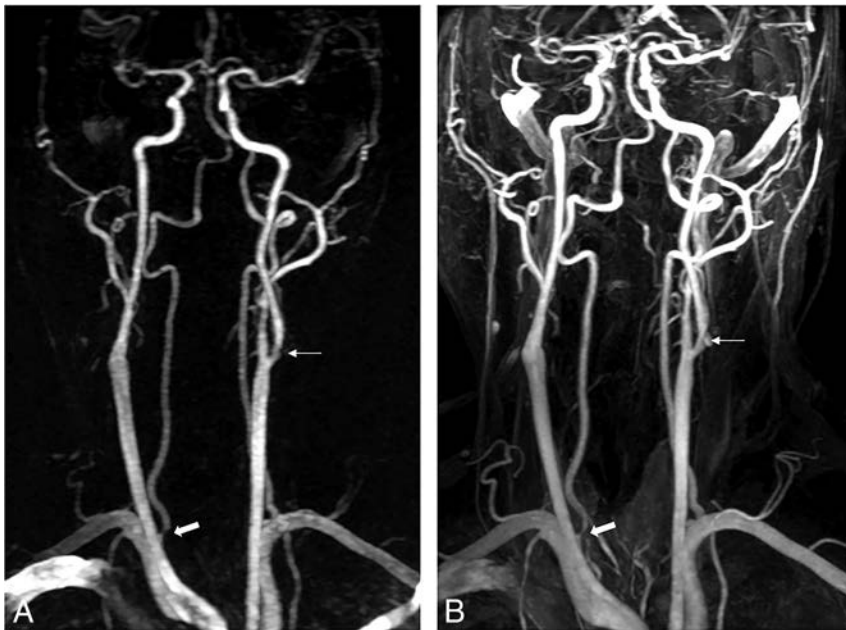


FIG 3. A 52-year-old man with suspected transient ischemic attack. TR-MRA with 1 mL of gadobutrol (A) and CE-MRA (B) show moderate stenosis at the origin of the right vertebral artery (*thick arrow*) and mild stenosis of the left proximal extracranial ICA (*thin arrow*).

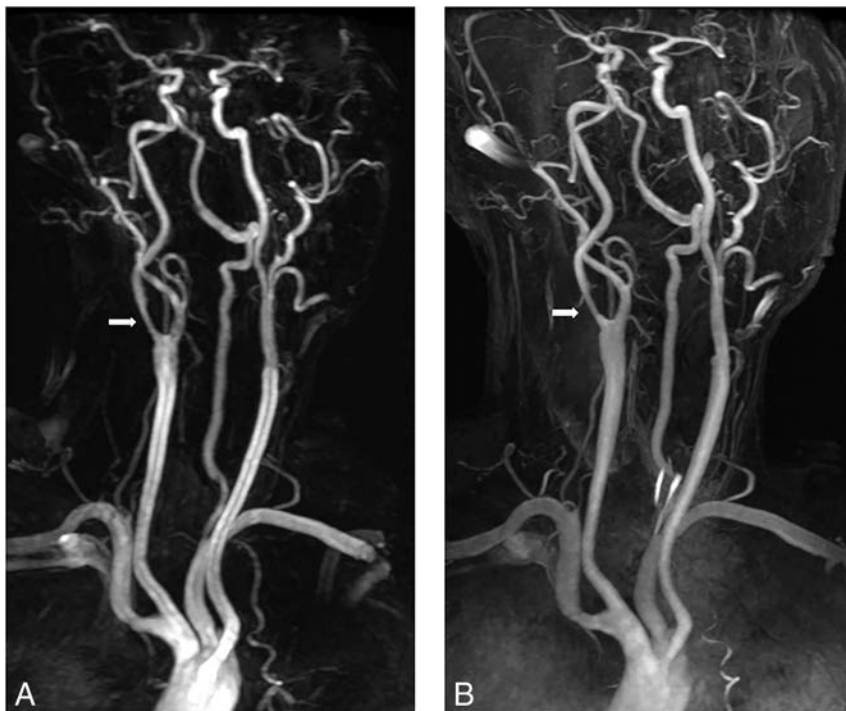


FIG 4. A 74-year-old man with suspected stroke. TR-MRA with 2 mL of gadobutrol (A) and CE-MRA (B) show moderate stenosis in the proximal extracranial ICA (*thick arrow*).

all groups, low-dose TR-MRA had good correlation for the assessment of stenosis compared with CE-MRA ($R = 0.957\text{--}0.991$) (Figs 3 and 4).

The key to the success of CE-MRA is the acquisition of the central lines of k -space during peak arterial enhancement.^{27,28} However, this is challenging because of rapid arterial-venous transit and the short duration of the arterial phase (~ 10 seconds) rather than the acquisition time for CE-MRA (~ 30 seconds).^{28,29}

On the other hand, TR-MRA enables visualization of the temporal dynamics of blood flow and captures a clear arterial phase with minimal venous contamination.^{16,30,31} Commercial TR-MRA techniques such as TRICKS, time-resolved imaging with stochastic trajectories (TWIST; Siemens, Erlangen, Germany), or 4D TR-MRA with Keyhole (4D-TRAK; Philips Healthcare, Best, the Netherlands) should provide a similar level of image quality.³² In this study, TRICKS was used. Venous contamination occurred 3 times more often on CE-MRA compared with TR-MRA. Venous contamination that influenced image interpretation was mostly seen in both the intracranial ICAs and basilar arteries on CE-MRA (Fig 2). In all 3 groups, image quality of both intracranial ICAs affected by venous enhancement was rated significantly lower for CE-MRA compared with TR-MRA ($P < .000$).

A high SNR is desirable to accurately depict arterial stenosis.²⁷ In our data, the mean SNR of TR-MRA with 1 and 2 mL of GBCA was inferior to the SNR of CE-MRA. TR-MRA effectively eliminated venous contamination, and background signal can be subtracted with the mask images.³² Thus, our study shows that the mean SNR was higher for TR-MRA with 3 mL of GBCA compared with CE-MRA (194.4 ± 77.3 for CE-MRA, 199.7 ± 82.9 for TR-MRA, $P = .004$) and an increased SNR of TR-MRA with a dose of 3 mL led to a similar score of image quality of arterial visualization compared with CE-MRA. Voth et al³³ demonstrated that full-dose gadolinium MRA results in higher SNR compared with a half dose. With regard to TR-MRA, the SNR increased as the dose increased (199.7 ± 82.9 for a dose of 3 mL, 170.8 ± 71.0 for a dose of 2 mL, and 107.7 ± 43.7 for a dose of 1 mL).

The present study has some limitations. First, the study retrospectively compared CE-MRA and TR-MRA, and TR-MRA for grading of stenosis

was not compared with DSA or CTA. CE-MRA has been validated as a credible criterion standard for supra-aortic artery imaging.^{20,25} However, CE-MRA was limited in the evaluation of some vessels. For example, CE-MRA has a tendency to overestimate arterial stenosis and has frequently shown pseudostenosis of the vertebral artery origin due to weak spatial resolution, intravoxel dephasing, and motion artifacts.³⁴ Validation in a prospective study will be necessary for comparison be-

tween low-dose TR-MRA and DSA regarding the accuracy in grading of the stenosis. However, the results of our study provide valuable information on the feasibility of low-dose TR-MRA with a relatively large number of patients. Second, there were a relatively small number of patients with stenosis because this study was retrospective and most patients underwent MRA for suspected intracranial or extracranial vascular lesions as well as screening. Third, venous contamination of CE-MRA may have been affected by previous TR-MRAs.

CONCLUSIONS

The image quality and diagnostic agreement for stenotic disease of TR-MRA were not inferior to those of CE-MRA for all 3 doses and appear better for 2- and 3-mL doses compared with a 1-mL dose. Patients with nephropathy and end-stage renal disease become more prevalent recently, and there is an increasing burden of complications associated with GBCA used for diagnosis and management of steno-occlusive disease,^{16,35} though it is unclear whether this finding is clinically significant relative to the risk of the contrast dose. TR-MRA with 2 or 3 mL of gadobutrol may be used as an alternative to CE-MRA for diagnostic techniques in high-risk populations.

REFERENCES

1. Krings T, Hans F. New developments in MRA: time-resolved MRA. *Neuroradiology* 2004;46(suppl 2):s214–22 CrossRef Medline
2. Lee YJ, Laub G, Jung SL, et al. Low-dose 3D time-resolved magnetic resonance angiography (MRA) of the supraaortic arteries: correlation with high spatial resolution 3D contrast-enhanced MRA. *J Magn Reson Imaging* 2011;33:71–76 CrossRef Medline
3. Lim RP, Shapiro M, Wang EY, et al. 3D time-resolved MR angiography (MRA) of the carotid arteries with time-resolved imaging with stochastic trajectories: comparison with 3D contrast-enhanced bolus-chase MRA and 3D time-of-flight MRA. *AJNR Am J Neuroradiol* 2008;29:1847–54 CrossRef Medline
4. Thiex R, Norbash AM, Frerichs KU. The safety of dedicated-team catheter-based diagnostic cerebral angiography in the era of advanced noninvasive imaging. *AJNR Am J Neuroradiol* 2010;31:230–34 CrossRef Medline
5. Tomasian A, Salamon N, Lohan DG, et al. Supraaortic arteries: contrast material dose reduction at 3.0-T high-spatial-resolution MR angiography—feasibility study. *Radiology* 2008;249:980–90 CrossRef Medline
6. Thomsen HS, Morcos SK, Almén T, et al; ESUR Contrast Medium Safety Committee. Nephrogenic systemic fibrosis and gadolinium-based contrast media: updated ESUR Contrast Medium Safety Committee guidelines. *Eur Radiol* 2013;23:307–18 CrossRef Medline
7. Zhang B, Liang L, Chen W, et al. An updated study to determine association between gadolinium-based contrast agents and nephrogenic systemic fibrosis. *PLoS One* 2015;10:e0129720 CrossRef Medline
8. Broome DR, Girguis MS, Baron PW, et al. Gadodiamide-associated nephrogenic systemic fibrosis: why radiologists should be concerned. *AJR Am J Roentgenol* 2007;188:586–92 CrossRef Medline
9. Collidge TA, Thomson PC, Mark PB, et al. Gadolinium-enhanced MR imaging and nephrogenic systemic fibrosis: retrospective study of a renal replacement therapy cohort. *Radiology* 2007;245:168–75 CrossRef Medline
10. Kallen AJ, Jhung MA, Cheng S, et al. Gadolinium-containing magnetic resonance imaging contrast and nephrogenic systemic fibrosis: a case-control study. *Am J Kidney Dis* 2008;51:966–75 CrossRef Medline
11. Marckmann P, Skov L, Rossen K, et al. Case-control study of gadodiamide-related nephrogenic systemic fibrosis. *Nephrol Dial Transplant* 2007;22:3174–78 CrossRef Medline
12. McDonald RJ, McDonald JS, Kallmes DF, et al. Intracranial gadolinium deposition after contrast-enhanced MR imaging. *Radiology* 2015;275:772–82 CrossRef Medline
13. Ramalho J, Semelka RC, Ramalho M, et al. Gadolinium-based contrast agent accumulation and toxicity: an update. *AJNR Am J Neuroradiol* 2016;37:1192–98 CrossRef Medline
14. Stojanov DA, Aracki-Trenkic A, Vojinovic S, et al. Increasing signal intensity within the dentate nucleus and globus pallidus on unenhanced T1W magnetic resonance images in patients with relapsing-remitting multiple sclerosis: correlation with cumulative dose of a macrocyclic gadolinium-based contrast agent, gadobutrol. *Eur Radiol* 2016;26:807–15 CrossRef Medline
15. Karabulut N. Gadolinium deposition in the brain: another concern regarding gadolinium-based contrast agents. *Diagn Interv Radiol* 2015;21:269–70 CrossRef Medline
16. Nael K, Moriarty JM, Finn JP. Low dose CE-MRA. *Eur J Radiol* 2011;80:2–8 CrossRef Medline
17. Nael K, Michaely HJ, Villablanca P, et al. Time-resolved contrast enhanced magnetic resonance angiography of the head and neck at 3.0 tesla: initial results. *Invest Radiol* 2006;41:116–24 CrossRef Medline
18. Kramer U, Fenchel M, Laub G, et al. Low-dose, time-resolved, contrast-enhanced 3D MR angiography in the assessment of the abdominal aorta and its major branches at 3 Tesla. *Acad Radiol* 2010;17:564–76 CrossRef Medline
19. Krishnam MS, Tomasian A, Lohan DG, et al. Low-dose, time-resolved, contrast-enhanced 3D MR angiography in cardiac and vascular diseases: correlation to high spatial resolution 3D contrast-enhanced MRA. *Clin Radiol* 2008;63:744–55 CrossRef Medline
20. Lohan DG, Tomasian A, Saleh RS, et al. Ultra-low-dose, time-resolved contrast-enhanced magnetic resonance angiography of the carotid arteries at 3.0 Tesla. *Invest Radiol* 2009;44:207–17 CrossRef Medline
21. Ferguson GG, Eliasziw M, Barr HW, et al. The North American Symptomatic Carotid Endarterectomy Trial: surgical results in 1415 patients. *Stroke* 1999;30:1751–58 CrossRef Medline
22. Bonvento MJ, Moore WH, Button TM, et al. CT angiography with gadolinium-based contrast media. *Acad Radiol* 2006;13:979–85 CrossRef Medline
23. Stojanov D, Aracki-Trenkic A, Benedeto-Stojanov D. Gadolinium deposition within the dentate nucleus and globus pallidus after repeated administrations of gadolinium-based contrast agents—current status. *Neuroradiology* 2016;58:433–41 CrossRef Medline
24. Remonda L, Senn P, Barth A, et al. Contrast-enhanced 3D MR angiography of the carotid artery: comparison with conventional digital subtraction angiography. *AJNR Am J Neuroradiol* 2002;23:213–19 Medline
25. Lee YJ, Kim BS, Koo JS, et al. Supra-aortic low-dose contrast-enhanced time-resolved magnetic resonance (MR) angiography at 3 T: comparison with time-of-flight MR angiography and high-resolution contrast-enhanced MR angiography. *Acta Radiol* 2015;56:673–80 CrossRef Medline
26. Haneder S, Kucharczyk W, Schoenberg SO, et al. Safety of magnetic resonance contrast media: a review with special focus on nephrogenic systemic fibrosis. *Top Magn Reson Imaging* 2015;24:57–65 CrossRef Medline
27. Carroll TJ, Korosec FR, Petermann GM, et al. Carotid bifurcation: evaluation of time-resolved three-dimensional contrast-enhanced MR angiography. *Radiology* 2001;220:525–32 CrossRef Medline
28. Du J, Fain SB, Korosec FR, et al. Time-resolved contrast-enhanced carotid imaging using undersampled projection reconstruction acquisition. *J Magn Reson Imaging* 2007;25:1093–99 CrossRef Medline
29. Watts R, Wang Y, Redd B, et al. Recessed elliptical-centric view-ordering for contrast-enhanced 3D MR angiography of the carotid arteries. *Magn Reson Med* 2002;48:419–24 CrossRef Medline
30. Raoult H, Ferré JC, Morandi X, et al. Quality-evaluation scheme for cerebral time-resolved 3D contrast-enhanced MR angiography techniques. *AJNR Am J Neuroradiol* 2010;31:1480–87 CrossRef Medline

31. Riederer SJ, Haider CR, Borisch EA, et al. **Recent advances in 3D time-resolved contrast-enhanced MR angiography.** *J Magn Reson Imaging* 2015;42:3–22 [CrossRef Medline](#)
32. Choi JW, Roh HG, Moon WJ, et al. **Time-resolved 3D contrast-enhanced MRA on 3.0T: a non-invasive follow-up technique after stent-assisted coil embolization of the intracranial aneurysm.** *Korean J Radiol* 2011;12:662–70 [CrossRef Medline](#)
33. Voth M, Michaely HJ, Schwenke C, et al. **Contrast-enhanced magnetic resonance angiography (MRA): evaluation of three different contrast agents at two different doses (0.05 and 0.1 mmol/kg) in pigs at 1.5 Tesla.** *Eur Radiol* 2011;21:337–44 [CrossRef Medline](#)
34. Kim S, Lee S, Choi HS, et al. **Pseudostenosis at the origin of the vertebral artery on contrast-enhanced MRA: correlation with aortic motion on dynamic 3D time-resolved contrast-enhanced MRA.** *J Korean Society of Magnetic Resonance in Medicine* 2012;16:236–42
35. Nael K, Krishnam M, Ruehm SG, et al. **Time-resolved MR angiography in the evaluation of central thoracic venous occlusive disease.** *AJR Am J Roentgenol* 2009;192:1731–38 [CrossRef Medline](#)

TIPIC Syndrome: Beyond the Myth of Carotidynia, a New Distinct Unclassified Entity

¹A. Lecler, ¹M. Obadia, ¹J. Savatovsky, ¹H. Picard, ¹F. Charbonneau, ¹N. Menjot de Champfleury, ¹O. Naggara, ¹B. Carsin, ¹M. Amor-Sahli, ¹J.P. Cottier, ¹J. Bensoussan, ¹E. Auffray-Calvier, ¹A. Varoquaux, ¹S. De Gaalon, ¹C. Calazel, ¹N. Nasr, ¹G. Volle, ¹D.C. Jianu, ¹O. Gout, ¹F. Bonneville, and ¹J.C. Sadik



ABSTRACT

BACKGROUND AND PURPOSE: The differential diagnosis of acute cervical pain includes nonvascular and vascular causes such as carotid dissection, carotid occlusion, or vasculitis. However, some patients present with unclassified vascular and perivascular changes on imaging previously reported as carotidynia. The aim of our study was to improve the description of this as yet unclassified clinico-radiologic entity.

MATERIALS AND METHODS: From January 2009 through April 2016, 47 patients from 10 centers presenting with acute neck pain or tenderness and at least 1 cervical image showing unclassified carotid abnormalities were included. We conducted a systematic, retrospective study of their medical charts and diagnostic and follow-up imaging. Two neuroradiologists independently analyzed the blinded image datasets.

RESULTS: The median patient age was 48 years. All patients presented with acute neck pain, and 8 presented with transient neurologic symptoms. Imaging showed an eccentric pericarotidian infiltration in all patients. An intimal soft plaque was noted in 16 patients, and a mild luminal narrowing was noted in 16 patients. Interreader reproducibility was excellent. All patients had complete pain resolution within a median of 13 days. At 3-month follow-up, imaging showed complete disappearance of vascular abnormalities in 8 patients, and a marked decrease in all others.

CONCLUSIONS: Our study improved the description of an unclassified, clinico-radiologic entity, which could be described by the proposed acronym: Transient Perivascular Inflammation of the Carotid artery (TIPIC) syndrome.

ABBREVIATIONS: PVI = perivascular infiltration; TIPIC = Transient Perivascular Inflammation of the Carotid artery; US = ultrasonography

Carotidynia was a clinical entity described by Fay in 1927,¹ characterized by tenderness and pain at the level of the carotid bifurcation. Initially classified as an idiopathic neck pain

syndrome in the first International Classification of Headache Disorders in 1988,² it was subsequently removed as a distinct entity in 2004.³ Indeed, the 2 clinical signs of carotidynia were neither specific nor constant, and other causes of neck pain might have the same clinical presentation. Biousse and Bousser⁴ described these controversial aspects in 1994 and considered carotidynia a myth.


However, since 2000, a few case reports have described imaging abnormalities in patients presenting with tenderness and pain at the level of the carotid bifurcation. Imaging techniques like ultrasonography (US),^{5,6} MR imaging,⁷ CT angiography, [¹⁸F] fluorodeoxyglucose positron-emission tomography,^{8,9} or associated modalities¹⁰ showed abnormal soft tissue surrounding the carotid artery and a thickened carotid wall, especially near its bifurcation. Differential diagnoses of carotid pain such as carotid

Received November 23, 2016; accepted after revision March 5, 2017.

From the Departments of Radiology (A.L., J.S., F.C., J.C.S.), and Neurology (M.O., G.V., O.G.), and Clinical Research Unit (H.P.), Fondation Ophtalmologique Adolphe de Rothschild, Paris, France; Department of Neuroradiology (N.M.d.C.), Montpellier University Hospital Center, Gui de Chauliac Hospital, Montpellier, France; Department of Radiology (B.C.), Centre Hospitalier Régional Universitaire de Rennes, Rennes, France; Department of Neuroradiology (O.N.), Centre Hospitalier Sainte-Anne, Paris, France; Department of Neuroradiology (M.A.-S.), Pitié-Salpêtrière Hospital, Paris, France; Centre D'imagerie Médicale Tourville (M.A.-S.), Paris, France; Department of Radiology (J.P.C.), Centre Hospitalier Régional Universitaire de Tours, Tours, France; Brain and Imaging Laboratory Unite Mixte de Recherche U930 (J.P.C.), Institut National de la Santé et de la Recherche Médicale, François-Rabelais University, Tours, France; Diagnostic and Interventional Neuroradiology Department (E.A.-C.) and Neurology Department (S.D.G.), Hôpital René et Guillaume-Laënnec, Centre Hospitalier Universitaire de Nantes, Saint-Herblain, France; Department of Radiology (J.B.), Hotel-Dieu Hospital, Paris, France; Department of Radiology (A.V.), Conception Hospital, Aix-Marseille University, Marseille, France; Departments of Neuroradiology (C.C., F.B.) and Neurology (N.N.), Hôpital Pierre-Paul-Riquet, Centre Hospitalier Universitaire Purpan, Toulouse, France; and Department of Neurology (D.C.J.), Victor Babes University of Medicine and Pharmacy, Timisoara, Romania.

Paper previously presented at: European Congress of Radiology, March 2–6, 2016; Vienna, Austria.

Please address correspondence to Augustin Lecler, MD, Department of Radiology, Fondation Ophtalmologique Adolphe de Rothschild, 25 Rue Manin, 75019 Paris, France; e-mail: alecler@for.paris

 Indicates article with supplemental on-line tables.

<http://dx.doi.org/10.3174/ajnr.A5214>

dissection, thyroiditis, vasculitis, head and neck inflammation or mass, sialadenitis, or cervical arthrosis were excluded. Hence, the authors suggested that a distinct entity of idiopathic carotid inflammation seemed to exist after all.

The goal of our study was to improve the clinico-radiologic description of this unclassified entity among patients presenting with acute neck pain and abnormal carotid and pericarotidian tissues on imaging.

MATERIALS AND METHODS

Research Design

We conducted a retrospective multicenter systematic chart review in centers specialized in head-and-neck and neurologic diseases. This study was approved by the institutional research ethics boards. All patients were contacted and given the opportunity to express their refusal to have their medical records used. This study follows the Strengthening the Reporting of Observational Studies in Epidemiology guidelines.¹¹

Patients

Two physicians, a senior neuroradiologist and a neurologist, both of whom are specialized in neurovascular diseases with 30 years of experience each (J.C.S. and M.O.), screened the clinical and radiologic files of all adult patients from 10 centers who presented from January 2009 through April 2016 with acute cervical pain and with at least 1 diagnostic image (MR imaging, CT, or US) including a dedicated vessel analysis. Among patients fulfilling these criteria, they excluded cases with inadequate or incomplete vessel exploration, cases with no vascular abnormality, and those in which a clearly identified and classified vascular disease was found. The final number of patients from these centers was 47, who all had symptomatology appropriate for the diagnosis of carotidynia and represent the study group.

Review of Clinical and Biologic Charts

Patient charts were systematically reviewed, and we collected the following clinical data: the date that pain began; the presence of major cardiovascular risk factors; medical history; medications; unilateral or bilateral cervical pain (as well as location, side, and pain scale score); a cervical swelling or a palpable abnormality over the carotid bifurcation; the presence of lymphadenopathy; the presence of associated head, neck, neurologic, or ophthalmologic symptoms; the treatment administered and its duration; the duration of pain; report of ≥ 1 relapse during follow-up; and the total duration of follow-up. All relevant biologic data on admission and during follow-up were collected. The following relevant biologic data were recorded on admission and during follow-up for all patients in the first center (A.Rotschild Foundation's Department of Radiology): erythrocyte sedimentation rate; C-reactive protein level; complete blood count; herpes simplex virus, varicella zoster virus, Epstein-Barr virus, chlamydia, mycoplasma, influenza, human immunodeficiency virus, hepatitis B virus, hepatitis C virus, Lyme disease, type 1 human T-cell lymphotropic virus, and syphilis serologies, including immunoglobulin-M and immunoglobulin-G; renal function; electrolyte level; glycemia; serum cholesterol level; comprehensive hepatic work-up; coagulation test; serum protein electrophoresis; thyroid hor-

mone level; autoimmune markers; angiotensin-converting enzyme level; and antineutrophil cytoplasmic antibody. The minimal biologic data recorded in the other centers included erythrocyte sedimentation rate, C-reactive protein level, complete blood count, renal function, electrolytes, glycemia, serum cholesterol level, comprehensive hepatic work-up, and coagulation test.

Diagnostic and Follow-Up Imaging Modalities

US was performed with Logic E9 (GE Healthcare, Milwaukee, Wisconsin) and Xario XG (Toshiba, Tokyo, Japan) machines. Cervical and intracranial vessels were examined in B-mode and color-coded duplex with spectrum analysis.

CTA examinations were performed with a Discovery 750 HD 64-section scanning system (GE Healthcare) in the first center, and with Discovery 750 HD 64-section or LightSpeed VCT 32-section (GE Healthcare) or Somatom 16-section (Siemens, Erlangen, Germany) scanners in the other centers.

MR imaging examinations were performed with a 3T Ingenia or a 1.5T Achieva imager (Philips Healthcare, Best, the Netherlands) with a 32-channel head coil covering the bifurcation in the first center and with 3T Skyra, 1.5T Avanto, 1.5T Sonata, 3T Verio (Siemens, Erlangen, Germany), 1.5T Signa Excite (GE Healthcare), or 3T Achieva (Philips Healthcare) scanners in the other centers.

Technical data are provided for the first center in On-line Tables 1 and 2.

Imaging Reading Criteria

Two neuroradiologists (A.L. and F.C. with 7 and 12 years of experience, respectively) independently analyzed the datasets in random order. The readers were blinded to the clinical and biologic data. Discrepancies were resolved by consensus.

For each diagnostic and follow-up imaging technique, the readers assessed the abnormalities as the following:

The presence of a perivascular infiltration (PVI) was defined as soft amorphous tissue replacing the fat surrounding the carotid artery, with a hazy aspect of the fat; its precise location; its dimensions (including largest axial diameter and span); its preferential side; the percentage of vessel circumference involvement; and the confidence in detecting the abnormalities (0 = very low level of confidence, 1 = relatively high confidence, 2 = extremely high confidence).

The presence of vascular abnormalities, such as an intimal soft plaque, defined as a well-delineated intimal plaque, hypoechogenic without posterior acoustic shadowing in US, hypodense or hypointense compared with a normal-sized lymph node on CT or MR imaging, respectively; or a calcified plaque, defined as a hyperechogenic intimal plaque with posterior acoustic shadowing on US, isodense to the bone in CT, with no signal on MR imaging; or the presence of a lumen caliber narrowing, and its quantification by using the North American Symptomatic Carotid Endarterectomy Trial criteria.¹²

For US, the readers assessed the presence of a vascularization of the PVI in Doppler or power Doppler mode and the presence of cervical carotid or intracranial vessel hemodynamic changes.

For MR imaging results, the readers assessed the fat-suppressed T1- and T2-weighted imaging signal intensity of the PVI

Table 1: Characteristics of patients

| Characteristics | Patients | % |
|--|--------------|------|
| No. of patients | 47 | |
| No. of carotid arteries | 49 | |
| Sex ratio (women/men) | 27/18; 1.5:1 | |
| Median age (yr) (IQR) | 48 (39–56) | |
| At least 1 vascular risk factor | 22 | 47% |
| High blood pressure | 8 | 17% |
| Dyslipidemia | 3 | 6% |
| Mellitus diabetes | 0 | 0% |
| Smoking | 19 | 40% |
| History of autoimmune disease | 8 | 17% |
| History of vascular event | 2 | 4% |
| Recent history of viral episode | 2 | 4% |
| Recent history of cervical chiropractic manipulation | 0 | 0% |
| Recent history of cervical trauma | 1 | 2% |
| Acute neck tenderness or cervical pain | 47 | 100% |
| Affected side (left/right) | 28/21 | |
| Bilateral involvement | 2 | 4% |
| Median pain intensity (10-point scale) (IQR) | 5 (3–6) | |
| Cervical swelling or palpable abnormality over the carotid bifurcation | 6 | 13% |
| Enlarged lymph nodes at palpation | 8 | 17% |
| Fever | 2 | 4% |
| Flu-like symptoms | 1 | 2% |
| Neurologic-associated symptoms | 8 | 17% |
| No abnormal biologic test findings | 42 | 89% |
| Biologic inflammatory syndrome (elevated ESR or CRP) | 3 | 6% |
| Positive serum IgM | 2/18 | 11% |
| Treatments | 37 | 79% |
| Anti-inflammatory treatment | 34 | 72% |
| Steroids | 3 | 6% |
| Follow-up | 47 | 100% |
| Median follow-up duration (days) (IQR) | 163 (88–354) | |
| Full clinical recovery (SD) | 47 | 100% |
| Mean recovery delay (days) (IQR) | 13 (10–15) | |
| Relapse | 9 | 19% |
| Median delay before relapse (mo) | 6 | |
| Persistence of abnormal laboratory test findings | 0 | 0% |

Note:—ESR indicates erythrocyte sedimentation rate; CRP, C-reactive protein; IgM, immunoglobulin-M; IQR, interquartile range.

compared with a contralateral normal-sized lymph node (1 = less intense, 2 = as intense, 3 = more intense) and the presence of cerebral ischemic lesions with diffusion-weighted imaging and fluid-attenuated inversion recovery sequences.

For CTA and MR imaging, the readers assessed the enhancement of the PVI compared with a contralateral normal-sized lymph node (0 = no enhancement, 1 = less enhancement, 2 = same enhancement, 3 = more enhancement) and the presence of inflammation of the pharyngeal or laryngeal mucosa.

Statistical Analysis

Results of systematic reviews were encoded on a spreadsheet and subsequently analyzed by a senior medical biostatistician (H.P.) with the R statistical package.¹³ Due to the descriptive design of this study, the analysis was focused on the description of patients' sociodemographic, clinical, biologic, and imaging characteristics. Interobserver agreement was assessed with nonweighted κ statistics, by using the Landis and Koch interpretation.¹⁴ Whenever quantitative imaging variables were measured with different imaging modalities, Bland-Altman plots were used to look for an intermodality measurement bias. A linear regression was conducted to evaluate the correlation between the symptom-to-

imaging delay and the following parameters: the percentage of arterial circumference involved, the presence of a lumen caliber narrowing and its severity, the PVI median largest diameter and median span, and the presence of a soft intimal plaque. A *P* value below .05 was considered significant.

RESULTS

Demographic, Clinical, and Biologic Characteristics

Forty-seven patients presented with cervical pain, including 45 with unilateral pain and 2 with bilateral pain. The mean patient age was 48 years, and the female/male ratio was 1.5:1. Twenty-two patients (47%) had at least 1 vascular risk factor. Eight patients (17%) had associated neurologic symptoms: transient dizziness and vertical diplopia with extrinsic ipsilateral oculomotor cranial nerve palsy in 1 patient, a contralateral-sided dysesthesia in 4 patients, a contralateral transient motor deficit in 1 patient, and an ipsilateral peripheral facial palsy in 2 patients. Two patients had fever. Eight patients (17%) had a clinical history of autoimmune disease: Two had ankylosing spondylarthritis, 1 had Hashimoto thyroiditis, 1 had Graves disease, 1 had systemic lupus erythematosus, 1 had Sjögren syndrome, and 2 had rheumatoid arthritis. Three patients overall (6%) had elevated erythrocyte sediment ratios or C-re-

active protein levels but normal blood counts. Two of eighteen (11%) had elevated serum immunoglobulin-M antibodies: against herpes simplex virus for 1 patient and against type B-influenza for the other. No other patients presented with an elevation in inflammatory markers (Table 1).

Diagnostic Imaging

The median delay between the onset of symptoms and the first imaging was 5 days. All patients except 4 presented with a PVI at the level of the carotid bifurcation, most often in a posterior and lateral location (Fig 1). Two patients presented with bilateral carotid abnormalities. The median largest axial diameter of the PVI ranged from 4 to 5 mm, and the median PVI span ranged from 15 to 28 mm. Self-assessed confidence in investigator detection was high in all examinations performed with US or MR imaging and in 69% of the CT reviews. An intimal soft plaque was observed in 14 US reviews (58%), 6 CT reviews (46%), and 12 MR imaging reviews (27%) (Fig 2). A mild lumen caliber narrowing was observed in US reviews of 9 patients (38%), CT reviews of 4 patients (31%), and MR imaging reviews of 12 patients (27%). No hemodynamic change was

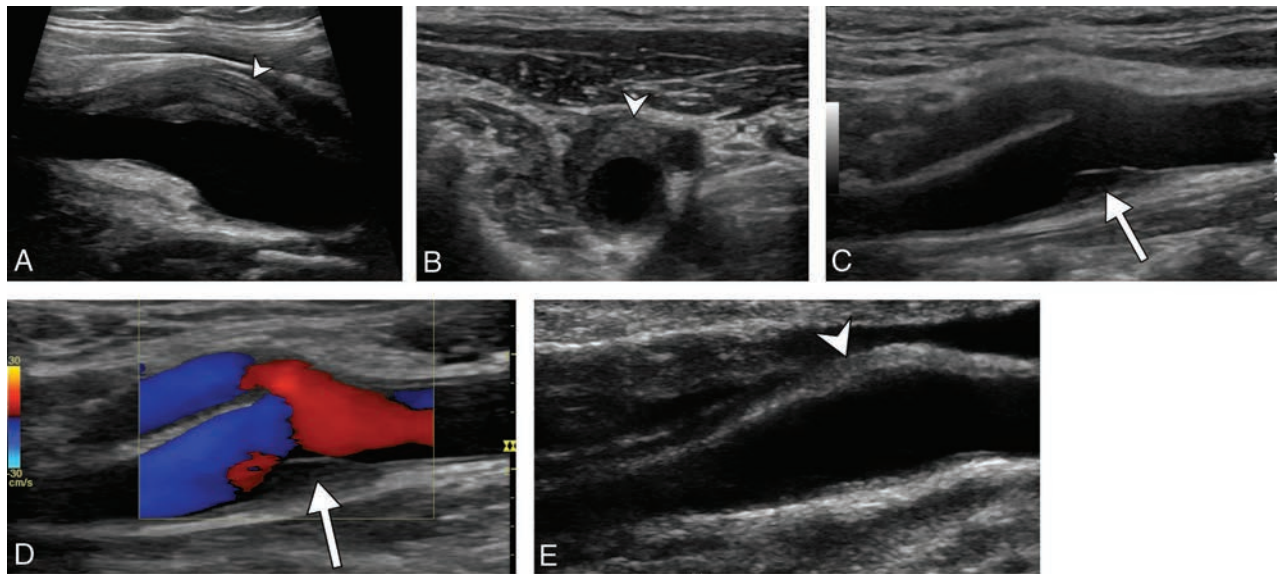


FIG 1. Diagnostic ultrasonography (A–D) shows an eccentric perivascular infiltration (arrowhead) at the level of bifurcation, with a soft intimal plaque (arrow) and a mild lumen narrowing without a hemodynamic change in Doppler mode. Follow-up ultrasonography (E) shows a marked decrease in the perivascular infiltration (arrowhead) and complete disappearance of the soft intimal plaque.



FIG 2. CTA shows a left posterolateral eccentric perivascular infiltration (arrowhead) surrounding the carotid artery, with a distinct low-density soft intimal plaque (arrow).

observed in color duplex Doppler. No cerebral parenchymal ischemia was seen with MR imaging.

Diagnostic imaging data are presented in Table 2.

Follow-Up

The mean follow-up duration was 3 months. All patients had a full clinical recovery, with a median delay of 13 days. Thirty-four patients received anti-inflammatory treatment, and 3 received steroids. Ten patients did not receive any treatment. Nine (19%) patients had a clinical relapse with exactly the same clinical and imaging abnormalities. Seven of these patients had a clinical history of autoimmune disease, and they presented with a simultaneously acute exacerbation of their autoimmune disease. All laboratory test results were within normal ranges during follow-up.

Twenty-five patients (53%) had follow-up imaging. Eleven (44%) had US, and 23 (92%) had MR imaging. No CTA was performed. All patients presented with a decrease or disappear-

ance of the PVI; a residual PVI was noted in all patients with US and 15 patients (65%) with MR imaging (Fig 3). Eight patients had complete disappearance of PVI on MR imaging. The median PVI diameter and span decrease ranged from 55% to 61% and 50% to 62%, respectively. Soft intimal plaque was persistent in 4 and 3 patients with US and MR imaging, respectively, and disappeared in 4 patients with US and 6 with MR imaging. Lumen caliber narrowing was persistent in 2 patients with US and 1 patient with MR imaging, respectively (Fig 4).

Follow-up imaging data are presented in Table 3.

Interobserver Agreement

Overall interobserver agreement was perfect ($\kappa = 1$) for the detection of a PVI, excellent for the PVI largest diameter or lumen caliber narrowing with US or MR imaging ($\kappa = 0.9$ and 0.83 , respectively), and good for the detection of soft intimal plaque ($\kappa = 0.75$). CT showed a smaller interobserver agreement for lumen caliber narrowing and the presence of soft intimal plaque ($\kappa = 0.6$ and 0.71 , respectively).

Associations with Symptom-to-Imaging Delay

There was a significant correlation between a longer symptom-to-imaging delay and a lower PVI median span ($P = .02$ and $P = .04$) and a lower PVI median largest diameter ($P = .04$) on sonography and a lower PVI median span ($P = .04$) on MR imaging. There was no significant correlation between the symptom-to-imaging delay and the presence of a lumen caliber narrowing or a soft intimal plaque or the percentage of the arterial circumference involved.

DISCUSSION

We report a multicenter series of 47 patients presenting with acute neck pain and strikingly similar unclassified perivascular and vascular abnormalities seen on imaging. These findings strongly support the existence of an as yet unclassified clinico-radiologic entity

Table 2: Diagnostic imaging data

| Characteristics | US | % | CT | % | MRI | % |
|---|------------|------|--------------|------|--------------|------|
| No. of patients | 23 | 49% | 13 | 28% | 43 | 91% |
| No. of carotid arteries | 24 | 49% | 13 | 27% | 45 | 92% |
| Median delay between onset of symptoms and diagnostic exam (days) (IQR) | | | 5 (3–7.5) | | | |
| High confidence in diagnosis | 24 | 100% | 9 | 69% | 45 | 100% |
| Preferential side of PVI: lateral/medial | | | 39/10: 3.9 | | | |
| Preferential side of PVI: posterior/anterior | | | 38/11: 3.5 | | | |
| Localization of PVI: carotid bifurcation | 23 | 96% | 12 | 92% | 41 | 91% |
| Circumferential | 0 | 0% | 0 | 0% | 2 | 4% |
| Percentage of carotid circumference involved (%) (IQR) | 40 (30–40) | | 30 (20–40) | | 40 (30–57.5) | |
| PVI | 24 | 100% | 13 | 100% | 45 | 100% |
| Pericarotid fat stranding | 24 | 100% | 13 | 100% | 45 | 100% |
| Lumen caliber narrowing | 9 | 38% | 4 | 31% | 12 | 27% |
| Mean percentage of carotid stenosis (%) (IQR) | 30 (20–30) | | 22.5 (18–26) | | 20 (14–30) | |
| Mean PVI span (mm) (IQR) | 15 (10–22) | | 15 (10–26) | | 28 (17–34) | |
| Median PVI largest diameter (mm) | 4 (2.4–6) | | 4 (3.6–4.8) | | 5 (4–7) | |
| Soft intimal plaque | 14 | 58% | 6 | 46% | 12 | 27% |
| Enlarged lymph nodes | 8 | 33% | 0 | 0% | 8 | 18% |
| PVI enhancement | NA | | 11 | 85% | 45 | 100% |
| Laryngeal or pharyngeal inflammation | 0 | 0% | 0 | 0% | 1 | 2% |

Note:—IQR indicates interquartile range; NA, not applicable.

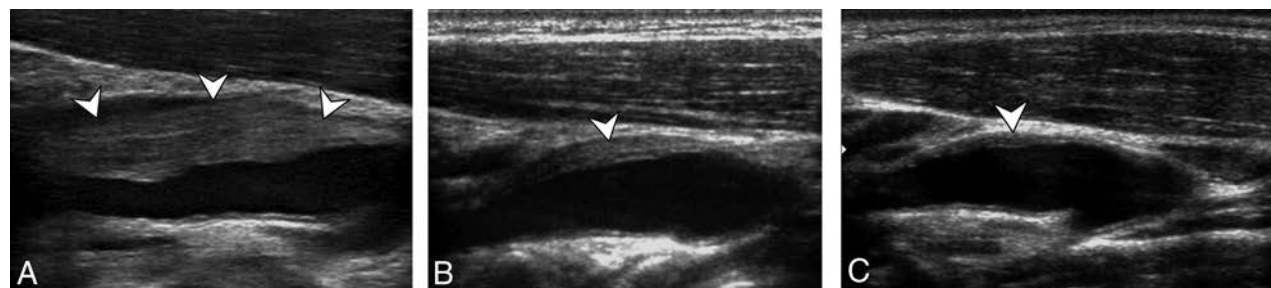


FIG 3. Initial diagnostic ultrasonography (A) and follow-up ultrasonography at 14 days (B) and 6 months (C) show a perivascular infiltration (arrowheads) at the level of the internal carotid artery just at the level of bifurcation, with a quick decrease at 14 days and the persistence of a thin abnormality at 6 months.

classically diagnosed as “carotidynia” in the literature dated before 2004.

Clinical and Imaging Characteristics

This entity was relatively rare in our study, with an estimated prevalence of 2.8% (18/654) among patients with acute neck pain in the first center. However, we can presume that this particular cluster of symptoms is underestimated because of the relatively mild clinical symptoms and the quick relief of pain and decrease of imaging abnormalities within 13 days. This entity has been previously reported on in a few small series as carotidynia, but we present the largest series published so far with 3 distinct imaging modalities and follow-up data.

Clinically, all our patients presented with acute pain directly around the level of the carotid bifurcation. Eight patients presented with previously undescribed, transient neurologic symptoms, which lacked explanation despite a brain parenchyma MR imaging. After imaging, the presence of a unilateral eccentric PVI at the level of bifurcation was the most striking feature described.^{6,7,10} Two patients presented with bilateral carotid involvement,⁹ though most were unilateral.^{6,7} PVI imaging characteristics were similar to those found in the literature, with a median diameter of 5 mm and a median span of 20 mm.^{7,15}

Some patients had a mild associated narrowing of the lumen,^{6,16} though most patients had no luminal change^{7,10} or any hemodynamic abnormality.

We report the presence of a self-limited, intimal soft plaque in half of our patients, which has been described in previous reports.^{6,17} These intimal changes might be induced by the healing phase of the carotid inflammatory process.

Nonsteroidal anti-inflammatory agents and high doses of aspirin were the most frequent treatment in our population and in the literature, with a complete median delay of pain relief in 13 days.^{5–7} Some authors reported full recovery with clopidogrel⁸ or without any treatment at all.⁷ All patients had complete clinical resolution during follow-up. Nine patients presented with ≥ 1 relapse with intervals ranging from 1 to 6 months, similar to what is found in the literature.¹⁸

Although early case reports described the complete disappearance of clinical and imaging abnormalities,⁷ more recent case reports showed a persistence of imaging abnormalities, similar to our findings.^{6,17,19} It could be explained by the development of early fibrosis associated with low-grade chronic active inflammation, as described in the only histologic study found during the literature review.²⁰

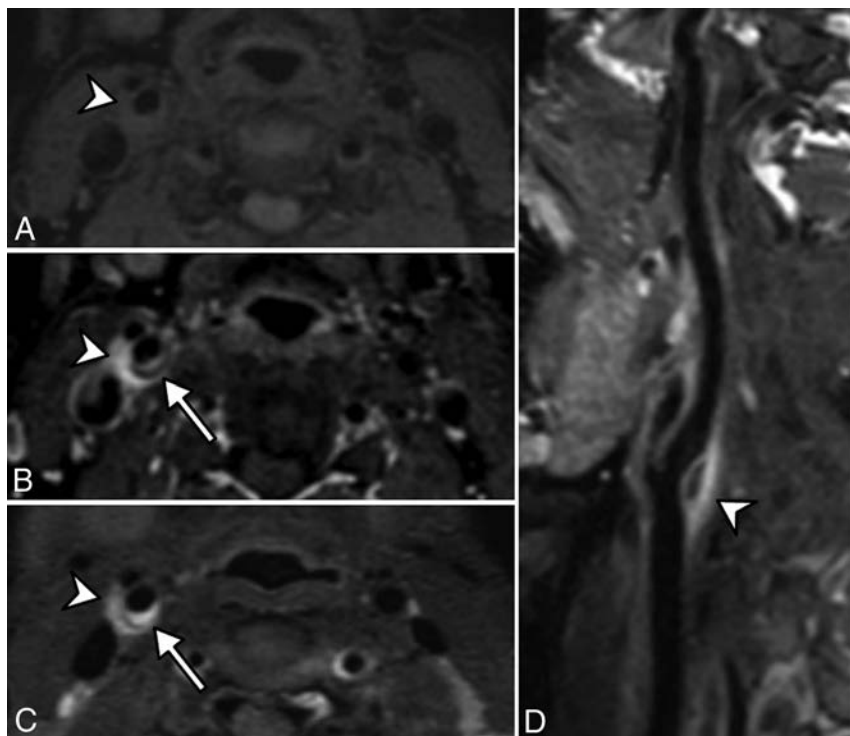


FIG 4. Pre (A) and post (B) contrast fat-suppressed 3D T1 and 3D T2-weighted (C) MR imaging in an axial plane shows T1 hypointense and T2 hyperintense perivascular infiltration (arrowhead) at the level of the carotid artery bifurcation, enhanced after gadolinium injection. A distinct soft intimal plaque (arrow) is visible at the posterior part of the carotid artery. A sagittal curvilinear reconstruction of the right internal carotid artery on the postcontrast T1-weighted imaging (D) shows the PVI (arrowhead) centered at the level of the right carotid artery bifurcation and extended to both the distal common carotid artery and proximal internal carotid artery. Note that there is no vascular or perivascular abnormality involving other parts of the common or the internal carotid arteries.

Table 3: Follow-up imaging data

| Characteristics | US | % | MRI | % |
|--|---------------|---------------|---------------|-----|
| No. of patients | 11 | 44% | 23 | 51% |
| Median delay between onset of symptoms and follow-up exam (days) (IQR) | | 89 (71.5–171) | | |
| PVI | 11 | 100% | 15 | 65% |
| Complete PVI disappearance | 0 | 0% | 8 | 35% |
| PVI decrease | 11 | 100% | 15 | 65% |
| PVI stability | 0 | 0% | 0 | 0% |
| PVI increase | 0 | 0% | 0 | 0% |
| Lumen caliber narrowing | 2 | 18% | 1 | 4% |
| Median PVI largest diameter (mm) (IQR) | 1.5 (0.9–2.4) | | 2.9 (2.0–3.5) | |
| Median decrease of the PVI largest diameter | 61% | | 55% | |
| Median PVI span (mm) (IQR) | 9 (5–10) | | 13 (9.5–16) | |
| Median decrease of the PVI span | 62% | | 50% | |
| Persistence of a soft intimal plaque | 4 | 50% | 3 | 33% |
| Disappearance of a soft intimal plaque | 4 | 50% | 6 | 67% |
| PVI enhancement | NA | | 12 | 52% |

Possible Pathophysiologic Mechanisms

Most case reports and small studies hypothesized that observed vascular and perivascular changes were consistent with inflammation.^{9,19} Clinical findings support this hypothesis, with ipsilateral lymph node enlargement and/or contiguous pharyngolaryngeal inflammation,²¹ as well as biologic findings, with a mild increase of the erythrocyte sedimentation rate or C-reactive protein.^{8,9,22,23} In our series, only 3 patients had a mild increase of the erythrocyte sedimentation rate or C-reactive protein levels. Eight patients had an autoimmune disease such as rheumatoid arthritis, systemic lupus erythematosus, ankylosing spondylarthritis,

Graves disease, Sjögren syndrome, or Hashimoto thyroiditis. Most interesting, 7 over these 8 patients presented with several simultaneous clinical relapses of the perivascular inflammation of the carotid artery and of their autoimmune disease, suggesting a link between the diseases. One study reported a case of fluoxetine-induced carotidynia, presumably explained by the inflammatory modulation induced by the antidepressants.²⁴ Some studies reported an increased activity corresponding to the region of soft-tissue thickening within the carotid sheath with FDG-PET-CT,^{8,9,25} though these findings were not specific for inflammation. Other hypotheses were discussed, such as vasculitis.²⁶ However, PET-CT with abnormally increased activity in neither the remainder of the body nor the vessels was described.^{8,9} In our center, none of the patients with biopsy-proved giant cell arteritis presenting with acute neck pain or tenderness had abnormalities of the carotid bulb on imaging, and no relationship between the 2 entities was reported in literature. Spontaneous resolution excludes neoplastic processes. Finally, 1 study reported histologically proved findings of chronic inflammation in 1 patient with pathologic changes consisting of vascular and fibroblast proliferation and predominantly lymphocytic low-grade chronic active inflammation.²⁰ Therefore, given that the pathogenesis remains unknown, this entity may be an inflammatory process of unknown origin or part of an autoimmune process.

Proposition for a New Entity

In 2004, carotidynia was removed from the International Classification of Headache Disorders.³ Causes of acute neck pain are numerous,²⁷ and we agree that the term “carotidynia” is confusing and should not be used anymore.⁴ However,

our study strongly suggests the existence of a clinical entity that was formerly poorly described (often under the “carotidynia” label) with very consistent clinical and imaging characteristics. In our study, the attempt to label this entity was shown to be dysfunctional and confusing among the different centers with at least 4 distinct labels used to describe the same entity (“carotidynia,” “carotidodynia,” “carotidobulbia,” or “carotiditis”). In the past, some authors proposed terms such as “idiopathic carotiditis”¹⁹ or “carotid periarteritis,”⁹ but these terms were not accurate because vascular and perivascular abnormalities occur simultaneously.

Consequently, we strongly support the need for a new label, and we suggest an acronym most apt for this entity: Transient Perivascular Inflammation of the Carotid artery (TIPIC) syndrome. This acronym was chosen by consensus of the neurologists, radiologists, internists, and vascular physicians working at the different centers that collaborated on this project.

We believe that this entity should be added to the International Classification of Headache Disorders-III.²⁸ We propose 4 major criteria as follows:

- 1) Presence of acute pain overlying the carotid artery, which may or may not radiate to the head
- 2) Eccentric PVI on imaging
- 3) Exclusion of another vascular or nonvascular diagnosis with imaging
- 4) Improvement within 14 days either spontaneously or with anti-inflammatory treatment.

Additionally, a minor criterion could be the presence of a self-limited intimal soft plaque.

Limitations of the Study

Our study has some limitations. First, it was a retrospective, descriptive study with a small number of patients, thus limiting its scope mostly in the descriptive and exploratory fields. Second, a non-negligible number of patients were probably not selected during the screening process because of a lack of diagnostic imaging or a delayed order for diagnostic imaging. Third, our median follow-up duration was short, and we could not say whether follow-up imaging would eventually show the complete disappearance of the PVI, relapses, or development of atherosclerosis. Fourth, because of the benign course of the disease, adding details from pathology is difficult and not feasible; thus, better comprehension of the physiopathology has been stalled for the moment.

Changes in Current Practice

We believe that clinicians should think about the TIPIC syndrome in the differential diagnosis of neck pain. They could set a precise diagnosis with adequate imaging modalities, to exclude other entities in the differential diagnosis and propose adequate treatment. Recognition of this syndrome would be cost-effective and avoid unnecessary, additional diagnostic examinations. US appears to be a suitable examination for screening because it can detect PVI with high accuracy, similar to other imaging methods, but without any exposure to radiation, high magnetic fields, or the administration of intravenous contrast agents. It is affordable and easily accessible, and it has excellent interreader concordance. Imaging diagnosis should be performed without delay because these abnormalities decrease very quickly. Follow-up could be made with US to assess PVI decrease and control lumen narrowing or soft intimal plaque.⁵

Our study raised concerns about 2 major issues. First, the neurologic risk may not be as low as previously reported in the literature because 8 of our patients had neurologic events. We do not have a convincing explanation regarding the possible relationship between this entity and the neurologic events encountered. The lumen caliber narrowing was mild, and there were no local or distal hemodynamic changes with cervical or transcranial US. Brain MR imaging performed at the time of the neurologic events

did not show any acute brain abnormality with diffusion or FLAIR-weighted imaging. Therefore, the hypothesis of a brain ischemia linked to the carotid artery narrowing, either due to distal embolism or low-flow, is unlikely. An inflammatory hypothesis involving both the carotid artery and intracranial arteries at the same time might be considered, but our imaging protocol was not designed to detect intracranial vessel wall inflammation.

Second, the persistence of vascular wall abnormalities, including an intimal soft plaque with imaging, suggest the hypothesis of a secondary development of atherosclerosis in these patients, therefore justifying a longer follow-up.

Recognition of this entity favors further, large prospective studies to answer these major questions and to elucidate the prevalence, pathophysiologic mechanisms, risk factors, etiologic processes, and potential therapies for this condition.

CONCLUSIONS

We describe more precisely a currently unclassified clinico-radiologic entity in patients presenting with acute cervical pain and strikingly similar perivascular and vascular abnormalities during diagnostic imaging. We suggest a suitable name to describe this entity: Transient Perivascular Inflammation of the Carotid artery (TIPIC) syndrome.

ACKNOWLEDGMENTS

Laura McMaster provided professional English-language medical editing of this article.












Disclosures: Julien Savatovsky—UNRELATED: Consultancy: Servier International Research Institute; Grants/Grants Pending: AIDS National Research Agency*; Payment for Lectures Including Service on Speakers Bureaus: Bayer, Medtronic, Philips Healthcare; Travel/Accommodations/Meeting Expenses Unrelated to Activities Listed: Bayer, Philips Healthcare, GE Healthcare. *Money paid to the institution.

REFERENCES

1. Fay T. **Atypical neuralgia.** *Arch Neurol Psychiatry* 1927;18:309–15
2. **Classification and diagnostic criteria for headache disorders, cranial neuralgias and facial pain: Headache Classification Committee of the International Headache Society.** *Cephalalgia* 1988;8(suppl 7): 1–96 [CrossRef Medline](#)
3. **Headache Classification Subcommittee of the International Headache Society: The International Classification of Headache Disorders—2nd edition.** *Cephalalgia* 2004;24(suppl 1):9–160 [CrossRef Medline](#)
4. Biousse V, Bousser MG. **The myth of carotidynia.** *Neurology* 1994; 44:993–95 [CrossRef Medline](#)
5. Behar T, Menjot N, Laroche J-P, et al. **Comparative evolution of carotidynia on ultrasound and magnetic resonance imaging.** *J Mal Vasc* 2015;40:395–98 [CrossRef Medline](#)
6. Arning C. **Ultrasonography of carotidynia.** *AJNR Am J Neuroradiol* 2005;26:201–02 [Medline](#)
7. Burton BS, Syms MJ, Petermann GW, et al. **MR imaging of patients with carotidynia.** *AJNR Am J Neuroradiol* 2000;21:766–69 [Medline](#)
8. Amaravadi RR, Behr SC, Kousoubri PD, et al. **[18F] fluorodeoxyglucose positron-emission tomography-CT imaging of carotidynia.** *AJNR Am J Neuroradiol* 2008;29:1197–99 [CrossRef Medline](#)
9. Hafner F, Hackl G, Haas E, et al. **Idiopathic carotidynia.** *Vasa* 2014; 43:287–92 [CrossRef Medline](#)
10. Kosaka N, Sagoh T, Uematsu H, et al. **Imaging by multiple modalities of patients with a carotidynia syndrome.** *Eur Radiol* 2007;17: 2430–33 [CrossRef Medline](#)
11. Vandenbroucke JP, von Elm E, Altman DG, et al; STROBE Initiative. **Strengthening the Reporting of Observational Studies in Epidemi-**

- ology (STROBE): explanation and elaboration. *PLoS Med* 2007;4:e297 [CrossRef Medline](#)
12. **Clinical alert: benefit of carotid endarterectomy for patients with high-grade stenosis of the internal carotid artery**—National Institute of Neurological Disorders and Stroke Stroke and Trauma Division. North American Symptomatic Carotid Endarterectomy Trial (NASCET) investigators. *Stroke* 1991;22:816–17 [CrossRef Medline](#)
13. R Foundation for Statistical Computing, Vienna, Austria. <http://www.R-project.org/>. 2016
14. Landis JR, Koch GG. An application of hierarchical kappa-type statistics in the assessment of majority agreement among multiple observers. *Biometrics* 1977;33:363–74 [CrossRef Medline](#)
15. Kuhn J, Harzheim A, Horz R, et al. MRI and ultrasonographic imaging of a patient with carotidynia. *Cephalalgia* 2006;26:483–85 [CrossRef Medline](#)
16. Wu Z, Yang H. Color Doppler imaging in the diagnosis and follow-up of carotid cavernous sinus fistulas. *Yan Ke Xue Bao* 1993;9:153–57 [Medline](#)
17. Woo JK, Jhamb A, Heran MK, et al. Resolution of existing intimal plaque in a patient with carotidynia. *AJNR Am J Neuroradiol* 2008;29:732–33 [CrossRef Medline](#)
18. Young JY, Hijaz TA, Karagianis AG. CT findings in a patient with bilateral metachronous carotidynia. *Clin Imaging* 2015;39:305–07 [CrossRef Medline](#)
19. Tardy J, Pariente J, Nasr N, et al. Carotidynia: a new case for an old controversy. *Eur J Neurol* 2007;14:704–05 [CrossRef Medline](#)
20. Upton PD, Smith JG, Charnock DR. Histologic confirmation of carotidynia. *Otolaryngol Head Neck Surg* 2003;129:443–44 [CrossRef Medline](#)
21. Comacchio F, Bottin R, Brescia G, et al. Carotidynia: new aspects of a controversial entity. *Acta Otorhinolaryngol Ital* 2012;32:266–69 [Medline](#)
22. da Rocha AJ, Tokura EH, Romualdo AP, et al. Imaging contribution for the diagnosis of carotidynia. *J Headache Pain* 2009;10:125–27 [CrossRef Medline](#)
23. Taniguchi Y, Horino T, Hashimoto K. Is carotidynia syndrome a subset of vasculitis? *J Rheumatol* 2008;35:1901–02 [Medline](#)
24. Jabre MG, Shahidi GA, Bejjani BP. Probable fluoxetine-induced carotidynia. *Lancet* 2009;374:1061–62 [CrossRef Medline](#)
25. Berzaczy D, Domenig CM, Beitzke D, et al. Imaging of a case of benign carotidynia with ultrasound, MRI and PET-CT. *Wien Klin Wochenschr* 2013;125:719–20 [CrossRef Medline](#)
26. Taniguchi Y, Horino T, Terada Y, et al. The activity of carotidynia syndrome is correlated with the soluble intracellular adhesion molecule-1 (sICAM-1) level. *South Med J* 2010;103:277–78 [CrossRef Medline](#)
27. Chambers BR, Donnan GA, Riddell RJ, et al. Carotidynia: aetiology, diagnosis and treatment. *Clin Exp Neurol* 1981;17:113–23 [Medline](#)
28. Headache Classification Committee of the International Headache Society (IHS): The International Classification of Headache Disorders—3rd edition (beta version). *Cephalalgia* 2013;33:629–808 [CrossRef Medline](#)

Carotid Bulb Webs as a Cause of “Cryptogenic” Ischemic Stroke

 P.I. Sajedi,  J.N. Gonzalez,  C.A. Cronin,  T. Kouo,  A. Steven,  J. Zhuo,  O. Thompson,  R. Castellani,  S.J. Kittner,  D. Gandhi, and  P. Raghavan

ABSTRACT

BACKGROUND AND PURPOSE: Carotid webs are intraluminal shelf-like filling defects at the carotid bulb with recently recognized implications in patients with recurrent ischemic stroke. We sought to determine whether carotid webs are an under-recognized cause of “cryptogenic” ischemic stroke and to estimate their prevalence in the general population.

MATERIALS AND METHODS: A retrospective review of neck CTA studies in young patients with cryptogenic stroke over the past 6 years ($n = 33$) was performed to determine the prevalence of carotid webs compared with a control group of patients who received neck CTA studies for reasons other than ischemic stroke ($n = 63$).

RESULTS: The prevalence of carotid webs in the cryptogenic stroke population was 21.2% (95% CI, 8.9%–38.9%). Patients with symptomatic carotid webs had a mean age of 38.9 years (range, 30–48 years) and were mostly African American (86%) and women (86%). In contrast, only 1.6% (95% CI, 0%–8.5%) of patients in the control group demonstrated a web. Our findings demonstrate a statistically significant association between carotid webs and ischemic stroke (OR = 16.7; 95% CI, 2.78–320.3; $P = .01$).

CONCLUSIONS: Carotid webs exhibit a strong association with ischemic stroke, and their presence should be suspected in patients lacking other risk factors, particularly African American women.

Carotid artery webs are shelf-like intraluminal protrusions in the carotid bulb with emerging implications related to recurrent ischemic stroke.^{1,2} Most carotid web cases have been previously described with conventional angiography.^{3,4} More recently, the imaging characteristics on CTA have also been established. The typical appearance of a carotid web on CTA is a focal, gracile intraluminal filling defect along the posterior wall of the carotid bulb.^{1,5} Superimposed thrombus has also been described, which is thought to be related to sluggish/turbulent blood flow produced by the filling defect.⁵

Carotid webs also have been referred to as an atypical variant of fibromuscular dysplasia, with intimal fibrosis and hyperplasia on histology in contrast to the classic, medial variant.^{3,6} Typical fibromuscular dysplasia occurs in middle-aged white women,

with a classic “string of beads” imaging appearance, and does not have a direct association with ischemic stroke.^{6,7}

Although considered a rare entity, a significant proportion of reported carotid web cases have been associated with recurrent ischemic strokes, most frequently in younger adults who lack other known risk factors.¹ Recent studies have revealed a mean age between 45 and 50 years in patients with carotid webs and associated ipsilateral carotid territory ischemic strokes, occurring more frequently in women than men.^{1,5,8} There is limited reporting on the prevalence of carotid webs in the stroke population. A recent report on an Afro-Caribbean population demonstrated a 23% prevalence of carotid webs in young patients with ischemic stroke and a 7% prevalence among control patients.⁸ Up to one-third of all patients presenting with ischemic strokes lack an identifiable cause and are classified as “cryptogenic” in etiology, with most of these cases occurring in younger patients.⁹ Webs may be an under-recognized entity because of their subtle morphology and a lack of familiarity amongst radiologists and clinicians with this lesion. They could account for a significant portion of cryptogenic strokes, particularly in young adults.

The purpose of our study was to determine the prevalence of carotid webs in a group of patients previously classified as having cryptogenic stroke.

Received December 26, 2016; accepted after revision February 27, 2017.

From the Departments of Diagnostic Radiology and Nuclear Medicine (P.R., P.I.S., T.K., J.Z.), Neurology (J.N.G., C.A.C., O.T., S.J.K.), and Interventional Neuroradiology (D.G.), University of Maryland School of Medicine, Baltimore, Maryland; Department of Diagnostic Radiology and Nuclear Medicine (A.S.), Ochsner Medical Center, New Orleans, Louisiana; and Department of Pathology (R.C.), University of Michigan Stryker M.D. School of Medicine, Kalamazoo, Michigan.

Please address correspondence to Prashant Raghavan, MBBS, Department of Diagnostic Radiology and Nuclear Medicine, University of Maryland School of Medicine, 22 South Greene St, Baltimore, MD 21201; e-mail: prashant.raghavan@gmail.com

<http://dx.doi.org/10.3174/ajnr.A5208>

MATERIALS AND METHODS

Patient Selection: Cryptogenic Stroke Group

This retrospective study was approved by our institutional review board; the need for informed consent was waived. A chart review of all patients presenting to the University of Maryland Medical Center with ischemic strokes from January 1, 2010 to August 31, 2015 ($n = 1738$) was undertaken. Patients between 18 and 55 years of age ($n = 590$) were examined in detail to identify those with anterior circulation cryptogenic stroke. Stroke etiology determination was modeled after the Causative Classification System, with patients characterized into one of the following categories after thorough work-up: large artery atherosclerotic, cardio-aortic embolism, small artery occlusion, other known cause, or cryptogenic.¹⁰ The work-up for these patients was as follows: all patients received transthoracic echocardiogram, with transesophageal echocardiogram and evaluation for right-to-left shunt performed if the etiology remained unknown after the initial evaluation. All patients had cardiac telemetry monitoring for arrhythmia, with prolonged ambulatory monitoring when indicated. Intracranial vascular imaging was performed with CTA or MRA, and extracranial vascular imaging was performed with CTA, MRA, or carotid duplex sonography. The potential for underlying dissection as the etiology was excluded by history and imaging. Lumbar puncture and laboratory testing to evaluate for appropriate etiologies, such as vasculitis, other autoimmune disorders, or hypercoagulable state, were performed when clinically indicated. A total of 119 patients between 18 and 55 years old with anterior circulation cryptogenic stroke were identified.

Forty of 119 patients with cryptogenic stroke had a diagnostic neck CTA performed during their admission and were included in the analysis. These neck CTA studies were transferred to the Aquarius Workstation (version 3.6.2.3; TeraRecon, San Mateo, California), an independent imaging viewer that enables multiplanar reformation as well as MIPs. Studies were then evaluated by a board-certified, fellowship-trained neuroradiologist with more than 10 years of experience to exclude patients with atherosclerotic calcification and/or greater than 3-mm carotid wall plaque within 2 cm above and below the level of the carotid bulb. This criteria was assigned because of recent studies that have shown that nonstenotic atherosclerotic disease above this threshold may account for cases of cryptogenic ischemic stroke.¹¹⁻¹³ Seven cases of atherosclerosis that met this criteria were identified by the reader, with 1 additional study deemed nondiagnostic because of inadequate contrast bolus timing, leaving a total of 33 neck CTA studies in our case population (Fig 1).

Patient Selection: Control Group

The control group was composed of patients between 18 and 55 years of age who had CTA of the neck performed during their admission and who presented for reasons other than ischemic stroke (including trauma, presurgical planning, etc). We excluded any CTA studies that demonstrated direct trauma to the neck (blunt or penetrating) or studies demonstrating a cervical spine fracture. Furthermore, patients with intracranial vascular lesions, including aneurysms and AVMs, were also excluded from the study because of a link between intracranial aneurysms and fibromuscular dysplasia.⁷ The control group was chosen to be compa-

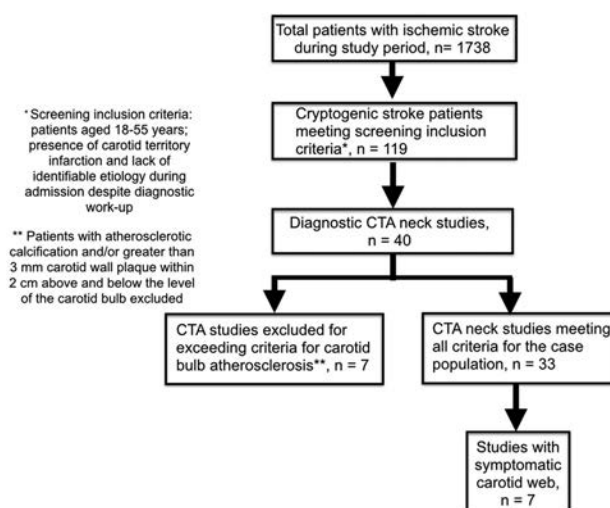


FIG 1. Algorithm of inclusion criteria.

Table 1: Demographic features of patients with cryptogenic stroke and control group patients

| Characteristic | Patients with Cryptogenic Stroke (n = 33) | Control Group Patients (n = 63) | P Value |
|-----------------------|---|---------------------------------|---------|
| Age, mean, SD | 39.2, 8.3 | 39.6, 8.4 | .82 |
| Sex, no. (%) | | | .83 |
| Male | 11 (33) | 21 (33) | |
| Female | 22 (67) | 42 (67) | |
| Ethnicity, no. (%) | | | .89 |
| African American | 18 (54) | 34 (54) | |
| White | 14 (43) | 28 (44) | |
| Other | 1 (3) | 1 (2) | |
| Carotid webs, no. (%) | 7 (21.2) | 1 (1.6) | .002 |

table with the case group with regard to age, sex, and ethnicity (Table 1). A total of 63 patients who met the inclusion criteria and had neck CTA studies done were acquired between November 6, 2012 and August 31, 2015. The following factors were assessed: patient age, sex, and indication for the CTA. As with the neck CTA studies in patients with ischemic stroke, these studies were transferred to the Aquarius Workstation.

Imaging Evaluation

CTA was chosen as the technique for interpretation because of its reliability in characterizing carotid webs^{1,5,8} as well as its ability to identify alternate pathologies such as atherosclerosis and vascular injury.⁵ Neck CTA was acquired from the aortic arch through the circle of Willis and performed on a 64-MDCT scanner with 1-mm thick sections. Scanning parameters included: pitch of 1; gantry rotation time, 0.5 seconds; 120 kVp; 350 mAs. Intravenous contrast material (100 mL of iohexol, 300 mg/mL; Omnipaque, GE Healthcare, Piscataway, New Jersey) and a 50-mL saline flush were administered at a rate of 4 mL/s with a power injector. Images were reconstructed with axial, coronal, and sagittal MIPs.

An independent review of these studies was then performed by 2 board-certified, fellowship-trained neuroradiologists with a range of 6–8 years of experience (T.K. and A.S.). The readers were blinded to patient age, sex, and laterality of stroke. The following parameters were assessed by each reader: presence of carotid web,

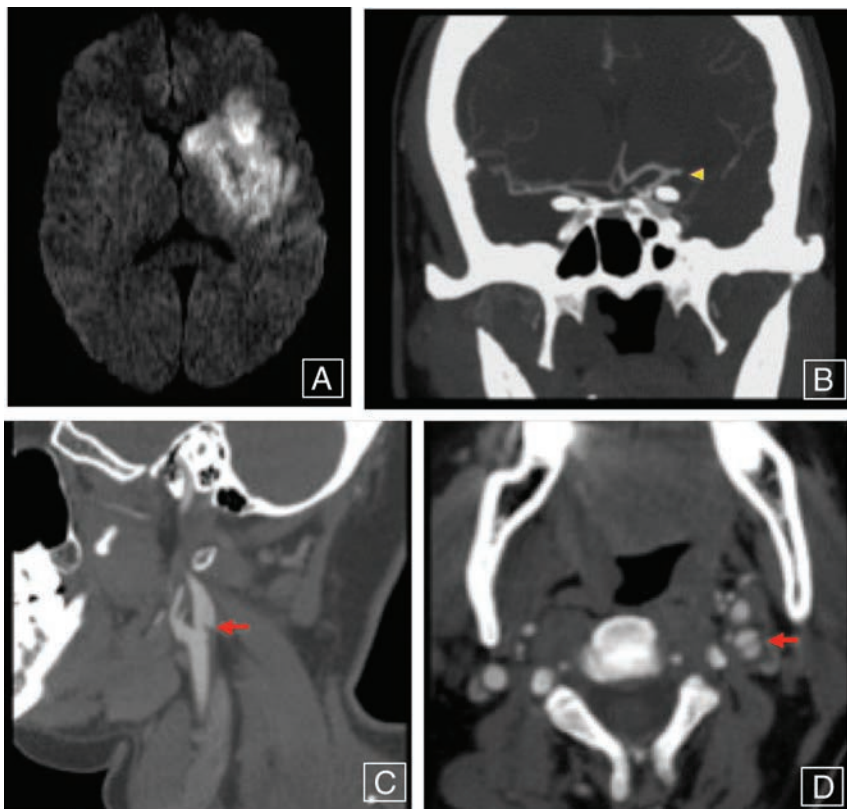


FIG 2. A patient presenting with right-sided weakness demonstrating an acute, large left MCA territory infarct as seen on diffusion-weighted imaging (A), with coronal CTA MIP image (B) showing abrupt occlusion involving the M1 segment of the left MCA (yellow arrowhead). Sagittal and axial neck CTA images (C and D) reveal a shelf-like intraluminal protrusion arising from the posterior wall of the left carotid bulb (red arrows), compatible with a carotid web.

atherosclerosis, and vascular injury. In patients with carotid web, laterality of the web, presence of superimposed clot, and presence of classic fibromuscular dysplasia were assessed. Disagreements were resolved by the third reader (P.R.), also a board-certified, fellowship-trained neuroradiologist with more than 10 years of experience.

Statistical Analysis

Carotid web prevalence was calculated by using a binomial distribution with 95% confidence intervals. The association of carotid webs with ischemic stroke was calculated by using logistic regression, where odds ratios were calculated with 95% confidence intervals. Interrater agreement of identifying carotid webs for all patients was assessed with Cohen κ score. Statistical significance was defined as $P < .05$. In addition, for both the cryptogenic stroke versus control populations, as well as positive carotid web versus nonweb in the stroke group, group differences in age were assessed by using a 2-tailed t test. For other categorical parameters (demographics and risk factors), group differences were assessed by using the Fisher exact test.

RESULTS

Of the 119 patients between the ages of 18 and 55 years who presented to our institution and were diagnosed with cryptogenic stroke during the study time period, 33 (27.7%) underwent a diagnostic neck CTA after accounting for patients with carotid

bulb atherosclerotic calcifications or wall thickness greater than 3 mm.^{11–13}

Both readers agreed on the presence and laterality of 6 (18.2%) cases of carotid web (Cohen κ coefficient, 0.78; 95% CI, 0.55–1) (Fig 2). Carotid webs were present bilaterally in half of these patients. Disagreement was encountered in 2 patients. Upon review of the studies by the third reader, 1 additional patient was deemed to have a web. Thus, a total of 7 (21.2%) positive cases of carotid web were ultimately identified within the cryptogenic stroke population (Table 2). One patient with a web demonstrated superimposed clot formation. No patients with coexistent typical, medial variant fibromuscular dysplasia were encountered.

Among the cases that were negative for carotid web, both readers agreed on 1 (3.8%) case with classic features of typical fibromuscular dysplasia. Features of prior carotid vascular injury, including pseudoaneurysm and dissection, were seen in 2 (7.7%) patients, though contralateral to the stroke. A thorough review of each patient's clinical presentation did not demonstrate a history suggestive of recent cervical vascular injury, such as neck pain, recent neck manipulation, hyperextension, or trauma.

Of the 63 patients in the control group, both readers agreed on 1 (1.6%) patient with incidental findings of carotid web. This patient was a 48-year-old African American woman whose imaging demonstrated no evidence of superimposed clot, atherosclerosis, or features of classic fibromuscular dysplasia. The prevalences of carotid webs in the cryptogenic stroke and control groups were 21.2% (CI, 8.9%–38.9%) and 1.6% (CI, 0%–8.5%), respectively, with a statistically significant association between webs and ischemic stroke (OR = 16.7; 95% CI, 2.78–320.3; $P = .01$). The mean age of patients with symptomatic carotid webs was 38.3 years (range, 30–41 years) compared with 42.5 years in patients with cryptogenic stroke without a carotid web (Table 3). The symptomatic patients with carotid web were 6 (86%) women and 1 (14%) man, and the remainder of the cryptogenic stroke population, those without carotid webs, consisted of 16 (62%) women and 10 (38%) men. With regard to ethnicity, 6 (86%) patients with carotid web and stroke were African American and 1 (14%) was white. In contrast, the ethnic makeup of the patients with noncarotid web included 12 African Americans (46%), 13 whites (50%), and 1 Asian (4%). There was no statistically significant difference in risk factors for patients with stroke such as hypertension; dyslipidemia; diabetes mellitus; and alcohol, cocaine, and tobacco use between the 2 groups (Table 3).

All symptomatic patients with carotid webs demonstrated MCA territory infarction ipsilateral to the carotid web. These in-

Table 2: Detailed demographic and imaging/clinical features, including work-up, of patients with positive carotid webs in the cryptogenic stroke population^a

| Patient No. | Ethnicity | Stroke Location | Thrombus Location | Web Location | Work-Up Methods ^b | Management after Initial Event | Recurrent Stroke |
|-------------|------------------|--|-----------------------------|--------------|------------------------------|--------------------------------|-------------------------|
| 1 | White | Near complete right MCA territory infarction | Right M1 | Bilateral | 1–3 ^c | Supportive care | No |
| 2 | African American | Near complete right MCA territory infarction | Right M1 | Right | 1–3 ^c | Clot retrieval | No |
| 3 | African American | Right basal ganglia and temporal lobe infarcts | Right distal M1/proximal M2 | Right | 1–3 | Supportive care | No |
| 4 | African American | Near complete left MCA territory infarction | Left distal M1/proximal M2 | Bilateral | 1–3 | Supportive care | Yes, multiple recurrent |
| 5 | African American | Near complete left MCA territory infarction | Left M1 | Bilateral | 1–3 ^c | Clot retrieval, then CEA | N/A |
| 6 | African American | Left basal ganglia and insular cortex infarcts | Left M2 | Left | 1–3 | Supportive care, then CEA | N/A |
| 7 | African American | Left basal ganglia and insular cortex infarcts | Left M2 | Left | 1–3 | Supportive care | No |

Note:—CEA indicates carotid endarterectomy; M1, segment from the origin to the bifurcation/trifurcation of the MCA; M2, segment from the MCA bifurcation/trifurcation to the insular circular sulcus; N/A, no follow-up available.

^a Patient ages ranged from 30–48 years, composed of 6 women and 1 man.

^b Work-up of patients with carotid web: 1, echocardiogram; 2, cardiac telemetry; 3, cross-sectional head/neck vascular imaging.

^c Interventional head/neck angiogram also performed.

Table 3: Demographic features and pertinent risk factors of patients with and without carotid webs in the cryptogenic stroke population^a

| Characteristics | Patients with Cryptogenic Stroke with Carotid Web (n = 7) | Patients with Cryptogenic Stroke without Carotid Web (n = 26) | P Value |
|-----------------------|---|---|---------|
| Age, mean, SD | 38.3, 5.6 | 39.4, 9.0 | .721 |
| Sex, no. (%) | | | |
| Male | 1 (14) | 10 (38) | .38 |
| Female | 6 (86) | 16 (62) | |
| Ethnicity, no. (%) | | | .16 |
| African American | 6 (86) | 12 (46) | |
| White | 1 (14) | 13 (50) | |
| Other | 0 (0) | 1 (4) | |
| Risk factors, no. (%) | | | |
| Hypertension | 0 (0) | 8 (31) | .15 |
| Dyslipidemia | 2 (29) | 4 (15) | .58 |
| Diabetes mellitus | 0 (0) | 7 (27) | .30 |
| Alcohol abuse | 0 (0) | 5 (19) | .56 |
| Cocaine | 0 (0) | 0 (0) | N/A |
| Tobacco | 3 (43) | 6 (23) | .39 |

Note:—N/A indicates not available.

^a Added P values for patient characteristics.

farcts ranged in size from involvement of the basal ganglia and insular cortex to involvement of greater than two-thirds of the MCA territory (Table 2). None of these patients had the appearance of a lacunar infarct. Of these 7 symptomatic patients with carotid web, 1 (14.3%) had multiple documented episodes of recurrent stroke. This patient was treated with intravenous tPA during each encounter, with the family refusing surgical intervention with carotid endarterectomy. In the remaining 6 patients, 4 were treated with supportive care during the initial episode and 2 with mechanical thrombectomy. After the presence of web was identified, 2 patients underwent carotid endarterectomy.

Seventy-eight patients were excluded from the case group given the lack of neck CTA imaging at presentation. Still, each of these patients did receive cervical vascular imaging in the form of MRA and/or carotid duplex sonography to rule out standard etiologies of stroke. An imaging review of these patients, performed

in retrospect, showed no patients with definite features of carotid web.

DISCUSSION

Our findings reveal a statistically significant association between carotid webs and ischemic stroke, particularly in younger African American women, with a prevalence of 21.2% in the cryptogenic stroke population as opposed to 1.6% in the control group, yielding an odds ratio of 10.6 (95% CI, 1.8–203.1). By comparison, a smaller case-control analysis of cryptogenic stroke in the Afro-Caribbean population of Martinique in the French West Indies found a prevalence of 37% in their 23 patients with cryptogenic stroke and a prevalence of 7% in their control patients, yielding an odds ratio of 5.0 (95% CI, 1.1–22.8).⁸ A more recent case-control analysis by Coutinho et al¹¹ also revealed similar findings, albeit with a lower prevalence of webs in cases (9.4%) compared with control patients (1%; OR = 8.0; 95% CI, 1.2–67; *P* = .032) compared with our series. They also noted a lack of significant difference in the prevalence of nonstenotic atherosclerotic disease between the case and control groups.

In our study, all patients with stroke who had carotid webs had them ipsilateral to the stroke; 3 had bilateral webs. All patients in this group had middle cerebral territory (MCA) infarcts, 5 (71.4%) with large territory involvement. These findings support our hypothesis that carotid webs are found more frequently in patients with cryptogenic strokes than in control patients and are likely causative. Our findings are in concordance with the emerging literature on this topic, with a higher prevalence of carotid webs in African American female patients with ischemic stroke who are of younger age and lack other identifiable risk factors.^{1,5,8} It should be noted that our 7 cases of cryptogenic stroke with carotid web included only 1 man and 1 person of white race. The mechanism of stroke in such patients, as suggested by Choi et al,⁵ may be related to local turbulence and subsequent thromboembolism. This is supported by the presence of a coexistent thrombus in 1 patient in our series.

CTA was used as the technique of choice in our study. Al-

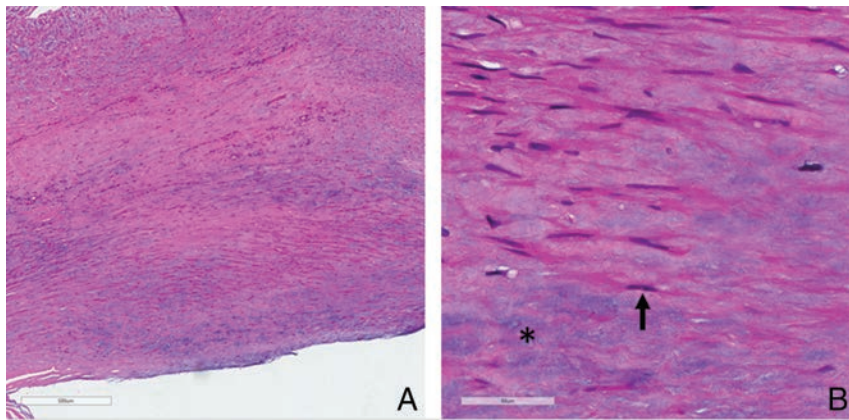


FIG 3. Low-magnification photomicrograph (A) shows extensive fibromuscular proliferation (scale bar = 500 μ). High magnification (B) shows proliferating smooth muscle cells (arrow) and myxoid degeneration (asterisk).

though descriptions of webs in conventional angiography, MR angiography, and sonography exist in the literature, CTA appears to be reliable in the detection and characterization of this entity.^{14,15} The advantages of CTA include rapid, high-resolution imaging as well as the ability to obtain reformatted images in multiple planes. Furthermore, CTA provides the added benefit of characterizing superimposed findings, such as thrombus, and aids in the exclusion of atherosclerosis or vascular injury. In the group of 78 patients with cryptogenic strokes who did not undergo CTA, no webs were found. This may have been because of limitations imposed by operator dependence (ultrasound), technique (TOF MRA), and artifacts. Therefore, based on our experiences, we suggest that all patients with cryptogenic stroke receive CTA imaging of the neck as part of the standard work-up.

Carotid webs can be distinguished from dissection and atherosclerotic plaques by their characteristic location and appearance, being gracile and focal in nature and exclusively located in the posterior wall of the carotid bulb. In contrast, dissection flaps typically propagate beyond the carotid bulb and may be associated with intramural hematomas and/or pseudoaneurysms. Soft carotid plaques present as focal areas of mural thickening, often, but not necessarily, confined to the posterior wall of the carotid bulb.

The prospective diagnosis of carotid webs will allow for targeted intervention to prevent recurrent ischemic events. Although 2 of our patients underwent carotid endarterectomy, there may also be a role for endovascular stent placement in the management of carotid webs, as described by Elmokadem et al.¹⁶ Histopathology in the patients who underwent surgery showed extensive intimal fibromuscular proliferation with fibrosis and myxoid degeneration. No frank atheromatous change was seen in either patient. These findings were most consistent with an atypical, intimal variant form of fibromuscular dysplasia, in keeping with prior descriptions of the histopathologic features of this entity (Fig 3).⁵

Our study had several potential limitations, including a retrospective study design and a small sample size. In addition, we included only patients between 18 and 55 years old, and it is conceivable that webs may be encountered in patients younger and older than our cohort. In fact, we have recently identified at least

2 patients with ischemic stroke with imaging features of carotid web who were older than 55 years. Another potential limitation of our study was evaluating only patients who had a CTA of the neck performed. Seventy-eight young patients with cryptogenic stroke were not included within the study population secondary to a lack of neck CTA imaging as detailed above. In addition, histopathologic correlation was available for only 2 patients in our series, though 1 patient's family refused surgical intervention, and several of the remaining cases had large territory infarcts, potentially limiting any benefit of an invasive procedure.

CONCLUSIONS

Carotid webs are an under-recognized cause of ischemic anterior circulation stroke, especially in younger African American women. CT angiography reliably depicts webs as gracile crescentic filling defects arising from the posterior wall of the carotid bulb and should be considered as part of the evaluation for patients with cryptogenic stroke. Histopathologically, they represent an intimal variant of fibromuscular dysplasia. Definitive treatment may require carotid endarterectomy or endovascular stent placement.

Disclosures: Steven Kittner—UNRELATED: Employment: University of Maryland, Veterans Administration; Grants/Grants Pending: National Institutes of Health, Veterans Administration*; Payment for Lectures (including service on Speakers Bureaus): National Institutes of Health. Dheeraj Gandhi—UNRELATED: Royalties: Cambridge Press. *Money paid to the institution.

REFERENCES

- Joux J, Chausson N, Jeannin S, et al. Carotid-bulb atypical fibromuscular dysplasia in young Afro-Caribbean patients with stroke. *Stroke* 2014;45:3711–13 CrossRef Medline
- Morgenlander JC, Goldstein LB. Recurrent transient ischemic attacks and stroke in association with an internal carotid artery web. *Stroke* 1991;22:94–98 CrossRef Medline
- Wirth FP, Miller WA, Russell AP. Atypical fibromuscular hyperplasia. Report of two cases. *J Neurosurgery* 1981;54:685–89 CrossRef Medline
- So EL, Toole JF, Moody DM, et al. Cerebral embolism from septal fibromuscular dysplasia of the common carotid artery. *Ann Neurol* 1979;6:75–78 CrossRef Medline
- Choi PM, Singh D, Trivedi A, et al. Carotid webs and recurrent ischemic strokes in the era of CT angiography. *AJNR Am J Neuroradiol* 2015;36:2134–39 CrossRef Medline
- Watanabe S, Tanaka K, Nakayama T, et al. Fibromuscular dysplasia at the internal carotid origin: a case of carotid web [in Japanese]. *No Shinkei Geka* 1993;21:449–52 Medline
- Touzé E, Oppenheim C, Trystram D, et al. Fibromuscular dysplasia of cervical and intracranial arteries. *Int J* 2010;5:296–305 CrossRef Medline
- Joux J, Boulanger M, Jeannin S, et al. Association between carotid bulb diaphragm and ischemic stroke in young Afro-Caribbean patients: a population-based case-control study. *Stroke* 2016;47:2641–44 CrossRef Medline
- Finsterer J. Management of cryptogenic stroke. *Acta Neurol Belg* 2010;110:135–47 Medline

10. Arsava EM, Ballabio E, Benner T, et al. **The Causative Classification of Stroke system: an international reliability and optimization study.** *Neurology* 2010;75:1277–84 [CrossRef Medline](#)
11. Coutinho JM, Derkatch S, Potvin AR, et al. **Carotid artery web and ischemic stroke: a case-control study.** *Neurology* 2017;88:65–69 [CrossRef Medline](#)
12. Gupta A, Baradaran H, Kamel H, et al. **Evaluation of computed tomography angiography plaque thickness measurements in high-grade carotid artery stenosis.** *Stroke* 2014;45:740–45 [CrossRef Medline](#)
13. Coutinho JM, Derkatch S, Potvin AR, et al. **Nonstenotic carotid plaque on CT angiography in patients with cryptogenic stroke.** *Neurology* 2016;87:665–72 [CrossRef Medline](#)
14. Lantos JE, Chazen JL, Gupta A. **Carotid web: appearance at MR angiography.** *AJNR Am J Neuroradiol* 2016;37:E5–E6 [CrossRef Medline](#)
15. Fu W, Crockett A, Low G, et al. **Internal carotid artery web: Doppler ultrasound with CT angiography correlation.** *J Radiol Case Rep* 2015;9:1–6 [CrossRef Medline](#)
16. Elmokadem AH, Ansari SA, Sangha R, et al. **Neurointerventional management of carotid webs associated with recurrent and acute cerebral ischemic syndromes.** *Interv Neuroradiol* 2016;22:432–37 [CrossRef Medline](#)

Solid Lymph Nodes as an Imaging Biomarker for Risk Stratification in Human Papillomavirus–Related Oropharyngeal Squamous Cell Carcinoma

T.J. Rath, S. Narayanan, M.A. Hughes, R.L. Ferris, S.I. Chiosea, and B.F. Branstetter IV

ABSTRACT

BACKGROUND AND PURPOSE: Human papillomavirus–related oropharyngeal squamous cell carcinoma is associated with cystic lymph nodes on CT and has a favorable prognosis. A subset of patients with aggressive disease experience treatment failure. Our aim was to determine whether the extent of cystic lymph node burden on staging CT can serve as an imaging biomarker to predict treatment failure in human papillomavirus–related oropharyngeal squamous cell carcinoma.

MATERIALS AND METHODS: We identified patients with human papilloma virus–related oropharyngeal squamous cell carcinoma and staging neck CTs. Demographic and clinical variables were recorded. We retrospectively classified the metastatic lymph node burden on CT as cystic or solid and assessed radiologic extracapsular spread. Biopsy, subsequent imaging, or clinical follow-up was the reference standard for treatment failure. The primary end point was disease-free survival. Cox proportional hazard regression analyses of clinical, demographic, and anatomic variables for treatment failure were performed.

RESULTS: One hundred eighty-three patients were included with a mean follow-up of 38 months. In univariate analysis, the following variables had a statistically significant association with treatment failure: solid-versus-cystic lymph nodes, clinical T-stage, clinical N-stage, and radiologic evidence of extracapsular spread. The multivariate Cox proportional hazard model resulted in a model that included solid-versus-cystic lymph nodes, T-stage, and radiologic evidence of extracapsular spread as independent predictors of treatment failure. Patients with cystic nodal metastasis at staging had significantly better disease-free survival than patients with solid lymph nodes.

CONCLUSIONS: In human papilloma virus–related oropharyngeal squamous cell carcinoma, patients with solid lymph node metastases are at higher risk for treatment failure with worse disease-free survival. Solid lymph nodes may serve as an imaging biomarker to tailor individual treatment regimens.

ABBREVIATIONS: HPV = human papilloma virus; OPSCC = oropharyngeal squamous cell carcinoma; rECS = radiologic evidence of extracapsular spread; TF = treatment failure; TNM = Tumor, Node, Metastasis

Human papillomavirus (HPV)–related oropharyngeal squamous cell carcinoma (OPSCC) is a distinct disease with more favorable locoregional control and survival outcomes compared with HPV-unrelated OPSCC.^{1–3} The favorable prognosis of

HPV-related OPSCC has prompted research directed at developing de-escalation treatment protocols that would offer reduced toxicity to patients at low risk of treatment failure (TF).⁴ Furthermore, the current anatomic-based Tumor, Node, Metastasis (TNM) Staging System is not well-suited to predicting outcome in HPV-related OPSCC.^{5,6} Despite its favorable prognosis, a subset of HPV-related OPSCCs recur primarily with distant metastases and frequently in atypical locations.^{3,7–10} Imaging biomarkers that stratify patients at risk for TF would be useful to identify patients who are not candidates for de-escalation therapy. HPV-related OPSCC is associated with cystic-appearing lymph nodes on CT, but some patients with HPV-associated disease have completely solid metastases.^{11,12} The purpose of this study was to determine whether solid and cystic lymph node metastases on staging neck CT could be used as an imaging biomarker to predict TF in patients with stage III or IV HPV-related OPSCC.

Received October 18, 2016; accepted after revision February 7, 2017.

From the Departments of Radiology (T.J.R., M.A.H., B.F.B.), Otolaryngology (T.J.R., M.A.H., R.L.F., B.F.B.), and Pathology (S.I.C.), University of Pittsburgh Medical Center, Pittsburgh, Pennsylvania; and Department of Radiology (S.N.), Children's Hospital of Pittsburgh of the University of Pittsburgh Medical Center, Pittsburgh, Pennsylvania.

Paper previously presented at: Annual Meeting of the American Society of Neuroradiology and Foundation of the ASNR Symposium, May 17–22, 2014; Montreal, Quebec, Canada: Number O-390.

Please address correspondence to Tanya J. Rath, MD, Department of Radiology, 200 Lothrop St, 2nd Floor, Suite 200 East Wing, Pittsburgh, PA 15213; e-mail: rathjt@upmc.edu

<http://dx.doi.org/10.3174/ajnr.A5177>

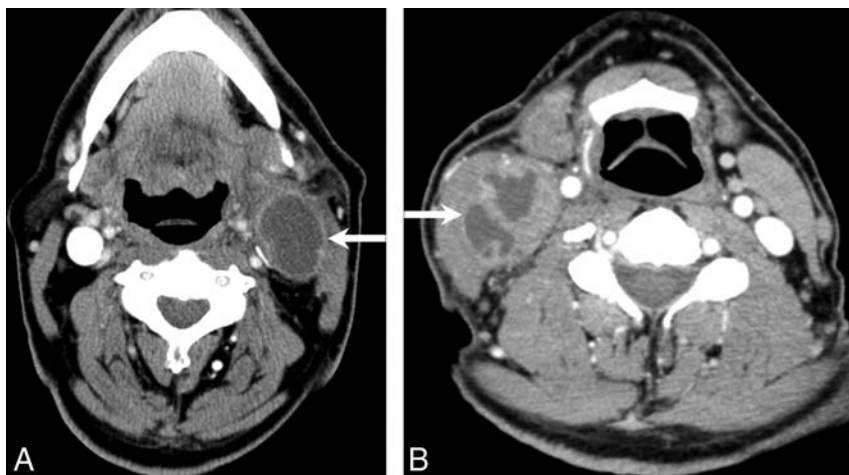


FIG 1. A and B, Two examples of metastatic lymph nodes (white arrows) classified as cystic.

MATERIALS AND METHODS

Study Sample

This retrospective Health Insurance Portability and Accountability Act–compliant single-institution study was approved by the institutional review board. Four hundred forty-one patients with HPV-positive OPSCC were identified from our head and neck cancer registry from 1984 to 2014.^{13,14} HPV positivity was determined by in situ hybridization by using probes targeting 37 HPV subtypes, including the following: 6, 11, 16, 18, 31, 33, 35, 39, 45, 51, and 52 (Y1404; Dako, Carpinteria, California). Five-micrometer tissue sections were deparaffinized and digested with proteinase K (Roche Diagnostics, Indianapolis, Indiana). Cases with punctate nuclear signal were considered positive.¹⁴ Before 2007, HPV positivity was determined retrospectively on available tissue blocks by a head and neck cancer pathologist (S.I.C.) blinded to clinical outcome.¹⁴ Exclusion criteria were the following: unavailable contrast-enhanced staging CT ($n = 221$), N0 disease on staging CT or pathology ($n = 21$), no clinical follow-up ($n = 10$), non-compliance with the prescribed treatment regimen ($n = 5$), and distant metastases at presentation ($n = 1$). The reference standard for nodal metastasis at staging was histologic confirmation or definitively abnormal-appearing lymph nodes on staging CT in a patient with biopsy-proved HPV-positive OPSCC.

Patient demographics, TNM classification as defined by the seventh edition of the *AJCC Cancer Staging Manual*, primary tumor site, tobacco use, treatment, and status at last follow-up (alive/died and disease-free or TF) were collected from the head and neck cancer registry, medical records, and death registry.¹⁵ For this study, TF was defined to include persistent residual disease 3 months following completion of definitive therapy, locoregional recurrence following a disease-free period, development of distant metastasis, or disease-related mortality of the patient. The reference standard for TF was histologic confirmation or unequivocal imaging evidence of locoregional recurrence or distant metastasis. TF was documented from the time of initial diagnosis. In cases without TF, follow-up was measured in months from diagnosis. The data were censored to the last follow-up in the medical record through July 29, 2016.

Neck CT Scans

Staging contrast-enhanced neck CT or the diagnostic contrast-enhanced neck CT portion of a staging PET/CT was reviewed for all subjects. The technique was variable, with staging neck CTs performed on 8-, 16-, or 64-channel CT scanners (GE Healthcare, Milwaukee, Wisconsin). A typical staging neck CT scan performed on a 64-channel scanner (GE Healthcare) 80 seconds following the administration of IV contrast (100-mL iopamidol, Isovue-370; Bracco, Princeton, New Jersey) used the following parameters: voltage = 120 kV(peak), tube current = 100–550 mA (automatic tube current modulation with a noise index of 9.1), pitch = 0.969 mm/rotation, gantry

rotation time = 0.8 seconds, detector collimation = 64×0.625 mm, FOV = 22 cm, 2.5 mm axial reconstructed section thickness with soft-tissue and bone algorithms. The neck CT for the diagnostic PET/CT examinations performed on 16- to 64-channel PET/CT scanners (Discovery; GE Healthcare) used the following parameters 30 seconds following the administration of IV contrast (125-mL iopamidol, Isovue-370): 120–30 kVp, variable mA (AutomA, GE Healthcare), 2.5-mm axial reconstructed section thickness through the neck, and 3.75-mm reconstructed section thickness through the body. All CT scans included in the study were deemed diagnostically adequate by both reviewing radiologists.

Image Analysis

Blinded consensus review of the CT scans was performed by 2 neuroradiologists (T.J.R. and B.F.B.). All morphologically abnormal lymph nodes in a patient were grouped together and classified as either cystic ($>20\%$ cystic change) or solid ($<20\%$ cystic change) (Figs 1 and 2). Cystic change was defined as a homogeneous low-attenuation area relative to normal muscle that was subjectively near-water attenuation with well-defined margins. Radiologic extracapsular spread (rECS) in metastatic cervical lymph nodes was defined as irregular nodal margins with invasion or distortion of surrounding soft tissues, regardless of nodal size, cystic change, or the number of pathologic nodes (Fig 3).

Treatment and Clinical Follow-Up

All patients were treated and followed according to standard institutional practice guidelines by a multidisciplinary head and neck cancer team. Patients underwent head and neck clinical examination 2 months after the conclusion of therapy and every 3 months thereafter for the first 2 years as long as they were free of disease. Subsequent follow-up typically includes clinical evaluation every 3 months for the third year and every 6 months for the fourth and fifth years following completion of treatment. All patients had a minimum of 1 posttreatment contrast-enhanced PET/CT or contrast-enhanced soft-tissue neck CT and a chest CT, starting 2–3 months after completion of therapy, with serial imaging thereafter at the discretion of the clinical team. Patients with suspicious radiologic or clinical findings underwent biopsy for

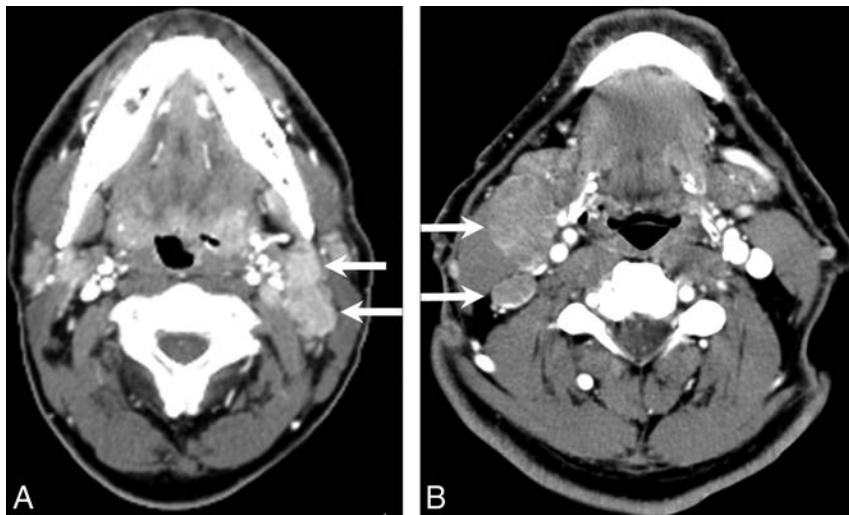


FIG 2. A and B, Two examples of metastatic lymph nodes (white arrows) classified as solid.

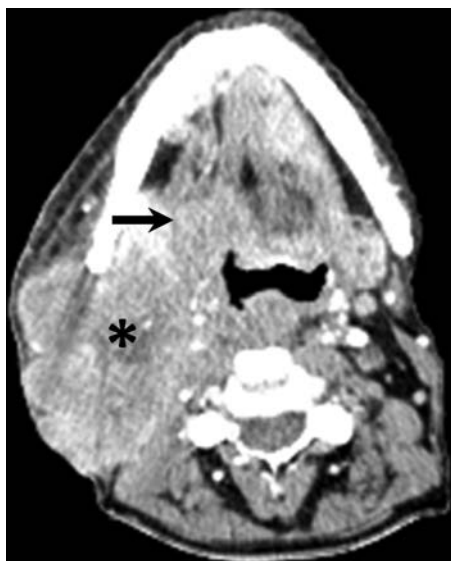


FIG 3. An example of radiographic extracapsular spread associated with a solid metastatic level II nodal mass (black asterisk) in a patient with right base of tongue oropharyngeal squamous cell carcinoma (black arrow).

confirmation or exclusion of recurrence when necessary for diagnosis.

Primary End Points and Statistical Analysis

Statistical analysis was performed by using SPSS statistics, Version 23 (IBM, Armonk, New York). Univariate Cox proportional hazard models were calculated to identify predictors of TF among the following variables: age (younger than 70 years versus 70 years and older), sex, T-stage, N-stage, primary tumor location (tonsil or tongue base), rECS, tobacco use (ever or never used tobacco products), calendar year of treatment, and solid-versus-cystic lymph nodes.⁵ A multivariate Cox proportional hazard model was performed by using the same variables with a forward inclusion threshold of 0.1. We used Pearson statistics to identify the correlation among variables that were included in the final Cox model. A *P* value significance threshold of .05 was used for all

statistics. Kaplan-Meier survival curves were plotted to visually compare disease-free survival in patients with solid-versus-cystic lymph nodes.

RESULTS

Patient Characteristics

Of 441 HPV-positive patients identified in the tumor registry from 1984 to 2014, 183 patients met the inclusion criteria (Fig 4). These 183 patients were treated between calendar years 2001 and 2014. Table 1 characterizes the patient demographics, tumor site, and staging information for all patients, categorized by solid and cystic patterns of nodal metastasis. There was no statistically significant correlation found among any of the listed

clinical and demographic variables compared with solid/cystic nodal status. Most patients were men (91.8%, 168/183), had a tonsil primary site (56.2%, 103/183), presented with N2b disease (53.0%, 97/183), and had a history of tobacco use (68.9%, 126/183). Solid and cystic patterns of nodal metastasis occurred in 42.6% (78/183) and 57.3% (105/183) of patients, respectively. The most frequent treatment technique was chemoradiotherapy (72.1%, 132/183).

Average follow-up of all patients was 38.2 months (range, 1–104 months). In the disease-free group, median follow-up from initial diagnosis was 45 months (range, 1–104 months) with 10.6% (15/141) having <24 months' follow-up. TF occurred in 42 patients (23.0% 42/183) at a mean of 14.6 months (range, 2–50 months) following initial diagnosis. Among patients with rECS, 55.6% (10/18) experienced TF.

Survival Analyses

Univariate Cox proportional hazard models showed significant differences at *P* < .05 for the following variables: solid-versus-cystic lymph nodes, T-stage, N-stage, and rECS. The multivariate Cox proportional hazard model resulted in a model that included solid-versus-cystic lymph nodes, T-stage, and rECS. A statistically significant correlation was found between rECS and solid-versus-cystic nodes (*P* = .03), but not between T-stage and solid-versus-cystic nodes (*P* = .66).

The Kaplan-Meier disease-free survival curves (Fig 5) demonstrate that overall disease-free survival was significantly lower among patients with solid metastatic regional lymph nodes at staging (*P* = .013; hazard ratio = 2.21; 95% confidence interval, 1.18–4.14). A univariate analysis of T-stages found a hazard ratio of 1.9 for T1 and T2 versus T3 and T4 (*P* < .001), and a univariate analysis of rECS found a hazard ratio of 3.3 (*P* = .001).

Table 2 lists the locations of TF. The most common pattern of TF was distant metastases alone (19/42, 45.2%). Most patients (90.4%, 38/42) experienced TF within 24 months of the initial diagnosis. Four patients (9.5%, 4/42) had TF >24 months following completion of therapy.

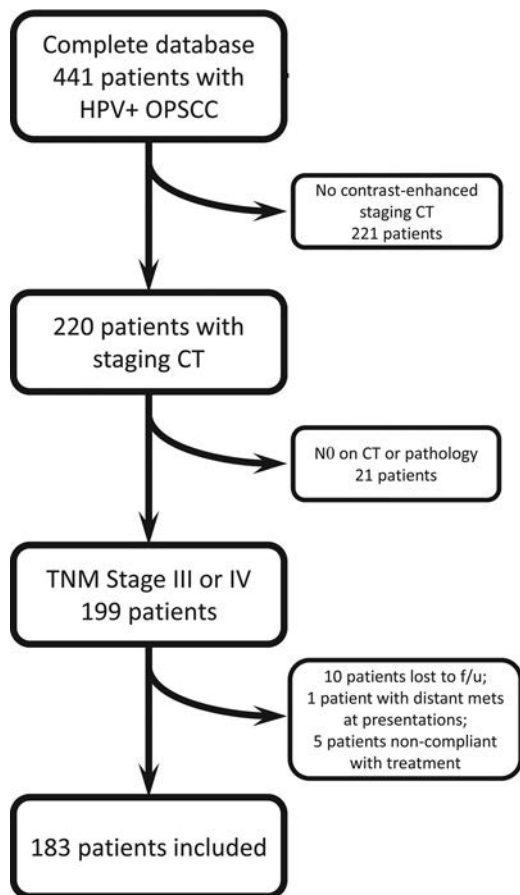


FIG 4. Data flow chart of patient selection.

DISCUSSION

In the era of rising HPV-related OPSCC affecting a population of young men, identifying reliable predictive imaging biomarkers is critical to developing tailored curative treatment regimens that minimize adverse effects. The goal of our study was to evaluate the prognostic value of the extent of cystic metastatic lymph node burden at staging for the prediction of TF in patients with stage III and IV (HPV)-related OPSCC. Our results suggest that the presence of solid lymph node metastases is an independent risk factor for TF in patients with HPV-associated OPSCC. Additionally, we found that T-stage and rECS remained independent predictors of TF in multivariate analysis. We hypothesize that greater overall solid nodal metastasis at staging more accurately reflects viable tumor burden, increasing the risk for locoregional failure and occult distant micrometastasis.

The prognostic utility of cystic-versus-solid metastatic lymph nodes in HPV-related OPSCC has not been previously reported, to our knowledge; however, the prognostic value of FDG PET/CT parameters in heterogeneous patient populations with OPSCC has been investigated. Alluri et al¹⁶ demonstrated that total metabolic tumor volume and primary metabolic tumor volume were associated with event-free survival in patients with stage III and IV HPV-related OPSCC. High standard uptake values of the primary tumor (standard uptake value > 8.0) and of nodal metastasis (standard uptake value > 10.4) have been associated with worse survival and greater rates of distant failure, respectively, in a heterogeneous population of patients with head and neck squamous

Table 1: Clinical and pathologic characteristics of patients^a

| Characteristic | All Patients (n = 183) (No.) (%) | Solid Node Group (n = 78) (No.) (%) | Cystic Node Group (n = 105) (No.) (%) |
|----------------------|--|--|--|
| Mean age (yr) | 56.1 | 56.2 | 56.1 |
| Male sex | 168 (91.8) | 75 (96.2) | 93 (88.6) |
| Smoking status | | | |
| Never smoked (<1 Py) | 56 (30.6) | 23 (29.4) | 33 (31.4) |
| Ever smoked | 120 (65.6) | 51 (65.3) | 69 (65.7) |
| <10 Py | 14 (7.7) | 4 (5.1) | 10 (9.5) |
| >10 Py | 68 (37.1) | 30 (38.5) | 38 (36.2) |
| Unknown Py | 38 (20.7) | 17 (21.8) | 21 (20.0) |
| Unknown | 1 (0.5) | 0 (0.0) | 1 (0.95) |
| Other tobacco | 6 (3.3) | 4 (5.1) | 2 (1.9) |
| T classification | | | |
| T1 | 74 (40.4) | 28 (35.9) | 46 (43.8) |
| T2 | 73 (39.9) | 35 (44.9) | 38 (36.2) |
| T3 | 16 (8.7) | 7 (8.9) | 9 (8.6) |
| T4 | 17 (9.3) | 7 (9.0) | 10 (9.5) |
| Unknown | 3 (1.6) | 1 (1.3) | 2 (1.9) |
| N classification | | | |
| N1 | 31 (16.9) | 13 (16.7) | 18 (17.1) |
| N2a | 24 (13.1) | 11 (14.1) | 13 (12.4) |
| N2b | 97 (53.0) | 37 (47.4) | 60 (57.1) |
| N2c | 26 (14.2) | 14 (17.9) | 12 (11.4) |
| N3 | 5 (2.7) | 3 (3.8) | 2 (1.9) |
| Overall stage | | | |
| Stage III | 28 (15.3) | 10 (12.8) | 18 (17.1) |
| Stage IV | 155 (84.7) | 68 (87.2) | 87 (82.9) |
| Primary tumor site | | | |
| Tonsil | 103 (56.2) | 41 (53.0) | 62 (60.0) |
| BOT | 76 (41.5) | 35 (44.9) | 41 (39.0) |
| Other | 2 (1.1) | 1 (1.3) | 1 (0.95) |
| Unknown | 2 (1.1) | 1 (1.3) | 1 (0.95) |
| Treatment | | | |
| CRT | 132 (72.1) | 57 (73.1) | 75 (71.4) |
| Operation | 12 (6.6) | 5 (6.4) | 7 (6.7) |
| Operation + MMT | 39 (21.3) | 16 (20.5) | 23 (21.9) |

Note:—Py indicates pack-year; BOT, base of tongue; CRT, chemoradiotherapy; MMT, multimodality therapy.

^aNo statistically significant correlation was found among any of the listed clinical and demographic variables compared with solid/cystic nodal status.

cell carcinoma.¹⁷ Cheng et al¹⁸ also determined that tumor total lesional glycolysis was an independent predictor of survival in patients with locally advanced OPSCC. The overall metastatic solid nodal metastasis volume on CT likely corresponds to FDG-avid viable nodal metastasis on FDG PET/CT. Our results are congruent with FDG PET/CT studies suggesting that viable tumor volume at staging impacts prognosis. However, there is no clear consensus on whether primary tumor volume, nodal metastatic tumor volume, or total viable tumor (primary + nodes) volume has the greatest prognostic value.

The prognostic value of other imaging parameters has been evaluated. Davis et al¹⁹ found that lower nodal volume was associated with greater disease-free survival in patients with HPV-related OPSCC, but did not distinguish solid-versus-cystic metastatic nodal volume. Spector et al⁹ reported that matted nodes, defined as “3 nodes abutting one another with loss of intervening fat plane,” are a novel imaging marker of poor prognosis in OPSCC, independent of HPV status. We did not evaluate matted nodes, given previously demonstrated poor interobserver agreement for this parameter.²⁰ The negative predictive value of rECS

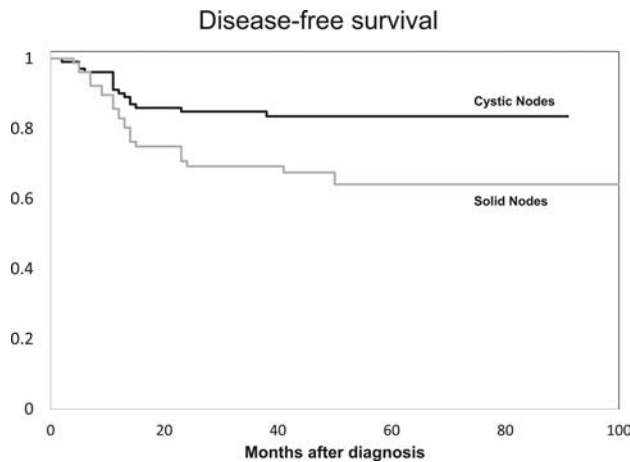


FIG 5. Kaplan-Meier survival curves. Overall disease-free survival was significantly lower among patients with cystic-versus-solid metastatic regional lymph nodes at staging ($P = .013$; hazard ratio = 2.21; 95% confidence interval, 1.18–4.14).

Table 2: Sites of treatment failure

| Site (n = 42) | No. (%) |
|------------------------------|-----------|
| Local | 3 (7.1) |
| Regional | 7 (16.7) |
| Distant | 19 (45.2) |
| Local and regional | 6 (14.3) |
| Local and distant | 1 (2.4) |
| Regional and distant | 3 (7.1) |
| Local, regional, and distant | 3 (7.1) |

on CT is poor; however, rECS on CT as evidenced by adjacent structure invasion has a good positive predictive value.^{20–23} We found, in multivariate analysis, that rECS with invasion of surrounding soft tissues was an independent predictor of TF and that rECS correlated significantly with solid lymph node metastasis. Recently Liu et al²⁴ did not find rECS to be an independent predictor of TF in a subset of patients with HPV-related OPSCC, though there was a trend toward worse survival in this group.

Kaka et al¹⁰ reported a predominance (>80%) of central tumor necrosis, evidence of extracapsular spread, and clustering of nodes (analogous to matted nodes) in their case series of 8 aggressive HPV-related OPSCCs. Joo et al²⁵ reported a significant positive correlation between lymph node size and high-risk HPV status and a significant positive correlation between lymph node size and cystic nodal metastases, yet with an overall better disease-specific survival rate in HPV-related head and neck squamous cell carcinoma compared with HPV-negative tumors. Huang et al⁵ also found that N2a disease had better overall survival compared with N1 disease, applying traditional TNM staging in a cohort of patients with HPV-related OPSCC. The results of Joo et al²⁵ and Huang et al⁵ support our hypothesis that solid or viable nodal metastatic burden may be prognostically more important, given the intranodal cystic changes frequently observed in HPV-related OPSCC.

We performed a multivariate analysis to address the possible covariance of radiologic and nonradiologic factors as prognosticators of TF. We could not confirm an association between TF and tobacco use, sex, or age, though an effect may exist but was too small to measure in the current study. Data on the impact of

smoking on TF in the literature are conflicting.^{26–28} Our results are similar to those of O’Sullivan et al,²⁸ who also found no effect of smoking on disease control in patients with HPV-related OPSCC, though overall survival among >10 pack-year smokers was reduced.

The results of the current study merit further investigation given the single-institution, retrospective nonrandomized nature of the study. We focused our study on HPV-related OPSCC and did not include non-HPV-related OPSCC, which constitutes an area of potential research. Due to the retrospective nature of this study, treatment regimens were variable, which can impact TF rates. Finally, we did not determine whether recurrences were treatable, and if treatable, whether treatment impacted overall survival.

CONCLUSIONS

Patients with HPV-related OPSCC who have solid lymph node metastases at staging CT have a higher risk for TF than patients with cystic lymph nodes. Larger scale, longer prospective studies are warranted to determine whether solid nodal metastasis is a useful imaging biomarker to risk-stratify patients for personalized treatment regimens in advanced-stage HPV-related OPSCC.

Disclosures: Srikala Narayanan—*UNRELATED: Employment:* work as an attending at Children’s Hospital of University of Pittsburgh Medical Center; *Other:* This work was presented at the American Society of Neuroradiology conference and won outstanding oral presentation for head and neck in 2014; prize money was given by the American Society of Neuroradiology. Robert L. Ferris—*UNRELATED: Board Membership:* Astra-Zeneca/Medimmune, Bristol-Myers Squibb, Eli Lilly and Company, Merck, Pfizer; *Grants/Grants Pending:* Astra-Zeneca/Medimmune, Bristol-Myers Squibb, Merck, VentiRx Pharmaceuticals*. *Money paid to the institution.

REFERENCES

- Gillison ML, Koch WM, Capone RB, et al. **Evidence for a causal association between human papillomavirus and a subset of head and neck cancers.** *J Natl Cancer Inst* 2000;92:709–20 [CrossRef](#) [Medline](#)
- Fakhry C, Westra WH, Li S, et al. **Improved survival of patients with human papillomavirus-positive head and neck squamous cell carcinoma in a prospective clinical trial.** *J Natl Cancer Inst* 2008;100:261–69 [CrossRef](#) [Medline](#)
- Ang KK, Harris J, Wheeler R, et al. **Human papillomavirus and survival of patients with oropharyngeal cancer.** *N Engl J Med* 2010;363:24–35 [CrossRef](#) [Medline](#)
- Mirghani H, Amen F, Blanchard P, et al. **Treatment de-escalation in HPV-positive oropharyngeal carcinoma: ongoing trials, critical issues and perspectives.** *Int J Cancer* 2015;136:1494–503 [CrossRef](#) [Medline](#)
- Huang SH, Xu W, Waldron J, et al. **Refining American Joint Committee on Cancer/Union for International Cancer Control TNM stage and prognostic groups for human papillomavirus-related oropharyngeal carcinomas.** *J Clin Oncol* 2015;33:836–45 [CrossRef](#) [Medline](#)
- Horne ZD, Glaser SM, Vargo JA, et al. **Confirmation of proposed human papillomavirus risk-adapted staging according to AJCC/UICC TNM criteria for positive oropharyngeal carcinomas.** *Cancer* 2016;122:2021–30 [CrossRef](#) [Medline](#)
- Huang SH, Perez-Ordóñez B, Liu FF, et al. **Atypical clinical behavior of p16-confirmed HPV-related oropharyngeal squamous cell carcinoma treated with radical radiotherapy.** *Int J Radiat Oncol Biol Phys* 2012;82:276–83 [CrossRef](#) [Medline](#)
- O’Sullivan B, Huang SH, Perez-Ordóñez B, et al. **Outcomes of HPV-related oropharyngeal cancer patients treated by radiotherapy**

- alone using altered fractionation. *Radiother Oncol* 2012;103:49–56 CrossRef Medline
9. Spector ME, Gallagher KK, Light E, et al; University of Michigan Head Neck Specialized Program of Research Excellence (SPORE) Program. **Matted nodes: poor prognostic marker in oropharyngeal squamous cell carcinoma independent of HPV and EGFR status.** *Head Neck* 2012;34:1727–33 CrossRef Medline
10. Kaka AS, Kumar B, Kumar P, et al. **Highly aggressive human papillomavirus-related oropharyngeal cancer: clinical, radiologic, and pathologic characteristics.** *Oral Surg Oral Med Oral Pathol Oral Radiol* 2013;116:327–35 CrossRef Medline
11. Goldenberg D, Begum S, Westra WH, et al. **Cystic lymph node metastasis in patients with head and neck cancer: an HPV-associated phenomenon.** *Head Neck* 2008;30:898–903 CrossRef Medline
12. Morani AC, Eisbruch A, Carey TE, et al. **Intranodal cystic changes: a potential radiologic signature/biomarker to assess the human papillomavirus status of cases with oropharyngeal malignancies.** *J Comput Assist Tomogr* 2013;37:343–45 CrossRef Medline
13. Chiosea SI, Grandis JR, Lui VW, et al. **PIK3CA, HRAS and PTEN in human papillomavirus positive oropharyngeal squamous cell carcinoma.** *BMC Cancer* 2013;13:602 CrossRef Medline
14. Maxwell JH, Ferris RL, Gooding W, et al. **Extracapsular spread in head and neck carcinoma: impact of site and human papillomavirus status.** *Cancer* 2013;119:3302–08 CrossRef Medline
15. Edge SB, Byrd DR, Compton CC, et al, eds. *AJCC Cancer Staging Manual*. 7th ed. New York: Springer; 2010:41–56
16. Alluri KC, Tahari AK, Wahl RL, et al. **Prognostic value of FDG PET metabolic tumor volume in human papillomavirus-positive stage III and IV oropharyngeal squamous cell carcinoma.** *AJR Am J Roentgenol* 2014;203:897–903 CrossRef Medline
17. Kubicek GJ, Champ C, Fogh S, et al. **FDG-PET staging and importance of lymph node SUV in head and neck cancer.** *Head Neck Oncol* 2010;2:19 CrossRef Medline
18. Cheng NM, Chang JT, Huang CG, et al. **Prognostic value of pretreatment ¹⁸F-FDG PET/CT and human papillomavirus type 16 testing in locally advanced oropharyngeal squamous cell carcinoma.** *Eur J Nucl Med Mol Imaging* 2012;39:1673–84 CrossRef Medline
19. Davis KS, Lim CM, Clump DA, et al. **Tumor volume as a predictor of survival in human papillomavirus-positive oropharyngeal cancer.** *Head Neck* 2016;38(suppl 1):E1613–17 CrossRef Medline
20. Chai RL, Rath TJ, Johnson JT, et al. **Accuracy of computed tomography in the prediction of extracapsular spread of lymph node metastases in squamous cell carcinoma of the head and neck.** *JAMA Otolaryngol Head Neck Surg* 2013;139:1187–94 CrossRef Medline
21. Branstetter BF, Rath TJ, Kubicek GJ. **Accuracy of computed tomography for predicting pathologic nodal extracapsular extension in patients with head and neck cancer undergoing initial surgical resection: in regard to Prabhu, et al.** *Int J Radiat Oncol Biol Phys* 2014;89:434–35 CrossRef Medline
22. Prabhu RS, Magliocca KR, Hanasoge S, et al. **Accuracy of computed tomography for predicting pathologic nodal extracapsular extension in patients with head-and-neck cancer undergoing initial surgical resection.** *Int J Radiat Oncol Biol Phys* 2014;88:122–29 CrossRef Medline
23. Maxwell JH, Rath TJ, Byrd JK, et al. **Accuracy of computed tomography to predict extracapsular spread in p16-positive squamous cell carcinoma.** *Laryngoscope* 2015;125:1613–18 CrossRef Medline
24. Liu JT, Kann BH, De B, et al. **Prognostic value of radiographic extracapsular extension in locally advanced head and neck squamous cell cancers.** *Oral Oncol* 2016;52:52–57 CrossRef Medline
25. Joo YH, Cho KJ, Park JO, et al. **High-risk human papillomavirus and lymph node size in patients with single node metastasis of oral and oropharyngeal cancer.** *Acta Otolaryngol* 2014;134:395–400 CrossRef Medline
26. Maxwell JH, Kumar B, Feng FY, et al. **Tobacco use in human papillomavirus-positive advanced oropharynx cancer patients related to increased risk of distant metastases and tumor recurrence.** *Clin Cancer Res* 2010;16:1226–35 CrossRef Medline
27. Gillison ML, Zhang Q, Jordan R, et al. **Tobacco smoking and increased risk of death and progression for patients with p16-positive and p16-negative oropharyngeal cancer.** *J Clin Oncol* 2012;30:2102–11 CrossRef Medline
28. O’Sullivan B, Huang SH, Siu LL, et al. **Deintensification candidate subgroups in human papillomavirus-related oropharyngeal cancer according to minimal risk of distant metastasis.** *J Clin Oncol* 2013;31:543–50 CrossRef Medline

The Central Bright Spot Sign: A Potential New MR Imaging Sign for the Early Diagnosis of Anterior Ischemic Optic Neuropathy due to Giant Cell Arteritis

 P. Remond,  A. Attyé,  A. Lecler,  L. Lamalle,  N. Boudiaf,  F. Aptel,  A. Krainik, and  C. Chiquet

ABSTRACT

BACKGROUND AND PURPOSE: A rapid identification of the etiology of anterior ischemic optic neuropathy is crucial because it determines therapeutic management. Our aim was to assess MR imaging to study the optic nerve head in patients referred with anterior ischemic optic neuropathy, due to either giant cell arteritis or the nonarteritic form of the disease, compared with healthy subjects.

MATERIALS AND METHODS: Fifteen patients with giant cell arteritis–related anterior ischemic optic neuropathy and 15 patients with nonarteritic anterior ischemic optic neuropathy from 2 medical centers were prospectively included in our study between August 2015 and May 2016. Fifteen healthy subjects and patients had undergone contrast-enhanced, flow-compensated, 3D T1-weighted MR imaging. The bright spot sign was defined as optic nerve head enhancement with a 3-grade ranking system. Two radiologists and 1 ophthalmologist independently performed blinded evaluations of MR imaging sequences with this scale. Statistical analysis included interobserver agreement.

RESULTS: MR imaging scores were significantly higher in patients with giant cell arteritis–related anterior ischemic optic neuropathy than in patients with nonarteritic anterior ischemic optic neuropathy ($P \leq .05$). All patients with giant cell arteritis–related anterior ischemic optic neuropathy (15/15) and 7/15 patients with nonarteritic anterior ischemic optic neuropathy presented with the bright spot sign. No healthy subjects exhibited enhancement of the anterior part of the optic nerve. There was a significant relationship between the side of the bright spot and the side of the anterior ischemic optic neuropathy ($P \leq .001$). Interreader agreement was good for observers ($\kappa = 0.815$).

CONCLUSIONS: Here, we provide evidence of a new MR imaging sign that identifies the acute stage of giant cell arteritis–related anterior ischemic optic neuropathy; patients without this central bright spot sign always had a nonarteritic pathophysiology and therefore did not require emergency corticosteroid therapy.

ABBREVIATIONS: AION = anterior ischemic optic neuropathy; FFE = fast-field echo; GCA = giant cell arteritis; GCA-AION = giant cell arteritis–related anterior ischemic optic neuropathy; NA-AION = nonarteritic anterior ischemic optic neuropathy

Anterior ischemic optic neuropathy (AION) is the most common acute optic neuropathy in individuals older than 50 years of age, with an incidence of 2–10 per 100,000 people per year.^{1,2} AION results from ischemic events within the optic nerve; these may be related to systemic vasculitis affecting large- and medium-caliber vessels in the arteritic form, due to giant cell arteritis (GCA-AION) or to blood flow disturbances associated with

nonarteritic ischemic optic neuropathy (NA-AION). A rapid identification of the etiology is crucial because it determines the therapeutic management; corticosteroids must be promptly administered in cases of GCA-AION. Establishing the diagnosis of giant cell arteritis (GCA) may be challenging. The histopathologic result of a temporal artery biopsy has been considered the diagnostic standard but should not delay the prompt institution of steroid therapy. Some clinical signs suggest an arteritic etiology, including amaurosis fugax and systemic symptoms; a marked deterioration of visual acuity; more extensive visual field defects; diplopia; and the findings of fundus examination and fluorescein or indocyanine green angiography.³ However, ophthalmologists require a rapid diagnostic test to definitively rule out this diagnosis in an emergency setting. In GCA-AION, the granulomatous inflammatory artery infiltrate consists of T-lymphocytes, macrophages, and multinucleated giant cells. The pathogenesis is still not fully understood, though there have been major advances in

Received November 3, 2016; accepted after revision February 25, 2017.

From the Department of Neuroradiology and MRI (P.R., A.A., A.K.), SFR RMN Neurosciences, and Department of Ophthalmology (P.R., F.A., C.C.), University Hospital of Grenoble, Grenoble, France; University Grenoble Alpes (A.A., L.L., N.B., A.K.), IRMaGe, Grenoble, France; and Department of Neuroradiology (A.L.), Rothschild Foundation, Paris, France.

The study was supported by Guerbet SA for MRI in Healthy Subjects.

Please address correspondence to Arnaud Attyé, MD, Neuroradiology and MR Unit, CS 10217, Grenoble University Hospital, F-38043, Grenoble Cedex 9, France; e-mail: aatty@chu-grenoble.fr

<http://dx.doi.org/10.3174/ajnr.A5205>

recent years. Cytotoxic mediators and growth factors trigger the remodeling of the arterial wall, leading to ischemic manifestations by luminal stenosis.⁴

An MR imaging examination is often used to narrow the differential diagnosis of optic disc edema and to highlight retrobulbar optic nerve enhancement in optic neuritis, a differential consideration of AION.^{5,6} In addition, imaging of branches of the external carotid artery may be useful in the diagnosis of GCA.⁷ In contrast, radiologic data have traditionally failed to obtain positive signs for diagnosing AION; the most common finding in these patients is brain leukoaraiosis, particularly in patients with the nonarteritic form of the disease.⁸ MR imaging is the technique of choice for studying subtle ischemic events, either with contrast media or diffusion imaging. However, diffusion-weighted MR imaging is prone to distortion and motion artifacts, which may be problematic for the study of the anterior optic pathway.

We raised the hypothesis that cytotoxic ischemia is more pronounced in GCA-AION compared with NA-AION, potentially leading to more permeable vessels in the former. We further hypothesized that damage to the anterior optic nerve microcirculation at the acute stage of AION might be revealed by contrast-enhanced MR imaging through a focal enhancement of the optic nerve head, the “central bright spot sign.”

MATERIALS AND METHODS

This was a multicenter, parallel-group imaging study that was registered with the ClinicalTrials.gov registry for healthy volunteers (NCT02529475). The study was approved by our institutional review board (6705/15-CHUG-02) for patients. It was conducted in accordance with the Declaration of Helsinki and international standards of Good Clinical Practice. Signed informed consent was obtained from all healthy volunteers.

Study Population and Design

Patients with typical MR imaging contraindications, such as implanted pacemakers, metallic foreign bodies, claustrophobia, contrast agent allergy, or renal dysfunction with a glomerular filtration rate of <30 mL/h, were excluded.

Patients 18 years of age or older were consecutively included in this study if they presented with acute onset of AION symptoms between August 2015 and May 2016. A diagnosis of AION was made following a recent appearance of a painless decrease in visual acuity and/or visual field defects and a clinical examination for diffuse or sectoral optic disc edema and peripapillary hemorrhages.⁴ Fluorescein angiography (Heidelberg Engineering, Heidelberg, Germany) was performed to detect the early stages of choroidal ischemia, and a visual examination (Humphrey Automated Field Analyzer 30–2 SITA-standard; Zeiss, Dublin, California) was performed at admission.

These patients were consecutively included if they had undergone MR imaging with a 3D radiofrequency-spoiled T1-weighted high-resolution, flow-compensated, fast-field echo (FFE) acquisition.

The diagnosis of GCA was based on being older than 50 years of age, systemic symptoms (anorexia, weight loss, jaw claudication, headache, scalp tenderness, abnormal temporal artery, neck pain, myalgia, malaise, and anemia), ophthalmologic examina-

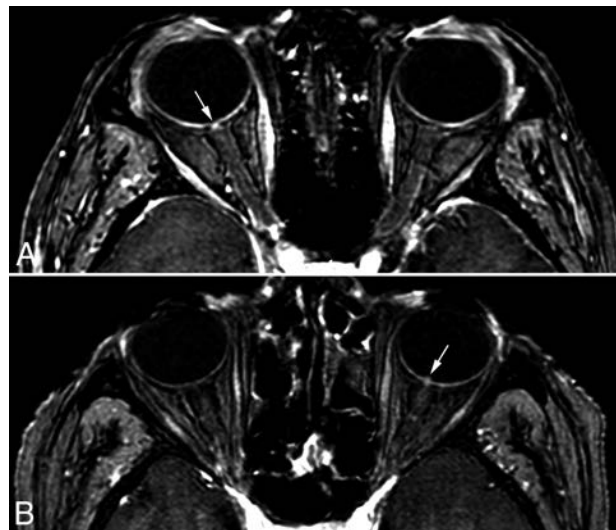


FIG 1. High-resolution T1 sequences in the axial plane showing the bright spot sign ranking score. *A*, The first patient was referred with right nonarteritic AION and a score of 1, with no optic nerve head intravitreal protrusion but local enhancement (white arrow). *B*, The second patient was referred with left GCA-related AION and both protrusion and local enhancement, defined as score 2 (white arrow).

tion, biologic inflammatory syndrome with erythrocyte sedimentation, elevated C-reactive protein, and a biopsy of the temporal artery positive for GCA.

Healthy volunteers were included in the control group and had undergone MR imaging with the same protocol, to ensure that normal vascularization of the optic nerve head could be distinguished from disease process.

Imaging Diagnosis

Two board-certified radiologists (A.A. and A.L.) and 1 ophthalmologist (P.R.) from 2 different university hospitals independently evaluated anonymized MR images of patients and healthy subjects. The readers were blinded to all clinical data. We performed the scans on a 3T MR imaging scanner, Achieva 3T TX (Philips Healthcare, Best, the Netherlands) with a 32-channel head coil. The MR imaging included a 3D radiofrequency-spoiled T1-weighted high-resolution, flow-compensated, FFE acquisition (magnitude image from a phase conventional angiography scan), by using the shortest TR and partial-echo TE (7.4 and 4.1 ms, respectively), 12° flip angle, 480-Hz/pixel readout gradient, transverse orientation, 95 sections, voxel size acquisition = $0.6 \times 0.7 \times 0.8$ mm³, voxel size reconstruction = 0.33, 0.33, and 0.40 mm³, right-left phase encoding, and scan time = 5 minutes 19 seconds. This evaluation was added to T2 spin-echo with whole-brain coverage.

MR Imaging Grading System

For qualitative analyses, we visually evaluated the intensity of the optic nerve head with a 3-grade ranking system. Each optic nerve head was assigned a score as follows:

Score 0: no optic nerve head enhancement

Score 1: optic nerve head enhancement without intravitreal protrusion (Fig 1A)

Score 2: both optic nerve head enhancement and intravitreal protrusion (Fig 1B).

Table 1: Number of patients with the bright spot sign for each reader

| Reader | Healthy Subjects (n = 15) | NA-AION (n = 15) | GCA-AION (n = 15) |
|----------|---------------------------|------------------|-------------------|
| Reader 1 | 0/15 | 7/15 | 15/15 |
| Reader 2 | 0/15 | 6/15 | 15/15 |
| Reader 3 | 0/15 | 6/15 | 15/15 |

In this study, score 0 represented physiologic features, and scores 1 and 2 represented active papillary disease.

Each observer rated the MR images of each patient as positive or negative for AION; for a positive MR imaging result, an optic nerve head score of 1 or 2 was required.

Statistical Analysis

Data were analyzed with SPSS software, Version 22.0 (IBM, Armonk, New York). Continuous data are presented as means with SDs. Age differences between healthy participants and patients were tested by using the Student *t* test. Categorical data were reported as frequency and percentages. The Pearson χ^2 test was used for the independence of the side of the central bright spot sign and the clinical side of the disease in the patient group. Sensitivity, specificity, positive/negative predictive values, and positive/negative likelihood ratios of the MR imaging examinations were calculated for each observer. The interobserver agreement was calculated by using the Fleiss κ test; a κ value > 0.80 represented outstanding agreement. We set the significance threshold (*P* values) at .05.⁹

RESULTS

Fifteen healthy volunteers (8 women, 7 men) were included in this study, with a mean age of 62 ± 6 years. Thirty patients (8 women, 22 men) were included with a mean age of 71 ± 11 years. Fifteen patients presented with NA-AION, while 15 presented with GCA-AION, confirmed with histopathologic examination. The delay between ocular symptoms and MR imaging was 3 ± 1.2 days. No adverse effects were observed after injection of gadoteric acid. There was no significant difference in the ages of healthy and patient groups.

Bright Spot Findings

With contrast-enhanced MR imaging, patients in the control group exhibited no enhancement of the optic nerve head. All patients with GCA-AION and 7 of 15 patients (46%) with NA-AION presented with the bright spot sign, a local enhancement of the optic nerve head on the high-resolution T1 sequence. The interobserver agreement for the 3-grade ranking system was high ($\kappa = 0.82$) (Table 1).

We found a significant relationship between the side of the bright spot and the side of clinical disease ($P \leq .001$). Table 2 summarizes the sensitivity, specificity, positive/negative predictive values, and positive/negative likelihood ratios of the MR imaging examinations.

MR imaging allows to distinguish GCA-AION from NA-AION with sensitivity of 100%, and specificity ranging from 53.3% to 60% for observer. Most important, all patients with AION and without a bright spot sign were diagnosed with NA-

AION (Table 2). This finding was supported by a negative likelihood ratio of <0.1 (ie, very useful for identifying patients who did not have GCA-AION).

In patients with NA-AION, MR imaging had a moderate sensitivity and high specificity and positive predictive value, compared with healthy volunteers (Table 2).

In patients with GCA-AION versus healthy subjects, the sensitivity, specificity, and negative and positive predictive values of MR imaging were 100% for each reader because the central bright spot sign was observed in all these patients.

The presence of the central bright spot sign was not significantly associated with age in either group.

DISCUSSION

Here, we have demonstrated the early presence of a new MR imaging sign in the acute phase of AION. All patients with GCA-AION exhibited optic nerve head enhancement, compared with only 50% of patients with NA-AION ($P \leq .05$) and 0% of healthy volunteers ($P \leq .01$). Therefore, in our series, the absence of optic nerve head enhancement in patients with AION precluded a diagnosis of giant cell arteritis.

In the clinical management of patients with AION, it is crucial to diagnose GCA promptly because early treatment with corticosteroids decreases both the risk of contralateral eye injury and recurrence on the original side^{1,3} and also decreases the risk of systemic complications. To date, there is limited evidence available regarding the value of MR imaging for patients with ischemic optic neuropathy. In a previous study with T1 inversion recovery—weighted imaging, Rizzo et al⁴ observed abnormalities in the clinically affected optic nerve of patients with optic neuritis (ie, associated with demyelinating brain disorders), whereas no abnormal signal was detected in patients with AION. Recently, an MR imaging study of 3 patients with AION highlighted possible optic nerve perineural sheath and optic chiasma enhancement.¹⁰ However, the optic nerve head was not studied in these patients.

This is the first MR imaging study that demonstrates an optic nerve head morphologic sign in patients with AION, to our knowledge. The negative predictive value of this sign strongly suggests that the absence of the bright spot sign rules out a diagnosis of GCA-AION.

In addition to morphologic brain examination, it was recently proposed that diffusion-weighted MR imaging and tractography postprocessing may help diagnose AION at the subacute stage.¹¹ Focusing on diffusion-weighted MR imaging, Bender et al¹² described 5 cases of acute optic ischemia with diffusion restriction and reduced apparent diffusion coefficient, while Wan et al¹¹ found only 2 cases of AION in a cohort of 42 patients. In a larger tractography study of 26 patients, Wang et al¹³ proposed several diffusion biomarkers in patients with AION that may serve as biomarkers of axonal and myelin damage in AION. However, diffusion-weighted MR imaging is prone to distortion and motion artifacts. This may be problematic for the study of optic pathways and extraction of quantitative values. Furthermore, the tensor model typically used for tractography in this area is particularly challenging to apply to the low signal-to-noise ratio areas.¹⁴ In addition, diffusion-weighted MR imaging depends on axonal

Table 2: Sensitivity, specificity, positive/negative predictive values, and positive/negative likelihood ratios of the MR imaging bright spot sign in healthy subjects and patients with GCA-AION or NA-AION

| | No. of Participants | TP Results | TN Results | FP Results | FN Results | Sensitivity (%) | Specificity (%) | PPV (%) | NPV (%) | PLR | NLR |
|------------------------------|------------------------|---------------|---------------|---------------|---------------|--------------------|--------------------|------------|------------|-----|-----|
| NA-AION vs GCA-AION | | | | | | | | | | | |
| Observer 1 | 30 | 15 | 8 | 7 | 0 | 100 | 53.3 | 68.2 | 100 | 2.1 | 0 |
| Observer 2 | 30 | 15 | 9 | 6 | 0 | 100 | 60 | 71.4 | 100 | 3.5 | 0 |
| Observer 3 | 30 | 15 | 9 | 6 | 0 | 100 | 60 | 71.4 | 100 | 3.5 | 0 |
| NA-AION vs healthy subjects | | | | | | | | | | | |
| Observer 1 | 30 | 7 | 15 | 0 | 8 | 46.7 | 100 | 100 | 65.2 | | 0.5 |
| Observer 2 | 30 | 6 | 15 | 0 | 9 | 40 | 100 | 100 | 62.5 | | 0.6 |
| Observer 3 | 30 | 6 | 15 | 0 | 9 | 40 | 100 | 100 | 62.5 | | 0.6 |
| GCA-AION vs healthy subjects | | | | | | | | | | | |
| Observer 1 | 30 | 15 | 15 | 0 | 0 | 100 | 100 | 100 | 100 | | 0 |
| Observer 2 | 30 | 15 | 15 | 0 | 0 | 100 | 100 | 100 | 100 | | 0 |
| Observer 3 | 30 | 15 | 15 | 0 | 0 | 100 | 100 | 100 | 100 | | 0 |

Note:—FN indicates false-negative; FP, false-positive; PLR, positive likelihood ratio; NLR, negative likelihood ratio; NPV, negative predictive value; PPV, positive predictive value; TN, true-negative; TP, true-positive.

integrity but also on other parameters such as axon diameter and the degree of myelination or the space between axons.¹⁵

A published case report of a patient with NA-AION has previously described this marked enhancement of the optic disc, similar to the bright spot sign.¹⁶ Friedland et al¹⁷ reported that this phenomenon could be associated with increased perfusion, a reparative reaction to ischemia. Hayreh¹⁸ determined that optic disc edema is always present in acute AION, due to 2 factors: an axonal ischemia mechanism with capillary leakage in the optic nerve head and a venous stasis secondary to the acute stroke. Optic nerve head enhancement on MR imaging assessment has previously been described in patients with pseudotumor cerebri compared with controls¹⁹ and in 1 patient at the acute stage of Leber hereditary optic neuropathy.²⁰

In our study, the bright spot sign was consistently observed in patients with GCA-AION and is concordant with the cytotoxic ischemia of this disease.²¹

We acknowledge that there are several limitations of this study. First, we should acknowledge a small sample size for patients with AION. While these results are encouraging, further multicenter studies that involve a large number of patients with AION, which is a rare disease in the context of GCA, should be performed to validate the early use of enhanced and high-resolution MR images.

In addition, we performed the scanning at the subacute phase with a mean delay of 3 ± 1.2 days. In the absence of other time points, however, we cannot currently determine the optimal delay for the examination, especially relating to the hours immediately after the clinical event. Follow-up studies would also be of interest to observe the evolution of the MR imaging signal with the time, with the potential limit of repeated injections of gadolinium which may be associated with contrast media accumulation in the brain parenchyma of healthy subjects.^{22,23} Here, we used a macrocyclic gadolinium chelate administration that, to date, has not been associated with the presence of hypersignal intensity in the dentate nucleus.²³

A long-term, clinical follow-up of patients would allow determining whether there is a correlation among the central bright spot sign, visual field defects, and/or involvement of the retinal nerve fiber layer of the optic nerve and macular ganglion cells, as has previously been demonstrated with optical coherence tomog-

raphy.²⁴ It might also reveal a possible predictive power for the likelihood of recovery or visual prognosis according to the absence or presence of the signal and its visual scale ranking.

CONCLUSIONS

This preliminary study suggests that patients with suspected ischemic optic neuropathy can potentially benefit from MR imaging in the emergency setting, to differentiate GCA-AION and NA-AION and definitively exclude the arteritic form.

ACKNOWLEDGMENTS

The authors acknowledge the valuable assistance of Patrice Jousse for editing the MR imaging pictures and drawings. We also thank Dr Louise Ball for critically editing the manuscript.

Disclosures: Arnaud Attyé—RELATED: Grant: Guerbet SA, Comments: The MRI for Healthy Subjects was funded by Guerbet SA*. Christophe Chiquet—UNRELATED: Board Membership: Allergan, Thea, ABBVIE. *Money paid to the institution.

REFERENCES

- Johnson LN, Arnold AC. Incidence of nonarteritic and arteritic anterior ischemic optic neuropathy: population-based study in the state of Missouri and Los Angeles County, California. *J Neuroophthalmol* 1994;14:38–44 Medline
- Hattenhauer MG, Leavitt JA, Hodge DO, et al. Incidence of nonarteritic anterior ischemic optic neuropathy. *Am J Ophthalmol* 1997; 123:103–07 CrossRef Medline
- Hayreh SS, Podhajsky PA, Zimmerman B. Occult giant cell arteritis: ocular manifestations. *Am J Ophthalmol* 1998;125:521–26 CrossRef Medline
- Rizzo JF 3rd, Andreoli CM, Rabinov JD. Use of magnetic resonance imaging to differentiate optic neuritis and nonarteritic anterior ischemic optic neuropathy. *Ophthalmology* 2002;109:1679–84 CrossRef Medline
- Hoorbakht H, Bagherkashi F. Optic neuritis, its differential diagnosis and management. *Open Ophthalmol J* 2012;6:65–72 CrossRef Medline
- Klink T, Geiger J, Both M, et al. Giant cell arteritis: diagnostic accuracy of MR imaging of superficial cranial arteries in initial diagnosis—results from a multicenter trial. *Radiology* 2014;273:844–52 CrossRef Medline
- Argyropoulou MI, Zikou AK, Tzovara I, et al. Non-arteritic anterior ischaemic optic neuropathy: evaluation of the brain and optic pathway by conventional MRI and magnetisation transfer imaging. *Eur Radiol* 2007;17:1669–74 CrossRef Medline

8. Hayreh SS. **Ischemic optic neuropathy.** *Prog Retin Eye Res* 2009;28:34–62 [CrossRef Medline](#)
9. Landis JR, Koch GG. **The measurement of observer agreement for categorical data.** *Biometrics* 1977;33:159–74 [CrossRef Medline](#)
10. D'Souza NM, Morgan ML, Almarzouqi SJ, et al. **Magnetic resonance imaging findings in giant cell arteritis.** *Eye (Lond)* 2016;30:758–62 [CrossRef Medline](#)
11. Wan H, Sha Y, Zhang F, et al. **Diffusion-weighted imaging using readout-segmented echo-planar imaging, parallel imaging, and two-dimensional navigator-based reacquisition in detecting acute optic neuritis.** *J Magn Reson Imaging* 2016;43:655–60 [CrossRef Medline](#)
12. Bender B, Heine C, Danz S, et al. **Diffusion restriction of the optic nerve in patients with acute visual deficit.** *J Magn Reson Imaging* 2014;40:334–40 [CrossRef Medline](#)
13. Wang MY, Qi PH, Shi DP. **Diffusion tensor imaging of the optic nerve in subacute anterior ischemic optic neuropathy at 3T.** *AJNR Am J Neuroradiol* 2011;32:1188–94 [CrossRef Medline](#)
14. Farquharson S, Tournier JD, Calamante F, et al. **White matter fiber tractography: why we need to move beyond DTI.** *J Neurosurg* 2013;118:1367–77 [CrossRef Medline](#)
15. Beaulieu C, De Crespigny A, Tong DC, et al. **Longitudinal magnetic resonance imaging study of perfusion and diffusion in stroke: evolution of lesion volume and correlation with clinical outcome.** *Ann Neurol* 1999;46:568–78 [Medline](#)
16. Yovel OS, Katz M, Leiba H. **Magnetic resonance imaging of luxury perfusion of the optic nerve head in anterior ischemic optic neuropathy.** *J Neuroophthalmol* 2012;32:256–58 [CrossRef Medline](#)
17. Friedland S, Winterkorn JM, Burde RM. **Luxury perfusion following anterior ischemic optic neuropathy.** *J Neuroophthalmol* 1996;16:163–71 [CrossRef Medline](#)
18. Hayreh SS. **Fluids in the anterior part of the optic nerve in health and disease.** *Surv Ophthalmol* 1978;23:1–25 [CrossRef Medline](#)
19. Brodsky MC, Vaphiades M. **Magnetic resonance imaging in pseudotumor cerebri.** *Ophthalmology* 1998;105:1686–93 [CrossRef Medline](#)
20. Lamirel C, Cassereau J, Cochereau I, et al. **Papilloedema and MRI enhancement of the prechiasmal optic nerve at the acute stage of Leber hereditary optic neuropathy.** *J Neurol Neurosurg Psychiatry* 2010;81:578–80 [CrossRef Medline](#)
21. Weyand CM, Goronzy JJ. **Immune mechanisms in medium and large-vessel vasculitis.** *Nat Rev Rheumatol* 2013;9:731–40 [CrossRef Medline](#)
22. Kanda T, Ishii K, Kawaguchi H, et al. **High signal intensity in the dentate nucleus and globus pallidus on unenhanced T1-weighted MR images: relationship with increasing cumulative dose of a gadolinium-based contrast material.** *Radiology* 2014;270:834–41 [CrossRef Medline](#)
23. Kanda T, Osawa M, Oba H, et al. **High signal intensity in dentate nucleus on unenhanced T1-weighted MR images: association with linear versus macrocyclic gadolinium chelate administration.** *Radiology* 2015;275:803–09 [CrossRef Medline](#)
24. Goto K, Miki A, Araki S, et al. **Time course of macular and peripapillary inner retinal thickness in non-arteritic anterior ischaemic optic neuropathy using spectral-domain optical coherence tomography.** *Neuroophthalmology* 2016;40:74–85 [CrossRef Medline](#)

Zuckerkanl Tubercle of the Thyroid Gland: Correlations between Findings of Anatomic Dissections and CT Imaging

 H.-J. Won,  H.-S. Won,  D.-S. Kwak,  J. Jang,  S.-L. Jung, and  I.-B. Kim

ABSTRACT

BACKGROUND AND PURPOSE: The Zuckerkanl tubercle is located at the posteromedial border of the thyroid lobe, and it may be confused with a neoplasm or other mass. This study was performed to clarify the position and morphologic characteristics of the Zuckerkanl tubercle by dissecting cadavers and to compare the findings with the corresponding CT images obtained in the same cadavers.

MATERIALS AND METHODS: One hundred thyroid lobes from 50 fresh cadavers were dissected for this study (20 males and 30 females; mean age at death, 77.3 ± 11.5 years). CT scans were obtained in 10 of the cadavers by using a 128-channel multidetector row CT scanner before dissection.

RESULTS: The Zuckerkanl tubercle of the thyroid gland was observed in 83% of the specimens. It was mostly located at the posteromedial border of the thyroid lobe and within the middle two quarters (2nd and 3rd) of the thyroid lobe. The Zuckerkanl tubercle was classified into 3 types based on its direction of extension: posteromedial in 64% of the specimens, posteromedial and superior in 13%, and posteromedial and inferior in 6%. On axial CT, the Zuckerkanl tubercle was usually continuous with the posteromedial part of the thyroid lobe and extended posteromedially to the esophagus. The parts of the Zuckerkanl tubercle that protrude posteromedially and superiorly or posteromedially and inferiorly from the thyroid lobe appeared separated from the thyroid gland by a thin, low-density string on axial CT.

CONCLUSIONS: Zuckerkanl tubercles that protrude toward the posteromedial and superior or inferior direction could cause confusion due to their separation when performing diagnoses with CT images.

ABBREVIATION: ZT = Zuckerkanl tubercle

Zuckerkanl¹ described a posterior projection of the thyroid lobe as the Zuckerkanl tubercle (ZT). The anatomic correlations of the ZT with the recurrent laryngeal nerve and the superior parathyroid gland were reported by Gilmour,² but this structure subsequently received little attention. Following the description of the ZT as a constant anatomic landmark of the recurrent laryngeal nerve and its classification into 4 grades according to its size,³ the topographic anatomy of these structures and the grading of the ZT have been studied both in patients during surgery⁴⁻⁸ and in cadavers.^{9,10} ZT has mostly been defined as a pos-

terior or lateral projection or a projection from the posterolateral border of the thyroid lobe in previous studies, but it was recently reported as a posteromedial projection in a normal anatomic position.¹¹ The lateral lobe of the thyroid gland is medially retracted to find the ZT during the surgery, which could be responsible for the differences in the position and shape of the ZT relative to a previous study that investigated fresh cadavers.¹¹

Most ZTs extend into the tracheoesophageal groove or posterior to the esophagus.^{8,11} Failing to remove the ZT in its entirety during total thyroidectomy may result in persistent unrelieved symptoms or recurrence^{4,12,13} as well as persistent radioiodine uptake on radioactive iodine scans.⁷ An enlarged ZT may increase pressure symptoms.^{4,14,15} Sonography is widely used for thyroid imaging, but CT is performed for nodules or nodule-like regions of the thyroid gland. ZT may be mistaken for a mass or lymph node on CT based on its morphology, resulting in unnecessary biopsies or additional imaging being performed.¹³

The aims of this study were to clarify the position and morphologic characteristics of the ZT by performing cadaver dissec-

Received September 7, 2016; accepted after revision February 9, 2017.

From the Department of Anatomy (H.-J.W., H.-S.W., D.-S.K., I.-B.K.), Catholic Institute for Applied Anatomy, College of Medicine, The Catholic University of Korea, Seoul, Korea; Department of Mortuary Science (H.-J.W.), Eulji University, Seongnam, Korea; Department of Anatomy (H.-S.W.), School of Medicine, Wonkwang University, Iksan, Korea; and Department of Radiology (J.J., S.-L.J.), Seoul St. Mary's Hospital, The Catholic University of Korea, Seoul, Korea.

Please address correspondence to In-Beom Kim, MD, PhD, Department of Anatomy, Catholic Institute for Applied Anatomy, College of Medicine, The Catholic University of Korea, Banpo-daero, Seocho-gu, Seoul 06591, Korea; e-mail: ibkimmd@catholic.ac.kr

<http://dx.doi.org/10.3174/ajnr.A5172>

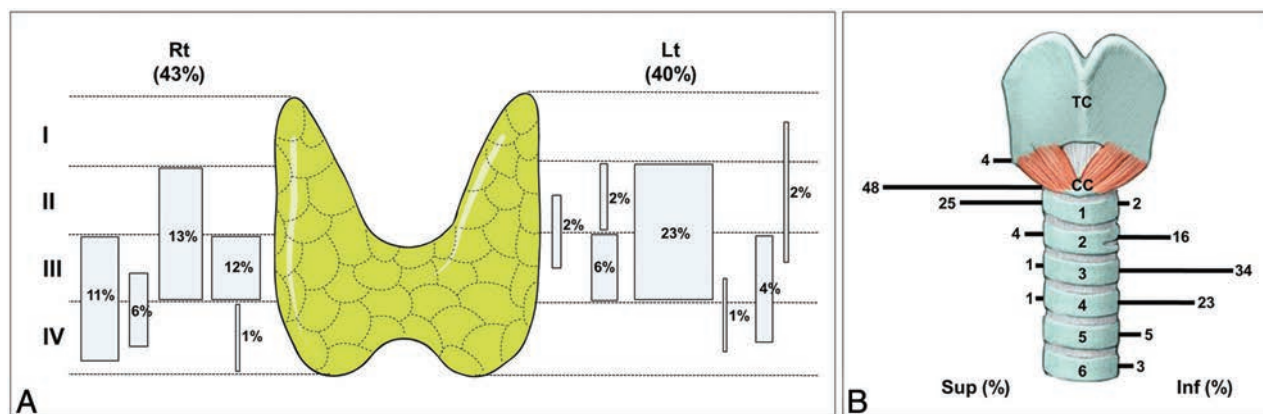


FIG 1. Location of the ZT and its superior and inferior borders according to the thyroid lobe (A) and the level of the tracheal rings (B). CC indicates cricoid cartilage; TC, thyroid cartilage; Rt, right; Lt, left; Sup, superior; Inf, inferior.

tions and to compare these findings with CT images obtained in the same cadavers.

MATERIALS AND METHODS

Cadavers

One hundred thyroid lobes from 50 fresh Korean cadavers were used for this study (20 males and 30 females; mean age at death, 77.3 years; age range, 51–103 years), and 10 of these cadavers were also used for CT imaging before dissection. No trauma-related morphologic changes were observed in the specimens during the dissection, and the medical histories related to thyroid disease were unknown. Examination of the external appearance of the thyroid glands revealed no enlargement, and pressure with the thumb and index finger was applied to all ZTs for detecting nodules. Due to the domestic law that cadavers must be donated and managed under an informed consent and ethical process, the institutional review board of our university has decreed that studies involving cadavers do not need to be reviewed. All cadavers stored at Catholic Institute for Applied Anatomy qualified as materials for education and research according to the domestic law.

Neck CT Scanning

CT was performed by using a 128-channel multidetector row CT scanner (Somatom Definition AS; Siemens, Erlangen, Germany) at 1–3 days after death. The neck of each cadaver was positioned in the center of the coil gantry in a neutral position, and axial images with a section thickness of 0.8 mm were obtained with following parameters: FOV, $200 \times 200 \text{ mm}^2$; matrix, 512×512 ; tube voltage, 150 kV(peak); tube current–time product = 160 mAs. Two radiologists specializing in head and neck radiology read the CT images. One is a professor with 30 years' experience in clinical diagnosis and research in head and neck radiology, and the other is a clinical fellow with 10 years' experience in clinical diagnosis and research.

Dissection

Thyroid glands were exposed after skin, platysma, and the sternocleidomastoid and infrahyoid muscles were sequentially removed. Then, each thyroid gland was removed with the trachea and esophagus en bloc by cutting above the thyroid cartilage, and it was immersed in fixative that included 5% formalin for 5 days. This produced a soft-state thyroid gland, which was then dissected.

The borders of the thyroid lobe and the direction of the projected part of the ZT were observed in their normal anatomic positions. Four thyroid glands with the trachea and esophagus were serially sectioned transversely at 2-mm intervals, and 2 of these were stained with hematoxylin-eosin to allow comparisons of the ZT tissues and those of the thyroid lobes. Cadaver dissection was performed by 5 anatomists specializing in human gross anatomy, and one of them, also specializing in histology, confirmed the histologic images. Three anatomists, including the corresponding author, are professors, and the other 2 anatomists are research fellows in the Department of Anatomy. All of the anatomists involved in the dissection have 10 to 50 years' experience in anatomic research. The pathologic conditions of the ZTs were confirmed by a pathologist, also a professor in the Department of Pathology, who has a board certification in pathology in the Korean Medical Association.

RESULTS

Dissected Specimens

The ZT of the thyroid gland was observed in 83% of the 100 thyroid lobes (40% left and 43% right; 34% male and 49% female), and it had no nodule. The ZT was located at the posteromedial border of the thyroid lobe in 77 specimens; in the other 6 specimens, it was identified at the posterior surface near the posteromedial border of the thyroid gland. The locations of the ZT and its superior and inferior borders was checked relative to the thyroid lobe (Fig 1A) and the level of the tracheal rings, respectively (Fig 1B). When the full longitudinal length of the thyroid lobe was divided equally into 4 parts, the ZT was found in ≥ 2 parts in 62% of the specimens: 2% in parts I–III, 38% in parts II and III, and 22% in parts III and IV. The ZT was located only in parts II, III, and IV in 2%, 18%, and 1% of the specimens, respectively. The superior border of the ZT was most frequently located on the inferior border of the cricoid cartilage (48% of the specimens), followed by the first tracheal ring (25%). The inferior border of the ZT was most frequently found at the level of the third tracheal ring (34%), followed by the fourth (23%) and second (16%) tracheal rings.

The ZT was classified into 3 types based on its direction of extension: posteromedial in 64% (31% left and 33% right), posteromedial and superior in 13% (9% left and 4% right), and posteromedial and inferior in 6% (only on right side) of the specimens (Fig 2). The long axes of the posteromedially and superiorly or inferiorly extended ZTs

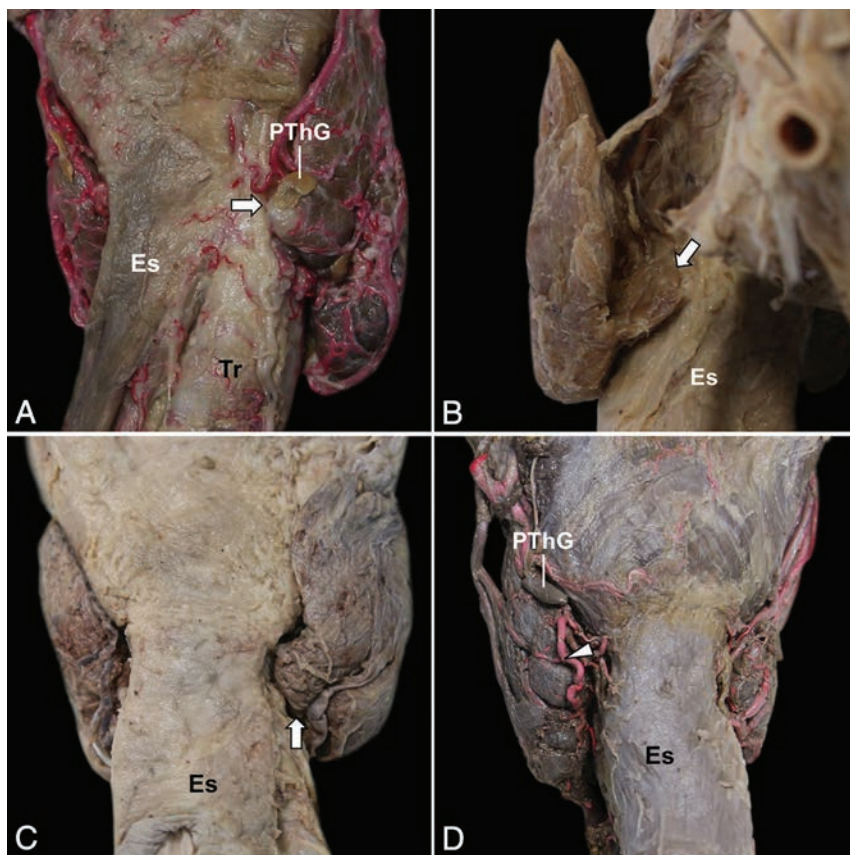


FIG 2. Types of ZTs based on the direction of extension: posteromedial (A), posteromedial and superior (B), and posteromedial and inferior (C). D, A specimen with an uneven ZT surface, which divides into 2 parts due to a deep groove (arrowhead) representing impressions of the blood vessels. Arrows indicate the ends of ZT extensions. Es indicates esophagus; PThG, parathyroid gland; Tr, trachea.

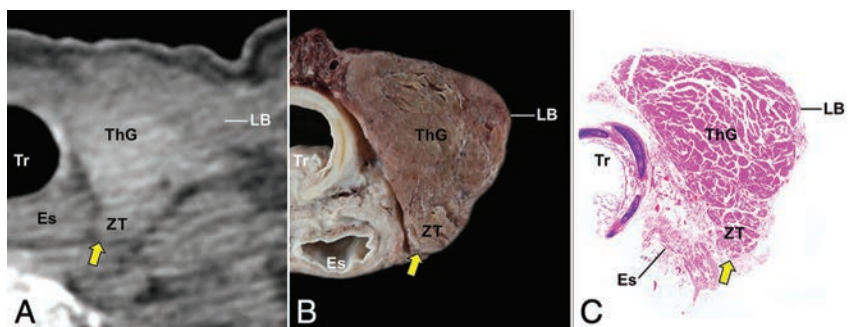


FIG 3. Comparison of ZT on axial CT (A), cross-sectional (B), and histologic (C) images of the same specimen. The ZT (arrows) is continuous with the posterior part of the thyroid lobe, extends posteromedially toward the posterior end of the esophagus, and is compatible with the other areas of thyroid tissue in the microscopic finding. LB indicates lateral border of the thyroid lobe; Es, esophagus; ThG, thyroid gland; Tr, trachea.

were angled at a mean of $20.0^\circ \pm 11.6^\circ$ and $24.2^\circ \pm 13.1^\circ$ relative to the thyroid lobes, respectively. The surface of the ZT was uneven in 22% of the specimens, which had 1 (14%), 2 (7%), and 3 (1%) deep grooves representing impressions of the blood vessels (Fig 2D). The microscopic findings of ZTs were compatible with the other areas of thyroid tissue (Fig 3C).

CT Findings

The ZT was observed in 14 of 20 thyroid lobes on axial CT images and was similarly identified in all the specimens when dissected.

The ZT was usually continuous with the posterior part of the thyroid lobe and extended posteromedially ($n = 10$) toward the tracheoesophageal groove or posterior end of the esophagus (Fig 3). Cases in which the ZT extended to the posteromedial and superior ($n = 3$) or inferior ($n = 1$) direction from the thyroid lobe were also detected in the series of axial CT images (Fig 4). When the ZT extended posteromedially and superiorly, it could be seen separately from the thyroid lobe in the upper level of the CT image, with the space between these structures appearing as a thin, low-density string. This string was not evident on the lower level of the CT image, where the ZT root merged with a thyroid lobe. When the ZT extended posteromedially and inferiorly, both it and the thyroid lobe were evident continuously in the upper level of the CT image, while the thin, low-density string appeared between them in the lower level of the CT image.

DISCUSSION

Most studies have found the incidence of ZT to lie within the range of 59%–87%,^{3,4,6,7,9–11,14,16,17} but there is 1 report of a very low incidence of 7%.¹⁸ Most investigators have detected the ZT more frequently in the right thyroid lobe.^{7,16,17,19,20} In the present study, the ZT was identified in 83% of the specimens, which is consistent with the incidence range reported by most authors, and it was also observed more frequently on the right side but with no sex difference.

The lateral lobe of the thyroid gland is retracted medially during thyroid surgery to reveal the ZT in the lateral aspect. Thus, the ZT might have been regarded as a lateral projection or a projection from the posterolateral border of the thyroid lobe for a long time.^{3,4,16,19}

However, its shape and position can differ according to the extent of thyroid lobe retraction and in excised thyroid

lobes because of the softness of the thyroid gland.¹¹ No lateral projection could be seen in previous anatomic studies reporting morphologic variations of the anterior view of the thyroid gland involving 60 white,²¹ 105 Indian,²² and 168 Korean²³ cadavers. Recently, Won et al¹¹ proposed descriptive terms for more accurate portrayal of the anatomic location and orientation of the ZT. The lateral border of the thyroid gland was defined as the most lateral margin of the anterior aspect of the thyroid in the anatomic position. The posteromedial border was defined as the margin

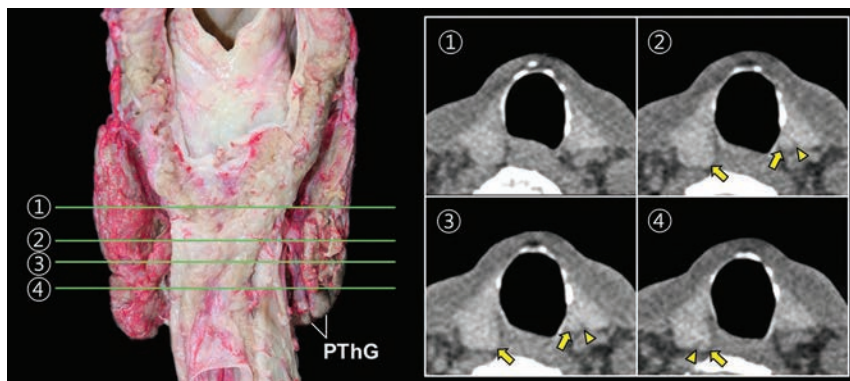


FIG 4. ZTs protruding posteromedially and superiorly (*left side*) and posteromedially and inferiorly (*right side*) in both thyroid lobes of the same cadaver, and their shapes on axial CT images at different levels. *Arrowheads and arrows* indicate the ZT and the slit between the ZT and the thyroid lobe, respectively. PTHG indicates parathyroid gland.

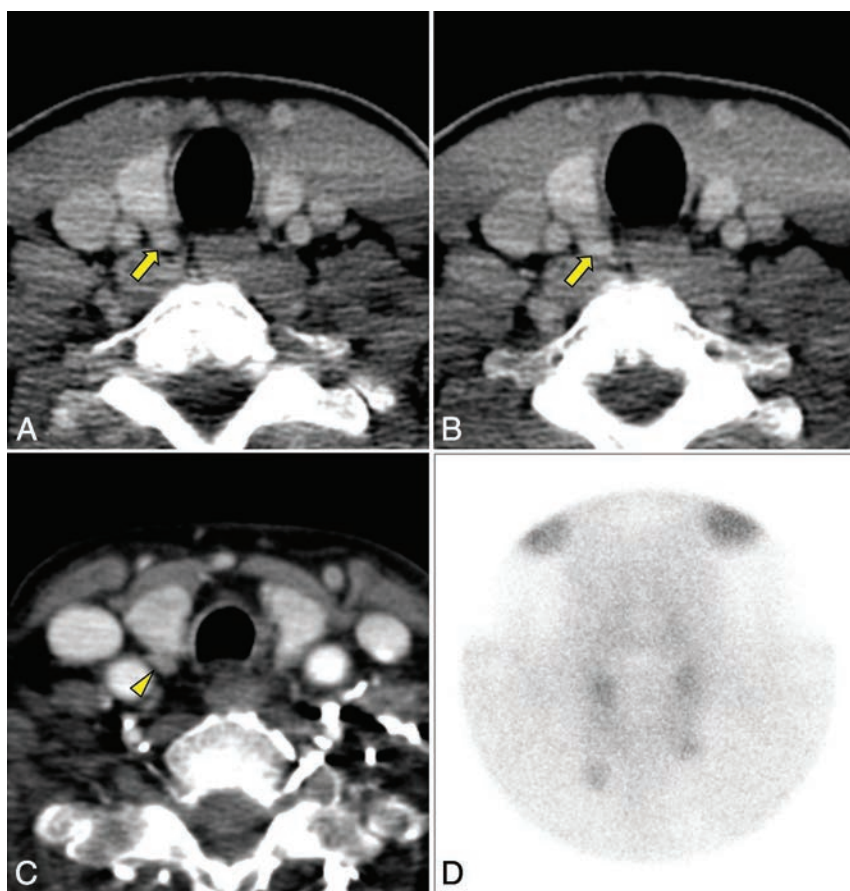


FIG 5. Comparison of clinically acquired axial CT images between the ZT appearing discontinuous from the thyroid gland and as a separate nodule or lymph node. A, Contrast-enhanced CT scan of a 33-year-old male patient who had undergone neck CT for work-up of lymphoma. There is a bulging structure (*arrow*) at the posterior aspect of the right thyroid lobe, and a fat plane between this structure and the thyroid lobe. The bulging structure protrudes toward the posterior and medial direction. The fat plane is not evident at the lower level of the CT image (B), which means that the bulging structure is a ZT protruding in the posteromedial and superior direction. C, Contrast-enhanced CT scan of a 65-year-old female patient who had hyperparathyroidism. An oval nodular lesion (*arrowhead*) separated from the thyroid gland with a fat plane is seen posterior to the right thyroid lobe and is protruding in the posterior and lateral direction. This nodule is suggested to be a parathyroid adenoma or hyperplasia in the delayed image of the parathyroid scan (D).

that exhibits the greatest projection toward the trachea or esophagus. This formed an angle on CT images through the isthmus of the thyroid gland. The posterior surface was between the lateral and posteromedial borders of the thyroid lobe. The posterolateral border was identifiable only in cases of compression by the common carotid artery in transverse sections of fixed cadavers and CT images. According to these terms, the ZT was mostly identified as a posterior or posteromedial projection at the posteromedial border of the thyroid lobe in a normal anatomic position. In the present study, the ZT also was not observed in the anterior view of the thyroid gland and was located at the posteromedial border of the thyroid lobe or posterior surface near the posteromedial border of the thyroid lobe.

The thyroid lobes are approximately conical and about 5 cm long. Their ascending apices diverge laterally to the level of the oblique lines on the laminae of the thyroid cartilage, and their bases are at the level of the fourth or fifth tracheal cartilage.²⁴ The ZT was usually found at the middle third of the thyroid lobe in previous studies^{9,16} but was mainly observed within the middle two quarters (2nd and 3rd) of the full longitudinal length of the thyroid lobe in the present study (Fig 1A). Its superior border was mainly located on the inferior border of the cricoid cartilage (48%), whereas its inferior border was diversely found at the levels of the second (16%), third (34%), and fourth (23%) tracheal rings (Fig 1B).

The shape of the ZT was previously described as sessile (56.4%) or pedunculated (23.1%) in 195 dissected thyroid lobes gained from 107 thyroidectomies,¹⁶ and the nodular-shaped ZT having a narrow neck or stalk from the posterior border of the thyroid lobe was reported as the most common, occurring in more than one-third of the CT scans of 96 patients.¹³ ZT has previously been defined on axial CT images as the part of the thyroid gland extending posteriorly to the tracheoesophageal groove, and the nodular-shaped ZT could appear discontinuous from the thyroid gland. When the ZT had a nodular shape and particularly when the low

neck was compromised by streak artifacts from the shoulders, it could be mistaken for a mass or lymph node.¹³

ZT can also be confused with a parathyroid adenoma, especially in patients with primary hyperparathyroidism. In a previous report reviewing primary hyperparathyroidism,²⁵ there were some cases in which the findings of a diagnostic imaging study such as [¹¹C]methionine PET/CT were positive but the surgeon could not locate the adenoma during the operation. We believe that some of these cases might have resulted from confusion of the ZTs with parathyroid adenomas. Theoretically, ZT has been described as the anatomic structure that separates the parathyroid glands into the superior and inferior parathyroid.³ Additionally, a previous report showed that the abnormal inferior parathyroid glands were more common than the abnormal superior glands in 810 parathyroidectomies reviewed.²⁶ We believe that these anatomic characteristics and statistical results should be considered when examining for parathyroid adenoma in patients with primary hyperparathyroidism.

In the present study, ZT usually appeared continuous with the posterior part of the thyroid lobe on axial CT and extended posteromedially toward the tracheoesophageal groove or posterior end of the esophagus (Fig 3B). ZT was also confirmed as being one part of the thyroid gland pathohistologically (Fig 3C), which implies that the ZT can be identified by gross inspection. However, none of the ZTs had a stalk, and they all protruded directly from the thyroid lobe. ZT extending to the posteromedial and superior or inferior direction could only appear discontinuous from the thyroid gland on axial CT images (Figs 4 and 5A); this appearance might result in it being confused with a separate nodule, lymph node, or parathyroid adenoma (Fig 5C).

CONCLUSIONS

This study has revealed the diverse positions and morphologies of the ZT based on anatomic dissections, which are also confirmed in the corresponding CT images. The information obtained in this study is expected to be helpful for reducing confusion between the ZT and other structures when performing diagnoses with CT.

ACKNOWLEDGMENTS

The authors thank Professor In-Hyuk Chung in the Department of Anatomy, Yonsei University College of Medicine, and Mr Seong-In John for their help in dissecting the specimens and preparing the figures. Also, the authors thank Professor Soo Young Kim in the Department of Pathology, The Catholic University of Korea, for confirming pathologic conditions of the specimens.

REFERENCES

- Zuckerkindl E. **Nebst Bemerkungen über die Epithelkörperchen des Menschen.** *Anat Hefte* 1902;LXI:61–82
- Gilmour JR. **The gross anatomy of the parathyroid glands.** *J Pathol Bacteriol* 1938;46:133–49
- Pelizzo MR, Toniato A, Gemo G. **Zuckerkindl's tuberculum: an arrow pointing to the recurrent laryngeal nerve (constant anatomical landmark).** *J Am Coll Surg* 1998;187:333–36 CrossRef Medline
- Gauger PG, Delbridge LW, Thompson NW, et al. **Incidence and importance of the tubercle of Zuckerkindl in thyroid surgery.** *Eur J Surg* 2001;167:249–54 CrossRef Medline
- Hisham AN, Lukman MR. **Recurrent laryngeal nerve in thyroid surgery: a critical appraisal.** *ANZ J Surg* 2002;72:887–89 CrossRef Medline
- Yun JS, Lee YS, Jung JJ, et al. **The Zuckerkindl's tubercle: a useful anatomical landmark for detecting both the recurrent laryngeal nerve and the superior parathyroid during thyroid surgery.** *Endocr J* 2008;55:925–30 CrossRef Medline
- Sheahan P, Murphy MS. **Thyroid tubercle of Zuckerkindl: importance in thyroid surgery.** *Laryngoscope* 2011;121:2335–37 CrossRef Medline
- Gil-Carcedo E, Menéndez ME, Vallejo LA, et al. **The Zuckerkindl tubercle: problematic or helpful in thyroid surgery?** *Eur Arch Otorhinolaryngol* 2013;270:2327–32 CrossRef Medline
- Yalçın B, Ozan H. **Relationship between the Zuckerkindl's tubercle and entrance point of the inferior laryngeal nerve.** *Clin Anat* 2007;20:640–43 CrossRef Medline
- Kaisha W, Wobenjo A, Saidi H. **Topography of the recurrent laryngeal nerve in relation to the thyroid artery, Zuckerkindl tubercle, and Berry ligament in Kenyans.** *Clin Anat* 2011;24:853–57 CrossRef Medline
- Won HS, Liu HF, Kim JH, et al. **Zuckerkindl's tubercle of the thyroid gland: its location in the anatomical position, and comparative morphology of the same specimens before and after fixation.** *Clin Anat* 2015;28:472–76 CrossRef Medline
- Reeve TS, Delbridge L, Cohen A, et al. **Total thyroidectomy: the preferred option for multinodular goiter.** *Ann Surg* 1987;206:782–86 CrossRef Medline
- Lee TC, Selvarajan SK, Curtin H, et al. **Zuckerkindl tubercle of the thyroid: a common imaging finding that may mimic pathology.** *AJNR Am J Neuroradiol* 2012;33:1134–38 CrossRef Medline
- Hisham AN, Aina EN. **Zuckerkindl's tubercle of the thyroid gland in association with pressure symptoms: a coincidence or consequence?** *Aust N Z J Surg* 2000;70:251–53 CrossRef Medline
- Delbridge L. **Total thyroidectomy: the evolution of surgical technique.** *ANZ J Surg* 2003;73:761–68 CrossRef Medline
- Gil-Carcedo Sañudo E, Menéndez Argüelles ME, Vallejo Valdezate LA, et al. **Zuckerkindl's tubercle. Location, shape and dimensions [in Spanish].** *Acta Otorrinolaringol Esp* 2012;63:443–49 CrossRef Medline
- Irkorucu O. **Zuckerkindl tubercle in thyroid surgery: is it a reality or a myth?** *Ann Med Surg (Lond)* 2016;7:92–96 CrossRef Medline
- Page C, Cuvelier P, Biet A, et al. **Thyroid tubercle of Zuckerkindl: anatomical and surgical experience from 79 thyroidectomies.** *J Laryngol Otol* 2009;123:768–71 CrossRef Medline
- Mehanna R, Murphy MS, Sheahan P. **Thyroid tubercle of Zuckerkindl is more consistently present and larger on the right: a prospective series.** *Eur Thyroid J* 2014;3:38–42 CrossRef Medline
- Rajakapsha A, Fernando R, Ranasinghe N, et al. **Morphology of the tubercle of Zuckerkindl and its importance in thyroid surgery.** *Ceylon Med J* 2015;60:23–24 CrossRef Medline
- Marshall CF. **Variations in the form of the thyroid gland in man.** *J Anat Physiol* 1895;29(Pt 2):234–39 Medline
- Ranade AV, Rai R, Pai MM, et al. **Anatomical variations of the thyroid gland: possible surgical implications.** *Singapore Med J* 2008;49:831–34 Medline
- Won HS, Chung IH. **Morphologic variations of the thyroid gland in Korean adults [In Korean with English abstract and explanation of figures].** *Korean J Phy Anthropol* 2002;15:119–25
- Gray H, Williams PL, Bannister LH. *Gray's Anatomy.* 38th ed. Edinburgh: Churchill Livingstone;1995:1892
- Noltes ME, Coester AM, van der Horst-Schrivers AN, et al. **Localization of parathyroid adenomas using 11C-methionine PET after prior inconclusive imaging.** *Langenbecks Arch Surg* 2017 Jan 14. [Epub ahead of print] CrossRef Medline
- LoPinto M, Rubio GA, Khan ZF, et al. **Location of abnormal parathyroid glands: lessons from 810 parathyroidectomies.** *J Surg Res* 2017;207:22–26 CrossRef Medline

The Role of Core Needle Biopsy for Thyroid Nodules with Initially Indeterminate Results on Previous Fine-Needle Aspiration: A Systematic Review and Meta-Analysis

C.H. Suh, J.H. Baek, C. Park, Y.J. Choi, and J.H. Lee



ABSTRACT

BACKGROUND: Sonography-guided fine-needle aspiration leads to relatively frequent cases of indeterminate cytology for the diagnosis of thyroid nodules.

PURPOSE: Our aim was to evaluate the efficacy and safety of core needle biopsy for the examination of thyroid nodules with initially indeterminate results on fine-needle aspiration.

DATA SOURCES: A computerized search of the MEDLINE and Embase databases was performed to identify relevant original articles.

STUDY SELECTION: Studies investigating the use of core needle biopsy for thyroid nodules with initially indeterminate results on previous fine-needle aspiration were eligible for inclusion.

DATA ANALYSIS: The pooled proportions for nondiagnostic results, inconclusive results, malignancy on core needle biopsy, the ability of core needle biopsy to diagnose malignancy, and the related complications of the procedure were analyzed.

DATA SYNTHESIS: The meta-analytic pooling was based on a random-effects model. Nine eligible studies, involving 2240 patients with 2245 thyroid nodules, were included. The pooled proportion for nondiagnostic results was 1.8% (95% CI, 0.4%–3.2%), and the pooled proportion for inconclusive results was 25.1% (95% CI, 15.4%–34.9%). The pooled proportion for malignancy was 18.9% (95% CI, 8.4%–29.5%). With regard to the diagnostic performance for malignancy, the sensitivity of core needle biopsy varied, ranging from 44.7% to 85.0%, but the specificity was 100% in all cases. No major complications of core needle biopsy were observed.

LIMITATIONS: The relatively small number of included studies and retrospective nature were limitations.

CONCLUSIONS: Core needle biopsy has low nondiagnostic result rates and high specificity for the diagnosis of malignancy. It is a safe diagnostic technique with a higher diagnostic yield, especially when molecular testing is not available or fine-needle aspiration did not yield enough cells for molecular testing.

ABBREVIATIONS: AUS = atypia of undetermined significance; CNB = core needle biopsy; FLUS = follicular lesion of undetermined significance; FNA = fine-needle aspiration; US = ultrasound


Sonography (US)-guided fine-needle aspiration (FNA) is an accurate and safe technique for the diagnosis of thyroid nodules. However, FNA leads to relatively frequent indeterminate cytology.^{1,2} According to the 2015 American Thyroid Association Management Guidelines, repeat FNA or molecular testing may be used to supplement the malignancy risk assessment of thyroid nodules with cytology findings of atypia of undetermined significance (AUS)/follicular lesion of undetermined significance


(FLUS).³ Moreover, if repeat FNA or molecular testing findings are deemed inconclusive, either surveillance or a diagnostic operation may be performed, given certain clinical risk factors, US patterns, and patient preferences.³ Nevertheless, repeat FNA has reportedly high rates of nondiagnostic (6.9%–9.9%) or inconclusive results (19.2%–52.5%) in the examination of thyroid nodules with initially indeterminate results on previous FNA.^{4–8}

Received November 21, 2016; accepted after revision February 13, 2017.

From the Department of Radiology and Research Institute of Radiology (C.H.S., J.H.B., Y.J.C., J.H.L.), University of Ulsan College of Medicine, Asan Medical Center, Seoul, Republic of Korea; Department of Radiology (C.H.S., C.P.), Namwon Medical Center, Jeollabuk-Do, Republic of Korea; and Department of Radiology (C.P.), Chonnam National University Hospital, Gwangju, Republic of Korea.

Please address correspondence to Jung Hwan Baek, MD, PhD, Department of Radiology and Research Institute of Radiology, University of Ulsan College of Medicine, Asan Medical Center, 86 Asanbyeongwon-Gil, Songpa-Gu, Seoul 138-736, Republic of Korea; e-mail: radbaek@naver.com

 Indicates article with supplemental on-line table.

 Indicates article with supplemental on-line photos.

<http://dx.doi.org/10.3174/ajnr.A5182>

Several recent studies have reported the advantages of using core needle biopsy (CNB) for the examination of thyroid nodules with initially indeterminate results on previous FNA.^{6–14} CNB has been reported to have low rates of nondiagnostic (0.5%–3.8%) and inconclusive (9.1%–45.3%) results compared with the inconclusive results of FNA (19.2%–52.5%).^{6,7,9,11,12,14} However, some physicians remain skeptical of the use of CNB for the examination of thyroid nodules with initially indeterminate results on previous FNA because most research has included observational or descriptive studies with small sample sizes. Furthermore, the American Thyroid Association guidelines do not recommend the routine use of CNB, possibly because of the high associated morbidity rates and the limited evidence elucidated thus far.³ Hence, it is essential to collect and review the currently available data regarding the prevalence of nondiagnostic results, diagnostic performance, and complications of CNB for the examination of thyroid nodules with initially indeterminate results on previous FNA.

To our knowledge, no studies have generated a comprehensive systematic summary of cases of thyroid nodules with initially indeterminate results on previous FNA. Accordingly, we aimed to systematically review the published literature and evaluate the prevalence of nondiagnostic results, diagnostic performance, and complications of CNB for thyroid nodules with initially indeterminate results on previous FNA, which could provide additional data to support standardized management of these lesions.

MATERIALS AND METHODS

Literature Search Strategy

A computerized search of the MEDLINE and Embase databases was performed to identify relevant original articles on the use of CNB for examining thyroid nodules with initially indeterminate results on previous FNA until May 15, 2016. We used the following search terms: (thyroid) AND (core-needle biopsy OR core needle biopsy OR CNB) AND (Bethesda category 3 OR atypia of undetermined significance OR AUS OR follicular lesion of undetermined significance OR FLUS OR indeterminate OR inconclusive). Our search was limited to English-language studies. The bibliographies of the selected articles were screened to identify other relevant articles.

Inclusion Criteria

Studies investigating the use of CNB for thyroid nodules with initially indeterminate results on previous FNA were eligible for inclusion. However, we included only studies that fulfilled all of the following criteria:

- 1) Population. Patients with thyroid nodules who underwent CNB evaluations following initially indeterminate results on previous FNA.
- 2) Reference Standard. Because the diagnostic criteria for CNB of thyroid nodules have not been standardized, the histologic results of CNB were grouped into the 6 categories of the Bethesda System^{6,9,15}: nondiagnostic results, benign, AUS or FLUS, follicular neoplasm or suspicious for follicular neoplasm, suspicious for malignancy, and malignant.¹⁶ We defined indeterminate results as those that at least fulfilled the criteria of thyroid nodules with Bethesda category 3 (AUS and FLUS), including cases with atypical cells that could not be

diagnosed as “suspicious for malignancy” or “malignancy,” or those with cellular follicular nodules that could not be diagnosed as “follicular neoplasm” or “suspicious for follicular neoplasm.” The malignant nodules were diagnosed after an operation or biopsy. In contrast, benign nodules were diagnosed after an operation, in cases in which at least 2 sets of benign findings were noted on FNA and/or CNB, or in cases in which benign cytology findings were noted on FNA or CNB and the nodule size remained stable after 1 year.

- 3) Outcomes. Results that were sufficiently detailed to evaluate the prevalence of nondiagnostic results, diagnostic performance, and complications of CNB.

Exclusion Criteria

The exclusion criteria were as follows: 1) case reports and case series with a sample size of <10; 2) review articles, editorials, letters, comments, and conference proceedings; 3) studies that did not focus on the use of CNB for thyroid nodules with initially indeterminate results on previous FNA; and 4) studies with partially overlapping patients and data. Two reviewers (C.H.S. and J.H.B.) independently selected the literature reports with a standardized form.

Data Extraction

These data were extracted from each of the following studies and entered into standardized data forms: 1) authors, year of publication, hospital or medical school, years of patient recruitment, study design, and sample size; 2) mean age, nodule size, and patient reference standards; 3) rates of nondiagnostic results, inconclusive results, and malignancy; 4) diagnostic performance of CNB for malignancy; and 5) complications, the size of the core needle, and patient anticoagulation status. One reviewer (C.H.S.) extracted the data from the studies, and the second reviewer (J.H.B.) confirmed the accuracy of the extracted data. There were a few disagreements, which were resolved by a unanimous decision.

Quality Assessment

The quality of the included studies was analyzed independently by 2 reviewers (C.H.S. and J.H.B.) with customized questionnaires based on the Quality Assessment of Diagnostic Accuracy Studies-2 (QUADAS-2) criteria.¹⁷ Very few disagreements were noted, which were resolved by consensus.

Data Synthesis and Statistical Analysis

The pooled proportions for the nondiagnostic results, inconclusive results, and malignancy on CNB following initially indeterminate results on previous FNA were adopted as the primary indices. The meta-analytic pooling was based on the inverse variance method for calculating weights, and the pooled proportions and their 95% confidence intervals were determined by using the DerSimonian-Laird random-effects model.^{18–20} Heterogeneity among the studies was determined by using following methods: The Cochran Q-test was performed for the pooled estimates with $P < .05$ indicating heterogeneity. In addition, we performed the Higgins inconsistency index (I^2) test: 0%–40%, might not be important; 30%–60%, may represent moderate heterogeneity;

50%–90%, may represent substantial heterogeneity; and 75%–100%, may represent considerable heterogeneity.^{21,22} The publication biases were visually assessed by using funnel plots. Thereafter, publication bias–adjusted pooled estimates—that is, adjusted pooled proportions—were obtained by using the trim-and-fill method.²³ If the original unadjusted pooled proportions and the trim-and-fill–adjusted pooled proportions were in agreement, the results were regarded as robust for publication bias.

The secondary indices of this study included the diagnostic performance of CNB for malignancy and complications. We estimated the descriptive statistics for the diagnostic performance of CNB, including sensitivity, specificity, positive predictive value, and negative predictive value. All statistical analyses were performed by using R statistical and computing software, Version 3.0.2 (<http://www.r-project.org/>) with the “metafor” and “mada” packages.

RESULTS

Literature Search

The study selection process is illustrated in Fig 1. A literature search of the Ovid MEDLINE and Embase databases identified 105 articles; after we removed the duplicates, 77 articles were screened for eligibility. Of those, 64 were excluded after a review of their titles and abstracts, including 35 review articles; 12 case reports; 9 letters, editorials, or conference abstracts; and 8 articles not related to the topic of interest of this study. The full texts of the remaining 13 articles were reviewed; a search of their bibliographies found no additional eligible studies. Of these 13 articles, 4 were further excluded after reviewing their full texts, due to the presence of partially overlapping patient cohorts.^{24–27} Finally, 9

eligible studies, involving 2240 patients with 2245 thyroid nodules, were included in this meta-analysis.^{6–14}

Characteristics of the Included Studies

The detailed characteristics of the 9 included studies are summarized in the On-line Table. All the included studies were retrospective in nature. The mean patient age ranged from 46 to 54.1 years. Of the 9 studies, only CNB was performed for the thyroid nodules in 6,^{9–14} whereas both CNB and repeat FNA were performed in 3.^{6–8} Among the studies, 2 included patients who simultaneously underwent repeat FNA and CNB of each nodule, wherein repeat FNA was performed before CNB.^{6,7} In those studies, real-time US guidance was used to determine that the CNB and repeat FNA were focusing on the same nodule. In 8 studies, the size of the core needle was 18 ga; 1 study was not explicit.¹³

The inclusion of thyroid nodules was slightly heterogeneous among the studies. Five studies included thyroid nodules with initial AUS or FLUS results at previous FNA,^{6,7,9,12,14} whereas Jang et al¹¹ included nodules with initial AUS results at previous FNA. Moreover, Trimboli et al¹³ included nodules with initial AUS or FLUS or follicular neoplasm/suspicious for follicular neoplasm results at previous FNA. Hahn et al¹⁰ included nodules with initial inconclusive results at previous FNA, and Park et al⁸ included initially indeterminate nodules at previous FNA. Hence, we finally included 6 studies (1836 nodules) that examined nodules with initial AUS or FLUS results at previous FNA in the quantitative synthesis of our meta-analysis.^{6,7,9,11,12,14} Among these 6 studies, 4 (496 nodules) included assessments of the diagnostic performance of thyroid malignancy.^{6,7,9,14} Two studies were excluded due to the presence of insufficient data for creating the diagnostic 2-by-2 table for CNB.^{11,12} The quality of the included studies, as assessed by the QUADAS-2 tool, was moderate overall, with all the studies satisfying ≥ 5 of the 7 items (On-line Fig 1).¹⁷

Prevalence of Nondiagnostic Results, Inconclusive Results, and Malignancy of CNB

Among the 6 studies included, 1836 nodules with initial AUS or FLUS results at previous FNA were examined. The pooled proportions for nondiagnostic results, inconclusive results, and malignancy on CNB are summarized in the Table, and the corresponding forest plots are shown in Fig 2. The pooled proportion for nondiagnostic results was 1.8% (95% CI, 0.4%–3.2%), and the pooled proportion for inconclusive results was 25.1% (95% CI, 15.4%–34.9%). The pooled proportion for malignancy was 18.9% (95% CI, 8.4%–29.5%). Considerable heterogeneity was observed among the studies in terms of the pooled proportions on CNB ($I^2 = 94.6\%$ – 98.3%). The funnel plots showed a publication bias for the pooled proportion for nondiagnostic results and ma-

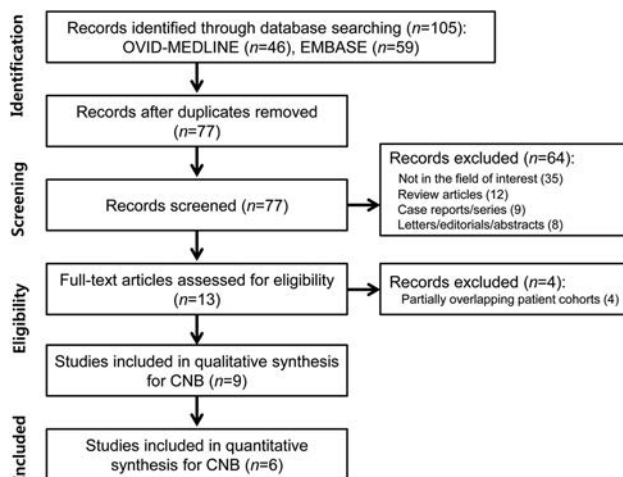


FIG 1. Flow diagram of the study selection process.

Summary of the meta-analytic pooled proportions for nondiagnostic results, inconclusive results, and malignancy on CNB

| | No. of Studies | Total No. of Cases | Summary Estimate | | | Trim-and-Fill Estimate | |
|-----------------------|----------------|--------------------|----------------------------|--|-----------------|------------------------|-------------------------------------|
| | | | Pooled Proportion (95% CI) | P Value for Heterogeneity ^a | I ^{2b} | No. of Missing Studies | Adjusted Pooled Proportion (95% CI) |
| Nondiagnostic results | 6 | 1836 | 1.8% (0.4%–3.2%) | <.01 | 94.6% | 2 | 0.8% (–0.8%–2.5%) |
| Inconclusive results | 6 | 1836 | 25.1% (15.4%–34.9%) | <.01 | 95.8% | 0 | |
| Malignancy | 6 | 1836 | 18.9% (8.4%–29.5%) | <.01 | 98.3% | 1 | 15.6% (4.4%–26.8%) |

^a P value by the Cochran Q method to test the heterogeneity of the pooled data, with $P < .05$ indicating substantial heterogeneity.

^b Higgins index for heterogeneity (0%–40%, might not be important; 30%–60%, may represent moderate heterogeneity; 50%–90%, may represent substantial heterogeneity; 75%–100%, may represent considerable heterogeneity).

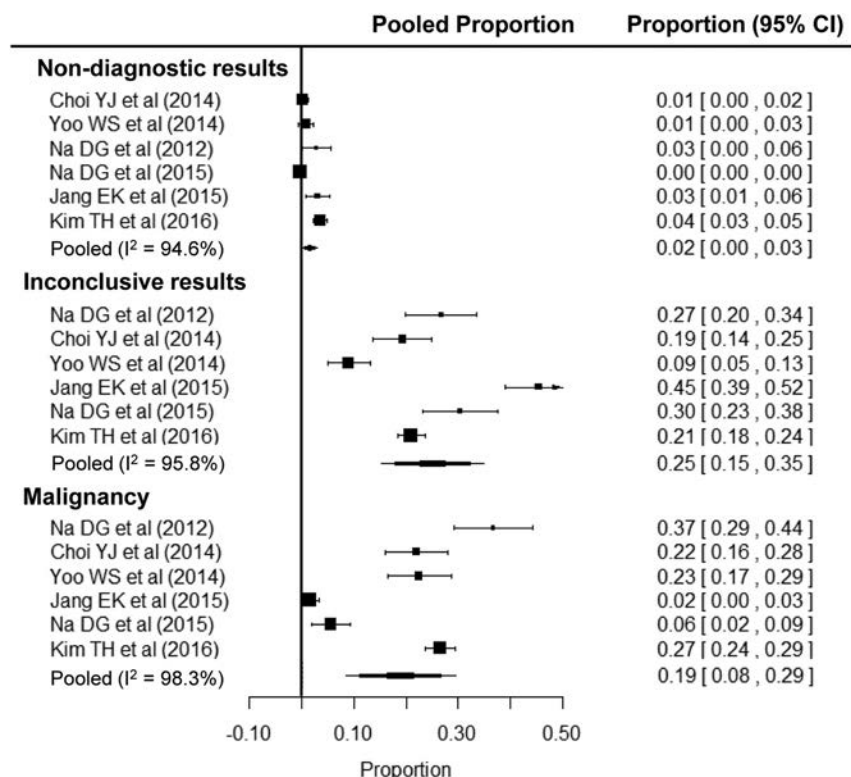


FIG 2. Forest plots for nondiagnostic results, inconclusive results, and malignancy of the CNB. Numbers are pooled estimates with 95% confidence intervals in parentheses. Horizontal lines indicate 95% CIs, and the black box on each line indicates the standardized mean difference for each study. The black diamond at the bottom of the plot shows the average effect size of the included studies.

lignancy on CNB (On-line Fig 2). After we adjusted for publication bias with the trim-and-fill approach, the adjusted pooled proportion for nondiagnostic results was 0.8% (95% CI, -0.8%–2.5%) and the adjusted pooled proportion for malignancy was 15.6% (95% CI, 4.4%–26.8%), which were in agreement with the unadjusted pooled estimates.

Diagnostic Performance of CNB for Malignancy

The diagnostic performance of CNB for malignancy was described in 4 studies involving 496 nodules. The diagnostic criteria for malignancy included a classification of Bethesda category 6 (malignancy). Pooling was not performed due to the relatively small number of studies included, the high risk of bias, and the inherent heterogeneity based on various study designs. The sensitivity varied from 44.7% to 85.0%; in fact, the lower margin of the 95% CI reached 25.2%. Nevertheless, the specificity was consistent, and all studies indicated a specificity of 100%; in fact, the lower margin of the 95% CI reached 89.1%. The positive predictive values were also consistent (100% in all 4 studies), whereas the negative predictive values varied (65.0%, 88.0%, 88.1%, and 94.0%).

Complications

Six of the 9 studies reported on the complications of CNB.^{6–10,12} In these 6 studies, no major complications, procedure-related deaths, or need for hospital admission or intervention was reported. One study reported a case (1/191) of neck swelling, pain, and perithyroid hematoma,⁹ whereas another study reported the

occurrence of minor complications, including small perithyroid hematomas in 8 patients (8/220) and mild transient parenchymal edema in 5 patients (5/220). All these patients had undergone simultaneous CNB and repeat FNA for each nodule in that study.⁶ They used 18-ga needles for CNB and 21-, 23-, or 25-ga needles for FNA. In case of patients receiving antiplatelet therapy, procedures were performed after discontinuing these medications for 1 week.

DISCUSSION

We performed a systematic review and meta-analysis to evaluate the efficacy and complications of CNB in the examination of thyroid nodules with initially indeterminate results on previous FNA. In the present study, we found that the pooled proportion for nondiagnostic results was 1.8% (95% CI, 0.4%–3.2%); for inconclusive results, it was 25.1% (95% CI, 15.4%–34.9%); and for malignancy, it was 18.9% (95% CI, 8.4%–29.5%). With regard to the diagnostic performance for malignancy, the sensitivity of CNB varied from 44.7% to 85.0%, but the specificity was constant at 100%. There were no major compli-

cations associated with CNB. Considering these findings, CNB is a safe diagnostic technique with higher diagnostic yield, especially when molecular testing is not available or FNA does not yield enough cells for molecular testing.

Several studies have reported that CNB is useful for evaluating thyroid nodules with initial “nondiagnostic results” on previous FNA.^{15,28,29} A recent meta-analysis demonstrated that CNB may serve as a complementary diagnostic technique for thyroid nodules with initial nondiagnostic results on previous FNA, including 4 studies.³⁰ Currently, the definite diagnosis and management of thyroid nodules with initially “indeterminate results” on previous FNA are commonly encountered problems in daily clinical practice. Therefore, we performed this systematic review and meta-analysis of thyroid nodules with initially indeterminate FNA results, including 9 studies. In the present study, CNB demonstrated low nondiagnostic result rates (1.8%; 95% CI, 0.4%–3.2%) and high specificities (100%) in the diagnosis of malignancy. The Korean Society of Thyroid Radiology guidelines mentioned that CNB might be useful for obtaining conclusive results in cases of thyroid nodules with initially indeterminate results on previous FNA.^{31,32} We believe that consistent evidence favoring the use of CNB, including the results of our systematic review with a meta-analysis, may be considered as a subsequent diagnostic approach for thyroid nodules with initially indeterminate results on previous FNA.

A gene-expression classifier is a molecular assay that was developed to improve surgical decision-making in cases of thyroid

nodules with initially indeterminate results on previous FNA. A previous prospective multicenter study reported on the ability of a gene-expression classifier to correctly identify indeterminate nodules (AUS/FLUS), with high sensitivity and negative predictive values (90% and 94%–95%, respectively) but low specificity (53%).³² In our present study, the specificities were 100% and the negative predictive values were variable, ranging from 65.0% to 94.0%. Moreover, a recent interinstitutional validation study showed that there were wide variations in the performance of the gene-expression classifier.³³ The cost of the gene-expression classifier is also high. Hence, although CNB shows slightly lower negative predictive values compared with those of the gene-expression classifier, CNB may serve as a better alternative method, with higher specificities and lower cost, in institutions in which the gene-expression classifier is not available.

CNB is reportedly more effective at obtaining large tissue samples, which enable molecular testing for the accurate diagnosis and assessment of the histologic architecture. Several recent articles have reported on molecular testing, which can be used for identification in CNB specimens of thyroid nodules with initially indeterminate results on previous FNA.^{11,12,24,27} Choi et al²⁴ revealed that the combination of *BRAF* V600E mutation analysis and CNB may add further value to the examination of thyroid nodules with initial AUS results on previous FNA. Furthermore, Kim et al¹² suggested a simple triage scheme involving US findings, CNB, or *BRAF* V600E mutation analysis, which can be used to identify a subpopulation of patients with a low or high likelihood of thyroid cancer among those with thyroid nodules with initial AUS/FLUS results on previous FNA. Jang et al¹¹ demonstrated that *NRAS* codon 61 mutation analysis along with CNB could be useful for achieving a clinical decision in cases of thyroid nodules with initial AUS results on previous FNA. Moreover, Trimboli et al²⁷ reported that galectin-3 and HBME-1 could improve the accuracy of CNB in cases of thyroid nodules with initially indeterminate results on previous FNA. Hence, it would be ideal for CNB to be integrated with radiologic, cytopathologic, or histologic approaches, along with certain patient factors, to optimize patient management. Moreover, further studies on long-term outcome data would help prove its clinical utility.

In our current systematic review, we did not observe any major complications of CNB. However, 1 case exhibited minor complications (1/191), including swelling, pain, and perithyroid hematomas after the CNB procedure.⁹ CNB is known to be a safe, well-tolerated method and is associated with a low complication rate.³⁴ Modern spring-activated biopsy needles (18–22 gauge) and US guidance can now be used to achieve high diagnostic accuracy and low complication rates. Despite such advances, CNB should be performed carefully under US guidance by experienced operators who are familiar with the US anatomy of the thyroid gland and perithyroid areas.^{30,31,35}

Our meta-analysis had several limitations of note. First, there were several inherent limitations of our study—that is, the relatively small number of included studies and its retrospective nature. Therefore, this meta-analysis should be interpreted cautiously if one wants to apply the findings. However, we used validated systematic review methods and reported results according to the standard reporting guidelines: the Preferred Reporting

Items for Systematic Reviews and Meta-Analyses³⁶ and the guidelines of the *Handbook for Diagnostic Test Accuracy Reviews* published by the Cochrane Collaboration.³⁷ Second, our meta-analysis showed considerable heterogeneity in the pooled proportions. These heterogeneities were possibly due to the technical variation among the institutions or operators, the nodule characteristics, the number of passes, or the absence of standardized pathologic criteria for CNB. Third, a comparison of diagnostic performance between CNB and repeat FNA could not be performed. Repeat FNA also provides definitive categorization of indeterminate nodules.³⁸ Fourth, the prevalence of malignancy in patients with nondiagnostic/indeterminate thyroid nodules and the mortality of thyroid cancer remains low. Therefore, the clinical impact of the observed higher conclusive results of CNB compared with repeat FNA could be controversial.^{39,40}

CONCLUSIONS

This systematic review and meta-analysis indicate that CNB has low nondiagnostic result rates and high specificities for the diagnosis of malignancy. CNB is a safe diagnostic technique with higher diagnostic yield, especially when molecular testing is not available or FNA did not yield enough cells for molecular testing.

REFERENCES

1. Baier ND, Hahn PF, Gervais DA, et al. **Fine-needle aspiration biopsy of thyroid nodules: experience in a cohort of 944 patients.** *AJR Am J Roentgenol* 2009;193:1175–79 [CrossRef Medline](#)
2. Wang CC, Friedman L, Kennedy GC, et al. **A large multicenter correlation study of thyroid nodule cytopathology and histopathology.** *Thyroid* 2011;21:243–51 [CrossRef Medline](#)
3. Haugen BR, Alexander EK, Bible KC, et al. **2015 American Thyroid Association Management Guidelines for Adult Patients with Thyroid Nodules and Differentiated Thyroid Cancer: The American Thyroid Association Guidelines Task Force on Thyroid Nodules and Differentiated Thyroid Cancer.** *Thyroid* 2016;26:1–133 [CrossRef Medline](#)
4. Yassa L, Cibas ES, Benson CB, et al. **Long-term assessment of a multidisciplinary approach to thyroid nodule diagnostic evaluation.** *Cancer* 2007;111:508–16 [CrossRef Medline](#)
5. Nayar R, Ivanovic M. **The indeterminate thyroid fine-needle aspiration: experience from an academic center using terminology similar to that proposed in the 2007 National Cancer Institute Thyroid Fine Needle Aspiration State of the Science Conference.** *Cancer* 2009;117:195–202 [Medline](#)
6. Na DG, Kim JH, Sung JY, et al. **Core-needle biopsy is more useful than repeat fine-needle aspiration in thyroid nodules read as nondiagnostic or atypia of undetermined significance by the Bethesda system for reporting thyroid cytopathology.** *Thyroid* 2012;22:468–75 [CrossRef Medline](#)
7. Na DG, Min HS, Lee H, et al. **Role of core needle biopsy in the management of atypia/follicular lesion of undetermined significance thyroid nodules: comparison with repeat fine-needle aspiration in subcategory nodules.** *Eur Thyroid J* 2015;4:189–96 [CrossRef Medline](#)
8. Park KT, Ahn SH, Mo JH, et al. **Role of core needle biopsy and ultrasonographic finding in management of indeterminate thyroid nodules.** *Head Neck* 2011;33:160–65 [CrossRef Medline](#)
9. Choi YJ, Baek JH, Ha EJ, et al. **Differences in risk of malignancy and management recommendations in subcategories of thyroid nodules with atypia of undetermined significance or follicular lesion of undetermined significance: the role of ultrasound-guided core-needle biopsy.** *Thyroid* 2014;24:494–501 [CrossRef Medline](#)
10. Hahn SY, Shin JH, Han BK, et al. **Ultrasonography-guided core needle biopsy for the thyroid nodule: does the procedure hold any ben-**

efit for the diagnosis when fine-needle aspiration cytology analysis shows inconclusive results? *Br J Radiol* 2013;86:20130007 CrossRef Medline

11. Jang EK, Kim WG, Kim EY, et al. Usefulness of NRAS codon 61 mutation analysis and core needle biopsy for the diagnosis of thyroid nodules previously diagnosed as atypia of undetermined significance. *Endocrine* 2016;52:305–12 CrossRef Medline
12. Kim TH, Jeong DJ, Hahn SY, et al. Triage of patients with AUS/FLUS on thyroid cytopathology: effectiveness of the multimodal diagnostic techniques. *Cancer Med* 2016;5:769–77 CrossRef Medline
13. Trimboli P, Nasrollah N, Amendola S, et al. A cost analysis of thyroid core needle biopsy vs. diagnostic surgery. *Gland Surg* 2015;4:307–11 CrossRef Medline
14. Yoo WS, Choi HS, Cho SW, et al. The role of ultrasound findings in the management of thyroid nodules with atypia or follicular lesions of undetermined significance. *Clin Endocrinol (Oxf)* 2014;80:735–42 CrossRef Medline
15. Yeon JS, Baek JH, Lim HK, et al. Thyroid nodules with initially non-diagnostic cytologic results: the role of core-needle biopsy. *Radiology* 2013;268:274–80 CrossRef Medline
16. Cibas ES, Ali SZ. The Bethesda System for Reporting Thyroid Cytopathology. *Am J Clin Pathol* 2009;132:658–65 CrossRef Medline
17. Whiting PF, Rutjes AW, Westwood ME et al. QUADAS-2: a revised tool for the quality assessment of diagnostic accuracy studies. *Ann Intern Med* 2011;155:529–36 CrossRef Medline
18. Suh CH, Park SH. Successful publication of systematic review and meta-analysis of studies evaluating diagnostic test accuracy. *Korean J Radiol* 2016;17:5–6 CrossRef Medline
19. Kim KW, Lee J, Choi SH, et al. Systematic review and meta-analysis of studies evaluating diagnostic test accuracy—a practical review for clinical researchers, part I: general guidance and tips. *Korean J Radiol* 2015;16:1175–87 CrossRef Medline
20. Lee J, Kim KW, Choi SH, et al. Systematic review and meta-analysis of studies evaluating diagnostic test accuracy—a practical review for clinical researchers, part II: statistical methods of meta-analysis. *Korean J Radiol* 2015;16:1188–96 CrossRef Medline
21. Higgins J, Green S. Cochrane Handbook for Systematic Reviews of Interventions. Version 5.1.0. Updated March 2011. The Cochrane Collaboration. <http://handbook.cochrane.org>. Accessed August 15, 2015
22. Higgins JP, Thompson SG, Deeks JJ, et al. Measuring inconsistency in meta-analyses. *BMJ* 2003;327:557–60 CrossRef Medline
23. Duval S, Tweedie R. Trim and fill: a simple funnel-plot-based method of testing and adjusting for publication bias in meta-analysis. *Biometrics* 2000;56:455–63 CrossRef Medline
24. Choi SH, Baek JH, Lee JH, et al. Evaluation of the clinical usefulness of BRAFV600E mutation analysis of core-needle biopsy specimens in thyroid nodules with previous atypia of undetermined significance or follicular lesions of undetermined significance results. *Thyroid* 2015;25:897–903 CrossRef Medline
25. Lee KH, Shin JH, Oh YL, et al. Atypia of undetermined significance in thyroid fine-needle aspiration cytology: prediction of malignancy by US and comparison of methods for further management. *Ann Surg Oncol* 2014;21:2326–31 CrossRef Medline
26. Nasrollah N, Trimboli P, Guidobaldi L, et al. Thin core biopsy should help to discriminate thyroid nodules cytologically classified as indeterminate: a new sampling technique. *Endocrine* 2013;43:659–65 CrossRef Medline
27. Trimboli P, Guidobaldi L, Amendola S, et al. Galectin-3 and HBME-1 improve the accuracy of core biopsy in indeterminate thyroid nodules. *Endocrine* 2016;52:39–45 CrossRef Medline
28. Suh CH, Baek JH, Lee JH, et al. The role of core-needle biopsy in the diagnosis of thyroid malignancy in 4580 patients with 4746 thyroid nodules: a systematic review and meta-analysis. *Endocrine* 2016;54:315–28 CrossRef Medline
29. Suh CH, Baek JH, Kim KW, et al. The role of core-needle biopsy for thyroid nodules with initially nondiagnostic fine-needle aspiration results: a systematic review and meta-analysis. *Endocr Pract* 2016;22:679–88 CrossRef Medline
30. Lee YH, Baek JH, Jung SL, et al; Korean Society of Thyroid Radiology (KSThR), Korean Society of Radiology. Ultrasound-guided fine needle aspiration of thyroid nodules: a consensus statement by the Korean Society of Thyroid Radiology. *Korean J Radiol* 2015;16:391–401 CrossRef Medline
31. Shin JH, Baek JH, Chung J, et al; Korean Society of Thyroid Radiology (KSThR) and Korean Society of Radiology. Ultrasonography diagnosis and imaging-based management of thyroid nodules: Revised Korean Society of Thyroid Radiology Consensus Statement and Recommendations. *Korean J Radiol* 2016;17:370–95 CrossRef Medline
32. Alexander EK, Kennedy GC, Baloch ZW, et al. Preoperative diagnosis of benign thyroid nodules with indeterminate cytology. *N Engl J Med* 2012;367:705–15 CrossRef Medline
33. Marti JL, Avadhani V, Donatelli LA, et al. Wide inter-institutional variation in performance of a molecular classifier for indeterminate thyroid nodules. *Ann Surg Oncol* 2015;22:3996–4001 CrossRef Medline
34. Nasrollah N, Trimboli P, Rossi F, et al. Patient's comfort with and tolerability of thyroid core needle biopsy. *Endocrine* 2014;45:79–83 CrossRef Medline
35. Ha EJ, Baek JH, Lee JH. Ultrasonography-based thyroidal and perithyroidal anatomy and its clinical significance. *Korean J Radiol* 2015;16:749–66 CrossRef Medline
36. Liberati A, Altman DG, Tetzlaff J, et al. The PRISMA statement for reporting systematic reviews and meta-analyses of studies that evaluate health care interventions: explanation and elaboration. *PLoS Med* 2009;6:e1000100 CrossRef Medline
37. Deeks JJ, Bossuyt PM, Gatsonis C, eds. Cochrane handbook for systematic reviews of diagnostic test accuracy. Version 1.0.0. 2013. The Cochrane Collaboration. <http://methods.cochrane.org/sdt/handbook-dta-reviews>. Accessed June 8, 2016
38. Espinosa De Ycaza AE, Lowe KM, Dean DS, et al. Risk of malignancy in thyroid nodules with non-diagnostic fine-needle aspiration: a retrospective cohort study. *Thyroid* 2016;26:1598–604 CrossRef Medline
39. Jooya A, Saliba J, Blackburn A, et al. The role of repeat fine needle aspiration in the management of indeterminate thyroid nodules. *J Otolaryngol Head Neck Surg* 2016;45:51 CrossRef Medline
40. Pyo JS, Sohn JH, Kang G. Core needle biopsy is a more conclusive follow-up method than repeat fine needle aspiration for thyroid nodules with initially inconclusive results: a systematic review and meta-analysis. *J Pathol Transl Med* 2016;50:217–24 CrossRef Medline

Nonmicrocephalic Infants with Congenital Zika Syndrome Suspected Only after Neuroimaging Evaluation Compared with Those with Microcephaly at Birth and Postnatally: How Large Is the Zika Virus “Iceberg”?

M.F.V.V. Aragao,¹ A.C. Holanda,² A.M. Brainer-Lima,³ N.C.L. Petribu,⁴ M. Castillo,⁵ V. van der Linden,⁶ S.C. Serpa,⁷ A.G. Tenório,⁸ P.T.C. Travassos,⁹ M.T. Cordeiro,¹⁰ C. Sarteschi,¹¹ M.M. Valenca, and A. Costello¹²



ABSTRACT

BACKGROUND AND PURPOSE: Although microcephaly is the most prominent feature of congenital Zika syndrome, a spectrum with less severe cases is starting to be recognized. Our aim was to review neuroimaging of infants to detect cases without microcephaly and compare them with those with microcephaly.

MATERIALS AND METHODS: We retrospectively evaluated all neuroimaging (MR imaging/CT) of infants 1 year of age or younger. Patients with congenital Zika syndrome were divided into those with microcephaly at birth, postnatal microcephaly, and without microcephaly. Neuroimaging was compared among groups.

RESULTS: Among 77 infants, 24.6% had congenital Zika syndrome (11.7% microcephaly at birth, 9.1% postnatal microcephaly, 3.9% without microcephaly). The postnatal microcephaly and without microcephaly groups showed statistically similar imaging findings. The microcephaly at birth compared with the group without microcephaly showed statistically significant differences for the following: reduced brain volume, calcifications outside the cortico-subcortical junctions, corpus callosum abnormalities, moderate-to-severe ventriculomegaly, an enlarged extra-axial space, an enlarged cisterna magna (all absent in those without microcephaly), and polymicrogyria (the only malformation present without microcephaly). There was a trend toward pachygyria (absent in groups without microcephaly). The group with microcephaly at birth compared with the group with postnatal microcephaly showed significant differences for simplified gyral pattern, calcifications outside the cortico-subcortical junctions, corpus callosum abnormalities, moderate-to-severe ventriculomegaly, and an enlarged extra-axial space.

CONCLUSIONS: In microcephaly at birth, except for polymicrogyria, all patients showed abnormalities described in the literature. In postnatal microcephaly, the only abnormalities not seen were a simplified gyral pattern and calcifications outside the cortico-subcortical junction. Infants with normocephaly presented with asymmetric frontal polymicrogyria, calcifications in the cortico-subcortical junction, mild ventriculomegaly, and delayed myelination.

ABBREVIATIONS: CZS = congenital Zika syndrome; IgM = immunoglobulin M; PRNT = plaque reduction neutralization test; STORCH = syphilis, toxoplasmosis, rubella, cytomegalovirus, herpes simplex; ZIKV = Zika virus

The Zika virus (ZIKV) is an arboviral disease with its main vector being *Aedes aegypti*.¹ There are also reports of sexual transmission and viral detection in urine² and tears.³ The first epidemic of ZIKV occurred in 2007 in the Yap Islands, Micronesia⁴; the second occurred in 2013, in French Polynesia⁵; and the

third began in Bahia, Northeast Brazil, in March 2015.⁶ In August 2015, in Pernambuco, Northeast Brazil, a significant increase in the number of congenital microcephaly cases was reported to the health authorities. Currently, the relationship between the ZIKV and microcephaly is well-established.⁷

The most characteristic findings of congenital Zika syndrome (CZS) include microcephaly, arthrogryposis, and ophthalmologic and hearing abnormalities.^{8–12} The major neuroimaging abnormalities reported by initial case series^{8,13,14} were calcifications

Received February 11, 2017; accepted after revision March 6.

From the Centro Diagnostico Multimagem (M.F.V.V.A.), Recife, Brazil; Federal University of Pernambuco (A.C.H.), Recife, Brazil; Pronto-Socorro Cardiológico de Pernambuco (Procape) (A.M.B.-L., M.M.V.), University of Pernambuco, Recife, Brazil; Barão de Lucena Hospital (N.C.L.P.), Recife, Brazil; Department of Radiology (M.C.), University of North Carolina, Chapel Hill, North Carolina; Association for Assistance of Disabled Children (V.v.d.L.), Recife, Brazil; Clínica de Apoio Ocupacional (S.C.S.), Jaboatão dos Guararapes, Brazil; Dom Malan Hospital (A.G.T.), Petrolina, Brazil; Laboratório Fernando Travassos (P.T.C.T.), Recife, Brazil; Centro de Pesquisas Aggeu Magalhães (M.T.C., C.S.), Fiocruz, Recife, Brazil; and Department of Maternal, Child, and Adolescent Health (A.C.), World Health Organization, Geneva, Switzerland.

Please address correspondence to Maria de Fatima Viana Vasco Aragão, MD, Rua Frei Matias Teves, 194 Ilha do Leite, Recife, PE, 50070-450 Brazil; e-mail: fatima.vascoaragao@gmail.com

Indicates open access to non-subscribers at www.ajnr.org

Indicates article with supplemental on-line tables.

<http://dx.doi.org/10.3174/ajnr.A5216>

in the cortico-subcortical white matter junction and malformations of cortical development, associated with other brain abnormalities.^{8,13,14}

These imaging features were reported on the basis of severe cases of microcephaly identified at birth.^{8,13-15} However, some of these patients⁸ did not have microcephaly at birth and were detected because in the beginning, microcephaly was defined as a head circumference of ≤ 33 cm, a cutoff that decreased 2 times before the establishment of the current criteria based on the Intergrowth-21st.¹⁶ Therefore, there is probably a disease spectrum that has only recently been recognized, with some patients presenting with less severe brain damage and even without microcephaly.

We reviewed the brain CT and MR imaging scans of infants 1 year of age or younger, to find cases of CZS without microcephaly and to compare them with infants with microcephaly. We hypothesized that these mild cases of CZS without microcephaly, not suspected before neuroimaging evaluation, have a milder degree of brain damage.

MATERIALS AND METHODS

We retrospectively evaluated all brain MR imaging and CT scans of infants 1 year of age or younger from December 2015 to November 2016, in the Centro Diagnostico Multimagem Radiology Clinic. This study was approved by the research ethics committee.

The imaging reports were divided into 3 groups: 1) healthy patients, 2) nonspecific or not related to ZIKV, and 3) cases of neuroimaging abnormalities consistent with CZS. The last group was further subdivided into 3 groups: 1) infants with microcephaly at birth, 2) infants with microcephaly developed a few months after birth, and 3) infants without microcephaly. The classification of microcephaly was based on the Intergrowth-21st.¹⁶

Clinical information and CSF tests (syphilis, toxoplasmosis, rubella, cytomegalovirus, herpes simplex [STORCH] infections and ZIKV-specific immunoglobulin M [IgM]) were retrospectively reviewed in infants with microcephaly. In infants without microcephaly, a history of arboviral infection during pregnancy was queried for support of the MR imaging diagnosis, and laboratory investigation was performed.

Infants in this study were possible (suspected), probable, or confirmed cases of CZS. According to the Brazilian Ministry of Health,¹⁶ probable cases involve the following: 1) the mother's rash during pregnancy, 2) brain imaging suggestive of congenital infection, and 3) laboratory exclusion of STORCH infections in the mother and/or infant. Confirmed cases have, in addition, 4) laboratory confirmation of ZIKV infection in the mother and/or infant (eg, real-time reverse transcription polymerase chain reaction, ZIKV-specific IgM, plate reduction neutralization test [PRNT] for ZIKV in the CSF and/or serum).¹⁷ Suspected cases were classified as possible CZS when the above-mentioned items 1 or 4 were unknown or not present but the infant was born in an epidemic area and there was microcephaly and brain imaging suggestive of CZS.^{8,13,14}

The group of infants with microcephaly at birth was compared with the group without microcephaly and with the group with postnatal microcephaly. We also joined groups and compared: 1) group with microcephaly at birth with group without microceph-

aly at birth (postnatal microcephaly + without microcephaly); and 2) group with microcephaly (microcephaly at birth + postnatal microcephaly) with group without microcephaly. The images were analyzed by 2 experienced neuroradiologists (M.F.V.V.A. and A.M.B.-L.), with the final interpretation determined by a consensus. CT scans were subjectively reviewed for reduced brain volume; brain stem and cerebellar hypoplasia; malformations of cortical development; the presence and location of brain calcifications; corpus callosum abnormalities (classified as hypogenesis, when it was incompletely formed, or hypoplasia, when it was complete but reduced in thickness)¹⁸; ventriculomegaly; an enlarged extra-axial CSF space; and an enlarged cisterna magna (largest diameters in 3 planes of ≥ 10 mm). Symmetry of brain damage was determined by visual comparison between the cerebral hemispheres. All features identified on CT scans were also reviewed on brain MR imaging. In addition, we evaluated myelination (normal or delayed, according to milestones determined by a previous study)¹⁸ and types of malformations of cortical development classified as periventricular heterotopia, agyria, pachygyria, polymicrogyria, and simplified gyral pattern.

Statistical Analysis

For association, we used the Fisher exact test. A *P* value $< .05$ was considered significant. The statistical analyses were performed by using SPSS software, Version 21.0 (IBM, Armonk, New York).

RESULTS

Regarding the neuroimaging diagnosis, among the 77 infants who underwent brain imaging scans (CT and/or MR imaging), 1) 18 (23.4%) had normal examination findings; 2) 40 (52.0%) had abnormalities considered nonspecific or not related to ZIKV infection; and 3) 19 (24.6%) had neuroimaging abnormalities consistent with CZS. In the CZS group, 9 (11.7%) infants had microcephaly at birth, 7 (9.1%) had postnatal microcephaly, and 3 (3.9%) did not have microcephaly. On-line Table 1 shows the individual clinical and laboratory data of the infants with CZS. The 3 infants without microcephaly were diagnosed as having probable CZS (On-line Table 2).

Clinical Information

The group with microcephaly at birth had more males (55.6%), while the groups with postnatal microcephaly and without microcephaly had more females (71.4% and 100.0%, respectively), without statistical significance. Six of 9 mothers of infants with microcephaly at birth reported rashes (66.7%), and 5 of 7 mothers of infants with postnatal microcephaly reported rashes (71.4%). Other clinical information is shown in On-line Table 1. Ages at imaging evaluation were an average of 139.4 ± 19.3 days for microcephaly at birth; a median of 129 days (interquartile range, 88–328) for postnatal microcephaly; and 253, 323, and 352 days for infants without microcephaly.

Laboratory Status

The laboratory tests were performed only once, shortly after birth for most infants (data from few of the infants could not be retrieved). For 2 infants with postnatal microcephaly and all with-

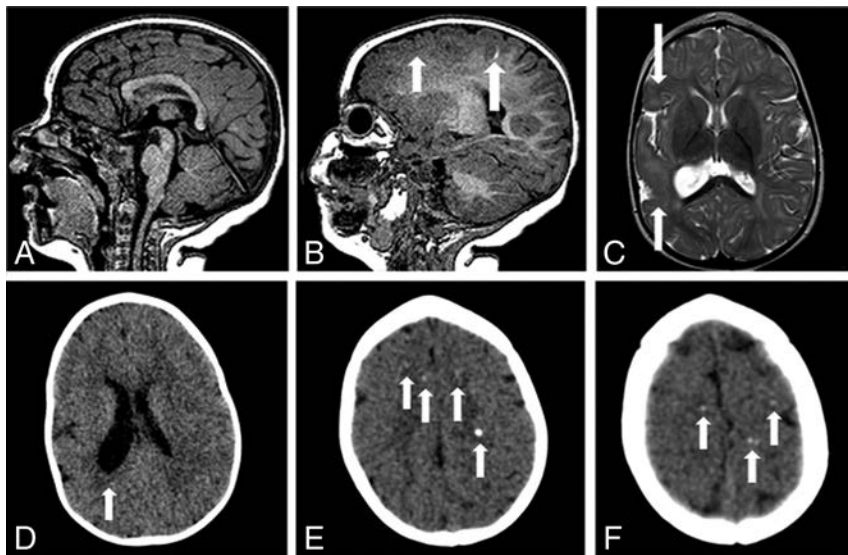


FIG 1. MR imaging and CT of an 8-month-old girl without microcephaly with probable congenital Zika syndrome. Sagittal T1-weighted image shows a normal corpus callosum and cisterna magna (A) and a small hyperintense focus of dystrophic calcification in the junction between the cortical and subcortical white matter (long white arrow) and left frontal polymicrogyria (short white arrow) (B). Axial T2-weighted image (C) shows right polymicrogyria (white arrows) and mildly decreased right hemisphere volume. CT scans show asymmetric hemispheres, with an enlarged right lateral ventricle (white arrow) (D) and small punctate foci, representing calcifications, at the cortico-subcortical white matter junction bilaterally in the frontal lobes (white arrows) (E and F).

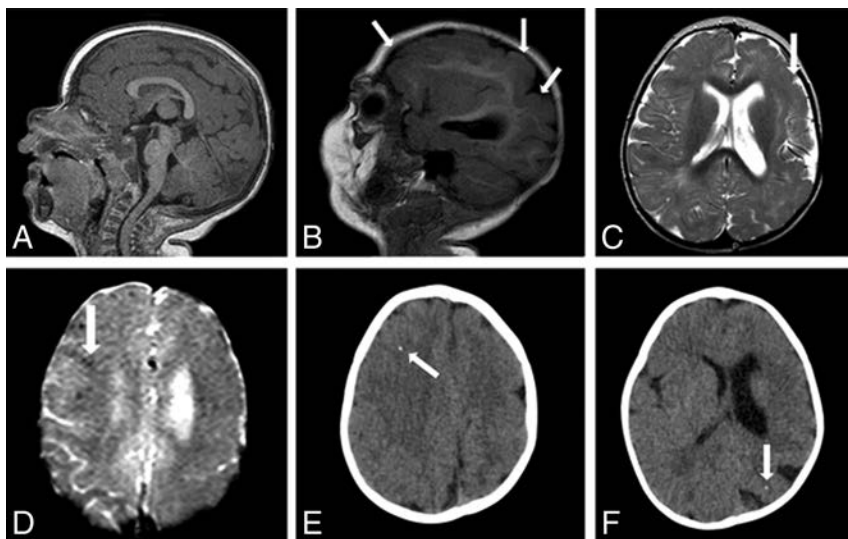


FIG 2. MR imaging and CT of an 11-month-old girl without microcephaly with probable congenital Zika syndrome. Sagittal T1-weighted image shows a normal corpus callosum and cisterna magna (A) and left polymicrogyria (white arrows) (B). Axial T2-weighted image (C) shows left polymicrogyria (white arrow) and mild left ventriculomegaly. A gradient-echo image (D) shows very few small and subtle punctate foci, representing calcifications, at the cortico-subcortical white matter junction (white arrow). Axial CT scans (E and F) show right frontal and left parietal punctate foci (white arrows).

out microcephaly (infants 15–19), tests were performed shortly before or after imaging evaluation; therefore, close to 1 year of age.

Findings of tests for STORCH and dengue in the CSF were negative in 18 infants (data not available for Infant 10) (On-line Table 1). In the microcephaly at birth group, 7/8 infants tested for Zika-specific IgM in the CSF had positive findings and just 1/8 had negative results (On-line Table 1). In the postnatal microcephaly group, 2/4 infants tested for Zika-specific IgM in the CSF

had positive findings. The other 2/4 who had negative results also had negative PRNT test findings in the CSF, but they were tested only several months after birth (On-line Table 1). All 3 infants with normal head circumferences had negative ZIKV-specific IgM and PRNT test findings in the CSF. However, the serologic PRNT test had positive results in both tested mothers of 2 infants without microcephaly (On-line Table 1).

Neuroimaging Features

Imaging abnormalities in the group without microcephaly (Figs 1–3) were not significantly different from those in the group with postnatal microcephaly (Fig 4).

The group without microcephaly was significantly different from the one with microcephaly at birth (Fig 5) for the following: reduced brain volume, calcifications outside the cortico-subcortical white matter junction, corpus callosum abnormalities, moderate-to-severe ventriculomegaly, an enlarged extra-axial CSF space, and an enlarged cisterna magna (Table). All these features were found only in microcephaly at birth. In addition, polymicrogyria was not present in the microcephaly at birth group, a finding that was significantly different from that in the group without microcephaly.

The group with microcephaly at birth was significantly different from the one with postnatal microcephaly in the following features: a simplified gyral pattern, calcifications outside the cortico-subcortical white matter junction, corpus callosum abnormalities, moderate-to-severe ventriculomegaly, and an enlarged extra-axial CSF space (Table). All these features were found more frequently in the microcephaly at birth group. In addition, polymicrogyria was not present in the microcephaly at birth group, with statistical differences from the group without microcephaly.

When the groups with and without microcephaly at birth were compared, significant differences were found for brain stem hypoplasia, simplified gyral pattern, calcifications outside the cortico-subcortical white matter junction, corpus callosum abnormalities, moderate-to-severe ventriculomegaly, an enlarged extra-axial CSF space, and an enlarged cisterna magna (Table). All these features were found more frequently or exclusively in the microcephaly at birth group. Polymicrogyria was not present in the microcephaly at birth

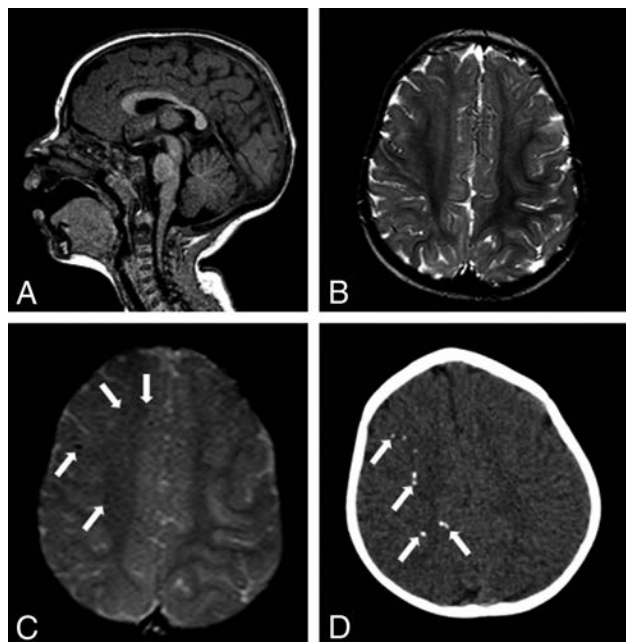


FIG 3. MR imaging and CT of an 11-month-old girl without microcephaly with probable congenital Zika syndrome. Sagittal T1-weighted image shows a normal corpus callosum and cisterna magna (A). Axial T2-weighted image (B) shows a normal cortex. A gradient-echo image (C) shows small and subtle punctate foci, representing calcifications, at the cortico-subcortical white matter junction (*white arrows*). Axial CT scan (D) shows punctate foci in the right hemisphere (*white arrows*).

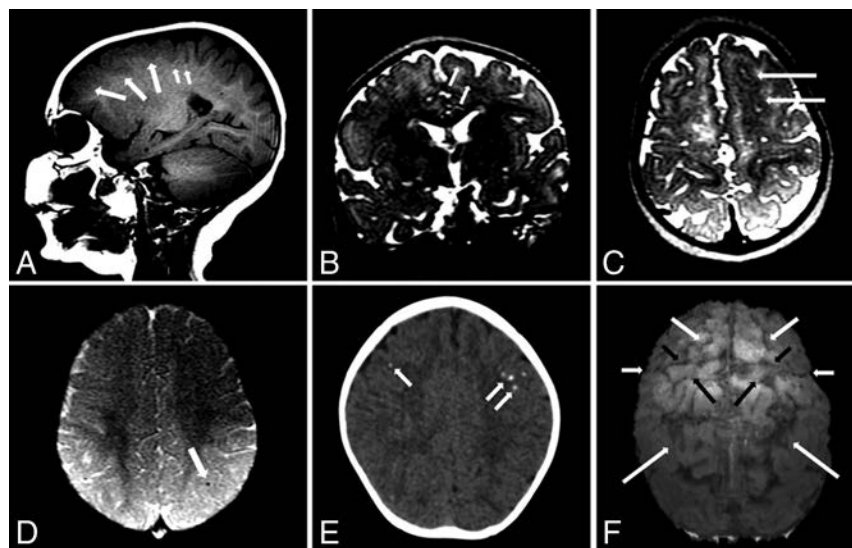


FIG 4. MR imaging and CT of a 10-month-old girl with microcephaly developed postnatally with possible congenital Zika syndrome. Sagittal T1-weighted image shows frontal polymicrogyria (*medium white arrows*) and very subtle hyperintense punctate foci, representing calcifications at the cortico-subcortical white matter junction (*small white arrows*). Coronal and axial T2-weighted images (B and C, respectively) show the thick and irregular cortex at the superior frontal sulcus (*white arrows*). Axial SWI (D) shows a small punctate focus, representing calcification at the cortico-subcortical white matter junction (*white arrow*). Axial CT scan (E) shows punctate foci in both frontal lobes. An echo-spoiled gradient-echo volumetric (3D reconstruction) image (F) shows malformation and prominence of brain high frontoparietal convexity gyri and sulci, predominantly at the left hemisphere: The superior frontal sulcus (*medium white arrows*) is well-identified bilaterally, as well as precentral (*short black arrows*), central (*short white arrows*), and intraparietal (*long white arrows*) sulci. The left hemisphere is more reduced than the right hemisphere; the left precentral gyrus (*large black arrows*) seems to be the most reduced in volume. These findings are located probably where the polymicrogyria is most severe, according to the T2-weighted images (B and C). These findings are better seen in a 3D reconstruction (F) than in sectional images (A–C), despite the presence of movement artifacts in the former.

group. Cerebellar hypoplasia was present in only 3 infants with microcephaly at birth, with a statistical trend.

When the groups with microcephaly were combined and compared with the group without microcephaly, statistically significant differences were found for reduced brain volume, an enlarged extra-axial CSF space, and an enlarged cisterna magna (Table). All of these features were found only in infants with microcephaly.

DISCUSSION

Among the 77 infants studied, 16 (20.8%) with microcephaly and 3 (3.9%) without microcephaly had evidence of CZS. This number could reflect the incidence of normocephalic CZS in the healthy population. However, this percentage could be either higher, because these cases are only starting to be detected, or lower, considering the higher chance of abnormalities in the population that undergoes imaging. The incidence of CZS in Pernambuco in 2015 was 0.19% (142,965 live births versus 268 confirmed CZS cases).^{10,19} This percentage in the Centro Diagnostico Multimagem radiologic center was higher because it is a referral center for neuropsychiatrists.

Neuroimaging Features of the Congenital Zika Syndrome Spectrum

Infants born with microcephaly presented with the highest number of abnormalities and more severe malformations, followed by those with postnatal microcephaly and then by the infants without microcephaly. However, significant differences were not observed between the last 2 groups.

Reduction in brain volume is present in all infants with microcephaly, while brain volume is preserved in infants without microcephaly with significant differences. Therefore, the normal head size in the normocephalic group is not due to hydrocephalus¹⁴ but due to less severe brain damage. Volumetric MR imaging studies could be useful for better characterizing the reduction of brain volume. This information could help in understanding the physiopathology of the disease, in the differential diagnosis, and in the prognosis and follow-up of these infants.

Moderate-to-severe ventriculomegaly was significantly more frequent in the group with microcephaly at birth compared with the other 2 groups, both separately and jointly. Ventricular enlargement is directly related to the reduction of brain volume, which is more severe in the group with microcephaly at birth and not due to hydrocephalus.

The frequency of enlarged extra-axial CSF spaces increases with the severity of the CZS spectrum. It was present in all infants with microcephaly at birth and

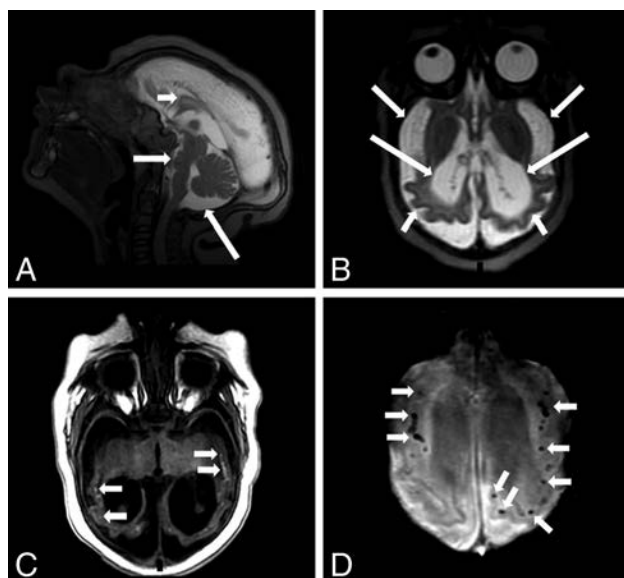


FIG 5. MR imaging of a 4-month-old boy with microcephaly with confirmed congenital Zika syndrome. Sagittal T2-weighted image (A) shows a hypogenetic corpus callosum (*short white arrow*), pons hypoplasia (*medium white arrow*), and an enlarged cisterna magna (*long white arrow*). An axial T2-weighted image (B) shows a diffuse simplified gyral pattern (note the thin cortex) (*short white arrows*), an enlarged extra-axial CSF space (*medium white arrows*), and severe ventriculomegaly (*long white arrows*). An axial T1-weighted image (C) shows hyperintense punctate foci, representing calcifications, at the cortico-subcortical white matter junction (*small white arrows*). Axial SWI (D) shows several punctate foci at the cortico-subcortical white matter junction (*short white arrows*).

absent in infants without microcephaly, with significant differences being directly related to reduced brain volume. Enlarged extra-axial space could also be the result of impaired CSF reabsorption.

The frequency of an enlarged cisterna magna also increases with the severity of the CZS spectrum. It was present in all infants with microcephaly at birth and absent in infants without microcephaly. Significant differences were found in most comparative analyses (microcephaly at birth versus postnatal microcephaly showed a statistical trend). An enlarged cisterna magna is not related to cerebellar hypoplasia because this was an infrequent finding.

Brain stem hypoplasia is mainly present in the most severe cases with microcephaly at birth. This group was significantly different from the combined group without microcephaly at birth. The decreased brain stem volume, especially of the pons, could represent more severe damage in microcephaly at birth, being possibly explained by a decreased number of descending fibers, supported by anatomic-pathologic studies.²⁰ Another hypothesis is direct viral action in brain stem nuclei. DTI studies could help in clarifying ZIKV damage not only in the brain stem but also to fibers in other sites.

A simplified gyral pattern was characteristic of microcephaly at birth, being exclusively found in this group and significantly different compared with the combined group without microcephaly at birth. This finding suggests that this type of malformation, resulting from diminished cell proliferation or white matter development in utero,¹⁸ is associated with more severe damage. In a simplified gyral pattern, few neurons are produced or too many undergo apoptosis.¹⁸

Comparison of brain MRI findings between microcephalic and normocephalic infants with congenital Zika syndrome

| MRI Findings | Microcephaly | | Without Microcephaly (n = 3) | P ₁ | P ₂ | P ₃ | P ₄ |
|--|---------------------|------------------------|---------------------------------|-------------------|-------------------|-------------------|-------------------|
| | At Birth (n = 9) | Postnatally (n = 7) | | | | | |
| Reduced brain volume | 8 (88.9%) | 5 (71.4%) | 0 (0.0%) | .018 ^a | .550 | .141 | .021 ^a |
| Brain stem hypoplasia | 6 (66.7%) | 1 (14.3%) | 0 (0.0%) | .182 | .060 | .020 ^a | .263 |
| Cerebellum hypoplasia | 3 (33.3%) | 0 (0.0%) | 0 (0.0%) | .509 | .213 | .087 | 1.000 |
| Malformations of cortical development ^b | | | | | | | |
| Simplified gyral pattern | 6 (66.7%) | 0 (0.0%) | 0 (0.0%) | .182 | .028 ^a | .009 ^a | .515 |
| Pachygyria | 6 (66.7%) | 4 (66.7%) | 0 (0.0%) | .182 | 1.000 | .637 | .069 |
| Polymicrogyria | 0 (0.0%) | 4 (66.7%) | 2 (66.7%) | .045 ^a | .011 ^a | .009 ^a | .245 |
| Normal cortex | 1 (11.1%) | 0 (0.0%) | 1 (33.3%) | .455 | 1.000 | 1.000 | .314 |
| Brain calcifications | | | | | | | |
| Cortico-subcortical white matter junction | 8 (88.9%) | 7 (100.0%) | 3 (100.0%) | 1.000 | 1.000 | .474 | 1.000 |
| Calcifications at other sites | 7 (77.8%) | 0 (0.0%) | 0 (0.0%) | .046 ^a | .003 ^a | .001 ^a | .263 |
| Basal ganglia | 4 (44.4%) | 0 (0.0%) | 0 (0.0%) | .491 | .103 | .082 | 1.000 |
| Thalamus | 3 (33.3%) | 0 (0.0%) | 0 (0.0%) | .509 | .229 | .206 | 1.000 |
| Periventricular | 3 (33.3%) | 0 (0.0%) | 0 (0.0%) | .509 | .229 | .206 | 1.000 |
| Brain stem | 4 (44.4%) | 0 (0.0%) | 0 (0.0%) | .491 | .103 | .082 | 1.000 |
| Cerebellum | 2 (22.2%) | 0 (0.0%) | 0 (0.0%) | 1.000 | .475 | .471 | 1.000 |
| Corpus callosum abnormalities | 9 (100.0%) | 2 (28.6%) | 0 (0.0%) | .005 ^a | .005 ^a | .001 ^a | .058 |
| Moderate-to-severe ventriculomegaly | 8 (88.9%) | 2 (28.6%) | 0 (0.0%) | .018 ^a | .035 ^a | .005 ^a | .087 |
| Enlarged extra-axial CSF space | 9 (100.0%) | 3 (42.9%) | 0 (0.0%) | .005 ^a | .019 ^a | .003 ^a | .036 ^a |
| Enlarged cisterna magna | 9 (100.0%) | 4 (57.1%) | 0 (0.0%) | .005 ^a | .063 | .008 ^a | .021 ^a |
| Delayed myelination ^b | 7 (77.8%) | 2 (33.3%) | 2 (66.7%) | 1.000 | .136 | .335 | 1.000 |
| Symmetry of abnormalities | 8 (88.9%) | 3 (42.9%) | 1 (33.3%) | .127 | .106 | .057 | .523 |

Note:—P indicates Fisher exact test; P₁, microcephaly at birth vs without microcephaly; P₂, microcephaly at birth vs microcephaly postnatally; P₃, microcephaly at birth vs without microcephaly at birth (microcephaly postnatally + without microcephaly); P₄, microcephaly (microcephaly at birth + microcephaly postnatally) vs without microcephaly. Microcephaly postnatally vs without microcephaly yielded no statistically significant results.

^a Statistically significant results.

^b Not assessed in Infant 14 (without MRI). For myelination assessment, infant 15 was considered born at term.

Pachygyria was present exclusively in infants in the combined group with microcephaly (at birth and postnatally). Despite these findings, only a trend was found when these groups were compared, possibly due to the small number of infants without microcephaly. Pachygyria, as a simplified gyral pattern, probably represents more severe brain damage, being associated with other abnormalities. When present in the same infant with microcephaly at birth, pachygyria was located in the anterior brain (a thick cortex mainly in the frontal lobes), and a simplified gyral pattern comprised mostly the posterior parts of the brain (parietal and occipital lobes).

Polymicrogyria was the only malformation of cortical development found in infants without microcephaly, and it was absent in infants with microcephaly at birth. This finding reinforces polymicrogyria being probably a less severe lesion, with consequent preservation of brain volume and the corpus callosum. In postnatal microcephaly, when polymicrogyria and pachygyria were found in the same infant, the former was located in the anterior brain (mainly in the frontal lobes), while the latter was located in the posterior parts of the brain (mainly in the parietal and occipital lobes).

Brain calcifications in the cortex and subcortical white matter were found in almost all CZS cases. Calcifications located at other sites (basal ganglia, thalamus, periventricular, brain stem, and cerebellum) were found only in microcephaly at birth, with significant differences compared with the other 2 groups, both separately and combined. When they are distributed in several structures of the brain, they suggest more severe damage and, consequently, probably more severe brain volume reduction. Even though CT has higher sensitivity to intracranial calcifications, MR imaging is also able to detect them. Calcifications appear as hyperintense foci on T1-weighted images, especially when the brain is not completely myelinated, and as hypointense on SWI, which is the best sequence to demonstrate them.^{8,21}

The frequency of corpus callosum abnormalities (hypogenesis and hypoplasia) is directly related to CZS severity. Corpus callosum abnormalities were absent in infants without microcephaly and very frequent in the infants with microcephaly at birth. Significant differences were found in most comparative analyses (patients with microcephaly versus those without microcephaly showed a statistical trend). Hypogenesis or hypoplasia of the corpus callosum with microcephaly at birth could be related to more severe parenchymal damage and cortical malformation, with a consequent decreased number of fibers crossing the cerebral hemispheres.

Lesions were more symmetric in infants with microcephaly at birth compared with infants without it, with a strong trend. Possibly this difference is because microcephaly at birth is related to more diffuse and severe lesions. In regards of the physiopathology, it is known that the ZIKV attacks neural progenitor cells and mature neural cells, causing downregulation of genes involved in cell cycle pathways, dysregulation of cell proliferation, and upregulation of genes involved in apoptotic pathways resulting in cell death.²² However, some authors suggest that vascular phenomena could also be involved in the pathophysiology.^{14,23} Heterogeneous material in the confluence of the sinuses, probably corresponding to thrombus, has already been described.^{14,23} As

the use of contrast is usually not recommended in infants, the frequency of cerebral venous thrombosis is unknown. Nevertheless, we hypothesize that, in CZS, there may exist an important damage to the cerebral vascular system, especially in the venous component, leading to cerebral venous thrombosis and cerebral venous hypertension during intrauterus development and continuing after birth. This could explain the cortico-subcortical calcifications, the development of hydrocephalus in some of the infants,²⁴ and changes in brain lesions,^{23,25} similarly to what happens in cerebral venous hypertension of the physiopathology of vein of Galen aneurysmal malformations.²⁶ The confirmation of this vascular hypothesis could lead to research for identifying treatment options during pregnancy and after birth, improving the prognosis of the infants and the evolution of the disease. The identification of changes in parenchyma thickness, ventricle size and calcifications^{23,25} indicates that these infants should be followed not only clinically, but also by laboratory tests (possibility of persistent viral activity) and by neuroimaging, especially if there are signs of disease progression.

In summary, the most severe group, with microcephaly at birth, presented with all the major abnormalities already described in the literature (reduced brain volume, brain stem hypoplasia, cerebellar hypoplasia, a simplified gyral pattern, pachygyria, calcifications at the cortico-subcortical white matter junction and at other sites, corpus callosum abnormalities, moderate-to-severe ventriculomegaly, an enlarged extra-axial CSF space, an enlarged cisterna magna, and delayed myelination), except for polymicrogyria.

In the intermediate group with postnatal microcephaly, the only abnormalities absent were simplified gyral pattern and calcifications outside the cortico-subcortical junction, compared with infants with microcephaly at birth. On the other hand, polymicrogyria was found in infants with postnatal microcephaly and without microcephaly but not in infants with microcephaly at birth.

In the less severe extreme, without microcephaly, there was only asymmetric polymicrogyria, mainly in the frontal lobes, calcifications restricted to the cortical/white matter junctions, mild ventricular enlargement, and delayed myelination.

Congenital Zika Syndrome without Microcephaly

The clinical signs of brain impairment in the 3 children without microcephaly were noticed by their mothers several months after birth. They were nonspecific, and the diagnosis could have been missed without accurate MR imaging interpretation. The 3 mothers remembered a rash during pregnancy, but 2 of them recognized it only when they were asked after the MR imaging report. Because about 75% of infected patients may be asymptomatic,²⁷ imaging becomes important in showing the “tip of the iceberg.”

Although other infections were excluded in all infants without microcephaly, Zika-specific tests did not confirm the ZIKV infection in these infants. However, these Zika-specific tests are not completely trustworthy, because they are not validated yet.²⁸ For IgM in the CSF, this negative result was expected due to the long period since the infection occurred because the children are currently close to 1 year of age. For PRNT (IgM and immunoglobulin G), the negative results in these infants are difficult to understand because the 2 mothers tested for PRNT (cases 18 and 19) had

positive results and all 3 had rashes during pregnancy, supporting ZIKV infection. Thus, although these 3 infants with negative specific tests are probable CZS,¹⁷ we suggest they be considered to have confirmed CZS.

The negative PRNT results and lower severity and number of brain lesions in infants without microcephaly need future experimental studies to be clarified. More severe ZIKV damage could be related to earlier vertical transmission during pregnancy, higher viral load, and a crossed immunologic response, among other hypotheses. Environmental factors could also be involved because the most severe cases are located in Northeast Brazil.¹⁴

Maternal infection during pregnancy was more frequent in the first trimester for microcephaly and in the second trimester for normocephaly, though without significant differences. One limitation is that the maternal ZIKV infection was based exclusively on recall of the mothers' rashes during pregnancy. Mothers may not remember the exact month in which they had the rash, and this drawback limits our interpretations. In addition, the literature has shown that the interval between maternal infection and sonographic evidence of fetal abnormalities can range from 2 to 27 weeks.²⁰

These are the first published cases in which CZS was not suspected by neuropsychiatrists because the patients had normal head circumferences and nonspecific neurologic signs and the diagnosis was only raised after MR imaging evaluation. They raise an important epidemiologic issue: How many children have less severe CZS brain damage and are being missed?

The radiologist's role is even more important in CZS without microcephaly: to recognize subtle suggestive findings and to indicate the probable diagnosis to the neuropsychiatrist. This early diagnosis allows rehabilitation to start as soon as possible, improving the development of these infants. Clinical and radiologic follow-up of the brains will be important to understand the pathophysiology of this new disease.

Our study has limitations, especially due to the small sample and retrospective method. Studies with a larger number of infants are needed to confirm the results and to reinforce information that was identified here. Nevertheless, the study was able to characterize brain abnormalities in 3 degrees of the CZS spectrum with statistically significant differences.

CONCLUSIONS

Infants without clinical suspicion of CZS (without microcephaly) can be first identified with neuroimaging studies. These cases represented 3.9% of the infants in our survey.

The spectrum of CZS comprises 3 different degrees of severity, with many statistically significant differences among the groups: 1) CZS with microcephaly at birth, which presented, except for polymicrogyria, with all abnormalities previously described in the literature; 2) CZS with postnatal microcephaly, in which, in relation to the group with microcephaly at birth, only a simplified gyral pattern and calcifications outside the cortical/white matter junctions were absent, but the infants presented with polymicrogyria; and 3) CZS without microcephaly, which presented with only asymmetric polymicrogyria mainly in the frontal lobes, calcifications restricted to the cortical/white matter junctions, mild ventricular enlargement, and delayed myelination.

ACKNOWLEDGMENTS

We thank Antônio Monteiro, Cristovam A de Lira Terceiro, Lucas Coelho Belfort Lustosa, Edineide Cristina Lopes, and Islane Martins for their inestimable help.

REFERENCES

1. Dick GW, Kitchen SF, Haddow AJ. **Zika virus, I: isolations and serological specificity.** *Trans R Soc Trop Med Hyg* 1952;46:509–20 CrossRef Medline
2. Gourinat AC, O'Connor O, Calvez E, et al. **Detection of Zika virus in urine.** *Emerg Infect Dis* 2015;21:84–86 CrossRef Medline
3. Miner JJ, Sene A, Richner JM, et al. **Zika virus infection in mice causes panuveitis with shedding of virus in tears.** *Cell Rep* 2016;16:3208–18 CrossRef Medline
4. Duffy MR, Chen TH, Hancock WT, et al. **Zika virus outbreak on Yap Island, Federated States of Micronesia.** *N Engl J Med* 2009;360:2536–43 CrossRef Medline
5. Cauchemez S, Besnard M, Bompard P, et al. **Association between Zika virus and microcephaly in French Polynesia, 2013–15: a retrospective study.** *Lancet* 2016;387:2125–32 CrossRef
6. Campos GS, Bandeira AC, Sardi SI. **Zika virus outbreak, Bahia, Brazil.** *Emerg Infect Dis* 2015;21:1885–86 CrossRef Medline
7. Rasmussen SA, Jamieson DJ, Honein MA, et al. **Zika virus and birth defects: reviewing the evidence for causality.** *N Engl J Med* 2016;374:1981–87 CrossRef Medline
8. de Fatima Vasco Aragao M, van der Linden V, Brainer-Lima AM, et al. **Clinical features and neuroimaging (CT and MRI) findings in presumed Zika virus related congenital infection and microcephaly: retrospective case series study.** *BMJ* 2016;353:i1901 CrossRef Medline
9. Leal MC, Muniz LF, Caldas Neto SD, et al. **Sensorineural hearing loss in a case of congenital Zika virus.** *Braz J Otorhinolaryngol* 2016 Jun 30. [Epub ahead of print] CrossRef Medline
10. Ventura CV, Maia M, Ventura BV, et al. **Ophthalmological findings in infants with microcephaly and presumable intra-uterus Zika virus infection.** *Arq Bras Oftalmol* 2016;79:1–3 CrossRef Medline
11. van der Linden V, Filho EL, Lins OG, et al. **Congenital Zika syndrome with arthrogryposis: retrospective case series study.** *BMJ* 2016;354:i3899 CrossRef Medline
12. Schuler-Faccini L, Ribeiro EM, Feitosa IM, et al; Brazilian Medical Genetics Society–Zika Embryopathy Task Force. **Possible association between Zika virus infection and microcephaly: Brazil, 2015.** *MMWR Morb Mortal Wkly Rep* 2016;65:59–62 CrossRef Medline
13. Hazin AN, Poretti A, Turchi Martelli CM, et al. **Computed tomographic findings in microcephaly associated with Zika virus.** *N Engl J Med* 2016;374:2193–95 CrossRef Medline
14. Soares de Oliveira-Szejnfeld P, Levine D, Melo AS, et al. **Congenital brain abnormalities and Zika virus: what the radiologist can expect to see prenatally and postnatally.** *Radiology* 2016;281:203–18 CrossRef Medline
15. Poretti A, Huisman TA. **Neuroimaging findings in congenital Zika syndrome.** *AJNR Am J Neuroradiol* 2016 Aug 4. [Epub ahead of print] CrossRef Medline
16. Ministério da Saúde (Brazil). Protocolo de vigilância e resposta à ocorrência de microcefalia e/ou alterações do sistema nervoso central (SNC). 2016. <http://combateaesds.saude.gov.br/images/sala-de-situacao/Microcefalia-Protocolo-de-vigilancia-e-resposta-10mar2016-18h.pdf>. Accessed April 15, 2017
17. Ministério da Saúde (Brazil). Orientações integradas de vigilância e atenção à saúde no âmbito da Emergência de Saúde Pública de Importância Nacional. 2016. <http://portalsauze.saude.gov.br/images/pdf/2016/dezembro/12/orientacoes-integradas-vigilancia-atencao.pdf>. Accessed December 20, 2016
18. Adachi Y, Poduri A, Kawaguchi A, et al. **Congenital microcephaly with a simplified gyral pattern: associated findings and their significance.** *AJNR Am J Neuroradiol* 2011;32:1123–29 CrossRef Medline
19. Agência Estadual de Planejamento e Pesquisas de Pernambuco.

- Natalidade: Anuário Estatístico de Pernambuco. 2015. <http://www.anuario.pe.gov.br/demografia/natalidade>. Accessed April 15, 2017
20. Melo AS, Aguiar RS, Amorim MM, et al. **Congenital Zika virus infection: beyond neonatal microcephaly.** *JAMA Neurol* 2016;73:1407–16 [CrossRef](#) [Medline](#)
 21. Livingston JH, Stivaros S, Warren D, et al. **Intracranial calcification in childhood: a review of aetiologies and recognizable phenotypes.** *Dev Med Child Neurol* 2014;56:612–26 [CrossRef](#) [Medline](#)
 22. Tang H, Hammack C, Ogden SC, et al. **Zika virus infects human cortical neural progenitors and attenuates their growth.** *Cell Stem Cell* 2016;18:587–90
 23. Aragão MF, Brainer-Lima AM, Holanda AC, Petribu NC de L. **Neuroimaging findings of congenital Zika syndrome.** In: Aragão MF, ed. *Zika in Focus*. Springer International Publishing; 2017:63–92
 24. van der Linden V, Filho EL, van der Linden A. **Congenital Zika syndrome: clinical aspects.** In: Aragão MF, ed. *Zika in Focus*. Springer International Publishing; 2017:33–45
 25. Petribu NC, Aragão MF. **Cases: Spectrum of Computed Tomography in Congenital Zika Syndrome.** In: Aragão MF, ed. *Zika in Focus*. Springer International Publishing; 2017:107–24
 26. Diebler C, Dulac O, Renier D, et al. **Aneurysms of the vein of Galen in infants aged 2 to 15 months: diagnosis and natural evolution.** *Neuroradiology* 1981;21:185–97
 27. Besnard M, Lastere S, Teissier A, et al. **Evidence of perinatal transmission of Zika virus, French Polynesia, December 2013 and February 2014.** *Euro Surveill* 2014;19 [Medline](#)
 28. de Araújo TV, Rodrigues LC, de Alencar Ximenes RA, et al; investigators from the Microcephaly Epidemic Research Group, Brazilian Ministry of Health, Pan American Health Organization, Instituto de Medicina Integral Professor Fernando Figueira, State Health Department of Pernambuco. **Association between Zika virus infection and microcephaly in Brazil, January to May, 2016: preliminary report of a case-control study.** *Lancet Infect Dis* 2016;16:1356–63 [CrossRef](#) [Medline](#)

Validation of an MRI Brain Injury and Growth Scoring System in Very Preterm Infants Scanned at 29- to 35-Week Postmenstrual Age

J.M. George, S. Fiori, J. Fripp, K. Pannek, J. Bursle, R.X. Moldrich, A. Guzzetta, A. Coulthard, R.S. Ware, S.E. Rose, P.B. Colditz, and R.N. Boyd



ABSTRACT

BACKGROUND AND PURPOSE: The diagnostic and prognostic potential of brain MR imaging before term-equivalent age is limited until valid MR imaging scoring systems are available. This study aimed to validate an MR imaging scoring system of brain injury and impaired growth for use at 29 to 35 weeks postmenstrual age in infants born at <31 weeks gestational age.

MATERIALS AND METHODS: Eighty-three infants in a prospective cohort study underwent early 3T MR imaging between 29 and 35 weeks' postmenstrual age (mean, $32^{+2} \pm 1^{+3}$ weeks; 49 males, born at median gestation of 28^{+4} weeks; range, 23^{+6} – 30^{+6} weeks; mean birthweight, 1068 ± 312 g). Seventy-seven infants had a second MR scan at term-equivalent age (mean, $40^{+6} \pm 1^{+3}$ weeks). Structural images were scored using a modified scoring system which generated WM, cortical gray matter, deep gray matter, cerebellar, and global scores. Outcome at 12-months corrected age (mean, 12 months 4 days $\pm 1^{+2}$ weeks) consisted of the Bayley Scales of Infant and Toddler Development, 3rd ed. (Bayley III), and the Neuro-Sensory Motor Developmental Assessment.

RESULTS: Early MR imaging global, WM, and deep gray matter scores were negatively associated with Bayley III motor (regression coefficient for global score $\beta = -1.31$; 95% CI, -2.39 to -0.23 ; $P = .02$), cognitive ($\beta = -1.52$; 95% CI, -2.39 to -0.65 ; $P < .01$) and the Neuro-Sensory Motor Developmental Assessment outcomes ($\beta = -1.73$; 95% CI, -3.19 to -0.28 ; $P = .02$). Early MR imaging cerebellar scores were negatively associated with the Neuro-Sensory Motor Developmental Assessment ($\beta = -5.99$; 95% CI, -11.82 to -0.16 ; $P = .04$). Results were reconfirmed at term-equivalent-age MR imaging.

CONCLUSIONS: This clinically accessible MR imaging scoring system is valid for use at 29 to 35 weeks postmenstrual age in infants born very preterm. It enables identification of infants at risk of adverse outcomes before the current standard of term-equivalent age.

ABBREVIATIONS: CA = corrected age; c- = corrected; CGM = cortical gray matter; DGM = deep gray matter; ICC = intraclass correlation coefficient; NSMDA = Neuro-Sensory Motor Developmental Assessment; PMA = postmenstrual age; TEA = term-equivalent age

Preterm infants are at risk of brain injury and impaired brain growth and consequently poorer outcomes in infancy and

childhood.^{1–6} Scoring of structural MR imaging to classify brain injury and growth has been validated for use at term-equivalent age (TEA) in infants born preterm.^{1,7} Initial systems were qualitative, focusing on classification of the severity of WM and cortical gray matter (CGM) injuries.^{7–9} The degree of WM abnormality demonstrated significant associations with concurrent motor, neurologic, and neurobehavioral performance^{10–13} and increas-

Received October 19, 2016; accepted after revision February 21, 2017.

From the Queensland Cerebral Palsy and Rehabilitation Research Centre (J.M.G., R.N.B.), Centre for Children's Health Research, Faculty of Medicine; University of Queensland Centre for Clinical Research (R.X.M., P.B.C.), Discipline of Medical Imaging (A.C.); and Queensland Centre for Intellectual and Developmental Disability (R.S.W.), The University of Queensland, Brisbane, Australia; Stella Maris Scientific Institute (S.F., A.G.), Department of Developmental Neuroscience, Pisa, Italy; Health and Biosecurity (J.F., K.P., S.E.R.), The Australian e-Health Research Centre, Commonwealth Scientific and Industrial Research Organisation, Brisbane, Australia; Department of Medical Imaging (J.B., A.C.) and Perinatal Research Centre (P.B.C.), Royal Brisbane and Women's Hospital, Brisbane, Australia; and Menzies Health Institute Queensland (R.S.W.), Griffith University, Brisbane, Australia.

This work was supported by grants from the Cerebral Palsy Alliance Research Foundation (IRG1413), the Financial Markets Foundation for Children (2014–074), and the Queensland Government (Smart State; Health Practitioner Stimulus Grant). The authors received funding from The University of Queensland (University of Queensland Research Scholarship, J.M.G.), the Queensland Government (Smart State PhD Scholarship, J.M.G.), and the National Health and Medical Research Council (Research Fellowship 1105038, R.N.B.).

Clinical Trial Registration: Australian New Zealand Clinical Trials Registry; Trial Registration Number: ACTRN12613000280707; Web address of trial: <http://www.ANZCTR.org.au/ACTRN12613000280707.aspx>.

Please address correspondence to Joanne M. George, Queensland Cerebral Palsy and Rehabilitation Research Centre, Centre for Children's Health Research, The University of Queensland, Level 6, 62 Graham St, South Brisbane, Queensland, 4101, Australia; e-mail: j.george2@uq.edu.au

Indicates open access to non-subscribers at www.ajnr.org

Indicates article with supplemental on-line tables.

Indicates article with supplemental on-line photos.

<http://dx.doi.org/10.3174/ajnr.A5191>

ing WM abnormality was associated with poorer motor and cognitive outcomes.^{1,2,5,7,14-16}

Scoring systems of MR imaging at TEA were further developed to include quantitative biometrics to measure the impact of secondary brain maturation and growth following preterm brain injury.¹⁷ These brain metrics correlated with brain volumes and differentiated preterm and term-born infants at TEA MR imaging.¹⁷ At TEA, transcerebellar diameter was associated with fidgety general movements at 3-month corrected age (CA),¹⁸ poorer cognitive outcomes at 12-month CA,¹⁹ and poorer motor and cognitive outcomes at 2-year CA.²⁰ Reduced deep gray matter area at TEA was associated with poorer motor and cognitive outcomes,¹⁹ and an increased interhemispheric distance independently predicted poorer cognitive development at 2-year CA.³ Reduced biparietal width at TEA predicted both motor and cognitive outcomes at 2-year CA in infants born very preterm.^{3,21}

Term-equivalent age MR imaging scoring systems have been further developed to include evaluation of deep gray matter (DGM) structures and the cerebellum.²² At TEA, global brain abnormality scores were significantly associated with motor outcomes at 2-years CA²³; and cognitive outcomes, at 7 years.^{24,25} Deep gray matter scores were significantly associated with poorer attention and processing speeds, memory, and learning.^{24,25}

With safe earlier MR imaging now possible with MR compatible incubators, valid scoring systems for use earlier than TEA are required. The aim of this study was to validate an MR imaging scoring system previously developed for very preterm infants at TEA in a cohort of infants born <31-weeks gestational age with MR imaging between 29 and 35 weeks' postmenstrual age (PMA).²² The study aimed to establish predictive validity for motor and cognitive outcomes at 12-months CA. Secondary aims were to examine inter- and intrarater reproducibility and to examine relationships between global brain abnormality categories and known perinatal risk factors. It was hypothesized that the scoring system would be valid and reliable for use at this earlier time point but with more infants classified with brain abnormalities, due to immaturity rather than injury.

MATERIALS AND METHODS

Study Design and Participants

This prospective cohort study of infants born at <31-weeks gestational age was conducted at the Royal Brisbane and Women's Hospital, Brisbane, Australia, between February 2013 and April 2015. Preterm infants were eligible if they had no congenital abnormality, and their parents/caregivers were English-speaking who lived within a 200-km radius of the hospital.²⁶ A reference sample of healthy term-born infants was simultaneously recruited to generate reference values and cut-points for the regional brain measurements that form part of the scoring system. Inclusion criteria for term-born infants were a gestational age at birth of 38–41 weeks; birthweight above the 10th percentile; an uncomplicated pregnancy, delivery, and postpartum period; and normal neurologic examination findings.²⁶ Ethics approval was obtained from the Royal Brisbane and Women's Hospital Human Research Ethics Committee (HREC/12/QRBW/245) and The University of Queensland (2012001060), and the trial was

registered with the Australian New Zealand Clinical Trials Registry (ACTRN12613000280707).

MR Imaging Acquisition

Brain MR imaging was performed during sleep without sedation between 30 and 32 weeks PMA or when the infant was medically stable (range, 29 to 35 weeks PMA, early MR imaging) and again at TEA (40 to 42 weeks PMA, term MR imaging). Infants were scanned by using a 3T MR imaging scanner, Tim Trio (Siemens Erlangen, Germany), using an MR compatible incubator with its dedicated neonatal head coil (Nomag incubator; LMT Lammers Medical Technology, Lübeck, Germany). Coronal, axial, and sagittal T2-weighted HASTE (TR/TE, 2000/90 ms; flip angle, 150°; FOV, 200 × 160 mm; matrix, 320 × 256; section thickness, 4 mm), axial T1 TSE (TR/TE, 1490/90 ms; flip angle, 150°; FOV, 200 × 160 mm; matrix, 256 × 180; section thickness, 2 mm), and axial multiecho T2 TSE images (TR/TE1/TE2/TE3, 10,580/27/122/189 ms; flip angle, 150°; FOV, 144 × 180 mm; matrix, 204 × 256; section thickness, 2 mm) were acquired.

MR Imaging Scoring

A standardized MR imaging scoring system according to Kidokoro et al²² was used to score all MRIs. An independent neurologist with training in radiology and experienced in neonatal MR imaging scoring (S.F.) performed the scoring. The scorer had no knowledge of any clinical characteristics of the infants except PMA at the time of scanning. Scoring was confirmed by a senior neuroradiologist (A.C.). Modifications to scoring cut-points were made by using the term reference data means and SDs.^{27,28} Scoring items and parameters are detailed in On-line Table 1, a scoring proforma is included in On-line Table 2, and On-line Figs 1–18 provide examples of lesion types and regional measurements.

Cerebral WM abnormality was rated on 6 components, with a maximum total score of 15: cystic degeneration, focal signal abnormalities, delayed myelination, thinning of the corpus callosum, dilated lateral ventricles, and reduction of WM volume.²² Myelination of the corpus callosum and posterior limb of the internal capsule was expected by 36-week PMA, so all infants were given a score of 2 for this item on early MR imaging. The CGM was rated on 3 components with a maximum total score of 8: signal abnormality, delayed gyration, and dilated extracerebral CSF space. Cerebellar and DGM abnormalities were rated on signal abnormality and volume reduction with maximum total scores of 6 for each.²² A total of WM, CGM, DGM, and cerebellar scores yielded a global brain abnormality score (0–35).²² Each of the WM, CGM, DGM, cerebellar, and global scores could be further categorized into no, mild, moderate, or severe brain abnormality categories.²² The WM total scores were categorized as none (0–2), mild (3–4), moderate (5–6), or severe (≥7) WM abnormalities. Cortical GM, DGM, and cerebellar categories used the following total scores: none (0), mild (1), moderate (2), and severe (≥3). Total global scores were classified as normal (0–3), mild (4–7), moderate (8–11), or severe (≥12) brain abnormalities.

Six regional measurements form part of the scoring: thickness of the corpus callosum (genu, body, and splenium), ventricular diameter, biparietal width, interhemispheric distance, DGM area,

and transcerebellar diameter. These measurements change with PMA at the time of MR imaging as a result of head and brain growth. To address this change and minimize the risk of confounding, we examined the relationship of each of these measures with PMA at MR imaging to derive a correction method for PMA at MR imaging. The PMA was determined on the basis of the obstetric estimate measure of gestation at delivery.²⁹ In the preterm group, early and term MR imaging data were pooled for each of the regional measures, and cases with focal brain lesions were removed to ensure that any linear relationship found was the result of age and not confounded by brain injury. For each measure that demonstrated a linear relationship with PMA at MR imaging, the regression coefficient (slope) was used to generate an equation for correction, written as: Corrected Value = Measured Value + Regression Coefficient \times (40-PMA at MR Imaging). The correction was then applied to the full cohort. On-line Figs 8–10 and 15 provide instructions for conducting regional measurements, correcting the raw values, and scoring.

The regional measurements were also obtained for the term reference sample, and examination of the relationship with PMA at MR imaging was performed separately from that of the preterm group. When linear relationships were found, measurements were corrected as per the equation above. Following correction of the term reference sample regional scores, means and SDs were calculated, and these were used to create cut-points for scoring each of the respective regional measurements.

Interrater reproducibility of MR imaging scoring was tested on a separate sample with 20 MR scans from each time point scored by a second blinded rater, a pediatric radiologist (J.B.). Intrarater reproducibility was tested with 20 MR scans from each time point rescored 1 month apart (S.F.).

Neurodevelopmental Outcome at 12-Months CA

All infants underwent neurodevelopmental assessment at 12-months CA by an experienced physiotherapist blinded to MR imaging findings and medical history. The Bayley Scales of Infant and Toddler Development, 3rd ed. (Bayley III), was performed, and composite scores for motor and cognitive performance were generated.³⁰ The Neuro-Sensory Motor Developmental Assessment (NSMDA) evaluates neurologic and sensory motor function in addition to gross and fine motor performance, with total scores and functional classifications used.^{31,32} The NSMDA at 12-months CA has good predictive validity for motor and cognitive outcomes and cerebral palsy at 4-years CA for very preterm infants^{33,34} and 24-month motor and functional outcomes for infants with cerebral palsy.³⁵

Statistical Analysis

Sample size calculations were based on qualitative evaluation of MR images at TEA predicting 12-month outcomes,⁴ with 69 infants required to reject the null hypothesis with 90% power (at $P < .05$). A sample of 80 infants was recruited to account for attrition and the earlier PMA at MR imaging (29 to 35 weeks PMA).

The association between each of the 6 regional measurements and PMA at MR imaging was analyzed by using mixed-effects regression models for the preterm sample data and separately for the term reference sample data with linear regression. When a

linear relationship was found, data were centered around the mean and the relationship was examined to determine whether it was quadratic. Correction equations were then applied to the raw regional measures. Term reference sample mean and SD data were used to generate scoring cut-points for each of the regional measures. Paired t tests were used to determine statistically significant differences between early and term MR imaging item scores in the preterm group.

The association between early MR imaging scores and 12-month outcomes and term MR imaging scores and 12-month outcomes was evaluated with univariable and multivariable linear regression. Multivariable regression included potential confounders of sex, social risk, and, for the NSMDA only, CA at assessment.

To examine the predictive validity of both early and term MR imaging, we calculated sensitivity, specificity, and accuracy (percentage of cases correctly classified). Dichotomized MR imaging and outcome data were used to construct 2×2 tables. MR imaging category scores were dichotomized into normal/mild or moderate/severe categories for each of the subscales and global scores. Bayley motor and cognitive composite scores were dichotomized (by < -1 SD) and the NSMDA functional classification scores, as normal/minimal versus mild/moderate/severe/profound.

Inter- and intrarater reliability was evaluated by using intraclass correlation coefficients (ICCs) (type 3, 1). Agreement was evaluated by using the percentage level of accuracy, in which the definition for accuracy was exact score ± 1 for the subscale scores and exact score ± 2 for the global scores.

When we investigated perinatal risk factors, differences across global brain abnormality score categories were determined by using Mann-Whitney U tests (dichotomous perinatal risk factors) and Kruskal Wallis 1-way ANOVAs (continuous perinatal risk factors). Analysis was performed by using the STATA statistical package, Version 14 (StataCorp, College Station, Texas).

RESULTS

Participants

Of 214 eligible preterm infants, parents or guardians of 110 consented to the study, of whom 83 had early MR imaging and 12-month outcomes available and were included in this analysis (16 with no early MR imaging: 5 medically unstable, 1 death, 4 cancellations due to MR imaging equipment failure, 3 with no MR imaging slots, 1 withdrawn, 2 with movement artefacts; 11 failed to return for 12-month follow-up). Of these, 77/83 had a second MR scan at term. Thirty-eight term-born infants were included in the reference sample. Demographic data and MR imaging scores are summarized in Tables 1–3; 12-month outcomes are summarized in Table 4. There were minimal differences between those participants with both early and term MR imaging and those with only early MR imaging, except that all 6 participants who did not undergo their term MR imaging were classified with a higher social risk.^{36,37} Given the established relationship between higher social risk and poorer neurodevelopmental outcome and an increased risk of cerebral palsy and to address this difference in our cohort between early and term MR imaging, all multivariable analyses included social risk as a potential confounder.^{38,39} All term reference sample infants had a normal global brain abnormality category score.

Table 1: Characteristics of preterm samples and term reference sample^a

| Birth and Maternal Data | Full Preterm Sample with Early MRI (n = 83) | Preterm Sample with Additional Term MRI (n = 77) | Term Reference Sample (n = 38) |
|--------------------------------|--|--|---|
| Gestational age at birth (wk) | 28 ⁺⁴ [26 ⁺⁶ –29 ⁺³], 23 ⁺⁶ –30 ⁺⁶ | 28 ⁺⁵ [26 ⁺⁶ –29 ⁺³], 23 ⁺⁶ –30 ⁺⁶ | 39 ⁺⁶ [39–40 ⁺³], 38 ⁺² –41 ⁺³ |
| Birth weight (g) | 1068 (312), 494–1886 | 1076 (322), 494–1886 | 3509 (317), 2932–4330 |
| Birth head circumference (cm) | 25.62 (2.38), 20.5–30.5, n = 80 | 25.64 (2.43), 20.5–30.5, n = 75 | 34.71 (1.12), 32.5–37, n = 31 |
| Males | 49 (59%) | 46 (60%) | 19 (50%) |
| Multiple births | 24 (29%) | 21 (27%) | 0 (0%) |
| Premature rupture of membranes | 19 (23%) | 18 (23%) | 4 (12%) n = 33 |
| Cesarean delivery | 60 (72%) | 56 (73%) | 9 (27%) n = 33 |
| Chorioamnionitis | 14 (17%) | 13 (17%) | |
| Antenatal steroids | 62 (75%) | 57 (74%) | |
| Magnesium sulphate | 43 (65%), n = 66 | 41 (65%), n = 63 | |
| Higher social risk | 40 (48%) | 34 (44%) | 5 (16%) n = 31 |

Note:—IQR indicates interquartile range.

^a Early MRI, 29 to 35 weeks PMA; term MRI, 40 to 42 weeks PMA. Data are No. (%), median [IQR] or mean (SD), range.

Table 2: Characteristics of preterm samples and term reference sample^a

| Acquired Medical Factors | From Birth to Early MRI (n = 83) | From Birth to Term MRI (n = 77) | Term Reference Sample (n = 38) |
|--|---|---|--|
| Patent ductus arteriosus | 39 (47%) | 36 (47%) | |
| IVH | 17 (20%) | 16 (21%) | |
| IVH grade 3 or 4 | 4 (5%) | 4 (5%) | |
| Periventricular leukomalacia | 2 (2%) | 2 (3%) | |
| Hydrocephalus | 2 (2%) | 2 (3%) | |
| NEC diagnosed or suspected | 3 (4%) | 2 (3%) | |
| Confirmed sepsis | 3 (4%) | 2 (3%) | |
| Total parenteral nutrition (days) | 11 [8–14], 0–30 | 11 [8–14], 0–30 | |
| Postnatal corticosteroids | 14 (17%) | 14 (18%) | |
| Ventilation (days) | 3 [0–12], 0–48 | 2 [0–12], 0–48 | |
| CPAP (days) | 15 [7–25], 0–47 | 30 [7–47], 0–81 | |
| Oxygen therapy (hr) | 12 [1–125], 0–1515, n = 69 | 29 [2–370], 0–3912, n = 67 | |
| 36-week PMA O ₂ requirement | | 23 (30%) | |
| PMA at MRI (wk) | 32 ⁺² (1 ⁺³), 29 ⁺³ –35 ⁺² | 40 ⁺⁶ (1 ⁺³), 38 ⁺³ –46 ⁺⁴ | 41 ⁺³ (1), 39 ⁺² –44 |
| Weight at MRI (g) | 1500 (352), 883–2715 | Early MRI 1505 (359), 883–2715 Term MRI 3127 (627), 1900–5150 | 3428 (378), 2500–4200, n = 31 |

Note:—IVH indicates intraventricular hemorrhage; NEC, necrotizing enterocolitis; CPAP, continuous positive airway pressure.

^a Data are No. (%), median [IQR] or mean (SD), range. Early MRI, 29 to 35 weeks PMA; term MRI, 40 to 42 weeks PMA.

Table 3: Characteristics of preterm sample and term reference sample^a

| MRI Scores | Early MRI | Term MRI | Term Reference Sample |
|----------------------|-----------|----------|-----------------------|
| White matter | 3 [2–4] | 1 [1–3] | 0 [0–0] |
| Cortical gray matter | 0 [0–1] | 0 [0–1] | 0 [0–0] |
| Deep gray matter | 0 [0–1] | 0 [0–1] | 0 [0–0] |
| Cerebellum | 0 [0–0] | 0 [0–1] | 0 [0–0] |
| Global score | 4 [3–7] | 3 [1–5] | 0 [0–0] |

^a Early MRI, 29 to 35 weeks PMA; term MRI, 40 to 42 weeks PMA. Data are median [IQR].

Table 4: Bayley III and NSMDA scores at 12-month corrected age (n = 83)

| Assessment | Scores |
|--|---------------------------------------|
| 12-mo outcomes (mean) (SD) | |
| Age at assessment | 12 months 4 days (1 ⁺² wk) |
| Bayley III motor composite | 96.96 (14.27) |
| Bayley III cognitive composite | 104.64 (12.07) |
| NSMDA total | 179.53 (18.81) |
| 12-mo outcomes dichotomized (No.) (%) | |
| Bayley III motor composite < –1 SD | 15 (18%) |
| Bayley III cognitive composite < –1 SD | 6 (7%) |
| NSMDA functional classification ≥2 | 7 (8%) |

Associations between Regional Brain Measurements and PMA at MR Imaging

All preterm regional measures except the body of the corpus callosum demonstrated linear relationships with PMA at MR imaging

($P < .01$). In the term reference sample, linear relationships were found only for transcerebellar diameter and the genu of the corpus callosum. Results of regression analyses and corrected regional measures for the early, term, and term reference sample MRIs are presented in On-line Tables 3 and 4.

Findings in Each Scoring Domain at Early and Term MR Imaging

Results for scoring items are presented in On-line Table 1. The incidence of WM cystic lesions, CGM signal abnormality, and WM volume reduction as measured by corrected biparietal width remained stable between early and term MR imaging. A proportion of signal abnormalities in the WM and DGM resolved between early and term MR imaging. A propensity to score worse at term compared with early MR imaging was evidenced for each of the following: ventricular dilation, interhemispheric distance, volume reduction of the DGM and cerebellum, and thinning of the corpus callosum. More infants had delayed gyral maturation at early MR imaging compared with term MR imaging.

Predictive Validity of Early MR Imaging

Results of univariable and multivariable regression analyses between early MR imaging scores and neurodevelopmental outcomes are presented in Fig 1 (first row); sensitivity, specificity, and accuracy, in Table 5. Global, WM, and DGM scores on early

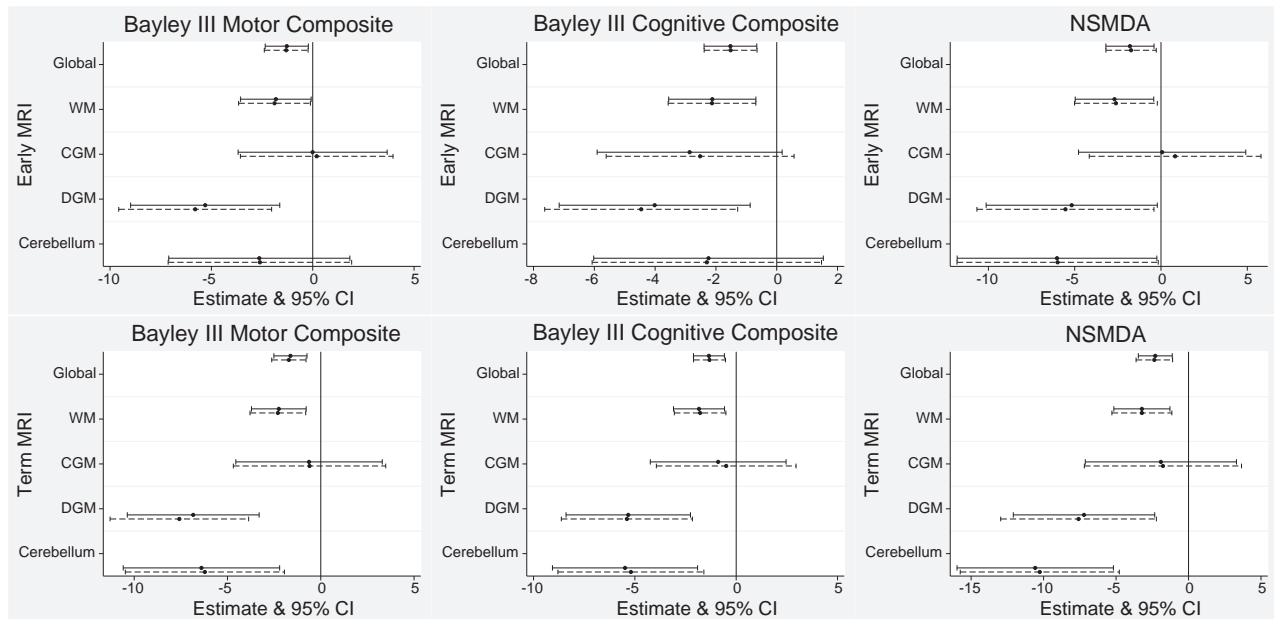


FIG 1. Associations between early (first row) and term (second row) MR imaging scores and neurodevelopmental outcome at 12-months corrected age for the preterm cohort. *Solid lines* represent univariable regression analyses, and *dashed lines* represent multivariable analyses for which sex, social risk and, for NSMDA only, corrected age at assessment were added.

Table 5: Sensitivity, specificity, and accuracy of early and term MRI scores categorized as moderate/severe to predict an outcome of < -1 SD on the Bayley III or NSMDA functional classification of mild-profound dysfunction^a

| | 12-Month Neurodevelopmental Outcome | | | | | | | | |
|--------------------|-------------------------------------|-------------|----------------------|--------------------------------------|-------------|----------------------|-------------|-------------|----------------------|
| | Bayley III Motor Composite Score | | | Bayley III Cognitive Composite Score | | | NSMDA | | |
| | Sensitivity | Specificity | Correctly Classified | Sensitivity | Specificity | Correctly Classified | Sensitivity | Specificity | Correctly Classified |
| Early MRI (n = 83) | | | | | | | | | |
| WM | 33 (12–62) | 78 (66–87) | 70 | 50 (12–88) | 78 (67–87) | 76 | 43 (10–82) | 78 (67–86) | 75 |
| CGM | 0 (0–22) | 81 (70–89) | 66 | 0 (0–46) | 83 (73–91) | 77 | 0 (0–41) | 83 (73–91) | 76 |
| DGM | 40 (16–68) | 94 (86–98) | 84 | 33 (4–78) | 90 (81–95) | 86 | 43 (10–82) | 91 (82–96) | 87 |
| Cerebellum | 13 (2–40) | 93 (84–98) | 78 | 17 (1–64) | 92 (84–97) | 87 | 29 (4–71) | 93 (85–98) | 88 |
| Global score | 33 (12–62) | 87 (76–94) | 77 | 50 (12–88) | 86 (76–93) | 83 | 43 (10–82) | 86 (76–93) | 82 |
| Term MRI (n = 77) | | | | | | | | | |
| WM | 14 (2–43) | 92 (82–97) | 78 | 33 (4–78) | 93 (84–98) | 88 | 29 (4–71) | 93 (84–98) | 87 |
| CGM | 21 (5–51) | 79 (67–89) | 69 | 0 (0–46) | 77 (66–87) | 71 | 29 (4–71) | 80 (69–89) | 75 |
| DGM | 36 (13–65) | 86 (75–93) | 77 | 33 (4–78) | 83 (72–91) | 79 | 71 (29–96) | 87 (77–94) | 86 |
| Cerebellum | 21 (5–51) | 92 (82–97) | 79 | 33 (4–78) | 92 (83–97) | 87 | 43 (10–82) | 93 (84–98) | 88 |
| Global score | 14 (2–43) | 90 (80–96) | 77 | 33 (4–78) | 92 (83–97) | 87 | 29 (4–71) | 91 (82–97) | 86 |

^a Sensitivity and specificity are percentage (95% CI); "Correctly Classified" is percentage; early MRI, 29 to 35 weeks PMA; term MRI, 40 to 42 weeks PMA.

MR imaging were associated with Bayley III motor outcome multivariably (global score: $\beta = -1.31$; 95% CI, -2.39 to -0.23 ; $P = .02$). Early MR imaging WM, DGM, and global scores were associated with Bayley III cognitive outcome (global $\beta = -1.52$; 95% CI, -2.39 to -0.65 ; $P < .01$). Early MR imaging WM, DGM, cerebellar, and global scores were associated with outcome on the NSMDA (global $\beta = -1.73$; 95% CI, -3.19 to -0.28 ; $P = .02$). The sensitivity of early MR imaging global scores to predict motor, cognitive, and NSMDA outcomes ranged from 33% to 50%, specificity ranged from 86% to 87%, with the percentage of accurately classified cases ranging from 77% to 83%.

Predictive Validity of Term MR Imaging

Univariable and multivariable regression analyses between term MR imaging scores and neurodevelopmental outcomes are presented in Fig 1 (second row). Sensitivity, specificity, and accuracy

are presented in Table 5. At term MR imaging, WM, DGM, cerebellar, and global scores were associated with Bayley III motor and cognitive and NSMDA scores. Global scores were associated with Bayley III motor outcome ($\beta = -1.71$; 95% CI, -2.63 to -0.79 ; $P < .01$), cognitive outcome ($\beta = -1.32$; 95% CI, -2.10 to -0.53 ; $P < .01$), and NSMDA ($\beta = -2.36$; 95% CI, -3.62 to -1.10 ; $P < .01$). The sensitivity of term MR imaging global scores to predict motor, cognitive, and NSMDA outcomes ranged from 14% to 33%, specificity ranged from 90% to 92%, with the percentage of accurately classified cases ranging from 77% to 87%.

Inter- and Intrarater Reproducibility

Reliability and agreement results are presented in On-line Table 5. At Early MR imaging, intrarater reliability ranged from 0.82 to 0.97 (ICC), and agreement, from 90% to 100%. Interrater reliability was low for CGM (ICC = 0.08) but excellent for the other

subscales (ICC = 0.76–0.86) and the global total (ICC = 0.89). Interrater agreement ranged from 70% to 95%. At term MR imaging, intrarater reliability ICCs ranged from 0.74 to 0.96, with a global score ICC of 0.97. Intrarater agreement ranged from 90% to 100%. Interrater reliability once again showed lower reliability for CGM (ICC = 0.66); however, the other subscale ICCs ranged from 0.86 to 0.93, and the global score ICC was 0.93. Interrater agreement ranged from 80% to 100%.

Perinatal Risk Factors

Perinatal risk factors were associated with increasing severity of the MR imaging global brain abnormality category scores (Online Table 6). Early MR imaging was associated with gestational age at birth, birth weight, patent ductus arteriosus, retinopathy of prematurity, postnatal corticosteroids, ventilation, and oxygen therapy. Term MR imaging was associated with gestational age at birth, birth weight, higher social risk, retinopathy of prematurity, ventilation, oxygen requirement at 36-weeks PMA, and the requirement for home oxygen.

DISCUSSION

This clinically accessible scoring system of structural brain MR imaging for use at 29 to 35 weeks PMA for infants born at <31-week gestational age is valid. Early MR imaging WM, DGM and global brain abnormality scores were associated with Bayley III motor and cognitive scores and outcome on the NSMDA at 12-months CA. Early cerebellar scores were also associated with the NSMDA outcome. These associations were reconfirmed at term MR imaging. In addition, term MR imaging cerebellar scores were associated with Bayley III motor and cognitive outcomes.

Early MR imaging was more strongly associated with cognitive than motor outcomes. The scoring system on which this study was based has been used in 2 studies examining the relationships between TEA MR imaging and cognitive outcomes at 7 years.^{24,25} Our results support previous findings at TEA and suggest that the brain changes associated with adverse cognitive outcomes are already present as early as 29 to 35 weeks PMA.⁷

Of all MR imaging subscale scores, at early and term MR imaging, DGM demonstrated the strongest relationship with outcome. This finding supports inclusion of DGM evaluation in qualitative and semiquantitative scoring systems in this population. Cerebellar scores on early MR imaging were associated with NSMDA scores but not the Bayley III motor score. This finding is interesting because the Bayley III motor scale focuses on motor achievement, while the NSMDA evaluates the quality of motor performance, including balance and postural reactions, functions known to be modulated by the cerebellum. The NSMDA also includes assessment of muscle tone, reflexes, and sensory motor function, and at 12 months CA, has been shown to predict motor and cognitive outcomes and cerebral palsy at 4 years in preterm infants.^{33,34}

The specificity of the scoring system is reasonable, indicating that those infants whose global scoring category is moderate or severe have a high probability of poor motor and cognitive outcomes at 12-months CA. The sensitivity is relatively low, so not all infants who progress to poor motor and cognitive outcomes will be identified by this scoring system at early or term MR imaging;

however, it also means that the risk of false-positives is low. Parents indicate a desire for prognostication and early identification of outcomes,⁴⁰ and a low false-positive rate is preferable to prolonged distress of a false-positive result causing parents to spend years waiting for an adverse outcome that does not occur.^{41,42} A combination of TEA MR imaging findings and 3-month CA general movement assessment demonstrates improved predictive validity over TEA MR imaging alone,^{43–45} so evaluation of the relationships between this early MR imaging scoring system and concurrent clinical measures and the combination of early MR imaging and clinical measures to predict later outcomes is warranted.

Our results indicate that term MR imaging scores demonstrate stronger associations with 12-month outcomes than early MR imaging scores. Term MR imaging associations described here are stronger than those found by another group using the original scoring system²³; this finding suggests that the modified scoring cut-points, based on term-born reference sample data, may be an improvement over the original scale.²⁷ Their outcome was at 2-years CA rather than 12-months CA in the present study. Stronger associations of term MR imaging with outcomes may be due to small focal lesions evident on early MR imaging having resolved by term MR imaging or volume reduction becoming more apparent. Both of these require further exploration. Term MR imaging scores presented here show a lower incidence of myelination delay compared with the cohort on which the scale was originally based. In the present study, the T1 sequence was performed at the end of the MR imaging when infants were often beginning to wake up; therefore, it had a higher incidence of motion artefacts. For this reason, T2-weighted images were used to score myelination delay with their improved contrast, and this may have resulted in an overestimation of myelination compared with the earlier study.²²

CONCLUSIONS

This study presents a clinically accessible MR imaging scoring system of brain injury and growth for use from 29 to 35 weeks' PMA in infants born at <31-weeks gestational age that has good reproducibility and significant associations with motor and cognitive outcomes at 12-months CA. The tool is suitable for use in research and for assisting clinical patient management.

ACKNOWLEDGMENTS

We acknowledge the families of infants who participated in this study; the staff of the neonatal unit and department of medical imaging; study personnel Dr Melissa Lai, Donna Hovey, Kellie McGrory, Kylie Smart, Christine Finn, and Kym Morris; and Dr Francisco Perales for statistical support.

Disclosures: Joanne M. George—*RELATED: Grant:* University of Queensland Research Scholarship, *Comments:* This is a PhD living stipend (June 2012 to December 2016). I also received a scholarship from the Queensland Government from June 2012 to December 2015 (Smart State PhD Scholarship). I was awarded a Health Practitioners Research Grant (Queensland Government), which provided funds to support the broader PPREMO study; *Support for Travel to Meetings for the Study or Other Purposes:* University of Queensland, *Comments:* support for travel to conferences; *Other:* grants provided to support the PPREMO Study, *Comments:* grants from the Cerebral Palsy Alliance Research Foundation (IRG1413), the Financial Markets Foundation for Children (2014–074), and the Queensland Government (Smart State; Health Practitioner Stimulus Grant) to support this project. The PPREMO study is the

broader project, a prospective cohort study, of which the current work is a part*;
 UNRELATED: Grants/Grants Pending: National Health and Medical Research Council of Australia, Comments: A separate study, PREBO (Preterm Brain Outcomes), has been awarded funding to progress work started by the PPREMO project. A number of participants in the present study have also consented to the PREBO study, which involves follow-up at later ages. I am listed as an associate investigator on that grant.*
 Jurgen Fripp—RELATED: Grant: National Health and Medical Research Council, Comments: The Commonwealth Scientific and Industrial Research Organisation received some funds to perform image analysis from the research grant.*
 Jane Bursle—UNRELATED: Employment: Royal Brisbane and Women's Hospital. Stephen E. Rose—RELATED: Grant: Cerebral Palsy Alliance Research Foundation (IRG1413).
 Paul B. Colditz—RELATED: Grant: National Health and Medical Research Council Project Grant, Comments: APPI084032*. Roslyn N. Boyd—RELATED: Grant: Financial Markets for Children, Comments: competitive funding for MRIs and Research Nurse.*
 *Money paid to the institution.

REFERENCES

- Woodward LJ, Anderson PJ, Austin NC, et al. Neonatal MRI to predict neurodevelopmental outcomes in preterm infants. *N Engl J Med* 2006;355:685–94 CrossRef Medline
- Woodward LJ, Clark CA, Bora S, et al. Neonatal white matter abnormalities an important predictor of neurocognitive outcome for very preterm children. *PLoS One* 2012;7:e51879 CrossRef Medline
- Kidokoro H, Anderson PJ, Doyle LW, et al. Brain injury and altered brain growth in preterm infants: predictors and prognosis. *Pediatrics* 2014;134:e444–453 CrossRef Medline
- Spittle AJ, Boyd RN, Inder TE, et al. Predicting motor development in very preterm infants at 12 months' corrected age: the role of qualitative magnetic resonance imaging and general movements assessments. *Pediatrics* 2009;123:512–17 CrossRef Medline
- Spittle AJ, Cheong J, Doyle LW, et al. Neonatal white matter abnormality predicts childhood motor impairment in very preterm children. *Dev Med Child Neurol* 2011;53:1000–06 CrossRef Medline
- Volpe JJ. The encephalopathy of prematurity—brain injury and impaired brain development inextricably intertwined. *Semin Pediatr Neurol* 2009;16:167–78 CrossRef Medline
- Miller SP, Ferriero DM, Leonard C, et al. Early brain injury in premature newborns detected with magnetic resonance imaging is associated with adverse early neurodevelopmental outcome. *J Pediatr* 2005;147:609–16 CrossRef Medline
- Inder TE, Wells SJ, Mogridge NB, et al. Defining the nature of the cerebral abnormalities in the premature infant: a qualitative magnetic resonance imaging study. *J Pediatr* 2003;143:171–79 CrossRef Medline
- Sie LT, Hart AA, van Hof J, et al. Predictive value of neonatal MRI with respect to late MRI findings and clinical outcome: a study in infants with periventricular densities on neonatal ultrasound. *Neuropediatrics* 2005;36:78–89 CrossRef Medline
- Spittle AJ, Brown NC, Doyle LW, et al. Quality of general movements is related to white matter pathology in very preterm infants. *Pediatrics* 2008;121:e1184–1189 CrossRef Medline
- Peyton C, Yang E, Kocherginsky M, et al. Relationship between white matter pathology and performance on the General Movement Assessment and the Test of Infant Motor Performance in very preterm infants. *Early Hum Dev* 2016;95:23–27 CrossRef Medline
- Brown NC, Inder TE, Bear MJ, et al. Neurobehavior at term and white and gray matter abnormalities in very preterm infants. *J Pediatr* 2009;155:32–38, 38.e1 CrossRef Medline
- Pineda RG, Neil J, Dierker D, et al. Alterations in brain structure and neurodevelopmental outcome in preterm infants hospitalized in different neonatal intensive care unit environments. *J Pediatr* 2014;164:52–60.e2 CrossRef Medline
- Iwata S, Nakamura T, Hizume E, et al. Qualitative brain MRI at term and cognitive outcomes at 9 years after very preterm birth. *Pediatrics* 2012;129:e1138–47 CrossRef Medline
- Hintz SR, Barnes PD, Bulas D, et al; SUPPORT Study Group of the Eunice Kennedy Shriver National Institute of Child Health and Human Development Neonatal Research Network. Neuroimaging and neurodevelopmental outcome in extremely preterm infants. *Pediatrics* 2015;135:e32–42 CrossRef Medline
- Skjold B, Vollmer B, Bohm B, et al. Neonatal magnetic resonance imaging and outcome at age 30 months in extremely preterm infants. *J Pediatr* 2012;160:559–66.e551 CrossRef Medline
- Nguyen The Tich S, Anderson PJ, Shimony JS, et al. A novel quantitative simple brain metric using MR imaging for preterm infants. *AJNR Am J Neuroradiol* 2009;30:125–31 Medline
- Spittle AJ, Doyle LW, Anderson PJ, et al. Reduced cerebellar diameter in very preterm infants with abnormal general movements. *Early Hum Dev* 2010;86:1–5 CrossRef Medline
- Melbourne L, Murnick J, Chang T, et al. Regional brain biometrics at term-equivalent age and developmental outcome in extremely low-birth-weight infants. *Am J Perinatol* 2015;32:1177–84 CrossRef Medline
- Park H, Yoon H-K, Han S, et al. Brain MRI measurements at a term-equivalent age and their relationship to neurodevelopmental outcomes. *AJNR Am J Neuroradiol* 2014;35:599–603 CrossRef Medline
- Tich SN, Anderson PJ, Hunt RW, et al. Neurodevelopmental and perinatal correlates of simple brain metrics in very preterm infants. *Arch Pediatr Adolesc Med* 2011;165:216–22 CrossRef Medline
- Kidokoro H, Neil JJ, Inder TE. New MR imaging assessment tool to define brain abnormalities in very preterm infants at term. *AJNR Am J Neuroradiol* 2013;34:2208–14 CrossRef Medline
- Brouwer MJ, van Kooij BJ, van Haastert IC, et al. Sequential cranial ultrasound and cerebellar diffusion weighted imaging contribute to the early prognosis of neurodevelopmental outcome in preterm infants. *PLoS One* 2014;9:e109556 CrossRef Medline
- Murray AL, Scratch SE, Thompson DK, et al. Neonatal brain pathology predicts adverse attention and processing speed outcomes in very preterm and/or very low birth weight children. *Neuropsychology* 2014;28:552–62 CrossRef Medline
- Omizzolo C, Scratch SE, Stargatt R, et al. Neonatal brain abnormalities and memory and learning outcomes at 7 years in children born very preterm. *Memory* 2014;22:605–15 CrossRef Medline
- George JM, Boyd RN, Colditz PB, et al. PPREMO: a prospective cohort study of preterm infant brain structure and function to predict neurodevelopmental outcome. *BMC Pediatr* 2015;15:123 CrossRef Medline
- Walsh JM, Doyle LW, Anderson PJ, et al. Moderate and late preterm birth: effect on brain size and maturation at term-equivalent age. *Radiology* 2014;273:232–40 CrossRef Medline
- Olsen JE, Brown NC, Eeles AL, et al. Early general movements and brain magnetic resonance imaging at term-equivalent age in infants born <30 weeks' gestation. *Early Hum Dev* 2016;101:63–68 CrossRef Medline
- Martin JA, Osterman MJ, Kirmeyer SE, et al. Measuring gestational age in vital statistics data: transitioning to the obstetric estimate. *Natl Vital Stat Rep* 2015;64:1–20 Medline
- Bayley N. *Bayley Scales of Infant and Toddler Development*. 3rd ed. San Antonio: Harcourt Assessment; 2006
- Burns YR, Ensby RM, Norrie MA. The Neuro-Sensory Motor Developmental Assessment, Part I: development and administration of the test. *Aust J Physiother* 1989;35:141–49 CrossRef Medline
- Burns YR, Ensby RM, Norrie MA. The Neuro Sensory Motor Developmental Assessment, Part II: predictive and concurrent validity. *Aust J Physiother* 1989;35:151–57 CrossRef Medline
- Burns Y, O'Callaghan M, McDonnell B, et al. Movement and motor development in ELBW infants at 1 year is related to cognitive and motor abilities at 4 years. *Early Hum Dev* 2004;80:19–29 CrossRef Medline
- Spittle AJ, Lee KJ, Spencer-Smith M, et al. Accuracy of two motor assessments during the first year of life in preterm infants for predicting motor outcome at preschool age. *PLoS One* 2015;10:e0125854 CrossRef Medline
- MacDonald J, Burns Y. Performance on the NSMDA during the first

- and second year of life to predict functional ability at the age of 4 in children with cerebral palsy. *Hong Kong Physiotherapy J* 2005;23:40–45 [CrossRef](#)
36. Hack M, Breslau N, Aram D, et al. The effect of very low birth weight and social risk on neurocognitive abilities at school age. *J Dev Behav Pediatr* 1992;13:412–20 [Medline](#)
 37. Roberts G, Howard K, Spittle AJ, et al. Rates of early intervention services in very preterm children with developmental disabilities at age 2 years. *J Paediatr Child Health* 2008;44:276–80 [CrossRef Medline](#)
 38. Treyvaud K, Ure A, Doyle LW, et al. Psychiatric outcomes at age seven for very preterm children: rates and predictors. *J Child Psychol Psychiatry* 2013;54:772–79 [CrossRef Medline](#)
 39. Solaski M, Majnemer A, Oskoui M. Contribution of socio-economic status on the prevalence of cerebral palsy: a systematic search and review. *Dev Med Child Neurol* 2014;56:1043–51 [CrossRef Medline](#)
 40. Ward K. Perceived needs of parents of critically ill infants in a neonatal intensive care unit (NICU). *Pediatr Nurs* 2001;27:281–86 [Medline](#)
 41. Pearce R, Baardsnes J. Term MRI for small preterm babies: do parents really want to know and why has nobody asked them? *Acta Paediatr* 2012;101:1013–15 [CrossRef Medline](#)
 42. Janvier A, Barrington K. Trying to predict the future of ex-preterm infants: who benefits from a brain MRI at term? *Acta Paediatr* 2012;101:1016–17 [CrossRef Medline](#)
 43. Skiöld B1, Eriksson C, Eliasson AC, et al. General movements and magnetic resonance imaging in the prediction of neuromotor outcome in children born extremely preterm. *Early Hum Dev* 2013;89:467–72 [CrossRef Medline](#)
 44. Bosanquet M, Copeland L, Ware R, et al. A systematic review of tests to predict cerebral palsy in young children. *Dev Med Child Neurol* 2013;55:418–26 [CrossRef Medline](#)
 45. Setänen S, Lahti K, Lehtonen L, et al. Neurological examination combined with brain MRI or cranial US improves prediction of neurological outcome in preterm infants. *Early Hum Dev* 2014;90:851–56 [CrossRef Medline](#)

Apparent Diffusion Coefficient Value Changes and Clinical Correlation in 90 Cases of Cytomegalovirus-Infected Fetuses with Unremarkable Fetal MRI Results

 D. Kotovich,  J.S.B. Guedalia,  C. Hoffmann,  G. Sze,  A. Eisenkraft, and  G. Yaniv



ABSTRACT

BACKGROUND AND PURPOSE: Cytomegalovirus is the leading intrauterine infection. Fetal MR imaging is an accepted tool for fetal brain evaluation, yet it still lacks the ability to accurately predict the extent of the neurodevelopmental impairment, especially in fetal MR imaging scans with unremarkable findings. Our hypothesis was that intrauterine cytomegalovirus infection causes diffusional changes in fetal brains and that those changes may correlate with the severity of neurodevelopmental deficiencies.

MATERIALS AND METHODS: A retrospective analysis was performed on 90 fetal MR imaging scans of cytomegalovirus-infected fetuses with unremarkable results and compared with a matched gestational age control group of 68 fetal head MR imaging scans. ADC values were measured and averaged in the frontal, parietal, occipital, and temporal lobes; basal ganglia; thalamus; and pons. For neurocognitive assessment, the Vineland Adaptive Behavior Scales, Second Edition (VABS-II) was used on 58 children in the cytomegalovirus-infected group.

RESULTS: ADC values were reduced for the cytomegalovirus-infected fetuses in most brain areas studied. The VABS-II showed no trend for the major domains or the composite score of the VABS-II for the cytomegalovirus-infected children compared with the healthy population distribution. Some subdomains showed an association between ADC values and VABS-II scores.

CONCLUSIONS: Cytomegalovirus infection causes diffuse reduction in ADC values in the fetal brain even in unremarkable fetal MR imaging scans. Cytomegalovirus-infected children with unremarkable fetal MR imaging scans do not deviate from the healthy population in the VABS-II neurocognitive assessment. ADC values were not correlated with VABS-II scores. However, the lack of clinical findings, as seen in most cytomegalovirus-infected fetuses, does not eliminate the possibility of future neurodevelopmental pathology.

ABBREVIATIONS: CMV = cytomegalovirus; feMRI = fetal head MR imaging; VABS-II = Vineland Adaptive Behavior Scales, Second Edition

Cytomegalovirus (CMV) infection is the most common intrauterine infection, with an overall birth prevalence of 1% (range, 0.2%–2.5%).^{1,2} Only 10%–15% of the infected fetuses are symptomatic at birth, presenting with typical clinical findings of congenital infection,^{3,4} while an additional 10%–15% of infants develop the symptoms during the first years of life.^{1,2,5,6} The

clinical findings include, but are not limited to, intrauterine growth restriction, periventricular calcifications, microcephaly, ventriculomegaly, hepatosplenomegaly, and cardiovascular system anomalies.^{3,4,7}

Most symptomatic infants will have long-term sequelae, including neurodevelopmental damage with intellectual disabilities, ranging up to severe decreases in cognitive capacity.^{2,4,5,8,9} Asymptomatic neonates constitute most cases, up to 90% of the infected fetuses, with outcomes still unclear due to limited research.^{1,5,6,8,9}

Sonography is a widely used prenatal screening tool and can show typical findings suggestive of CMV infection. Recent studies have shown that sonography is not sensitive enough for the entire spectrum of neuropathologies, mainly brain maturation.^{10,11} Fetal head MR imaging (feMRI) is accepted as a complementary test for the evaluation of the brain. Studies have shown that feMRI produces much more information, including improved spatial resolution, visualization of the entire brain parenchyma, and detection of white matter maturation and pathologies earlier and better than sonogra-

Received December 14, 2016; accepted after revision March 6, 2017.

From The Faculty of Medicine (D.K., A.E.), Institute for Research in Military Medicine, The Hebrew University of Jerusalem, Jerusalem, Israel; The Israel Defense Forces Medical Corps (D.K., A.E.), Chevy Chase, Maryland; Neuropsychology Unit (J.S.B.G., G.Y.), Shaare Zedek Medical Center, Jerusalem, Israel; Department of Diagnostic Imaging (C.H.) and Dr. Pinchas Bornstein Talpiot Medical Leadership Program (G.Y.), Sheba Medical Center, Tel HaShomer, Ramat Gan, Israel; and Department of Radiology and Biomedical Imaging (G.S., G.Y.), Yale School of Medicine, New Haven, Connecticut.

Please address correspondence to Gal Yaniv, MD, PhD, 154 Willard St, New Haven, CT 06515; e-mail: Gal.yaniv@yale.edu



Indicates article with supplemental on-line tables.



Indicates article with supplemental on-line photos.

<http://dx.doi.org/10.3174/ajnr.A5222>

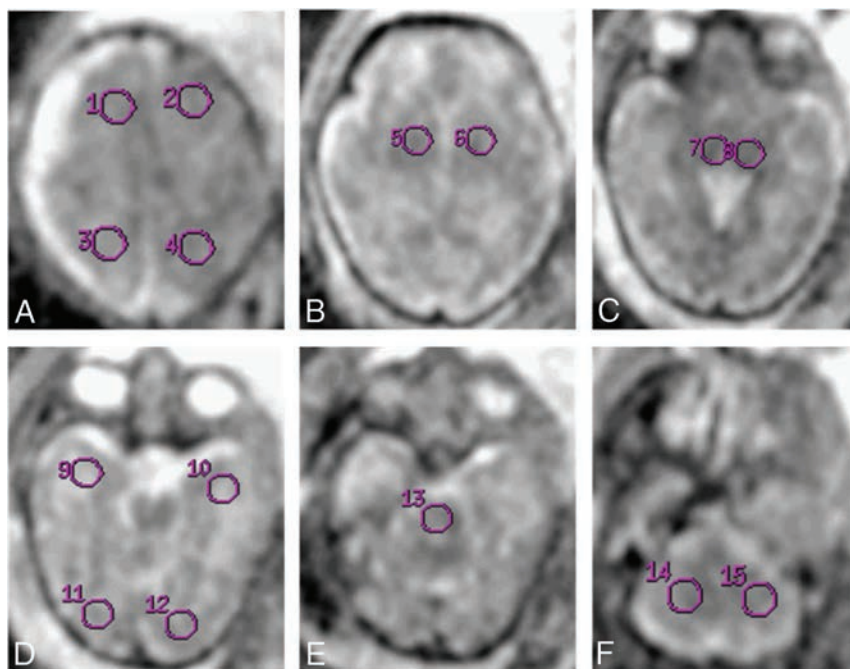


FIG 1. ROI analyzed for apparent diffusion coefficient. ROI placement example. A, 1, 2 = frontal lobe; 3, 4 = parietal lobe. B, 5, 6 = basal ganglia. C, 7, 8 = thalami. D, 9, 10 = temporal lobe; 11, 12 = occipital lobe. E, 13 = pons. F, 14, 15 = cerebellum.

phy.¹⁰⁻¹³ However, even with both techniques combined, it is still unclear how to accurately predict the extent of the neurodevelopmental impairment in the prenatal period, especially in cases without any notable imaging pathology.^{10,11,13,14}

Diffusion-weighted imaging (DWI, DTI) was studied extensively for its utility in the evaluation of the normal development of the fetal brain.¹⁵⁻²⁰ One of the DWI metrics, the apparent diffusion coefficient, allows quantitative evaluation of cerebral maturation and intracellular changes in utero.^{15,18-22} Very little research has been done examining the ADC values in CMV-infected fetal brains, and even less research has focused on fetuses with normal fMRI results.^{14,18}

In our current study, we compared ADC values in several anatomic brain areas of CMV-infected fetuses with unremarkable fMRI results and an age-matched control group with normal MR imaging findings. For neurodevelopmental assessment, the Vineland Adaptive Behavior Scales, Second Edition (VABS-II)^{23,24} was performed on children from the CMV-infected group.

Our hypothesis was that CMV-infection causes diffusional changes in fetal brains and that those changes may be correlated to the severity of neurodevelopmental deficiencies.

MATERIALS AND METHODS

This retrospective study was approved by the institutional review board of Tel HaSomer Hospital.

Subjects and Procedures

A retrospective analysis was performed on 90 sequential fMRI scans of 83 polymerase chain reaction-validated CMV-infected fetuses obtained between 2004 and 2014. Five fetuses had 2 scans, and one fetus had 3 scans. Any fetus with a major abnormality on the fMRI scan was excluded from this study.

The control group included 68 fetuses scanned between 2006 and 2013 who had unremarkable fMRI results, with no clinical or laboratory evidence of chromosomal abnormalities or intra-uterine infection. The indications for the fMRI scan were the following: a sibling with perinatal neurologic findings, previous abnormal pregnancy, prenatal sonography with abnormal findings not confirmed by fMRI, or a suspected CMV infection without confirmation by polymerase chain reaction testing of the amniotic fluid.

MR Imaging

Technical parameters and protocol of the scan are identical to those of our previous published work.²⁵ ROIs were placed as shown in Fig 1. No significant difference between the ADC values of the 2 sides (except for the basal ganglia and the occipital lobe in the CMV group and the temporal lobe in the control group) was shown.

Vineland Adaptive Behavior Scales, Second Edition

The VABS-II test was performed on 58 children from the CMV-infected group whose parents agreed to participate in the study and whom we were able to contact. The questionnaire was performed by telephone with the mother of the child in all the cases, except one with the father alone.

Statistical Methods

To compare ADC values of the CMV and control groups, we applied the *t* test. The χ^2 test was used for the comparison of the observed and expected frequency of each VABS-II adaptive level. The comparison of ADC values with VABS-II adaptive levels was performed by either applying the ANOVA model with the Scheffe procedure for post hoc comparisons or the Kruskal-Wallis nonparametric test. Nonparametric tests were used when the groups compared were small and the distribution of the variables was not normal.

All tests were 2-tailed, and a *P* value of $\leq 5\%$ was considered statistically significant. The statistical analysis was performed with SPSS, Version 21 (IBM, Armonk, New York).

RESULTS

Group Characteristics

The CMV-infected fetuses group consisted of 90 fMRI scans (Table 1) with a mean maternal age of 31.3 ± 4.2 years, while the control group consisted of 68 fetal scans with a mean maternal age of 32.2 ± 4.8 years ($P > .05$).

The mean ROI size was 83.5 ± 4.3 for the control group and 82.6 ± 3.34 for the CMV-infected group ($P > .05$).

All the CMV-infected fetuses had unremarkable fMRI reports (On-line Table 1).

The Vineland Adaptive Behavior Scales test was performed on 58

children (32 males and 26 females) of the 90 patients in the CMV-infected group, with a mean age of 60.1 ± 30.8 months. Eight of the children had hearing disabilities (14%) (Table 1 and On-line Table 1).

Effect of CMV Infection on Regional ADC

CMV infection was accompanied by a highly significant decrease in ADC in all brain regions except in the temporal lobes (Table 2 and On-line Table 2). ADC values were significantly reduced in the frontal ($P = .005$), parietal ($P = .008$), and occipital ($P = .022$) lobes; basal ganglia ($P = .016$); thalamus ($P < .001$); cerebellum ($P = .005$); and pons ($P = .011$). The temporal lobes had no significant decrease, yet they showed a high correlation trend ($P = .057$) (Fig 2 and On-line Table 2).

VABS-II Results

The VABS-II scores are summarized in On-line Table 3 for all the domains, subdomains, and the Adaptive Behavior Composite.

Table 1: Descriptive data of the fetuses included in the study

| | Controls | CMV Group |
|----------------------------|------------------|--------------------|
| No. (feMRI) | 68 | 90 |
| Maternal age (mean) (yr) | 32.05 ± 4.43 | 31.58 ± 4.23 |
| GA (MRI) (mean) | 31.8 ± 2.3 | 33.1 ± 2.0 |
| GA (infection, No.) | NA | |
| 1st trimester | | 25 |
| 2nd trimester | | 43 |
| 3rd trimester | | 15 |
| Unknown | | 7 |
| VABS-II | NA | 58 |
| Child's age (mean) (mo) | | 60.12 ± 30.774 |
| Male (No.) | | 32 |
| Mean age (mo) | | 50.75 ± 26.3 |
| Female (No.) | | 26 |
| Mean age (mo) | | 71.65 ± 32.4 |
| Hearing disabilities (No.) | | 8 (14%) |

Note:—GA indicates gestational age; NA, not applicable.

Table 2: Regional effects of cytomegalovirus infection on fetal brain ADC^a

| Region | Controls \pm SD | CMV Group \pm SD | P Value |
|----------------|--------------------|--------------------|---------|
| Frontal lobe | 1762.3 ± 191.6 | 1675.0 ± 190.3 | .005 |
| Parietal lobe | 1733.9 ± 228.9 | 1637.2 ± 220.5 | .008 |
| Occipital lobe | 1700.2 ± 193.7 | 1629.9 ± 186.7 | .022 |
| Temporal lobe | 1687.5 ± 172.5 | 1636.7 ± 159.1 | .057 |
| Basal ganglia | 1448.5 ± 212.3 | 1375.2 ± 147.3 | .016 |
| Thalamus | 1354.2 ± 220.7 | 1247.2 ± 155.3 | <.001 |
| Cerebellum | 1486.3 ± 198.7 | 1407.5 ± 152.5 | .005 |
| Pons | 1359.2 ± 189.3 | 1286.3 ± 164.7 | .011 |

^a Data are means. ADC units are 10^6 mm²/s.

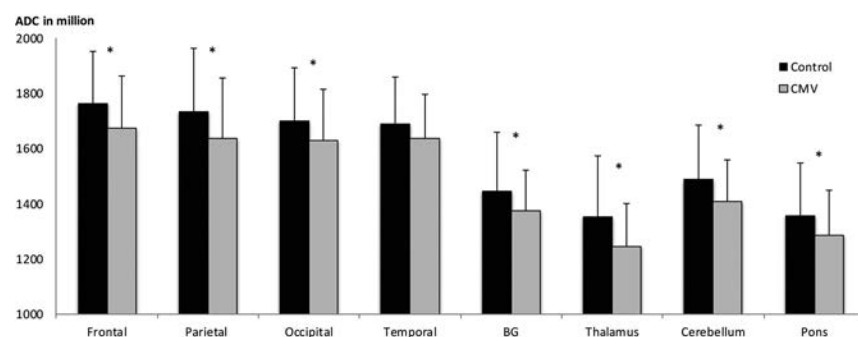


FIG 2. Comparison between ADC values (in millions) of different brain regions from CMV-infected fetuses (gray) and a control group (black). A significant difference is shown with an asterisk.

Significant differences were observed in the following subdomains between the standard score and the CMV-infected results distribution (Fig 3): Written ($P = .001$) and Coping Skills ($P < .001$) with a tendency toward lower scores, and in the Receptive subdomain ($P < .001$) with a tendency toward higher scores. Significant differences were observed in the Daily Living Skills ($P = .011$) and Socialization ($P = .009$) domains with the scores accumulating in the adequate category, thus creating a statistically significant difference from the expected normal distribution. The Adaptive Behavior Composite also showed a significant difference ($P = .005$), with the results again accumulating in the adequate category. The Interpersonal Relationships subdomain was not significantly different, yet it showed a high tendency ($P = .054$), with a small tendency toward lower scores.

The categories with significance did not change when the statistical analysis was performed with only the 50 children without hearing disabilities.

Correlation between ADC Values and VABS-II: 50 Children (No Hearing Disabilities)

Correlation between the ADC values and the VABS-II showed a significant difference for the following: pons and Written subdomain ($P = .052$) with a general negative trend; pons and Daily Living Skills subdomain ($P = .013$) with a positive trend; basal ganglia and Coping Skills subdomain ($P = .049$) with no clear trend; and a tendency in the temporal lobe ($P = .065$) with a general positive trend; temporal lobe and Socialization domain ($P = .043$) with a tendency in the thalamus ($P = .076$); frontal/parietal/temporal lobes and the pons with Fine Motor Skills subdomain ($P = .009$, $P = .05$, and $P = .005$ and $P = .048$, respectively) with no clear trend and a tendency in the thalamus and occipital lobe ($P = .06$ and $P = .074$, respectively) with no clear trend; and the pons and Motor Skills domain ($P = .037$) with no clear trend. A tendency had been shown between the thalamus and the Play and Leisure Time subdomain ($P = .06$) with a general positive trend and the parietal lobe with Gross Motor subdomain ($P = .064$) with a general positive trend (Fig 4).

DISCUSSION

Because the leading intrauterine infection has no effective vaccination in sight and with up to 20%–25% of infected fetuses eventually with some degree of damage,^{1–6,8,26,27} prenatal CMV infection remains a major concern.

To determine the pathology and predict future sequelae, sonography and feMRI are used complementarily. However, the lack of findings, as seen in most CMV-infected fetuses, does not eliminate the possibility of future neurodevelopmental pathology.^{7,10–13,17} This possibility raises the need for more reliable and objective imaging tools for neonatal evaluation to aid clinicians and parents in making more accurate and evidence-based decisions.

ADC measurements could be the tool in this evaluation. As a quantitative value

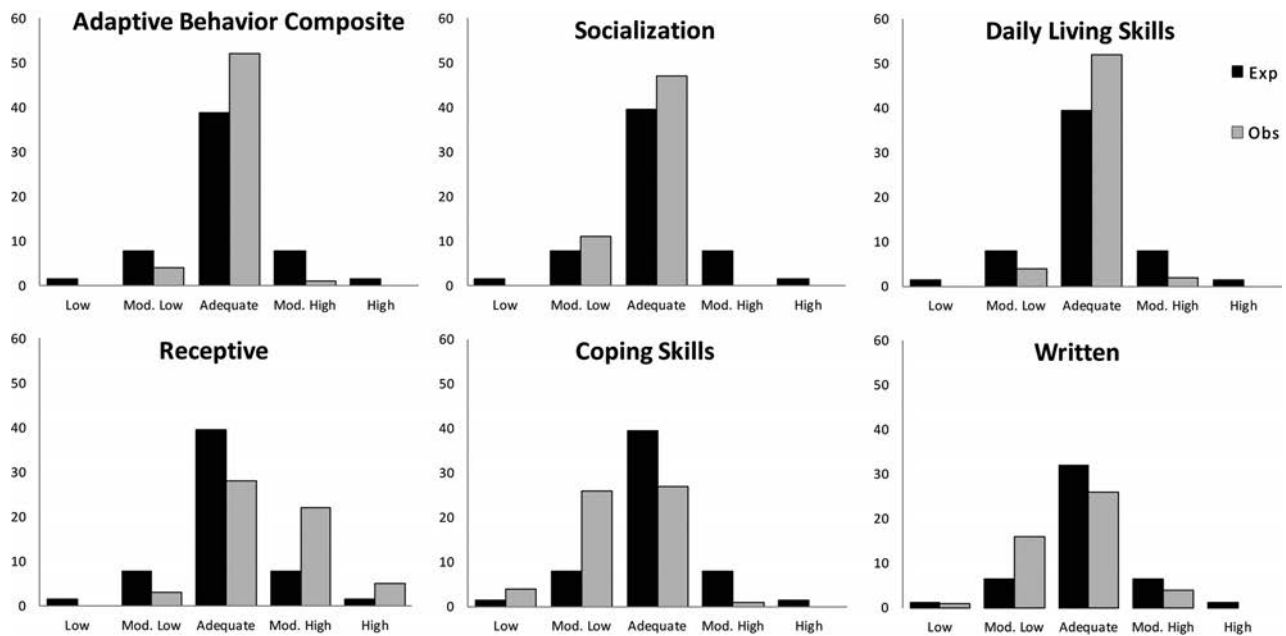


FIG 3. Vineland domains and subdomain absolute results distribution by category of the CMV-infected group (gray) compared with the normal expected distribution (black). Only significant results are shown.

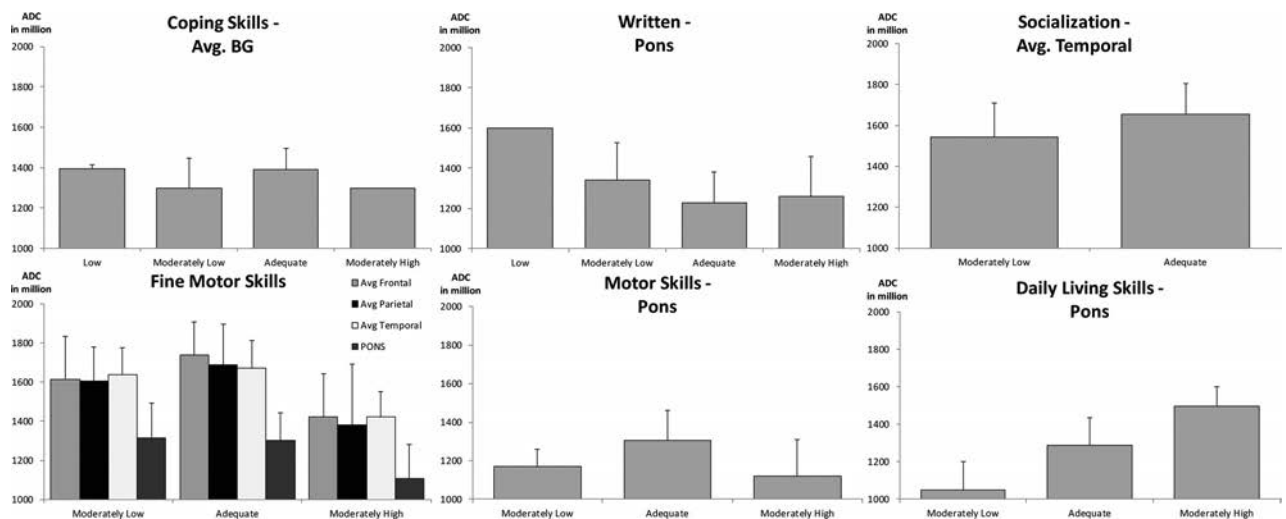


FIG 4. Correlation between ADC values (in millions) by brain regions and Vineland results by domains or subdomains of neonatal CMV-infected children, including only children without hearing disabilities and Vineland results. Only significant results are shown. BG indicates basal ganglia; Avg., average.

measuring voxel diffusion changes, it allows identification of tissue changes at an early stage and quantitative follow-up.^{14,16-19,22}

To date, only 3 studies^{14,28,29} have been performed evaluating ADC values in congenital CMV-infected brains, with 2 of them^{28,29} having a sample size of only 4 and 5 neonates, respectively. The third study¹⁴ was performed by our department, and part of its sample was included in this study (51/90). However, this is the first time, to our knowledge, that ADC studies of the CMV-infected fetal brains have focused on fMRI scans with unremarkable findings.

We compared the ADC values of confirmed CMV-infected fetal brain regions with unremarkable fMRI findings with those of a matched healthy control group and found significantly diffuse decreased ADC values throughout the fetal brain in the CMV-infected group, except for the temporal lobes ($P = .057$).

These findings are similar to those in previous studies,^{14,28} though we emphasize that the difference exists even if the fMRI findings are unremarkable.

Analysis of the ADC values shows a significant difference among trimesters in most of the areas examined, excluding the basal ganglia and the pons (On-line Fig 1). Those findings are thought to correspond with previous studies showing a decrease in ADC with fetal brain maturation, mostly due to the ongoing process of myelination. However, this decrease may also reflect microgliosis, which is the hallmark of neuroinflammation of all causes.^{14,15,18-22,30,31} These results are shown in unremarkable fMRI findings of CMV-infected fetuses and may imply an underlying inflammatory process within the fetal brain, unrecognized by conventional imaging.

To assess neurocognitive development in the CMV-infected group, we used the VABS-II, the most commonly used tool for adaptive function assessment,^{23,24,32} and compared the results with the test standardized distribution. The results showed no tendency toward lower or higher scores in the major domains or the composite score. Analysis of the subdomains showed a tendency toward lower scores in the Written and Coping Skills subdomain and a tendency for higher scores in the Receptive subdomain. These results align with some previous studies showing no major difference between neurodevelopmental outcomes of asymptomatic children with CMV and the healthy population,^{9,33} yet they raise the possibility of a deficit as shown in the Written and Coping skills subdomains. A possible explanation for those findings may be higher scores in the Receptive subdomain, which in turn cause the lower scores in the Coping skills subdomain because the child has problems integrating the overflow of information he or she perceives. Future studies focusing on these categories should be performed for further evaluation.

Comparison of the children from the CMV-infected group treated at birth with ganciclovir with the other children showed a benefit for the treatment in the Gross Motor subdomain, with the treated children scoring slightly higher within the normal distribution (On-line Fig 2), thus supporting the current policy of treatment with ganciclovir of asymptomatic neonates. Comparison of the children with hearing disabilities between the CMV-infected group and the other children showed no marked trend, though the small size of the hearing disability group should be borne in mind.

ADC values were evaluated as a potential prognostic factor by matching them with the corresponding Vineland scores. Significant correlation with a coherent trend has been shown for the Daily Living Skills domain and the pons and for the Community domain and the frontal lobe, with lower ADC values matching lower Vineland scores. The remainder of the significant correlation scores of ADC and Vineland have shown no coherent trend.

This work has a few limitations. First, although the CMV and control ADC values statistically differ, the SDs overlap; therefore, no absolute cutoff to distinguish the groups can be used. Nevertheless, single patient follow-up might be useful with further research. The second is the lack of an intellectual function assessment for the CMV-infected children. Intellectual functioning is an essential part of intellectual disability assessment combined with the adaptive behavior, which was assessed with the Vineland test. The third limitation is the number of CMV-infected children with Vineland scores. Due to most children falling into the adequate category, the number of children in the other categories was low; therefore, this number limits the statistical analysis of the results for correlation to ADC values.

CONCLUSIONS

This is the largest work to date to evaluate the influence of congenital CMV infection on ADC values in the brain on fMRI scans with unremarkable findings and the first to search for a correlation between those values and the cognitive outcome in children. We observed reduced ADC values in most brain areas studied. Neurodevelopmental assessment of the CMV-infected children with unremarkable fMRI findings showed no trend for the major

domains or the composite score, with a trend toward lower results in the Coping skills and Written subdomains and a trend toward higher results in the Receptive subdomain. A benefit for treating asymptomatic neonates with ganciclovir was observed for Gross Motor functions.

REFERENCES

1. Elliott SP. **Congenital cytomegalovirus infection: an overview.** *Infect Disord Drug Targets* 2011;11:432–36 Medline
2. Naing ZW, Scott GM, Shand A, et al. **Congenital cytomegalovirus infection in pregnancy: a review of prevalence, clinical features, diagnosis and prevention.** *Aust N Z J Obs Gynaecol* 2016;56:9–18 CrossRef Medline
3. Ornoy A, Diav-Citrin O. **Fetal effects of primary and secondary cytomegalovirus infection in pregnancy.** *Reprod Toxicol* 2006;21:399–409 CrossRef Medline
4. Dreher AM, Arora N, Fowler KB, et al. **Spectrum of disease and outcome in children with symptomatic congenital cytomegalovirus infection.** *J Pediatr* 2014;164:855–59 CrossRef Medline
5. Zhang XW, Li F, Yu XW, et al. **Physical and intellectual development in children with asymptomatic congenital cytomegalovirus infection: a longitudinal cohort study in Qinba mountain area, China.** *J Clin Virol* 2007;40:180–85 CrossRef Medline
6. Goderis J, De Leenheer E, Smets K, et al. **Hearing loss and congenital CMV infection: a systematic review.** *Pediatrics* 2014;134:972–82 CrossRef Medline
7. Fink KR, Thapa MM, Ishak GE, et al. **Neuroimaging of pediatric central nervous system cytomegalovirus infection.** *Radiographics* 2010;30:1779–96 CrossRef Medline
8. Fowler KB, Boppana SB. **Congenital cytomegalovirus (CMV) infection and hearing deficit.** *J Clin Virol* 2006;35:226–31 CrossRef Medline
9. Temple RO, Pass RF, Boll TJ. **Neuropsychological functioning in patients with asymptomatic congenital cytomegalovirus infection.** *J Dev Behav Pediatr* 2000;21:417–22 Medline
10. Benoist G, Salomon LJ, Mohlo M, et al. **Cytomegalovirus-related fetal brain lesions: comparison between targeted ultrasound examination and magnetic resonance imaging.** *Ultrasound Obs Gynecol* 2008;32:900–05 CrossRef Medline
11. Picone O, Simon I, Benachi A, et al. **Comparison between ultrasound and magnetic resonance imaging in assessment of fetal cytomegalovirus infection.** *Prenat Diagn* 2008;28:753–58 CrossRef Medline
12. Lipitz S, Hoffmann C, Feldman B, et al. **Value of prenatal ultrasound and magnetic resonance imaging in assessment of congenital primary cytomegalovirus infection.** *Ultrasound Obs Gynecol* 2010;36:709–17 CrossRef Medline
13. Capretti MG, Lanari M, Tani G, et al. **Role of cerebral ultrasound and magnetic resonance imaging in newborns with congenital cytomegalovirus infection.** *Brain Dev* 2014;36:203–11 CrossRef Medline
14. Yaniv G, Hoffmann C, Weisz B, et al. **Region-specific reductions in brain apparent diffusion coefficient in cytomegalovirus-infected fetuses.** *Ultrasound Obs Gynecol* 2016;47:600–67 CrossRef Medline
15. Schneider JF, Confort-Gouny S, Le Fur Y, et al. **Diffusion-weighted imaging in normal fetal brain maturation.** *Eur Radiol* 2007;17:2422–29 CrossRef Medline
16. Bydder GM, Rutherford MA. **Diffusion-weighted imaging of the brain in neonates and infants.** *Magn Reson Imaging Clin N Am* 2001;9:83–98, viii Medline
17. Abdelhalim AN, Alberico RA. **Pediatric neuroimaging.** *Neurol Clin* 2009;27:285–301, x CrossRef Medline
18. Huppi PS, Inder TE. **Magnetic resonance techniques in the evaluation of the perinatal brain: recent advances and future directions.** *Semin Neonatol* 2001;6:195–210 CrossRef Medline
19. Schneider MM, Berman JI, Baumer FM, et al. **Normative apparent diffusion coefficient values in the developing fetal brain.** *AJNR Am J Neuroradiol* 2009;30:1799–803 CrossRef Medline

20. Gropman A. **Imaging of neurogenetic and neurometabolic disorders of childhood.** *Curr Neurol Neurosci Rep* 2004;4:139–46 [Medline](#)
21. Counsell SJ, Allsop JM, Harrison MC, et al. **Diffusion-weighted imaging of the brain in preterm infants with focal and diffuse white matter abnormality.** *Pediatrics* 2003;112(1 pt 1):1–7 [Medline](#)
22. Miller SP, Vigneron DB, Henry RG, et al. **Serial quantitative diffusion tensor MRI of the premature brain: development in newborns with and without injury.** *J Magn Reson Imaging* 2002;16:621–32 [CrossRef Medline](#)
23. Sparrow SS, Cicchetti DV. **Diagnostic uses of the Vineland Adaptive Behavior Scales.** *J Pediatr Psychol* 1985;10:215–25 [CrossRef Medline](#)
24. Scattone D, Raggio DJ, May W. **Comparison of the Vineland Adaptive Behavior Scales, Second Edition, and the Bayley Scales of Infant and Toddler Development, Third Edition.** *Psychol Rep* 2011;109:626–34 [CrossRef Medline](#)
25. Yaniv G, Katorza E, Bercovitz R, et al. **Region-specific changes in brain diffusivity in fetal isolated mild ventriculomegaly.** *Eur Radiol* 2016;26:840–48 [CrossRef Medline](#)
26. Kenneson A, Cannon MJ. **Review and meta-analysis of the epidemiology of congenital cytomegalovirus (CMV) infection.** *Rev Med Virol* 2007;17:253–76 [CrossRef Medline](#)
27. Townsend CL, Forsgren M, Ahlfors K, et al. **Long-term outcomes of congenital cytomegalovirus infection in Sweden and the United Kingdom.** *Clin Infect Dis* 2013;56:1232–39 [CrossRef Medline](#)
28. Hoffmann C, Weisz B, Lipitz S, et al. **Regional apparent diffusion coefficient values in 3rd trimester fetal brain.** *Neuroradiology* 2014;56:561–67 [CrossRef Medline](#)
29. van der Voorn JP, Pouwels PJ, Vermeulen RJ, et al. **Quantitative MR imaging and spectroscopy in congenital cytomegalovirus infection and periventricular leukomalacia suggests a comparable neuropathological substrate of the cerebral white matter lesions.** *Neuropediatrics* 2009;40:168–73 [CrossRef](#)
30. Hüppi PS, Dubois J. **Diffusion tensor imaging of brain development.** *Semin Fetal Neonatal Med* 2006;11:489–97 [Medline](#)
31. Lodygensky GA, West T, Moravec MD, et al. **Diffusion characteristics associated with neuronal injury and glial activation following hypoxia-ischemia in the immature brain.** *Magn Reson Med* 2011;66:839–45 [CrossRef Medline](#)
32. Ray-Subramanian CE, Huai N, Ellis Weismer S. **Brief report: adaptive behavior and cognitive skills for toddlers on the autism spectrum.** *J Autism Dev Disord* 2011;41:679–84 [CrossRef Medline](#)
33. Farkas N, Hoffmann C, Ben-Sira L, et al. **Does normal fetal brain ultrasound predict normal neurodevelopmental outcome in congenital cytomegalovirus infection?** *Prenat Diagn* 2011;31:360–66 [CrossRef Medline](#)

Quantitative Folding Pattern Analysis of Early Primary Sulci in Human Fetuses with Brain Abnormalities

 K. Im,  A. Guimaraes,  Y. Kim,  E. Cottrill,  B. Gagoski,  C. Rollins,  C. Ortinau,  E. Yang, and  P.E. Grant



ABSTRACT

BACKGROUND AND PURPOSE: Aberrant gyral folding is a key feature in the diagnosis of many cerebral malformations. However, in fetal life, it is particularly challenging to confidently diagnose aberrant folding because of the rapid spatiotemporal changes of gyral development. Currently, there is no resource to measure how an individual fetal brain compares with normal spatiotemporal variations. In this study, we assessed the potential for automatic analysis of early sulcal patterns to detect individual fetal brains with cerebral abnormalities.

MATERIALS AND METHODS: Triplane MR images were aligned to create a motion-corrected volume for each individual fetal brain, and cortical plate surfaces were extracted. Sulcal basins were automatically identified on the cortical plate surface and compared with a combined set generated from 9 normal fetal brain templates. Sulcal pattern similarities to the templates were quantified by using multivariate geometric features and intersulcal relationships for 14 normal fetal brains and 5 fetal brains that were proved to be abnormal on postnatal MR imaging. Results were compared with the gyrification index.

RESULTS: Significantly reduced sulcal pattern similarities to normal templates were found in all abnormal individual fetuses compared with normal fetuses (mean similarity [normal, abnormal], left: 0.818, 0.752; $P < .001$; right: 0.810, 0.753; $P < .01$). Altered location and depth patterns of sulcal basins were the primary distinguishing features. The gyrification index was not significantly different between the normal and abnormal groups.

CONCLUSIONS: Automated analysis of interrelated patterning of early primary sulci could outperform the traditional gyrification index and has the potential to quantitatively detect individual fetuses with emerging abnormal sulcal patterns.

ABBREVIATIONS: GI = gyrification index; GW = gestational weeks

In the human cerebral cortex, primary sulci are important anatomic landmarks for predicting several primary, secondary, and higher order cortical areas.¹ Their global patterning (arrangement, number, and size of primary sulcal folds) has been hypothesized to relate to the optimal organization of functional areas and

their white matter connections.^{2–4} Interestingly, the primary sulcal pattern is prenatally determined and appears to show little individual variability in healthy patients in early fetal life before 30 gestational weeks (GW).^{5–8} However, in many brain malformations and psychiatric/neurologic disorders, defects in the neurodevelopmental process result in a disrupted primary sulcal pattern, which may appear in early fetal life.^{9–13} Therefore, sulcal folding analysis in the fetal brain may provide a useful tool for identifying the early signs of developmental brain disorders.


Previous studies using MR imaging have quantified cortical folding development in human fetal and preterm brains. The temporal changes of the gyrification index (GI) were observed during fetal life,^{14,15} and cortical surface curvatures at the global level have been measured to quantify the overall degree of cortical folding from 22–39 GW.^{15–20} The curvature and depth changes of cortical folding at the vertex level have also been observed for the


Received October 21, 2016; accepted after revision March 13, 2017.

From the Fetal Neonatal Neuroimaging and Developmental Science Center (K.I., A.G., Y.K., E.C., B.G., P.E.G.), Division of Newborn Medicine (K.I., P.E.G.) and the Departments of Neurology (C.R.) and Radiology (B.G., E.Y., P.E.G.), Boston Children's Hospital, Boston, Massachusetts; Harvard Medical School (K.I., B.G., C.R., C.O., E.Y., P.E.G.), Boston, Massachusetts; Department of Pediatrics Newborn Medicine (C.O.), Brigham and Women's Hospital, Boston, Massachusetts; and Faculdade de Medicina da USP (A.G.), Sao Paulo, Brazil.

This work was supported by National Institutes of Health grants 1R21HD083956-01A1, 1R01EB017337-01, and 1U01 HD087211-01; a Boston Children's Hospital Faculty Career Development Award; a Scholar Award from the Pediatric Heart Network supported by the National Heart, Lung, and Blood Institute of the National Institutes of Health (U10HL068270); a Neurological Sciences Academic Developmental Award from the National Institutes of Neurological Disorders and Stroke; and the Mend a Heart Foundation.

Please address correspondence to Kiho Im, PhD, Boston Children's Hospital, 1 Autumn St, Boston, MA 02115; e-mail: Kiho.Im@childrens.harvard.edu

 Indicates open access to non-subscribers at www.ajnr.org

 Indicates article with supplemental on-line photos.

<http://dx.doi.org/10.3174/ajnr.A5217>

entire cortical area.^{18,21,22} However, no quantitative analysis of the interrelated arrangement and global patterning of primary sulci in the human fetal brain exists. We previously developed a comprehensive and quantitative analytical method for comparing primary sulcal patterns by using not only the regional features of sulci folds themselves, but also the intersulcal geometric and topologic relationships.²³ This method provided an effective means for detecting genetically influenced abnormal sulcal patterns in pediatric patients with cerebral malformations^{10,12} and developmental dyslexia.¹³

We hypothesized that the global pattern of primary sulci may be disrupted early in fetal brain development in fetuses destined to have abnormal sulcation at birth. Therefore, by using normal fetal brain templates to define normal sulcal patterning, we set out to measure early differences of sulcal pattern in fetuses with brain abnormalities confirmed by MR imaging at birth. The biologic motivation behind this hypothesis is that cortical arealization and connectivity begin early in fetal brain development and, if defective, might give rise to atypical sulcal topology. We also compared our method with an established metric, the GI, which has been used to quantify the development of human cortical folding.^{18,24}

MATERIALS AND METHODS

Patients

For this pilot feasibility study, fetuses with confirmed brain abnormalities were identified retrospectively from the existing clinical MR imaging data at Boston Children's Hospital. We searched for fetal MRIs performed between 18 and 30 GW with reports raising a concern for cerebral malformations and included only those fetuses who had the cerebral malformation confirmed by a follow-up postnatal brain MR imaging. The clinical imaging diagnoses were confirmed by 2 pediatric neuroradiologists (E.Y. and P.E.G.). Among approximately 40 fetuses identified by using this process, most were excluded because of serious head motion in the fetal MRIs, which could not be sufficiently processed to yield accurate fetal brain surfaces. Thus, 5 fetuses with confirmed brain malformations were included in the final analysis (male/female, 3/2; age [mean \pm SD], 20–30 GW [25.3 \pm 3.8]; maternal age [mean \pm SD], 29–37 years [33.8 \pm 2.7]) (1 Chiari II malformation [subject ID: M1] with sacral myelomeningocele, 3 polymicrogyria [M2, M3, and M5], and 1 atypical gyral folding [M4]). Fetuses M1 and M2 were initially thought to have a normal sulcal folding, but neonatal MR imaging identified atypical sulcal folding and polymicrogyria, respectively. One patient with polymicrogyria was longitudinally scanned with fetal MR imaging at 22 and 29 GW [M5a and M5b].

Healthy control patients were recruited from mothers referred to the Advanced Fetal Care Center at Boston Children's Hospital because of a family history of congenital heart disease, but for whom fetal echocardiogram was normal. Inclusion criteria were the following: maternal age of 18–45 years and gestational age of 18–30 GW. We excluded multiple gestation pregnancies and fetuses with dysmorphic features on sonography, brain malformations, other brain lesions, known chromosomal abnormalities, other identified organ anomalies, and known congenital infections. We also excluded patients as healthy controls if the fetal MR imaging identified these conditions as being present. Using these

criteria, 21 healthy control fetuses were recruited and scanned, but 7 fetuses were excluded because of serious head motion. Fourteen healthy fetuses were finally included in this study (male/female, 4/10; age [mean \pm SD], 21–30 GW [25.5 \pm 2.3]; maternal age [mean \pm SD], 25–39 years [29.9 \pm 4.0]).

This study was approved by the institutional review board committee of Boston Children's Hospital.

MR Imaging Acquisition and Processing and Reconstruction of Cortical Plate Surface

Fetal brain MR imaging was performed by using a T2-weighted HASTE MR imaging sequence on a 3T scanner (Skyra; Siemens, Erlangen, Germany) equipped with the body matrix array (18 coil elements used) in combination with the spine array (12–18 coil elements) for a total of 30–36 coil elements. The following sequence was used for each patient: TR, \sim 1.5 seconds; TE, 120 ms; FOV, 256 mm; in-plane resolution, 1 mm; section thickness, 2–4 mm. The HASTE acquisition was performed at least 3 times in different orthogonal orientations with respect to the fetal brain for reliable image processing.

Fetal head motion was corrected, and 0.75 mm isotropic volume images were reconstructed from the multiple scans.²⁵ The volume images were manually aligned along the anterior/posterior commissure points by using AFNI (<http://afni.nimh.nih.gov/afni>),²⁶ and the cortical plate was semi-automatically segmented by using FreeView (<http://surfer.nmr.mgh.harvard.edu>). The cortical plate was painted on each section by using intensity value ranges and corrected via examination on orthogonal views. To reconstruct smooth surface models, the inner volume of the cortical plate was binarized and smoothed by using a $3 \times 3 \times 3$ mean filter. The 3D inner cortical plate surface was then reconstructed by using the isosurface function with the isovalue of 0.5 in Matlab software (MathWorks, Natick, Massachusetts) (Fig 1). Although small folds similar in size to a voxel might be eliminated, our smoothing was effective to avoid noisy features and voxelized representation of the surface.

We used 9 previously published fetal brain templates from 23–31 GW that were constructed from 80 normal fetuses (<http://brain-development.org/brain-atlases>)²⁷ as a reference for our sulcal pattern analysis. The cortical plate surfaces of the fetal templates were reconstructed by using the same process (Fig 2).

Identification and Geometric Measurements of Sulcal Catchment Basins

Early sulcal catchment basins were used for sulcal pattern analysis because they are relatively invariant between patients and hypothesized to relate to functional areas and activations.^{28,29} Sulcal basins are concave substructures decomposed from one large part of cortical folds.²⁹ Cortical mean curvature and depth on a surface model were measured by using FreeSurfer (<http://surfer.nmr.mgh.harvard.edu>), and sulcal basins were automatically identified by using a watershed algorithm based on the curvature map^{12,13,23,29} (Fig 1). A minimum bounding box for a given surface model was defined, and an average 3D relative position (x , left–right [0–1]; y , posterior–anterior [0–1]; z , inferior–superior [0–1]) was calculated for each sulcal basin. We also computed

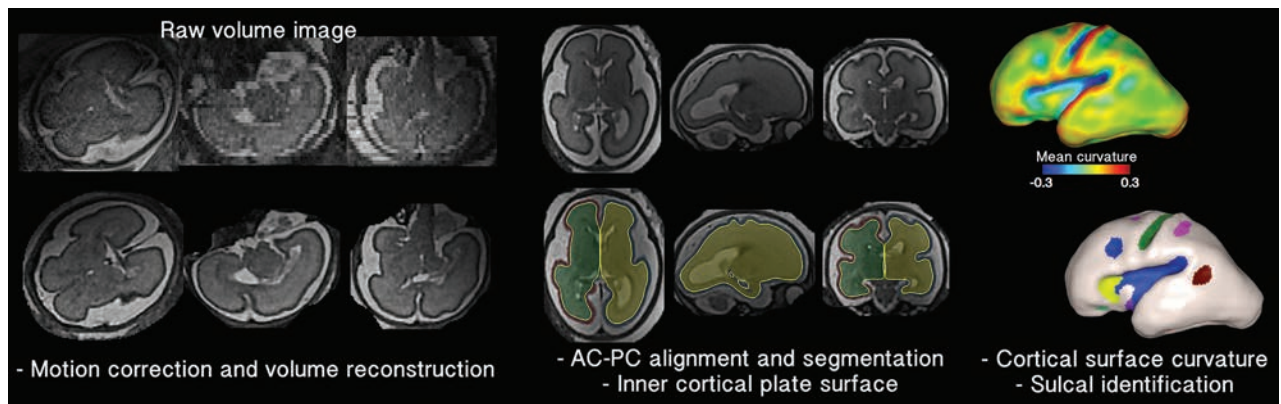


FIG 1. Processing overview for the identification of sulcal basins on the cortical plate surface. A raw volume image of an individual fetal brain (26 GW) is reconstructed to a motion-corrected, high-resolution volume. The reconstructed volume image is aligned along the anterior/posterior commissure (AC–PC) points. The inner volume of the cortical plate is semi-automatically segmented, its 3D surface is reconstructed, and its mean curvature is represented by a *color map*. Sulcal catchment basins are identified on the cortical plate surface based on the curvature and identified with different colors.

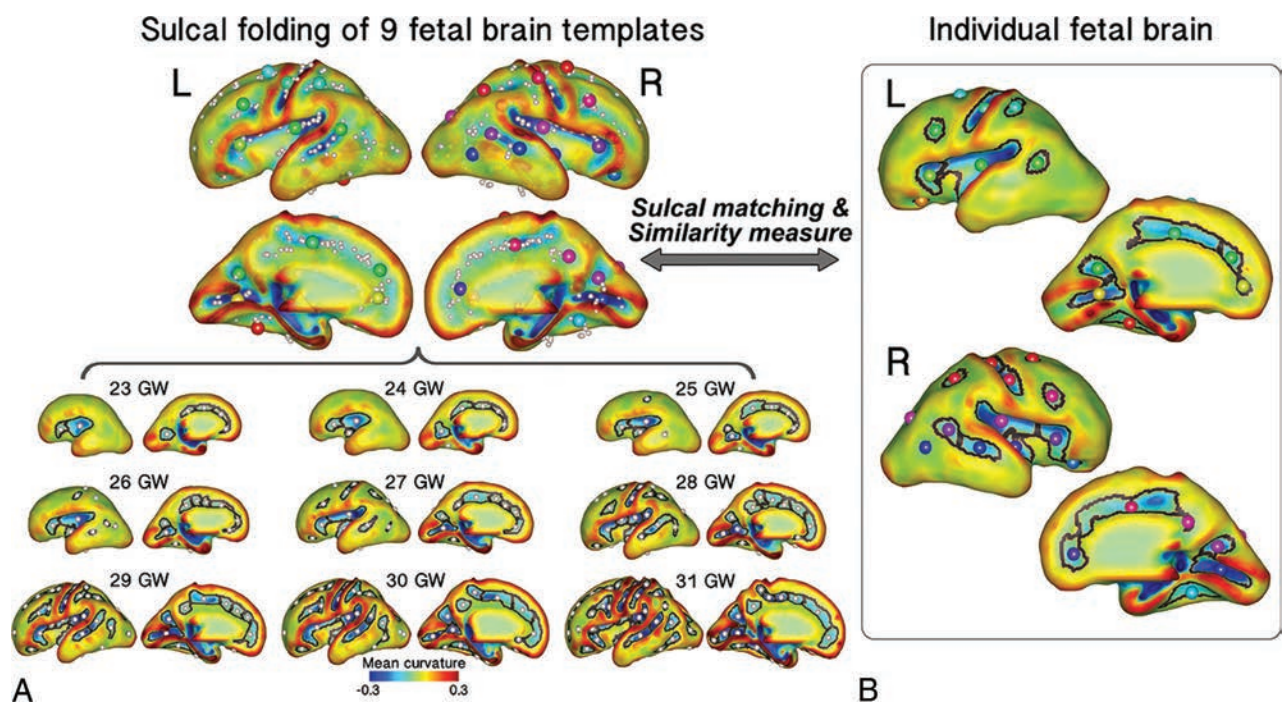


FIG 2. Sulcal matching overview. *A*, The combined set of sulcal folds (*top*) identified and generated from 9 fetal brain templates (*bottom*). Sulcal basins and their average positions are represented by *black line* and *sphere*, respectively. *B*, Sulcal matching result for an individual fetal brain (26 GW). Each sulcal basin of the individual brain is optimally matched with 1 of the sulcal basins of the 9 template brains. The *spheres* with the same color represent the matched corresponding sulcal basins between the templates and the individual brain.

normalized surface area (s) and mean sulcal depth (d) for sulcal geometry.

Sulcal Pattern Matching and Similarity to the Templates and Automatic Sulcal Labeling

Sulcal pattern was represented with a feature set of sulcal basins including not only the local sulcal features, but also the inter-sulcal geometric relationships in the left and right hemispheres.²³ To quantify the deviation from the normal pattern of sulcal folding for each fetus, individual brains were matched and compared with the combined set of all 9 fetal brain templates (Fig 2). Sulcal sets P (individual brain) and Q (9 template

brains) containing m and n sulcal basins, respectively, were represented as follows:

$$P = \{p_1, p_2, \dots, p_m\} \text{ and } Q = \{q_1, q_2, \dots, q_n\}$$

For the comparison, we used a spectral matching technique to determine the optimal match having the minimum difference of the features between 2 sulcal sets.^{13,23,30} We constructed a matrix M to store the affinities of all candidate matches and chose a subset matrix A , determining the optimal match and maximum affinity between P and Q by calculating the principal eigenvector of M . For a more detailed explanation of the methodologic procedures, see Im et al.²³ Through this process, each sulcal basin of an individual brain was

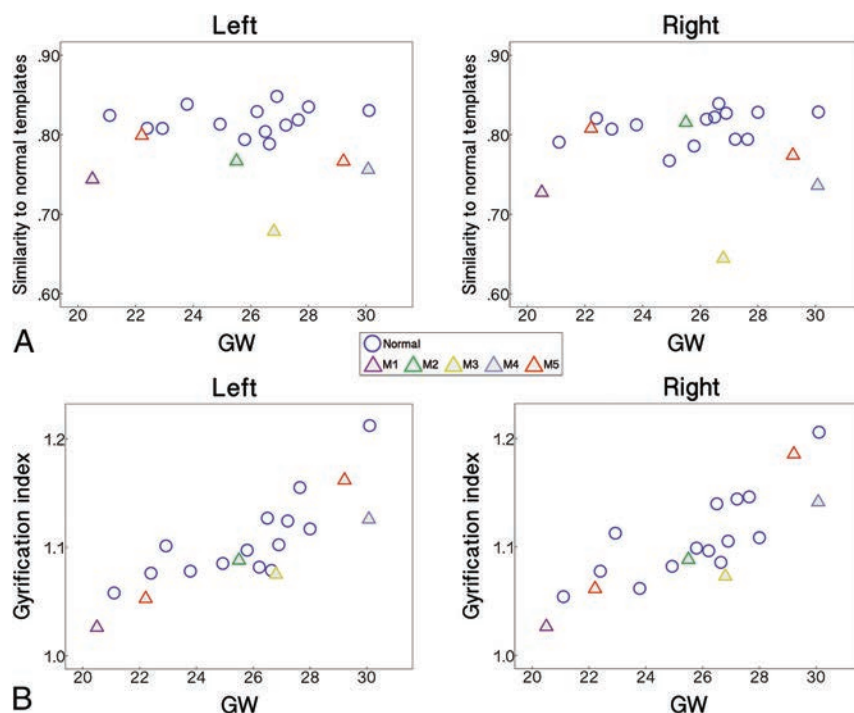


FIG 3. Scatterplots of the similarity to normal templates computed with A, the whole feature set and B, GI against GW for the left and right hemispheres.

optimally matched with 1 of the sulcal basins of the 9 template brains (Fig 2), and the similarity to the templates was calculated, which ranged from 0–1^{23,30} (On-line Fig 1). For the similarity measure, we used variable weighting of features to assess their relative importance on sulcal pattern similarity. First, all 3 features were optimally weighted in the sulcal pattern matching and similarity measure ($w_{x,y,z} = 3$; $w_s = 8$; $w_d = 0.8$). Then, we evaluated the impact of each individual feature on similarity measures by setting all weights of the other features to 0.

Because the 3D position of the sulcal basin was required for optimal sulcal matching, we aligned the orientation of the cortical surface along the anterior/posterior commissure line. Although this is not a perfect spatial normalization, it was considered sufficient for measuring the scale-free value of relative position. Moreover, our method is insensitive to the spatial normalization because the intrinsic sulcal pattern characterized by intersulcal relationships is used for computing a large part of the sulcal pattern similarity and minimally affected by the spatial alignment.²³

3D Global Gyrification Index

A GI is defined as the ratio between the whole areas of the cortical surface and its convex hull in 3D.^{14,31} First, the inner volume of the cortical plate surface was isolated and constructed, and the 3D morphologic closing operation was performed by using a sphere of 15 mm diameter as the structural element to close the sulcal folding.³¹ The outer hull surface wrapping the cortical plate surface was created from the binary closed volume by using the iso-surface function (On-line Fig 2). We then calculated the 3D global GI of the left and right whole cerebral hemispheres.

Statistical Group and Individual Analysis

Using the sulcal pattern matching and comparison method, the sulcal pattern similarities to the set of 9 normal templates were

computed with the 4 different feature sets for each fetus in the left and right hemispheres (whole feature, 3D position, sulcal area, and sulcal depth). The similarities to the templates were statistically compared between normal fetuses and fetuses with brain abnormalities with an independent 2-sample *t* test. The Pearson correlation and Mann-Whitney *U* test were used in normal fetuses to test the effects of gestational age and sex, respectively, on the sulcal pattern similarity. The group difference in GI was statistically assessed by using linear regression analysis. The dependent variable was the GI, and the independent variable was the group. Age and sex were used as covariates to control for their effects. Because 1 patient with an abnormal brain had repeated longitudinal measurements (M5a and M5b), the group comparisons in the sulcal pattern similarity and GI were performed 2 times, including either M5a or M5b, to comply with the assumption of statistical tests.

We examined if the similarity of each individual abnormal brain to the templates deviated from the normal range by measuring its relative position in the distribution of all 14 normal individual fetuses. We counted the number of normal patients who had a lower similarity and expressed that value as a ratio to the total number of normal individual patients (histogram ranking). If an individual abnormal fetus showed a ratio of 0, meaning none of the normal individual fetuses had a lower similarity to the normal template, that patient was tagged as presenting an “abnormal” pattern of sulcal folding. If the ratio value was smaller than 0.1, the sulcal folding was deemed “suspicious” for an abnormal sulcal pattern.

RESULTS

Sulcal Pattern Similarity to the Normal Templates

The fetuses with abnormal brains showed significantly lower sulcal pattern similarities to the templates compared with the normal fetuses in both hemispheres measured with the whole set of features (Fig 3A). In the statistical tests for each individual feature, significantly low similarities were observed in the abnormal group for the relative position, area, and depth of cortical folding in the left hemisphere. In the right hemisphere, sulcal position and depth pattern similarities were significantly lower in the abnormal fetal brains. All statistical results for the group comparisons with M5a or M5b are presented in Table 1. We confirmed that sulcal pattern similarities were not significantly associated with GW (left: correlation coefficient $r = 0.075$, $P = .80$; right: $r = 0.334$, $P = .24$) and not different between male and female patients (left: $P = .37$; right: $P = .84$).

Regression analysis showed that global GI of the fetal brains increased with GW (statistical results including M5a [a] and M5b [b], left and right: $P < .001$), but there was no significant

Table 1: Statistical results for the comparisons of the sulcal pattern similarity with the templates between normal and abnormal groups with different feature sets

| | Normal | Abnormal | P^{abc} |
|-------------------|---------------|---------------|---------------------------------|
| Left | | | |
| Whole feature | 0.818 ± 0.017 | 0.752 ± 0.040 | $[a] < .001^b$; $[b] < .001^b$ |
| 3D position | 0.871 ± 0.022 | 0.824 ± 0.046 | $[a] = .01^c$; $[b] < .001^b$ |
| Sulcal basin area | 0.921 ± 0.019 | 0.895 ± 0.029 | $[a] = .006^c$; $[b] = .04^c$ |
| Sulcal depth | 0.928 ± 0.021 | 0.896 ± 0.022 | $[a] = .02^c$; $[b] = .007^c$ |
| Right | | | |
| Whole feature | 0.810 ± 0.020 | 0.753 ± 0.066 | $[a] = .009^c$; $[b] = .002^b$ |
| 3D position | 0.862 ± 0.020 | 0.812 ± 0.068 | $[a] = .03^c$; $[b] = .001^b$ |
| Sulcal basin area | 0.921 ± 0.027 | 0.901 ± 0.037 | $[a] = .14$; $[b] = .12$ |
| Sulcal depth | 0.930 ± 0.013 | 0.910 ± 0.016 | $[a] = .01^c$; $[b] = .02^c$ |

^a[a], statistical analysis with M5a; [b], statistical analysis with M5b.

^b $P < .005$.

^c $P < .05$.

Table 2: Demographic data, qualitative assessments of fetal and neonatal MRIs, and quantitative assessments of fetal MRIs for fetuses with brain abnormalities

| ID | Age (GW) | Sex | Qualitative Fetal MRI Assessment | Qualitative Neonatal MRI Assessment | Quantitative Fetal MRI Assessment |
|-----|----------|-----|----------------------------------|-------------------------------------|-----------------------------------|
| M1 | 20 | F | N | A (Chiari II) | A (L, R) |
| M2 | 25 | F | N | A (Polymicrogyria) | A (L) |
| M3 | 26 | M | A | A (Polymicrogyria) | A (L, R) |
| M4 | 30 | M | A | A (Atypical gyral folding) | A (L, R) |
| M5a | 22 | M | A | A (Polymicrogyria) | S (L), A (R) |
| M5b | 29 | | A | | A (L, R) |

Note:—A indicates abnormal sulcal folding; L, left; N, normal sulcal folding; R, right; S, suspicious for abnormal sulcal folding.

sex effect ($[a]$ left: $P = .38$, right: $P = .67$; $[b]$ left: $P = .45$, right: $P = .78$). The GI was not statistically different between the normal and abnormal fetal groups in either hemisphere ($[a]$ left: $P = .18$, right: $P = .22$; $[b]$ left: $P = .33$, right: $P = .48$) (Fig 3B).

Individual analysis based on the ratio quantifying the deviation from the normal showed that all abnormal fetal brains had an abnormal sulcal pattern with the ratio 0 in 1 or more feature sets in at least 1 hemisphere (left: M1, M2, M3, M4, and M5b determined as abnormal; right: M1, M3, M4, M5a, and M5b determined as abnormal). The similarity measures for all individual hemispheres and the ratio values for each abnormal fetal brain hemisphere are shown, along with 5 normal fetal brains for example, in On-line Fig 3. Our quantitative assessment for each abnormal fetal brain was compared with the qualitative assessment of fetal MR imaging. An abnormal sulcal pattern was detected for individual fetal brains that were judged to have abnormal gyrification by qualitative assessment (M3, M4, and M5). Moreover, high deviation from the normal was also quantitatively observed for fetal brains that were judged to have normal gyrification by qualitative fetal MR imaging assessment (M1 and M2). Demographic data and qualitative and quantitative assessments of fetal/neonatal MRIs are shown in Table 2. Specifically, abnormal brain M2, initially misjudged to have normal sulcal folding in qualitative fetal MR imaging but postnatally confirmed to have abnormal folding (false-negative), was assessed to be abnormal in left hemispheric sulcal pattern in our quantitative analysis (true-positive).

DISCUSSION

We used a novel automatic sulcal pattern comparison method to quantify sulcal pattern similarities of individual fetal brains

against normal fetal brain templates by using multivariate geometric sulcal features and detected not only group differences between abnormal and normal fetal brains, but also individual differences in sulcal patterns in all abnormal fetuses. Although the entire set of features (3D position, area, and depth of sulcal basin) showed the highest statistical significance for the group comparison, the 3D position and depth of the sulcal basin were the major driving factors. The common cortical folding measurement GI was also used for the group analysis, but showed no significant difference between the groups. In our pilot data, our approach, based on sulcal location and depth patterns, outperformed the more traditional GI, previously thought to be the most sensitive measure for evaluation of the developing human brain.²⁴ This suggests that in brain abnormalities associated with abnormal sulcal folding, the relative sulcal locations and depths are altered more than the overall amount of cortical folding during early fetal brain development.

Atypical patterns of sulcal locations and folding depths in fetal brains may indicate defective regulation of spatiotemporal dynamics of early cortical surface expansion and folding. Cortical areas do not develop independently, but in strong relation to other functional areas with optimized white matter connections, and accordingly show specific locations and size.^{3,32} It has been proposed that cortical functional arealization and organization may be related to the specific spatial pattern of early primary sulci in fetal brains.^{1,4} Similarly, the gyrogenesis theory suggests that areas of rapid growth form gyri at the center of a functional zone and underlie the formation of the first major folds during the early stage of cortical growth.^{33,34} The areal expansion and folding of the human cerebral cortex are precisely regulated processes in time during fetal life.⁵⁻⁸ The normal stereotypical pattern of gyrogenesis likely results in regular intersulcal relationships and folding depth at each fetal stage. In fact, the positional identity of cortical functional regions is defined by the combinatorial expression pattern of various genes, with their areal expansion also under tight genetic control with distinct spatiotemporal characteristics.^{32,35-37} Therefore, atypical patterns of sulcal locations and folding depths in fetal brains before 30 GW likely are associated with defects in genetic control of cortical arealization and expansion.

In 2 cases (M1 and M2), our individual quantitative analysis detected an abnormal sulcal pattern not detected on qualitative fetal MR imaging assessment yet confirmed postnatally. Thus, our quantitative analysis shows the feasibility and potential for detecting emerging subtle abnormalities in sulcal patterns that are difficult to perceive visually. Future studies will be aimed at obtaining true sensitivity and specificity data in a larger cohort that

includes postnatal imaging of normal fetuses because this pilot study could not show the full distribution of typical sulcal patterns because of the small number of normal fetuses. In addition, we will explore the ability of such quantitative analyses to decrease variation in clinical interpretations. Finally, comparison of quantitative assessments with genetic studies and follow-up clinical/behavioral outcomes is needed to further evaluate the potential applicability of our method in understanding the ability to detect and distinguish different genetic disorders and predict outcomes.

Limitations of MR imaging–based sulcal analysis on fetal brains include the low success rate (5/40 [12.5%]) for triplane reconstruction in clinically acquired fetal datasets and the current need for manual segmentations. However, because healthy control fetuses were scanned with a research MR imaging protocol that acquired more sets of triplane images, the success rate for our healthy fetal MR imaging processing was higher (14/21 [66.7%]). Future accelerations in image acquisition and improvements in postprocessing techniques are likely to increase success rates moving forward. Another limitation is the delay in the detection of cerebral sulci in MR imaging studies compared with histopathology. At least 1-week discrepancy has been reported between anatomic and qualitative MR imaging studies because of limitations in the resolution and contrast of in utero fetal MR imaging.^{38,39} If cerebral sulci are identified by using automatic and quantitative image processing techniques, sulcal detection is more delayed. For example, 1 small sulcus, the olfactory sulcus, was reported to appear before 20 weeks,^{7,8} but here it was not identified at such an early stage not only on the templates, but also on individual fetal brains. Delayed sulcal detection on fetal MR imaging has also been shown in previous quantitative studies.^{21,40} Ongoing innovations in this area as mentioned above are also likely to improve early sulcal detection.

CONCLUSIONS

Our quantitative sulcal pattern analysis with a focus on relative spatial location and depth of sulci has the potential to detect not only group differences in cortical folding, but also individual differences in fetuses destined to develop cortical malformations. Our method outperformed GI, which was dominated by gestational age. In addition, our method outperformed blinded expert qualitative fetal MR imaging assessments.

Disclosures: Kiho Im—*RELATED: Grant:* National Institutes of Health, Boston Children's Hospital. Caitlin Rollins—*RELATED: Grant:* National Institutes of Health, *Comments:* Scholar Award from the Pediatric Heart Network and K12 training award*; *UNRELATED: Stock/Stock Options:* Biogen. Cynthia Ortin—*RELATED: Mend A Heart Foundation;* *UNRELATED: Payment for Lectures (including service on Speakers Bureaus):* Academy of Neonatal Nursing. Edward Yang—*RELATED: Grant:* National Institutes of Health, *Comments:* principal investigator for National Institutes of Health grant 1R21HD083956–01A1*; *UNRELATED: Consultancy:* Corticometrics LLC; *Grants/Grants Pending:* National Institutes of Health*. *Money paid to the institution.

REFERENCES

1. Fischl B, Rajendran N, Busa E, et al. **Cortical folding patterns and predicting cytoarchitecture.** *Cereb Cortex* 2008;18:1973–80 [CrossRef Medline](#)
2. Van Essen DC. **A tension-based theory of morphogenesis and compact wiring in the central nervous system.** *Nature* 1997;385:313–18 [CrossRef Medline](#)
3. Klyachko VA, Stevens CF. **Connectivity optimization and the positioning of cortical areas.** *Proc Natl Acad Sci U S A* 2003;100:7937–41 [CrossRef Medline](#)
4. Sun T, Hevner RF. **Growth and folding of the mammalian cerebral cortex: from molecules to malformations.** *Nat Rev Neurosci* 2014;15:217–32 [CrossRef Medline](#)
5. Kostovic I, Vasung L. **Insights from in vitro fetal magnetic resonance imaging of cerebral development.** *Semin Perinatol* 2009;33:220–33 [CrossRef Medline](#)
6. Garel C, Chantrel E, Brisse H, et al. **Fetal cerebral cortex: normal gestational landmarks identified using prenatal MR imaging.** *AJNR Am J Neuroradiol* 2001;22:184–89 [CrossRef Medline](#)
7. Chi JG, Dooling EC, Gilles FH. **Gyral development of the human brain.** *Ann Neurol* 1977;1:86–93 [CrossRef Medline](#)
8. White T, Su S, Schmidt M, et al. **The development of gyrification in childhood and adolescence.** *Brain Cogn* 2010;72:36–45 [CrossRef Medline](#)
9. Nakamura M, Nestor PG, McCarley RW, et al. **Altered orbito-frontal sulcogyral pattern in schizophrenia.** *Brain* 2007;130:693–707 [CrossRef Medline](#)
10. Bae BI, Tietjen I, Atabay KD, et al. **Evolutionarily dynamic alternative splicing of GPR56 regulates regional cerebral cortical patterning.** *Science* 2014;343:764–68 [CrossRef Medline](#)
11. Barkovich AJ, Guerrini R, Kuzniecky RI, et al. **A developmental and genetic classification for malformations of cortical development: update 2012.** *Brain* 2012;135:1348–69 [CrossRef Medline](#)
12. Im K, Pienaar R, Paldino MJ, et al. **Quantification and discrimination of abnormal sulcal patterns in polymicrogyria.** *Cereb Cortex* 2013;23:3007–15 [CrossRef Medline](#)
13. Im K, Raschle NM, Smith SA, et al. **Atypical sulcal pattern in children with developmental dyslexia and at-risk kindergarteners.** *Cereb Cortex* 2016;26:1138–48 [CrossRef Medline](#)
14. Zilles K, Armstrong E, Schleicher A, et al. **The human pattern of gyrification in the cerebral cortex.** *Anat Embryol (Berl)* 1988;179:173–79 [CrossRef Medline](#)
15. Lefevre J, Germanaud D, Dubois J, et al. **Are developmental trajectories of cortical folding comparable between cross-sectional datasets of fetuses and preterm newborns?** *Cereb Cortex* 2016;26:3023–35 [CrossRef Medline](#)
16. Wright R, Kyriakopoulou V, Ledig C, et al. **Automatic quantification of normal cortical folding patterns from fetal brain MRI.** *Neuroimage* 2014;91:21–32 [CrossRef Medline](#)
17. Hu HH, Chen HY, Hung CI, et al. **Shape and curvedness analysis of brain morphology using human fetal magnetic resonance images in utero.** *Brain Struct Funct* 2013;218:1451–62 [CrossRef Medline](#)
18. Clouchoux C, du Plessis AJ, Bouyssi-Kobar M, et al. **Delayed cortical development in fetuses with complex congenital heart disease.** *Cereb Cortex* 2013;23:2932–43 [CrossRef Medline](#)
19. Clouchoux C, Kudelski D, Gholipour A, et al. **Quantitative in vivo MRI measurement of cortical development in the fetus.** *Brain Struct Funct* 2012;217:127–39 [CrossRef Medline](#)
20. Dubois J, Benders M, Cachia A, et al. **Mapping the early cortical folding process in the preterm newborn brain.** *Cereb Cortex* 2008;18:1444–54 [CrossRef Medline](#)
21. Habas PA, Scott JA, Roosta A, et al. **Early folding patterns and asymmetries of the normal human brain detected from in utero MRI.** *Cereb Cortex* 2012;22:13–25 [CrossRef Medline](#)
22. Scott JA, Habas PA, Rajagopalan V, et al. **Volumetric and surface-based 3D MRI analyses of fetal isolated mild ventriculomegaly: brain morphometry in ventriculomegaly.** *Brain Struct Funct* 2013;218:645–55 [CrossRef Medline](#)
23. Im K, Pienaar R, Lee JM, et al. **Quantitative comparison and analysis of sulcal patterns using sulcal graph matching: a twin study.** *Neuroimage* 2011;57:1077–86 [CrossRef Medline](#)
24. Shimony JS, Smyser CD, Wideman G, et al. **Comparison of cortical**

- folding measures for evaluation of developing human brain. *Neuroimage* 2016;125:780–90 CrossRef Medline
25. Kuklisova-Murgasova M, Quaghebeur G, Rutherford MA, et al. **Reconstruction of fetal brain MRI with intensity matching and complete outlier removal.** *Med Image Anal* 2012;16:1550–64 CrossRef Medline
 26. Cox RW. **AFNI: what a long strange trip it's been.** *Neuroimage* 2012; 62:743–47 CrossRef Medline
 27. Serag A, Aljabar P, Ball G, et al. **Construction of a consistent high-definition spatio-temporal atlas of the developing brain using adaptive kernel regression.** *Neuroimage* 2012;59:2255–65 CrossRef Medline
 28. Derrfuss J, Brass M, von Cramon DY, et al. **Neural activations at the junction of the inferior frontal sulcus and the inferior precentral sulcus: interindividual variability, reliability, and association with sulcal morphology.** *Hum Brain Mapp* 2009;30:299–311 CrossRef Medline
 29. Im K, Jo HJ, Mangin JF, et al. **Spatial distribution of deep sulcal landmarks and hemispherical asymmetry on the cortical surface.** *Cereb Cortex* 2010;20:602–11 CrossRef Medline
 30. Leordeanu M, Hebert M. **A spectral technique for correspondence problems using pairwise constraints.** In: *ICCV'05 Proceedings of the Tenth IEEE International Conference on Computer Vision*, Washington, DC. October 17–21, 2005 CrossRef
 31. Schaer M, Cuadra MB, Tamarit L, et al. **A surface-based approach to quantify local cortical gyrification.** *IEEE Trans Med Imaging* 2008; 27:161–70 CrossRef Medline
 32. O'Leary DD, Chou SJ, Sahara S. **Area patterning of the mammalian cortex.** *Neuron* 2007;56:252–69 CrossRef Medline
 33. Hasnain MK, Fox PT, Woldorff MG. **Structure–function spatial covariance in the human visual cortex.** *Cereb Cortex* 2001;11:702–16 CrossRef Medline
 34. Welker W. **Why does cerebral cortex fissure and fold? A review of determinants of gyri and sulci.** In: Jones EG, Pertes A, eds. *Cerebral Cortex* vol. 8B. New York: Plenum; 1990:3–136 CrossRef
 35. Chen CH, Gutierrez ED, Thompson W, et al. **Hierarchical genetic organization of human cortical surface area.** *Science* 2012;335: 1634–36 CrossRef Medline
 36. Stahl R, Walcher T, De Juan Romero C, et al. **Trnp1 regulates expansion and folding of the mammalian cerebral cortex by control of radial glial fate.** *Cell* 2013;153:535–49 CrossRef Medline
 37. Miller JA, Ding SL, Sunkin SM, et al. **Transcriptional landscape of the prenatal human brain.** *Nature* 2014;508:199–206 CrossRef Medline
 38. Nishikuni K, Ribas GC. **Study of fetal and postnatal morphological development of the brain sulci.** *J Neurosurg Pediatr* 2013;11:1–11 CrossRef Medline
 39. Garel C, Chantrel E, Elmaleh M, et al. **Fetal MRI: normal gestational landmarks for cerebral biometry, gyration and myelination.** *Childs Nerv Syst* 2003;19:422–25 CrossRef Medline
 40. Rajagopalan V, Scott J, Habas PA, et al. **Local tissue growth patterns underlying normal fetal human brain gyrification quantified in utero.** *J Neurosci* 2011;31:2878–87 CrossRef Medline

Lumbar Puncture Test in Normal Pressure Hydrocephalus: Does the Volume of CSF Removed Affect the Response to Tap?

S.K. Thakur, Y. Serulle, N.P. Miskin, H. Rusinek, J. Golomb, and A.E. George

ABSTRACT

BACKGROUND AND PURPOSE: There is limited evidence to support the use of high-volume lumbar taps over lower-volume taps in the diagnosis of normal pressure hydrocephalus. The purpose of this study is to detect whether the volume of CSF removed from patients undergoing high-volume diagnostic lumbar tap test for normal pressure hydrocephalus is significantly associated with post-lumbar tap gait performance.

MATERIALS AND METHODS: This retrospective study included 249 consecutive patients who underwent evaluation for normal pressure hydrocephalus. The patients were analyzed both in their entirety and as subgroups that showed robust response to the lumbar tap test. The volume of CSF removed was treated as both a continuous variable and a discrete variable. Statistical tests were repeated with log-normalized volumes.

RESULTS: This study found no evidence of a relationship between the volume of CSF removed during the lumbar tap test and subsequent gait test performance in the patient population (Pearson coefficient $r = 0.049 - 0.129$). Log normalization of the volume of CSF removed and controlling for age and sex failed to yield a significant relationship. Subgroup analyses focusing on patients who showed greater than 20% improvement in any of the gait end points or who were deemed sufficiently responsive clinically to warrant surgery also yielded no significant relationships between the volume of CSF removed and gait outcomes, but there were preliminary findings that patients who underwent tap with larger-gauge needles had better postprocedure ambulation among patients who showed greater than 20% improvement in immediate time score ($P = .04$, $n = 62$).

CONCLUSIONS: We found no evidence to support that a higher volume of CSF removal impacts gait testing, suggesting that a high volume of CSF removal may not be necessary in a diagnostic lumbar tap test.

ABBREVIATIONS: FAP = functional ambulation performance; LTT = lumbar tap test; NPH = normal pressure hydrocephalus

Idiopathic normal pressure hydrocephalus (NPH) is a debilitating disorder characterized by a triad of gait disturbance, cognitive impairment, and urinary incontinence.^{1,2} Patients correctly diagnosed with NPH who undergo ventricular shunt placement may have marked improvement of their symptoms.¹ Selection of patients who will undergo ventricular shunt may be challenging. When based

solely on patient history, basic neuroimaging with MR imaging or CT, and neurologic testing, the positive predictive value of patient improvement after shunting ranges from less than 50% to 61%.³

The diagnosis of NPH is characterized by several neuroimaging features, including ventricular dilation in the presence of normal gray matter volume, but despite a very large number of publications since 1964, the role of neuroimaging in predicting the response to shunting remains uncertain.^{4,5} Tarnaris et al⁶ performed a literature review of 69 studies published between 1980 and 2006 to examine the role of structural as well as functional imaging in providing biomarkers of favorable surgical outcome in NPH. The papers reviewed included studies of structural CT and MR imaging features;^{4,6-9} phase-contrast MR imaging studies of aqueductal CSF velocity and stroke volumes;¹⁰⁻¹² and functional studies including xenon-enhanced CT,¹³ FDG-PET,^{14,15} single-photon emission CT,¹⁶ and MR imaging spectroscopy.¹⁷ Studies showing the value of the individual techniques are often coun-

Received September 22, 2016; accepted after revision February 15, 2017.

From the Departments of Radiology (S.K.T., H.R., A.E.G.) and Neurology (J.G.), New York University School of Medicine, New York, New York; Department of Radiology (Y.S.), University of Maryland Medical Center, Baltimore, Maryland; and Department of Radiology (N.P.M.), Brigham and Women's Hospital, Boston, Massachusetts.

Paper previously presented at: American Society of Neuroradiology Annual Meeting and the Foundation of the ASNR Symposium, May 18–23, 2013; San Diego, California.

Please address correspondence to Ajax E. George, MD, 560 First Ave, New York, NY 10016; e-mail: ajax.george@nyulmc.org

<http://dx.doi.org/10.3174/ajnr.A5187>

tered by studies showing contradictory results. The authors conclude that at present, no single imaging technique may assist clinicians in selecting patients for shunt placement and that invasive studies will remain the mainstay of the process of selecting patients for CSF diversion procedures.⁶

The high-volume lumbar tap test (LTT) is one of the most widely used invasive tests to predict shunt response. It consists of a lumbar puncture wherein a large volume (typically 40–50 mL) of CSF is removed, with gait testing occurring before, 1–4 hours after, and 24 hours after the LTT. Transient recovery in gait after the LTT has been considered a positive prognostic indicator for surgery, but no response after the LTT warrants further investigation.^{18–24} A 2016 review by Mihalj et al²⁵ found the LTT to have an average published sensitivity of 58%, specificity of 75%, and accuracy of 62% in predicting positive response to shunt over 8 included studies. Complications that may compromise the effectiveness of high-volume LTT include headache and pain that may be pronounced enough to compromise gait testing.²¹

External lumbar drainage testing requires hospital admission and placement of a lumbar intrathecal catheter for CSF drainage at 10 mL per hour for 72 hours. Studies evaluating external lumbar drainage routinely exclude patients who responded to the LTT, making it difficult to directly compare external lumbar drainage and LTT.²⁴ External lumbar drainage has a reported sensitivity between 60% and 100% and a specificity between 80% and 100%.²⁶

There are several protocols for invasive testing of Ro, the impedance of CSF flow by absorption pathways, to predict shunt response. Given the heterogeneity of techniques and limited studies, sensitivity ranges from 58%–100% and specificity ranges from 44%–92% between protocols and research series.^{24,27,28} Complication rates similarly vary, with up to 20% in 1 series of 107 patients reporting headaches after fluid infusion for impedance testing.^{24,29}

Given the relative ease of administration and low incidence of complications, the LTT is routinely performed as the first test to determine whether a patient will respond to shunting. Those patients who do not respond to the LTT can progress to external lumbar drainage for further evaluation.²⁶ Although the LTT is commonly performed with large-volume CSF removal, to our knowledge, no study has addressed the optimal amount of CSF required to be removed to have an accurate test. Contrary to the high-volume LTT used today, in the original description of NPH by Hakim and Adams,¹ they noted improvement the next day in patients after an LTT removing only 10–15 mL of CSF. In 1982, Wikkelsø et al³⁰ proposed the drainage of 50 mL of CSF, but future studies did not corroborate that this was an optimum volume. We examined the relationship between the volume of CSF removed and change in gait patterns among patients with clinically diagnosed NPH.

MATERIALS AND METHODS

Institutional Review Board Status

This anonymous, retrospective, single-center study was exempt from institutional review board approval and patient informed consent.

Patients and Protocol

We analyzed 249 consecutive patients with a clinical diagnosis of NPH who were treated by a standard protocol at an academic center that specializes in brain aging, between 2000 and 2013.

Patients were referred from a variety of academic and outside clinical sources to an academic specialty clinic that has focused on NPH for more than 20 years. Patients were referred for evaluation because of symptoms related to NPH, especially gait impairment with associated urinary incontinence or gait impairment with associated enlarged ventricles on MR or CT studies concerning for hydrocephalus. Patients received detailed neurologic and medical evaluation by a neurologist who specialized in NPH diagnosis and management. Patients were referred for an LTT if the clinical judgment suggested NPH to determine whether the spinal tap resulted in gait improvement. Image analysis was performed by neuroradiologists who were asked to evaluate for NPH and imaging evidence of other etiologies of dementia and were not blinded to patient history. Lumbar taps were performed by attending neuroradiologists or neuroradiology fellows under direct supervision. All taps were performed under fluoroscopic guidance. The neuroradiologists performing the LTTs were instructed to remove up to 50 mL of CSF and had no stated minimum volume of CSF to remove; the designated spinal needle was 18G as per procedure protocol. In a subset of cases, a 20G needle was used as per the performing neuroradiologist's preference. The volume of CSF removed was determined by summing the fluid in each of the vials used to collect the fluid; the vials were calibrated with volume markers 1–8 mL.

The volume of CSF removed was measured during the procedure and recorded in the clinical notes. We excluded patients who required multiple attempts to obtain a lumbar tap, including those patients who required 2 or more appointments because of unsuccessful taps and those patients who required multiple attempts within the same appointment. The number of attempted taps was based on postprocedure medical notes. Clinical diagnosis was based on the presence of ventriculomegaly on imaging and clinical symptoms of incontinence, gait disturbance, and dementia. Patients received gait testing before, 1–2 hours after, and 24 hours after the LTT. Gait testing consisted of the time it took to walk 30 meters (time score) and a composite functional ambulation performance (FAP) score calculated by a Gaitrite machine (CIR Systems, Franklin, New Jersey). FAP ranged from 0 (unable to walk) to 100 (optimal walking ability).³¹ Both time score and FAP score were measured 2–5 times at each gait test; we used the mean score of each test. Thus, we had a total of 4 assessment values for gait after LTT: time and FAP scores immediately after the LTT and time and FAP scores 24 hours after the LTT. Both velocity³² and Gaitrite FAP³¹ have been found to improve in patients with NPH after LTT, with those patients showing larger improvement more likely to respond to shunt surgery.

Statistics

We used IBM SPSS 20 (IBM, Armonk, New York) and R Studio (<http://rstudio.org/download/desktop>) for our statistical analyses. We analyzed all 249 patients as a group. We created 4 additional overlapping subgroups consisting of patients who showed a 20% or greater improvement in any of the 4 LTT measures. We

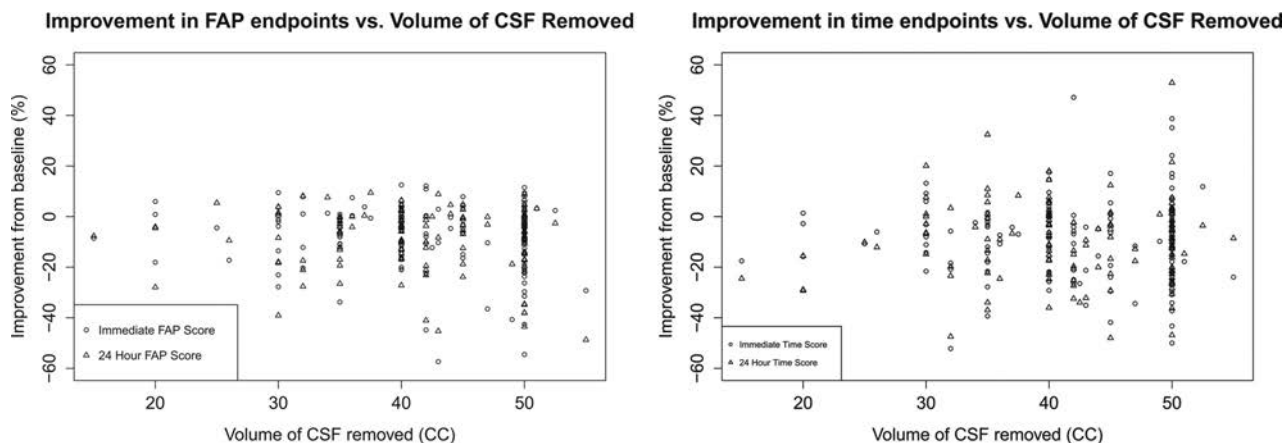


FIG 1. Percentage improvement in 4 end points versus volume of CSF removed. For each end point, there was no significant relationship between the volume of CSF removed and percentage improvement from baseline ($r = 0.049$ – 0.129).

created an additional subgroup of patients who were deemed clinically responsive to the LTT and subsequently advanced to shunt surgery. Clinical response reflected the treating neurologist's judgment on whether the patient showed sufficient improvement in measured outcomes like gait, as well as in patient-reported measures such as urinary incontinence, to warrant placement of a shunt. The current literature is ambiguous about defining what merits an effective response to an LTT, with no definitive guidelines followed by clinicians.^{19,21,32} We defined our cutoffs to maximize the magnitude of improvement while maintaining a sufficient sample size to do meaningful statistical analyses.

We used regression analysis on our total sample and our subgroups to look for a correlation between the volume of CSF removed in LTT and the percentage change in any of our 4 gait assessments (relative to baseline time and FAP scores recorded before the LTT.) A partial correlation was run to determine the relationship between the volume of CSF removed and a patient's gait improvement measures while controlling for age and sex. We used Student *t* tests to examine whether needle gauge (18G versus 20G) had any association with the gait assessments. We used χ^2 analysis to look for an association between LTT volume ("high" or "low," where high was defined as ≥ 40 mL) and response to LTT ("response" or "no response," using 20% improvement as a cutoff for response).

RESULTS

Patient Characteristics

Patients had an average age of 77.4 years (range, 52–91 years) at the time of LTT; 45% were female and 55% were male.

Patients had an average of 41.2 mL of CSF removed during the LTT (range, 8–55 mL; 25th percentile, 35 mL; median, 40 mL; 75th percentile, 50 mL). Approximately 71% of patients had 40 mL or greater of CSF removed, and 29% had less than 40 mL of CSF removed. The volume of CSF removed was not related to patient age or sex (per multiple regression, $P = .255$ – $.861$) or needle gauge (per *t* test comparing mean mL removed between 20G and 18G patients, $P = .5086$). Patients showed a 10.6% (95% CI, 8.1%–13.0%) and 11.1% (95% CI, 9.0%–13.3%) improvement in time score immediately and 24 hours after the LTT. Patients showed an average improvement of 8.1% (95% CI, 6.2%–

9.9%) and 8.6% (95% CI, 7.0%–10.2%) in FAP score immediately and 24 hours after the LTT.

Entire Sample Analysis

Regression analysis was performed to assess the relationship between the volume of CSF removed and the percentage change in each of the following tests: time and FAP scores immediately after the LTT and time and FAP scores 24 hours after the LTT. Pearson coefficients ranged from $r = 0.049$ – 0.129 . Given the skew in the volume of CSF removed, the analysis was repeated with logarithmic normalization of the volume of CSF removed. This correction yielded no significant changes in these results. Using partial correlations that control for age and sex, we found no relationship between CSF removed and the 4 measures of gait changes: $\Delta T\%$ ($r = 0.006$, $P = .935$), $\Delta T24\%$ ($r = -0.034$, $P = .658$), $\Delta FAP\%$ ($r = 0.121$, $P = .131$), and $\Delta FAP24\%$ ($r = 0.128$, $P = .126$). Next, we assessed the importance of the needle gauge used for the LTT (18 versus 20). There was no significant association between needle gauge and improvement ($P = .283$ – $.410$).

Subset Analysis

Given that not all patients in our cohort responded to the LTT, the analyses of the possible effects of the volume of CSF removed on response were repeated on subsets of patients who showed robust response. Thus, subsets of patients were created based on either showing a 20% improvement in any of the 4 gait tests or proceeding to shunt surgery. The 5 overlapping subsets, therefore, were patients who showed a response to time score immediately after the LTT ($n = 62$), patients who showed a response 24 hours after the LTT ($n = 60$), patients who showed a response to FAP score immediately after the LTT ($n = 31$), patients who showed a response to FAP score 24 hours after the LTT ($n = 23$), and patients who underwent shunt surgery ($n = 97$).

Regression analysis yielded no significant correlation between volume of CSF removed and any of the 4 end points, with no significant change in results with log normalization of the volume of CSF removed. The Figure shows 4 plots of improvement in the end point versus the volume of CSF removed of the nonnormalized data. There was a significant finding, however, between needle gauge and certain end points in some of the subgroups.

Among patients who showed an improvement in time score immediately after the LTT, patients whose taps involved a larger-bore needle showed a statistically significantly greater improvement in immediate time score (95% CI, $33.1\% \pm 5.0\%$ for 18G versus $27.0\% \pm 2.5\%$ for 20G; $P = .04$). An analysis of subgroup characteristics showed no significant difference between the 18G and 20G groups in terms of the volume of CSF removed ($P = .43$), sex ($P = .17$), and age ($P = .18$). Among patients who showed improvement in time score 24 hours after the LTT, patients whose taps involved a larger-bore needle had a nonsignificant tendency to have greater improvement in 24-hour time score (95% CI, $32.3\% \pm 3.7\%$ for 18G, $26.5\% \pm 4.4\%$ for 20G; $P = .06$). Again, groups were similar in the volume of CSF removed ($P = .72$) and sex ($P = .99$), but this time differed significantly in age (mean of 20G patients was 87.5 years versus 82.1 years for 18G patients; $P = .021$).

In our final subgroup analysis, we divided patients into those who received higher-volume LTTs (≥ 40 mL; $n = 176$) or lower-volume (< 40 mL; $n = 73$) LTTs. There was no difference between these groups in terms of age ($P = .93$) or sex ($P = .40$). χ^2 analysis was performed to assess for a relationship between higher or lower volume of CSF removed and response to the LTT ("response" or "no response"). No statistically significant relationship was found ($P = .19-.90$) for any of the 4 LTT end points.

DISCUSSION

This study examined the relationship between the volume of CSF removed in an LTT and changes in patient gait. As prior studies noted, gait disturbance is the symptom that shows the most dramatic improvement after an LTT and shunting.¹⁹ The main conclusion of the current study is that within the 28–50 mL range (values between the 5th and 95th percentile), there is no significant association between the volume of CSF removed and gait outcomes.

Although high-volume spinal tap has been established as an accurate method to diagnose NPH and to identify patients who will likely benefit from shunt surgery, to our knowledge, there is no consensus on the amount of CSF required to be removed. The first formal study of the LTT by Wikkelsø et al³⁰ in 1982 removed 40–50 mL of CSF in LTT, but the authors noted that there was no prior evidence that this was the ideal range. Prior reports, including the original description by Hakim and Adams¹, frequently removed much smaller volumes of CSF.

In the current study, there was no association between the volume of CSF removed and improvement of gait testing after an LTT. The range of CSF removed in patients who showed a $\geq 20\%$ improvement in a gait test was 15–55 mL. Our results indicate that as little as 15 mL removed in an LTT may be enough to have a good outcome.

This study took several steps to reduce the probability that a significant relationship between the volume of CSF removed and gait outcomes was missed. First, this study looked at a sample ($n = 249$) that was much larger than typical NPH studies. In choosing a large sample, we had significantly more statistical power to detect weak relationships.

Second, several steps were taken to ensure that the distribution of the volume of CSF removed did not impact results. Given that

practitioners currently aim for LTTs to remove 50 mL of fluid, the distribution of volume removed was skewed toward higher volumes of CSF. This skew, in turn, could impact regression analysis. Log normalization of the data, however, failed to produce significant results. Furthermore, the χ^2 analysis treated the volume of CSF removed as a categorical variable, which would minimize the effects of skew on results. The χ^2 analysis also failed to show a significant relationship.

Third, given that the data from patients who did not respond to an LTT may mask trends in patients who did respond, a subset analysis was performed that looked only at patients who showed response to an LTT. There is no consensus on what cutoff should be used to determine response, so this study chose 20%, the highest cutoff the authors found in the literature. Because of the high cutoff, these subsets consisted only of patients who showed a very robust response to an LTT. These were the patients we suspected would most likely show a relationship between the volume of CSF removed and LTT outcomes if such a relationship existed. Regardless, there was no such evidence from these subsets.

Fourth, given that some patients may show a response to an LTT that manifested in ways that were appreciated clinically but not necessarily demonstrated in gait testing, this study looked at a subset of patients who went on to receive shunts. As with the other subsets, this subset failed to demonstrate a significant relationship between the volume of CSF removed and any of the gait outcomes.

Given the lack of evidence that the volume of CSF removed by an LTT correlates to gait outcomes, an alternative explanation for why patients show improved gait after an LTT is that there is passive flow of CSF from the puncture site created by the needle. If this were the case, then the data would show that an 18G needle (which has twice the surface area as a 20G needle) might lead to better gait outcomes. In line with this theory, we found preliminary evidence for a potential role of needle gauge in determining LTT outcomes. There was a relationship between larger-bore needles and improved immediate time score among patients who showed a $\geq 20\%$ improvement in immediate time score ($P = .04$) and between larger-bore needles and 24-hour time score in patients who showed a $\geq 20\%$ improvement in 24-hour time score ($P = .06$). Of note, there was no difference in baseline features between the 18G and 20G patients who showed a significant response in immediate time score. Among the patients who showed response at 24 hours, the 20G patients were significantly older (87.5 years versus 82.1 years).

The major weakness in this study is its retrospective nature and lack of randomization. Although we demonstrated no difference in age or sex between the groups that had higher or lower volumes of LTT, other differences may exist between the subgroups (eg, failed taps) that may confound the data. The ideal follow-up study should have a randomized, prospective design to demonstrate the lack of clinical benefit in draining 50 mL rather than 30–35 mL of CSF. In our data analysis, however, we did find that no patient characteristics such as age, sex, or needle gauge correlated with CSF removed, so the volume of CSF removed was essentially a random variable in this retrospective investigation.

CONCLUSIONS

The main conclusion of the current study is that within the 28–50 mL range (values between the 5th and 95th percentile), there is no significant association between the volume of CSF removed and gait outcomes. Future studies should use a prospective, randomized, and controlled methodology to evaluate whether a higher volume of CSF removal is necessary in the LTT and, separately, whether the use of a larger needle bore size improves performance in subsequent gait testing.

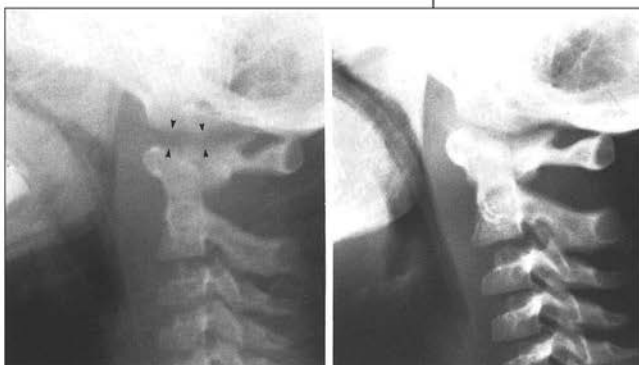
Disclosures: Ajax George—UNRELATED: Employment: NYU Langone Medical Center, Comments: full-time attending neuroradiologist; Patents (Planned, Pending or Issued): polynomial prediction of NPH using MRI (pending); Travel/Accommodations/Meeting Expenses Unrelated to Activities Listed: NYU, Comments: travel funds to attend academic meetings.

REFERENCES

1. Hakim S, Adams RD. The special clinical problem of symptomatic hydrocephalus with normal cerebrospinal fluid pressure. Observations on cerebrospinal fluid hydrodynamics. *J Neurol Sci* 1965;2: 307–27 CrossRef Medline
2. Larsson A, Wikkelsö C, Bilting M, et al. Clinical parameters in 74 consecutive patients shunt operated for normal pressure hydrocephalus. *Acta Neurol Scand* 1991;84:475–82 CrossRef Medline
3. Klinge P, Marmarou A, Bergsneider M, et al. Outcome of shunting in idiopathic normal-pressure hydrocephalus and the value of outcome assessment in shunted patients. *Neurosurgery* 2005;57(3 Suppl):S40–52; discussion ii–v CrossRef Medline
4. Serulle Y, Rusinek H, Kirov II, et al. Differentiating shunt-responsive normal pressure hydrocephalus from Alzheimer disease and normal aging: pilot study using automated MRI brain tissue segmentation. *J Neurol* 2014;261:1994–2002 CrossRef Medline
5. Miskin N, Serulle Y, Wu W, et al. Post-shunt gait improvement correlates with increased cerebrospinal fluid peak velocity in normal pressure hydrocephalus: a retrospective observational phase-contrast magnetic resonance imaging study. *Int J Sci Study* 2015;3:48–54
6. Tarnaris A, Kitchen ND, Watkins LD. Noninvasive biomarkers in normal pressure hydrocephalus: evidence for the role of neuroimaging. *J Neurosurg* 2009;110:837–51 CrossRef Medline
7. Golomb J, de Leon MJ, George AE, et al. Hippocampal atrophy correlates with severe cognitive impairment in elderly patients with suspected normal pressure hydrocephalus. *J Neurol Neurosurg Psychiatry* 1994;57:590–93 CrossRef Medline
8. Holodny AI, George AE, de Leon MJ, et al. Focal dilation and paradoxical collapse of cortical fissures and sulci in patients with normal-pressure hydrocephalus. *J Neurosurg* 1998;89:742–47 CrossRef Medline
9. Holodny AI, Waxman R, George AE, et al. MR differential diagnosis of normal-pressure hydrocephalus and Alzheimer disease: significance of perihippocampal fissures. *AJNR Am J Neuroradiol* 1998;19: 813–19 Medline
10. Bradley WG Jr, Whittemore AR, Kortman KE, et al. Marked cerebrospinal fluid void: indicator of successful shunt in patients with suspected normal-pressure hydrocephalus. *Radiology* 1991; 178:459–66 CrossRef Medline
11. Bradley WG Jr, Scalzo D, Queralt J, et al. Normal-pressure hydrocephalus: evaluation with cerebrospinal fluid flow measurements at MR imaging. *Radiology* 1996;198:523–29 CrossRef Medline
12. Bradley WG, Safar FG, Furtado C, et al. Increased intracranial volume: a clue to the etiology of idiopathic normal-pressure hydrocephalus? *AJNR Am J Neuroradiol* 2004;25:1479–84 Medline
13. Tamaki N, Kusunoki T, Wakabayashi T, et al. Cerebral hemodynamics in normal-pressure hydrocephalus. Evaluation by ^{133}Xe inhalation method and dynamic CT study. *J Neurosurg* 1984;61:510–14 CrossRef Medline
14. Jagust WJ, Friedland RP, Budinger TF. Positron emission tomography with ^{18}F fluorodeoxyglucose differentiates normal pressure hydrocephalus from Alzheimer-type dementia. *J Neurol Neurosurg Psychiatry* 1985;48:1091–96 CrossRef Medline
15. George AE, de Leon MJ, Miller J, et al. Positron emission tomography of hydrocephalus. Metabolic effects of shunt procedures. *Acta Radiol Suppl* 1985;369:435–39 Medline
16. Waldemar G, Schmidt JF, Delecluse F, et al. High resolution SPECT with $^{99\text{m}}\text{Tc}$ -d,l-HMPAO in normal pressure hydrocephalus before and after shunt operation. *J Neurol Neurosurg Psychiatry* 1993; 56:655–64 CrossRef Medline
17. Kizu O, Yamada K, Nishimura T. Proton chemical shift imaging in normal pressure hydrocephalus. *AJNR Am J Neuroradiol* 2001;22: 1659–64 Medline
18. Ahlberg J, Norlén L, Blomstrand C, et al. Outcome of shunt operation on urinary incontinence in normal pressure hydrocephalus predicted by lumbar puncture. *J Neurol Neurosurg Psychiatry* 1988; 51:105–08 CrossRef Medline
19. Ravdin LD, Katzen HL, Jackson AE, et al. Features of gait most responsive to tap test in normal pressure hydrocephalus. *Clin Neurol Neurosurg* 2008;110:455–61 CrossRef Medline
20. Shprecher D, Schwalb J, Kurlan R. Normal pressure hydrocephalus: diagnosis and treatment. *Curr Neurol Neurosci Rep* 2008;8:371–76 CrossRef Medline
21. Virhammar J, Cesarini KG, Laurell K. The CSF tap test in normal pressure hydrocephalus: evaluation time, reliability and the influence of pain. *Eur J Neurol* 2012;19:271–76 CrossRef Medline
22. Sand T, Bovim G, Grimse R, et al. Idiopathic normal pressure hydrocephalus: the CSF tap-test may predict the clinical response to shunting. *Acta Neurol Scand* 1994;89:311–16 CrossRef Medline
23. Walchenbach R, Geiger E, Thomeer RT, et al. The value of temporary external lumbar CSF drainage in predicting the outcome of shunting on normal pressure hydrocephalus. *J Neurol Neurosurg Psychiatry* 2002;72:503–06 Medline
24. Marmarou A, Bergsneider M, Klinge P, et al. The value of supplemental prognostic tests for the preoperative assessment of idiopathic normal-pressure hydrocephalus. *Neurosurgery* 2005;57(3 Suppl):S17–28; discussion ii–v CrossRef Medline
25. Mihalj M, Dolić K, Kolić K, et al. CSF tap test - obsolete or appropriate test for predicting shunt responsiveness? A systemic review. *J Neurol Sci* 2016;362:78–84 CrossRef Medline
26. Mori E, Ishikawa M, Kato T, et al. Guidelines for management of idiopathic normal pressure hydrocephalus: second edition. *Neurol Med Chir (Tokyo)* 2012;52:775–809 CrossRef
27. Malm J, Kristensen B, Karlsson T, et al. The predictive value of cerebrospinal fluid dynamic tests in patients with the idiopathic adult hydrocephalus syndrome. *Arch Neurol* 1995;52:783–89 CrossRef Medline
28. Takeuchi T, Kasahara E, Iwasaki M, et al. Indications for shunting in patients with idiopathic normal pressure hydrocephalus presenting with dementia and brain atrophy (atypical idiopathic normal pressure hydrocephalus). *Neurol Med Chir (Tokyo)* 2000;40:38–46; discussion 46–47 CrossRef
29. Meier U, Bartels P. The importance of the intrathecal infusion test in the diagnosis of normal-pressure hydrocephalus. *Eur Neurol* 2001;46:178–86 CrossRef Medline
30. Wikkelsø C, Andersson H, Blomstrand C, et al. The clinical effect of lumbar puncture in normal pressure hydrocephalus. *J Neurol Neurosurg Psychiatry* 1982;45:64–69 CrossRef Medline
31. Williams MA, Thomas G, de Lateur B, et al. Objective assessment of gait in normal-pressure hydrocephalus. *Am J Phys Med Rehabil* 2008;87:39–45 CrossRef Medline
32. Warnecke K. Analysis of gait before and after cerebrospinal fluid lumbar tap test in idiopathic normal pressure hydrocephalus: a literature review and case report. *Top Geriatr Rehabil* 2009;25:203–10 CrossRef

Celebrating 35 Years of the AJNR

July 1982 edition



Traumatic Longitudinal Atlanto-occipital Distraction Injuries in Children

Traumatic atlanto-occipital dislocation with survival is possible and, in fact may be relatively more common than once thought. The spectrum of neurologic manifestations is broader than previously described and does not necessarily end in death or tragic neurologic deficit. Radiographic diagnosis of this injury may be difficult, particularly in the longitudinal distraction-dislocation type. Although several methods have been proposed to evaluate the atlanto-occipital relationship, none of these is infallible in the recognition of distraction injury in children. Immobilization rather than skeletal traction provides sufficient immediate stabilization when the dislocation at the atlanto-occipital junction is of the longitudinal distraction type. Three cases are reported; in one, death occurred early; in the second, recovery was partial, but sudden death occurred 2 years later; the third child recovered fully.

Traumatic atlanto-occipital dislocation is a rare injury of the craniovertebral junction and is thought to be immediately fatal in most instances [1]. There are but 16 well documented cases of survival following this injury; in three, death occurred within 36 hr. Nine of these 16 cases were adults. We report three children who were seen recently, two of whom survived this injury. The importance of longitudinal atlanto-occipital distraction is stressed, and several new aspects of this injury, its radiographic evaluation, and its treatment are suggested.

Case Reports

Case 1

A 5½-year-old girl was a passenger in the front seat of an auto when it hit a tree. Her head hit the dashboard and she slumped unresponsive in the front seat. She became apneic and cyanotic and immediate cardiopulmonary resuscitation (CPR) led to improvement in color.

On arrival at Children's Hospital Medical Center (CHMC) emergency room she had no palpable blood pressure, no spontaneous movement, and no spontaneous respiration. Neurologic examination revealed flaccid paralysis and absent deep tendon reflexes, but a positive response to deep pain in the lower extremities. Slight toe flexion occurred in response to plantar stimulation. Cranial nerves were intact. Her blood pressure responded to intravenous fluids and manual ventilation by resuscitation bag. She was cautiously intubated and placed on a ventilator, her neck immobilized. Bedside radiographs of the cervical spine showed longitudinal atlanto-occipital distraction (Fig. 1), and the child was thought to have a brain stem contusion as well.

Within the first 10 days of admission she awoke and could respond to communication by blinking. There was some recovery of deep tendon reflexes in her lower extremities. She required posterior wiring of C1 to the occiput for atlanto-occipital stabilization. During the next 10 months she progressed slowly and eventually could vocalize weakly and move all four extremities weakly. She was alert and oriented and her mental status was normal. However, she suffered from speech difficulties and was unable to swallow solid foods. She continued to experience occasional nocturnal dusky episodes and required an apnea monitor at home. She died suddenly 2 years after injury. No autopsy was performed.

Received June 12, 1981; accepted after revision January 6, 1982.

¹Department of Radiology, University of Cincinnati College of Medicine, Children's Hospital Medical Center, Eland & Bethesda Ave., Cincinnati, OH 45229. Address reprint requests to R. A. Kaufman.

²Department of Radiology, University of Cincinnati College of Medicine, Cincinnati General Hospital, Cincinnati, OH 45267.

³Department of Surgery, University of Cincinnati College of Medicine, Cincinnati, OH 45267.

AJNR 3:379-385, July/August 1982
0195-6108/82/0304-0379\$05.00
© American Roentgen Ray Society

Computed Tomographic Anatomy of the Temporal Bone

Chat Virapongse¹
Stephen L. G. Rothman
E. Leon Kier
Mahammad Sarwar

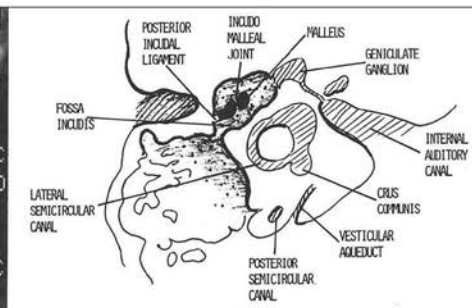
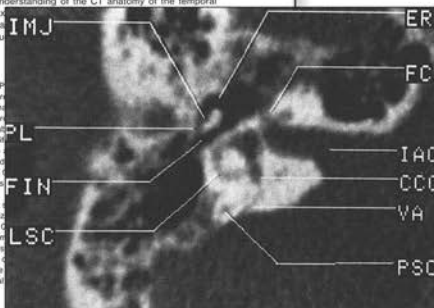
With the recent development of high-resolution computed tomography (CT), there is a growing need to explore the full potential of this new method in demonstrating the detailed anatomy of the temporal bone. For this purpose, dry skulls with intact ossicles were scanned in axial and coronal projections. The detailed CT anatomy of the temporal bone was documented, complemented by images from live patients. Because of its superior contrast resolution, CT was able to demonstrate numerous structures, such as the tympanic membrane, ossicles, and supporting structures, hitherto never or poorly visualized by any other method. In addition, the ease by which axial sections of the temporal bone could be obtained is of great benefit in displaying several structures previously difficult to evaluate.

Computed tomographic (CT) scanning has proven to be indispensable in the evaluation of intracranial pathology, but its role in the evaluation of the temporal bone anatomy and pathology has not been fully explored [1]. Recent improvements in CT scanners have made available detailed information of the temporal bone [2], and certain structures that were previously poorly visible by other methods are now clearly seen [1-6]. The wealth of anatomic data displayed in various projections on CT poses a diagnostic challenge to neuroradiologists and clinicians. Furthermore, the understanding of the CT anatomy of the temporal bone is difficult due to complex anatomy. Our system was designed to demonstrate and document the anatomy of the temporal bone.

Materials and Methods

All scans were obtained with a PDP-11 scanner. The scanner contains a detector array of 128 channels. The detectors are collimated to the beam. The x-ray beam width is narrow and is collimated to 2 mm by a removable collimator. The scanning algorithm is modified and by decreasing the translation two software modifications and of resolution allowing visualization of small structures in the temporal bone in the usual manner.

Hounsfield [3] suggested that degraded by graininess at pixel size projected the epitympanum into the middle ear. This disadvantage recomputing the opposite temporal bone is difficult due to complex anatomy. Our system was designed to demonstrate and document the anatomy of the temporal bone.



This article appears in the July/August 1982 issue of AJNR and the October 1982 issue of AJNR.

Received March 5, 1981; accepted after revision January 6, 1982.

Presented at the annual meeting of the American Society of Neuroradiology, Chicago, April, 1981.

*All authors: Department of Diagnostic Radiology, Section of Neuroradiology, Yale University School of Medicine, 333 Cedar St., New Haven, CT 06510. Address reprint requests to C. Virapongse.

AJNR 3:379-385, July/August 1982
0195-6108/82/0304-0379\$05.00
© American Roentgen Ray Society

3D-Printed Patient-Specific Models for CT- and MRI-Guided Procedure Planning



Image-guided, minimally invasive percutaneous ablations of primary and metastatic tumors are increasingly being performed in the head/neck and the spine. Thermal (radiofrequency, laser, microwave, cryoablation) and nonthermal (irreversible electroporation) ablation techniques provide symptomatic relief in patients considered to be poor surgical candidates, but are associated with a steep learning curve and often require careful planning given the individual patient's anatomy.¹ Safety is also a concern,² particularly as new application sites are explored, such as the posterior spinal elements.³

3D printing is an emerging technology for presurgical planning and simulation, intraoperative navigation, and physician training.⁴ Models of patient anatomy that are 3D-printed from medical images provide spatial comprehension and tactile feed-

back with the ability to peel away layers of anatomy, providing insight into underlying pathology. To date, 3D-printed simulation of minimally invasive procedures has been limited to conventional angiography procedures, where hollow, radiopaque vascular models can be readily 3D-printed. The next barrier to overcome in this technology is the development of 3D-printing materials and printing techniques that yield models visible with other imaging modalities.

Last year, we began searching for polymeric materials⁴ that possess protons with sufficient mobility to escape substantial dipolar broadening and ultrashort T2 values, so as to enable imaging of 3D-printed models in clinical MR imaging systems.⁵ We aimed to leverage such materials to produce models exhibiting different image characteristics for distinct tissues in both CT and MR imaging.

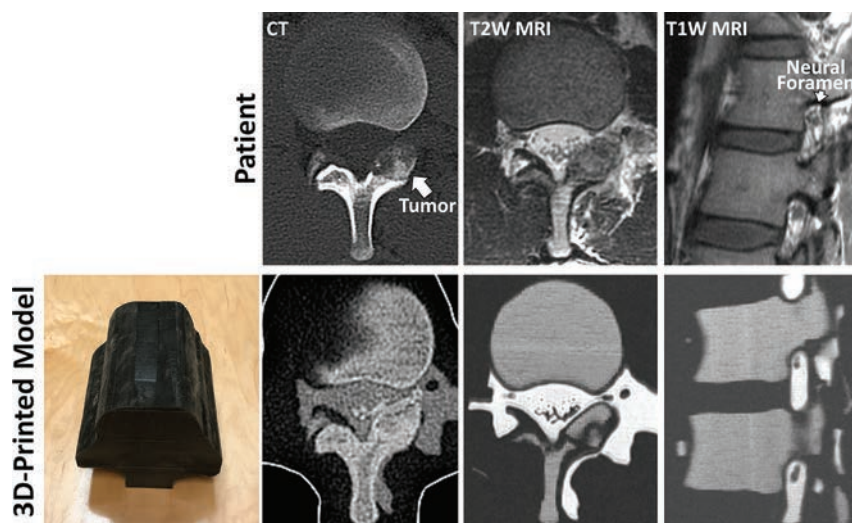


FIGURE. 3D-printed model of the lumbar spine (*bottom left panel*) of a patient with L1 left lamina osteoblastoma, designed to replicate the patient's anatomy as seen in the patient's diagnostic CT and MR imaging (*top row*). The outer *black* shell of the model is printed in a soft material to mimic soft tissue properties. CT of the 3D-printed model demonstrates cortical and cancellous bone with differential CT Hounsfield units, whereas MR imaging of the model demonstrates cancellous bone with intermediate and cortical bone with dark signal. Neural foramen and nerve root, key structures monitored during MR imaging-guided cryoablation as this patient underwent, are clearly visualized in the MR imaging of the printed model.

Indicates open access to non-subscribers at www.ajnr.org

<http://dx.doi.org/10.3174/ajnr.A5189>

We now bring to your attention this new technique to 3D-print models replicating patient-specific, complex intertwined anatomy in both CT and MR imaging. A model of a patient with an L1 left lamina osteoblastoma was 3D-printed from the patient's diagnostic CT and MR imaging. Tissues visualized (ie, segmented) in each of the 2 diagnostic scans were spatially aligned to produce a single model combining them. Different mixtures of one MR imaging–visible⁵ and one non-MR imaging–visible material, both of which are radiopaque, were used to produce a model displaying the patient's cortical and cancellous bone and osteoblastoma (as visualized in the patient's CT), spinal nerves, CSF, and epidural fat (as visualized in the patient's MR imaging) with distinct signal characteristics in each imaging modality (Figure).

This model can be used to simulate CT-guided power drilling and subsequent MR imaging–monitored cryoablation (as ice ball formation is not readily visualized on CT in vivo). This is, in fact, the procedure that this patient underwent at our institution. The signal intensity of the model in MR imaging allowed visualization of the neural foramen and nerve root, key structures monitored during this procedure.

Much further research remains in the field, including the development of 3D-printed materials that better match tissue properties and image characteristics (eg, MR relaxation rates and CT Hounsfield units). However, this new 3D-printing technique holds great promise for image-guided procedure planning toward assessing safety and efficacy and also, importantly, for hands-on training where, at present, limited options, such as virtual reality systems, are currently being explored.

Dr. Dimitrios Mitsouras received research funding from the National Institutes of Health–National Institute of Biomedical Imaging and Bioengineering, grant number: K01 EB015868 and Vital Images, a Toshiba Medical Systems Company. Dr. Thomas C. Lee received research funding from the National Institutes of Health–National Institute of Biomedical Imaging and Bioengineering, grant number: U41 RR019703.

REFERENCES

1. Hinshaw JL, Lubner MG, Ziemlewicz TJ, et al. **Percutaneous tumor ablation tools: microwave, radiofrequency, or cryoablation—what should you use and why?** *Radiographics* 2014;34:1344–62 [CrossRef Medline](#)
2. Kurup AN, Morris JM, Schmit GD, et al. **Neuroanatomic considerations in percutaneous tumor ablation.** *Radiographics* 2013;33:1195–215 [CrossRef Medline](#)
3. Philip A, Gupta S, Ahrar K, et al. **A spectrum of nerve injury after thermal ablation: a report of four cases and review of the literature.** *Cardiovasc Intervent Radiol* 2013;36:1427–35 [CrossRef Medline](#)
4. Mitsouras D, Liacouras P, Imanzadeh A, et al. **Medical 3D printing for the radiologist.** *Radiographics* 2015;35:1965–88 [CrossRef Medline](#)
5. Mitsouras D, Lee TC, Liacouras P, et al. **Three-dimensional printing of MRI-visible phantoms and MR image-guided therapy simulation.** *Magn Reson Med* 2017;77:613–22 [CrossRef Medline](#)

 **E. George**

Department of Radiology
Brigham and Women's Hospital
Boston, Massachusetts

 **P. Liacouras**

Walter Reed National Military Medical Center
Bethesda, Maryland

 **T.C. Lee**

 **D. Mitsouras**

Department of Radiology
Brigham and Women's Hospital
Boston, Massachusetts

3D T2-SPACE versus T2-FSE or T2 Gradient Recalled-Echo: Which Is the Best Sequence?

We read with interest the paper published on-line by Chokshi et al¹ regarding whether 3D T2 sampling perfection with application-optimized contrasts by using flip angle evolution (SPACE) could replace T2 FSE in spinal imaging.

We agree with the authors that 3D T2-SPACE is an excellent sequence when the aim is to evaluate changes in the relationship between the diameter of the spinal canal and its contents, in particular to confirm cord compression related to stenosis of the spinal canal caused by degenerative changes, to analyze very small normal or pathologic structures (roots, rootlets, root sheaths, superficial spinal cord vessels, denticulate ligaments), or to better depict the wall of cystic lesions. However, this sequence is not capable of discriminating abnormalities of the spinal cord or of the brachial plexus distal to the spinal ganglion. We think the question should not be “which is the best sequence,” but rather, “which is the best application for each sequence?”

Sequences such as in T2 gradient recalled-echo (GRE)^{2, 3} (multiecho recombined gradient echo [MERGE], multiecho data image combination [MEDIC], fast-field echo [FFE]), or even proton-density and 2D T2 fast spin-echo, have long proved to be superior in the axial and sagittal plane for better visualization of spinal cord abnormalities in case of degenerative myelopathy, demyelination plaques, or other kinds of myelopathies. The 3D T2-SPACE sequence is only able to demonstrate intramedullary lesions with high water content (cystic tumors, syringomyelia, necrotic areas, dilation of the ependymal canal), but proves unsatisfactory in identifying the hyperintense signal intensity associated with demyelination plaques, edematous contusion, or ischemia.

We agree with the authors that 3D T2-SPACE is less sensitive

to susceptibility and flow artifacts than 2D T2 spin-echo and T2 gradient-echo.⁴

3D T2-SPACE is an excellent sequence, but it should not be used alone. Instead, it should be used in conjunction with the T2-FSE or T2-GRE sequences, depending on the clinical indication.

Furthermore, we think it would be useful for the reader if some of the limitations of 3D T2-SPACE were mentioned, such as the visualization of false superficial siderosis, which can randomly appear in the sagittal, coronal, or axial planes, as illustrated in Fig 1.

REFERENCES

1. Chokshi FH, Sadigh G, Carpenter W, et al. **Diagnostic quality of 3D T2-SPACE compared with T2-FSE in the evaluation of cervical spine MRI anatomy.** *AJNR Am J Neuroradiol* 2017 Feb 2 [Epub ahead of print] CrossRef Medline
2. Yousem DM. **Point: Don't call me a DOC!** *AJNR Am J Neuroradiol* 2016;37:2180 CrossRef Medline
3. Sundarakumar DK, Smith CM, Hwang WD, et al. **Evaluation of focal cervical spinal cord lesions in multiple sclerosis: comparison of white matter-suppressed T1 inversion recovery sequence versus conventional STIR and proton density-weighted turbo spin-echo sequences.** *AJNR Am J Neuroradiol* 2016;37:1561–66 CrossRef Medline
4. Vargas MI, Delavelle J, Kohler R, et al. **Brain and spine MRI artifacts at 3Tesla.** *J Neuroradiol* 2009;36:74–81 CrossRef Medline

● M.I. Vargas

Division of Neuroradiology, DISIM
Geneva University Hospital
Geneva, Switzerland

● J.L. Dietemann

Department of Radiology
University Hospital of Strasbourg
Strasbourg, France

<http://dx.doi.org/10.3174/ajnr.A5190>

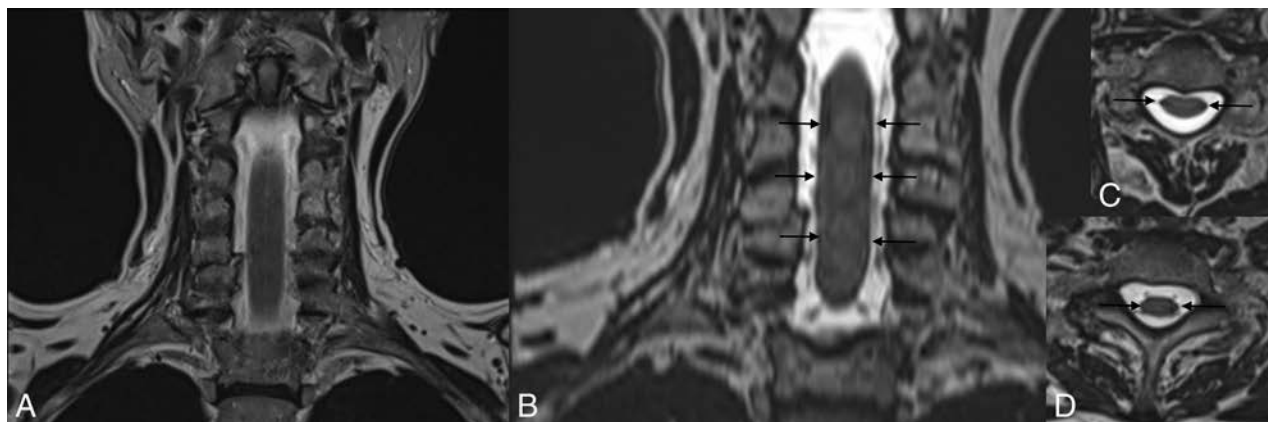


FIG 1. T2 TSE (A) and 3D T2-SPACE (B) in the coronal plane. Note linear low signal intensity on both sides of the spinal cord (arrows, B) on 3D T2-SPACE, also visible on the axial plane (C and D), mimicking superficial siderosis.

REPLY:

We thank Drs. Vargas and Dietemann for their interest in our article “Diagnostic Quality of 3D T2-SPACE Compared with T2-FSE in the Evaluation of Cervical Spine MRI Anatomy”¹ and their thoughtful comments and suggestions.

We agree with Drs. Vargas and Dietemann that T2-FSE is relatively a good sequence for the visualization of intrinsic spinal cord abnormality. However, to our knowledge, there have been no previous studies directly comparing its performance with T2-SPACE. The results of our study for the visualization of cord signal comparing the 2 sequences have been debated among our research team.

We do agree that the visualization of intrinsic cord signal and pathology is suboptimal with the T2-SPACE sequence; however, this was not the primary focus of this study. Subsequent studies should evaluate the role of T2-SPACE imaging as an adjunct sequence to visualize or not visualize cord pathology. This, however, was outside of the scope of our project.

Our study is not sufficient to provide guidance on the full range of imaging situations where T2-SPACE could be useful, but rather fills a void related to assessing the visualization of anatomic (not pathologic) cervical spine structures on MR imaging. We did not assess the diagnostic accuracy of T2-SPACE versus T2-FSE

sequences in assessing degenerative changes, which would be a separate analysis and paper. We have also noticed the “false superficial siderosis” appearance in some, but not all, T2-SPACE images. We did not feel it was as pronounced as the authors’ images show in their letter. With some training on visualizing T2-SPACE images, we believe that this appearance would not be problematic in clinical use.

Future well-designed diagnostic accuracy and comparative effectiveness studies will better inform radiologists of the uses and limitations of T2-SPACE for C-spine imaging.

REFERENCE

1. Chokshi FH, Sadigh G, Carpenter W, et al. **Diagnostic quality of 3D T2-SPACE compared with T2-FSE in the evaluation of cervical spine MRI anatomy.** *AJNR Am J Neuroradiol* 2017 Feb 2. [Epub ahead of print] CrossRef Medline

✉ **F.H. Chokshi**

Department of Radiology and Imaging Sciences, Division of Neuroradiology
Department of Biomedical Informatics

✉ **G. Sadigh**

Department of Radiology and Imaging Sciences, Division of Neuroradiology

✉ **W. Carpenter**

Department of Radiology and Imaging Sciences, Division of
Musculoskeletal Radiology

✉ **J.W. Allen**

Department of Radiology and Imaging Sciences, Division of Neuroradiology
Department of Neurology
Emory University School of Medicine
Atlanta, Georgia

<http://dx.doi.org/10.3174/ajnr.A5202>